Uncovering the natural history of cystic fibrosis progression within human pancreas and the potential role of the stellate cell as a mediator of β-cell dysfunction in cystic fibrosis-related diabetes

Yara Al-Selwi

Thesis submitted for the degree of Doctor of Philosophy

Newcastle University

Faculty of Medical Sciences

Institute of Cellular Medicine

August 2024

Declaration

I hereby declare that all work submitted in this thesis is entirely my own and the data gathered have not been submitted previously for any alternative degrees. All work was performed by me and any collaborations and contributions from colleagues have been acknowledged in the respective sections. All sources of information have been acknowledged by means of references.

-Yara Al-Selwi

Abstract

Cystic fibrosis (CF) is the commonest life-shortening autosomal recessive inherited disease. It is caused by mutations in the CF transmembrane conductance regulator gene (*CFTR*). This encodes the CFTR protein, which forms an ion channel mediating the secretion of chloride ions, sodium absorption and water transport across the cell membrane in epithelial cells. Loss of CFTR function leads to thickened fluid secretions particularly affecting the lungs and pancreas. Cystic fibrosis-related diabetes (CFRD) is a common non-pulmonary co-morbidity in CF affecting 2% of children increasing to 20% in adolescents and 50% in adults. Yet, the underlying pathogenesis is not fully understood.

To understand how pancreatic changes during CF may impact on the islet compartment leading to CFRD development, this project aimed to investigate the morphological changes within CF pancreata as the disease progresses. Also, it explored whether a semi-quantitative scoring of histopathological changes in CF, including duct dilatation, fibrosis, and fat replacement could meaningfully elucidate the course of the disease. AI quantitative analysis (HALO) was employed to further quantify the changes in exocrine and endocrine compartments of CF pancreata. Following on, this thesis aimed to establish an *in vitro* primary human islet stellate cell (ISC) model, which could mimic the cell-mediated 'stress' environment which islets are exposed to in CF and or CFRD pancreata. Subsequently, transcriptomic analysis of CF pancreatic tissue and EndoC-βH1 cells following treatment with ISC secretome was conducted.

A total number of 29 human pancreata biopsied at *post-mortem* from individuals with CF with age range 0–27-year-old were provided from Exeter Archival Diabetes Biobank (EADB) and a pathology bank collected by Prof. Günter Klöppel, Technical University of Munich, Germany. Fifty-eight control human pancreata were obtained from EADB and Quality in Organ Donation (QUOD) donors with age range of 0-29 year-old. Pancreatic tissue was stained with haematoxylin and eosin (H&E). In addition, a sub-cohort was stained with Sirius Red / Fast Green (SRFG), and immunohistochemistry staining for four endocrine hormones, chromogranin A, inflammatory cell markers CD45 and CD68, endothelial cell marker CD31 and α-smooth muscle actin (α-SMA).

CF pancreata were classified into: fibroatrophic pattern alone (CF Pattern 1); fibroatrophic and lipoatrophic pattern (CF Pattern 2); and lipoatrophic pattern alone (CF Pattern 3). Semi-quantitative scoring revealed an increase in ductal dilation in later-stage CF in fibrotic regions, severe ductal loss in adipocyte-rich regions and an increase islet remodelling as the disease

progresses from Pattern 1 to Pattern 3. AI-driven image analysis revealed islets to be increasingly disorganised with disease progression with significantly decreased insulin$^+$ area [%]. In CF, peri-islet fibrosis was significant in CF Pattern 2 with associated α-SMA$^+$ stellate cells. NanoString nCounter analysis in CF and control *post-mortem* tissue confirmed an increase in fibrosis-related gene expression including *TGF-β1* in CF.

As a potential mediator of pancreatic fibrosis, it was hypothesised that pancreatic stellate cells may secrete cytokines driving β-cell dysfunction in CF. *In vitro* primary human ISC model was established, characterised and ISC-secretome was shown to decrease EndoC-βH1 insulin content and secretion in the presence of high glucose. Deeper molecular phenotyping with bulk RNA sequencing revealed downregulation of β-cell transcription factors including *MafA*, *NKX 6.1* and *PDX1* in EndoC-βH1 treated with ISC secretome.

Collectively, these studies offered meaningful insights on pancreatic pathology natural history in CF, supporting a role of pancreatic stellate cells as potential mediators of endocrine dysfunction.

Dedication

I would like to dedicate this thesis to my father Fuad Al-Selwi and my mother Samia Al-Selwi and my sister Neamah Al-Selwi for nurturing me with unconditional love and support throughout my journey. I also dedicate this work to my family back home in Yemen.

Acknowledgment

Firstly, I thank Allah for giving me this opportunity to serve humanity with my humble knowledge and skills, for surrounding me with great people and for giving me the strength to wake up every day to pursue this journey.

I would like to thank Newcastle University in partnership with the Cystic Fibrosis Trust for funding this PhD project. I would like to thank all deceased donors and their families. This work would not have been achieved without them.

I would like to give my sincere gratitude to my supervisor, Professor James Shaw for giving me his support, guidance, advice, understanding and encouragement throughout my PhD journey, and for being a great and responsible role model. Secondly, I would like to thank my second supervisor Dr. Nicole Kattner for her friendly attitude, guidance, support and companion throughout my PhD. This work would not have been possible without their positive contributions.

I would like thank Exeter Archival Diabetes Biobank (EADB), Quality in Organ Donation (QUOD) and Professor. Günter Klöppel for providing pancreatic tissue/scans. I would also like pass my gratitude to Professor. Günter Klöppel for his kindness, willingness to share his knowledge and experience and for all the fruitful discussions we had together.

I sincerely thank Professor. Dina Tiniakos for sharing her experience and skills, for explaining the histology of the pancreas and for training me to be able to interpret pathological changes within diseased pancreatic tissue.

Further, I sincerely thank Professor. Sarah Richardson and her team for their collaboration with the AI-driven analysis. I would like to thank our lab manager Minna Honkanen-Scott, Megan Shaw and Dr. Nicola Dyson within our Translational Regenerative Medicine Laboratories for pancreatic biopsy handling, islets isolation and arrangements for isolated islet transportation. I would like to thank Michelle Thursby for her kindness and help throughout my PhD journey. I thank Rowan Coulthard and her colleagues at the NovoPath Newcastle Laboratories for their helpful service.

A special thank you to Professor. Lena Eliasson, Professor. Anna Wendt, Anna-Maria Ramsay and their outstanding PhD student Efraim Westholm for hosting me in their laboratory in Sweden, equipping me with the essential training and knowledge to conduct *in vitro* cell culture

studies using EndoC-βH1 cell line and supporting me with glucose-stimulated insulin secretion experiments. It has been an absolute pleasure to have the opportunity to collaborate with them.

I would like to thank Dr. Catherine Arden and Dr. Brain Ford for providing INS-1E cells. I would like to thank our lab technician Catlin Brack, Dr. Lee Borthwick and Dr. Jonathan Coxhead for their collaborations and service. Further, I would like to thank Dr. Olivier Govaere and James Clarck for their staining guidance during first and second year.

A warm thank you to my friends and lab/office colleagues (Sarah, Shireen, Michalina, Tarek, Fahad, Salma, Alaa, Sarah and Amelia) who became my second family over the last few years. Their support, random jokes, deep motivational talks, random presents, coffee dates and food sessions made this journey more enjoyable and fun. I am also grateful to Dr. Afie Leslie for his support and kindness.

I would like to deeply thank my family and friends here in the UK and back home in Yemen. To my parents and sister with her baby girl Rooh, my uncle Mohi El-Deen and my best friend Ruth Jeyaraj, thank you- for being there for me through the happy moments and hard times and what lies within the two. I would like to thank my grandmothers Neamah and Rayhana for keeping me in their thoughts and prayers and showering me with endless love and support. I would like to thank my cousins (especially Malak and Maria) for looking up to me and always inspiring me to be a better version of myself.

Finally, I thank myself and thank you for reading this work.

Published abstracts and awards

Diabetes UK Professional Conference (Oral presentation and Poster). **"Establishing an *in vitro* human model of islet-derived pancreatic stellate cells to study endocrine-exocrine cross-talk."** Kattner, Nicole., **Al-Selwi Yara.**, Brack, Caitlin., Westholm, Efraim., Honkanen-Scott, Minna., Dyson, Nicola., Wendt, Anna., Eliasson, Lena., Shaw, James. London, UK. April 2024.

17th European CF Young Investigators Meeting (Oral presentation). **"In depth characterisation of incremental pathological changes in Cystic Fibrosis pancreata using robust semi-quantitative and AI quantitative analysis." Y. Al-Selwi**, S. Richardson, L.A. Russell, R. Coulthard, D. Tiniakos, G. Klöppel, N. Kattner, J.A.M. Shaw. Paris, France. March 2024. **Best Oral Presentation Award**

European Association for the Study of Diabetes (EASD) (Oral presentation). "**Progressive pancreatic morphological changes and pro-inflammatory cell density in Cystic Fibrosis is associated with islet atrophy." Al-Selwi, Yara**., Kattner, Nicole., Bury, Yvonne., Coulthard, Rowan., Tiniakos, Dina., Klöppel, Günter., Govaere, Olivier., Shaw, James. Stockholm, Sweden. September 2022.

Future Investigators of Regenerative Medicine (Oral presentations and Poster). **"Progressive pancreatic morphological changes and pro-inflammatory cell density in cystic fibrosis is associated with islet atrophy." Y. Al-Selwi**, O. Govaere, Y. Bury, R. Coulthard, D. Tiniakos, G. Klöppel, J.A.M. Shaw, N. Kattner. Darlington, UK. May 2022.

Publications

Accepted in Principle. Westholm, Efraim., Karagiannopoulos, Alexandros., Kattner, Nicole., **Al-Selwi, Yara**., Merces, George., Shaw, James., Wendt, Anna., Eliasson, Lena. Islet insulin-like growth factor binding protein 7 is upregulated in type 2 diabetes and decreases insulin secretion.

Published. **Al-Selwi, Y**., Shaw, J., & Kattner, N. (2021). Understanding the Pancreatic Islet Microenvironment in Cystic Fibrosis and the Extrinsic Pathways Leading to Cystic Fibrosis Related Diabetes. Clinical Medicine Insights. Endocrinology and Diabetes, 14, 11795514211048812. https://doi.org/10.1177/11795514211048813

Publications for the data generated in this thesis are in preparation.

Table of Contents

List of Figures

List of Tables

List of Abbreviations

Abbreviation	Description
α	Alpha
%	Percentage
<	Less than
>	Greater than
±	Plus/minus
≤	Less equal or equal
≥	Greater than or equal
µm	Micrometre
mm	Millimetre
AAV	Adeno-associated virus
ACACB	Acetyl-CoA carboxylase beta
ACSM3	Acyle-CoA synthetase medium-chain family member-3
ACTA2	Actin Alpha 2, Smooth Muscle
ADH1B	Alcohol dehydrogenase 1B
ADIPOR1	Adiponectin receptor-1
AECs	Airway epithelial cells
AGEs	Advanced glycation end products
AI	Artificial intelligence
AMOTL2	Angiomotin like-2
ANGPTL4	Angiopoietin-like-4
ATP6V1E1	ATPase H+ transporting V1 subunit E1
BCA	Bicinchoninic acid
BCL2	B-cell lymphoma-2
BSA	Bovine serum albumin
C5	Complementary activation complement component-5
CASP	Caspase
CBL	Casitas B-lineage lymphoma
CCK	Cholecystokinin

CCL-2	Chemokine ligand-2
CDH11	Cadherin-11
CF	Cystic fibrosis
CF Pattern 1 (CF-P1)	Fibroatrophic
CF Pattern 2 (CF-P2)	Fibroatrophic and lipoatrophic
CF Pattern 3 (CF-P3)	Lipoatrophic
CFRD	CF related diabetes
CFTR	CF transmembrane conductance regulator
CGA	Chromogranin A
CGM	Continuous glucose monitoring
cm	Centimetre
COL1A1	Collagen Type I Alpha 1 Chain
CP-DM	Chronic pancreatitis- diabetes mellitus
CRP	C-reactive protein
CT	Computerised tomography
Ctrl	Control
CXCL	C-X-C motif chemokine ligand
CXCR4	CXC receptor-4
DAMPs	Damage-associated molecular patterns
DAPI	4′,6-diamidino-2-phenylindole
DDIT3	DNA damage inducible transcript 3
dL	Decilitre
DLL4	Delta-like-4
EADB	Exeter Archival Diabetes Biobank
ECM	Extracellular matrix
ELN	Elastin
ELX	Elexacaftor
EMT	Epithelial-mesenchymal-transition
FABP4	Fatty acid-binding protein
FASN	Fatty acid synthase
FBS	Fetal bovine serum
FFPE	Formalin-fixed paraffin embedded

FGA	Fibrinogen alpha chain
FGCGR3A/B	Fc gamma receptor 1A and 3B
FGD2	Faciogenital dysplasia-2
GLP1R	Glucagon-like peptide-1 receptor
GREM1	Germlin-1
GSIS	Glucose-stimulated insulin secretion
H&E	Haematoxylin and Eosin
HIF3A	hypoxia including hypoxia-inducible factor 3 alpha
HMGB1	High-mobility group box 1
HSPG2	Heparan sulphate proteoglycan 2
IF	Immunofluorescence
IFN-γ	Interferon- gamma
IGF1	Insulin-like growth factor 1
IHC	Immunohistochemistry
IL-1β	Interleukin-1beta
Ins1	Insulin 1
Ins2	Insulin 2
IPA	Ingenuity pathway analysis
ISCs	Islet stellate cells
IVA	Ivacaftor
KRT	Keratin-7
L	Litre
LAMCI	Laminin C1
LMEM	Linear mixed effect model
LSD	Least significant difference
LUM	Lumacaftor
MafA	V-maf musculoaponeurotic fibrosarcoma oncogene homolog A
MAPILC3A	Microtubule-associated protein 1 light chain 3 alpha
MCP-1	Monocyte chemoattractant protein 1

mg	Milligram
MHC	Histocompatibility complex
Min	Minutes
MIP-1α	Macrophage inflammatory protein-1 alpha
mmol	Millimole
MMP2	Matrix metalloproteinase-2
MMUT	Methylmalonyl-CoA mutase
MODY	Maturity-onset diabetes of young
MRI	Magnetic resonance imaging
MSD	Meso Scale Discovery
MSD	Multidimensional scaling
mTOR	Mechanistic target of rapamycin
MTS	3-[4,5-Dimethylthiazol-2-yl]-5-[3-carboxymethoxyphenyl]-2-[4-sulfophenyl]-2H-tetrazolium
MTT	3-[4,5-dimethylthiazol-2-yl]-2,5 diphenyl tetrazolium bromide
NETs	Neutrophil extracellular traps
NeuroD1	Neurogenic differentiation 1
NF-κB	Nuclear factor kappa-light-chain-enhancer of activated B cells
ng/ml	Nanograms per milliliter
NICE	National Institute for Health and Care Excellence
NID2	Nidogen-2
NK cells	Natural killer cells
NKX 6.1	NK6 homeobox 1
NOD	Non-obese diabetic
NOTCH3	Neurogenic locus notch homolog protein 3
NRIH3	Nuclear receptor interacting protein-3
NRP2	Neuropilin-2
NSAIDs	Non-steroidal anti-inflammatory drugs
°C	Celsius

OCLN	Ocludin
OGTT	Ooral glucose tolerance test
P4HB	Prolyl 4-hydroxylase beta subunit
PaSCs	Pancreatic stellate cells
PBS	Phosphate buffered saline
PCA	Principal component analysis
PCK1	Phosphoenolpyruvate carboxykinase-1
PDE2A	Phosphodiesterase
PDGFRB	Platelet-derived growth factor receptor beta
Pdx1	Pancreatic and duodenal homebox 1
PEI	Pancreatic exocrine insufficiency
PGP	Proline-glycine-proline
pH	Potential of hydrogen
PI3K-Akt	Phosphoinositide 3-kinase protein kinase B
PLCG2	Phospholipase C gamma-2:
PLIN4	Perilipin-4
pmol/L	Picomoles per liter
POSTN	Periostin
PPAR	Peroxisome proliferator-activated receptor
PSEN2	Presenilin
QUOD	Quality in Organ Donation
RBX1	Ring-box protein-1
rER	Rough endo plasmic reticulum
RIPA	Radio-immunoprecipitation assay
RNF152	Ring Finger protein-152
ROS	Reactive oxygen species
RPLP0	Ribosomal protein, large, R0
rtq-RT PCR	Real-time quantitative reverse transcription-polymerase chain reaction
SAB	Secretion assay buffer
SCNT	Somatic cell nuclear transfer
Sec	Seconds

SERPINF1	Serpin family F member-1
SERPING1	Serpin family G member-1
Slc2a2	Glucose transporter protein type 2 (GTR2)
Slc30a8	Solute carrier family 30 member 8 (zinc transporter)
SREBF1	Sterol regulatory element-binding transcription factor-1
SRFG	Picro-sirius red fast green
STAT 3/5	Signal transducer and activator of transcription-3/5
T1D	Type 1 diabetes
T2D	Type 2 diabetes
T3cD	Type 3c diabetes mellitus
T_{eff}	Effector T cells
TEZ	Tezacaftor
TGF-β	Tumour growth factor-beta
THBS1	Thrombospondin-1
TNF-α	Tumour necrosis factor-alpha
TRAF3	TNF Receptor Associated Factor 3
T_{reg}	Regulator T cells
TRIS/EDTA	Tirs/ Ethylenediaminetetraacetic acid,
TTN	Titin
VAMP8	Vesicle associated membrane protein-8
VCAM1	Vascular cell adhesion molecule-1
VEGF	Vascular endothelial growth factor
VIM	Vimentin
WHO	World Health Organisation
WWC1	Ww domain containing-1
X	Times
XBP1	X-box binding protein 1
α-SMA	Alpha-smooth muscle actin
β	Beta

δ	Delta
ε	Epsilon

Chapter 1: Introduction

1.1 The human pancreas

The pancreas is a complex organ that undertakes key roles within the digestive and the endocrine systems. In adults, the pancreas usually weighs around 100 g and is about 14-20 cm long (Longnecker, 2021). The pancreas is divided into three main parts: the head; which lies within the loop of the duodenum, the tail; which lies near the hilum of the spleen, and the body; which is the largest portion, lying behind the stomach ***(Figure 1.1)*** (Pandol, 2010; Longnecker, 2021).

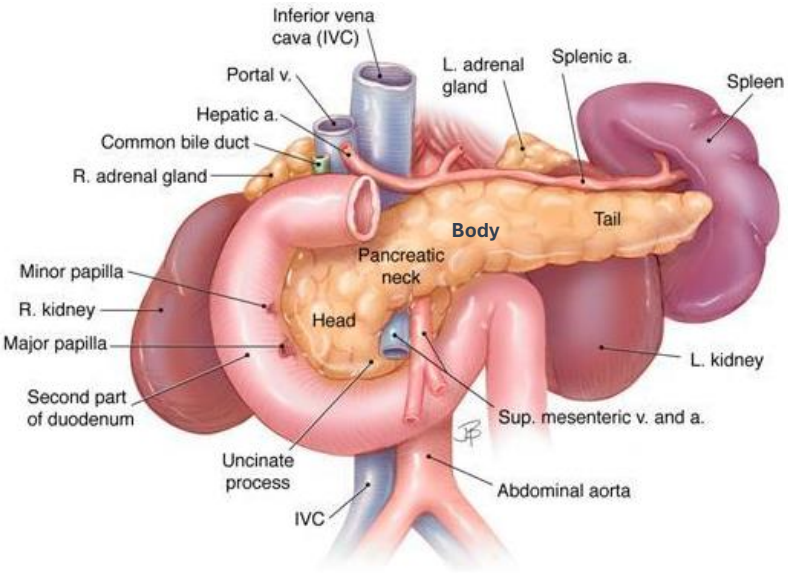

Figure 1.1: The Pancreas.

Anatomic relationships of the pancreas with respect to the surrounding organs. L: left, R: right, v: vein and a: artery. Adapted from Longnecker (2021).

The pancreas consists of two morphologically and functionally distinct components: the exocrine and the endocrine pancreas ***(Figure 1.2)*** (The Endocrine Pancreas | Anatomy and Physiology II, 2021). The exocrine part of the pancreas constitutes approximately 84% of the total mass; while the endocrine part takes up approximately 2-5% of the organ; blood vessels comprise around 4% of the pancreas and the remaining 10% is composed of extracellular matrix (ECM) including collagen fibres, reticular fibres, and fibroblasts (Longnecker, 2021).

The exocrine pancreas is composed of ductal and acinar cells, which produce a wide range of digestive enzymes, including lipases, proteinases, and amylases, that are secreted into the pancreatic duct and flow into the small intestine to break down fats, proteins, and carbohydrates for absorption (Zhou & Melton, 2018). The endocrine pancreas consists of islets of Langerhans,

which are clusters of vascularised micro-organs and are spread throughout the pancreas and contain five major types of islet cells (Zhou & Melton, 2018). Each islet cell type synthesises and secretes specific hormones playing key roles in regulating blood glucose homeostasis: α-cells secrete glucagon, β-cells secrete insulin, δ-cells secrete somatostatin, PP-cells secrete pancreatic polypeptide and ε-cells secrete ghrelin (El Sayed & Mukherjee, 2023).

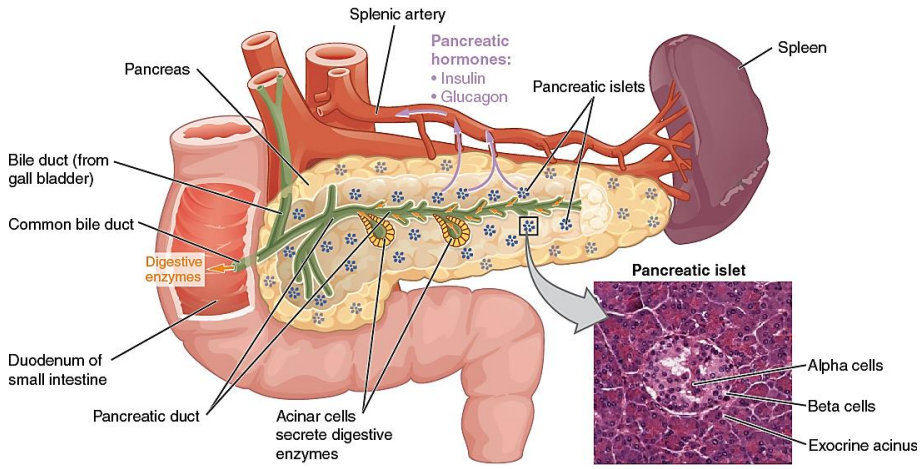

Figure 1.2: Tissue structure of the pancreas.

Illustration of the digestive and hormonal secretion by the exocrine and endocrine compartments of the pancreas. Adapted from The Endocrine Pancreas | Anatomy and Physiology II (2021).

Changes in islet microenvironment along with extrinsic stress within the exocrine compartment are associated with pancreatic diseases including diabetes, pancreatitis, cystic fibrosis (CF) and CF-related diabetes (CFRD) (Rickels et al., 2020). Below, different pancreatic pathologies are reviewed and their impact on pancreas morphology and function is summarised.

1.2 Diabetes mellitus

Diabetes mellitus is a complex metabolic disorder encompassing various diseases adversely affecting the glucose status of the human body (Tsalamandris et al., 2019). The clinical diagnostic features are hyperglycaemia driven by absolute or relative insulin deficiency with or without insulin-resistance dependent on diabetes type (Tsalamandris et al., 2019). Since 1980, the number of adults living with diabetes has almost quadrupled to 422 million adults and these figures are expected to rise to 552 million by 2030, according to the World Health Organisation (WHO) global report on diabetes that was published in 2016 (Whiting et al., 2011; WHO, 2016). These high figures highlight the critical importance of developing potential effective therapeutic approaches to enable the treatment and / or the prevention of diabetes and associated diabetes-related complications including atherosclerotic cardiovascular disease

(Booth et al., 2006; Beckman et al., 2013). The majority of diabetes cases mainly fall into two broad pathogenic categories: type 1 diabetes (T1D) and type 2 diabetes (T2D) (Tsalamandris et al., 2019).

1.2.1 Type 1 diabetes mellitus

Historically, T1D is said to be one of the most common chronic illnesses of childhood whereby incidences peak occurs at 5-7 years of age and at or near puberty (Gale, 2005; Harjutsalo et al., 2008). However, over the past decade it has become clear that T1D can present at any age. (Leslie, 2010). Nevertheless, the age of onset plays a significant role in T1D heterogeneity along with other factors including the severity of autoimmune response (Bottazzo et al., 1974; Willcox et al., 2009; Atkinson et al., 2011).

T1D is characterised by insulin deficiency resulting from a specific and selective autoimmune-mediated destruction of insulin-producing β-cells in the islet of Langerhans, by self-reactive T cells and macrophages that infiltrate the islets without visible pathological alterations of other pancreatic endocrine cells (Atkinson et al., 2014). Moreover, both humoral and cellular immunity are reported to be involved in the pathogenesis of T1D (Bottazzo et al., 1974; Willcox et al., 2009; Atkinson et al., 2011).

The triggers to the immune response in T1D remain unclear, but there are genetic and environmental factors that are involved and can influence this immune response. Genetically, there are approximately 40 loci that have been reported to impact on disease susceptibility and the majority of these loci are thought to be involved in the development of the autoimmune response in T1D (Concannon et al., 2009). Haplotypes DRB1*0401 and DQB1*0302 of the HLA class II genotype are associated with the greatest susceptibility to T1D (Concannon et al., 2009). With that being said, T1D development is not dependent on a single gene (Haller et al., 2005). Moreover, the risk of T1D is believed to be influenced by environmental factors including but not limited to diet, vitamin D deficiency, bacterial and viral infections (Kukko et al., 2005; Daneman, 2006; Harjutsalo et al., 2008; Atkinson et al., 2014). The pathological and physiological responses to these environmental factors might also be influenced by the genetic susceptibility (Cooper et al., 2011; Winkler et al., 2011). Other factors such as geographical location, which influence the environmental factors, can further affect the incidence of T1D, however the underlying mechanisms are unknown (Atkinson et al., 2014; Xia et al., 2019). In addition, months or years before the onset of symptomatic T1D, it is

thought that seasonal synchronisation is apparent regarding the development of T1D-related autoimmunity evidenced by islet autoantibody formation (Kukko et al., 2005).

1.2.1.1 Inflammation and immune cell infiltration

The predominant pathophysiology of T1D is the inflammation of pancreatic islets (insulitis) throughout the disease progression (Tsalamandris et al., 2019). A study demonstrated that the arrival of autoreactive T cells in the circulating blood of non-obese diabetic (NOD) mice is mediated by a failure in both central and peripheral immune tolerance (Anderson & Bluestone, 2004). Peripheral immune tolerance regulators, T regulatory cells (T_{regs}), have also been demonstrated to be dysfunctional in T1D (Anderson & Bluestone, 2004). In addition, studies in animal models have demonstrated the participation of effector T cells (T_{eff}) $CD4^+$ and $CD8^+$ in the development of T1D, where they target specific β-cells autoantigens and associated peptide epitopes (Miller et al., 1988; El-Sheikh et al., 1999; Phillips et al., 2009; Richardson et al., 2014). T-cell subtypes have been reported to have the ability to induce peri-islet inflammatory infiltrates and overt diabetes using adoptive T-cell transfer models of T1D (Healey et al., 1995; Katz et al., 1995). The presence of effector T cells has been further shown in *post-mortem* human pancreata from donors with recent-onset T1D (Willcox et al., 2009; Arif et al., 2014).

Islet inflammation is influenced by macrophages which produce reactive oxygen species (ROS) and secrete cytokines including interleukin-1β (IL-1β) and tumour necrosis factor-α (TNF-α) (Willcox et al., 2009; Hutchings et al., 1990). Similarly, other immune cells such as lymphocytes and neutrophils have been demonstrated to be abundant in the exocrine tissue of T1D pancreata and these cells are suspected to play a role in the development of T1D (Valle et al., 2013; Rodriguez-Calvo et al., 2014). Other studies have shown the presence of dendritic cells, natural killer cells (NK) and NK T-cells (a subset of T cells that exhibits properties of both NK cells and T cells) in the islet infiltrate (Dotta et al., 2007; Lehuen et al., 2010). The interactions between this wide range of inflammatory cells mediate diabetes progression and the synergic effect of interferon- gamma (IFN-γ) and the innate inflammatory cytokines TNF-α and IL-1β appears to drive β-cell inflammation (Dotta et al., 2007; Lehuen et al., 2010).

1.2.1.2 Pathological and morphological changes in T1D pancreata

Reported pathological and morphological observations in T1D include a reduction in overall pancreas weight, atrophy of dorsal region, exocrine atrophy, lobular loss of β-cells, alterations of insulin, somatostatin, glucagon and pancreatic polypeptide secretion as well as

heterogeneous lobular insulitis (Atkinson et al., 2014; Alexandre-Heymann et al., 2019). Other observations noted in islets in T1D include insulitis comprising immune cell presence of T-cells, B-lymphocytes and macrophages located adjacent and/or within islets, overexpression of major histocompatibility complex (MHC) Class I, loss of β-cells which is reported to increase as the disease progresses. Beta-cell necrosis, apoptosis and diminished insulin content in remaining β-cells have all been postulated (Atkinson et al., 2014).

1.2.2 Type 2 diabetes mellitus

T2D is the most common form of diabetes accounting for 90-95% of all diabetes cases and prevalence is continuously increasing at a significant rate, with an associated rise in morbidity and mortality that increases the burden on health-care systems (American Diabetes Association, 2018; Ying et al., 2020). Genetic and environmental factors both influence the epidemiology of T2D and generally the genetic factors appear to exert their effect after the exposure to an environmental 'stress' factor such as low physical activity and high-calorie intake (Galicia-Garcia et al., 2020).

Insulin-resistance is commonly believed to be the primary defect in T2D development whereas a relative insulin deficiency is considered as a secondary but necessary factor in the development of T2D (American Diabetes Association, 2018). During the initial state of insulin resistance, in individuals who are at a high risk of T2D, there is a hypersecretion of insulin in β-cells, however by the time these individuals are diagnosed with T2D their β-cells are no longer capable of secreting enough insulin to maintain normal glucose levels (Jallut et al., 1990).

1.2.2.1 Inflammation and immune cell infiltration

Chronic activation of proinflammatory pathways in insulin target cells is believed to contribute to obesity, insulin-resistance and related metabolic disorders including T2D (Marques-Vidal et al., 2012). Mouse models and human studies have established that islet inflammation is present in patients with obesity and/or T2D raising the possibility of a contribution of islet inflammation to β-cell dysfunction in T2D (Ying et al., 2020). However, the detailed mechanisms leading to islet inflammation are not fully understood (Ying et al., 2020). $CD68^+$ macrophages including both tissue-resident and infiltrating monocyte-derived macrophages are the dominant immune cell causing inflammation in islets in obese and/or T2D individuals (Böni-Schnetzler & Meier, 2019a; Ying et al., 2020). This is in contrast to T1D whereby adaptive in addition to innate immune cells are strongly involved. In T2D, local proliferation

of resident macrophages further enhances macrophage accumulation which increases signals potentially stimulating β-cell hyperplasia (Ying et al., 2020). Moreover, a phenotypic shift in predominantly anti-inflammatory M2-type macrophages switching to elevated proportions of pro-inflammatory classical M1-type macrophages in T2D, further supports their significant role in the initiation and amplification of islet inflammation (Sell et al., 2012). Therefore, it has been proposed that islet-resident macrophages underlie the inflammatory state in obesity and T2D leading to β-cell dysfunction (Böni-Schnetzler & Meier, 2019).

In vitro experiments have reported that some inflammatory cytokines and chemokines including IL-6, IL-8, C-X-C motif chemokine ligand 1 (CXCL-1) and macrophage inflammatory protein-1α (MIP-1α) were released from islets isolated from T2D individuals, and the increase of these inflammatory cytokines was shown to have a correlation with the abundance of macrophages (Ehses et al., 2007). However, the cellular origin of these inflammatory cytokines and their impact on β-cell function is still undetermined (Böni-Schnetzler & Meier, 2019).

In obesity and T2D studies, increased numbers of intra-islet macrophages, increased β-cell proliferation, increased IL-β and TNF production, lowered expression of end-differentiated β-cell-specific genes as well as suppressed glucose-stimulated insulin secretion were reported (Ying et al., 2020). Moreover, activated pancreatic stellate cells (PaSCs) in a rat model have been postulated to lead to islet fibrosis in T2D, however when PaSCs activation was reduced by pirfenidone, islet fibrosis was reduced, but there was no observed effect on glucose tolerance or on β-cell function, suggesting that PaSCs activation itself might not contribute significantly to progressive β-cell dysfunction in T2D (Lee et al., 2017).

1.2.2.2 Pathological and morphological changes in T2D pancreata

Ultrasound imaging studies in T2D pancreata reported a decrease in pancreas volume by 33% versus matched controls with normal glucose tolerance (Macauley et al., 2015). Morphological observations on T2D pancreata reported reduced islet numbers, loss of β-cell mass and the presence of fat infiltration in the exocrine parenchyma, which may be associated with insulin resistance and is implicated in islet lipotoxicity (Yagihashi, 2017; Atkinson et al., 2020). The detected elevated fat deposition has been suggested to contribute to an irregular border of the pancreas on imaging, which is thought to be a distinctive feature of diabetes in T2D individuals that is not observed in the pancreas of T1D individuals (Al-Mrabeh et al., 2016). The presence

of fibrotic tissue and islet amyloidosis (develops from the extracellular deposition of islet amyloid polypeptide) are observed in T2D pancreas (Yagihashi, 2017; Atkinson et al., 2020).

1.2.3 Complications of T1D and T2D

The onset and progression of macrovascular complications in T1D and T2D are determined by the combination of multiple risk factors such as high fat intake, obesity, smoking and low physical activity (Avogaro & Fadini, 2019). These complications include coronary heart complications, cerebro-vascular and peripheral vascular diseases (Avogaro & Fadini, 2019). Moreover, microvascular complications including nephropathy, neuropathy and retinopathy are mainly induced by hyperglycaemia through mechanisms including the production of advanced glycation end products (AGEs), the formation of a proinflammatory microenvironment and the induction of oxidative stress (Papatheodorou et al., 2016).

1.2.4 Diabetes mellitus diagnosis clinical management

T1D and T2D can be diagnosed by a fasting glucose concentration greater than 7.0 mmol/L (126 mg/dL) or a random blood glucose concentration higher than 11.1 mmol/L (200 mg/dL) with symptoms of hyperglycaemia (American Diabetes Association, 2018; Butler & Misselbrook, 2020). A 2 h plasma glucose value greater than 11.1 mmol/L (200 mg/dL) during an oral glucose tolerance test (OGTT) using a 75 g glucose load (Butler & Misselbrook, 2020) is also diagnostic. A less sensitive criterion is elevated glycosylated haemoglobin (HbA_{1C}, a form of haemoglobin non-enzymatically linked to glucose) above 48 mmol/mol (American Diabetes Association, 2018; Butler & Misselbrook, 2020). Being obese or having a higher body fat percentage, predominantly distributed in the abdominal area, are typical characteristics of patients with T2D, however, not all obese individuals develop T2D and not all people with T2D are overweight (Galicia-Garcia et al., 2020).

1.2.5 Diabetes mellitus clinical management

Up until now, there is no cure for T1D. The primary treatment is life-long exogenous administration of insulin (Atkinson et al., 2014). In addition to pharmacological therapies, both T1D and T2D patients have to estimate their carbohydrate, protein and fat intake as well as monitoring their blood glucose frequently and undertake sufficient physical activity (Tsalamandris et al., 2019).

In addition to primary glucose-lowering action, some current therapies targeting T2D have potential anti-inflammatory characteristics as their main mode of action. These include

thiazolidinediones and metformin, which also has metabolic actions (Atkinson et al., 2014). Moreover, when oral agents cease to be sufficient in T2D, insulin therapy is required (Atkinson et al., 2014). Importantly, the use of inflammatory biomarkers can potentially help in defining optimal management for diabetes and related metabolic disorders (Goldfine et al., 2011; Kengne et al., 2012).

Macrovascular complications of diabetes need to be addressed by altering patients' lifestyle and incorporating healthy management factors such as low-fat diet, weight control, frequent physical activity, smoking cessation and maintaining normal blood pressure and lipid profile (Daneman, 2006). Microvascular complications are targeted by lowering glucose towards normal levels using insulin treatment in T1D and oral agents / insulin in T2D (D. M. Nathan & Group, 2014).

1.2.6 Other forms of diabetes

As many factors such as genetic, immunological or neuroendocrinological pathways together play a role in the cellular and molecular mechanisms involved in disease development, some diabetes cases do not fall into the common two classifications (Tsalamandris et al., 2019). For example, gestational diabetes where glucose intolerance is developed during pregnancy and usually resolves post-delivery; maturity-onset diabetes of young (MODY) where the development and maturation of β-cells are affected due to inherited genetic mutations presenting most commonly in young adults before the age of 25; and neonatal diabetes affecting new-borns under the age of 6 months (Alfadhli, 2015; Anik et al., 2015; Lemelman et al., 2018).

1.3 Pancreatitis

Pancreatitis is a disease continuum formed by acute pancreatitis, recurrent pancreatitis and eventually chronic pancreatitis (Mayerle et al., 2019). Pancreatitis is a multifactorial, proinflammatory condition and is the most common form of injury to the exocrine pancreas (Q. Zhou & Melton, 2018). It is distinguished by a painful inflammation triggered by genetic factors including genes predisposing to pancreas-targeting autoimmune reaction, cystic fibrosis or various environmental factors including injury, alcohol, smoking or high fat diet (Q. Zhou & Melton, 2018). Chronic pancreatitis is characterised by repetitive episodes of pancreatic inflammation that lead to severe loss of exocrine parenchyma that is extensively replaced by fibrotic tissue, resulting in irreversible tissue damage that results in chronic pain, exocrine and

endocrine pancreatic insufficiency as well as reduced life-quality and life expectancy (Beyer et al., 2020).

Pancreatogenic diabetes is now termed type 3c diabetes mellitus (T3cD). It is characterised by pancreatic exocrine insufficiency (PEI) and accounts for up to 5-10% of the overall diabetes population (often being misdiagnosed as T2D) with 79% of cases arising from chronic pancreatitis (CP-DM) and 4% of cases arising from CF (Ewald et al., 2012).

Imaging modalities used to diagnose pancreatitis include X-ray, ultrasound, computerised tomography (CT), and magnetic resonance imaging (MRI) (Beyer et al., 2020). Pancreatitis is treated with medications to ease the pain, artificial digestive enzymes are prescribed for individuals with PEI, and insulin administration is the primary treatment for patients who develop diabetes (Beyer et al., 2020). Endoscopy is used in cases to remove any blockages within the pancreatic ducts and relieve pain. Surgery is also a treatment option, especially for chronic pancreatitis, to remove part of the pancreas, unblock pancreatic ducts and to drain cysts, when medications are not effective in reducing the pain (Beyer et al., 2020).

1.3.1 Inflammation and immune cell infiltration

The early cellular events that take place after the initial onset of acute pancreatitis are independent activation of intra-acinar protease and nuclear factor kappa-light-chain-enhancer of activated B cells (NF-κB), which is resident normally in the cytoplasm, and its main function is to regulate the immune response (Baldwin, 1996; Gukovsky et al., 1998; Steinle et al., 1999). In addition, it has been reported that prolonged activation of NF-κB promoted progression of CP (Huang et al., 2013). NF-κB is a central mediator of the innate and adaptive mechanisms, and its activation can lead to a chronic infiltration of immune cells (Mayerle et al., 2019). However, an external stimulus such as injury is required for pancreatitis to develop, as the presence of immune cell infiltration in the pancreas is not sufficient to develop pancreatitis because these immune cells need to be activated to play a significant role in pancreatitis severity and its prognosis (Johnson & Abu-Hilal, 2004; Aleksic et al., 2007; Baumann et al., 2007; Gukovsky et al., 2013; Sendler et al., 2013; Habtezion, 2015).

The majority of immune cell infiltrate is made up of innate immune cells: neutrophil granulocytes, monocytes, and macrophages (Liu et al., 2017). In pancreatitis, NF-κB activation and cholecystokinin (CCK) stimulation induce acinar cells to release various cytokines and chemokines including IL-6, TNF-α, and/or monocyte chemoattractant protein 1 (MCP-1) (Gukovskaya et al., 1997; Sendler et al., 2018). Necrotic acinar cells also release damage-

associated molecular patterns (DAMPs) including free DNA, histones, and free adenosine triphosphate that meditate the activation of immune cells (Gukovskaya et al., 1997; Hoque et al., 2011; Sendler et al., 2018; Zhao et al., 2018a). These cytokines and DAMPS lead to NFκB p65 and p50 translocation within the infiltrating immune cells, further enhancing tissue cytokine storm via the secretion of proinflammatory mediators, which further increases pancreatic damage and enhance systematic inflammation (Gukovskaya et al., 2002; Sendler et al., 2013, 2018).

Pancreatitis inflammation markers include neutrophil granulocytes, which are considered a major source of ROS production and are able to induce oxidative damage in acinar cells and elevate trypsinogen activation, which can lead to autodigestion of the pancreatic gland (Gukovskaya et al., 2002). The biochemical marker for pathological granulocyte polymorphonuclear neutrophil-elastase also contributes to acinar cell dissociation and tissue damage (Mayerle et al., 2005). Neutrophils are believed to have a direct effect on pancreatitis severity, whereby studies investigated the effect of neutrophil depletion via antineutrophil serum and reported that, pancreatic tissue damage was reduced following neutrophil depletion protease activation (Gukovskaya et al., 2002; Sendler et al., 2013). Moreover, the formation of neutrophil extracellular traps (NETs) is critical in bile stone development and contributes significantly to ductal obstruction which further impacts on pancreatitis severity (Schauer et al., 2014; Leppkes et al., 2016).

Other cellular markers include monocytes and macrophages. Classic activated M1 macrophages are reported to be associated with multiorgan dysfunction syndrome and increased mortality (Johnson & Abu-Hilal, 2004). M1 macrophages exhibit proinflammatory characteristics whereby they secrete large amounts of TNF-α, IL-6, IL-12 and IL-1β, and express elevated levels of inducible nitric oxide synthase, which increases the release of nitric oxide that activates NFκB pathway (Gordon & Taylor, 2005). Additionally, TNF-α is reported to have a direct effect on pancreatic acinar cells whereby it mediates pancreatic damage and the activation of digestive proteases (Perides et al., 2011; Guo et al., 2012). Further, *in vitro* experiments demonstrated that NF-κB promoted the activation of PaSCs and the secretory response of M1 chronic pancreatitis-associated macrophages and fibrosis-related factors (Wu et al., 2021).

Interestingly, pancreatic damage and necrosis correlate to a greater extent with macrophage infiltration rather than neutrophil infiltration as macrophages are needed for removing necrotic

cells (Sendler et al., 2018). In various models of acute and chronic pancreatitis phagocytosing macrophages were observed (Gukovskaya et al., 2002; Koh et al., 2010; Guo et al., 2012; Diakopoulos et al., 2015; Mareninova et al., 2015; Cobo et al., 2018; Sendler et al., 2013, 2018). Moreover, activated M2 macrophages act as anti-inflammatory cells and promote organ regeneration but also fibrogenesis in chronic pancreatitis via the production of IL-10 and/or TGF-β (Criscimanna et al., 2014; Sendler et al., 2015; Xue et al., 2015). M2 fibrogenesis is reported to be dependent on IL-4 and IL-3 signalling and PaSCs are demonstrated to be a source of IL-4 and IL-3 (Xue et al., 2015).

1.4 Cystic fibrosis

CF is a monogenic chronic condition that is inherited in an autosomal recessive manner and is caused by loss-of-function mutations in the *CFTR* gene coding for the CF transmembrane conductance regulator (CFTR) (Riordan et al., 1989). The CFTR protein forms a chloride channel that mediates the secretion of chloride ions, sodium absorption and water transport across the cell membrane in epithelial cells, mainly in the lungs, pancreas (on the apical membrane of epithelial cells in the pancreatic ductal epithelium), gut and genital tract (Riordan et al., 1989; Stoltz et al., 2015; Norris et al., 2019). Mutations in the *CFTR* gene impair this critical role of CFTR leading to mucus hyper-concentration along with decreased muco-ciliary clearance, which is the primary innate defence mechanism of the respiratory system airways (Stoltz et al., 2015).

CF cases have been reported from all ethnicities and nationalities whereby the estimated prevalence rate in Asians, native Hawaiians and pacific Islanders is 1:31,000 to 1:100,000; in African Americans is 1:15,100; in Hispanics is 1:3,500 and in white individuals is 1:2,500 (Rubin, 2014). Globally, there are approximately 70,000 to 100,000 individuals with CF including about 10,600 people in the UK with an estimated 200-300 diagnosed new cases annually (Taylor-Robinson et al., 2018; Kelsey et al., 2019).

1.4.1 Cystic fibrosis genotype/phenotype

There are six predominant functional classes of CFTR mutations that give rise to multiple phenotypes ***(Figure 1.3)*** (Boyle & De Boeck, 2013). Mutations of classes I-III have partial or no CFTR function and are present in severe CF cases, whereas mutations of classes IV-VI are associated with mild CF cases; as they maintain some residual CFTR function and are reported to be more usually associated with pancreatic exocrine-sufficient CF (Lopes-Pacheco, 2016; Turcios, 2020). Class I mutations account for 12% of CFTR mutations and are caused by

nonsense and/or frame-shift mutations that result in a non-functional CFTR protein (Feldmann et al., 2003; Lopes-Pacheco, 2016; Turcios, 2020). Class II mutations, with the highest prevalence of all mutations at 87%, are caused by missense and/or amino acid deletion (e.g ΔF508) mutations leading to misfolding of the protein, whereby it gets trapped and degraded in the endoplasmic reticulum and fails to arrive at the cell surface (Turcios, 2020). The third class of mutations is classified by abnormal channel function with failure to open due to missense mutations (Turcios, 2020). Class IV mutations also have abnormal channel function but, in this case, there is a reduced ion conductance, whereas class V mutations are missense and/or splicing mutations that reduce CFTR synthesis (Feldmann et al., 2003; Lopes-Pacheco, 2016; Turcios, 2020). Class VI missense mutations are rare with a shortened CFTR half-life decreasing its stability (Turcios, 2020).

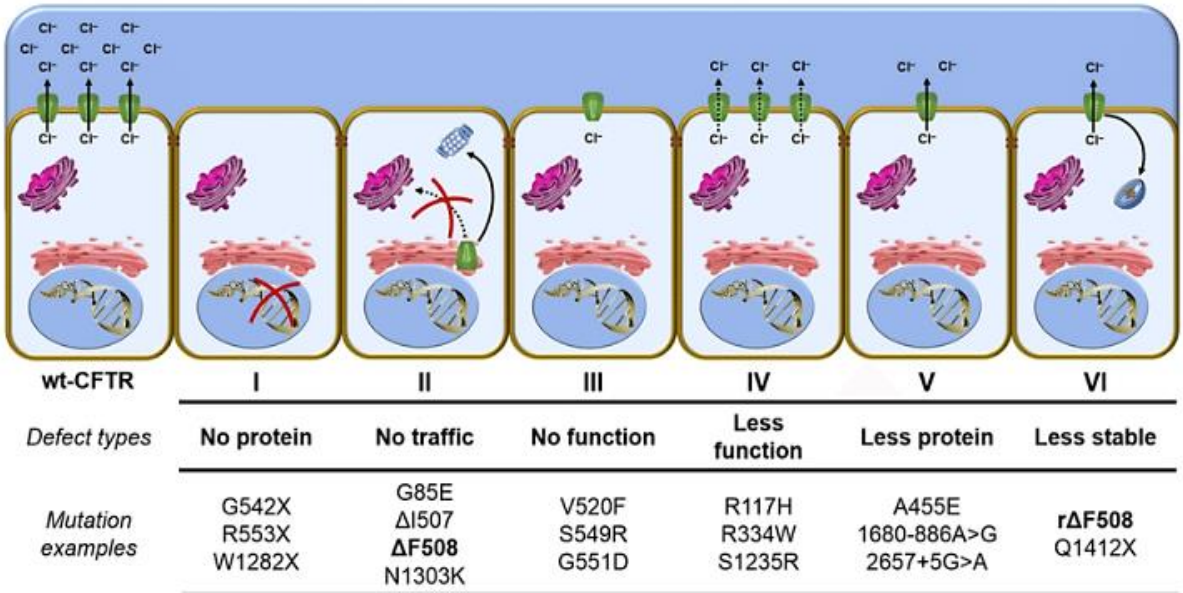

Figure 1.3: Functional classes of CFTR mutations.

Adapted from (Lopes-Pacheco, 2016).

1.4.2 Cystic fibrosis complications

Some complications including gastrointestinal and nutritional pathology develop in early life (Turcios, 2020). Approximately 15% of new-borns with CF have 'meconium ileus' due to the intestines being blocked leading to rectal prolapse (Turcios, 2020). Other non-pulmonary clinical complications of CF caused by thick mucus secretion include chronic inflammation in different tissue including the pancreas (Collins, 2018; Turcios, 2020). Pancreatic pathology is CF is initiated by obstruction of pancreatic ducts leading to damage of exocrine tissue which can result in PEI as well as CFRD (Collins, 2018; Turcios, 2020). Approximately 85-90% of

people with CF have PEI (Kalnins et al., 2007; Baker et al., 2005; Hegyi et al., 2016). Mutations of classes I to IV lead to PEI due to substantial loss of acinar cells within the pancreas and as a result a decline in the production of digestive enzymes (Kerem et al., 2010). Lack of digestive enzyme activity leads to the clinical syndrome of PEI due to malabsorption of fat in addition to of fat-soluble vitamins and proteins (Collins, 2018; Turcios, 2020).

The majority of males with CF develop infertility due to the absence of congenital bilateral and vas deferens, whereas females with CF develop infertility due to obstruction of the cervical opening which prevents sperm penetration into the uterus (Turcios, 2020). Blockage of the common bile duct can lead to gall stone formation and potentially biliary hepatic cirrhosis (Turcios, 2020).

Respiratory failure is the dominant cause of mortality and morbidity in CF (Turcios, 2020). Individuals of the same CF genotype can manifest different phenotypes making it difficult to predict lung function over time for any given individual (Vanscoy et al., 2007). Defects in chloride ion and bicarbonate anion secretion, due to defects in CFTR function, lead to fluid hyperabsorption within the airway epithelium and increased osmotic pressure in the mucus layer compared to the periciliary layer, which in turn depletes the airway surface of fluid resulting in dehydrated mucus, mucus transport impairment, and the adhesion of mucus to airway surfaces (Boucher, 2019). Moreover, the formation of endobronchial mucus plaques and plugs narrows the airways, due to dehydrated mucus secretions, and become the site of chronic airway infection with persistent high-intensity inflammatory response, characterised by increased levels of neutrophil elastase (Rubin, 2014; Cantin et al., 2015; Chalmers et al., 2017). This further enhances the development of severe bronchiectasis (abnormal widening and thickening of lung bronchi) by contributing to excess mucus adhesiveness and cohesiveness and ultimately resulting in pulmonary insufficiency and respiratory failure ***(Figure 1.4)*** (Rubin, 2014; Cantin et al., 2015; Chalmers et al., 2017).

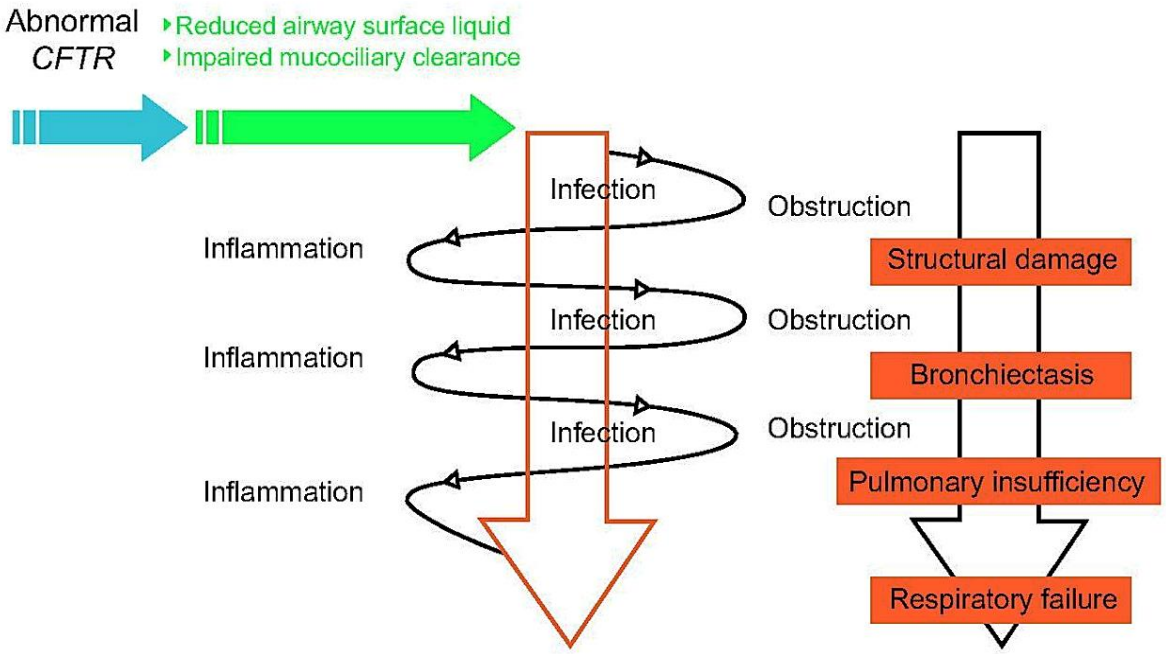

Figure 1.4: CF-related lung pathology.

The common characteristics of CF lung disease include air-flow obstruction and recurrent infections, which further result in inflammation response that damages the airways structural integrity and the development of bronchiectasis. Adapted from (Turcios, 2020).

1.4.2.1 Inflammation and immune cell infiltration - CF lungs

Airway inflammation in CF is characterised by the activation of innate immune cells including airway epithelial cells (AECs) and macrophages during the onset stages, then followed by neutrophils (Ralhan et al., 2016). The release of chemo-attractants such as soluble bacterial products (N-formyl-methionyl-leucyl-phenylalanine), fragments of the 5th component of the complement system (C5a and C5 adesArg), cellular proinflammatory cytokines (IL-8, IL-7 and leukotriene B4), and high-mobility group box 1 (HMGB1) together with proline-glycine-proline (PGP) as well as N-acetyl PGP, recruits neutrophils into the CF airway (Rose, 2002; Castellani et al., 2018). During the inflammatory response, neutrophils in CF airways undergo necrosis further releasing high quantities of intracellular contents including actin and long-stranded DNA fragments, which contribute to the viscosity of CF sputum (Sanders et al., 2009; Duncan et al., 2016;). Within the CF lung microenvironment, high levels of proinflammatory markers including IL-8, IL-6, IL-1β and TNF-α were present compared to healthy control, whereas IL-10 levels were reduced (Bruscia & Bonfield, 2016). In CF lung pathophysiology, abnormal macrophage function can impact on the adaptive immune system, whereby macrophage MHC class II expression is reduced impacting on T-cell response to pathogens, with defective natural killer T-cell activity, elevated B-lymphocyte activity and dysregulated

cytokine production (Bruscia & Bonfield, 2016). These defects further contribute to the recurrent infection / inflammatory state in CF lungs.

1.4.3 Diagnosis of CF

The genetic screening test for the *CFTR* gene has been the definitive diagnostic test for CF for the past 30 years (Françoise & Héry-Arnaud, 2020). Measuring serum immunoreactive trypsinogen (a specific pancreatic enzyme) level is commonly used as a new-born screening diagnostic approach (Farrell et al., 2017). If an elevated positive screening result is reported and/or a family history of CF is present and/or any CF symptoms are observed, then a diagnostic sweat test should be carried out (Farrell et al., 2017). A clinical diagnosis of CF is established when the level of sweat chloride is higher than 60 mmol/L in children and adults and > 40 mmol/L in infants (Turcios, 2020). Genetic analysis is essential when sweat chloride level is within the intermediate range (30-59 mmol/L) (Turcios, 2020). Normal measurement (< 29 mmol/L) of sweat chloride indicates that a CF diagnosis is unlikely; however, this normal level can still be reported even in the presence of some CFTR mutations (Feldmann et al., 2003; Strong et al., 1991).

Sometimes CF is mistaken for asthma in countries where neonatal screening is not provided and, as a result, appropriate management and treatment is delayed (Turcios, 2020). Some factors that influence the diagnosis of CF in non-screened individuals, include the age of onset, the possible development of partial or complete pancreatic insufficiency and the absence of established CF clinical complications (Sosnay et al., 2017).

Early diagnosis, a better understanding of the disease mechanisms and improvement of therapeutic approaches have contributed to a marked increase in survival with CF, whereby in 2015 the median predicted survival rate of CF individuals born in that year was 41.2 years compared to the following year where it increased to 47.7 years (Bethesda, 2017; Turcios, 2020). Some of the main aspects involved in successfully managing CF include timely and effective treatment of pulmonary exacerbations along with anti-inflammatory and anti-microbial therapy, enhanced mucociliary clearance as well as mucus drainage, controlled intense nutritional support, the availability of measures to control CF infections, as well as rapid diagnosis and treatment of any complications (Jaques et al., 2020).

1.4.4 Clinical management of CF

CFTR modulators are orally administered drugs designed to improve the quality of life and health outcomes of people with CF (Taylor-Cousar et al., 2023). A CFTR modulator, Ivacaftor (IVA), was first introduced into clinical practice in 2012 and was approved by the National Institute for Health and Care Excellence (NICE) in 2013 (Taylor-Cousar et al., 2023; NICE, 2024). CFTR modulators are categorized into five main groups depending on the effects on CFTR mutations: potentiators, correctors, stabilizers, read-through agents, and amplifiers (Lopes-Pacheco, 2019). Different combinations of CFTR modulators that can be used for CF individuals with specific CFTR mutations have been reported to improve patients' clinical outcome and life-expectancy, and these combinations include IVA, lumacaftor (LUM), tezacaftor (TEZ) and elexacaftor (ELX) (Despotes & Donaldson, 2022; Lopes-Pacheco, 2019; Turcios, 2020). The triple combination therapy ELX/TEZ/IVA (kown as Kaftrio or ETI) was approved as a standard-of-care drug by NICE in 2020 (NICE, 2024).

Conventional treatments and intensive management do not prevent but rather delay the progression of lung disease (Turcios, 2020). Bronchodilators (such as β-agonists) are prescribed to reduce viscoelasticity and to alleviate thick sticky mucus that builds up in the lungs in addition to dilating the airway. CF lung infections are mainly treated with antibiotics and non-steroidal anti-inflammatory drugs (NSAIDs) which can be used to control airway inflammation (Rafeeq & Murad, 2017).

1.5 Cystic fibrosis-related diabetes

As life expectancy for people with CF has increased due to the incremental improvements in clinical care, so has the prevalence of CFRD, whereby it now affects approximately 50% of CF adult patients and 2% of CF children increasing to 20% in adolescence (Moran et al., 2009; Kelsey et al., 2019; Olesen et al., 2020). CF patients who develop CFRD have poor prognosis, a significantly higher risk of chronic lung infections leading to a more rapid decline in pulmonary function, and overall 6-fold increased morbidity and mortality compared to CF individuals without CFRD, regardless of the decreased morbidity due to improvements in diabetes management to date (Moran et al., 2009; Kelsey et al., 2019; Olesen et al., 2020). The connections that link CFRD and accelerated pulmonary function decline are not yet fully understood. Lung function is negatively impacted by chronic hyperglycaemia via impeding bacterial clearance and elevating oxidative stress leading to reduced pulmonary function and eventually pulmonary failure (Ntimbane et al., 2008; Moran et al., 2009; Hunt et al., 2014).

Clinical experimental medicine studies have concluded that CFRD is primarily caused by reduced β-cell function leading to insufficient insulin secretion, however the detailed pathophysiology is complex and not yet fully elucidated (Nathan et al., 2010; Street et al., 2012; Cano-Megías et al., 2015; Norris et al., 2019). There are different proposed hypotheses regarding the pathogenesis of impaired insulin secretion in CFRD:

1) Cell intrinsic CFTR-dependent mechanisms of insulin secretion resulting in β-cell dysfunction (Edlund et al., 2014; J. Guo et al., 2014; Koivula et al., 2016).

2) Oxidative stress and islet inflammatory-based remodelling during and after exocrine pancreas decline leading to β-cell dysfunction (Kelly & Moran, 2013; Barrio, 2015; Yi et al., 2016).

3) Pancreas-extrinsic CFTR defects such as intestinal pathology leading to altered incretin responses resulting in β-cell dysfunction (Kelly & Moran, 2013; Barrio, 2015).

Correspondingly, CFRD is currently viewed as a multifactorial condition resulting from multiple changes within the endocrine and exocrine CF pancreas.

Interestingly, both T1D and T2D share a number of common complications with CFRD including (increasingly recognised) PEI, multi-organ dysfunction, malabsorption, malnutrition, chronic infection, insulin resistance of differing degrees as well as microvascular complications including retinopathy, nephropathy and neuropathy (Blackman et al., 2013; Couce et al., 1996; Kelly & Moran, 2013; Konrad et al., 2013; Moran et al., 2010; O'riordan et al., 2008). However, macrovascular complications in CFRD have to date rarely been present unlike T1D and T2D (Doan & Madison, 2020). However, due to the reversal from a catabolic state to potentially pathological weight gain in the era of CFTR modulator therapy, macrovascular complications are now predicted to increase significantly (Sandouk et al., 2021).

1.5.1 Diagnosis of CFRD

The American Diabetes Association has recommended screening CF patients annually from as young as 6-9 years of age and certainly over the age of 10 for impaired glucose tolerance with an OGTT (Mohan et al., 2008; Moran et al., 2009; Olesen et al., 2020). In 20% of CFRD cases, exclusively testing fasting glucose gives a false negative diagnosis for CFRD, as fasting hyperglycaemia may only ensue some years after an initial CFRD diagnosis is established (Mueller-Brandes et al., 2005). The usual tests such as fasting blood glucose test and HbA1c, that are used to diagnose diabetes mellitus, are thus unsuitable for diagnosing CFRD (Kayani

et al., 2018). Moreover, as early insulin deficiency in CF patients is present prior to the positive CFRD diagnosis by OGTT; continuous glucose monitoring (CGM) can be used to take frequent measures of glucose in order to establish a real-time glucose trend detecting early rise in glucose after eating which can normalise by the time of a formal OGTT time point. (Prentice et al., 2016; Cystic Fibrosis Trust UK, 2021). Recent studies have reported that the use of CGM by CF adults enabled the earlier identification of impaired glucose metabolism than the 2 h OGTT (Soliman et al., 2014). Yet, there is a need to develop new accurate methods for diagnosing CFRD including the development of novel biomarkers to enable early diagnosis (Rickels et al., 2020).

1.5.2 Clinical management of CFRD

CFRD is a life-long condition with no established cure, but it is a manageable disorder through insulin therapy (Moran et al., 2009). CF and CFRD mortalities have significantly been decreased with the implementation of annual diabetes screening and early admission of insulin therapy, which helped in reducing airway glucose and improving nutritional status (Moran et al., 2009; Kayani et al., 2018). CFRD patients report a decline in pulmonary and nutritional performance, therefore it is recommended that insulin therapy is administrated early for CFRD patients or even in individuals who are developing CFRD, as β-cell function and glucose tolerance inexorably decline in CFRD (Brennan & Beynon, 2015).

The use of CFTR modulators IVA and a dual treatment of LUM/IVA has been proposed to improve glucose tolerance (Bellin et al., 2013a; Kelly et al., 2019; Misgault et al., 2020). However, other studies have contradicted these results (Colombo et al., 2021; Moheet et al., 2021; Thomassen et al., 2018). Yet, treatments with a dual combination of first generation CFTR modulators TEZ/IVA exhibited no association with glucose tolerance nor insulin secretion in CF adults. However, CFTR modulators were suggested that they may still impact positively on insulin sensitivity (Ekblond et al., 2023). Additional studies to investigate the impact of different combinations of CFTR modulators on glucose tolerance and insulin sensitivity could be further conducted along with providing a better understanding of the disease development and progression, to provide a more effective CFRD treatment and management (Ekblond et al., 2023).

1.5.3 CFTR expression

In human pancreas, CFTR has been reported to be predominantly expressed in ductal cells ***(Figure 1.5)*** (Sun et al., 2017; Hart et al., 2018; White et al., 2020). Other studies have reported

that CFTR protein expression is hardly detected in human islets with no detectable levels of CFTR protein expression in human endocrine cells (Sun et al., 2017; Hart et al., 2018; White et al., 2020). However, contradicting studies have demonstrated that low levels of CFTR mRNA and protein expression were present in a small number of endocrine cells, single human β-cells and isolated islets (Edlund et al., 2014; Di-Fulvio et al., 2020). In addition, CFTR expression has previously been observed in endocrine cells in rodent models (Boom et al., 2007; Guo et al., 2014; Edlund et al., 2014, 2019; Ntimbane et al., 2016; Di-Fulvio et al., 2020;).

In situ studies using ferret pancreas as well as *in vitro* studies using isolated human and ferret islets, using single-molecule fluorescent *in situ* hybridization reported the co-localization of CFTR mRNA with Keratin-7 ($KRT7^{+}$) in ductal cells and not endocrine cells (Sun et al., 2017; White et al., 2020). These findings suggest that the impact of CFTR mutations on β-cell function in CFRD is mediated via paracrine mechanisms that involve proinflammatory signals secreted from islet-associated exocrine-derived cells (Sun et al., 2017).

To fully understand the impact of CFTR and CFTR modulators on β-cell function and both endocrine and exocrine compartments of the pancreas, longer cohort studies with larger and more varied CF and CFRD cases need to be conducted (Bellin et al., 2013; Hayes et al., 2014; Tsabari et al., 2016; Thomassen et al., 2018; Kelly et al., 2019; Gaines et al., 2021).

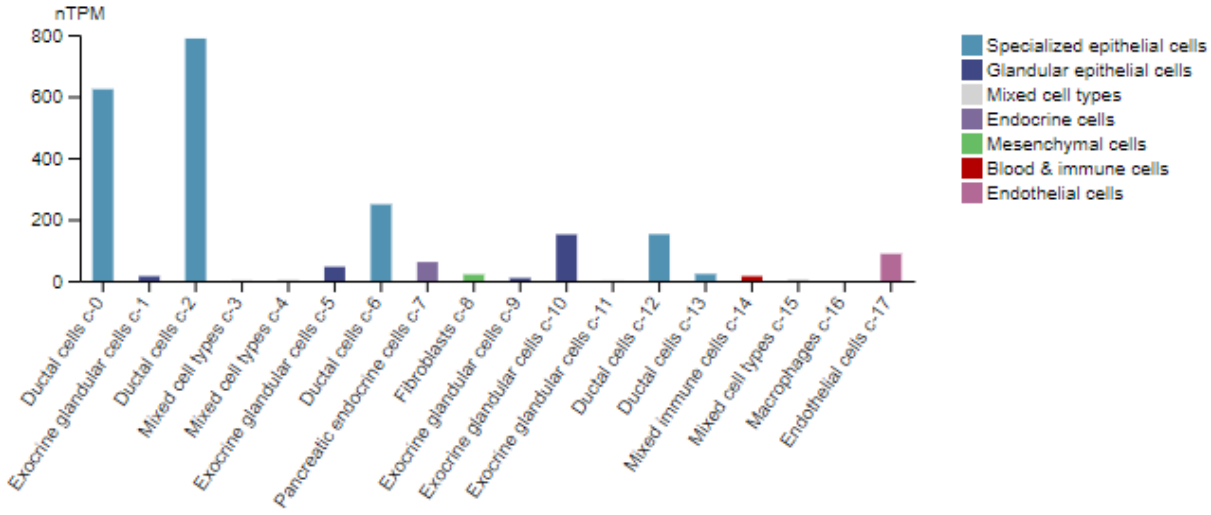

Figure 1.5. The expression of cftr in pancreatic cells.

Normalised transcriptome data showing the average TPM (Transcript Per Million) values per sample scaled to a sum of 1 million TPM (pTPM) used to estimate cftr gene expression level, of all individual samples for each pancreatic cell type that is represented by a c-value (Cell type atlas - CFTR - The Human Protein Atlas, 2021).

1.5.4 Exocrine changes in CF and CFRD pancreata

In the exocrine compartment of CF and CFRD pancreata, architectural remodelling and morphological changes have previously been observed and reported. *Post-mortem* pancreata from CF patients over the age of 5 years with reported relatively advanced pathology showed cystic dilatation with the absence or the presence in reduced quantity of exocrine acinar and duct cells, using qualitative histological analysis (Löhr et al., 1989). Further, there have been two distinct reported patterns of exocrine pancreas pathology during CF: a fibrotic pattern whereby fibrotic tissue predominantly replaced the exocrine tissue, and a lipofibrotic pattern where fatty tissue (adipocytes) predominantly replaced the exocrine tissue (Löhr et al., 1989; Rotti et al., 2018). In one study in young CFRD patients, total loss of exocrine pancreas and fat replacement of the exocrine parenchyma was observed (Iannucci et al., 1984). However, in young children of age less than 1 year with CF, the absence of exocrine lipofibrotic replacement but early pancreatic duct dilatation was reported, while CF children of 1-4 years-old displayed more severe exocrine changes (Bogdani et al., 2017).

As there is limited human tissue availability and only cross-sectional studies are possible, it has been difficult to systematically elucidate the progression of early CF-related pancreatic pathologies. CF and non-CF ferret models of different clinical age groups have been used, however, for this purpose (Rotti et al., 2018). A CF ferret model that shares several characteristics with clinical CF pancreatic pathology has been genetically engineered. Initially, an adeno-associated virus (AAV) mediated gene targeting technique was used to introduce CFTR gene mutation, then somatic cell nuclear transfer (SCNT) was used to create embryos that were implanted into surrogate maternal ferrets resulting in the birth of ferret clones with mutated CFTR gene (Sun et al., 2008). Neonatal CF ferrets have been reported to exhibit mild pancreas pathology with little sign of inflammation and fibrosis (Yi et al., 2016; Olivier et al., 2012; Rotti et al., 2018). In new-born CF ferrets there was increased apoptosis of acinar and pancreatic duct cells illustrating early exocrine parenchyma destruction, which has been proposed to lead to reduction in islet mass in neonatal CF, together with an impact on endocrine pancreas morphological structure (Olivier et al., 2012a). Histological pancreatic analysis was reported as showing mild inflammatory cell infiltration with acinar lumen ectasia (dilatation) graded mild to moderate in CF ferrets ages 3-4 weeks (Rotti et al., 2018). As age increases, a significant reduction in pancreatic exocrine tissue with a dilatated ductal cross-sectional area and increased replacement of exocrine parenchyma with fibrotic and fatty tissues were observed in CF ferrets compared to wild-type ferrets (Sun et al., 2014; Rotti et al., 2018). In 2-

3 month-old CF ferrets, which seems comparable to 1-2-year-old CF children, there was a significant increase in inflammatory cell infiltration and proinflammatory factors, as well as observed fibrosis within the exocrine parenchyma, in parallel with a marked disorganisation and restructuring of islets in the endocrine pancreas (Olivier et al., 2012; Yi et al., 2016). The significant increase of fat tissue within the exocrine parenchyma during the inflammatory response due to exocrine injury has been proposed to initiate an adipogenic programme (Rotti et al., 2018).

CFRD also shares some histological and imaging features with diabetes secondary to chronic pancreatitis including acinar loss, pancreatic duct dilatation with plugs, infiltration of fibrotic tissue as well as fatty tissue, overall islet anatomical preservation and the progression to pancreatic atrophy (Rickels et al., 2020a). However, clinically, chronic pancreatitis presents differently with significant pancreas-related pain which is not reported in CFRD (Rickels et al., 2020a).

1.5.5 Endocrine changes in CF and CFRD pancreata

Exocrine damage, collagen deposition and frank fibrosis in the islet microenvironment of the CF pancreas have been reported to impact on islet morphology and number (Couce et al., 1996; Bogdani et al., 2017). Islets in CF pancreata have been reported to be highly fragmented with the presence of intra-islet fibrosis as well as perisinusoidal sclerosis (presence of fibrous tissue around small blood vessels) (Löhr et al., 1989; Hull et al., 2018).

Using primary mouse islets, and β-cell lines, CFTR expression has been shown to impact on insulin secretion and electrophysiological responses (Boom et al., 2007; Edlund et al., 2014, 2019; Guo et al., 2014; Ntimbane et al., 2016; Di Fulvio et al., 2020). In a rodent β-cell line study, an increase in oxidative stress and impaired glucose-stimulated insulin secretion were observed due to loss of CFTR function (Ntimbane et al., 2016). Further, CFTR inhibition studies in human and mouse isolated islets demonstrated that priming and exocytosis of insulin granules was impaired when CFTR was inhibited (Edlund et al., 2014). In addition, a study used a mouse model where CFTR phenylalanine 508 (F508) was deleted mimicking this clinical genotype leading to defective CFTR function, reported a possible defect in proinsulin cleavage and the secretion of immature insulin, whereby there was a reduction in exocytosis and the number of insulin-containing granules ‘docked’ at the cell membrane (Edlund et al., 2019). The study also reported an increase in glucagon secretion (Edlund *et al.*, 2019).

Mouse CFTR inhibitor studies demonstrated that impairing CFTR function for a short period of time can impact on islet size with no observed impact on insulin secretion and/or glucose tolerance; suggesting that to impact on β-cell function, reduced CFTR function needs to last for a longer period of time (Khan et al., 2019). Studying insulin secretion in response to glucose levels, research studies have used CFTR knock-out animal models and conducted *in vivo* and *in vitro* investigations (Olivier et al., 2012; Yi et al., 2016; Sun et al., 2017). In ferrets during CF development, changes in β-cell mass correlated with changes in blood glucose levels (Yi et al., 2016b). In meal tolerance tests, it was demonstrated that first-phase insulin response was impaired whereby insulin secretion was reduced (Olivier et al., 2012; Yi et al., 2016).

An *in vitro* study using isolated islets from five human CF pancreata and control samples, it was reported that there were comparable insulin and glucagon secretions between the isolated islets of both groups (Hart et al., 2018). This study also conducted whole-islet RNA sequencing to investigate key transcripts in islet cell identity, maintenance and hormone secretion, whereby results reported that both islets isolated from CF pancreata, and islets of healthy pancreata had comparable gene expression suggesting that islets' genetic identity was preserved despite CF (Hart et al., 2018). However, due to the small sample size used as well as other factors such as islet isolation procedure which might have impacted islet gene expression and function, the true effect of CF *in vivo* may have been masked / missed (Hart et al., 2018).

Compared to intact normal islets, endocrine cells located in ductal and acinar epithelium of CF pancreata have been shown to have more variable hormone composition including an elevated occurrence of PP^+ cells in young CF individuals (Iannucci et al., 1984). Furthermore, in some CF human fibrotic pancreata, endocrine cells were observed budding off from ductal epithelium, which has also been observed in pancreata of CF ferrets with some of the cells displaying markers for neogenesis (Löhr et al., 1989; Hull et al., 2018). These findings further support previous studies suggesting the possibility of neogenesis in pancreata of adult and diseased individuals, which may have the potential to enhance β-cell functional mass in CFRD pancreata (Wang et al., 1995; Bonner-Weir et al., 2008). In addition, in 38-69% of CFRD pancreata, amyloid deposition within islets (only in individuals with known CFRD) along with simultaneous islets apoptosis and β-cell loss have been reported (Couce et al., 1996; Bogdani et al., 2017; Hull et al., 2018). Increased β-cell apoptosis and reduced β-cell area have been reported to be influenced by abnormal amyloid deposition in islets of T2D – a potential further contributor to β-cell dysfunction in CFRD (Jurgens et al., 2011)

1.5.6 Key non-endocrine cellular players in CF and CFRD pancreata

1.5.6.1 Immune cell infiltration

In young human CF tissue, there was an observed islet immune cell infiltration of leukocytes, whereas this islet immune infiltration was less in adult CF and CFRD tissue samples (Bogdani et al., 2017; Hart et al., 2018). In young CF donors, islet immune infiltrate was mainly made up of T-cells and macrophages, which appeared to be absent in islets of adult CF donors (Bogdani et al., 2017). Independent of CF donor age, leukocytes, T-cells and macrophages were observed in the exocrine compartment (Bogdani et al., 2017; Hart et al., 2018). Some studies reported that the fibrotic exocrine compartment exhibited more immune cells compared to the lipoatrophic pattern (Löhr et al., 1989; Bogdani et al., 2017). Considering these findings, it is suggested that the presence of peri-islet and intra-islet immune infiltration in CF impacts on β-cell dysfunction via immune mechanisms similar to those of T1D and T2D (Lehuen et al., 2010; Marchetti, 2016). Additionally, impaired CFTR function along with the changes within the islet microenvironment and the persistent presence of the immune infiltration within islets and around the islets in the exocrine compartment may present a continuous state of stress impacting on islet function and remodelling and further exacerbating islet dysfunction (Bogdani et al., 2017; Hart et al., 2018).

1.5.6.2 Proinflammatory markers

In CF ferret pancreas, there is a detected increase in inflammatory markers including IL-8, IL-6 and CXCL-10, during glycaemic crisis (a metabolic imbalance in growing ferret kits associated with marked insulin deficiency) and these inflammatory markers have been reported to be associated with acute pancreatitis (Frossard et al., 2001; Granger & Remick, 2005; Ness-Otunnu & Hack, 2013; Yi et al., 2016). CFTR-expressing exocrine-derived cells have been demonstrated to impact β-cell function via the secretion of pro-inflammatory markers such as IL-6, in a study that used CFTR inhibitors and islets from CF ferret model (Sun et al., 2017). In addition, when compared to wild-type islets, IL-6 level was shown to increase in CF ferrets which was associated with a decrease in total insulin content and an increase in insulin content percentage that was secreted at basal (rather than high) glucose levels (Sun et al., 2017).

Hart et al. (2018) study demonstrated the characterisation of the adaptive immune infiltrate by sorting T cells isolated from CF islets and reported that adaptive immune infiltration of CF islets mediated the production of inflammatory cytokines including INF-γ and TNF-α, which have been reported to impair *in vivo* β-cell function (Wang et al., 2010; Hart et al., 2018). Also,

chemokines and cytokines including IL-6, IL-1β, TNF-α, IFN-γ, and CXCL-10 have been reported to be secreted from stimulated T-cells that were isolated from CF islets, suggesting that the removal of CF islets from this inflammatory environment may limit the effect on β-cell function enabling more normal secretion of insulin and glucagon *in vitro* (Hart et al., 2018). Moreover, IL-1β has been shown to be present in islets of CF children of less than 10-year-old, CF adolescents and adults with CFRD (Hull et al., 2018). Several studies have reported that β-cell function can be impaired due to chronic inflammation, whereby β-cell can undergo apoptosis or dedifferentiate in the presence of the previously mentioned pro-inflammatory cytokines such as IL-1β (Cnop et al., 2005; Donath et al., 2010; Wang et al., 2010; Lopes et al., 2014; Collier et al., 2017; Nordmann et al., 2017; Hart et al., 2018). Interestingly, β-cells are capable of secreting chemokines that enhance immune cell recruitment and the overall cytokine-mediated signalling within and around the islets. This is thought to play a significant role in regulating β-cell function in conditions including T2D, obesity and metabolic syndrome (Haugen et al., 2001; Asensio et al., 2004; Maedler et al., 2004; Xu et al., 2005; Haider et al., 2006; Janet et al., 2007; LaPensee et al., 2008; Carnegie et al., 2010; Wang et al., 2010; Collier et al., 2017; Sun et al., 2017).

A recent study reported that miRNA-29 / TNF Receptor Associated Factor 3 (TRAF3) / CXCL10 pathways in β-cells facilitate the recruitment of monocytes and macrophages when metabolic stress promotes islet inflammation, which further suggests a possible pathway for islet dysfunction in CF pancreata with elevated levels of β-cell microRNA-29 having been associated with the development of T2D in elderly (Sun et al., 2021).

1.5.6.2 Pancreatic stellate cells

PaSCs are cells that are found in endocrine and exocrine pancreatic tissue and represent 7% of parenchymal pancreatic cells (Erkan et al., 2019). PaSCs in their quiescent state lay down the basement membrane in order to support the formation of epithelial cell structure and parenchymal function (Means, 2013). However, in their pathological state, PaSCs become activated, lose their stored fat droplets, and transdifferentiate into proliferating myofibroblasts, which play a significant role in pathological pancreatic fibrosis associated with pancreatic diseases such as pancreatic cancer, where these myofibroblasts are proposed to contribute to tumour progression and β-cell dysfunction (Omary et al., 2007; Phillips, 2012). Activated PaSCs in CF ferrets express α-smooth muscle actin (α-SMA) and desmin evidencing their proinflammatory active state compared to quiescent state in wild-type CF ferrets (Sun et al., 2017). Various studies have established that activated PaSCs synthesise and secrete different

extracellular matrix (ECM) proteins such as fibronectin, collagen type I and III, pro-inflammatory cytokines and growth factors (Apte et al., 1998, 1999; Elsässerm et al., 1989; Kuroda et al., 1998; Gabbiani, 2003). In addition to this, during injury and/or inflammation, acinar cells, platelets, inflammatory cells, and endothelial cells can produce cytokines as well as growth factors that can induce the activation of PaSCs (Masamune & Shimosegawa, 2009). Further, during pancreatic injury or inflammation, *in vitro* studies have demonstrated that cytokines and growth factors produced by acinar cells, inflammatory cells, platelets and endothelial cells including TGF-β, IL-1, IL-6, TNF-α, activin A, oxidative stress, ethanol and its metabolites, could activate PaSCs (Omary et al., 2007; Vonlaufen et al., 2008; Masamune et al., 2009; Masamune & Shimosegawa, 2009; Erkan et al., 2012).

Moreover, it has been reported that in CF ferrets of 1-4 months age range, activated PaSCs were observed around ductal epithelium, and this observation was not seen in wild-type ferrets, suggesting PaSCs to be the source of myofibroblasts during CF pancreatic remodelling (Rotti et al., 2018). In addition, it was proposed that myofibroblasts in fibrotic regions of ferret pancreata may be a possible source of adipocytes in CF, which was further supported by mouse lineage-trancing studies where it was demonstrated that myofibroblasts could transdifferentiate into adipocytes (Plikus et al., 2017; Rotti et al., 2018).

Alongside the presence of pro-inflammatory environment in islet cultures from CF ferrets, gene expression analysis reported elevated expression of activated PaSC, fibrosis, inflammation and remodelling markers such as *cxcl10*, *acta1*, *acta2*, and *tgf-β1*. (Sun et al., 2017). These findings were postulated to contribute to islet dysfunction in CF (Sun et al., 2017).

1.6 Aims

Diabetes is manifested as a secondary complication of a range of pancreatic diseases, where pancreatic ducts and the exocrine compartment are affected and damaged. Although islets do survive such environments in a dysfunctional state, their function eventually is impaired, and endocrine insufficiency ensues. The physiological, molecular, and cellular mechanisms that play the most significant roles in exocrine-endocrine communication leading to β-cell dysfunction are not yet fully understood, mainly due to limited access to human CF and CFRD pancreatic tissue.

Therefore, to understand how pancreatic changes during CF influence islet impairment leading to CFRD development, this thesis aimed to investigate the morphological changes within human CF pancreata as the disease progresses, and its relation to donor age. Also, it addressed

whether a semi-quantitative scoring of histopathological changes in CF, including duct dilatation, fibrosis, and fat replacement could elucidate the natural history of the disease. Robust AI quantitative analysis (HALO) was employed to further characterise the changes in exocrine and endocrine compartments of CF pancreata and shed light on the following questions:

1) Is there evidence for a decrease in islet number/density and β-cell number/density in CF?

2) Do islets undergo fibrotic changes?

3) Are cellular constitution changes including the presence of activated PaSCs associated with the changes within islets and islet niche?

Moreover, as the activation on PaSCs and transdifferentiation into proliferating myofibroblasts is reported to mediate pancreatic fibrosis and could eventually be associated with β-cell malfunction, I hypothesised that establishing an *in vitro* primary human islet stellate cell (ISC) model could mimic the cell-mediated 'stress' environment which islets are exposed to in CF and or CFRD pancreata. This model could enable the assessment of β-cell function under the impact of proinflammatory components produced due to the activation of ISCs.

Subsequently, the previous questions were explored by undertaking a transcriptome analyses of CF pancreatic tissue with different patterns of CF disease and a human β-cell line after treatment with conditioned media from the established ISC model. This could uncover the possible associated pathways involved in exocrine-endocrine cell-mediated cross-talk, further enhancing understanding of CFRD pathophysiology.

To address these questions, the following aims and objectives were proposed:

Aim 1: To analyse pancreatic histopathological changes in human *post-mortem* CF tissue and identify associated cell phenotypes with potential aetiological roles in CFRD to answer three main questions:

1) What is the natural history of CF pancreatic pathology within the exocrine compartment?

2) How are exocrine compartment changes associated with changes in the endocrine compartment?

3) Is there any spatial relationship between fibrosis and stellate cells around the islets in CF?

- **Objective 1.1:** Evaluate the histopathological changes in the exocrine parenchyma and categorise the CF pancreatic tissue blocks into patterns based on the morphological changes observed.
- **Objective 1.2:** Use H&E-stained pancreatic tissue sections to assess the changes in CF pancreata over the course of the disease and potential associations with donor age at *post-mortem.*
- **Objective 1.3:** Establish a semi-quantitative scoring system to investigate the changes in the exocrine and endocrine compartments based on the established morphological patterns.
- **Objective 1.4:** Assess proportion of specific endocrine cell phenotypes, fibrosis and activated PaSCs in diseased and control pancreata and quantify these changes using immunohistochemistry staining and AI deep learning.

Aim 2: To establish an *in vitro* primary human islet-derived stellate cell (ISC) model and examine the impact of its secretome on β-cell line viability and function.

- **Objective 2.1:** Confirm the establishment of activated ISCs in culture:

  1) Undertaking immunofluorescent staining for activated stellate cells markers
  2) Performing real-time quantitative reverse transcription-polymerase chain reaction (rtq-RT PCR) for genes associated with stellate cell activation.

- **Objective 2.2:** Examine ISC secretome for the presence of proinflammatory molecules, by performing a multiplex immunoassay to quantify proteins, Meso Scale Discovery (MSD) and COL1A1 ELISA.
- **Objective 2.3:** Investigate the impact of ISC secretome on (rat) INS-1E cell viability, insulin transcription and genes associated with stimulus-secretion coupling.
- **Objective 2.4:** Investigate the impact of ISC secretome on (human) EndoC-βH1 cell function assessed by glucose-stimulated insulin secretion assay and insulin / pro-insulin content.

Aim 3: To conduct transcriptomic phenotyping of CF pancreatic tissue and EndoC-βH1 cells following treatment with ISC secretome.

- **Objective 1:** Investigate the differentially expressed genes and identify possible signalling pathways associated with the morphological and cellular changes across CF pancreatic tissue of different morphological patterns, by performing a NanoString nCounter analysis.
- **Objective 2:** Investigate the impact of ISC secretome on EndoC-βH1 cell transcriptome by performing bulk-RNA sequencing and exploring possible upregulated and downregulated gene expression pathways.

Chapter 2: Materials and methods

All chemicals and tissue culture consumables were purchased from Sigma-Aldrich (Missouri, USA) and Thermo Fisher Scientific (Waltham, USA), unless otherwise stated.

2.1 Human Cohort Studies

2.1.1 Human cohort

A total number of 58 control human pancreata were obtained from Exeter Archival Diabetes Biobank (EADB) and Quality in Organ Donation (QUOD) donors with an age range of 0-29 years-old ***(Table 2.1)***. Twenty-nine human pancreata biopsied at *post-mortem* from individuals with CF with an age range of 0-27 years-old were obtained from EADB and a pathology bank collected by Professor. Günter Klöppel, Technical University of Munich, Germany ***(Table 2.2)***.

Deceased donor organs for the QUOD Expand Whole Pancreas Biobank were taken after written donor-relative consent in compliance with the UK Human Tissue Act of 2004 under specific ethical approvals by the UK Human Research Authority (05/MRE09/48 and 16NE0230). Donors from the EADB were used with full ethical permission from the West of Scotland Research Ethics Committee (ref: 20/WS/0074; IRAS project ID: 28362015/WS/0258). An ethical approval established by local ethic committee of the University Hospital 'rechts der Isar', Munich, Germany (document number: 281/19 s) was issued to approve all studies on archival material.

Table 2.1: Control cohort donor details including case number, biobank, age and sex if known.

Case number	Biobank	Age	Sex
1	EADB	Premature	NA
2	EADB	7 days	NA
3	EADB	7 days	NA
4	EADB	7 days	NA
5	EADB	7 days	NA
6	EADB	13 days	NA
7	EADB	3 weeks	NA
8	EADB	3 weeks	NA
9	EADB	3 weeks	NA
10	EADB	3 weeks	NA
11	EADB	6.2 weeks	NA
12	EADB	4 months	NA
13	EADB	8 months	NA
14	EADB	1 year	NA
15	EADB	2 years	NA
16	EADB	2 years	NA
17	EADB	2 years	NA
18	EADB	2 years	NA
19	EADB	2 years	NA
20	EADB	2 years	NA
21	EADB	2 years	NA
22	EADB	2.5 years	NA
23	EADB	3 years	NA
24	EADB	3 years	NA
25	EADB	3 years	NA
26	EADB	4 years	NA
27	EADB	4 years	NA
28	EADB	5 years	NA
29	EADB	5 years	NA
30	EADB	5 years	NA

31	QUOD	6 years	Female
32	EADB	6 years	NA
33	EADB	6 years	NA
34	EADB	6 years	NA
35	EADB	6 years	NA
36	EADB	7 years	NA
37	EADB	7 years	NA
38	EADB	7 years	NA
39	EADB	7 years	NA
40	EADB	8 years	NA
41	EADB	8 years	NA
42	EADB	9 years	NA
43	EADB	9 years	NA
44	EADB	10 years	NA
45	EADB	10 years	NA
46	EADB	10 years	NA
47	EADB	10 years	NA
48	EADB	12 years	NA
49	EADB	12 years	NA
50	QUOD	13 years	Male
51	QUOD	18 years	Female
52	QUOD	18 years	Female
53	QUOD	19 years	Male
54	QUOD	24 years	Male
55	QUOD	27 years	Male
56	QUOD	27 years	Male
57	QUOD	27 years	Male
58	QUOD	29 years	Male
		Mean age: 7.1 years Standard deviation: 7.7 years	

EADB cohort: Exeter Archival Diabetes Biobank. QUOD: Quality in Organ Donation. NA: Not available

Table 2.2: Donor details of CF cohort: case number, biobank, age, sex if known and the number of blocks provided.

Cases number	Biobank	Age	Sex	Number of blocks	CF Pattern
1	Klöppel	0	Female	1	Pattern 1
2	Klöppel	0	Female	3	Pattern 1
3	Klöppel	2 days	Male	1	Pattern 1
4	EADB	3 days	NA	1	Pattern 1
5	EADB	10 days	NA	1	Pattern 1
6	EADB	3 months	NA	1	Pattern 1
7	EADB	3 months	NA	1	Pattern 1
8	EADB	4 months	NA	1	Pattern 1
9	Klöppel	4 months	Male	2	Pattern 1
10	EADB	6 months	NA	1	Pattern 1
11	EADB	2 years	NA	1	Pattern 1
12	EADB	2 years	NA	1	Pattern 1
13	EADB	3 years	NA	1	Pattern 1
14	EADB	3 years	NA	1	Pattern 2
15	EADB	4 years	NA	1	Pattern 1
16	EADB	4 years	NA	1	Pattern 1
17	EADB	4 years	NA	1	Pattern 2
18	EADB	7 years	NA	1	Pattern 2
19	EADB	7 years	NA	1	Pattern 3
20	Klöppel	7 years	Male	1	Pattern 2
21	EADB	12 years	NA	1	Pattern 3
22	Klöppel	13 years	Female	7	Predominant Pattern 3*
23	EADB	14 years	NA	1	Pattern 2
24	EADB	14 years	NA	1	Pattern 2
25	Klöppel	14 years	Female	1	Pattern 1
26	EADB	19 years	NA	1	Pattern 3
27	Klöppel	19 years	Male	2	Pattern 2

28	Klöppel	27 years	Male	3	Pattern 3
29	Klöppel	27 years	Male	6	Predominant Pattern 2**
		Mean age: 7 years Standard deviation: 8.2 years			

*Pattern 1= Fibroatrophic, Pattern 2= Fibroatrophic and lipoatrophic, Pattern 3= Lipoatrophic. * This case has 2 blocks with pattern 2. ** This case has 2 blocks with pattern 3. NA: Not available. EADB cohort: Exeter Archival Diabetes Biobank*

2.1.2 Haematoxylin and Eosin (H&E) and immunohistochemistry (IHC) staining

All staining was carried out by NovoPath Newcastle Laboratories, Royal Victoria Infirmary, Newcastle upon Tyne, UK. To evaluate tissue morphology and fibrosis, 4 μm of tissue sections were stained manually for H&E and picro-sirius red fast green (SRFG). Immunohistochemistry (IHC) staining was carried out using the Discovery Ultra Auto-Stainer (Roche Diagnostic, Indianapolis, USA) for various antibodies at the specific dilutions ***(Table 2.3)***. Pancreatic stained sections were scanned either using an Akoya Biosciences Vectra® Polaris™ Automated Quantitative Pathology Imaging System using a Brightfield x 40 scanning protocol or Leica DMR microscopy with the Leica DFC310 FX 1.4-megapixel digital colour camera (Leica Microsystems, Wetzlar, Germany). Images of stained scanned sections were captured using ImageScope (v12.4.6.5003) (Leica Biosystems, Illinois, USA).

Table 2.3: Details of antibodies used for IHC staining.

Antibody	**Dilution**	**LOT No.**	**Company**
Insulin	1:1000	BSH-2010-100	Nordic Biosite, Täby, Sweden
Glucagon	1:1500	EP74	Cell Marque, California, USA
Pancreatic polypeptide	1:2000	ab113694	Abcam, Cambridge, UK
Somatostatin	1:300	EP130	Cell Marque, California, USA
Chromogranin A	1:5000	ab254557	Abcam, Cambridge, UK
CD45	1:250	2B11+PD7/26	Dako, Agilent Technologies, Santa Clara, USA
CD31	1:2000	ab182981	Abcam, Cambridge, UK
α-SMA	1:200	ab150301	Abcam, Cambridge, UK
CD68	1:200	M0876	Dako, Agilent Technologies, Santa Clara, USA

2.1.3 Artificial intelligence (AI) quantification

AI quantification was performed by Prof. Sarah Richardson and her team at the University of Exeter, UK. Prior to section analysis using HALO V3.0 image analysis software (Indica Labs, Albuquerque, USA), quality control on sections was performed and the following areas were excluded: sections of spleen, intestinal cell wall, lymph nodes, blurred regions, mucus within large ducts and any tears and regions of nonspecific staining. Individual DenseNet V2 classifiers (Version 3.2.1851.354) were made for the H&E and the SRFG stained sections. The H&E classifier included six annotations: 'Background', 'Fibrosis', 'Acinar', 'Ducts', 'Islets' and 'Fat' ***(Figure 2.1)***.

In control donors, the hierarchy of tissue types was as above, because occasionally fat was visible within the islets. However, in the CF donors, especially those with a lipoatrophic disease pattern, islets were often located within a large amount of fat ***(Figure 2.1 C*** and ***D)***. Therefore, for CF donors, the hierarchy 'Background', 'Fibrosis', 'Acinar', 'Ducts', 'Fat' and then 'Endocrine' was used. The classifiers were trained on donors with a range of CF pathology, relatively 'normal' pancreas, a fibrotic disease pattern and a lipoatrophic disease pattern. In control donors, three donors encompassing a range of ages were used for training: < 1 week old, 6 months and 3-year-old. Every example of the different tissue phenotype was drawn around to ensure accurate training. The classifier was based on tissue colour, shape, and texture differences. Each classifier, once made, was trained to 50,000 iterations and until cross-entropy (a mathematical tool to measure the difference between predicted probabilities and true class labels in classification tasks) fluctuated between 0.2 and 0.6. Only islets with an area > 1000 μm^2 (typically > 8-10 cells) were included.

The peri-islet AI pipeline using SRFG staining was established following the study of fibrosis in a separate 52-year-old QUOD donor pancreata ***(Figure 2.2)***. The largest distance from the islet basement membrane to the outer edge of peri-islet fibrosis across 25 randomly selected islets was assessed. The peri-islet ring, used to assess $SRFG^+$ area in this region, was defined as a 33.1 μm ring around the islet ***(Figure 2.2)***. After running the DenseNet V2 classifier in HALO, the islet annotation was manually expanded by this amount and further analysis was run within this annotation layer. The area quantification module (Version 3.2.1851.354) was used to collect the area of specific stains. This was performed on either the whole section or in specific annotation layers generated by the DenseNet V2 classifier to calculate the area of each

stain. The same settings for the area quantification module were used on every sample to ensure consistency and reproducibility. Other pipelines were developed and classifiers were trained to calculate chromogranin A^+ (CGA^+), $CD31^+$ area ***(Figure 2.3)*** and α-SMA^+ areas ***(Figure 2.4)***.

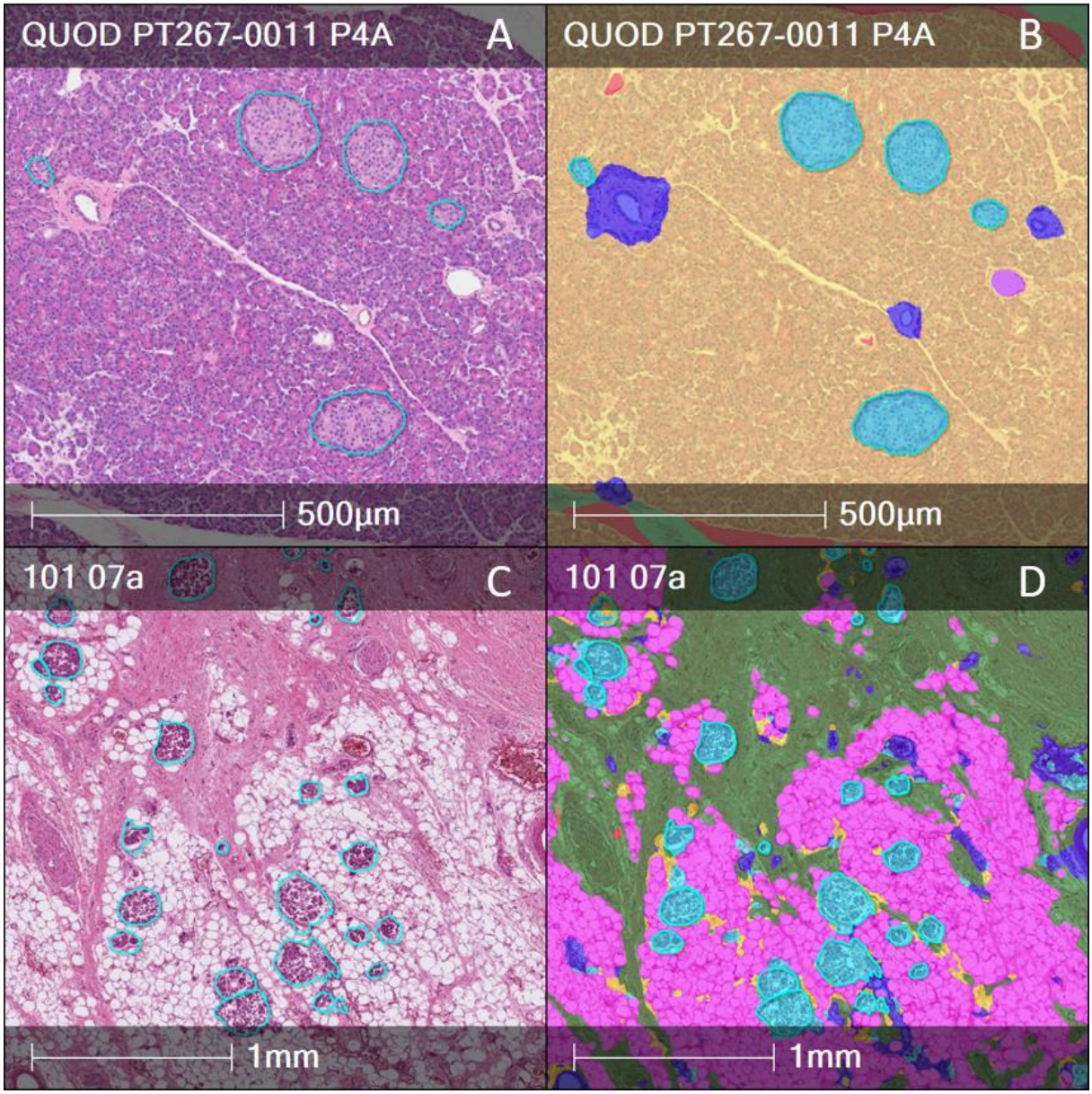

Figure 2.1: AI classifier illustration of H&E area quantification of a 27-year-old male QUOD control (Case number:29) (A and B) and a 27-year-old male CF donor (C and D).

Tissue classifier colours: islets (cyan); ducts (blue); fat (pink); acinar (yellow); background (red); fibrosis (green).

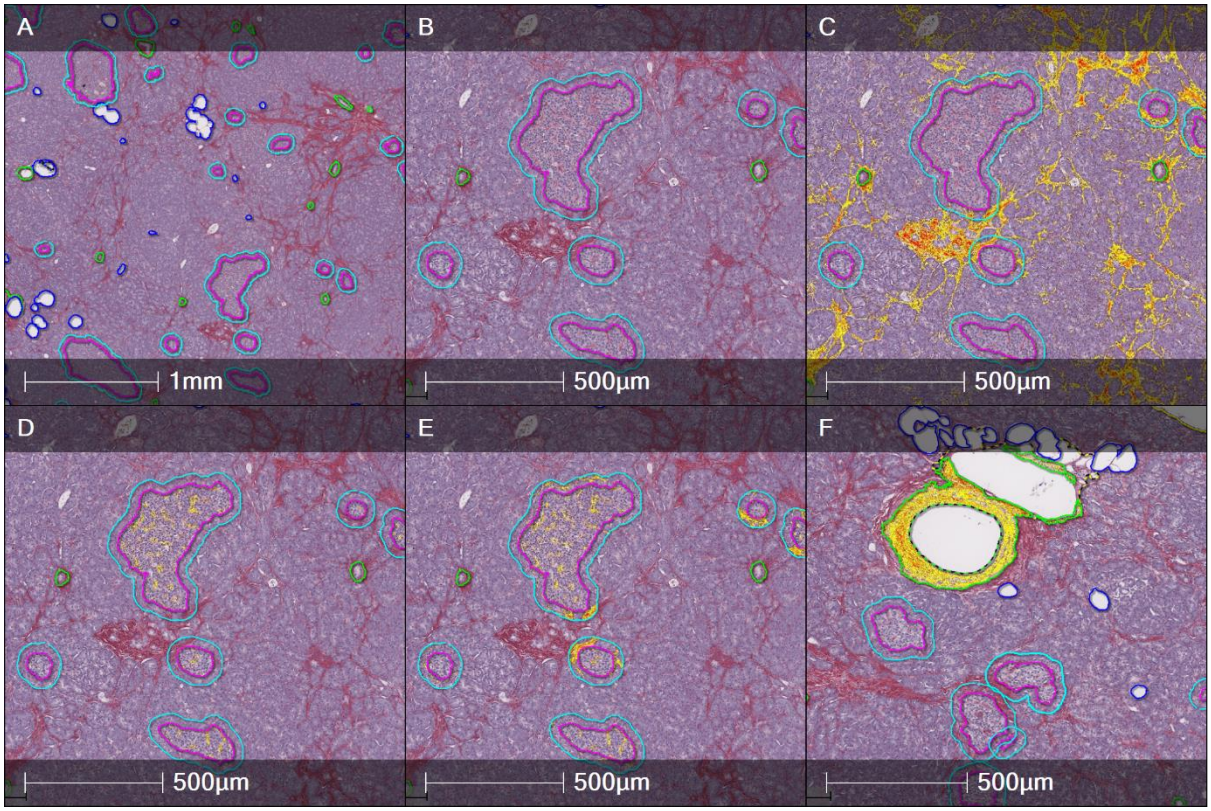

Figure 2.2: AI classifier illustration of SRFG$^+$ area (yellow/orange labelling) quantified in different compartments of a 52- year-old male QUOD control.

(A) *Tissue with classifier: fat (blue); islet (pink); peri-islet/ islet (cyan); duct and other (green).* ***(B)*** *Tissue classifier – higher magnification.* ***(C)*** *SRFG$^+$ area quantification within acinar layer.* ***(D)*** *SRFG$^+$ area quantification within islet.* ***(E)*** *SRFG$^+$ area quantification within peri-islet/ islet. Peri-islet SRFG$^+$ area was calculated by subtracting islet area (pink) from peri-islet/islet area (cyan).* ***(F)*** *SRFG$^+$ area quantification within duct and other (blood vessels).*

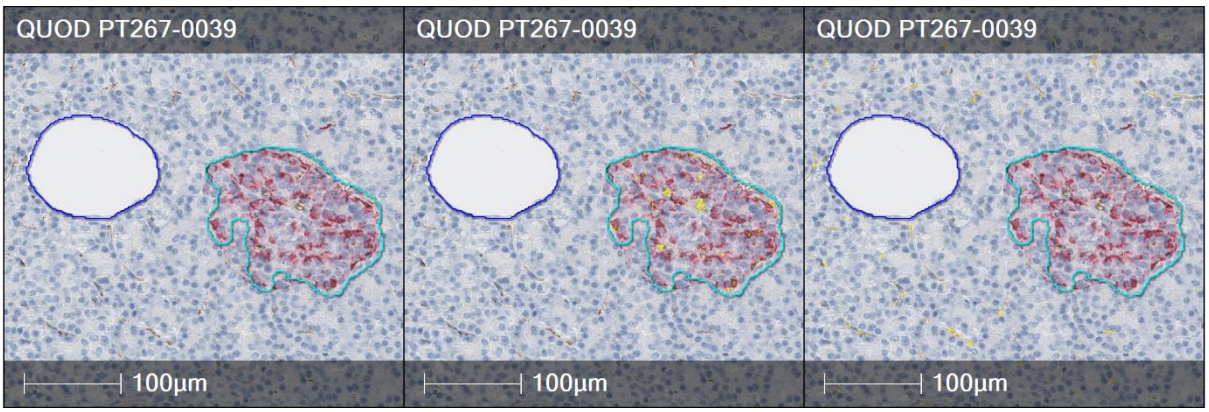

Figure 2.3: AI classifier illustration of CD31$^+$ area quantification (yellow/ orange labelling) in a 27-year-old male QUOD control (Case number: 56).

(A) *Tissue with classifier: fat (blue) and islet (cyan).* ***(B)*** *CD31$^+$ area quantification within islet layer (yellow).* ***(C)*** *CD31$^+$ area quantification within acinar layer (yellow).*

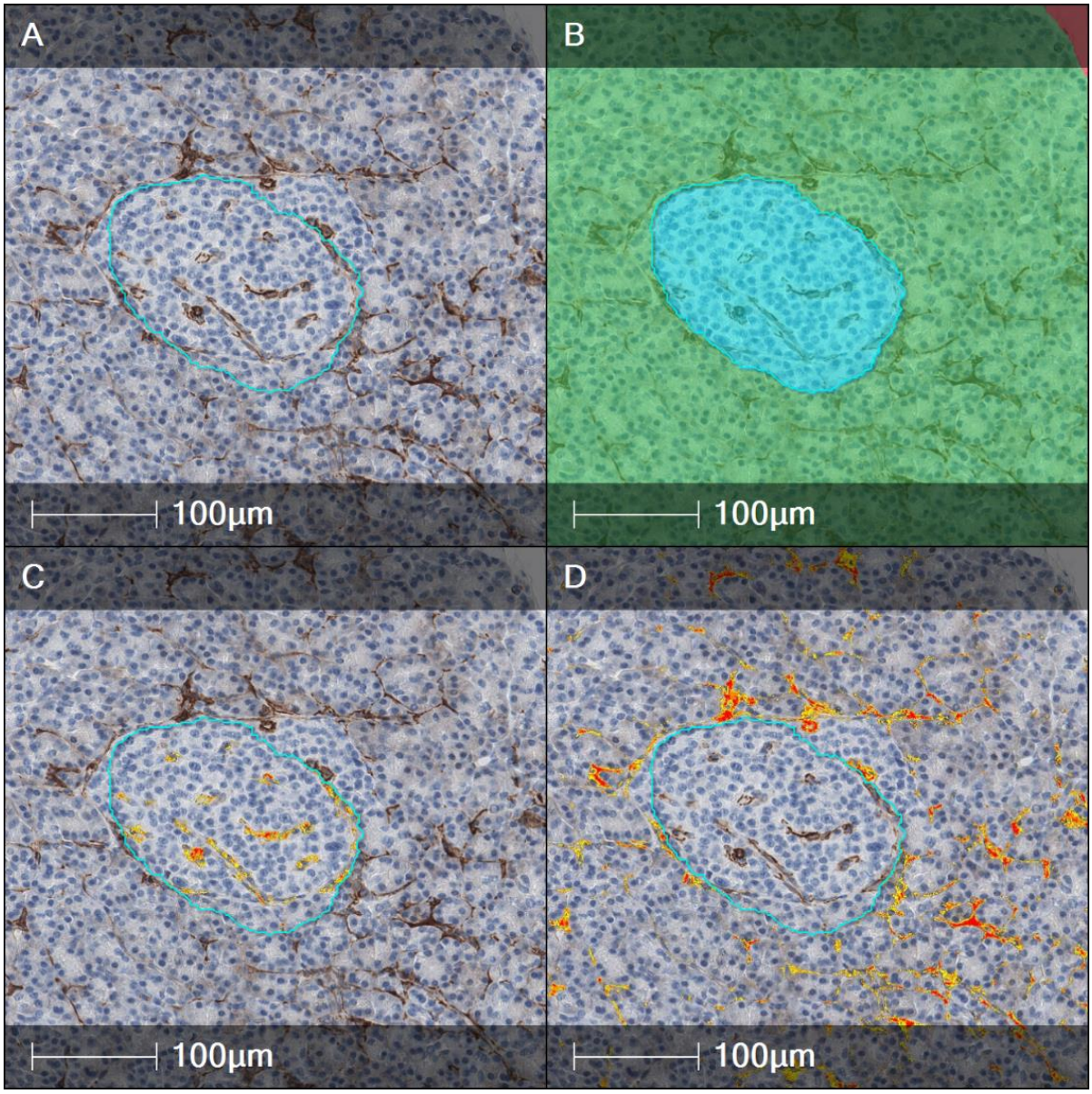

Figure 2.4: AI classifier illustration for α-SMA$^+$ area (yellow/orange) staining in a 27-year-old male QUOD control (Case number: 56).

(A) *α-SMA in brown and islet circled with cyan.* ***(B)*** *Classification of tissue: acinar (green); islet (cyan).* ***(C)*** *α-SMA$^+$ area quantification in islet.* ***(D)*** *α-SMA$^+$ area quantification in acinar.*

2.1.4 Molecular studies

2.1.4.1 RNA extraction from formalin-fixed paraffin tissue

For transcriptomic analysis, RNA was extracted from both CF and control tissue blocks successfully using The High Pure FFPE RNA Isolation Kit (Roche, Basal, Switzerland), according to manufacturer's protocol. RNA was then quantified using Qubit^{TM} RNA HS Assay Kit (Thermo Fisher Scientific, Waltham,USA). Samples were stored at -80 $^{\circ}$C.

2.1.4.2 Bulk RNA sequencing and Nanostring analysis

RNA samples extracted (**2.1.4.1)** from ten QUOD donors (n=10 blocks) and ten CF cases (n=20 blocks) obtained from Professor. Klöppel ***(Table 2.1*** and ***Table 2.2)***, were sent to Genomic Core Facility, Newcastle University for Bulk RNA sequencing using TruSeq Standard mRNA library prep kit.

NanoString nCounter analysis was conducted in the Human Dendritic Cell Laboratory, Newcastle University Medical School. The nCounter Master® Kit and the NanoString nCounter® predesigned gene expression Human Fibrosis V2 Panel were used according to manufacturer's specifications, to profile gene expressions of human pancreatic FFPE RNA samples obtained from three healthy donors (n=3 blocks) and seven CF donors (n=9 blocks) of different morphological pathologies ***(Table 2.4)***.

Table 2.4: Details of donors used for NanoString nCounter analysis including case number, sex and age.

Sample ID.	**Case Number**	**Sex**	**Age**
Control 1	55	Male	27 years
Control 2	31	Female	6 years
Control 3	53	Male	19 years
CF Pattern 1.1	1	Female	Premature
CF Pattern 1.2	2	Female	Premature
CF Pattern 1.3	9	Male	4 months
CF Pattern 2.1	27	Male	19 years
CF Pattern 2.2	29	Male	27 years
CF Pattern 2.3	22	Female	13 years
CF Pattern 3.1	28	Male	27 years
CF Pattern 3.2	29	Male	27 years
CF Pattern 3.3	22	Female	13 years

2.2 Human islet stellate cell model (ISC)

2.2.1 Human islets

Primary isolated human islets were coded with an internal identification number (LDIS). All donor families had provided written informed consent for research use of donated tissue and the work was carried out following full ethical approval under REC number 05/MRE0948 adhering to all HTA requirements for research at Newcastle University. Donor characteristics, pancreas ischaemic time and islet purity / viability are provided in ***(Table 2.5)***.

Deceased donor pancreata were retrieved at UK donor hospitals by the NHS Blood and Transplant National Organ Retrieval Service, with islets isolated at Oxford Diabetes and Endocrinology Centre, Newcastle Transplant Regenerative Medicine Laboratories or King's College Cell Isolation Unit, preserved in 37 °C tissue culture at the isolation site when necessary, and shipped to Newcastle University Medical School for the current studies.

Table 2.5: Islet donor information.

Donor ID	Age [years]	Sex	BMI [kg/m^2]	Donor Type	CIT	WIT [min]	Purity [IVF]	Viability	Isolation site
LDIS326	55	Female	23.15	DBD	32 h 31 min	0	70%	63%	Newcastle
LDIS328	53	Female	24.54	DBD	24 h 36 min	0	60%	60%	Newcastle
LDIS335	53	Male	28.41	DBD	NA	0	70%	77%	Oxford
LDIS354	53	Female	32.15	DBD	NA	0	60%	57%	Oxford
LDIS355	38	Male	22.45	DBD	NA	0	30%	77%	King's
LDIS359	73	Male	29.76	DCD	5 h 42 min	40	50%	80%	Newcastle

Donor ID represented by LDIS number, age (years), sex, body mass index (BMI, kg/m^2), donor type (DBD: donor after brain death, DCD: donor after circulatory death), cold ischemia time (CIT), warm ischemia time (WIT, min), purity measured by islet volume fraction (IVF), viability (%) and isolation site (Oxford Diabetes and Endocrinology Centre or Newcastle Transplant Regenerative Medicine Laboratories or King's College Cell Isolation Unit. Not available (NA).

2.2.2 Establishment of ISCs in primary culture

Isolated islets were cultured in Connaught Medical Research Laboratories (CMRL) 1066 medium (Mediatech Inc., Manassas, USA) supplemented with 2% human serum albumin (Gemini Bio-Products, West Sacramento, USA), 1.2% 1 M HEPES solution and 1.2% 100 x

penicillin/streptomycin. Islets were cultured at 37 °C and 5% CO_2, in T175 suspension flasks with an islet equivalent (IEQ) of 200 IEQ/cm^2, until further experiments were carried out.

Setting up ISC cultures is summarised in ***Figure 2.5***. Once islets were received, samples for time point Day 0 were taken for RNA analysis as well as formalin fixation. First, islets were washed twice with PBS (phosphate buffered saline), before resuspending in 750 µl lysis buffer containing 7.5 µl 2-β-mercaptoethanol and pipetted into 1.5 ml Eppendorf tubes, then snap frozen in liquid nitrogen before storing at -80 °C ready for RNA extraction.

In preparation for fixation, islets were resuspended in 1.5 ml of 4% formalin and stored overnight at 4 °C, followed by discarding formalin and adding 2 ml PBS. Then, to embed islets, PBS was discarded carefully, and the islet pellet was re-suspended in 200 µl of fresh PBS and was allowed to settle for 5 min before adding agarose gel. Next, this agarose chip containing the islets was transferred into a tissue cassette placed inside a 50 ml Universal container filled with 10% formalin to ensure the tissue is covered. Embedding and sectioning of the tissue was performed by NovoPath Newcastle Laboratories.

To set up ISCs in primary culture, islets isolated from donors LDIS326, LDIS328 and LDIS335 ***(Table 2.5)*** were re-suspended in RPMI medium (#21875-034, Gibco, Thermo Fisher, Waltham, USA) containing L-Glutamine and supplemented with 10% fetal bovine serum (FBS) (#10500-64, Gibco, Thermo Fisher, Waltham, USA) and 1% penicillin/streptomycin. Isolated islets from donors LDIS354, LDIS355 and LDIS359 ***(Table 2.5)*** were re-suspended in fresh RPMI 1640 medium (#R8758, Sigma-Aldrich, Missouri, USA) containing 10 mM glucose, L-Glutamine and sodium bicarbonate and supplemented with 5% FBS, 1 mM sodium pyruvate solution (#RNBK5893, Sigma-Aldrich, Massouri, USA), 5 ul/l β- Mercaptoethanol 75 mg/l penicillin and 50 mg/l streptomycin. Re-suspended islets at a density 200 IEQ/well were cultured in adherent 12-well cell culture plates (#E211239E, CELLSTAR ®, Greiner Bio-One, Kremsmünster, Austria) or on circular coverglasses of 13 mm diameter (#L46R13-1, Agar Scientific, Stansted, UK) in alcohol sterilised 12-well suspension cell culture plates (#E18023CK, CELLSTAR ®, Greiner Bio-One, Kremsmünster, Austria), for up to seven days, ready for RNA extraction (**2.2.4**) or IF staining (**2.2.7.2**), respectively.

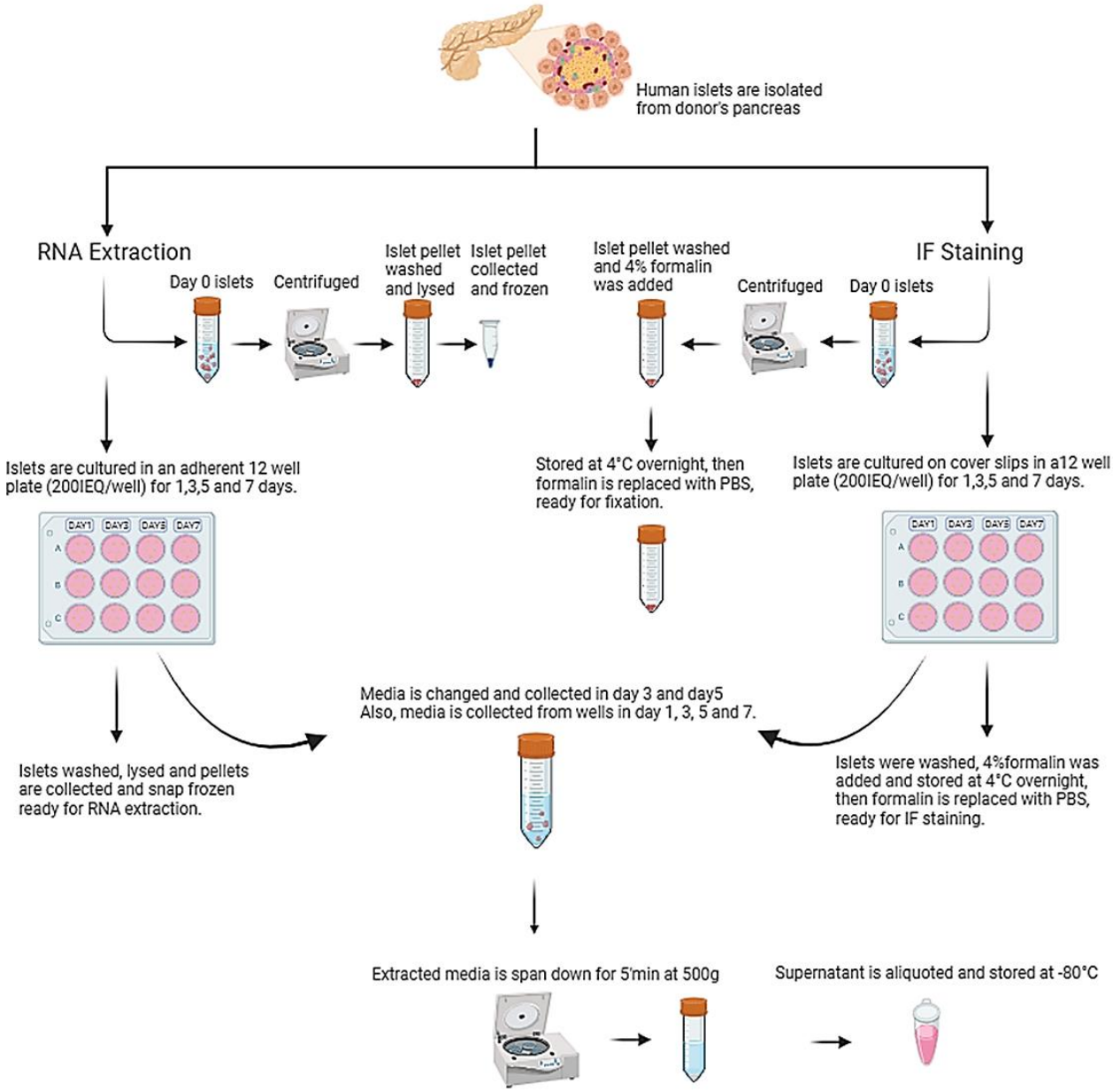

Figure 2.5: ISC model set-up for medium extraction, RNA extraction and IF staining.

Image created using Bio-render.

2.2.3 ISC medium collection

ISC medium collection was carried out on Day 1, 3, 5 and 7 with total volume media changes on Day 3 and Day 5. Medium was collected from designated wells into 15 ml Falcon tubes and then spun down for 5 min at 500 xg. Supernatant was aliquoted into 1.5 ml Eppendorf tubes and stored at -80 °C, until further experiments were conducted.

2.2.4 RNA extraction

After media collection, islets were washed twice with 500 µl/well PBS. Then, 250 µl of RNA lysis buffer was added and wells were scraped into 1.5 ml Eppendorf tubes, which were snap frozen in liquid nitrogen and stored at -80 °C.

RNA extraction was performed using the GenElute TM Total RNA Purification Kit according to manufacturer's instructions (Sigma-Aldrich, Massouri, USA). Samples were thawed and lysate was pipetted into a GenElute Filtration Column and centrifuged at 14,000 xg for 2 min. All centrifugation steps were carried out at speed of 14,000 xg. The Filtration column was discarded and an equal volume of 70% ethanol solution was added and mixed thoroughly with the lysate before transferring onto a GenElute binding column, followed by centrifuging for 15 sec and discard of the flow-through. The retained collection tube and column were washed with 250 µl Wash Solution 1 and centrifuged for 15 sec. Tubes were then incubated at room temperature for 15 min after the addition of 10 µl of DNase I and 30 µl Digest buffer mixture. A second wash of the membrane with 500 µl Wash Solution 1 and centrifuging for 15 sec followed. The column was then transferred into a new collection tube and washed with 500 µl of Wash Solution 2 and centrifuged for 15 sec before discarding the wash solution and repeating the washing step with 250 µl of Washing Solution 2 and centrifuging for 2 min, to remove ethanol, and discarding the flow-through. This was followed by a 1 min centrifuging before transferring the column into a new collection tube and adding 50 µl of elusion solution into the column and centrifuging for 1 min. Collection tubes containing eluted RNA samples were retained and labelled correctly before storing at -80 °C until further experiments were performed.

2.2.5 Complementary DNA (cDNA) synthesis

RNA samples (1 µl) were quantified using NanoDrop spectrophotometer (NanoDrop TM-2000; Thermo Fisher, Waltham, USA) and RNA purity was assessed using the A260/280 ratio, which ranged from 1.77-3.40 with most samples having an A260/280 ratio around 2.0, in keeping with highly pure RNA. To normalise the concentration of all RNA samples, a value of 2 ng/ µl was subtracted from the smallest value measured of an RNA sample, then the resulted value was used to normalise all the other measured RNA samples. Samples were then topped up with elusion buffer to make a final volume of 20 µl. To convert RNA samples into complementary DNA (cDNA), a high-capacity cDNA reverse transcription kit (Applied Biosystems, Foster City, USA) was used to make a total volume of 20 µl per reaction, whereby 10 µl of master

mix was prepared ***(Table 2.6)***. Prepared master mix was added and mixed well with 10 µl of each RNA sample following concentration normalisation. To test for possible contamination within each reaction, a blank control was prepared using an RNA sample and a master mix substituting Nuclease-Free H_2O for MultiScribe^{TM} Reverse Transcriptase (Roche, Basal, Switzerland). All samples were then placed inside a TC-512 gradient thermal cycler (Techne Inc., Burlington, UK) that has been set up with the optimised cycling conditions to generate cDNA ***(Table 2.7)***. cDNA samples were then stored at -20 $^{\circ}$C until quantitative real-time PCR was performed.

Table 2.6: Master-mix reagents and volume to make up 10 µl per reaction.

Reagent	**Volume (µl)**
10x RT buffer	2
25x dNTP Mix (100 mM)	0.8
10x RT Random Primers	2
MultiScribe^{TM} Reverse Transcriptase	1
Nuclease Free H_2O	4.2

Table 2.7: Thermal cycler optimised conditions for cDNA synthesis.

Steps/Settings	**Temperature [$^{\circ}$C]**	**Time [min]**
Step 1	25	10
Step 2	37	120
Step 3	85	5
Step 4	4	∞

2.2.6 Real-time quantitative reverse transcription-polymerase chain reaction (rtq-RT PCR)

To assess the changes in gene expression, real-time quantitative reverse transcription-polymerase chain reaction (rtq-RT PCR) was undertaken. Prior to taking cDNA samples, prepared in **2.2.5**, out of the freezer, surfaces, pipettes and tube racks were cleaned with 70% ethanol. Then, TE buffer pH 8.0 (Ambion^{TM}, Thermo Fisher Scientfic, Waltham,USA), H_2O, 0.5 ml PCR tubes, pipettes, LightCycler® Multiwell Plate 96 (Starlab, Hamburg, Germany) were all placed inside a UV hood for 20 min. Then, master mix (0.5 µl DNA probe, 0.5 µl TE buffer, 10 µl LightCycler® 480 Probes Master (Roche, Basel, Switzerland) and 7 µl H_2O) was

prepared for each DNA probe ***(Table 2.8)*** with duplicates for each cDNA sample. Following this, 18 µl of master mix was reverse pipetted into the bottom of designated wells followed by 2 µl of cDNA, which was pipetted onto the side of the well using a fresh tip. The plate was then sealed with polyolefin film (Starlab, Hamburg, Germany) and briefly centrifuged for 18 sec. The plate was run using a LightCycler® 480 PCR machine (Roche Diagnostics, Rotkreuz, Switzerland) with an optimised protocol. The cycling conditions initially started with a pre-incubation cycle of 95 °C for 10 min, followed by 50 cycles of 95 °C for 15 sec, 60 °C for 1 min and 40 °C for 10 sec. Data generated from each reaction were normalised to the reference gene RPLP0, then the fold change in gene expression was calculated using the double delta Ct analysis method.

Table 2.8: DNA probes for qrt-RT PCR with human gene name, gene symbol, species and detected transcripts.

Gene	Gene Symbol	Species	Transcript detected
Ribosomal protein, large, R0	*RPLP0*	Human	Hs00420895_gH
Collagen Type I Alpha 1 Chain	*COL1A1*	Human	Hs00164004_m1
Vimentin	*VIM*	Human	Hs00185584_m1
Actin Alpha 2, Smooth Muscle	*ACTA2*	Human	Hs00901479_m1
Cadherin-11	*CDH11*	Human	Hs00901479_m1

2.2.7 Immunofluorescence (IF) staining

Primary and secondary antibodies used are listed in ***Table 2.9***.

2.2.7.1 Tissue IF staining

Four µm tissue sections were cut from paraffin embedded and formalin fixed islets (collected at Day 0) and placed on glass slides. Sections were deparaffinised by placing in Histo-Clear™II (National Diagnostics, Atlana, USA) for 10 min and were then placed in a decreasing ethanol concentration gradient (100%, 90%, 70% and 50%) for 3 min each to rehydrate the tissue. Slides were then placed in deionised water until antigen retrieval with pH 9 TRIS/EDTA (Tris/ Ethylenediaminetetraacetic acid) buffer. To block non-specific binding, tissues were incubated with blocking buffer 20% FBS in PBS for 1 h. Primary antibodies ***(Table 2.9)*** were prepared by diluting in 0.05% FBS in PBS and pipetted onto the tissues, with 0.05% FBS in PBS alone used as negative antibody control. All slides were incubated in a humid and light-proof container overnight at 4 °C. Prior and after to secondary antibody incubation ***(Table 2.9)*** for 1

h at room temperature, slides were washed three times with 1X PBS for 5 min/wash. Following this, all slides were stained with 4′,6-diamidino-2-phenylindole (DAPI) for 15 min to visualise nuclei. Subsequently, slides were mounted using mounting medium containing DAPI (Vectashield®, Burlingame, USA). To prevent stained sections from dehydrating, slides were covered with 22x40 mm glass coverslips and nail polish was applied around the glass slips. All slides were kept in a light-proof box to prevent the fluorescence signal fading and stored at 4 °C before visualising using Leica SP8 Digital Light Sheet confocal microscope (Leica, Wetzlar, Germany).

2.2.7.2 Cell culture IF staining

Following medium collection, cultured islets were washed twice with 500 µl PBS, then 500 µl/well of 4% formalin was added and plates were kept at 4 °C overnight. Then, formalin was removed, and 1 ml of PBS was added, and plates were covered and stored at 4 °C.

To perform IF staining, the glass coverslips with adherent islet cells facing upwards were transferred into wells of a 12-well plate containing 300 µl of 0.2% Triton solution and the plate was placed on a shaker for 30 min. Then, Triton was replaced by 300 µl of 20% FBS in PBS and incubated on a shaker for 1 h. Post incubation, wells were washed with 500 µl PBS and glass coverslips were placed, with islets facing downwards, onto a droplet of 50 µl primary antibody ***(Table 2.9)*** prepared solutions on a parafilm surface that was placed in a hydration box. All air bubbles were removed, and the box was covered with foil and placed over night at 4 °C. Afterwards, all glass coverslips, with islet cells facing up, were transferred into a 12-well plate containing 500 µl PBS and incubated on a shaker for 15 min with changes of PBS every 5 min. Another box with parafilm covered surface and 50 µl secondary antibody ***(Table 2.9)*** solution droplets was prepared. Glass coverslips were placed on the secondary solution with cells facing downwards, all air bubbles were removed, and glass coverslips were incubated for 1 h in the dark at room temperature. Following, glass coverslips were transferred into a 12-well plate and washed 3X with PBS every 5 min in the dark. Then, 500 µl of DAPI solution was added and incubated in the dark on the shaker for 20 min. Excess DAPI solution was dabbed off and cover slips were dipped in PBS briefly and excess PBS was removed by dapping the edge of the cover glass gently on tissue paper. Glass coverslips were mounted using mounting medium containing DAPI on adhesive microscopic slides 25x75 mm (#J1800AMNZ, Thermo Fisher Scientific, California, USA) and sealed with nail polish. All slides were kept in a light-proof box to prevent the fluorescence signal fading and stored at 4 °C, before visualising using

Leica SP8 DLS confocal microscope (Leica, Wetzlar, Germany).

Table 2.9: Details of primary and secondary antibodies used for IF staining.

Antibody	**Primary/ Secondary**	**Dilution**	**Catalogue number (#)**	**LOT number.**	**Company**
Polyclonal guinea pig anti-insulin IgG	Primary	1:5	IR002	11590944	Dako, Agilent Technologies, Santa Clara, USA
Polyclonal rabbit anti-alpha smooth muscle actin IgG	Primary	1:200	Ab5694	GR3356867-3	Abcam, Cambridge, UK
Monoclonal anti-glucagon IgG antibody produced in mouse	Primary	1:100	G2654-2ML	000080611	Sigma Aldrich, Merck, Dorset, USA
Anti-vimentin antibody raised in goat	Primary	1:100	V4630	085K4869	Sigma-Aldrich, Merck, Dorset, USA
Alexa Fluor™ 568 goat anti- guinea pig IgG	Secondary	1:500	A11075	2160073	Invitrogen, Thermo Fisher, Massachusetts, USA
Alexa Fluor™ 488 goat anti-rabbit IgG	Secondary	1:500	A11008	2284595	Invitrogen, Thermo Fisher, Massachusetts, USA
Alexa Fluor™ 647 donkey anti-mouse	Secondary	1:500	A31571	2260928	Invitrogen, Thermo Fisher, Massachusetts, USA

2.2.8 ISC secretome analysis

In collaboration with Caitlin Brack, a lab technician at Transplant and Regenerative Medicine Laboratories of Newcastle University, ISC secretome samples collected at Culture Days 1, 3, 5, and 7 were analysed using a Human Pro-Collagen I α1 (COL1A1) sandwich ELISA (#DY6220-05, R&D Systems, Minneapolis, USA). Further, in collaboration with Dr. Lee Borthwick within Newcastle University, a custom made Meso Scale Discovery (MSD) multiplex assay was performed (Meso Scale Discovery, Maryland, USA).

2.3 Tissue culture studies

2.3.1 INS-1E cell line culture

Rat insulinoma INS-1E were kindly provided by Dr Catherine Arden and Dr. Brian Ford, Newcastle University. Passages between No. 84 and 89 were used for all experiments. The cells were cultured routinely in standard RPMI 1640 growth medium (#R8758, Sigma-Aldrich, Mssouri, USA) containing 10 mM glucose, L-Glutamine and sodium bicarbonate, supplemented with 5% FBS, 1 mM sodium pyruvate solution (#RNBK5893, Sigma-Aldrich, Massouri, USA), 5 µl/l β-mercaptoethanol, 75 mg/l penicillin and 50 mg/l streptomycin. Cells were cultured in 75 cm^2 tissue culture flasks, at 37 $^{\circ}C$ and 5% CO_2, with change of medium every two days.

2.3.2 INS-1E cell line treatment

Upon reaching 80% confluence, INS-1E cells were seeded in a 500 µl cell suspension at a density of 250,000-300,000 cells/well in a 24-well standard cell culture plate (#83.3922, SARSTEDT, Nümbrecht, Germany). Cells were incubated overnight in a humidified atmosphere with 5% CO_2 at 37 $^{\circ}C$. At 24 h post-plating, cells were incubated with collected ISC medium from Days 1, 3, 5 and 7 that were diluted in a 1:1 ratio with INS-1E culture medium and added to wells of plated INS-1E cells, following removal (by suction) of original medium from wells and washing cells gently with 500 µl pre-warmed PBS. In parallel, cells were treated with a range of concentrations (1 ng/ml – 50 ng/ml) of human cytokine mixture containing: IL-1β (#201-LB-070/CF), INF-γ (#285-IF-100/CF) and TNF-α (#210-TA-005/CF) (R&D Systems, Minneapolis, USA). Treated cells were incubated for 24 h in a humidified atmosphere with 5% CO_2 at 37 $^{\circ}C$, followed by RNA extraction or MTT cell viability assay.

2.3.3 INS-1E RNA extraction and rtq-RT PCR

RNA extraction of treated INS-1E was carried out using RNA lysis buffer, followed by cDNA synthesis and rtq-RT PCR that carried out using methods described in **2.2.4**, **2.2.5** and **2.2.6**, respectively. DNA probes used to perform rtq-RT PCR are summarised in ***Table 2.10***.

Table 2.10: DNA probes for rtq-RT PCR with rat gene name, gene symbol, species and detected transcripts.

Gene	Gene Symbol	Species	Transcript detected
Ribosomal protein, large, R0	*RPLP0*	Rat	Rn03302271_gH
Insulin 1	*Ins1*	Rat	Rn02121433-g1
Insulin 2	*Ins2*	Rat	Rn01774648_g1
Pancreatic and duodenal homebox 1	*Pdx1*	Rat	Rn00755591_m1
Solute carrier family 30 member 8 (zinc transporter)	*Slc30a8*	Rat	Rn00555793_m1
Glucose transporter protein type 2 (GTR2)	*Slc2a2*	Rat	Rn00563565_m1

2.3.4 Cell viability MTT assay

MTT (3-[4,5-dimethylthiazol-2-yl]-2,5 diphenyl tetrazolium bromide) reagent (#8A/265741, Tocris bioscience, Bristol, UK) was used to determine cell viability colorimetrically based on mitochondrial metabolic activity, whereby the number of viable cells is directly proportional to the intensity of colour generated. MTT aliquots were prepared in a concentration of 5 mg/ml in sterile PBS and stored at -20 $^{\circ}$C for subsequent use. Post INS-1E plating and treatment, MTT prepared aliquots were thawed and diluted (1:10) in INS-1E RPMI medium ready for use. Briefly, media was removed by suction from the plate and 500 µl/well of diluted MTT reagent was added followed by an incubation at 37 $^{\circ}$C for 2 h in a humidified, 5% CO_2 atmosphere. Then, MTT reagent was discarded by suction from wells and 500 µl/well acidified isopropanol was added. The plate was left on shaker for 15 min then, a 100 µl/well of mixture was transferred into a designated well of a 96 well plate, in duplicate. The plate was then spectrophotometrically read using a Multiskan Spectrum Thermo Labsystems (Thermo Fisher Scientific, Massachusetts, USA) at 570 nm and 690 nm, whereby the absorbance was calculated after subtracting the reading at 690 nm from 570 nm.

2.3.5 EndoC-βH1 cell line culture

Experiments using EndoC-βH1 cells were conducted under the training and supervision of Professor. Lena Elisson and her laboratory team members (Department of Clinical Sciences, Malmö, Sweden).

Tissue culture flasks were first coated using Dulbecco's Modified Eagle Medium (DMEM) High Glucose medium (24.97 mM/l) (#41965-039, Life Technology, Thermo Fisher Scientific, California, USA), supplemented with 2 µg/ml fibronectin (#F1141, Sigma-Aldrich, Massouri, USA), 1% penicillin /streptomycin, 100 µg/ml ECM (#E1270, Sigma-Aldrich, Massouri, USA). Then, coated tissue flasks were incubated for 2 h in a humidified atmosphere with 5% CO_2 at 37 °C, prior to culturing EndoC-βH1 cells.

EndoC-βH1 cells were cultured in T75 or T175 coated tissue culture flasks at densities of 5.25 million cells or 12.25 million cells, respectively. Cells were cultured in DMEM Low Glucose medium (5.55 mM/l) (#31885023, Life Technology, Thermo Fisher Scientific, California. USA) supplemented with 2% bovine serum albumin (BSA) fraction V (#10775835001, Roche Diagnostics, Basel Switzerland), 10 mM/l nicotinamide (#481907, VWR International, Pennsylvania, USA), 0.05 mM/l β-mercapthoethanol, 1% penicillin /streptomycin, 6.7 ng/ml sodium selenite (#S1382, Sigma-Aldrich, Massouri, USA) and 5.5 µg/ml human transferrin (#T8158, Sigma-Aldrich, Massouri, USA).

EndoC-βH1 cells between Passage Number 75 and 80 were used for all experiments. Upon reaching confluence, cells were seeded in a 200 µl cell suspension with a density of 180,000 cell/well in a coated 48-well plate (Nunc™ Cell-Culture Treated Multidishes, #150687, Thermo Fisher Scientific, California, USA). Cells were incubated overnight in a humidified atmosphere with 5% CO_2 at 37 °C.

2.3.6 EndoC-βH1 cell line treatment

After 24 h post plating, EndoC-βH1 cells were treated with collected ISC medium dilutions of Days 1, 3, 5 and 7 that were prepared in a 1:1 ratio with EndoC-βH1 culturing medium and added to wells, following removal (by suction) of original medium from wells and washing cells gently with 500 µl pre-warmed PBS. Also, cells were treated with a human cytokine mixture containing: 1 ng/ml IL-1β (#201-LB-070/CF), 20 ng/ml INF-γ (#285-IF-100/CF) and 20 ng/ml TNF-α (#210-TA-005/CF) (R&D Systems, Minneapolis, USA) (Tsonkova et al., 2018). Then, cells were incubated for 72 h in a humidified atmosphere with 5% CO_2 at 37 °C,

until performing glucose stimulated insulin secretion, extraction of cells for bicinchoninic acid (BCA) assay or RNA extraction.

2.3.7 Glucose-stimulated insulin secretion (GSIS)

After 72 h incubation with ISC medium, human cytokine mixture or control medium, confluent EndoC-βH1 plates were inverted to remove media and washed with 1 ml of pre-warmed and prepared secretion assay buffer (SAB), pH 7.3 (1.16 mM MgSO4, 4.7 mM KCl, 1.2 mM KH_2PO_4, 114 mM NaCl, 2.5 mM $CaCl_2$, 25.5 mM $NaHCO_3$, 20 mM HEPES, and 0.2% BSA) containing 1 mM glucose (#G-8270, Sigma-Aldrich, Massouri, USA). Then, cells were pre-incubated for 2 h with 500 µl SAB containing 1 mM glucose. Next, pre-incubation buffer was aspirated by suction from each well with a 200 µl tip fixed to the tip of a 2 ml polystyrene serological pipette (#86.1252.001, SARSTEDT, Nümbrecht, Germany). Then, designated wells for stimulation with low glucose (1 mM) or high glucose (20 mM) were incubated with 250 µl of corresponding SAB buffer for 1 h at 37 °C. Following this, 180 µl aliquots of cell medium were collected into 1.5 ml Eppendorf tubes which were kept on ice and then centrifuged at 200 xg for 5 min at 4 °C, followed by 130 µl of supernatant being transferred into a new carefully labelled 1.5 ml Eppendorf tubes and stored at -20 °C. Immediately after collecting these samples, plates were inverted, and wells were washed with 250 µl PBS of 4 °C. Plates were inverted again and 80 µl/well of 4 °C radio-immunoprecipitation assay (RIPA) buffer (0.1% SDS, 150 nM NaCl, 1% Triton X-100, 50 mM Tris-Cl, pH 8, and cOmplete ™, EDTA-free Protease Inhibitor Cocktail (#11873580001, Roche Diagnostics, Basel Switzerland) was added to extract protein. Plates were left on ice on an orbital shaker for 20 min. Then, wells were scraped vigorously using pipette tips, samples were collected into labelled 1.5 ml Eppendorf tubes and stored at -20 °C, ready for total insulin quantification and BCA assay.

2.3.8 BCA protein quantification assay

RIPA protein-extracted samples in **2.3.7** were thawed and centrifuged at 14,000 xg for 15 min and supernatant was carefully transferred to new labelled 1.5 ml Eppendorf tubes, ready for analysing protein content using Pierce™ BCA Protein Assay Kit (Pierce, Rockford, IL, USA). Working reagent was prepared in a 50 ml Falcon tube according to protocol (1 part of Reagent B and 50 parts of Reagent A) and protected from light using foil. Standard curve samples were prepared and vortexed according to protocol using 100% RIPA buffer as diluent. 25 µl of cell lysate samples were added using reverse pipetting into designated wells. 25 µl of standard curve samples were added to designated wells on the pate. Following this, 200 µl/well working

reagent was added then plate was sealed using Acetate foil for micro-test well plates (SARSTEDT, New York, USA), shaken gently, and incubated for 30 min in 37 °C incubator followed by a 10 min rest at room temperature. Plate was read at 562 nm using CLARIOstar® Plus Microplate Reader (BMG LABTECH, Ortenberg, Germany).

2.3.9 Human insulin ELISA

Insulin secretion and total insulin content were measured using human Mercodia Insulin direct sandwich ELISA (#10-1113-01, Uppsala, Sweden). The assay was carried out following manufacturer's protocol. Briefly, all secretion samples were thawed on ice and vortexed for a few seconds. Then, a 1:40 dilution was prepared by pipetting 2.5 µl of secreted samples and adding 97.5 µl SAB. 25 µl of each diluted sample prepared was then pipetted into the ELISA plate. Total insulin samples were diluted at 1:1250 dilution, whereby 5 µl of sample was added into 495 µl of SAB, then 2 µl of this sample was further diluted within the ELISA plate with 23 µl of SAB. Two µl of each standard curve sample was added into designated wells on the plate. Afterwards, conjugated enzyme 100 µl /well was prepared and added onto all wells on the plate, which was sealed with tape and incubated for 1 h on Reciprocating Shaker (OHAUS, New Jersey, USA) at 800 rpm at room temperature. Then, plate was inverted and washed 6X with 350 µl of previously prepared Washing Buffer. 200 µl of Tetramethylbenzidine (TMB) substrate was then added into each well and plate was left covered on the bench for 15 min, followed by addition of 50 µl STOP solution. The plate was sealed again and shaken on Reciprocating Shaker briefly at 400 rpm, then read at 450 nm on a CLARIOstar® Plus Microplate Reader (BMG LABTECH, Ortenberg, Germany). Cubic spline regression was used to produce a standard curve using CLARIOstar® MARS software (BMG LABTECH, Ortenberg, Germany). Insulin secretion and insulin content measured values were normalised to total protein content of the corresponding wells.

2.3.10 Human proinsulin ELISA

Proinsulin secretion and total proinsulin content were measured using human Mercodia Proinsulin direct sandwich ELISA (#10-1118-01, Uppsala, Sweden). The assay was carried out following manufacturer's protocol. Secretion samples were diluted in a 1:5 in SAB and total proinsulin samples were diluted in a 1:200 dilution in SAB. The remaining procedures were similar to **2.3.9**.

2.3.11 Cell viability MTS assay

EndoC-βH1 cells were seeded at a density of 70,000 cells/well in a 96-well plate and incubated overnight at 37 °C. Then, media was changed, and cells were treated with ISC conditioned medium (1:1) dilution with a final volume of 100 µl/well then plate was incubated for 72 h at 37 °C. Subsequently, cell viability was assessed via the colorimetric MTS assay (3-[4,5-Dimethylthiazol-2-yl]-5-[3-carboxymethoxyphenyl]-2-[4-sulfophenyl]-2H-tetrazolium) using CellTiter 96® AQueous One Solution Cell Proliferation Assay (#G3580, Promega, Wisconsin, USA). The assay was performed as manufacturer's protocol. Briefly, 20 µl of MTS reagent was added to each well. Blank wells were treated with 100 µl of 1:1 dilution (DMEM media: RPMI media) to ensure background subtraction when analysing the results. Then the plate was incubated at 37 °C for 3 h in a humidified, 5% CO_2 atmosphere. Afterwards, absorbance was read at 490 nm using CLARIOstar® Plus Microplate Reader (BMG LABTECH, Ortenberg, Germany). After this, the plate was inverted to remove solution and cells were washed twice with 100 µl PBS. Then, 50 µl/well of RIPA buffer was added to perform a BCA assay to enable cell viability data normalisation to total protein content for each well.

2.3.12 RNA extraction for bulk RNA sequencing

RNA samples from EndoC-βH1 cells were extracted using QIAzol ® Lysis Reagent (57208428, QIAGEN Sciences, Maryland, USA) inside a fume cabinet. Following incubation for 72 h with ISC-conditioned medium, this was aspirated carefully by suction with a 200 µl tip fixed to the tip of a 2 ml polystyrene serological pipette attached to the automatic suction device. Promptly, wells were washed slowly with 250 µl pre-warmed PBS using an automated single channel pipette to avoid cells from drying out. PBS was then aspirated and 350 µl/well of QIAzol was added (2 wells pooled together in 700 µl provided 1 sample per condition). Wells were scraped thoroughly with a plastic pipette tip and mixture was transferred to 1.5 ml RNAase Eppendorf tubes that were labelled and frozen on dry ice for at least 10 min before storing at -20 °C until RNA extraction. Empty wells were covered carefully with sealing film to avoid any exposure to any harmful Qiazol residues, before being rinsed twice with 500 µl PBS.

RNA purification was then performed using miRNAeasy® Mini Kit (#217004, Qiagen, Hilden, Germany). Firstly, samples were taken out of the -20 °C and incubated at room temperature for 5 min. Samples were then incubated at room temperature for 2-3 min after being shaken vigorously for 15 sec following the addition of 140 µl chloroform. Then, samples were centrifuged for 15 min at 12,000 xg at 4 °C. Without disturbing the interphase, the upper

aqueous phase was collected into a new collection tube and 450 µl of 100% ethanol was added and mixed thoroughly by pipetting. Then, 700 µl of the sample was pipetted into an RNeasy® Mini column in a 2 ml collection tube and centrifuged at 8000 xg for 15 sec at room temperature. After discarding the flow-through, 700 µl of Buffer RWT was added to the column followed by 15 sec centrifugation at 8,000 xg. Flow-through was discarded. Then, 500 µl of Buffer RPE was added and tubes were centrifuged at 8,000 xg for 15 sec. This step was repeated with centrifugation at the same speed for 2 min then at 12,000 xg for 1 min with open lid to dry the membrane. Prior to final centrifugation at 8,000 xg for 1 min to elute RNA, the column was transferred to a new 1.5 ml collection tube and 50 µl of RNase-free water was added directly onto the membrane and incubated for 2 min. Samples were stored at -20 $^{\circ}$C ready to be sent to the Genomic Core Facility, Newcastle University for Bulk RNA sequencing using TruSeq Standard mRNA library prep kit.

2.4 Data and statistical analysis

Statistical analyses were carried out using Prism version 9.5.0 and version 10.1.2 (GraphPad Inc, California, USA). Non-linear or simple linear regression analyses were used to visualise the trend in the changes observed in CF and control pancreata. Two-tailed Student's t test, one-way or two-way ANOVA tests were used to test the differences between means of different groups. Least significant difference (LSD) Fisher's post hoc test was used when investigating the significance difference between 3 groups. Tukey post-hoc test was used when investigating the significance difference between the mean of more than 3 groups. Statistical significance was deemed to be evidenced by $p < 0.05$.

To analyse the AI-generated data from stained pancreatic tissue sections obtained from human control and CF donors, some with multiple blocks, a mixed-linear model was implemented using IBM SPSS® Statistics Data software package (IBM, New York, USA). The mixed-linear model considered the morphological pattern as fixed effects and the donor ID as random effects to accommodate the nested structure of the data. Then, Bonferroni post-hoc test was used to test for the significance, indicated by $p < 0.05$. Where this model was not applicable due to the small number of blocks per pattern, one-way ANOVA tests followed by Bonferroni post-hoc testing was conducted.

Chapter 3: Systematic semi-quantitative and AI-driven quantitative analysis of pancreatic exocrine and endocrine compartments in CF

3.1 Introduction

Cystic fibrosis (CF) results from mutations in the CF transmembrane conductance regulator (*CFTR*) gene, which leads to the impairment of chloride ion secretion, sodium absorption and water transportation across epithelial cell membranes in organs including the lungs and the pancreas (Riordan et al., 1989). In CF pancreata, the production of sticky mucin in the ducts obstructs the drainage of digestive enzymes, a process that induces apoptosis, atrophy and loss of acinar cells that are replaced by fibrosis and/ or lipomatosis resulting in pancreatic enzyme insufficiency (PEI) (Löhr et al., 1989). As CF progresses, what remains in the pancreas are the mucin-filled dilated ducts and islets which aggregate in the fibrotic and/or fatty tissue and form complexes of different sizes, that are irregularly distributed in the fibrotic and lipomatous tissue (Iannucci et al., 1984; Löhr et al., 1989; Couce et al., 1996; Hart et al., 2018).

Diabetes mellitus occurring in conjunction with CF used to be rare. However, in association with increasing survival of people with CF, there is a rising incidence of overt diabetes whereby, up to 50% of adults and 20% of adolescents with CF develop CF-related diabetes (CFRD) (Moran et al., 2009; Kelsey et al., 2019; Olesen et al., 2020). CFRD is characterized by a gradually decreasing insulin secretion that cannot be explained by insulin resistance or mechanisms other than a gradual loss of β-cell function (Nathan et al., 2010; Street et al., 2012; Cano-Megías et al., 2015; Norris et al., 2019). Yet the underlying pathogenesis of CFRD is not fully understood.

In CF pancreata, two distinct pathological patterns - 'fibrotic' (parenchymal replacement with fibrotic tissue) and 'lipoatrophic' (parenchymal replacement with fatty tissue) have been reported and have been used to describe the exocrine compartment changes in CF pancreata (Iannucci et al., 1984; Abdul-Karim et al., 1986; Soejima & Landing, 1986; Löhr et al., 1989; Couce et al., 1996; Bogdani et al., 2017; Cory et al., 2018; Hull et al., 2018). In both patterns, islets appear to survive either individually or as clusters of aggregated islets (Abdul-Karim et al., 1986; Hart et al., 2018; Löhr et al., 1989). Although, underlying mechanisms of CFRD development remain unclear, it is increasingly accepted that exocrine-endocrine cross-talk plays a part in mediating endocrine dysfunction through oxidative stress and islet inflammation-based remodelling (Kelly & Moran, 2013; Barrio, 2015; Yi et al., 2016). Löhr et

al. (1989) reported the presence of moderate intra-islet fibrosis and in cases where severe intra-islet fibrosis was present, the islets appeared to be fragmented (Löhr et al., 1989). Bogdani et al. (2017) reported that CF islets embedded in fatty tissue surrounded by collagen exhibited more apparent changes in morphology and density compared to islets embedded in CF fibrotic tissue (Bogdani et al., 2017).

It remains unclear whether CFRD development is due to gradual loss of pancreatic islets or the loss of β-cells within remaining islets, or a combination between the two processes. Also, due to the limited human CF tissue availability, the lack of age-matched controls it remains unclear whether the end-stage of CF can be either fibrosis and fat replacement; or whether there is progression from fibrosis to virtually total fat replacement.

In a series of histological and AI-based quantification studies, I set out to evaluate histopathological changes in 29 human *post-mortem* CF pancreata with a wide age range (perinatal death-27-year-old) in comparison to 58 age-matched controls (0 months-29-year-old) with no overt pancreatic pathology. Following qualitative histological evaluation of exocrine and endocrine compartments, a systematic semi-quantitative scoring system was established. In collaboration with Professor Sarah Richardson and her team, University of Exeter, Artificial Intelligence-driven (AI) HALO deep learning pancreatic-based image analysis software was developed as a powerful tool, to provide further insights into the pathological changes within CF and CFRD pancreatic tissue. It employed mathematical and AI techniques to design and train classifiers to extract quantitative data from stained pancreatic tissue. This enabled quantitative analysis of morphological and pathological exocrine and endocrine changes necessary to understand disease progression with age.

3.2 Aim

To analyse pancreatic histopathological changes in human *post-mortem* CF tissue and identify associated cell phenotypes with potential aetiological roles in CFRD to answer three main questions:

1) What is the natural history of CF pancreatic pathology within the exocrine compartment?

2) How are exocrine compartment changes associated with changes in the endocrine compartment?

3) Is there any spatial relationship between fibrosis and stellate cells around the islets in CF?

- **Objective 1.1:** Evaluate the histopathological changes in the exocrine parenchyma and categorise the CF pancreatic tissue blocks into patterns based on the morphological changes observed.
- **Objective 1.2:** Use H&E-stained pancreatic tissue sections to assess the changes in CF pancreata over the course of the disease and potential associations with donor age at *post-mortem.*
- **Objective 1.3:** Establish a semi-quantitative scoring system to investigate the changes in the exocrine and endocrine compartments based on the established morphological patterns.
- **Objective 1.4:** Assess proportion of specific endocrine cell phenotypes, fibrosis and activated PaSCs in diseased and control pancreata and quantify these changes using immunohistochemistry staining and AI deep learning.

3.3 Results

3.3.1 Histological evaluation of control and CF pancreata

3.3.1.1 Initial qualitative evaluation of pancreatic morphology in CF in comparison to normal control pancreas

H&E-stained pancreatic tissue sections of 58 control donors (58 blocks) obtained from EADB and QUOD tissue banks with an age range of (0–29-year-old) ***(Table 2.1)*** and 29 CF donors (46 blocks) obtained from EADB and a pathology bank collected by Professor Günter Klöppel, Technical University of Munich, Germany ***(Table 2.2)*****,** were evaluated qualitatively and findings were reported.

A representative pancreas of a 19-year-old donor without overt pancreatic disease (control) illustrated an overall normal pancreatic morphology, whereby the lobular architecture is easily defined and exocrine parenchyma is well-preserved ***(Figure 3.1 A)***. Acinar cells appeared normal and fully intact demonstrating a cytoplasm with a basophilic characteristic at the basal pole and eosinophilic appearance at the apical pole ***(Figure 3.1 B)***. Islets (examples indicated with black arrows) appeared ovoid in shape and were easily identified and scattered individually within the pancreatic lobules ***(Figure 3.1 C)***. Ducts appeared normal (no dilation) with no presence of eosinophilic mucus secretion ***(Figure 3.1 D)***.

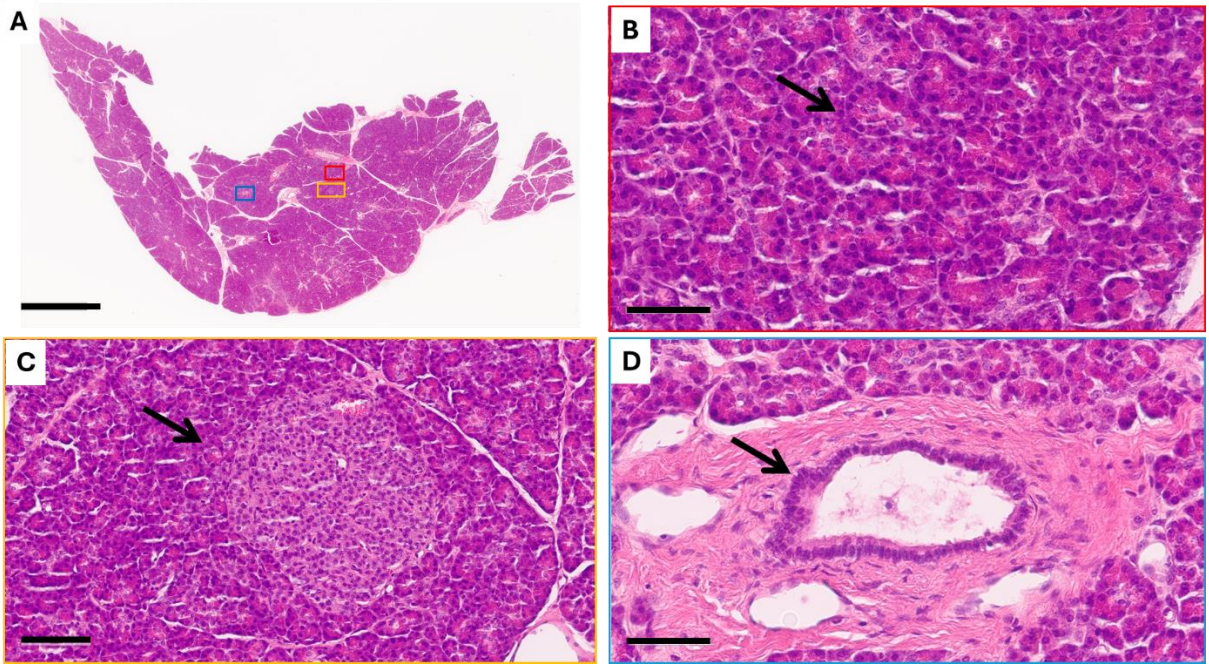

Figure 3.1: Representative H&E images of a 19-year-old control pancreas (Table 2.1: Case number: 53) illustrating intact exocrine parenchyma with well-defined lobule architecture.

(A) *A whole pancreas section illustrating the preserved lobular architecture of the pancreas.* ***(B)*** *A magnified section of* ***A*** *(red rectangle) showing acini.* ***(C)*** *A magnified section of* ***A*** *(yellow rectangle) showing an islet (indicated by black arrows) surrounded by acinar cells.* ***(D)*** *A magnified section of* ***A*** *(blue rectangle) illustrating an example of an intralobular duct. Scale bars represent 3 mm* ***(A)****, 60 µm* ***(B*** *and* ***D)*** *and 200 µm* ***(C)****.*

Evaluation of CF pancreata revealed exocrine and endocrine morphological changes that were observed at low and high magnifications. A pancreatic section from a young CF donor that was born prematurely ***(Table 2.2:*** Case number 1***)*** and died peri-natally illustrated some alteration to pancreatic lobule architecture represented by larger inter-lobular spaces (***Figure 3.2 A***). At a higher magnification, the exocrine parenchyma was preserved with some acinar lumen dilation, mild acinar atrophy and some presence of abnormal intra-lobular collagen deposition ***(Figure 3.2 B)***. Islets were surrounded by fibrous tissue, were varied in size and were less-well defined from surrounding acini ***(Figure 3.2 C)***. Ductal dilation was observed with some presence of eosinophilic mucus secretion ***(Figure 3.2 D)***. Morphological changes in CF pancreata of 16 CF donors (19 blocks) with an age range of (0–14-year-old) were reported similarly to these observations and the blocks were classified by a fibroatrophic pathological pattern (CF Pattern 1). This pattern was reported previously by (Löhr et al., 1989).

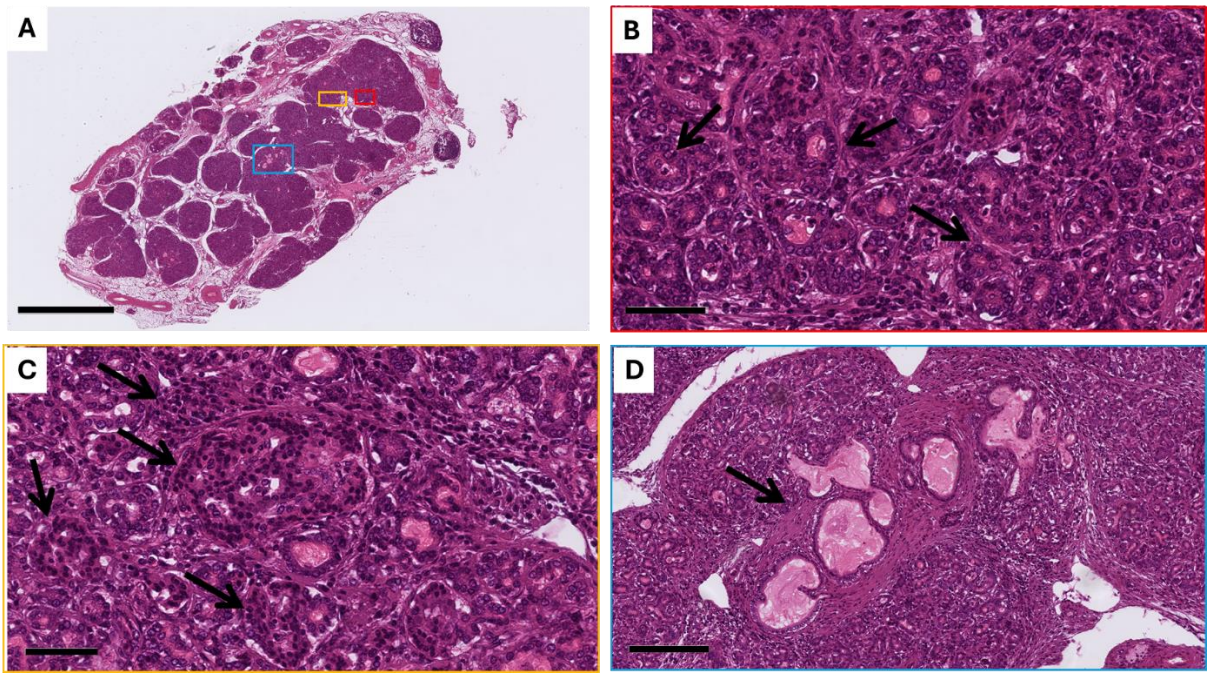

Figure 3.2: Representative H&E images of a CF pancreas of a pre-mature donor (Table 2.2: Case number: 1) illustrating a fibroatrophic pattern (CF Pattern 1).

(A) *A whole pancreas section illustrating the preserved lobular architecture of the pancreas.* ***(B)*** *A magnified section of* ***A*** *(yellow rectangle) showing acini lumen dilation.* ***(C)*** *A magnified section of* ***A*** *(yellow rectangle) showing example islets of different sizes (indicated by black arrows) surrounded by abnormal collagen deposition.* ***(D)*** *A magnified section of* ***A*** *(blue rectangle) illustrating ductal dilation and the presence of eosinophilic mucus secretion. Scale bars represent 3 mm* ***(A)****, 60 µm* ***(B*** *and* ***C)*** *and 200 µm* ***(D)****.*

Histological evaluation of 13 CF cases (3–27-year-old) illustrated severe damage to the exocrine pancreas ***(Figure 3.3 and Figure 3.4)***. Eight of the 13 cases illustrated an extensive disruption of lobule architecture, whereby the exocrine parenchyma was extensively replaced by a mixture of fibrous and fatty tissue ***(Figure 3.3 A and B)***. Islets (examples indicated with black arrows) were still present embedded in fibrous tissue or surrounded by peri-islet collagen strands with adjacent adipocytes, some islets appeared round in shape whereas some islets appeared 'disturbed' with some presence of intra-islet collagen strands (example islet 1) ***(Figure 3.3 C)***. Ducts appeared severely dilated with eosinophilic secretions (often thick mucus) and extensive peri-ductal fibrosis ***(Figure 3.3 D)***. The changes reported here were similar in all eight CF cases (14 blocks) with an age range of 3–27-year-old and tissue blocks of these cases were classified as having a combined fibroatrophic and lipoatrophic pattern (CF Pattern 2).

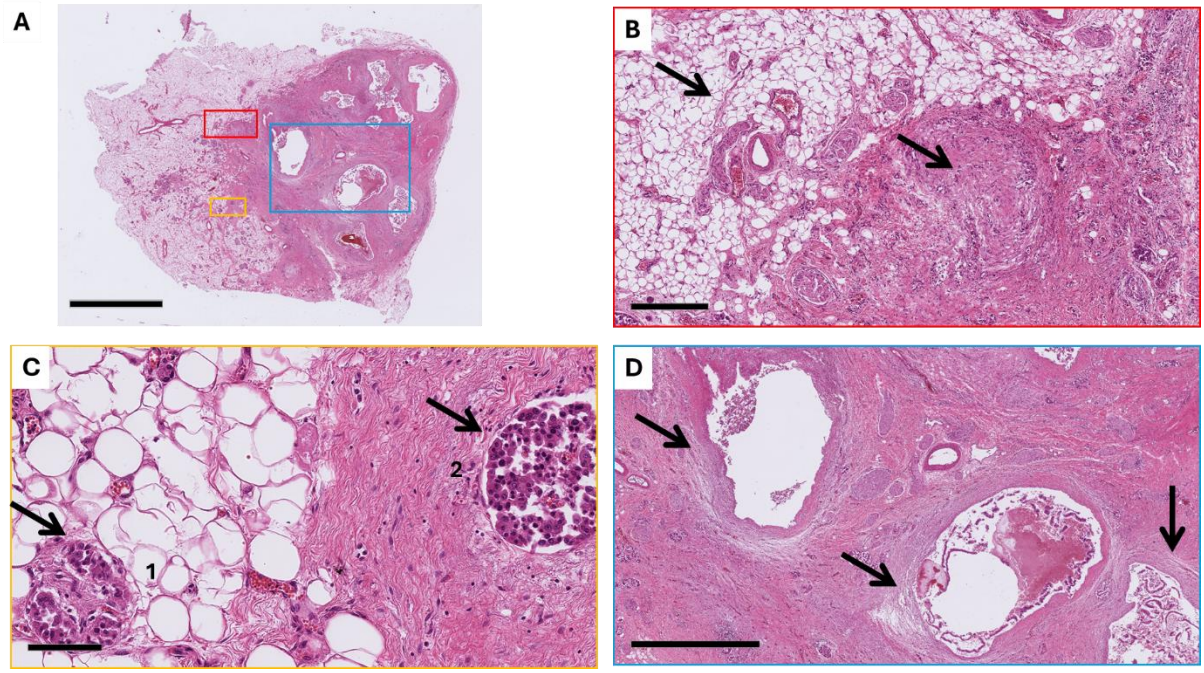

Figure 3.3: Representative H&E images of CF pancreas of a 27 year-old donor (Table 2.2: Case number: 29) illustrating a fibroatrophic and lipoatrophic pattern (CF Pattern 2).

(A) *A whole pancreas section illustrating the total loss of lobular architecture and the exocrine parenchyma being replaced by abnormal collagen deposition and fatty tissue.* ***(B)*** *A magnified section of* ***(A)*** *(red rectangle) showing acinar atrophy.* ***(C)*** *A magnified section of* ***(A)*** *(yellow rectangle) showing islets surrounded by peri-islet collagen strands with adjacent adipocytes (1) or dense fibrosis (2).* ***(D)*** *A magnified section of* ***(A)*** *(blue rectangle) illustrating an example of ductal dilation and the presence of eosinophilic mucus secretion. Scale bars represent 5 mm* ***(A)****, 400 µm* ***(B)****, 100 µm* ***(C)*** *and 200 µm* ***(D)****.*

Five out of the 13 CF cases had a similar degree of severe damage to the exocrine pancreas in terms of total loss of acinar tissue, but the tissue was predominantly replaced by adipocytes ***(Figure 3.4 A*** and ***B).*** Islets were present but they appeared as clusters with irregular shapes and sizes and were surrounded by peri-islet collagen strands surrounded by adipocytes ***(Figure 3.4 C)***. In these cases, ductal loss was observed within fatty tissue and remaining ducts appeared to be small-medium in size and dilated surrounded by peri-ductal fibrosis and adjacent adipocytes ***(Figure 3.4 D)***. These changes observed within these five CF cases (13 tissue blocks) with an age range of 7–27-year-old were histologically evaluated and classified as having a lipoatrophic CF pattern (CF Pattern 3). This pattern was reported previously by (Löhr et al., 1989).

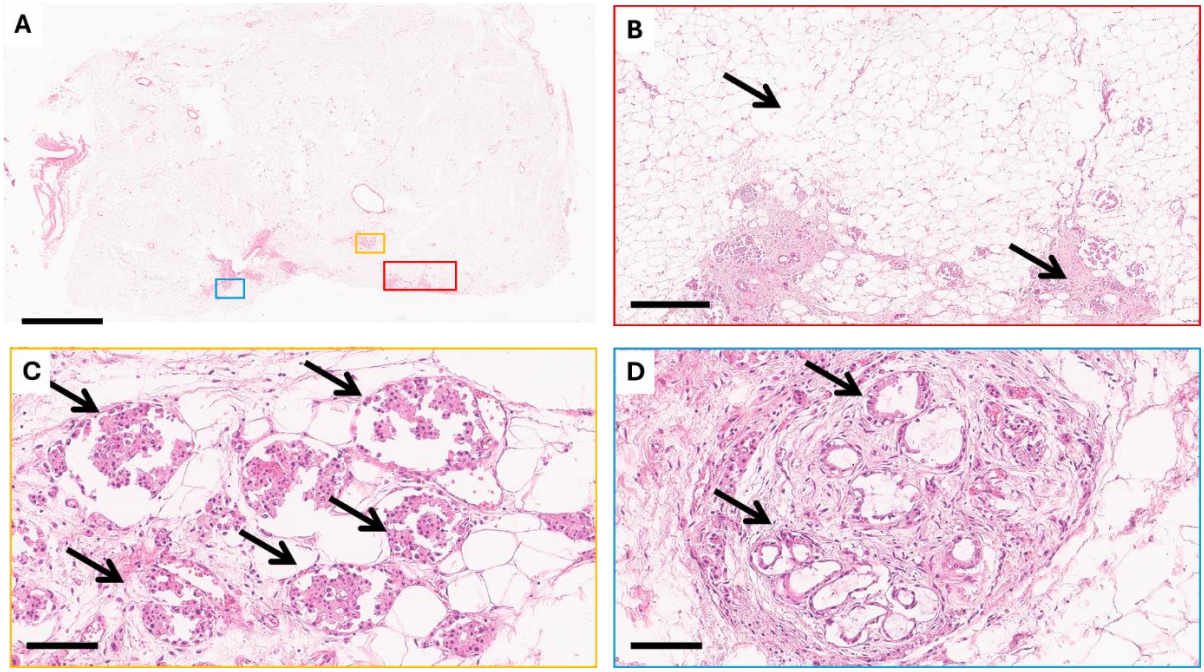

Figure 3.4: Representative H&E images of CF pancreas of a 27-year-old donor (Table 2.2: Case number: 28) illustrating a lipoatrophic pattern (CF Pattern 3).

(A) *A whole pancreas section illustrating the total loss of lobular architecture, absence of severely dilated ducts and the exocrine parenchyma predominantly being replaced by fatty tissue.* ***(B)*** *A magnified section of* ***(A)*** *(red rectangle) showing acinar atrophy and replacement with fatty tissue with some mild presence of fibrotic tissue.* ***(C)*** *A magnified section of* ***(A)*** *(yellow rectangle) showing example islet clusters of different sizes (indicated by black arrows) surrounded by collagen strands adjacent to adipocytes.* ***(D)*** *A magnified section of* ***(A)*** *(blue rectangle) illustrating an example of mini ductal clusters surrounded by collagen and the presence. Scale bars represent 5 mm* ***(A)****, 500 µm* ***(B)****, 100 µm* ***(C*** *and* ***D)****.*

3.3.2 Histopathological semi-quantitative scoring of morphological changes within control and CF pancreata

3.3.2.1 Developing and validating a semi-quantitative integer scoring system

Löhr et al., (1989) study has previously reported some semi-quantitative scoring on ductal dilation. Building on this and informed by the qualitative microscopic evaluation of morphological changes in CF pancreata, I developed a histopathological semi-quantitative integer scoring system (0-3) for a wider range of parameters including ductal dilation, ductal loss, exocrine fibrosis, acinar atrophy, islet remodelling and inflammatory cell infiltration. The scoring system was validated in discussions with experienced clinical pathologists Professor Dina Tiniakos (University of Athens, Greece and Newcastle University, UK) and Professor Günter Klöppel (Technical University Munich, Germany), whereby scoring descriptors were refined and iterated based on the changes and patterns reported during the morphological assessment. The scoring was undertaken on tissue slides stained with H&E in parallel with

SRFG staining to assess fibrosis, when available; CGA-stained slides were used to identify islets, when available; CD45 staining was used to assess inflammatory infiltration, when available. For each parameter, the scoring integer value (0-3) was agreed using the QUOD control cohort with an age range 6–29-year-old, and EADB and Klöppel CF cohorts with an age range of premature–27-year-old ***(Table 2.1*** and ***Table 2.2***, respectively***)***.

For each scored parameter an example image was illustrated for each integer score (0-3) to provide a key. Ductal lumen dilation was scored based on presence of ductal dilation, severity of dilation and the presence of mucus within dilated ducts ***(Figure 3.5)***. Ductal loss was scored based on whether there was focal ductal loss observed within an area of the tissue or whether ductal loss was global across the tissue area ***(Figure 3.6)***. Exocrine pancreas fibrosis was assessed based on the presence and the severity of abnormal collagen deposition replacing the exocrine parenchyma ***(Figure 3.7)***. Acinar atrophy was scored based on the degree of acinar tissue area loss ***(Figure 3.8)***. Islet remodelling was scored based on islet size, shape and distribution within the exocrine parenchyma either as solitary islets or as aggregated clusters/complexes ***(Figure 3.9)***. Inflammation was scored based on the presence and severity of inflammatory cells within the tissue ***(Figure 3.10)***. Only the Klöppel CF cohort could be scored for inflammation due to unavailability of EADB slides stained for CD45. After, validating all scores, the scoring system was finalised as shown in ***Table 3.1***.

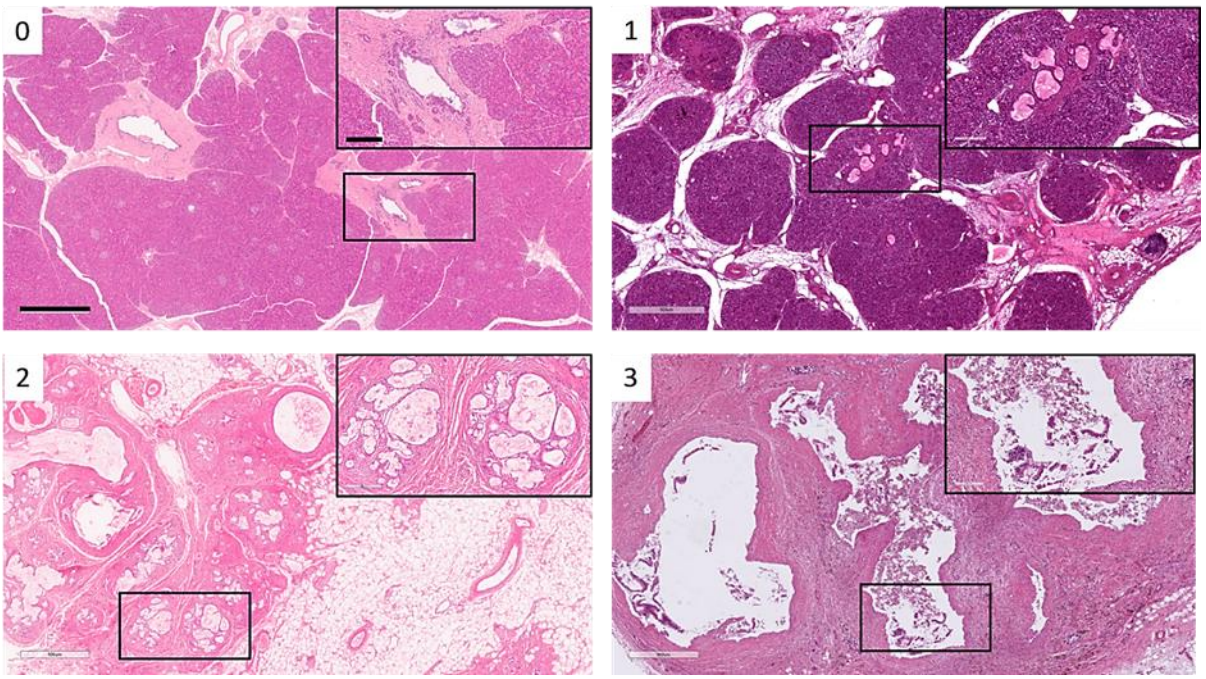

Figure 3.5: Representative H&E-stained control (0) and CF (1-3) pancreatic tissue to demonstrate the semi-quantitative scoring system for ductal lumen dilation, represented by a score of 0-3.

0= non-dilated, 1= mild dilation sometimes filled with mucus, 2= ducts dilated and often filled with mucus, 3= massive dilation. Scale bars 900um and 200 µm for magnified images (black rectangle).

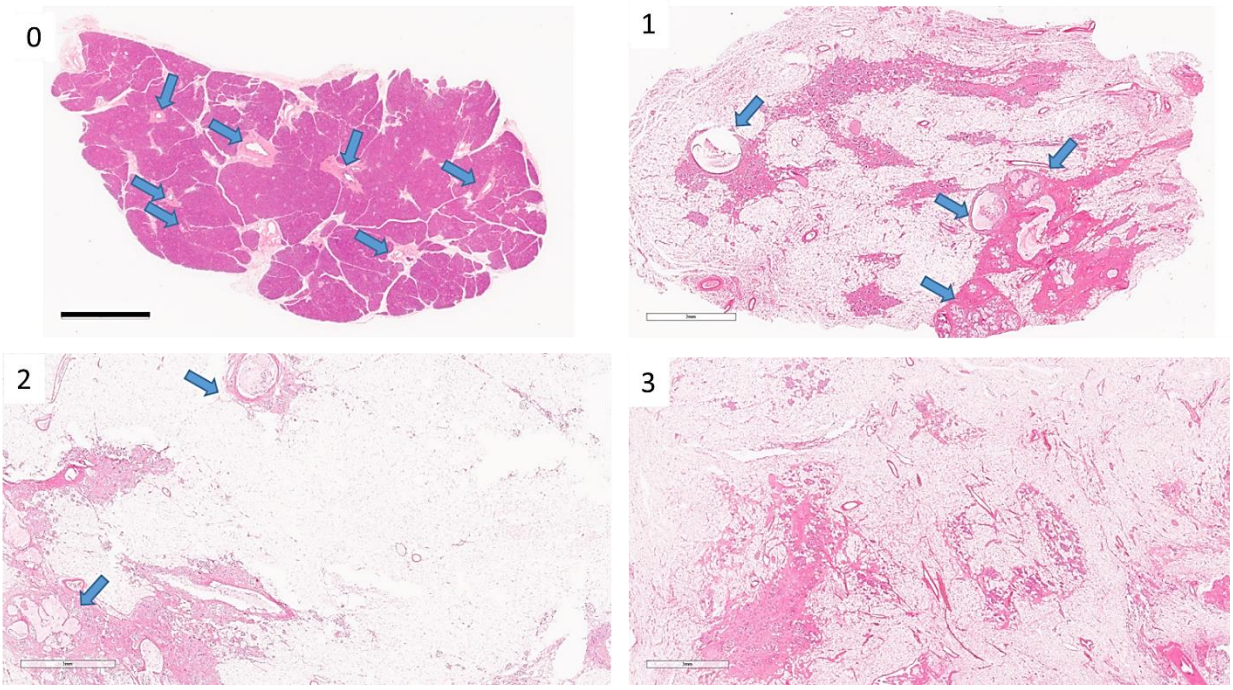

Figure 3.6: Representative H&E-stained control (0) and CF pancreatic tissue (1-3) to demonstrate the semi-quantitative scoring system for ductal loss, represented by a score of 0-3.

0= no ductal loss, 1= focal loss, 2= moderate loss, 3= severe loss. Blue arrows indicating ducts. Scale bar 3 mm. representative for all images.

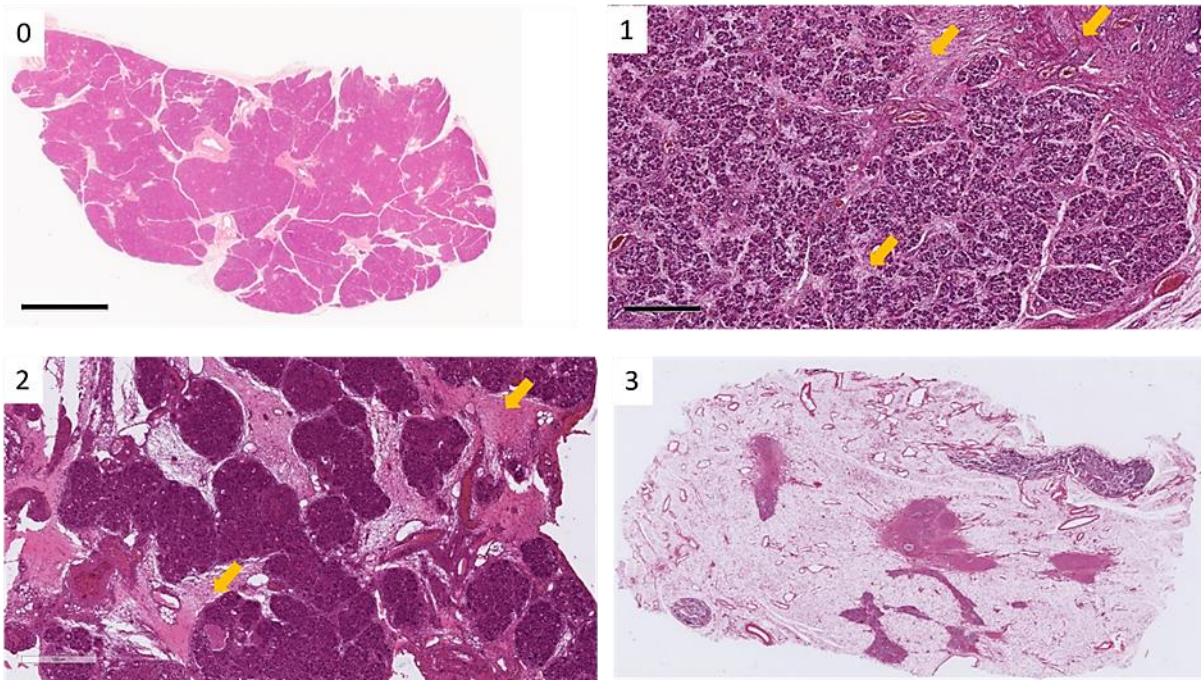

Figure 3.7: Representative H&E-stained control (0) and CF pancreatic tissue (1-3) to demonstrate the semi-quantitative scoring system for acinar atrophy, represented by a score of 0-3.

Yellow arrows indicated example areas of acinar atrophy. 0= no acinar atrophy, 1= < 1/3 of acini lost, 2= 1/3 – 2/3 acini loss, 3= >2/3 acini loss. Scale bar 500 µm (1 & 2) and 4 mm (0 & 3).

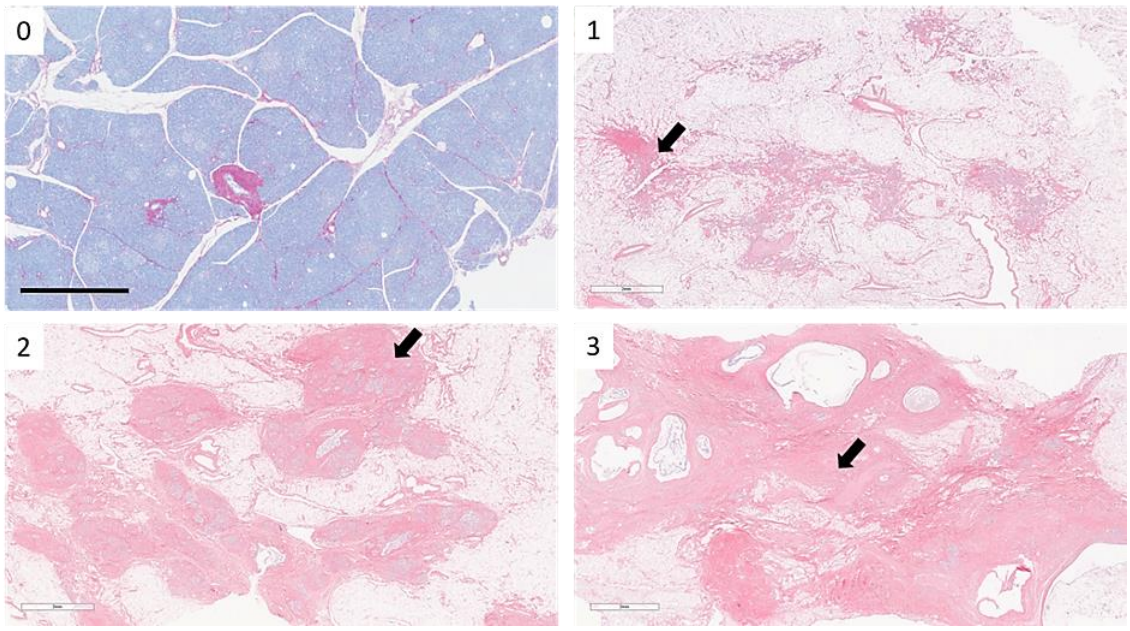

Figure 3.8: Representative SRFG-stained control (0) and CF pancreatic tissue (1-3) to demonstrate the semi-quantitative scoring system for exocrine pancreas fibrosis, represented by a score of 0-3.

Black arrows indicated red/pink collagen stained areas illustrating fibrotic areas stained red/pink. 0= no abnormal presence of fibrotic tissue, 1= mild presence of fibrotic tissue, 2= moderate presence of fibrotic tissue, 3= massive presence of fibrotic tissue. Scale bar 2 mm, representative for all images.

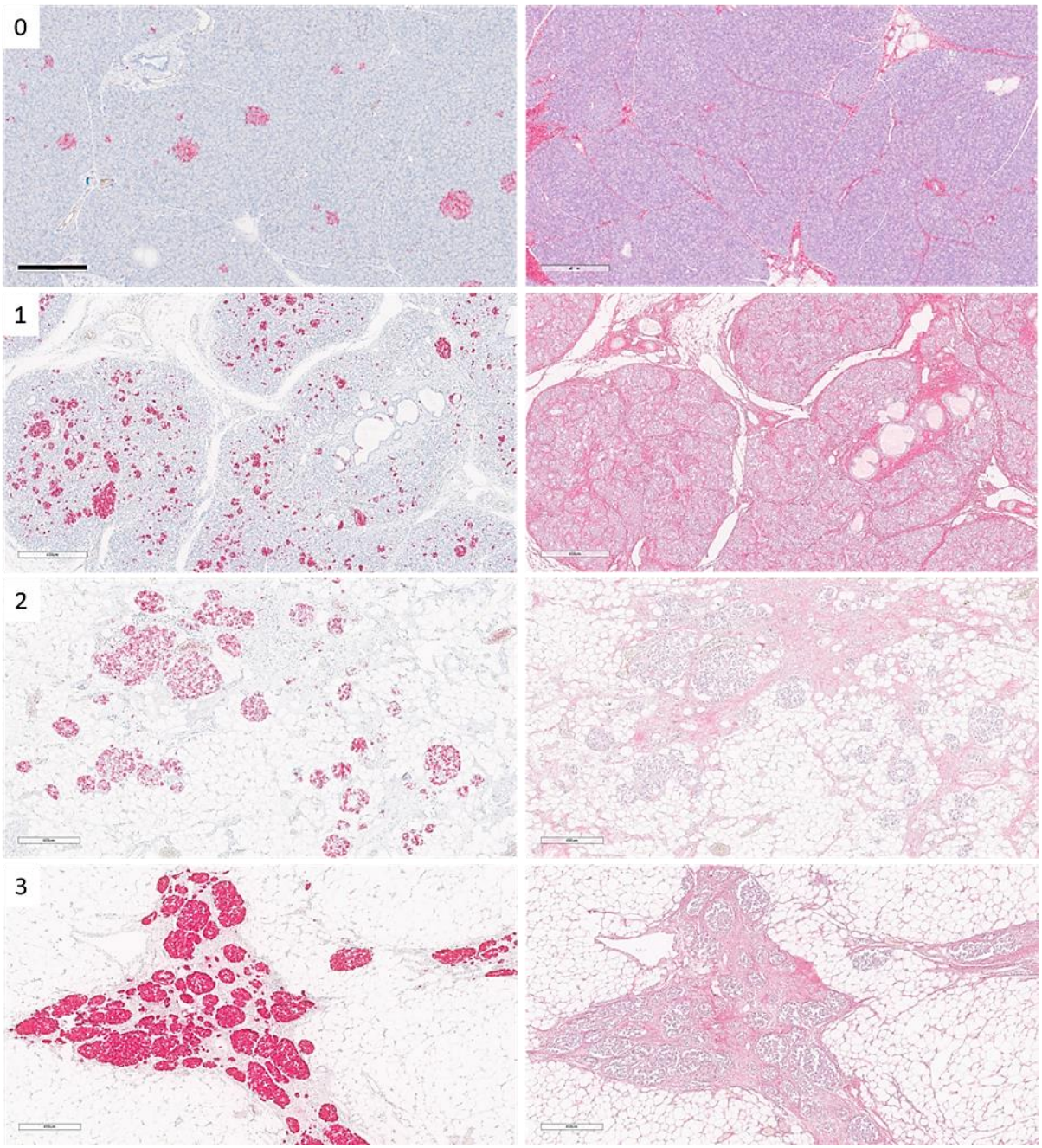

Figure 3.9: Representative Chromogranin A (red) (left column) and SRFG (right column) stained control (0) and CF pancreatic tissue (1-3) to demonstrate the semi-quantitative scoring system for islet remodelling, represented by a score of 0-3.

0= no abnormal size or distribution, 1= presence of some solitary islets surrounded by fibrosis, 2= many islets are aggregated in complexes, 3= most islets of variable size and shape are aggregated in complexes. Scale bar 400 µm, representative for all images.

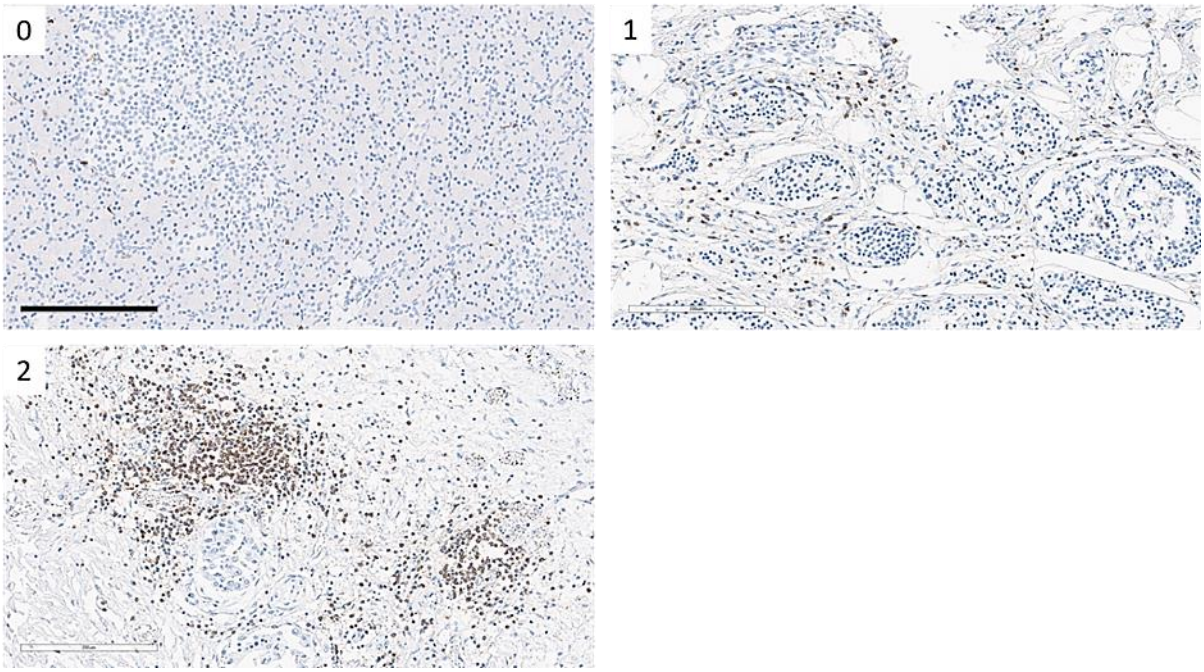

Figure 3.10: Representative CD45 (in brown) stained control (0) and CF pancreatic tissue (1-2) to demonstrate the semi-quantitative scoring system for inflammation, represented by a score of 0-3.

0= no abnormal inflammatory cell infiltration, 1= mild presence of inflammatory cells, 2= moderate presence of inflammatory cells, 3= severe presence of inflammatory cells (was not observed). Scale bar 200 µm, representative for all images.

Table 3.1: Semi-quantitative scores (0-3) definitions for ductal lumen dilation, ductal loss, exocrine pancreas fibrosis, acinar atrophy, islet remodelling and inflammation.

Score	**0**	**1**	**2**	**3**
Ductal lumen dilation	Non-dilated	Little dilatation sometimes filled mucus	Dilated and often filled with mucus	Massive dilatation often filled with mucus
Ductal loss	No ductal loss	Focal ductal loss	Moderate ductal loss	Severe ductal loss
Exocrine pancreas fibrosis	No abnormal presence of fibrotic tissue	Mild presence of fibrotic tissue	Moderate presence of fibrotic tissue	Massive presence of fibrotic tissue
Acinar atrophy	No acinar atrophy	<1/3 acini lost	1/3 – 2/3 acini loss	>2-3 acini loss
Islet remodelling	No abnormal size or distribution	Presence of some solitary islets surrounded by fibrosis	Many islets are aggregated in complexes	Most islets of variable size and shape are aggregated in complexes
Inflammation	No pathological inflammatory cell infiltration	Mild inflammatory cell infiltration	Moderate inflammatory cell infiltration with some presence of inflammatory foci	Severe inflammation with extensive presence of inflammatory foci

3.3.2.2 Semi-quantitative integer scoring of CF pancreatic biopsies in comparison to age matched control donors

Following the development of semi-quantitative integer scoring system, I implemented the scoring to score all blocks from QUOD control cohort (10 blocks) in parallel with EADB and Klöppel CF pancreatic biopsies (46 blocks; some donors had multiple blocks) ***(Table 2.1*** and ***Table 2.2*** respectively***)***, with the exception of inflammation, which was scored in 10 controls and 26 CF blocks.

Following the unbiased scoring, blocks were grouped according to the classified Pathological Patterns and statistical analysis was undertaken ***(Figure 3.11)***. Ductal dilation was present in all CF patterns and was greatest in Pattern 2 prior to total adipocyte replacement (Pattern 3) ***(Figure 3.11 A)***. Ductal loss was observed to be present parallel to adipocyte replacement and was more apparent in CF Pattern 3 ***(Figure 3.11 B)***. Fibrosis was apparent in all CF biopsies regardless of the pathological pattern and persisted even with exocrine tissue total replacement with adipocytes ***(Figure 3.11 C)***. Acinar atrophy was present in all CF patterns with complete acinar tissue loss in CF Pattern 2 and 3, where fibrotic and fatty tissue replaced the exocrine parenchyma ***(Figure 3.11 D)***. CF progression from fibrosis alone (Pattern 1), through a combined fibrotic/ adipocyte replacement phenotype (Patten 2), to total adipocyte replacement (Pattern 3) was also supported by islet remodelling score illustrating greater islet dysmorphology presented by varied islet sizes and shapes that appeared to be clustered in complexes ***(Figure 3.11 E)***.

Semi-quantitative scores for all parameters were significantly higher in all CF pathological patterns compared with control except for inflammation score, which could be due to $CD45^+$ inflammatory cells being scattered within the exocrine parenchyma in both control and CF biopsies without a significant presence of confluent inflammatory foci in any of the pathological patterns ***(Figure 3.11 F)***.

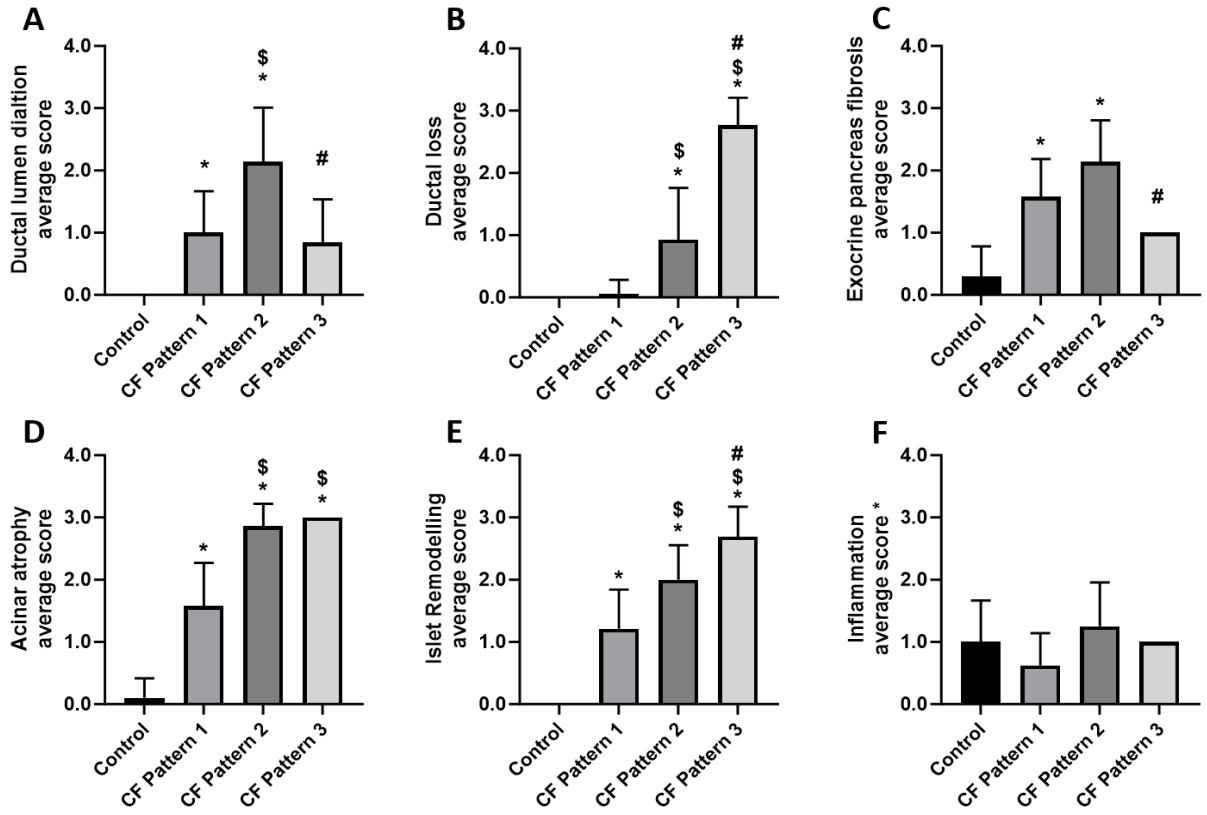

Figure 3.11: Pattern-based histopathological semi-quantitative analysis to assess control and CF pancreata for different morphological parameters.

(A) *Ductal lumen dilation,* ***(B)*** *ductal loss,* ***(C)*** *exocrine pancreas fibrosis,* ***(D)*** *acinar atrophy,* ***(E)*** *islet remodelling, and* ***(F)*** *inflammation****.*** *Graphs show the mean±SD. Linear mixed effect model (LMEM) was used with pancreata pattern set as fixed effect, donor as random effect and Bonferroni post hoc test was utilised for statistical analysis. Significant difference is represented by p<0.05, (*) indicates the significant difference compared to control, $ is significantly different compared to CF Pattern 1, # is significantly different compared to CF Pattern 2. Graphs* ***(A)****,* ***(B)****,* ***(C)****,* ***(D)*** *and* ***(E)****: Control n = 10 blocks, and CF pancreata n = 46 blocks (Pattern 1 n = 19 blocks, Pattern 2 n = 14 blocks and Pattern 3 n = 13 blocks). For Graph* ***(F)*** *control n=10 blocks, and CF pancreata n = 26 blocks (Pattern 1 n = 8 blocks, Pattern 2 n = 8 blocks and Pattern 3 n = 10 blocks).*

For six CF cases (Case number: 2, 9, 22, 27, 28 and 29) obtained from Professor. Günter Klöppel, multiple blocks per donor (2-7 blocks) were available and different pathological patterns were observed in one donor ***(Table 2.2)***. A summary of the semi-quantitative scores in the donors with more than one block was compiled ***(Figure 3.12)***. Donor cases are presented according to increasing age, whereby CF Case 2 was a premature donor and Case 29 was a 27-year-old CF donor. Semi-quantitative scores of ductal lumen dilation, ductal loss and exocrine pancreas fibrosis varied between the blocks of most of the donors, illustrating how these parameters varied according to overall Pathological Pattern. Acinar atrophy, islet remodelling,

and inflammation illustrated minimal variation between blocks in any individual donor ***(Figure 3.12)***.

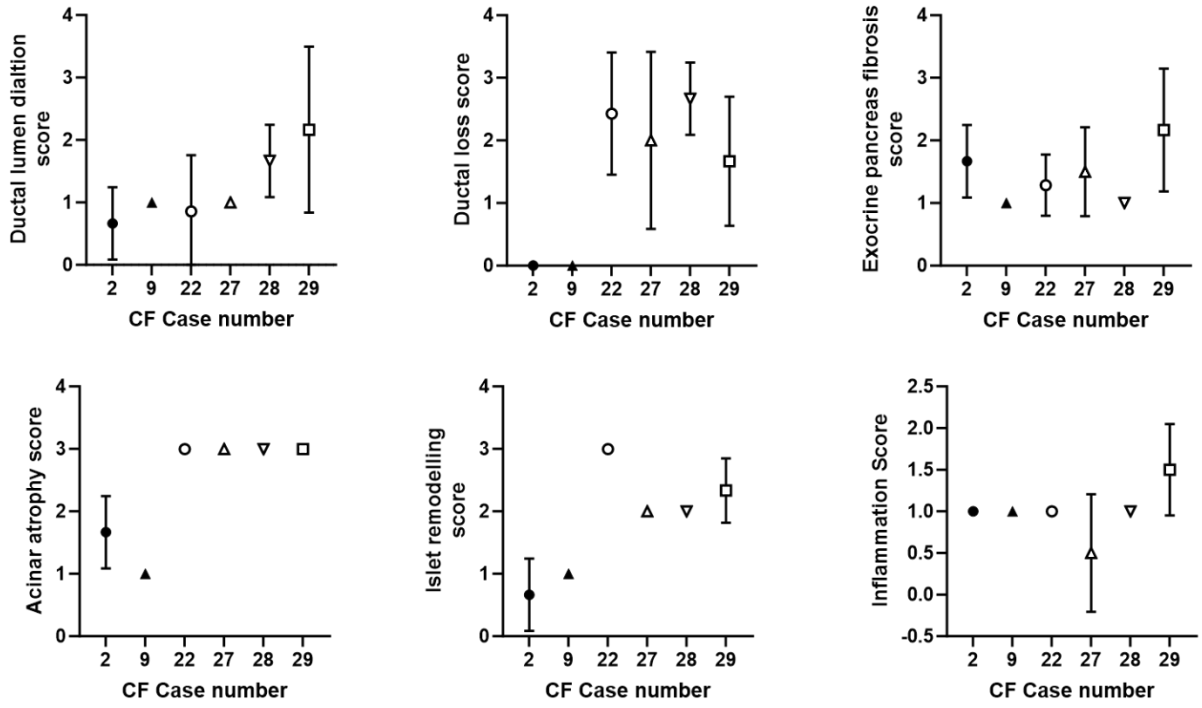

Figure 3.12: Average semi-quantification scoring for CF donors of multiple blocks to show the heterogeneity of changes within the tissue.

Graphs show the mean±SD. Case 2: 3 blocks (CF Pattern 1); Case 9: 2 blocks (CF Pattern 1); Case 22: 7 blocks (2 blocks CF Pattern 2 and 5 block CF Pattern 3); Case 27: 2 blocks (CF Pattern 2); Case 28: 3 blocks (CF Pattern 3); Case 29: 6 blocks (4 blocks CF Pattern 2 and 2 blocks CF Pattern 3).

3.3.3 AI HALO analysis confirms pathological changes as CF progresses

In collaborations with Professor Sarah Richardson and her team at the University of Exeter, UK, AI quantification was validated and performed using HALO V3.0 image analysis software (Indica Labs, Albuquerque, USA) on H&E, SRFG and IHC stained tissue as described previously in Chapter 2 (**2.1.3**). Analyses were carried out based on:

1) Donor quantification values and for donors with multiple blocks the average value was calculated and used.
2) Block quantification values grouped by Pathological Pattern.

3.3.3.1 Exocrine pancreata- AI HALO image assessment

Using H&E-stained tissue sections from 58 control and 25 CF pancreata (unless stated otherwise), AI quantification was used to calculate the proportion of acinar area, endocrine area, collagen area and fat area within the tissue section (Chapter 2 ***Figure 2.1***). Each individual area was calculated by dividing its measured value (mm^2) within a section by the total tissue area (mm^2) then multiplying by 100 to provide percentage proportion.

3.3.3.1.1 Significant decrease in proportion of acinar area in CF pancreata

Acinar area [%] of both control and CF pancreata of young donors < 1 year of age was in the range of 50-70%. As age increased, acinar area [%] of most control pancreata showed a steady increase up to 80-90% of total tissue area. In contrast, the proportion of acinar area of CF pancreata (age 2–4-years-old) illustrated a gradual decrease to around 20% and this reduction in acinar area continued to be close to 0% by the age of 12 years ***(Figure 3.13 A)***.

Following statistical comparison using an unpaired t-test, the proportion of acinar area in CF pancreata was significantly reduced compared to control ($p < 0.001$) ***(Figure 3.13 B)***. A mixed linear model analysis based on pancreatic morphological patterns demonstrated that acinar area [%] of CF Patterns 1, 2 and 3 were significantly lower than control ($p < 0.001$). Also, CF Patterns 2 and 3 had significantly lower percentage acinar area compared with CF Pattern 1 ($p < 0.001$) ***(Figure 3.13 C)***.

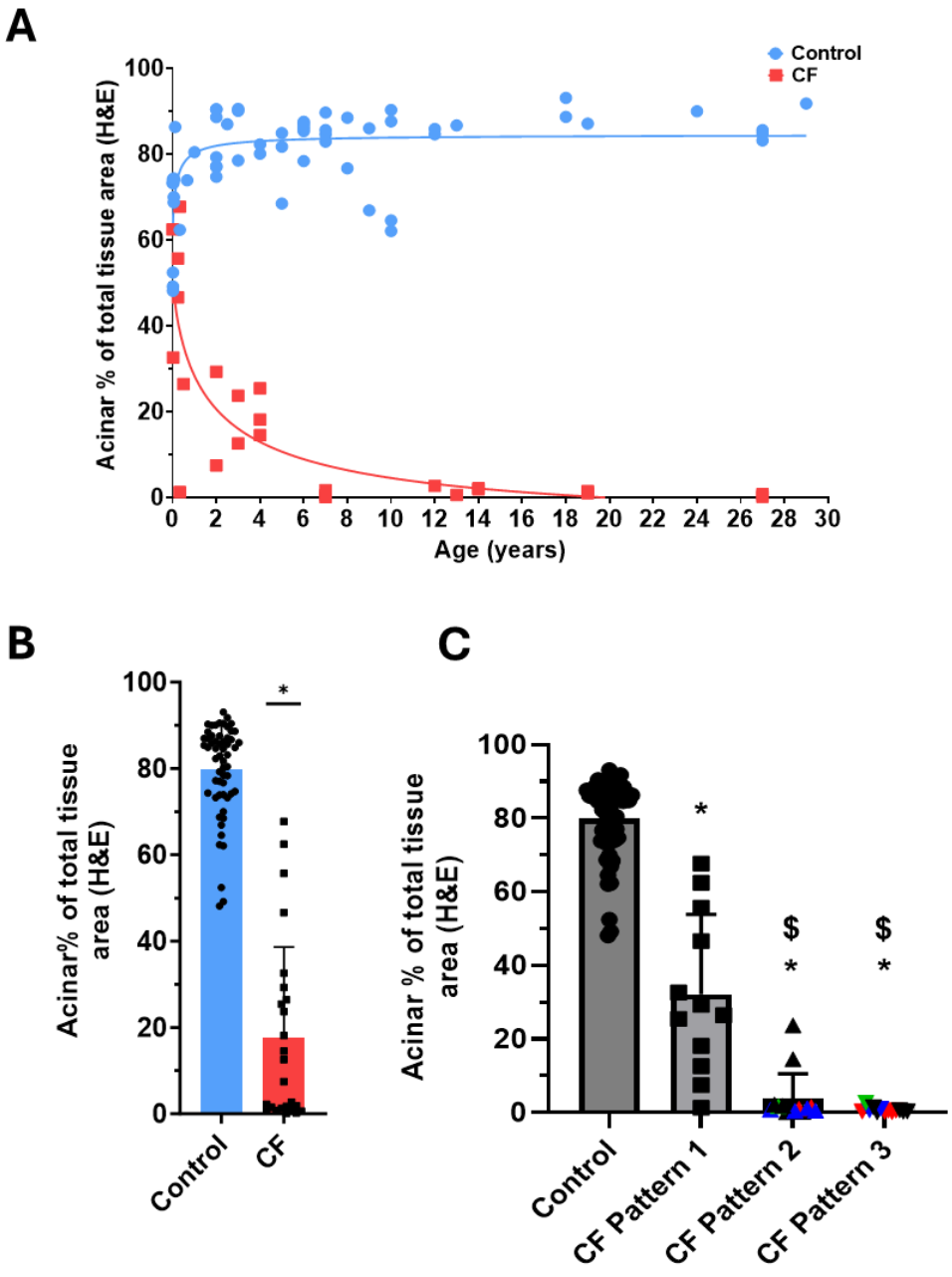

Figure 3.13: Acinar area [%] of total tissue area (mm^2) quantification on H&E-stained control and CF pancreata.

Donor-based analysis vs age presented by nonlinear regression analysis, control n = 58 donors and CF n = 25 donors. ***(B)*** *Donor-based analysis of control vs CF using Unpaired Student's t statistical test control n = 58 donors and CF n = 25).* ***(C)*** *Block-based analysis of control vs CF pattern 1, 2 and 3, control n = 58 and CF n = 39 blocks (Pattern 1 n = 12; Pattern 2 n = 14; Pattern 3 n = 13 blocks). Linear mixed effect model (LMEM) was used with Pancreatic Pattern set as fixed effect, donor as random effect and Bonferroni post hoc test was utilised for statistical analysis. Graphs show the mean±SD. Significant difference is represented by p < 0.001, (*) indicates the significant difference compared to control, ($) is significantly different compared to CF Pattern 1.* ***(C)*** *Red colour represents Case 22 and blue colour represents Case 29, both donors have multiple blocks of different patterns. Green colour represents CF Cases 21 and 24 with diagnosed CFRD.*

3.3.3.1.2 Significant increase in proportion of collagen area in CF pancreata (Patterns 1 and 2)

Collagen proportional area was at its highest (20-60%) in young CF pancreata (0–4 years-old) and this proportion tended to decrease as donor age increased ***(Figure 3.14 A)***. Collagen area [%] of control pancreata (6–29-year-old) was less than 10% ***(Figure 3.14 A)***. Unpaired t-test confirmed a significant increase in collagen proportion in CF pancreata compared to control approximately 45% greater ($p < 0.0001$) ***(Figure 3.14 B)***. *Collagen* area [%] of total area was significantly higher in CF Pattern 1 and 2 compared to control ($p < 0.001$) ***(Figure 3.14 C)***. Collagen area [%] in CF Pattern 3 was not significantly higher compared to control but significantly lower compared to CF Patterns 1 and 2 ($p < 0.001$) ***(Figure 3.14 C)***. Collagen area [%] data of EADB control donors was not available.

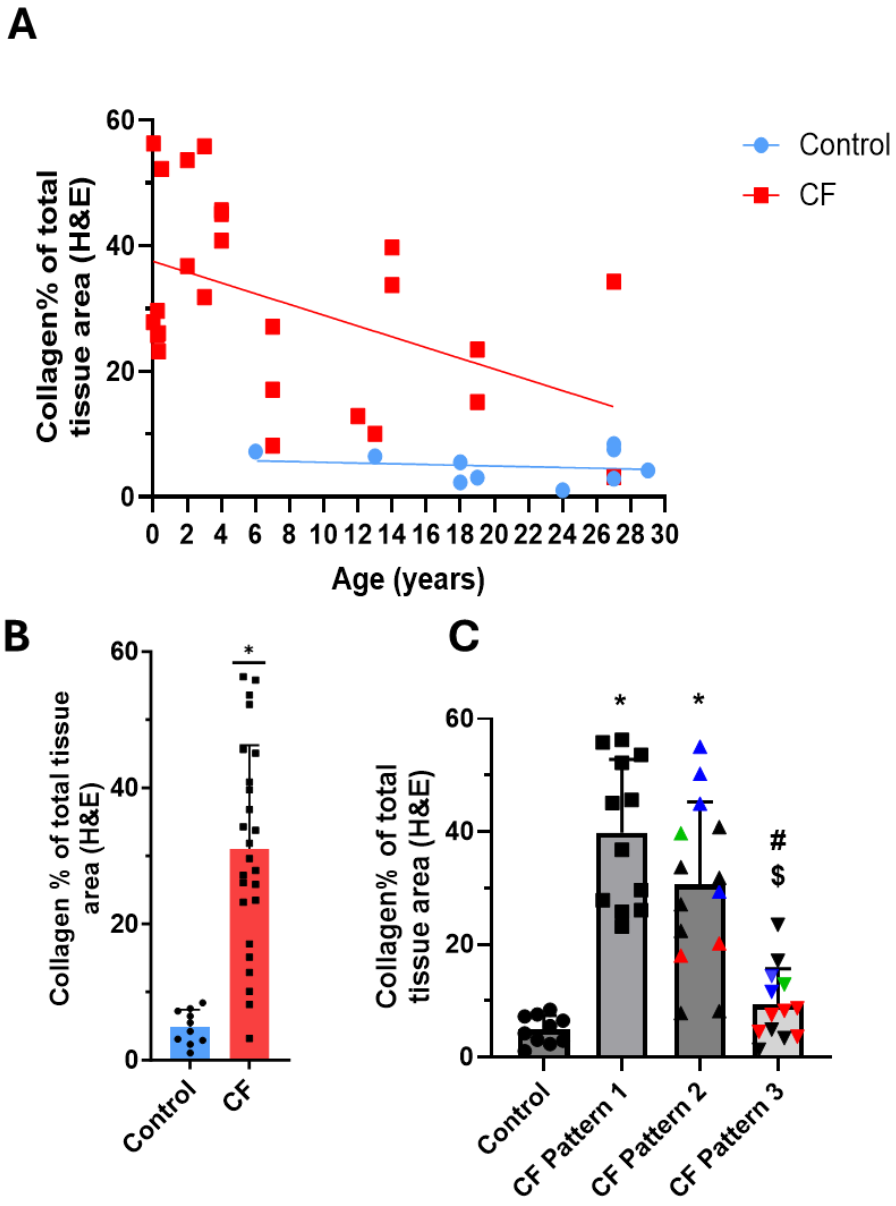

Figure 3.14: Collagen area [%] of total tissue area (mm^2) quantification on H&E-stained control and CF pancreata.

(A) *Donor-based analysis vs age presented by simple linear regression analysis, control n = 10 donors and CF n = 25 donors.* ***(B)*** *Donor-based analysis of control vs CF using Unpaired Student's t statistical test (control n = 10 donors and CF n = 25 donors).* ***(C)*** *Block-based analysis of control vs CF pattern 1, 2 and 3. Control n = 10 and CF n = 39 blocks (Pattern 1 n = 12; Pattern 2 n = 14; Pattern 3 n = 13 blocks). Linear mixed effect model (LMEM) was used with pancreata pattern set as fixed effect, donor as random effect and Bonferroni post hoc test was utilised for statistical analysis. Graphs show the mean±SD. Significant difference is represented by p < 0.05, (*) indicates the significant difference compared to control, ($) is significantly different compared to CF Pattern 1, # is significantly different compared to CF Pattern 2.* ***(C)*** *Red colour represents Case 22 and blue colour represents Case 29, both donors have multiple blocks of different patterns. Green colour represents CF Cases 21 and 24 with diagnosed CFRD.*

3.3.3.1.3 Significant increase in proportion of fat area in CF pancreata

In CF, adipocyte area [%] positively correlated with age whereby it increased as age increased. In young donors of 0-1 years old percentage of fat area was around 10% and this had incresaed to at least 85% at 27-year-old ***(Figure 3.15)***. In all control pancreata (0–29-years-old), percentage fat area was less than 10% ***(Figure 3.15 A)***. Unpaired t-test illustrated a significant increase ($p < 0.0001$) in fat area (% of total tissue area) in CF pancreata when compared to controls ***(Figure 3.15 B)***. Fat area [%] in the three CF Patterns was significantly higher compared to control ($p = 0.010$, $p < 0.001$ and $p < 0.001$, respectively) ***(Figure 3.15 C)***. Fat area [%] in CF Pattern 2 and 3 were significantly higher compared to CF Pattern 1 ($p < 0.001$) and CF Pattern 3 was also significantly higher compared to CF Pattern 2 ($p < 0.001$) ***(Figure 3.15 C)***.

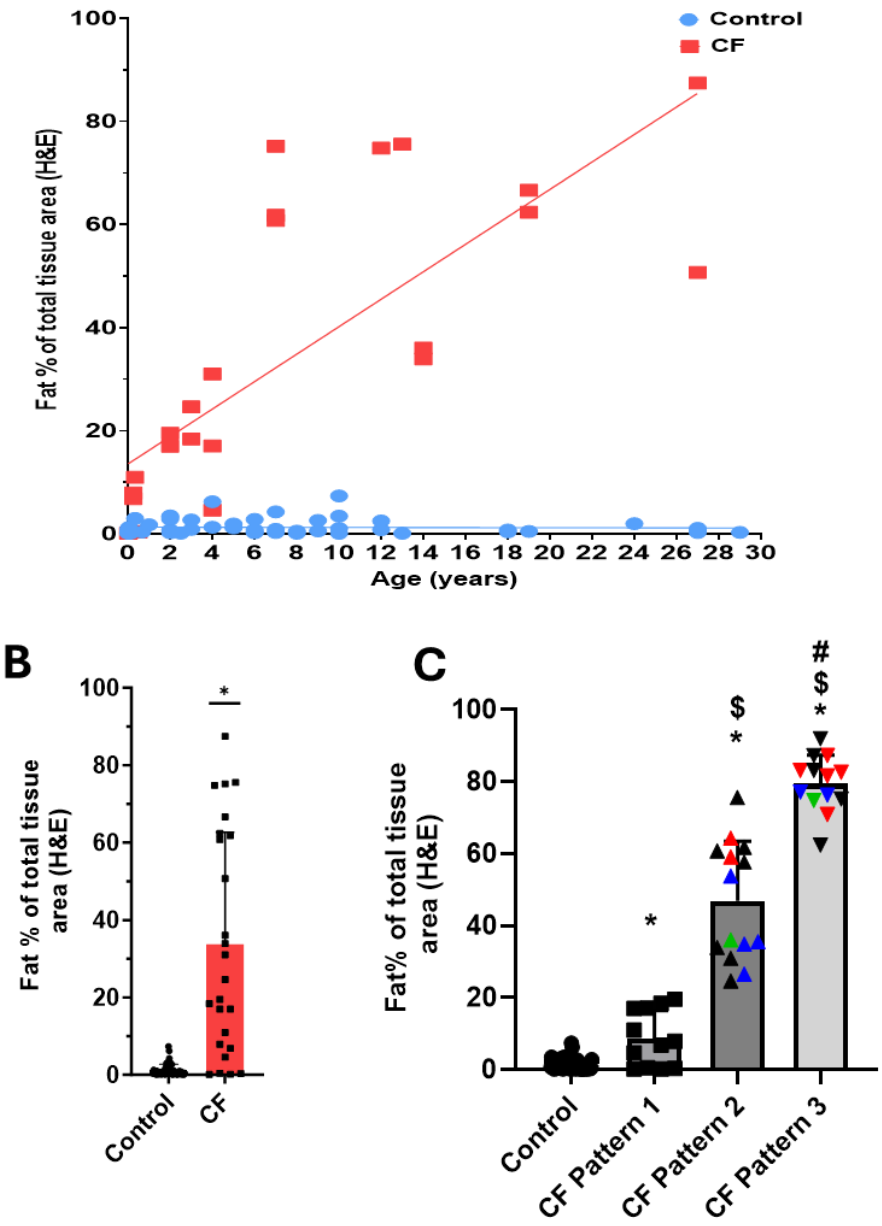

Figure 3.15: Fat area [%] of total tissue area (mm^2) quantification on H&E-stained control and CF pancreata.

(A) *Donor-based analysis vs age presented by simple linear regression analysis,* *control n = 58 donors and CF n = 25 donors.* ***(B)*** *Donor-based analysis of control vs CF (control n = 58 donors and CF n = 25). Unpaired Student's t statistical test was used.* ***(C)*** *Block-based analysis of control vs CF pattern 1, 2 and 3. Control n = 58 and CF n = 39 blocks (Pattern 1 n = 12; Pattern 2 n = 14; Pattern 3 n = 13blocks). Linear mixed effect model (LMEM) was used with pancreata pattern set as fixed effect, donor as random effect and Bonferroni post hoc test was utilised for statistical analysis. Graphs show the mean±SD. Significant difference is represented by p < 0.05, (*) indicates the significant difference compared to control, ($) is significantly different compared to CF Pattern 1, # is significantly different compared to CF Pattern 2.* ***(C)*** *Red colour represents Case 22 and blue colour represents Case 29, both donors have multiple blocks of different patterns. Green colour represents CF Cases 21 and 24 with diagnosed CFRD.*

3.3.3.2 Endocrine compartment- AI HALO image assessment

Using H&E-stained control and CF pancreata, islets with an area greater than 1000 μm^2 were quantified (as described in Chapter 2 **2.1.3**) and the following parameters were quantified: endocrine area [%], islet density (islet number/mm^2), median islet circularity, islet diameter (µm) and median islet area/size (μm^2). For individual endocrine cell phenotype AI quantification, IHC-stained slides were used to quantify the proportion of hormone positive cells with the islets. The variability between the number of donors and blocks used for the statistical analyses was due to AI difficulties in respect to morphological changes and accurately locating islets within young donor CF tissue.

3.3.3.2.1 Reduction in proportion of endocrine area with age

Percentage of endocrine area of 58 control and 25 CF pancreata was calculated by dividing the measured endocrine area (mm^2) within a section by the total tissue area. Interestingly, proportion of endocrine area decreased with age in both control and CF tissue ***(Figure 3.16 A)***. Proportion of endocrine area in CF was not significantly different to control ***(Figure 3.16 B)***. There was no significant difference in proportion of endocrine between control and CF Pattern 1, 2 and 3 and among CF Patterns ***(Figure 3.16 C)***.

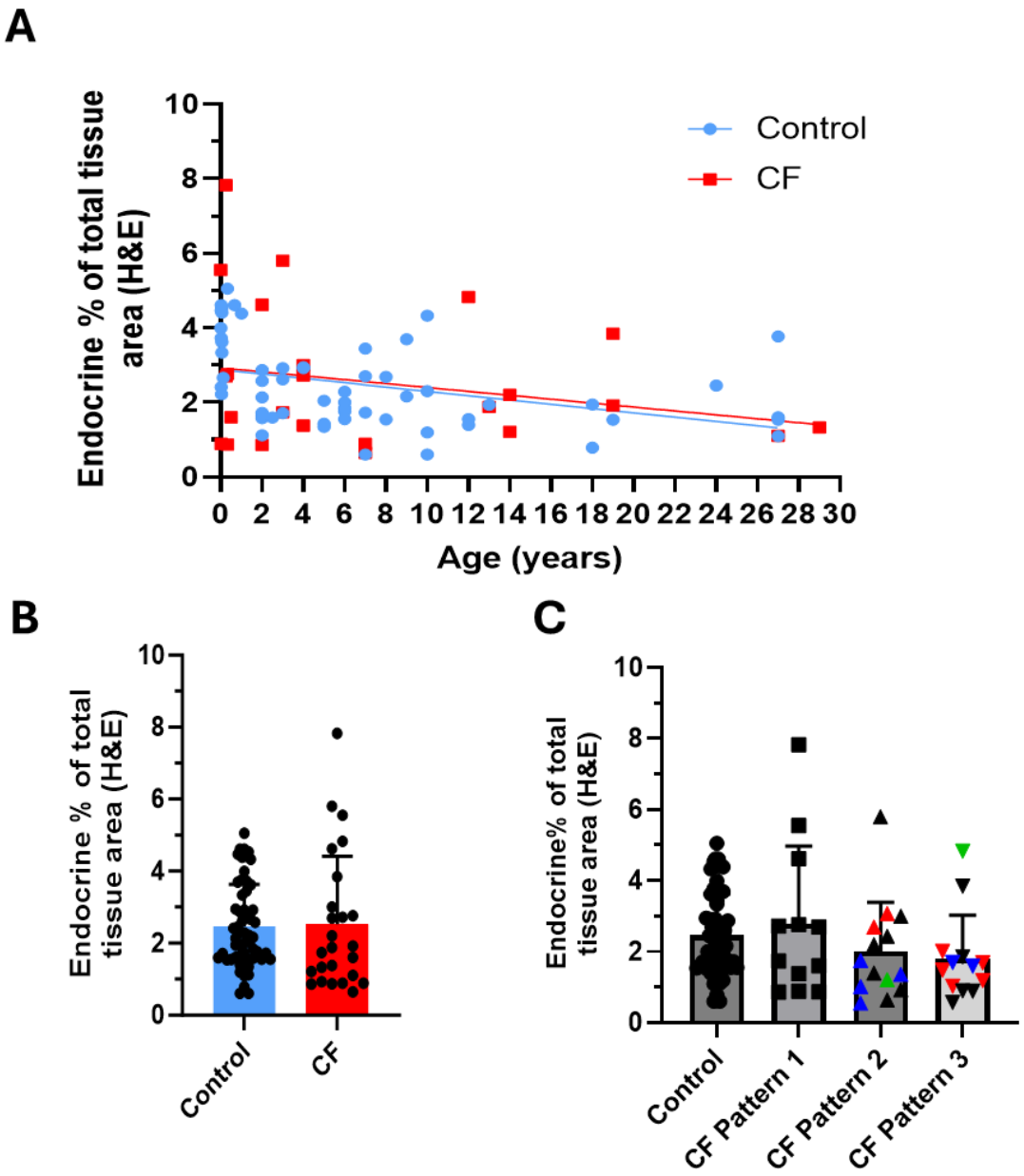

Figure 3.16: Endocrine area [%] of total tissue area (mm^2) quantification on H&E-stained control and CF pancreata.

(A) *Donor-based analysis vs age presented by simple linear regression analysis control n = 58 donors and CF n = 25 donors.* ***(B)*** *Donor-based analysis of control vs CF using Unpaired Student's t statistical test (control n = 58 donors and CF n = 25 donors).* ***(C)*** *Block-based analysis of control vs CF pattern 1, 2 and 3. Control n = 58 and CF n = 39 blocks (Pattern 1 n = 12; Pattern 2 n = 14; Pattern 3 n = 13 blocks). Linear mixed effect model (LMEM) was used with pancreata pattern set as fixed effect, donor as random effect and Bonferroni post hoc test was utilised for statistical analysis. Graphs show the mean±SD. Significant difference is represented by p < 0.05, (*) indicates the significant difference compared to control, ($) is significantly different compared to CF Pattern 1, # is significantly different compared to CF Pattern 2.* ***(C)*** *Red colour represents Case 22 and blue colour represents Case 29, both donors have multiple blocks of different patterns. Green colour represents CF Cases 21 and 24 with diagnosed CFRD.*

3.3.3.2.2 Significant decrease in islet density in CF Pattern 2 and Pattern 3 compared to CF Pattern 1

Using H&E-stained pancreatic tissue of 58 control and 24 CF donors, islet density represented by islet number/mm^2 decreased as age increased from 3-15 islets /mm^2 at the age of 0-year-old to 1 islet/mm^2 at 27-year-old (CF) and 29-years-old (control) ***(Figure 3.17 A)***. Donor-based analysis illustrated no significant change between control and CF islet density ***(Figure 3.17 B)***. However, block-based analysis illustrated a significant decrease in islet density in CF Pattern 2 and 3 compared to CF Pattern 1 ($p = 0.006$ and $p = 0.002$, respectively) ***(Figure 3.17 C)***.

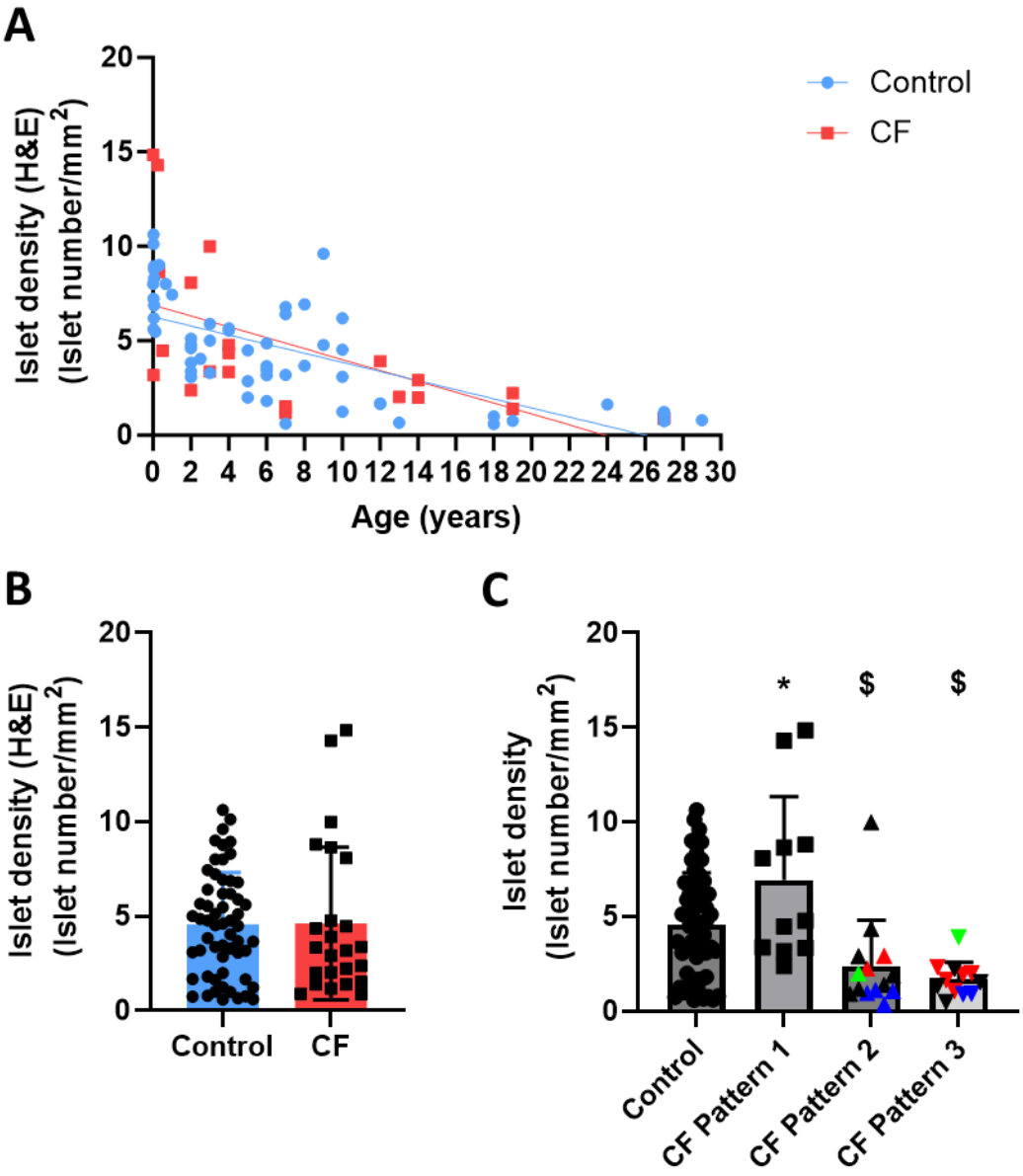

Figure 3.17: Islet density (islet number/mm^2) quantification on H&E-stained control and CF pancreata.

(A) *Donor-based analysis vs age presented by simple linear regression analysis, control n = 58 donors and CF n = 24 donors.* ***(B)*** *Donor-based analysis of control vs CF using Unpaired Student's t statistical test (control n = 10 donors and CF n = 24 donors).* ***(C)*** *Block-based analysis of control vs CF pattern 1, 2 and 3. Control n = 58 and CF n = 37 blocks (Pattern 1 n = 11; Pattern 2 n = 14; Pattern 3 n = 12 blocks). Linear mixed effect model (LMEM) was used with pancreata pattern set as fixed effect, donor as random effect and Bonferroni post hoc test was utilised for statistical analysis. Graphs show the mean±SD. Significant difference is represented by $p < 0.05$, (*) indicates the significant difference compared to control and ($) is significantly different compared to CF Pattern 1.* ***(C)*** *Red colour represents Case 22 and blue colour represents Case 29, both donors have multiple blocks of different patterns. Green colour represents CF Cases 21 and 24 with diagnosed CFRD.*

3.3.3.2.3 Significant reduction in median islet circularity in CF pancreata

Using H&E-stained pancreatic tissue of 58 control and 24 CF donors, islet circularity was calculated based on a previously published method (Seiron et al., 2019). Then, the median of all quantified islet circularity assessments within a single section was calculated and used for analysis. There was a possible trend towards increasing islet circularity with age ***(Figure 3.18 A)***. Donor-based analysis demonstrated a significant reduction in median islet circularity of CF donors compared to control ($p = 0.0221$) ***(Figure 3.18 B)***. Block-based analysis, however, did not show significant reduction in circularity compared with controls ***(Figure 3.18 C)***.

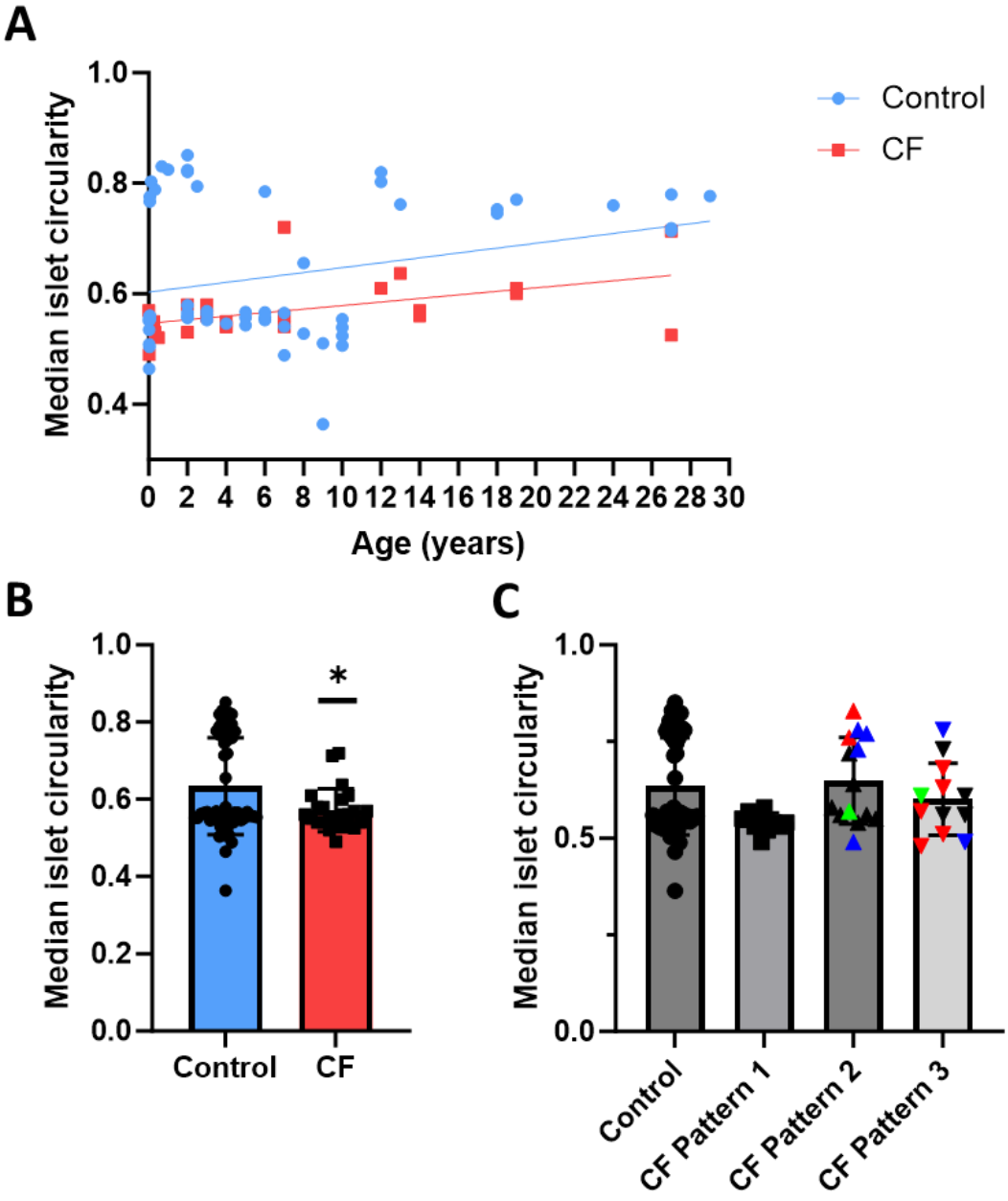

Figure 3.18: Median islet circularity quantification on H&E-stained control and CF pancreata.

Donor-based analysis vs age presented by simple linear regression analysis, control n = 58 donors and CF n = 25 donors. ***(B)*** *Donor-based analysis of control vs CF, using Unpaired Student's t statistical test (control n = 58 donors and CF n = 24 donors).* ***(C)*** *Block-based analysis of control vs CF pattern 1, 2 and 3. Control n = 58 and CF n = 37 blocks (Pattern 1 n = 11; Pattern 2 n = 14; Pattern 3 n = 12 blocks). Linear mixed effect model (LMEM) was used with pancreata pattern set as fixed effect, donor as random effect and Bonferroni post hoc test was utilised for statistical analysis. Graphs show the mean±SD. Significant difference is represented by p < 0.05, (*) indicates the significant difference compared to control.* ***(C)*** *Red colour represents Case 22 and blue colour represents Case 29, both donors have multiple blocks of different patterns. Green colour represents CF Cases 21 and 24 with diagnosed CFRD.*

3.3.3.2.4 Significant increase in islet diameter (µm) in CF Pattern 2 and 3

Using H&E-stained pancreatic tissue of 58 control and 24 CF donors, islet diameter was quantified for all islets within the tissue, then the median was calculated and used for analysis. Median islet diameter (µm) for both control and CF donors started at around 20–100 µm and increased up to 125–135 µm as age increased ***(Figure 3.19 A)***. Donor-based analysis illustrated no significant change in between control and CF islet diameter (µm) ***(Figure 3.19 B)***. Block-based analysis illustrated no significant change in islet diameter of CF Pattern 1 compared to control, but islet diameter (µm) increased significantly in of CF Patterns 2 and 3 compared to control ($p = 0.028$ and $p < 0.001$, respectively) and CF Pattern 1 ($p = 0.002$ and $p < 0.001$, respectively) ***(Figure 3.19 C)***.

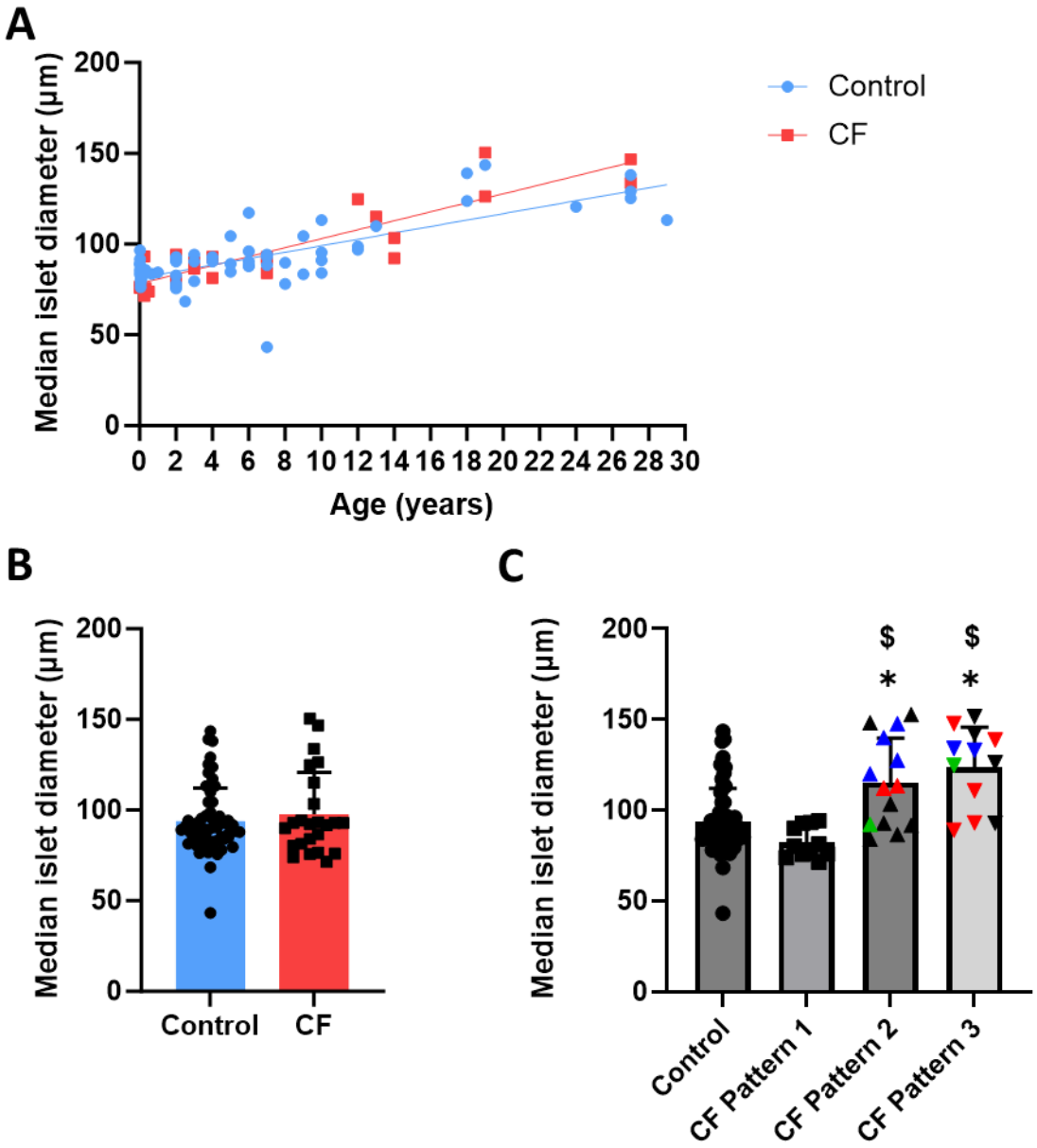

Figure 3.19: Median islet diameter (µm) quantification on H&E-stained control and CF pancreata.

(A) *Donor-based analysis vs age presented by simple linear regression analysis, control n = 58 donors and CF n = 24 donors.* ***(B)*** *Donor-based analysis of control vs CF, using Unpaired Student's t statistical test (control n = 58 donors and CF n = 24 donors).* ***(C)*** *Block-based analysis of control vs CF pattern 1, 2 and 3. Control n = 10 and CF n=37 blocks (Pattern 1 n = 11; Pattern 2 n = 14; Pattern 3 n = 12 blocks). Linear mixed effect model (LMEM) was used with pancreata pattern set as fixed effect, donor as random effect and Bonferroni post hoc test was utilised for statistical analysis. Graphs show the mean±SD. Significant difference is represented by p < 0.05, (*) indicates the significant difference compared to control and ($) indicates the significant difference compared to CF Pattern 1.* ***(C)*** *Red colour represents Case 22 and blue colour represents Case 29, both donors have multiple blocks of different patterns. Green colour represents CF Cases 21 and 24 with diagnosed CFRD.*

3.3.3.2.5 Increase in median islet area (µm^2) with age

Using H&E-stained pancreatic tissue of 58 control and 24 CF donors, islet area was quantified and data was plotted. Islet area for both control and CF donors increased as age increased ***(Figure 3.20 A)***. Donor-based analysis illustrated no significant change between control and CF islet diameter (µm^2) ***(Figure 3.20 B)***. Block-based analysis illustrated a significant increase in islet area of CF Pattern 3 compared to control ($p = 0.018$), with a significant increase in islet area in CF Patterns 2 and 3 compared to CF Pattern 1 ($p = 0.008$ and $p < 0.001$, respectively) ***(Figure 3.20 C)***.

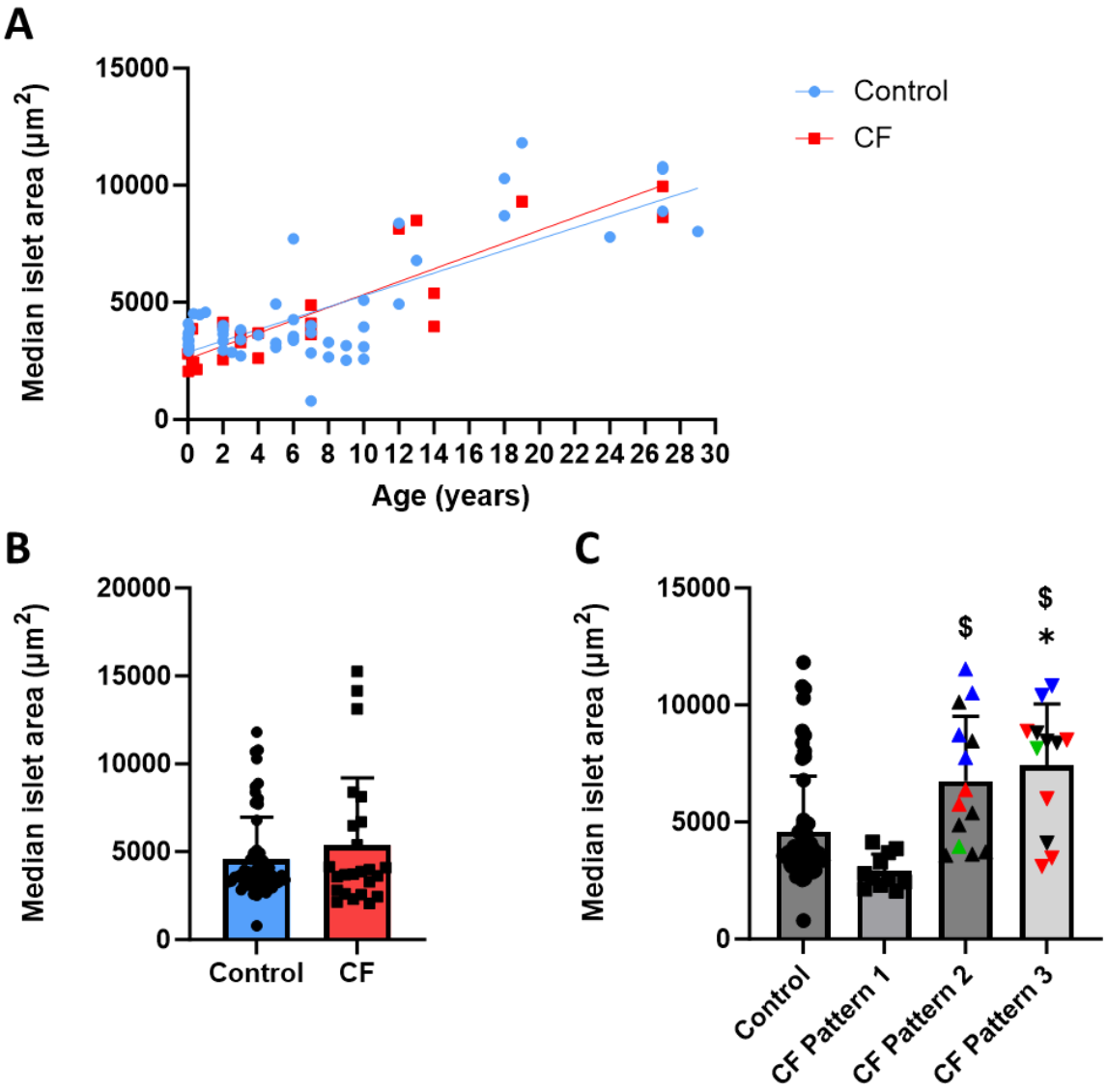

Figure 3.20: Median islet area (µm²) quantification on H&E-stained control and CF pancreata.

Donor-based analysis vs age presented by simple linear regression, control n = 58 donors and CF n = 24 donors. ***(B)*** *Donor-based analysis of control vs CF, using Unpaired Student's t statistical test (control n = 58 donors and CF n = 24 donors).* ***C)*** *Block-based analysis of control vs CF pattern 1, 2 and 3. Control n = 58 and CF n = 37 blocks (Pattern 1 n = 11; Pattern 2 n = 14; Pattern 3 n = 12 blocks). Linear mixed effect model (LMEM) was used with pancreata pattern set as fixed effect, donor as random effect and Bonferroni post hoc test was utilised for statistical analysis. Graphs show the mean±SD. Significant difference is represented by p < 0.05, (*) indicates the significant difference compared to control and ($) indicates the significant difference compared to CF Pattern 1.* ***(C)*** *Red colour represents Case 22 and blue colour represents Case 29, both donors have multiple blocks of different patterns. Green colour represents CF Cases 21 and 24 with diagnosed CFRD.*

3.3.3.2.6 Decreased endocrine microvascular in CF pancreata

Islet vascularisation was assessed via IHC staining for the endothelial marker CD31 as illustrated in Chapter 2 ***Figure 2.3***. With respect to age, endocrine CD31$^+$ area (mm^2) in 10 control donors appeared to decrease with age (6-29-years-old), whereas in eight CF donors endocrine CD31$^+$ area (mm^2) appeared unchanged as age increased (0-27-year-old) ***(Figure 3.21 A)***. Although CF endocrine CD31$^+$ area (mm^2) trended towards being lower than in control donors, donor-based and block-based analyses demonstrated no significant difference compared to control or among CF patterns ***(Figure 3.21 B*** and ***C)***.

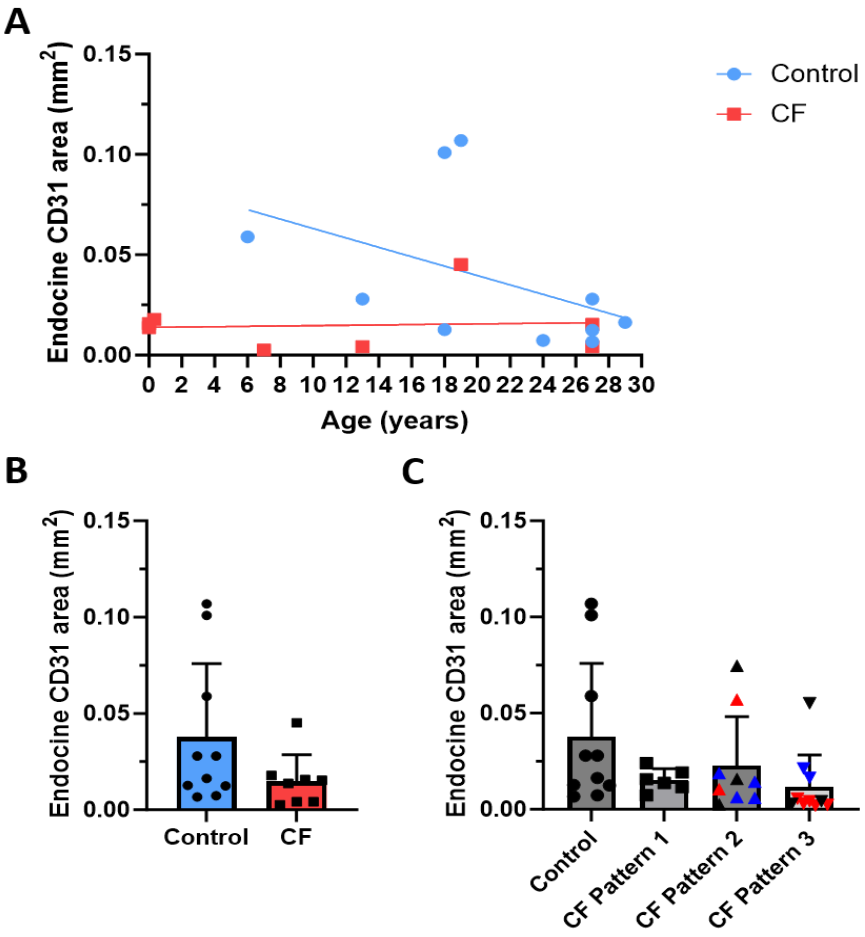

Figure 3.21: Endocrine CD31$^+$ area (mm^2) quantification on CGA&CD31 stained control and CF pancreata.

(A) *Donor-based analysis vs age presented by simple linear regression analysis, control n = 10 donors and CF n = 8 donors.* ***(B)*** *Donor-based analysis of control vs CF, using Unpaired Student's t statistical test (control n = 10 donors and CF n = 8 donors).* ***(C)*** *Block-based analysis of control vs CF pattern 1, 2 and 3. Control n = 10 and CF n = 25 blocks (Pattern 1 n = 6; Pattern 2 n = 9; Pattern 3 n= 10 blocks). Linear mixed effect model (LMEM) was used with pancreata pattern set as fixed effect, donor as random effect and Bonferroni post hoc test was utilised for statistical analysis. Graphs show the mean±SD.* ***(C)*** *Red colour represents Case 22 and blue colour represents Case 29, both donors have multiple blocks of different patterns.*

3.3.3.3 Endocrine hormone expression

3.3.3.3.1 IHC staining

Pancreatic serial sections in 10 control and nine CF donors were co-stained for insulin (INS) and pancreatic polypeptide (PP) (brown and pink respectively) and then glucagon (GCG) and somatostatin (SST) (brown and pink respectively). Representative images from a 27-year-old CF donor with CF Pattern 2 exemplify a proportional decrease in insulin^{+} cells and an increase in glucagon^{+} cells, when compared to a 19-year-old control. Pancreatic polypeptide-expressing cells in both donors appeared to be virtually absent in this example islet. In contrast, there were more somatostatin^{+} endocrine cells compared with the control donor ***(Figure 3.22)***.

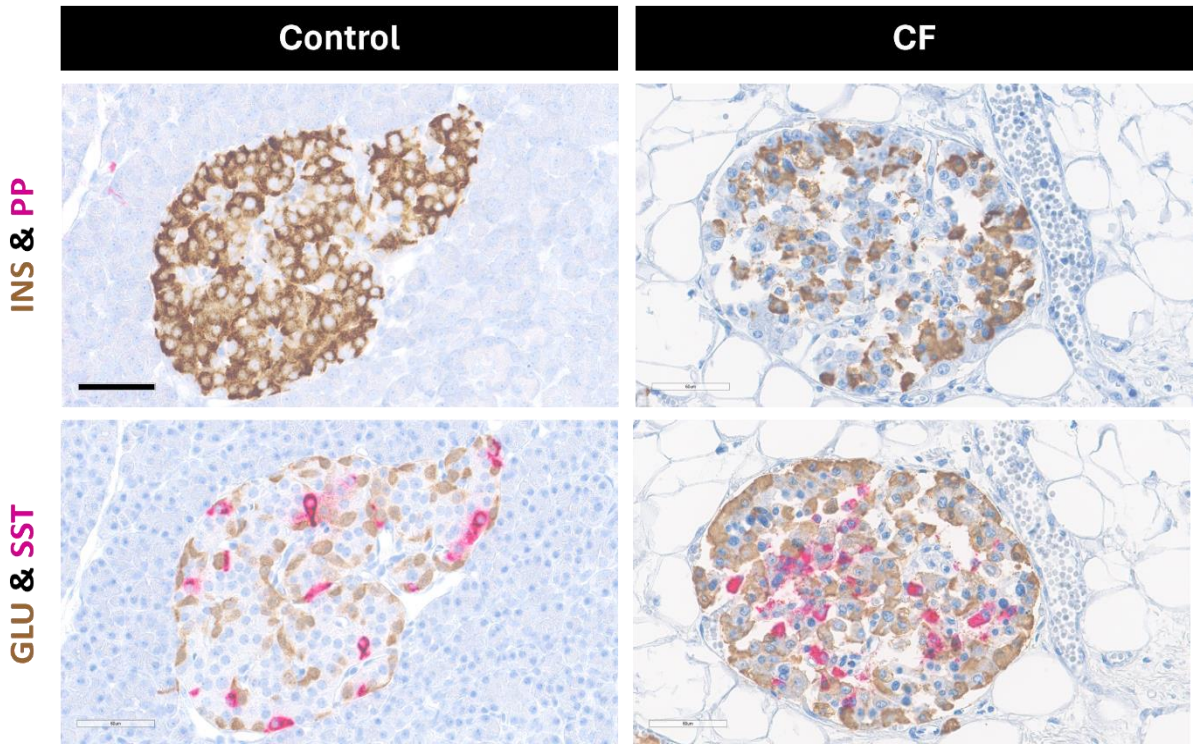

Figure 3.22: IHC co-visualisation of endocrine hormones of a control and CF pancreata.

Control: a 19-year-old control (Case number: 53, left panel) and CF: a 27-year-old CF pancreata Pattern 2 (Case number: 29, right panel). Insulin and polypeptide (INS: brown, PP: pink) top row images, glucagon, and somatostatin (GLU: brown, SS: pink) bottom row images. Staining was carried out in serial tissue section slides. Scale bar represents 60 µm (scale bar in control INS & PP applies to all panels).

3.3.3.3.2 AI quantification

Using AI pipeline created to quantify dual hormonal staining within two serial sections, quantification of proportions of each hormone-expressing cell phenotype was conducted. Analyses were carried out for eight CF donors and 10 control donors. Individual hormone positive staining area was calculated as a percentage of the four hormones' area within the islet. Proportion of insulin^{+} cells was significantly lower in CF (20-70%) compared to ten control (70-90%) ($p < 0.001$) ***(Figure 3.23 A)***. Insulin proportion in CF Patterns 1, 2 and 3 was significantly reduced compared to control donors ($p < 0.001$, $p = 0.0002$ and $p = 0.0142$, respectively) ***(Figure 3.24 A)***. Pancreatic polypeptide [%] appeared lower in CF compared with control donors but there were no significant differences at donor or block level ***(Figure 3.23 B*** and ***Figure 3.24 B)***. Glucagon [%] significantly increased in CF (15-45%) compared to control (5-12%) ($p < 0.0001$) ***(Figure 3.23 C)***. Block-based analysis reported proportion of glucagon in CF Patterns 1, 2 and 3 to be significantly higher compared to control ($p = 0.0152$, $p < 0.0001$ and $p = 0.0032$ respectively) ***(Figure 3.24 C)***. Somatostatin [%] was significantly higher in CF (12-35%) compared to control (1-17%) ($p < 0.0001$) ***(Figure 3.23 D)***. This significant increase was seen in CF Pattern 1 ($p < 0.0001$), whereas CF Patterns 2 and 3 were significantly lower compared to CF Pattern 1 ($p < 0.0001$ and $p = 0.0002$, respectively) ***(Figure 3.24 D)***.

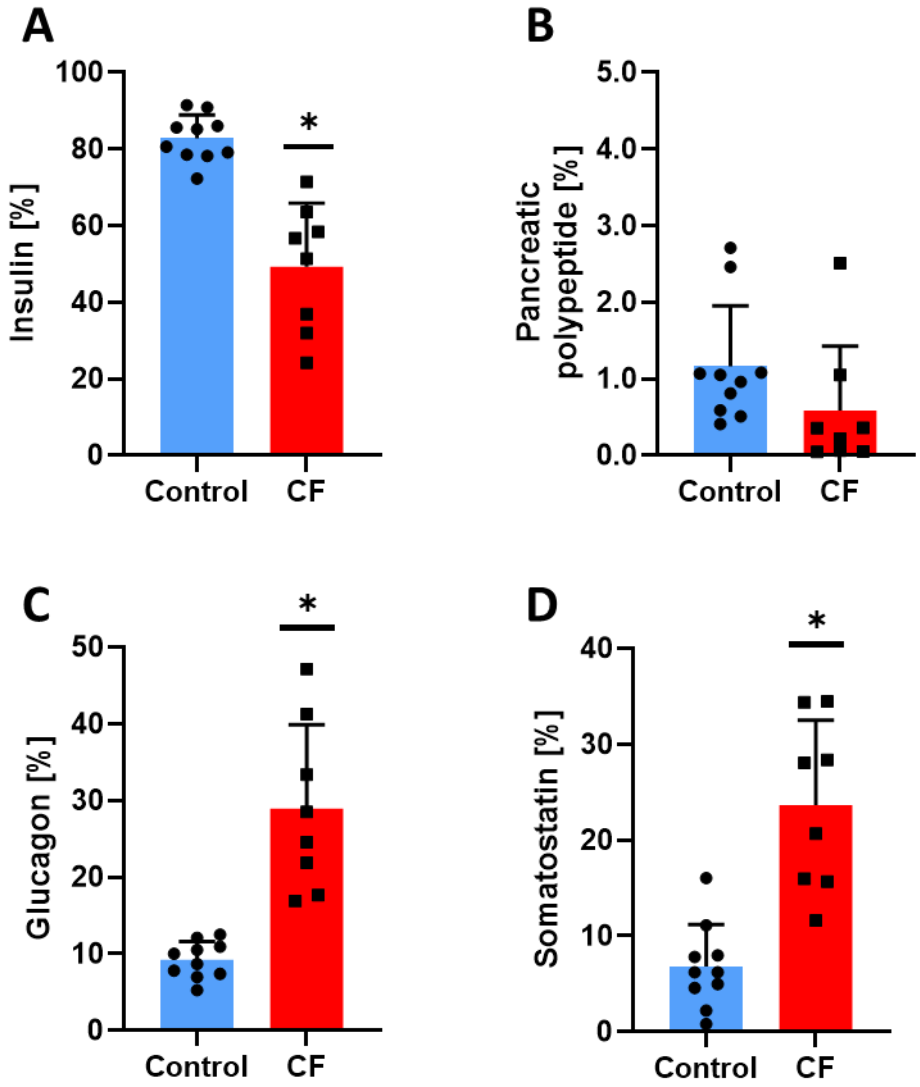

Figure 3.23: Donor-based AI quantification of endocrine hormonal proportion [%] within islets of control and CF pancreata.

(A) *Insulin,* ***(B)*** *pancreatic polypeptide,* ***(C)*** *glucagon and* ***(D)*** *somatostatin proportion [%] area within islets. Control n = 10 donors, CF n = 8 donors. Statistical analyses were carried out using unpaired student's t test. Graphs show the mean±SD. Significant difference is represented by p < 0.05, (*) indicates the significant difference compared to control.*

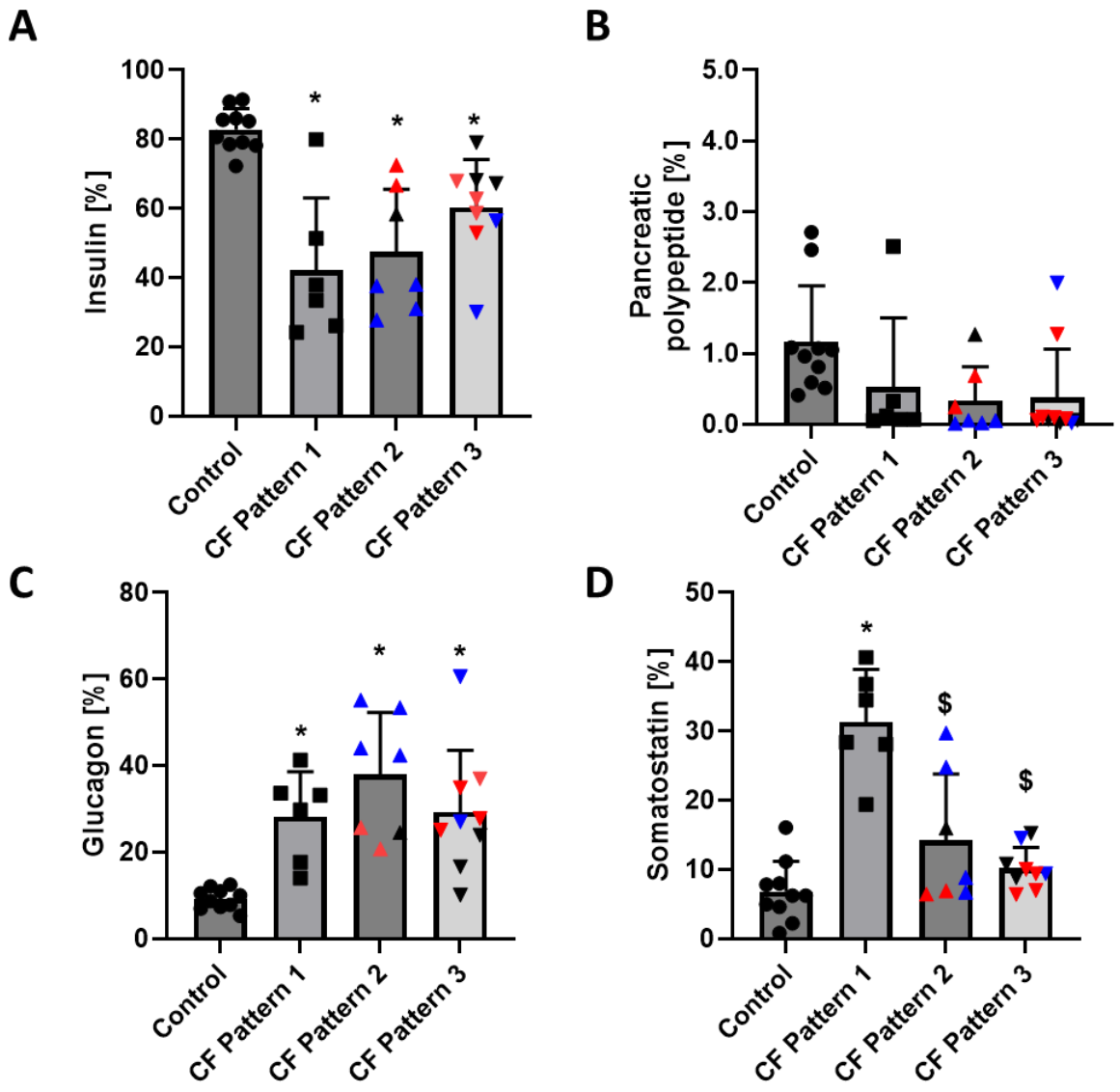

Figure 3.24: Block-based AI quantification of endocrine hormone proportion area within islets of control and CF pancreata.

(A) *Insulin,* ***(B)*** *pancreatic polypeptide,* ***(C)*** *glucagon and* ***(D)*** *somatostatin proportion [%] area within islets. Control n = 10 blocks, CF n = 22 blocks (Pattern 1 n = 6, Pattern 2 n = 7 and Pattern 3 n = 9). Statistical analyses were carried out one-way ANOVA statistical test with Bonferroni post hoc test. Graphs show the mean±SD. Significant difference is represented by p < 0.05, (*) indicates the significant difference compared to control and ($) is significantly different compared to CF Pattern 1. Red colour represents Case 22 and blue colour represents Case 29, both donors have multiple blocks of different patterns.*

3.3.3.4 Peri-ductal fibrosis and α-SMA expression

3.3.3.4.1 IHC staining

Representative IHC staining for α-SMA, SRFG and CD45 in a 6-year-old control donor and a 27-year-old CF donor demonstrated that, in CF, ductal α-SMA was observed in higher prevalence compared to control and this was associated with extensive fibrotic regions and some presence of inflammatory cell clusters (CD45) around the ducts of CF pancreata compared to control ***(Figure 3.25)***. Peri-ductal fibrosis and presence of peri-ductal α-SMA^{+} cells were further confirmed by conducting an IHC staining for macrophage marker CD68, whereby CD68^{+} cells within the peri-ductal fibrotic tissue were observed more frequently compared to leukocytes CD45^{+} cells ***(Figure 3.26 C*** and ***D)***.

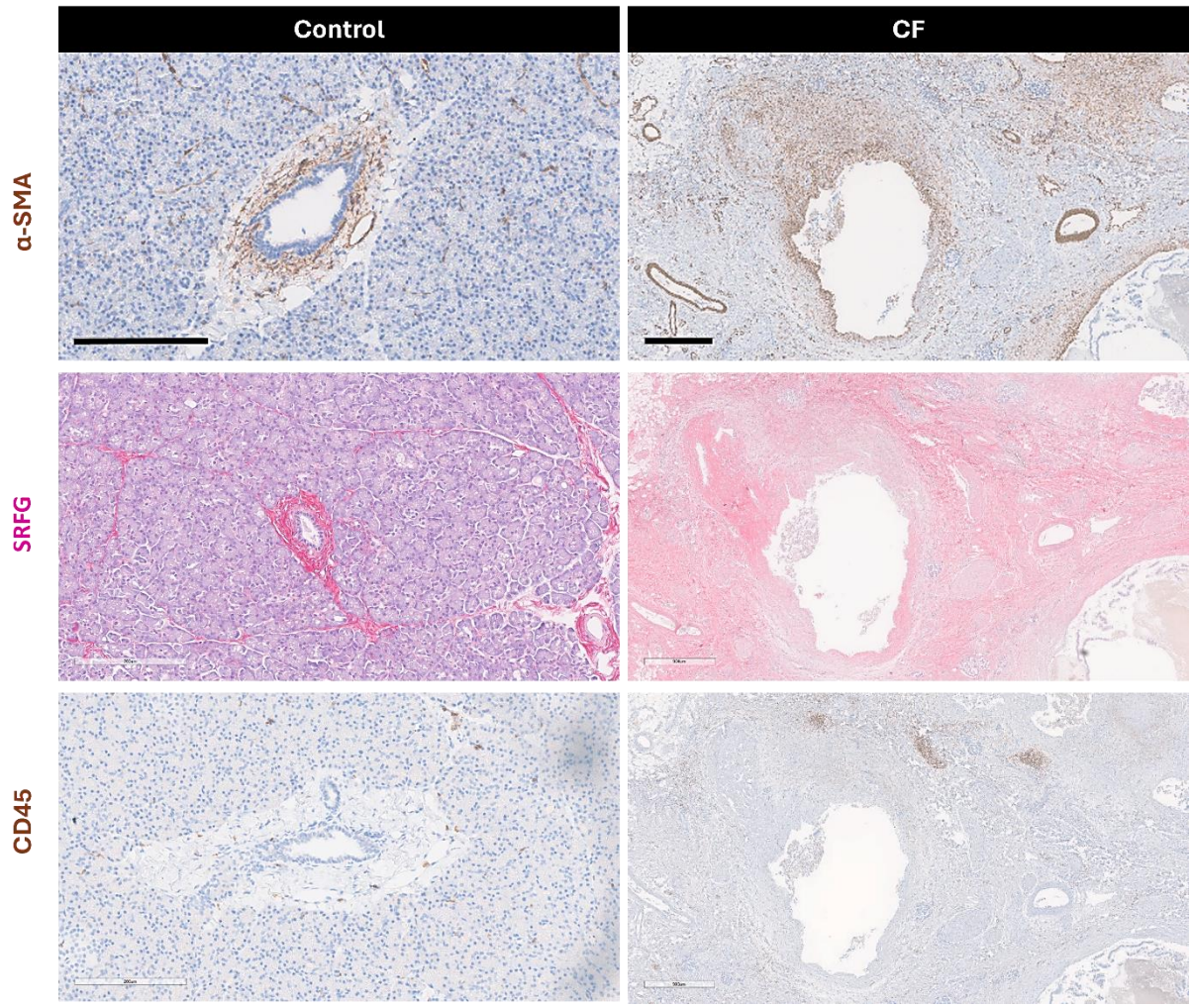

Figure 3.25: Representative illustration of pancreatic ductal environment using SRFG staining and IHC staining for α-SMA and CD45 of control and CF pancreata.

Control (a 6-year-old donor) and CF (a 27-year-old donor with CF pattern 2, case 29). IHC staining for CF was carried out on close serial section slides, but this was not the case for the control donor. Scale bars: 200 µm (control) and 900 µm (CF).

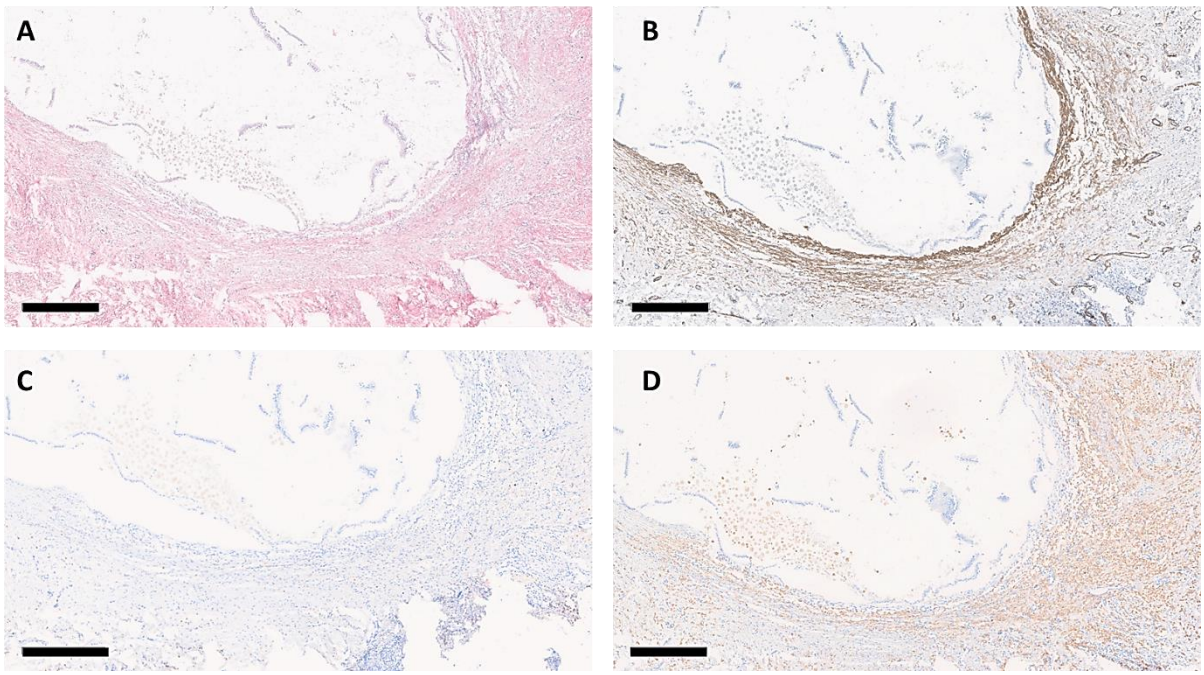

Figure 3.26: Representative illustration of pancreatic ductal environment in CF pancreata.

(A) *SRFG staining. IHC staining for α-SMA* ***(B)****, CD45* ***(C)*** *and CD68* ***(D)*** *of a CF (a 27-year-old donor with CF pattern 2, Case number: 29). IHC staining for CF sections was carried out on close or serial section slides. Scale bars: 500 µm.*

3.3.3.4.2 AI quantification

AI quantitative analysis illustrated that measured ductal α-SMA area (mm^2) increased slightly as age increased in both CF (nine donors) and control (10 donors) pancreata ***(Figure 3.27 A)***. Donor-based analysis illustrated an increase in CF ductal a-SMA vs control, yet this increase was not significant ***(Figure 3.27 B)***. CF Pattern 1 ductal α -SMA area appeared similar to those of control, whereas in CF Pattern 2 and 3 it appeared to have some blocks with higher ductal α-SMA area compared to most control blocks ***(Figure 3.27 C)***.

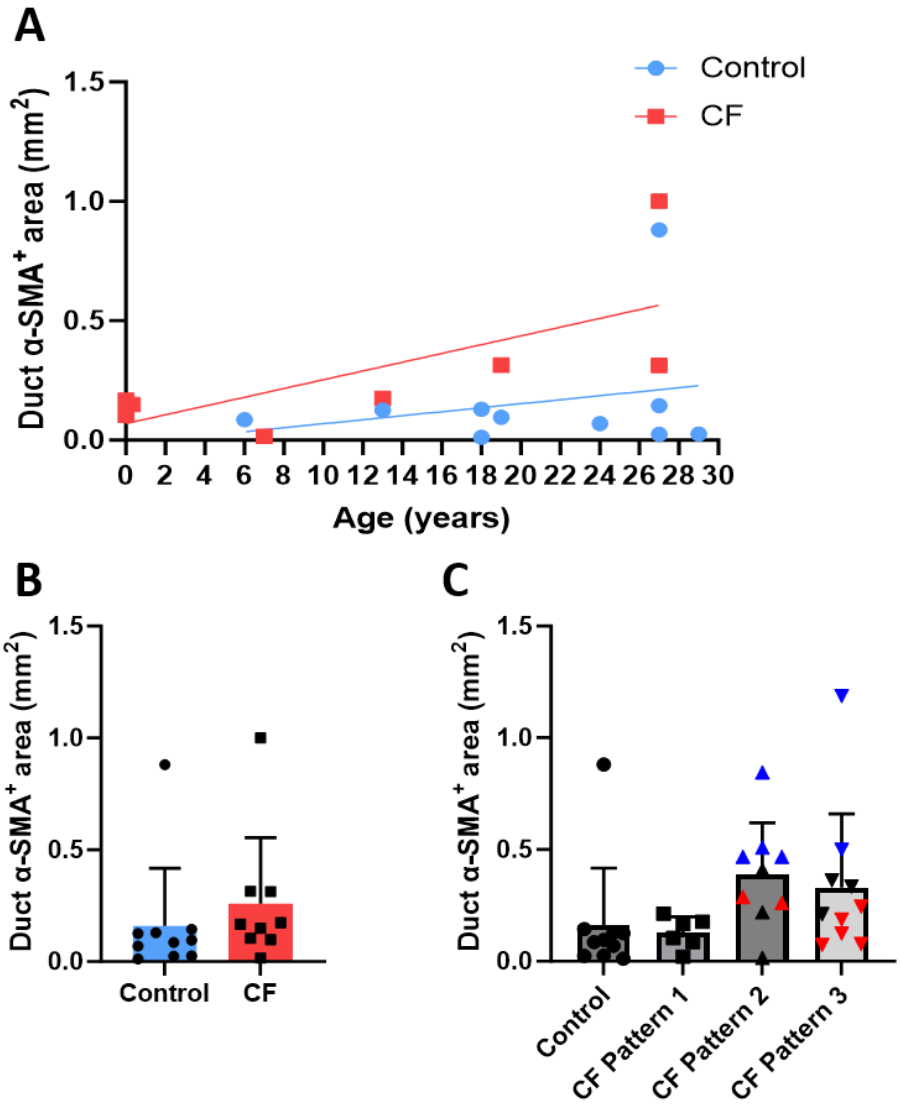

Figure 3.27: AI assessment for ductal α-SMA⁺ area (mm²) for control and CF pancreata.

(A) *Simple linear regression analysis to represent expression of ductal α-SMA⁺ area (mm²) vs age (years).* ***(B)*** *Donor-based analysis of ductal α-SMA⁺ area (mm²) in control and CF pancreata.* ***(C)*** *Block-based analysis of ductal α-SMA⁺ area (mm²) in control and CF pancreata of different patterns. Statistical analyses were carried out using Unpaired Student's t test and Linear mixed effect model (LMEM) with pancreata pattern set as fixed effect, donor as random effect and Bonferroni post hoc test. Graphs show the mean±SD. Graph* ***(A)*** *and* ***(B)****: control n = 10 donors and CF n = 9 donors. Graph* ***(C)****: control n = 10 blocks, CF n = 25 blocks (Pattern 1 n = 6; Pattern 2 n = 9; Pattern 3 n = 10 blocks). Red colour represents Case 22 and blue colour represents Case 29, both donors have multiple blocks of different patterns.*

3.3.3.5 Peri-and intra-islet inflammation

3.3.3.5.1 IHC staining

In addition to conducting an IHC staining for $CD45^+$ cells and α-SMA, fibrotic regions surrounding the islets, indicated by SRFG staining, were further investigated by assessing the presence of macrophages $CD68^+$ cells, which appeared more abundant compared to $CD45^+$ cells ***(Figure 3.28)***.

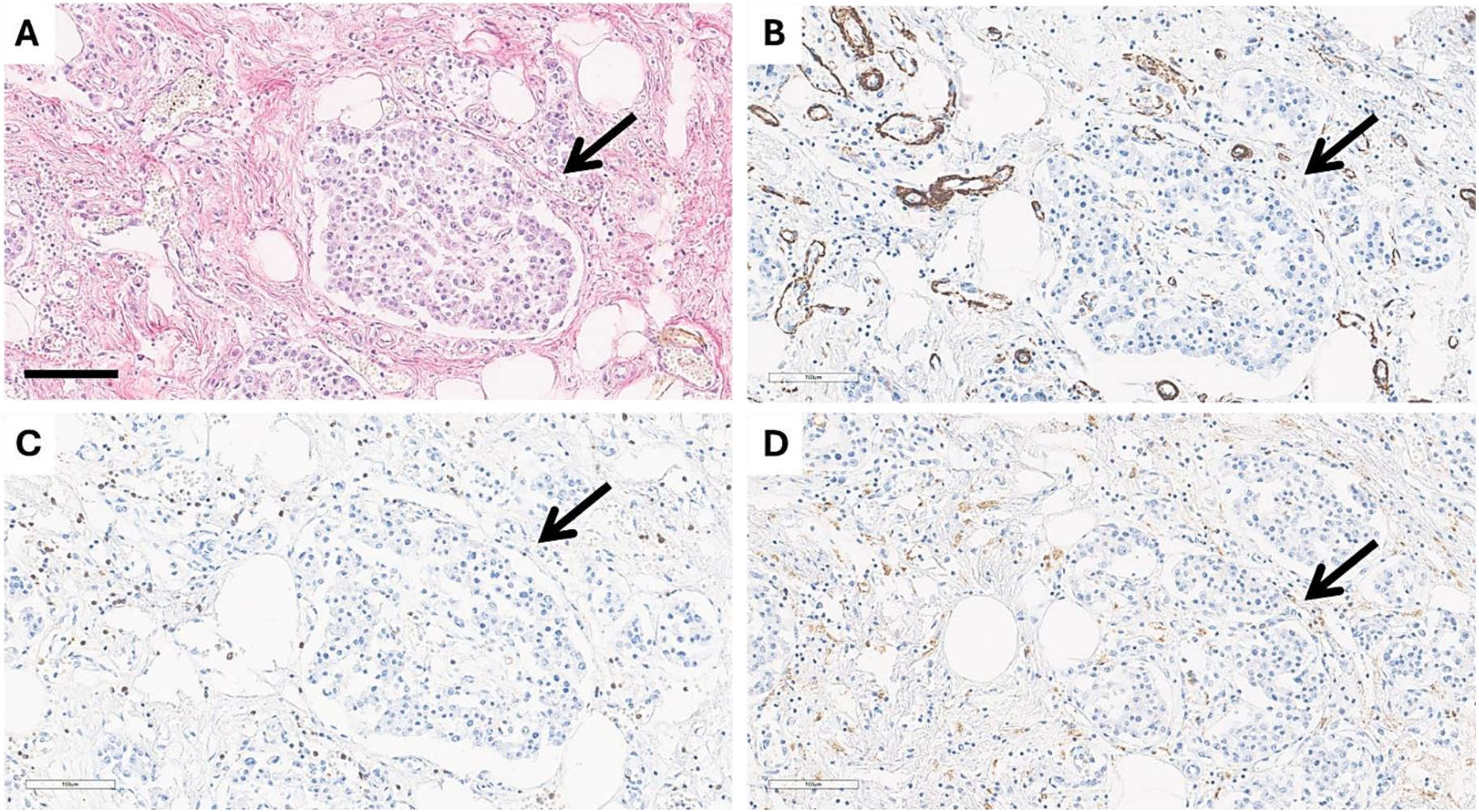

Figure 3.28: Representative illustration of fibrotic environment surrounding islets in CF.

(A) *SRFG staining. IHC staining in brown for α-SMA* ***(B)****, CD45* ***(C)*** *and CD68* ***(D)*** *of a CF (a 27-year-old donor with CF Pattern 2, Case number: 29). An example islet is indicated with black arrows. IHC staining was carried out on close serial section slides. Scale bar represents 100 µm (scale bar in* ***(A)*** *applies to all panels).*

3.3.3.6 Peri-islet fibrosis and α-SMA expression

3.3.3.6.1 IHC staining

Peri-islet fibrosis was observed in CF pancreata, where islets (examples indicated by black arrows) are embedded within collagen-rich areas ***(Figure 3.29)***. This was mirrored by the presence of α-SMA^{+} cells within fibrous tissue representing activated stellate cells ***(Figure 3.29)***. A representative image of control islets (examples indicated by dotted line) demonstrated a healthy exocrine parenchyma surrounding islets with the absence to mild presence of abnormal peri-islet collagen and islet α-SMA^{+} cells ***(Figure 3.29)***.

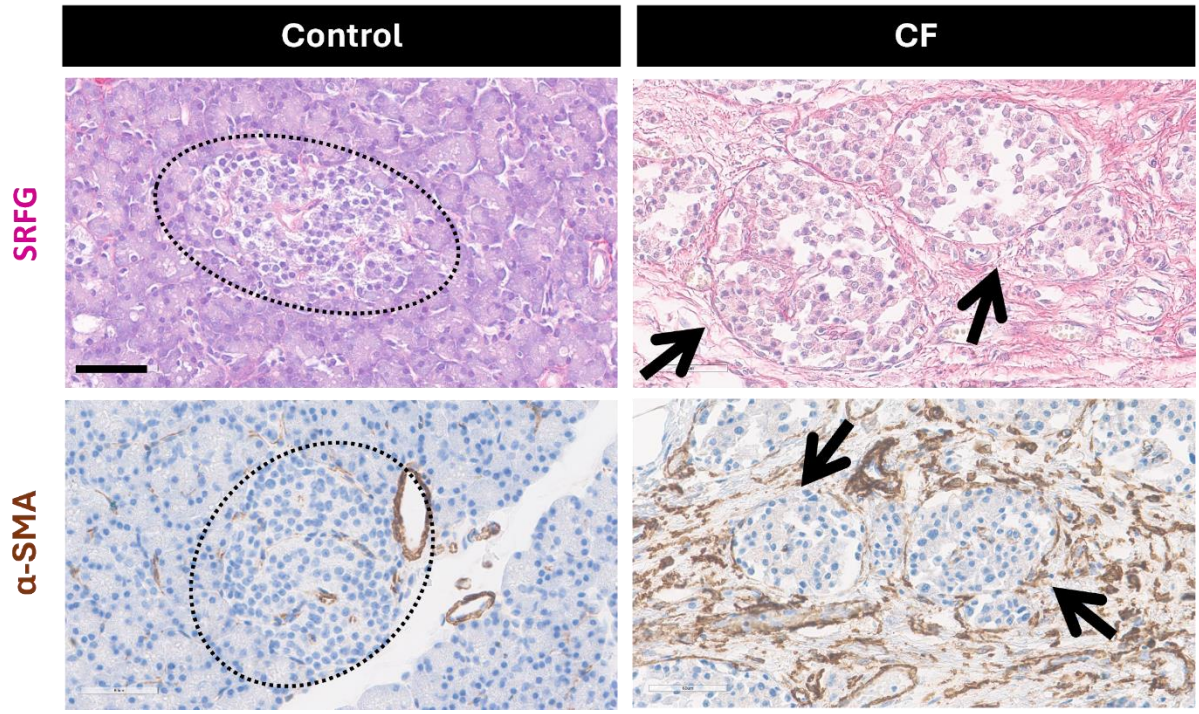

Figure 3.29: Representative illustration of peri-islet fibrosis (SRFG: pink) and activated stellate cells (brown) in the environment surrounding islets in control and CF pancreata.

Control: a 6-year-old donor pancreas (Case number: 31) and CF: a 19-year-old donor with CF Pattern 2 pancreas (Case number: 27). Examples of control islets indicated by a dotted black circle with examples of CF islets indicated by black arrows. Scale bar represents 60 µm (scale bar in control SRFG applies to all panels).

3.3.3.6.2 AI quantification

Using SRFG stained slides, an AI-driven classifier trained on a separate QUOD donor (52-year-old) was to quantify peri-islet SRFG^{+} area by first measuring intra-islet SRFG^{+} area indicated by a pink colour and illustrated in Chapter 2 (**2.1.3**) ***Figure 2.2 E***, then measuring total area within a peri-islet SRFG^{+} ring of 33.1 µm diameter around each islet, indicated by a

cyan colour in ***Figure 2.2 E***. Following, peri-islet SRFG$^+$ area was calculated by subtracting islet area (pink) from peri-islet/islet area (cyan).

AI quantification illustrated a significant increase in peri-islet fibrosis represented by proportion SRFG$^+$ area in five CF donors when compared to ten controls ($p < 0.0139$) ***(Figure 3.30 A)***. Peri-islet fibrosis was significantly higher in CF Pattern 2 compared to control ($p < 0.005$), whereas islets embedded in fatty tissue and surrounded by collagen strands represented in CF Pattern 3, illustrated a higher peri-islet proportion SRFG$^+$ area compared to control, although this was not statistically significant ***(Figure 3.30 B)***. AI data for peri-islet proportion SRFG$^+$ area for CF Pattern 1 pancreata were not available as AI classifier was trained on the QUOD control donor and had difficulties working on young diseased tissue.

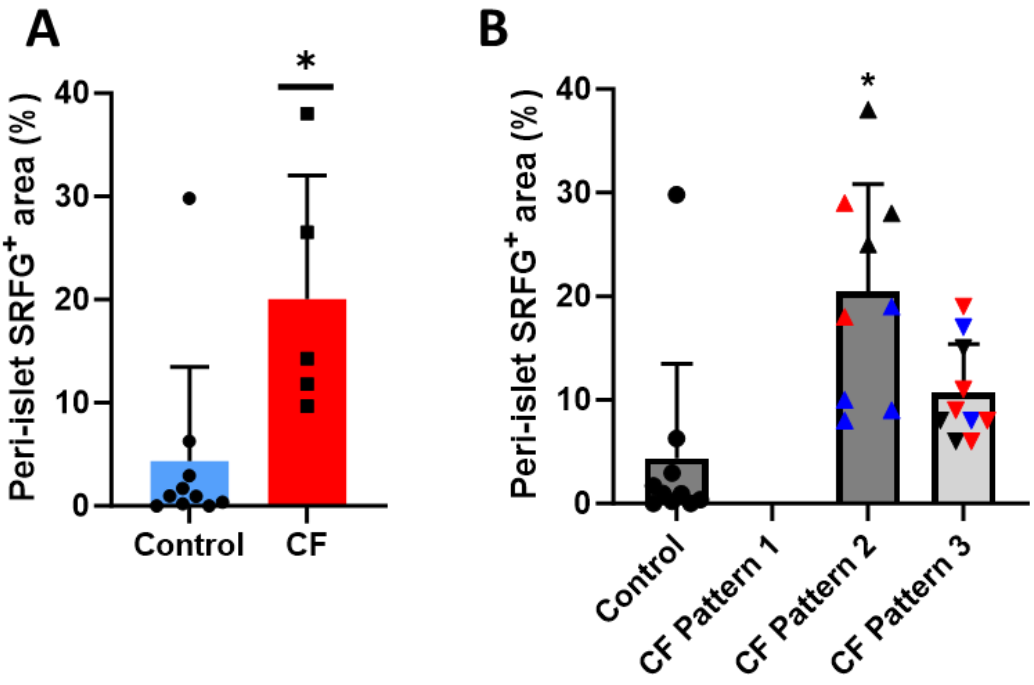

Figure 3.30: AI quantification of peri-islet fibrosis [%] using SRFG stained control and CF pancreata.

(A) *Donor-based analysis of control n = 10 donors, and CF n = 5 donors, carried out using unpaired student's t test.* ***(B)*** *Block-based analysis of control n = 10 and CF n = 19 blocks (Pattern 2 n = 9; Pattern 3 n = 10 blocks), performed using linear mixed effect model (LMEM) with pancreata pattern set as fixed effect, donor as random effect and Bonferroni post hoc test. There was unavailable data for CF Pattern 1. Graphs show the mean±SD. Significant difference is represented by p < 0.05, (*) indicates the significant difference compared to control.* ***(B)*** *Red colour represents Case 22 and blue colour represents Case 29, both donors have multiple blocks of different patterns.*

3.3.3.7 Intra-islet fibrosis and α-SMA expression

3.3.3.7.1 IHC staining

Using SRFG staining, control islets illustrated no to mild presence of collagen strands within islets, whereas intra-islet fibrosis was observed more frequently in CF pancreata. A representative illustration from a 13-year-old CF donor with CF Pattern 2, demonstrated the presence of intra-islet fibrosis (example indicated by black arrows) when compared to islets in a 13-year-old control donor (example indicated by dotted line) ***(Figure 3.31)***.

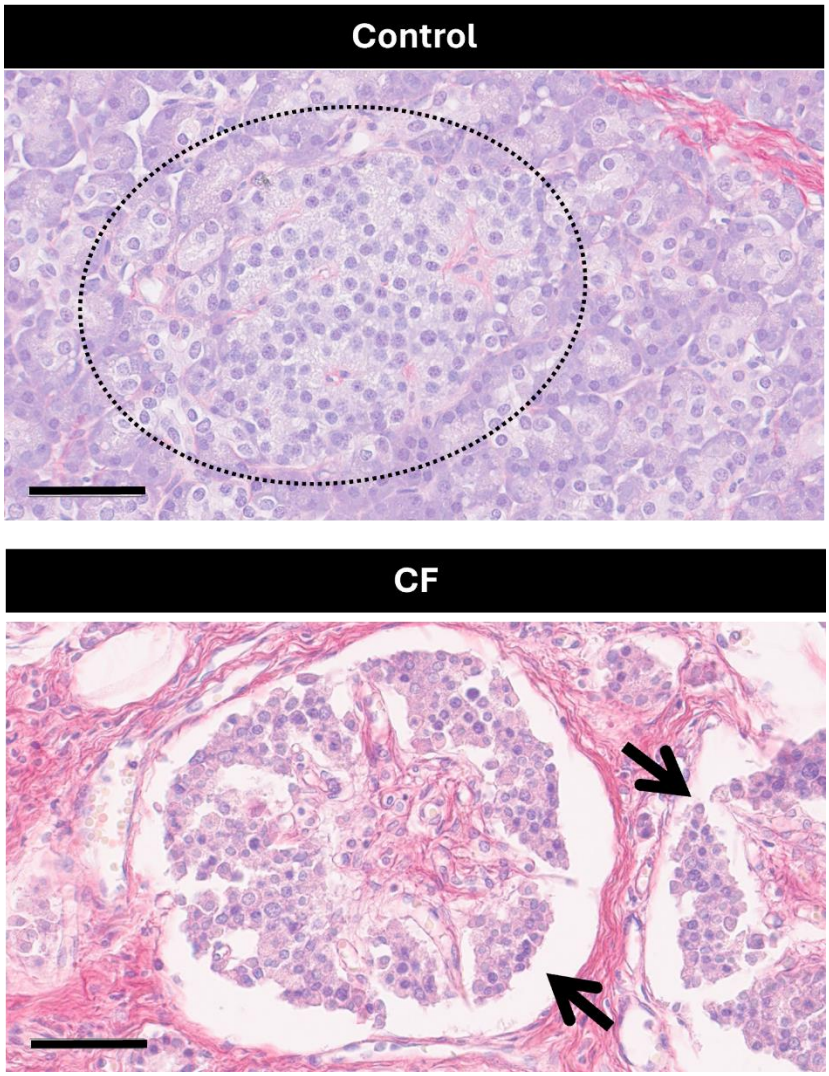

Figure 3.31: Illustration of a representative intra-islet SRFG^{+} area in islets of Control and CF pancreata.

Images from a 13-year-old control donor (dotted line, Case number: 50) and a 13-year-old donor with CF Pattern 2 pancreas (black arrows, Case number: 22). Scale bar represents 60 µm.

3.3.3.7.2 AI quantification

Using SRFG-stained slides, the AI classifier quantified intra-islet $SRFG^+$ area within islets indicated by a yellow colour and illustrated in Chapter 2 ***Figure 2.2 D***. Donor-based analysis showed a significant increase in the proportion of intra-islet $SRFG^+$ area in seven CF pancreata compared to 10 control organs ($p < 0.0215$) ***(Figure 3.32 A)***. Block-based quantification, demonstrated a significant increase in intra-islet $SRFG^+$ area (%) of CF Pattern 2 islets compared with controls ($p < 0.006$) ***(Figure 3.32 B)***. Interestingly, proportion of intra-islet α-SMA^+ area (quantified as illustrated in Chapter 2.1.3 ***Figure 2.4 C***) that was corrected to islet area was significantly lower in CF compared to control ***(Figure 3.32 C)*** with a reduced trend across all patterns ***(Figure 3.32 D)***.

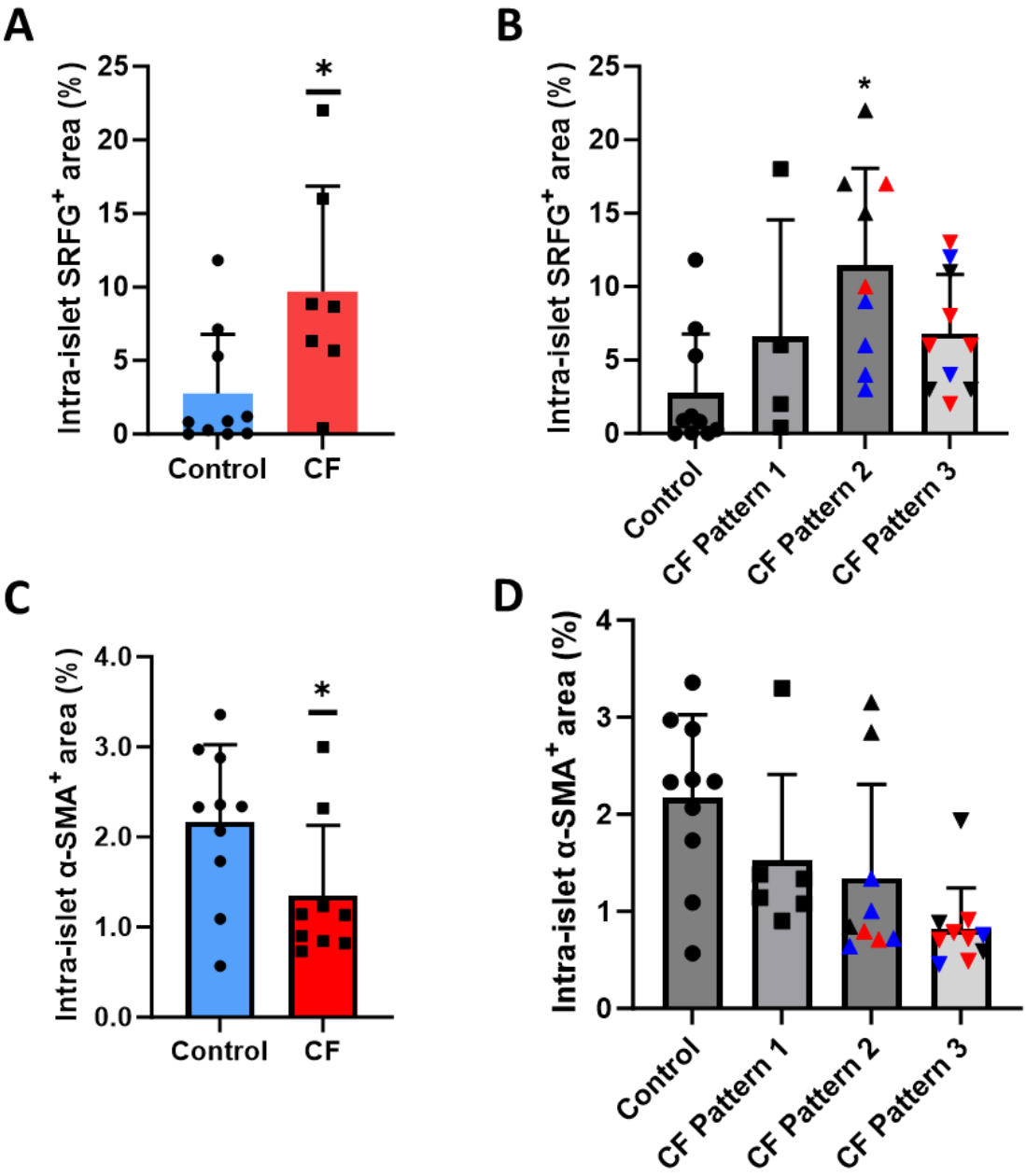

Figure 3.32: AI quantification of intra-islet SRFG⁺ and α-SMA⁺ area [%] on control and CF SRFG and α-SMA stained pancreatic tissue.

(A) *Donor-based intra-islet SRFG⁺ area [%] assessment, control n = 10, CF n = 7 donors.* ***(B)*** *Block-based intra-islet SRFG⁺ area [%] assessment for control and CF pancreata of different patterns, control n = 10, CF n = 23 (Pattern 1 n = 4; Pattern 2 n = 9; Pattern 3 n = 10) blocks.* ***(C)*** *Donor-based intra-islet α-SMA⁺ area [%] assessment for control and CF pancreata of different patterns, control n= 10 and CF n = 9 donors.* ***(D)*** *Block-based islet α-SMA⁺ area [%] assessment for control and CF pancreata of different patterns, control n = 10 and CF n = 25 blocks (Pattern 1 n = 6; Pattern 2 n = 9; Pattern 3 n = 10) blocks. Donor-based statistical analyses were carried out using unpaired student's t test and block-based analyses were conducted using linear mixed effect model (LMEM) with pancreata pattern set as fixed effect, donor as random effect and Bonferroni post hoc test. Graphs show the mean±SD. Significant difference is represented by $p<0.05$, (*) indicates the significant difference compared to control. Red colour represents Case 22 and blue colour represents Case 29, both donors have multiple blocks of different patterns.*

3.4 Discussion

3.4.1 Overview

Studying the progression of CF-related diabetes in man and elucidating the disease pathogenesis have been challenging due to the highly limited tissue availability. The work in this chapter was carried out on rare CF pancreas tissue kindly provided by Professor. Günter Klöppel and the EADB. After being trained and supported by experienced clinical pathologists Professors Günter Klöppel and Dina Tiniakos, I undertook systematic histopathological evaluation of a wide range of disease in a total of 29 CF donors, which could then provide context for deeper molecular phenotyping studies world-wide. Importantly, age-matched control cohorts (58 donors) with no pancreatic pathologies provided by QUOD and EADB were included in the study.

This chapter focused on analysing pancreatic histopathological changes in human *post-mortem* CF tissue and identifying associated cell phenotypes with potential role in CFRD pathogenesis. I set out to answer three main questions:

1) What is the natural history of CF pancreatic pathology within the exocrine compartment?

2) How are exocrine compartment changes associated with changes in the endocrine compartment?

3) Is there any spatial relationship between fibrosis and stellate cells around the islets in CF?

The following sections addressed these questions.

3.4.2 What is the natural history of CF pancreatic pathology within the exocrine compartment?

Although there are limited human studies and some animal studies that address the changes within CF and CFRD pancreata, natural history remains incompletely understood. To address this gap in respect to CFRD pathogenesis, initially changes in CF pancreata over the course of the disease were histologically evaluated using H&E-stained pancreatic tissue sections from 29 human CF donors (two CFRD diagnosed cases) and 58 age-matched control donors with no known pancreatic pathology.

Histological evaluation of young CF cases (premature–14-year-old) classified by CF Pattern 1 (fibroatrophic changes only) and represented in ***Figure 3.2*** revealed some mild alteration to pancreatic lobules, whereas the exocrine parenchyma was still preserved. Intra-lobular abnormal collagen presence was observed in addition to the presence of some dilated ducts and mild acinar lumen dilation and acinar atrophy. Islet size and shape varied and there was some presence of peri-islet fibrosis. A quantitative evaluation of the development of CF infant exocrine pancreas reported that changes in acinar volume in CF infants above 42 weeks' post-conceptional age was distinguishable compared to control (Imrie et al., 1979). Whereby, a decrease in acinar volume to connective tissue ratio following 52 weeks post-conceptional age (around 3 months after birth) was reported, when compared to age-matched control pancreata. The study also reported the increase in acinar and ductal lumen dilation in CF infants compared to control. Iannucci et al. (1984) reported that young CF children of age less than 1 year illustrated the absence of exocrine fat replacement and severe ductal dilation. These findings aligned with our observations of young CF pancreata and supported the establishment of an early-stage CF Pathology Pattern.

Later-stage CF was designated after the evaluation of CF cases (3–27-year-old) which illustrated severe histopathological changes. These cases were histologically classified by CF Pattern 2 (fibroatrophic and lipoatrophic) and CF Pattern 3 (lipoatrophic) ***(Figure 3.3*** and ***Figure 3.4***, respectively***)***. Both patterns illustrated an extensive loss of the exocrine parenchyma and the presence of both abnormal collagen and adipocytes or predominantly adipocytes alone. In both patterns, islets of different sizes appeared spared but disrupted and surrounded by collagen deposition or collagen strands with adjacent adipocytes. These findings aligned with those of a qualitative histological analysis, whereby CF *post-mortem* pancreata over the age of 5 years exhibited more cystic ductal dilation with the absence of acinar tissue and exocrine compartment being replaced with fibrotic and/or fatty tissue (Löhr et al., 1989).

The semi-quantitative scoring system developed and validated in this chapter, inspired by the Löhr et al. (1989) study, supported the previous histological evaluations and systematically characterised the degree of variation in histopathological changes across the disease patterns, as the disease progresses ***(Figure 3.11)***. Ductal dilation in CF has been reported to be more apparent (Iannucci et al., 1984; Soejima & Landing, 1986; Löhr et al., 1989; Bogdani et al., 2017; Hart et al., 2018). Our scoring system revealed that ductal lumen dilation appeared to be associated with fibrotic changes within CF exocrine parenchyma whereby it was significantly higher in end-stage CF Pattern 2 (3–27-year-old) compared to early-stage CF Pattern 1

(premature–14-year-old) and became less severe in later-stage CF with total fat replacement ($p < 0.001$) ***(Figure 3.11 A)***. Ductal loss was more apparent in the lipoatrophic areas of CF tissue demonstrated by the later-stage CF Pattern 3 ($p < 0.001$ vs CF Pattern 1 and 2) ***(Figure 3.11 B)***. This raised the question whether lipogenesis had an impact on ductal existence. Exocrine pancreatic fibrosis was significantly higher in the fibroatrophic regions of CF rather than the lipoatrophic tissue (CF Pattern 1 vs 3: $p = 0.013$ and CF Pattern 2 vs 3: $p < 0.001$) ***(Figure 3.11 C)***. Acinar atrophy and islet remodelling were significantly higher in CF compared to control ($p < 0.001$), with advanced CF cases all manifesting severe acinar atrophy (CF Patterns 2 and 3 vs 1: $p < 0.001$) and islet remodelling (CF Pattern 2 vs 1: $p = 0.005$ and CF Pattern 3 vs 1 $p < 0.001$) ***(Figure 3.11 D*** and ***E)***. Islet remodelling in the later-stage CF of the lipoatrophic Pattern 3 was significantly higher compared to islets of fibroatrophic-associated Patterns 1 and 2 ($p < 0.001$ and $p < 0.008$, respectively) ***(Figure 3.11 E)***. There was no significant change in inflammatory cell infiltration between control and CF pancreata and between CF pancreata of different patterns.

Considering the histological findings and the semi-quantitative scoring reported data, AI quantitative analysis further provided further insights into the changes within the exocrine parenchyma over the course of the disease. H&E-stained pancreatic tissue of 25 human CF and 58 age-matched controls were used to quantify the changes associated with acinar atrophy and exocrine parenchyma replacement with abnormal collagen deposition and fatty tissue.

In keeping with the semi-quantitative scoring, the proportion of acinar area in CF pancreata was significantly lower than in controls. This significant decrease was observed across the three CF Patterns with the later-stage CF showing greater reduction in acinar area when compared to early-stage CF ***(Figure 3.13)***. These findings aligned with the semi-quantitative analysis of acinar atrophy ***(Figure 3.11 D)***. AI data demonstrated that, in controls up to the age of 30 years, proportion of acinar area remained consistent. However, in CF including premature and donors of < 1 week of age, acinar area [%] was around a third of that in controls ***(Figure 3.13 A)***. The severity of *CFTR* mutation has been proposed to impact on acinar cell development during gestation, which is exacerbated by autolysis post-birth (Imrie et al., 1979). The study reported that acinar volume was reduced at pre-term and at full term birth in CF pancreata compared to control (Imrie et al., 1979).

AI quantification of fibrotic changes and abnormal collagen deposition area in CF confirmed a significant increase compared to controls ($p < 0.0001$) and seemed to be associated with

fibroatrophic changes in both early- and later-stage CF rather than lipoatrophic changes ***(Figure 3.14)***. These findings supported the semi-quantitative analysis of exocrine pancreas fibrosis across the three patterns ***(Figure 3.11 C)***. Proportion of fat area replacing the exocrine parenchyma significantly increased in CF compared to control ($p < 0.0001$) and was greatly associated with CF cases representing the later-stage of the disease (CF Pattern 2 and CF Pattern 3), whereby more than 60-90% of tissue was replaced with fatty tissue ***(Figure 3.15)***.

Although, Löhr et al. (1989) established the fibrotic and the lipoatrophic patterns when describing the early- and end-stage CF, respectively, our study proposed that the fibrotic pattern alone is mainly associated with young and early-stage CF, whereby there was an absence of fatty tissue replacing the exocrine parenchyma. This could highlight the natural history of CF progression is associated with age and the severity of the disease illustrated by early-stage fibrotic pattern alone through the later-stage illustrated by a mixed fibrotic/lipoatrophic pattern and a total fatty tissue replacement of the exocrine parenchyma. It is important to highlight that fat replacement of the exocrine parenchyma increased linearly with age, again in keeping with a steady progression of the disease. This could suggest that the later-stage of the disease could be divided into two stages: advanced-stage represented by CF Pattern 2, which then progresses into end-stage represented by CF Pattern 3. The systematic semi-quantitative scoring system analyses performed based on Pathological Patterns further elucidated CF progression via ductal dilation/loss; acinar cell loss and pancreatic fibrosis along with islet remodelling. AI quantification of acinar area [%] in parallel with exocrine parenchyma replacement with collagen and or fatty tissue alone, further supported our semi-quantitative findings in respect to disease progression based on phenotypic classification.

3.4.3 How are exocrine compartment changes associated with changes in the endocrine compartment?

H&E-stained pancreatic sections were assessed to further investigate the endocrine compartment and undertake quantitative analysis of islet parameters including endocrine proportion area, islet density, median islet circularity, median islet diameter and median islet area/size.

Interestingly, H&E-stained pancreatic sections of CF and aged-matched controls showed no change of endocrine area [%] or in islet density in CF when compared to control, yet both cohorts illustrated a gradual decrease of endocrine area [%] and islet density as age increased ***(Figure 3.16*** and ***Figure 3.17)***. This possibly due to the overall reduction in pancreatic volume

as age increases (Löhr et al., 1989). In addition, another study of 115 non-diabetic autopsied pancreatic tissue proposed that islet density decreased as age increased (Mizukami et al., 2014). Although this work did not show a reduction in islet number in CF/CFRD pancreata compared to control, illustrating islet survival in such damaged neighbourhood, a *post-mortem* CF study has suggested a decrease in islet number (Löhr et al., 1989). Some studies reported no change in relative endocrine mass in CF cases compared to control (Löhr et al., 1989, Couce et al., 1996, Bogdani et al., 2017). Yet, endocrine mass in CFRD cases was reported to be lower compared to CF cases (Iannucci et al., 1984, Soejima and Landing, 1986, Bogdani et al., 2017).

Having observed no change in endocrine area [%] in our CF cohort compared to controls, further islet parameters were investigated. In early-stage CF (CF Pattern 1), some cases illustrated the presence of some solitary islets within pancreatic lobule and some islets were surrounded by abnormal collagen deposition, identified by CGA^+ staining and SRFG staining, respectively ***(Figure 3.9 Score 1)***. These findings contradicted Bogdani et al. (2017) study that reported islets of young CF donors that exhibited less severe exocrine changes to be larger compared to those with more severe exocrine changes (Bogdani et al., 2017). However in this chapter, the frequent presence of solitary islets in young CF cases could be further supported by islet density, which appeared to be significantly higher compared to later-stage CF cases of Patterns 2 and 3 ($p = 0.006$ and $p = 0.002$, respectively) ***(Figure 3.17 C)***.

Donor-based analysis of median islet circularity illustrated a significant reduction of islet circularity in CF compared to control ($p = 0.0221$) with no significant change in the pattern-based analysis ***(Figure 3.18 B)***. Also, donor-based analysis reported that median islet diameter ***(Figure 3.21 A*** and ***B)*** and median islet area (size) ***(Figure 3.19 A*** and ***B)*** increased gradually with age with no significant change in CF when compared to control pancreata. Yet, pattern-based analysis illustrated a significant increase in median islet diameter in later-stage CF when compared to control (CF Pattern 2: $p = 0.028$ and CF Pattern 3: $p < 0.001$) and early-stage CF (CF Pattern 2: $p = 0.002$ and CF Pattern 3: $p < 0.001$) ***(Figure 3.20 C)***. Whereas, median islet area was significantly higher in later-stage CF compared to early-stage islets (CF Pattern 2 and 3 vs 1: $p = 0.008$ and $p < 0.001$, respectively), and islets area of the lipoatrophic pattern was significantly higher compared to control ($p = 0.018$) ***(Figure 3.22 C).*** These quantitative findings supported the qualitative observation of bigger islets observed using CGA and SRFG staining ***(Figure 3.9*** Score 2 and 3***)*** and the semi-quantitative scoring illustrating a greater islet remodelling in the advanced- and end-stage CF compared to the early-stage CF ***(Figure 3.11 E)***. These observations are supported by reported findings that islets in CFRD pancreata exhibit

different sizes and appear disorganised (Iannucci et al., 1984, Abdul-Karim et al., 1986). Another study reporting that lipoatrophic pattern was associated with greater altered islet morphology (Bogdani et al., 2017). Also, lipoatrophy of the exocrine pancreas has also been proposed to be associated with β-cell dysfunction via lipotoxicity (Lee et al., 1994).

Reduction in β-cell function leading to impaired insulin release in people with CF is considered essential in the development of CFRD (Moran et al., 1991; Mohan et al., 2009; Merjaneh et al., 2015; Sheikh et al., 2017). Some studies reported that β-cell area is reduced in CFRD cases compared to CF cases (Iannucci et al., 1984; Abdul-Karim et al., 1986; Soejima and Landing, 1986; Löhr et al., 1989). Yet, Bogdani et al. (2017) study contradicted these findings by reporting no difference in β-cell area in CFRD and CF.

To assess the endocrine hormonal composition in CF pancreata, IHC for endocrine hormones was carried out on eight CF cases (0–27-year-old) and 10 control cases (6–29-year-old). Visual histological assessment of CF islets illustrated differences in hormonal^{+} cell proportions when compared to controls. Endocrine hormonal quantitative analysis revealed the significant reduction in β-cell area represented by insulin^{+} area in CF cases (20-70%) when compared to control (70-90%) ($p < 0.001$) and this reduction was also observed in both the early- and later-stage CF ***(Figure 3.23 A*** and ***Figure 3.24 A)***. The reduction in β-cell in CF observed in this study was supported by studies on pancreatic specimen from adult human donors with CF, which have reported the decrease in β-cell area (Abdul-Karim et al., 1986; Löhr et al., 1989; Couce et al., 1996; Hart et al., 2018). Exocrine pathological changes demonstrated by fibrotic and fatty tissue replacement have been reported to exhibit similar impact on β-cell loss (Löhr et al., 1989). Bogdani et al. (2017) reported that β-cell loss, demonstrated by loss of insulin^{+} area, in younger CF cases was greater compared to older CF cases, this finding aligned with the early-stage CF fibrotic pattern exhibiting lower insulin^{+} [%] compared to the later-stage CF pattern 2 and 3 ***(Figure 3.24 A)***. These presented changes in islet composition specifically β-cell loss in the early-stage CF should be further investigated to determine the underlying factors contributing to β-cell loss/dysfunction leading to the development of CFRD. Molecular studies to determine the impact of the associated fibrotic changes on β-cell identity and function could further provide an idea of the possible treatments to limit this impact and prevent CFRD. During pancreatic injury pancreatic fibrosis resulted from reoccurring necrosis, apoptosis and inflammation of the exocrine parenchyma has been associate with endocrine changes and islet dysfunction, eventually leading to diabetes (Klöppel et al., 2004).

On the other hand, compared to control, α-cell quantification presented by the proportion of glucagon$^+$ area within islets was significantly higher in CF donor-based ($P < 0.0001$) and pattern-based analyses (CF Patterns 1, 2 and 3 $p = 0.0152$, $p < 0.0001$ and $p=0.0032$, respectively) ***(Figure 3.23 C*** and ***Figure 3.24 C)***. Immunobiological studies have reported similar findings of increased α-cells abundance in human CF islets with and without CFRD (Löhr et al., 1989; Bogdani et al., 2017; Hart et al., 2018; Hull et al., 2018). Together these findings could shed the light into understanding the association between islet cell's identity and function in CF pancreas.

Proportion of pancreatic polypeptide$^+$ area appeared decreased in CF islets compared to control, but this was not significant ***(Figure 3.23 B*** and ***Figure 3.24 B)***. Contradictory findings of higher pancreatic polypeptide$^+$ area in CF compared to control have been reported (Löhr et al., 1989). Other studies have reported the increase being observed in young CF islets compared to controls (Bogdani et al., 2017; Hull et al., 2018).

Similarly, δ-cells represented by somatostatin$^+$ area was significantly increased in CF islets compared to control and this significant increase was prominently observed in early-stage CF of a fibroatrophic pattern ($p < 0.0001$) ***(Figure 3.23 D*** and ***Figure 3.24 D)***. Also, early-stage somatostatin$^+$ [%] was significantly higher compared to later-stage CF (CF Patterns 2 and 3: $p < 0.0001$ and $p = 0.0002$, respectively) ***(Figure 3.24 D)***. Similar observations of elevated δ-cell area in CF compared to control have been reported (Löhr et al., 1989; Bogdani et al., 2017; Hull et al., 2018). Some studies have reported contradictory findings on whether there was an increase in δ-cells area in CFRD cases compared to CF cases (Iannucci et al., 1984; Bogdani et al., 2017; Hart et al., 2018; Hull et al., 2018).

Any differences from published work in reported observations regarding endocrine cell composition, via AI quantification on IHC stained tissue for endocrine hormone, could be due to the small size of CF (eight cases: 22 blocks) and control (10 cases: 10 blocks) cohorts used. Also, unlike the CF cohort there was limited availability of very young (<1 year old) control tissue.

3.4.4 Is there any spatial relationship between fibrosis and stellate cells around the islets in CF?

To investigate islet vascularisation and peri-islet pathology including inflammation, fibrosis and presence of activated PaSCs, control and CF sub-cohorts were further stained with endothelial marker CD31, inflammatory markers CD45 and CD68, collagen stain SRFG and

activated PaSCs marker α-SMA, respectively. The islet microvascular capillary network is a key mediator of islet function whereby it acts as a channel for nutrient transportation to endocrine cells, as well as necessary components such as growth factors and ECM proteins to regulate islet β-cell function. It also regulates the delivery of hormones to the peripheral tissue (Richards et al., 2010; Peiris et al., 2014; Hogan & Hull, 2017; Jansson & Carlsson, 2019). Our donor-based analysis showed a reduction in endocrine $CD31^+$ area in CF when compared to control but this reduction was not significant ***(Figure 3.21 B)***. Yet, it appeared to decrease as the disease progresses from CF Pattern 1 to CF Pattern 3 ***(Figure 3.21 C)***. A preliminary study illustrated a decrease in islet capillary density and in exocrine capillaries with an additional molecular study of islets from CF donors reporting an increase of endothelial inflammatory markers such as SELE and IL6, illustrating the possibility of endothelial cells inflammation (Castillo et al., 2022; Hart et al., 2018).

Semi-quantitative scoring showed that ductal dilation was significantly associated with pathological fibrotic changes within CF pancreas ***(Figure 3.11 A)***. Further staining for inflammatory cells demonstrated moderate presence of leukocytes ($CD45^+$ cells) within these fibrotic areas around the ducts ***(Figure 3.25)***. Leukocytes - T-cells and macrophages were observed in the CF exocrine pancreas, independent of donor age (Bogdani et al., 2017; Hart et al., 2018). Compared to the lipoatrophic CF Pattern, immune cells in the fibrotic exocrine compartment were reported to be more present (Löhr et al., 1989; Bogdani et al., 2017). Extensive presence of activated PaSCs represented by a positive staining for α-SMA within fibrotic periductal fibrotic areas has been established ***(Figure 3.25*** and ***Figure 3.26 B)***. In the CF ferret model, activation of PaSCs has also been demonstrated by α-SMA expression (Sun et al., 2017). Also, Rotti et al. (2018) study has observed the activation of PaSCs around ductal epithelium in CF ferrets of 1-4 months age (< 3.5 years human age) when compared to wild-type ferrets. Together these observations support the hypothesis that PaSCs are the source of myofibroblasts during CF pancreatic remodelling further making them a key target in CFRD treatment (Rotti et al., 2018).

CD45 and CD68 IHC staining revealed the presence of inflammatory cells within the fibrotic areas surrounding ducts and islets, with some $CD68^+$ macrophages infiltrating the islets ***(Figure 3.26*** and ***Figure 3.28****,* respectively***)***. $CD68^+$ macrophage cells have been reported to play a coordinating role in stellate cells activation, whereby they secrete cytokines including TNF-α that stimulates collagen synthesis by activated stellate cells (Stalnikowitz & Weissbrod, 2003). Progressive inflammation and fibrosis have been reported to be implicated in the decline

of β-cell function (Bridges et al., 2018). Although significant fibrotic pathological changes associated with islets were reported in the later-stage CF, it is critical to investigate these changes during early-stage CF to enable better management of the disease before irreversible progression.

Also, α-SMA$^+$ PaSCs were found in the fibrotic areas surrounding the islets ***(Figure 3.29)***. With fibrosis seen to be a predominant pathology in the islet neighbourhood even following virtually complete adipocyte replacement of the parenchyma, we propose that α-SMA$^+$ stellate cells are a key cellular player in mediating fibrotic changes and possibly impacting on islet function. PaSCs are known to play a key role in pathological pancreatic fibrosis and β-cell dysfunction (Omary et al., 2007; Apte et al., 2012; Phillips, 2012). Therefore, peri- and intra-islets fibrotic changes were further investigated using SRFG staining ***(Figure 3.29*** and ***Figure 3.31)***. AI quantification of collagen area [%] illustrated the significant increase in peri-islet and intra-islet fibrosis in CF when compared to control donors ($p < 0.0139$ and $p < 0.0215$) ***(Figure 3.30 A*** and ***Figure 3.32 A)***. This increase was associated with fibrotic changes represented by advanced CF Pattern 2 ***(Figure 3.30 B*** and ***Figure 3.32 B)***. Our findings of increased presence of peri- and intra-islet fibrosis along with the semi-quantitative scoring illustrating increased islet remodelling ***(Figure 3.11 E)***, as the disease progresses, were further supported by Löhr et al. (1989) and Hull et al. (2018) studies, whereby CF islets were reported to be highly fragmented with presence of intra-islet fibrosis (Löhr et al., 1989; Hull et al., 2018).

In summary we have demonstrated the presence of α-SMA$^+$ PaSCs in the fibrotic regions of the tissue ***(Figure 3.28)*** in parallel with CF progressing to the advanced-stage Pattern 2 and end-stage CF Pattern 3 in conjunction with partial to total replacement of the exocrine parenchyma by adipocytes, of unknown source, respectively ***(Figure 3.3***, ***Figure 3.4*** and ***Figure 3.15 C***, respectively***)***; and increased islet remodelling as the disease progresses ***(Figure 3.11 A)***. Informed by CF ferret and mouse studies, it has been proposed that myofibroblasts, equivalent to activated PaSCs, in the fibrotic regions could be a possible source of adipocytes in CF (Plikus et al., 2017; Rotti et al., 2018). This could give a rise to lipotoxicity further impacting on β-cell function (Lee et al., 1994).

Together, the findings presented in this chapter suggest that activated PaSCs could be one of the key cellular players mediating the changes observed in human CF with a possible pivotal role in mediating exocrine-endocrine crosstalk leading to β-cell dysfunction and eventually CFRD. Further spatial and functional *in vitro* studies were thus planned (Chapters 4 and 5).

3.4.5 Study limitations

There were several limitations to this study. There were staining-quality challenges, when working with the CF tissue, provided kindly by Professor Günter Klöppel (the sub-cohort), as these were from historic *post-mortem* (1979-2008) cases, limiting successful staining of all blocks leading to challenges with accurate AI-driven quantification. The designed AI classifiers to quantify fibrotic changes within CF sections faced challenges when analysing grossly fibrotic pancreata due to difficulty in differentiating tissue phenotypes affected by collagen fibres. Therefore, some of the early-stage H&E and SRFG stained fibrotic samples were not included in the quantification procedure. Generally, AI classifiers had difficulties working on CF tissue, compared to control pancreas, due to the variation in the extensive damage present. Although I was trained by expert pathologists to score the CF and control cohorts, semi-quantitative analysis remained user-dependent and with unavoidable subjective limitations.

There were no available data regarding the diagnosis of CFRD in the sub-cohort investigated in this study. Therefore, for future studies, it would be essential to explore CFRD cases to able to format an overall picture of the disease development. There was limited access to tissue blocks further limiting additional staining for all cases in both control and CF cohorts.

CFTR genotype is directly linked to the severity of exocrine pancreatic status (Kerem et al., 1990; Kristidis et al., 1992; Wilschanski & Novak, 2013). Although the proposed findings in this chapter in respect to the stage of the disease, age and morphological pattern were powerful, it is critical to determine the CFTR mutation in CF cases (which was impossible to conduct successfully using the historic CF tissue blocks provided by Professor. Günter Klöppel). Identifying mutation type could aid the understanding of pathological change severity and establishment of a truly well-defined natural history of disease progression. This would facilitate drug development studies to design treatment strategies to target the changes of early-stage disease and, by limiting acinar loss and fibrosis progression, lessen mechanical damage to exocrine and endocrine parenchyma, further reducing the severity and thus complications of CFRD.

Chapter 4: Establishment of a human primary islet-derived stellate cell (ISC) model and investigating the impact of its secretome on β-cell viability and function

4.1 Introduction

4.1.1 Insulin biosynthesis and secretion

Insulin is produced by pancreatic β-cells within islets of Langerhans and it is a key hormone responsible for regulating blood glucose levels by mediating glucose uptake by insulin-sensitive tissue (Weiss, 2009; Fu et al., 2013). Insulin biosynthesis shown in ***Figure 4.1*** is regulated at the transcriptional level by proteins (transcription factors) including pancreatic and duodenal homeobox-1 (*PDX1*), neurogenic differentiation 1 (*NeuroD1*) and V-maf musculoaponeurotic fibrosarcoma oncogene homolog A (*MafA*) (Fu et al., 2013; Tokarz et al., 2018). In response to elevated blood glucose levels, the *INS* gene encoding insulin is transcribed into pre-mRNA, which is spliced to form mature mRNA that is translated via ribosomes attached to the rough endo plasmic reticulum (rER) to produce a 110 amino acid precursor called preproinsulin (Weiss, 2009; Fu et al., 2013). Insulin biosynthesis is also regulated at the translational level to produce a stable protein (Weiss, 2009; Fu et al., 2013). Preproinsulin is translocated across rER membrane into the lumen via cytosolic ribonucleoprotein signal recognition particles (SRP), which are located at the surface of the rER (Chan et al., 1976; Lomedico et al., 1977; Egea et al., 2005). Then, a signal peptidase cleaves off the peptide of preproinsulin resulting in proinsulin, which consists of A-chain and B-chain and a C-peptide (Patzelt et al., 1978; Fu et al., 2013). Proinsulin is then transported from the ER to the Golgi apparatus to be packed into secretory granules, in which it undergoes further cleavage at amino acids 31 and 64 to release C-peptide (Weiss, 2009; Fu et al., 2013). The remaining chains A and B are joined by disulphide bonds to form 51 amino acids that make up insulin which is stored in immature secretory granules (less electron-dense and contain some proinsulin that continues to be processed), that mature by becoming more electron-dense due to insulin crystallisation and containing minimal to no proinsulin ***(Figure 4.1)*** (Weiss, 2009; Fu et al., 2013; Tokarz et al., 2018).

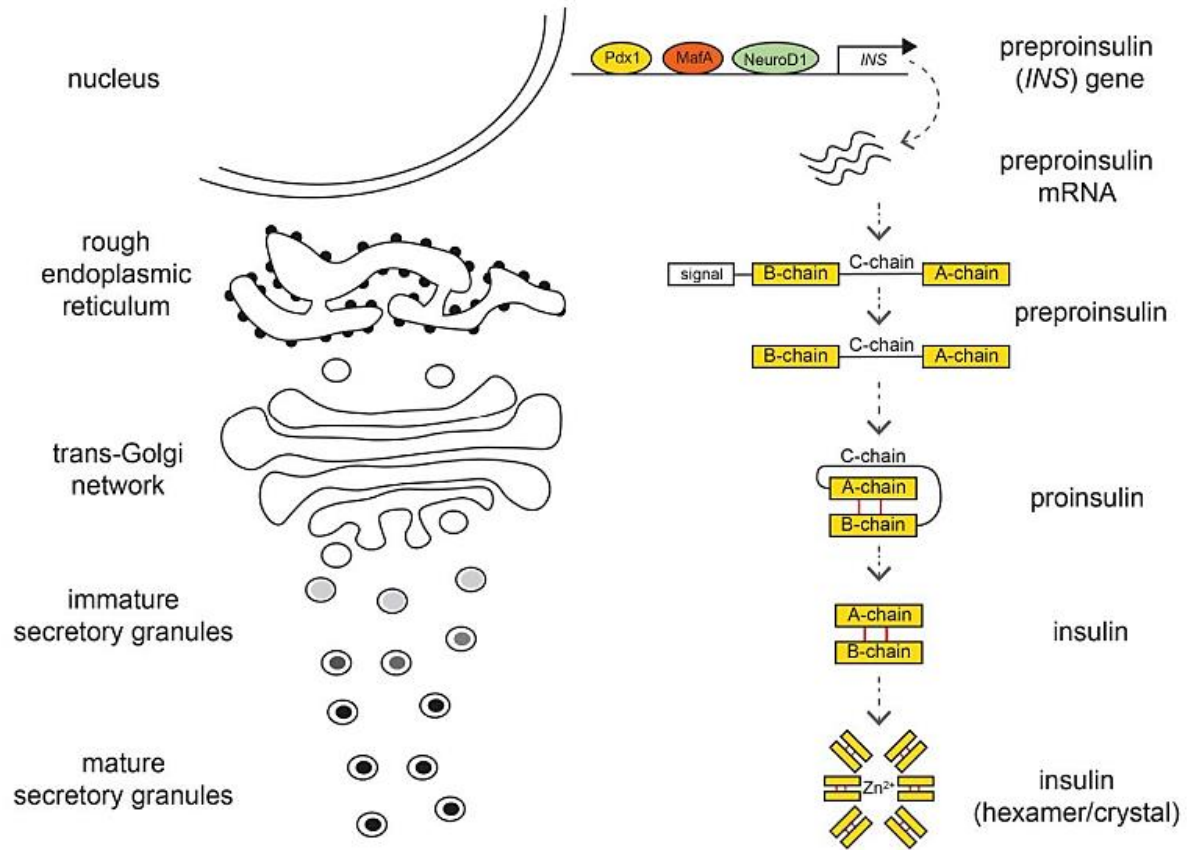

Figure 4.1: An illustration of insulin biosynthesis.

Adopted from (Tokarz et al., 2018).

Insulin secretion from the secretory granules shown in ***Figure 4.2*** is mediated by various physiological stimuli. Initially, in response to glucose stimulation, glucose transporters GLUT-2 in rodent and GLUT-1 and GLUT-3 in humans, on the surface of β-cell open and allow the entry of glucose into the cell (Weiss, 2009; Fu et al., 2013; Thorens & Mueckler, 2014). Glucose comprising six carbon molecules undergoes sequential enzymatic reactions that are mediated at the level of three irreversible reactions to generate two molecules of pyruvate (three carbon molecules) during a mechanism termed glycolysis (Galindo et al., 2022). Then pyruvate undergoes a chain of reactions via the Kreb's cycle (Tricarboxylic Acid Cycle also known as Citric Acid Cycle), whereby ATP is produced (Weiss, 2009; Fu et al., 2013). An increase in intracellular ATP:ADP ratio leads to the closure of ATP-sensitive potassium channels. This depolarises the membrane, which in turn causes the voltage-dependent calcium channels to open, allowing an influx of calcium ions. The increase in intracellular calcium ion concentration triggers the exocytosis of insulin from mature secretory granules via fusion with plasma membrane of β-cell ***(Figure 4.2)***. To clinically assess β-cell function, C-peptide is typically used as an endogenous marker of insulin secretion, as it is secreted in equimolar levels

to insulin and has a better stability (half-life of 20-30 min) compared to insulin (half-life of 3-5 min) (Leighton et al., 2017; Thota et al., 2017). Unlike insulin, which is metabolised by the liver, C-peptide is partly metabolised by the liver and is primarily excreted by the kidneys after circulating in the blood (Leighton et al., 2017; Thota et al., 2017).

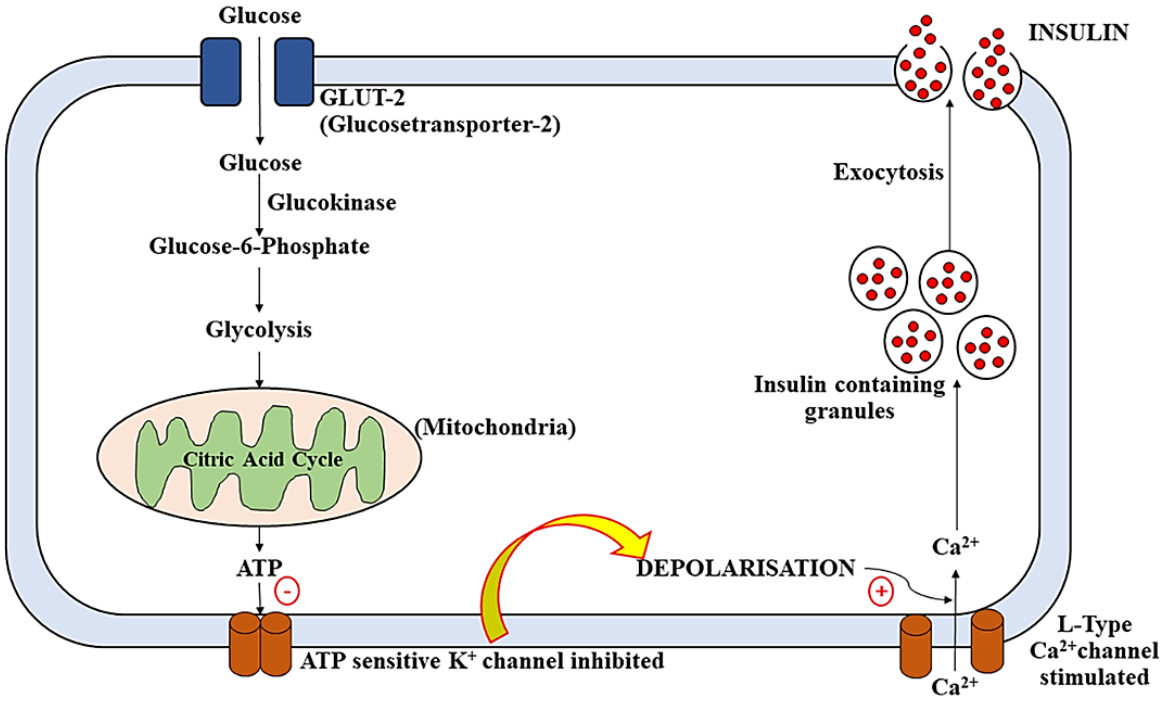

Figure 4.2: An illustration of insulin secretion following glucose stimulation.

Adopted form Arora et al (2021).

4.1.2 Type 3c diabetes and stellate cells

Type 3c (T3c) diabetes also known as pancreatogenic diabetes mellitus accounts for 5-10% of all diabetes cases. Underlying causes include chronic pancreatitis (79% of cases), pancreatic ductal adenocarcinoma (8%), haemochromatosis (7%), CF cases (4%) and previous pancreatic surgery (2%) (Hart et al., 2016). Islet β-cell dysfunction characterised by insufficient insulin secretion in parallel with pancreatic fibrosis is believed to contribute to the development of type 3c diabetes, yet the underlying mechanisms remain unknown (Phillips, 2012). A recent study investigating T3c diabetes in people with CF (CFRD) reported a progressive impairment of insulin secretion as the disease progressed (Nielsen et al., 2023). Also, CFRD was demonstrated to be associated with β-cell stress indicated by incrementally rising fasting proinsulin-insulin ratio (Nielsen et al., 2023). Changes in β-cell mass has been demonstrated to be correlated with changes in blood glucose levels in ferrets during CF development (Yi et al., 2016). First-phase insulin response was impaired with a reduction in insulin secretion

during a meal tolerance test (Olivier et al., 2012; Yi et al., 2016). In islets isolated from CFTR knock out ferrets, total insulin content was lower in CF compared to wild-type islets (Sun et al., 2017).

Pancreatic stellate cells (PaSCs) were first reported in 1982 in mouse pancreatic ducts as lipid-storing cells, identified using autofluorescence and electron microscopy techniques (Watari et al., 1982). Six years later, PaSCs were identified in sections from healthy rat and human pancreata (Ikejiri, 1990). In 1998, Ape et al and Bachem et al were successful in developing *in vitro* methods to isolate and culture PaSCs from rat and human pancreata and study their physiological and pathological phenotypes (Apte et al., 1998; Bachem et al., 1998).

In normal physiological conditions, PaSCs are called quiescent PaSCs. These are rich in intracellular vitamin A lipid-droplets and identified by expression of intermediate filament proteins such as desmin and glial fibrillary acidic protein (GFAP). They do not express α-SMA (microfilament protein) (Erkan et al., 2012). PaSCs represents 4-7% of all parenchymal cells in the pancreas and are situated close to the basal aspect of acinar cells, appearing with a central cell body and long cytoplasmic projections lining along the base of adjacent acinar cells (Erkan et al., 2012). Quiescent PaSCs contribute to the maintenance of pancreatic architecture and play a role in ECM regulation, to contribute to the elasticity and tensile strength of pancreatic tissue by maintaining mechanical stability of the basement membrane (Erkan et al., 2012; Omary et al., 2007).

In pathological states in response to pancreatic injury, quiescent PaSCs become activated whereby they lose their stored fat droplet and express α-SMA (Bachem et al., 1998). Activated PaSCs have been reported to transdifferentiate into proliferating myofibroblast-like cells and secrete ECM proteins including fibronectin, collagen I, collagen III, growth factors such as platelet derived growth factor (PDGF), TGF-β, connective tissue growth factor (CTGF), IL-1 and IL-6, that also further perpetuate PaSC activation (Elsässerm et al., 1989; Apte et al., 1998, 1999; Bachem et al., 1998; Kuroda et al., 1998; Gabbiani, 2003; Erkan et al., 2012).

It has been proposed that PaSC activation is induced by cytokines and growth factors produced by acinar cells, inflammatory cells, platelets and endothelial cells during pancreatic injury or inflammation (Vonlaufen et al., 2008; Masamune et al., 2009; Masamune & Shimosegawa, 2009; Omary et al., 2007; Erkan et al., 2012). *In vivo* and *in vitro* studies have reported that injured acinar cells, ductal cells and leukocytes produce paracrine factors including TGF-β, TNF-α, IL-1, IL-6 and activin A, ethanol and its metabolites, that induce the activation of

PaSCs (Vonlaufen et al., 2008; Masamune et al., 2009; Masamune & Shimosegawa, 2009; Omary et al., 2007; Erkan et al., 2012). Also, hypoxia has been reported to activate PaSCs (Masamune et al., 2008). A recent *in vitro* study using isolated islets and primary PaSCs from rats, demonstrated that PaSCs activation within islets was induced by hypoxia (Kim et al., 2020). The study also showed that islet apoptosis increased when islets were cultured with conditioned medium from PaSCs cultured in hypoxia (1% O_2) (Kim et al., 2020). Additional rodent *in vitro* studies have demonstrated that co-culturing with activated PaSCs exhibited a direct impact on β-cell function by decreasing insulin secretion and inducing apoptosis (Kikuta et al., 2013; Zang et al., 2015; Zha et al., 2014).

Stellate cells isolated from mouse, rat and human islets using collagenase digestion, have been designated islet stellate cells (ISCs) and were reported as a sub-type of PaSCs, whereby they expand from within the islets rather than the islet periphery (Zha et al., 2014). A study undertaken by Li et al. (2016) proposed that an activated type of PaCS that is associated with islet dysfunction and fibrosis in pancreatitis is termed an islet stellate cell (ISC).

Compared to PaSCs, ISCs have been reported to contain less lipid-droplets, be easily activated by stimulators and exhibit a reduced proliferation and migration abilities (Wang et al., 2018). Other studies confirmed the presence of stellate cells in islets using single-cell transcriptome analysis (Lawlor et al., 2017; Li et al., 2016). Together, these studies proposed that ISCs could potentially be associated with islet fibrosis and impact on islet function. A study reported that islet malfunction was associated with loss of vitamin A during ISC activation (Zhou et al., 2019). ISCs have been proposed to be activated by the diabetic environment characterised by hyperglycaemia, oxidative stress, macrophage infiltration and elevated levels of inflammatory molecules including IL-1, IL-6, TNF-α, MCP-1 and MIP-1α (Zha et al., 2014; Zha et al., 2016).

A role for PaSCs as a potential mediator of pancreatic fibrosis has been postulated in the pathogenesis of chronic pancreatitis and pancreatic cancer (Omary et al., 2007). ISCs have been reported to be activated during diabetes (Yang et al., 2020). In pancreata of CF ferrets, activated PaSCs expressing α-SMA and desmin were reported compared to a quiescent state in wild-type CF ferrets (Sun et al., 2017). A study by Rotti et al., (2018) also reported the presence of activated PaSCs around the epithelium of dilated ducts in the CF ferrets. However, the role of activated PaSCs and ISCs in the development of islet fibrosis and β-cell dysfunction in CF remains incompletely understood.

Following the results obtained in Chapter 3, demonstrating the presence of peri- and intra-islet fibrosis as well as activated stellate cells expressing α-SMA within the CF tissue, this chapter focused on establishing an *in vitro* primary human ISC model. We hypothesised that this model could mimic the interplay between activated stellate cells and endocrine β-cells in CF and CFRD pancreata and could enable the assessment of β-cell function under the impact of proinflammatory molecules secreted due to the activation of ISCs in culture.

4.2 Aim

The studies reported in this chapter aimed to establish an *in vitro* primary human islet-derived stellate cell (ISC) model and examine the impact of its secretome on β-cell line viability and function.

- **Objective 1:** Confirm the establishment of activated ISCs in culture:

  1) Undertaking immunofluorescent staining for activated stellate cells markers
  2) Performing real-time quantitative reverse transcription-polymerase chain reaction (rtq-RT PCR) for genes associated with stellate cell activation.

- **Objective 2:** Examine ISC secretome for the presence of proinflammatory molecules, by performing a multiplex immunoassay to quantify proteins (Meso Scale Discovery (MSD) and COL1A1 ELISA.

- **Objective 3:** Investigate the impact of ISC secretome on (rat) INS-1E cell viability, insulin transcription and genes associated with stimulus-secretion coupling.

- **Objective 4:** Investigate the impact of ISC secretome on (human) EndoC-βH1 cell function assessed by glucose-stimulated insulin secretion assay and insulin / pro-insulin content.

4.3 Results

4.3.1 Establishment of human ISCs in primary culture

Islets were isolated from 6 separate human pancreas organ donors none of whom had diagnosed diabetes (Chapter 2 ***Table 2.5***). Isolated islets were resuspended in media, seeded at a density of 200 IEQ/well in adherent tissue culture plates and cultured for up to 7-days (Chapter 2 **2.2.2**). Light microscopic phase contrast images of cultured isolated islets were captured over this period ***(Figure 4.3)***. On Day 0, islets in suspension appeared to be regular in shape with well-identified edges ***(Figure 4.3 A)***. On Day 1, islets started to adhere to the bottom of the culture plate ***(Figure 4.3 B)*** and islets on Day 3 demonstrated the presence of cells growing from the edges of the islets, which continued to proliferate and expand through Day 5 and Day 7, to form a confluent monolayer of cells ***(Figure 4.3 C-E)***. These cells were bipolar in shape exhibiting a more fibroblast-like morphology and therefore were suspected to be stellate cells emanating from the adherent islets.

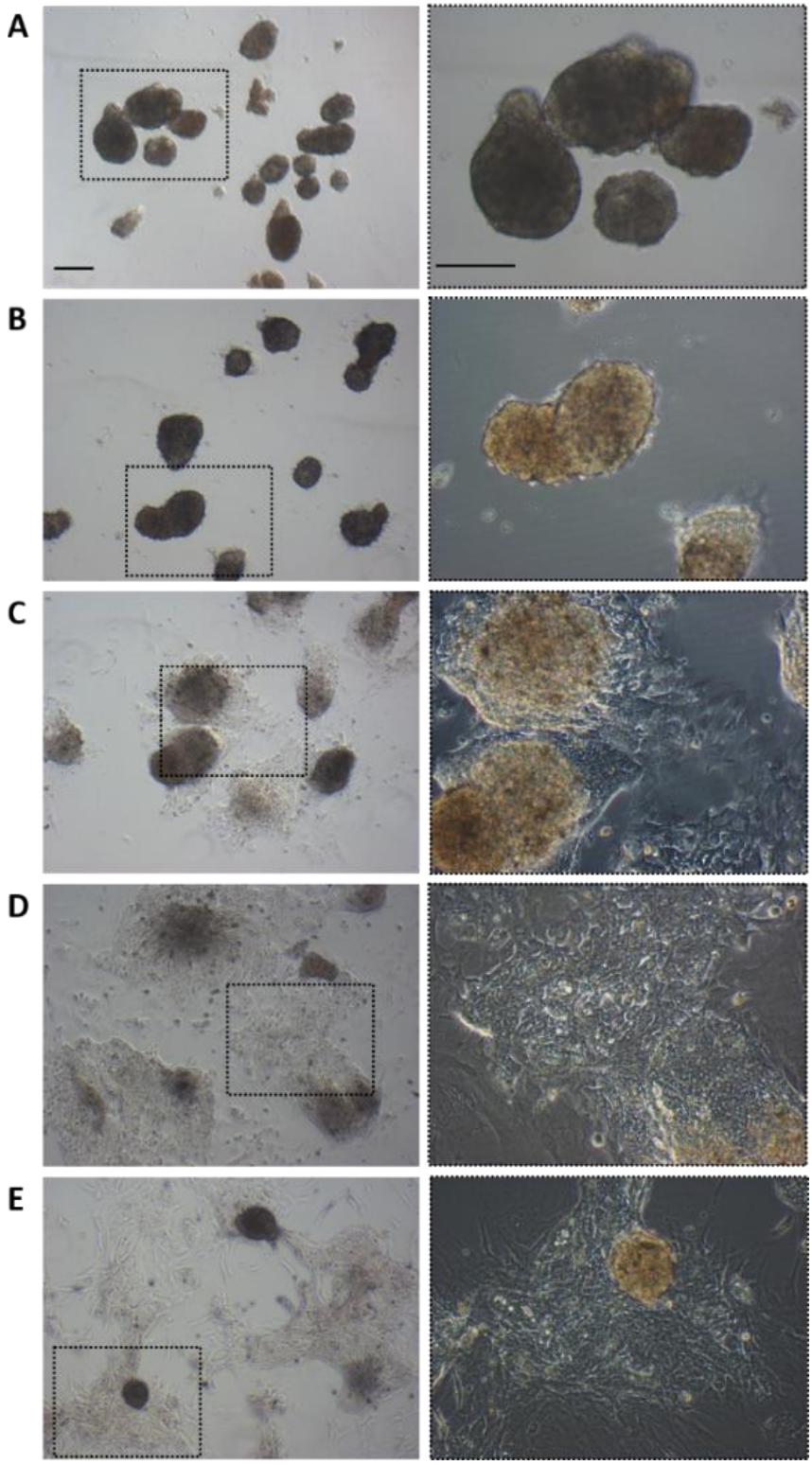

Figure 4.3: Representative light microscopic images of the ISC model using isolated islets from a 38-year-old male control donor (LDIS355) during the selected culture time points.

Pictures show the ISC model on Day 0 ***(A)****, Day 1* ***(B)****, Day 3* ***(C)****, Day 5* ***(D)*** *and Day 7* ***(E)****. Scale bars: 300 µm and 600 µm. Scale bars in panel A images represent the rest of the figures of the corresponding column.*

4.3.1.1 Presence of stellate cells confirmed by vimentin^{+} and α-SMA^{+} IF staining

To primarily investigate the phenotype of the progressively outgrown proliferating cells from the edges of the islets, immunofluorescence staining of isolated, formalin fixed, paraffin-embedded sectioned Day 0 islets was performed (Chapter 2 **2.2.7.1**) with the fibroblast marker vimentin alongside insulin and glucagon staining ***(Figure 4.4 A)***. Day 0 islets showed positive staining for insulin, glucagon and vimentin. Vimentin staining appeared as elongated or circular positive staining within islets with no co-localisation with insulin or glucagon. To confirm the specificity of the staining for insulin, glucagon and vimentin of Day 0 islets, 0.05% FBS in PBS alone was used as negative primary antibody control ***(Figure 4.4 B).***

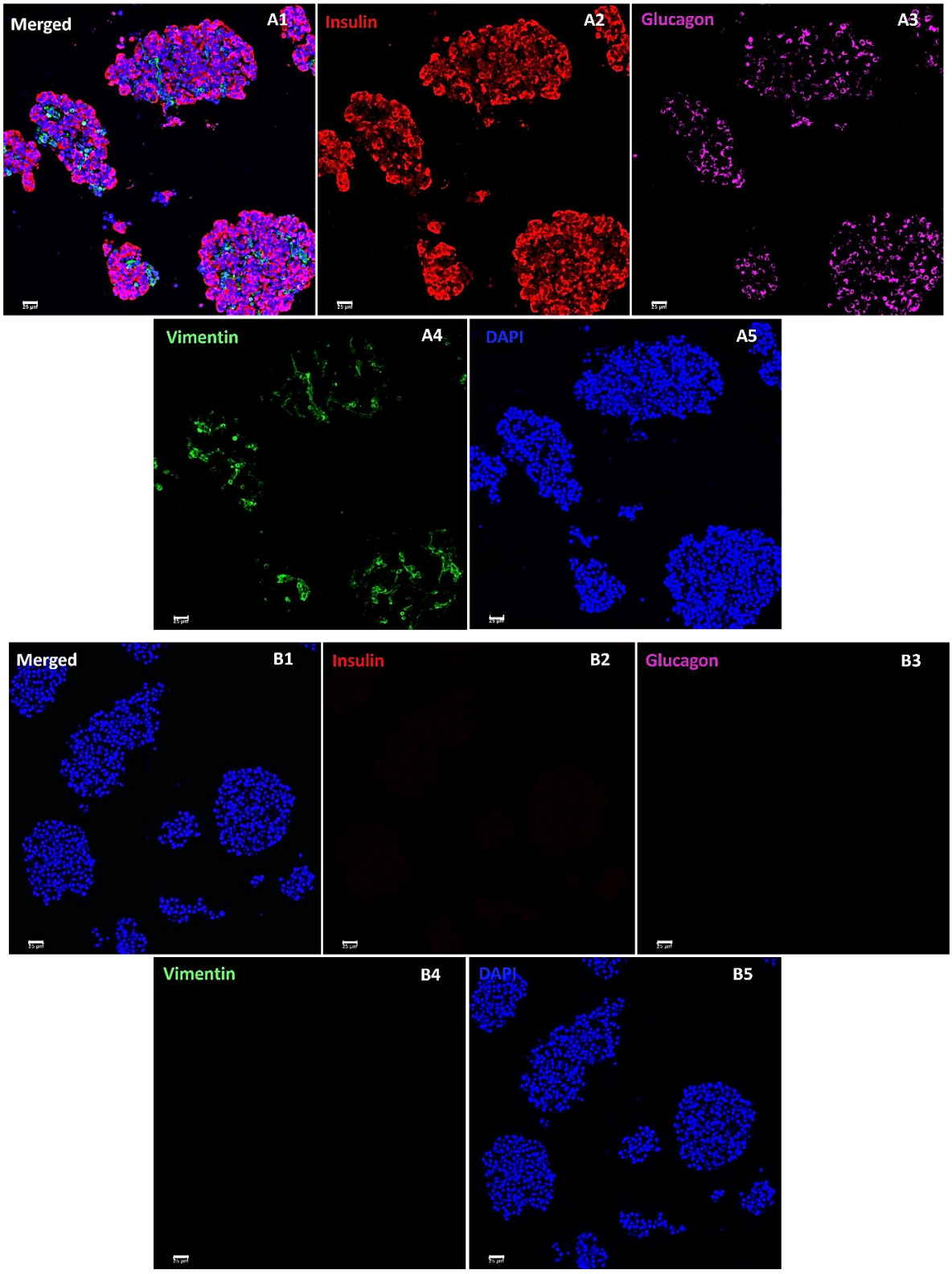

Figure 4.4: Representative immunofluorescence staining of Day 0 formalin fixed and paraffin-embedded islets from a pancreas donor without diabetes (LDIS335). Islets stained for insulin (red), glucagon (purple), vimentin (green) and DAPI (blue).

(A1-A5) *Primary antibody stains.* ***(B1-B5)*** *No primary antibody control stains. Representative of studies undertaken in three separate donors. Scale bars 25 µm.*

Insulin, glucagon and vimentin staining was undertaken following formalin fixation in ISCs over 7 days' culture in adherent culture plates as described in Chapter 2 (**2.2.7.2**). At Day 1, fixed cells exhibited positive staining for insulin, glucagon and vimentin ***(Figure 4.5 A2-4,*** respectively***)*** in keeping with the presence of mesenchymal cells within islets. The vimentin^{+} staining was also observed in the out-grown proliferating cells around islets at Day 3, Day 5 and Day 7 showing spindle like cytoskeleton appearance ***(Figure 4.5 B4-D4***, respectively***)***. Over time in primary culture, intensity of insulin and glucagon staining diminished and vimentin^{+} proliferating cells did not express insulin or glucagon ***(Figure 4.5 B2-D2*** *and* ***B3-D3)***. No primary antibody controls for insulin, glucagon and vimentin of Days 1, 3, 5 and 7, confirmed the specificity of antibody stains ***(Figure 4.6)***.

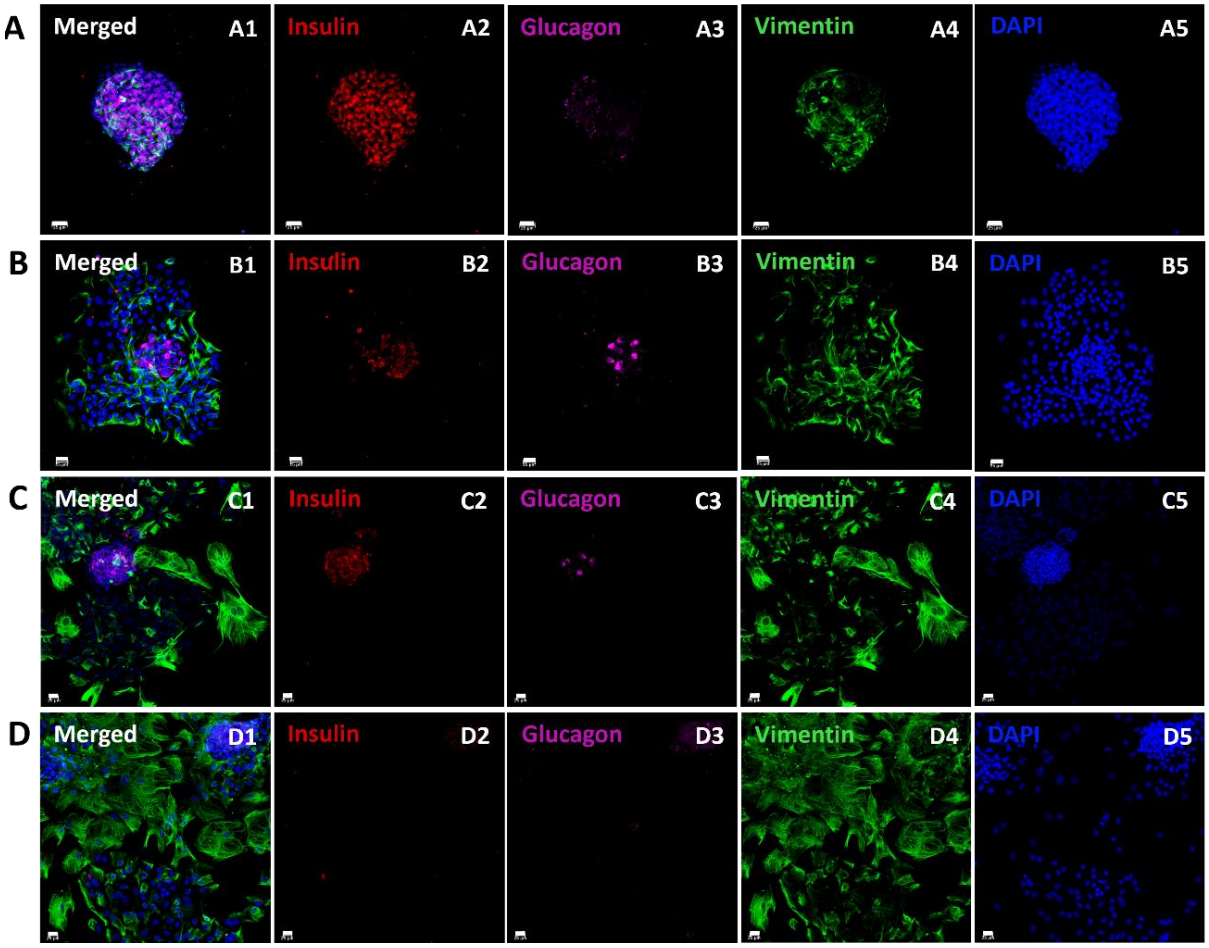

Figure 4.5: Representative immunofluorescence staining of isolated, cultured and formalin fixed islets from a pancreas donor without diabetes (LDIS335).

Islet culturing period: Day 1 ***(A)****, Day 3* ***(B)****, Day 5* ***(C)*** *and Day 7* ***(D)****. Islets stained with primary antibodies: insulin in column 2 (red), glucagon in column 3 (purple), vimentin in column 4 (green) and DAPI in column 5 (blue). Merged images are shown in column 1. Representative of studies undertaken in three separate donors. Scale bars 25 µm.*

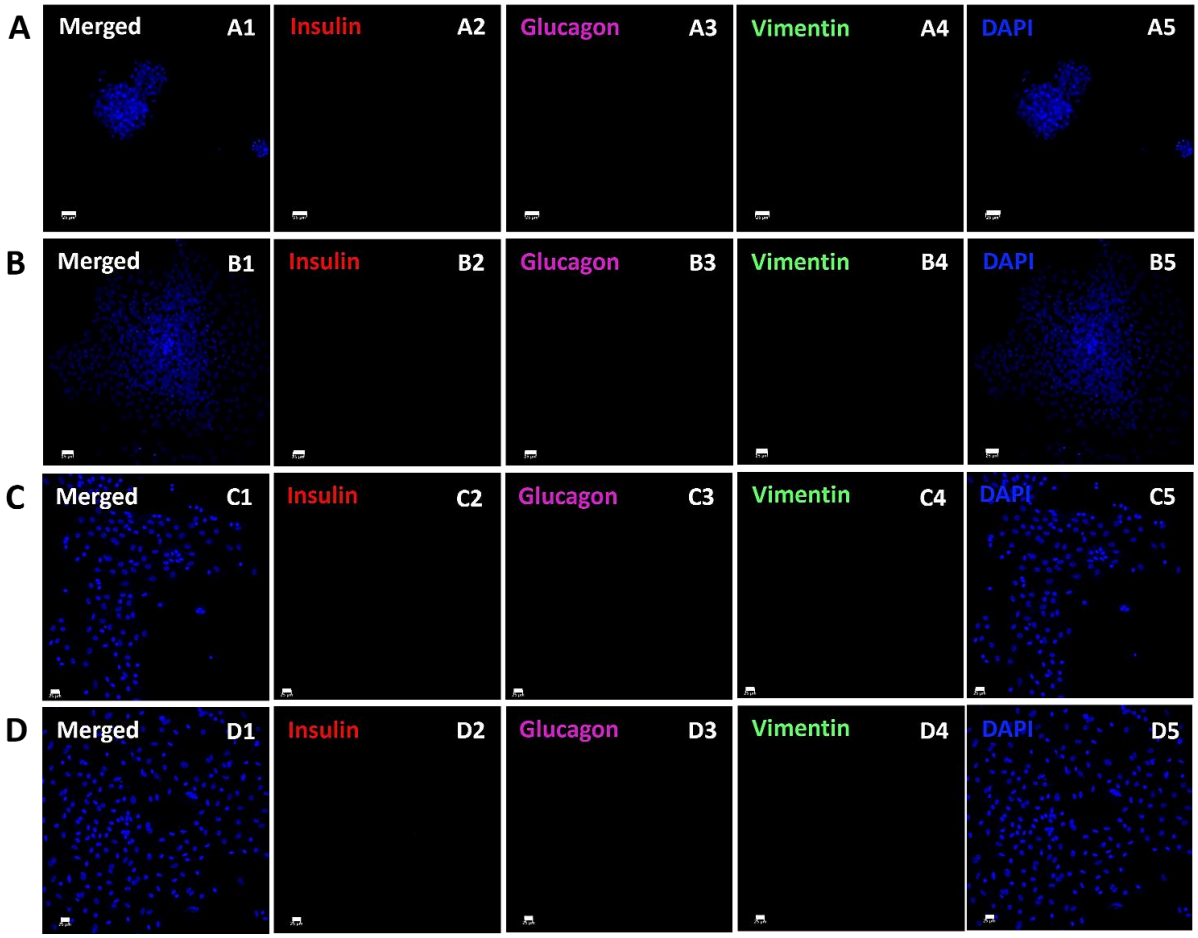

Figure 4.6: Representative no primary antibody immunofluorescence staining of isolated, cultured and fixed islets from a pancreas donor without diabetes (LDIS335).

*Islet culturing period: Day 1 (**A**), Day 3 (**B**), Day 5 (**C**) and Day 7 (**D**). Insulin in column 2 (red), glucagon in column 3 (purple), vimentin in column 4 (green) and DAPI in column 5 (blue). Merged images are shown in column 1. Representative of studies undertaken in three separate donors. Scale bars 25 µm.*

To further confirm the nature of vimentin^{+} cells within islets and the out-growing fibroblast-like cells ***(Figure 4.4 A*** and ***Figure 4.5)***, staining for α-SMA, a stellate cell activation and myofibroblast marker, was conducted. Positive staining for insulin and glucagon was observed in ***Figure 4.7 A2*** *and* ***A3.*** Interestingly, before culturing the islets, these paraffin-embedded Day 0 islets of the non-diabetic donors illustrated a positive staining for α-SMA which appeared to stain islet vasculature without co-localisation with endocrine hormones insulin or glucagon ***(Figure 4.7 A4*** *and* ***A5)***. To confirm the specificity of the staining for insulin, glucagon and α-SMA of Day 0 islets, 0.05% FBS in PBS alone was used as negative primary antibody control ***(Figure 4.7 B)***.

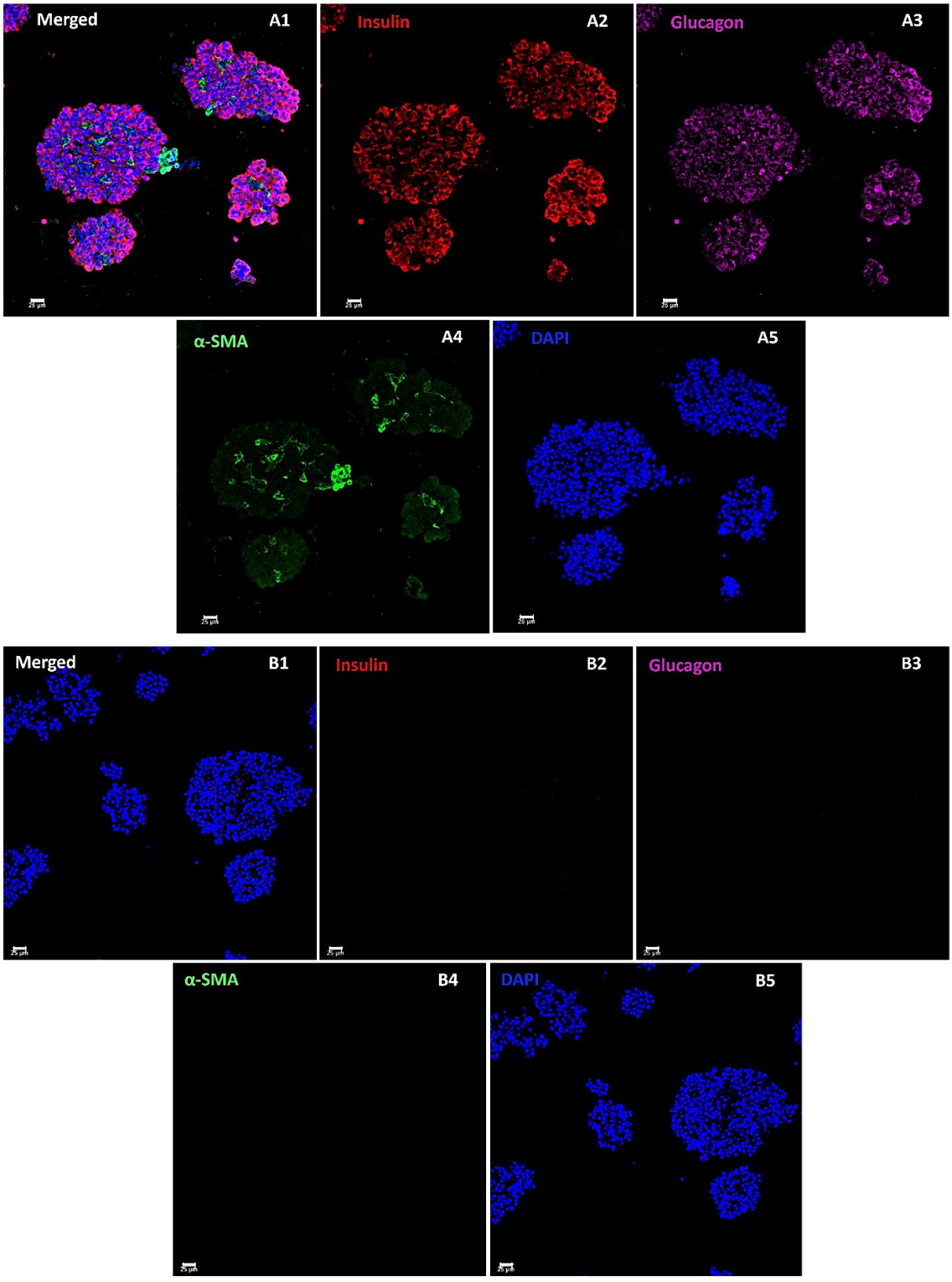

Figure 4.7: Representative immunofluorescence staining of Day 0 formalin fixed and paraffin-embedded islets from a pancreas donor without diabetes (LDIS335). Islets stained for insulin (red), glucagon (purple), α-SMA (green) and DAPI (blue).

(A1-A5) *Primary antibody stains.* ***(B1-B5)*** *No primary antibody control stains. Representative of studies undertaken in three separate donors. Scale bars 25 µm.*

Similarly, staining for insulin, glucagon and α-SMA in the cultured and formalin-fixed ISCs over 7 days' culture in adherent culture plates as described in Chapter 2 (**2.2.7.2**). ***Figure 4.8 A2*** and ***A3*** illustrated positive staining of Day 1 islets for insulin and glucagon. Alpha-SMA positive staining was also observed suggesting the presence of mesenchymal cells within islets (***Figure 4.8 A4*)**. Out-grown proliferating cells around islets of Day 3, Day 5 and Day 7 showed positive staining for α-SMA with a spindle-like morphology ***(Figure 4.8 B4-D4***, respectively***)***. These cells were insulin and glucagon negative ***(Figure 4.8 B2-D2*** *and* ***Figure 4.8 B3-D3****,* respectively***)***. This suggested that these out-grown cells from the edges of islets that are positive for both vimentin and α-SMA can be identified as ISCs. No primary antibody controls for insulin, glucagon and α-SMA Days 1, 3, 5 and 7, confirmed the specificity of antibody stains ***(Figure 4.9)***.

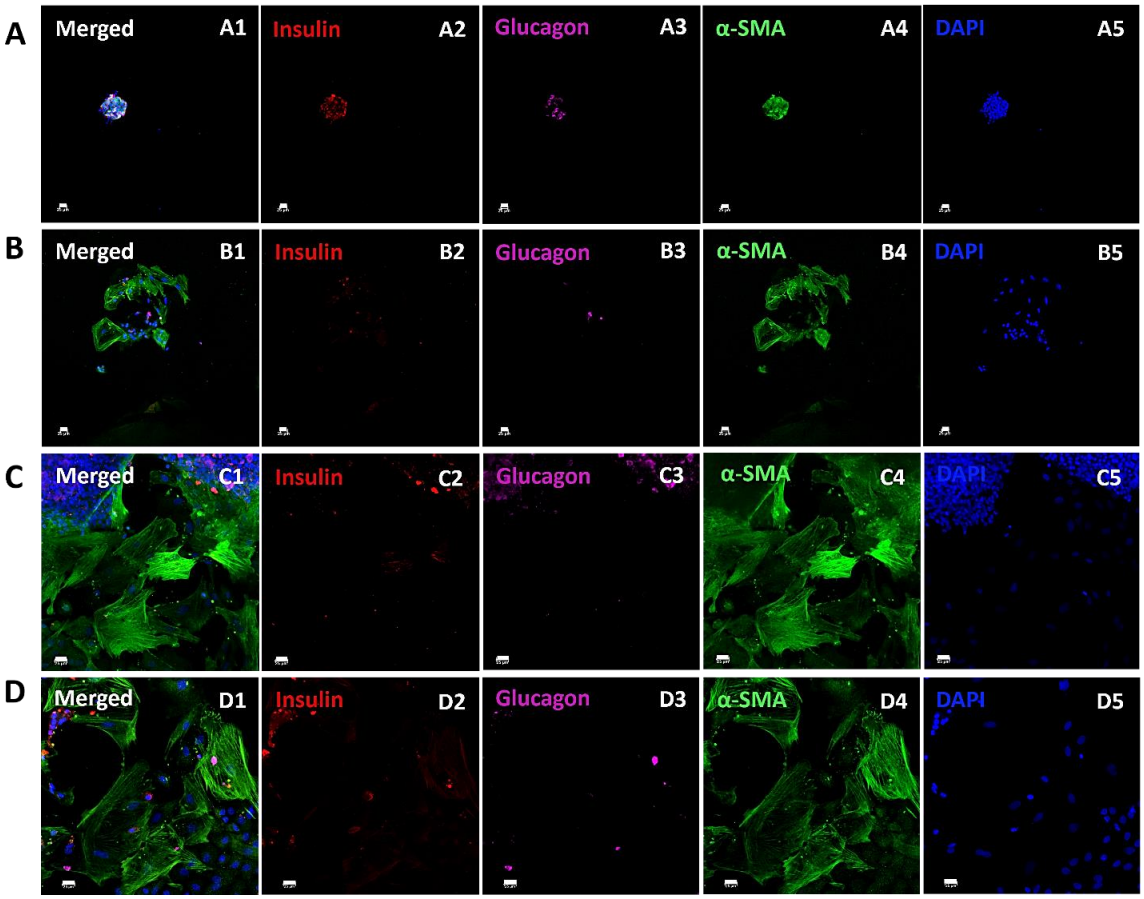

Figure 4.8: Representative immunofluorescence staining of isolated, cultured and formalin fixed islets from a pancreas donor without diabetes (LDIS335).

*Islet culturing period: Day 1 (**A**), Day 3 (**B**), Day 5 (**C**) and Day 7 (**D**). Islets stained for primary antibodies: insulin in column 2 (red), glucagon in column 3 (purple), α-SMA in column 4 (green) and DAPI in column 5 (blue). Merged images are shown in column 1. Representative of studies undertaken in three separate donors. Scale bars 25 µm.*

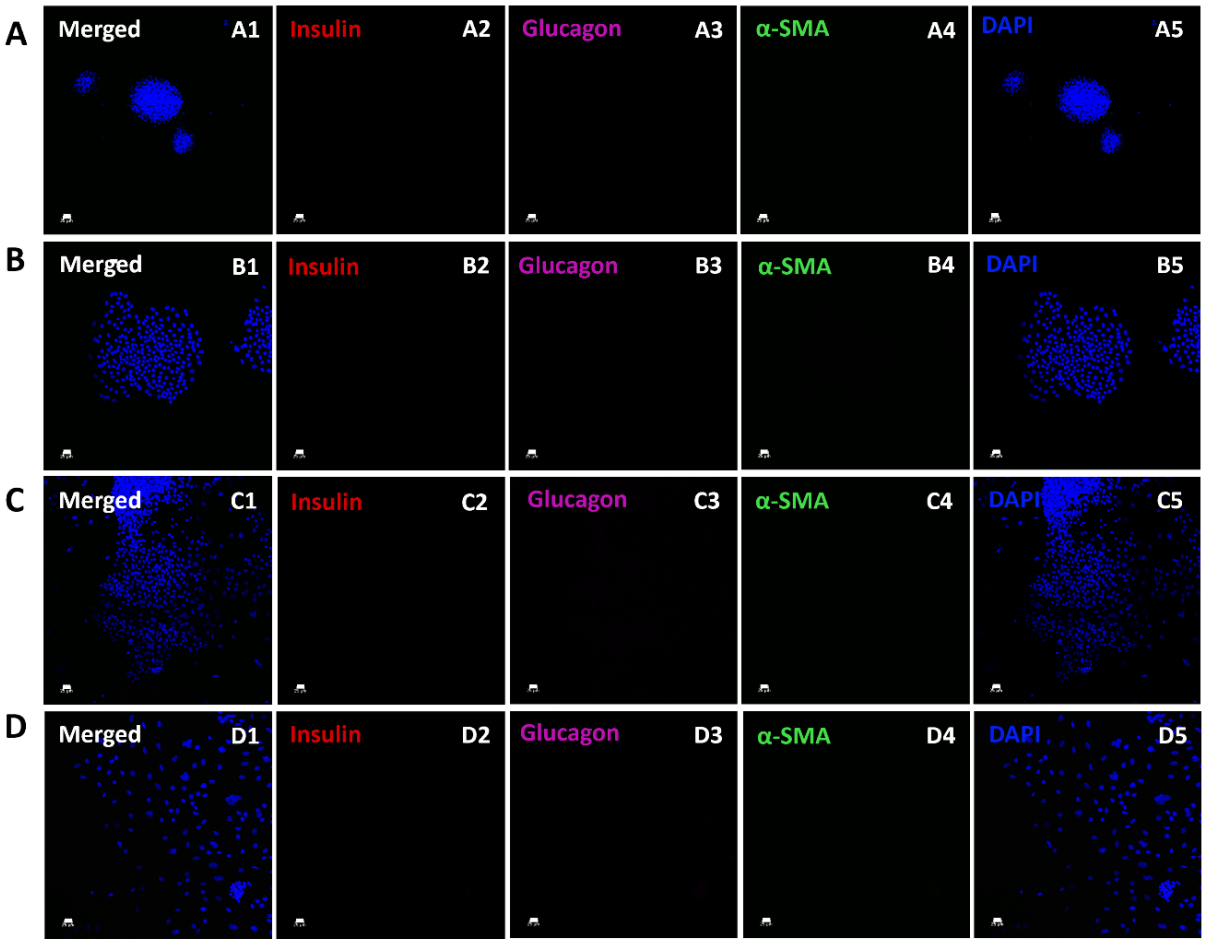

Figure 4.9: Representative no primary antibody immunofluorescence staining of isolated, cultured and fixed islets from a pancreas donor without diabetes (LDIS335).

*Islet culturing period: Day 1 (**A**), Day 3 (**B**), Day 5 (**C**) and Day 7 (**D**). Insulin in column 2 (red), glucagon in column 3 (purple), α-SMA in column 4 (green) and DAPI in column 5 (blue). Merged images are shown in column 1. Representative of studies undertaken in three separate donors. Scale bars 25 µm.*

4.3.1.2 Increase in the expression of genes associated with stellate cell identity and function

Further characterisation of the ISC model was undertaken via rtq-RT PCR gene analysis (Chapter 2 **2.2.5** and **2.2.6**) to investigate the expression of different markers associated with stellate cell activation and function. Across the culturing period of isolated islets from the donor LDIS355, ***Figure 4.10*** shows that there was a gradual increase in the expression of mesenchymal markers vimentin (*VIM*) and cadherin-11 (*CDH11*), which is also a cell surface marker associated with stellate cell activation and function. Increased expression over time in culture was also seen for other markers including the gene encoding smooth muscle alpha-actin (*ACTA2*) and the connective tissue gene collagen type 1 alpha (*COL1A1*) in keeping with stellate cell activation and function. This increase in gene expression was significant ($p < 0.05$)

on culture Day 5 and Day 7, when compared to Day 0 control, Day 1 and Day 3 samples. Gene expression at Day 7 was significantly higher ($p<0.05$) than at Day 5.

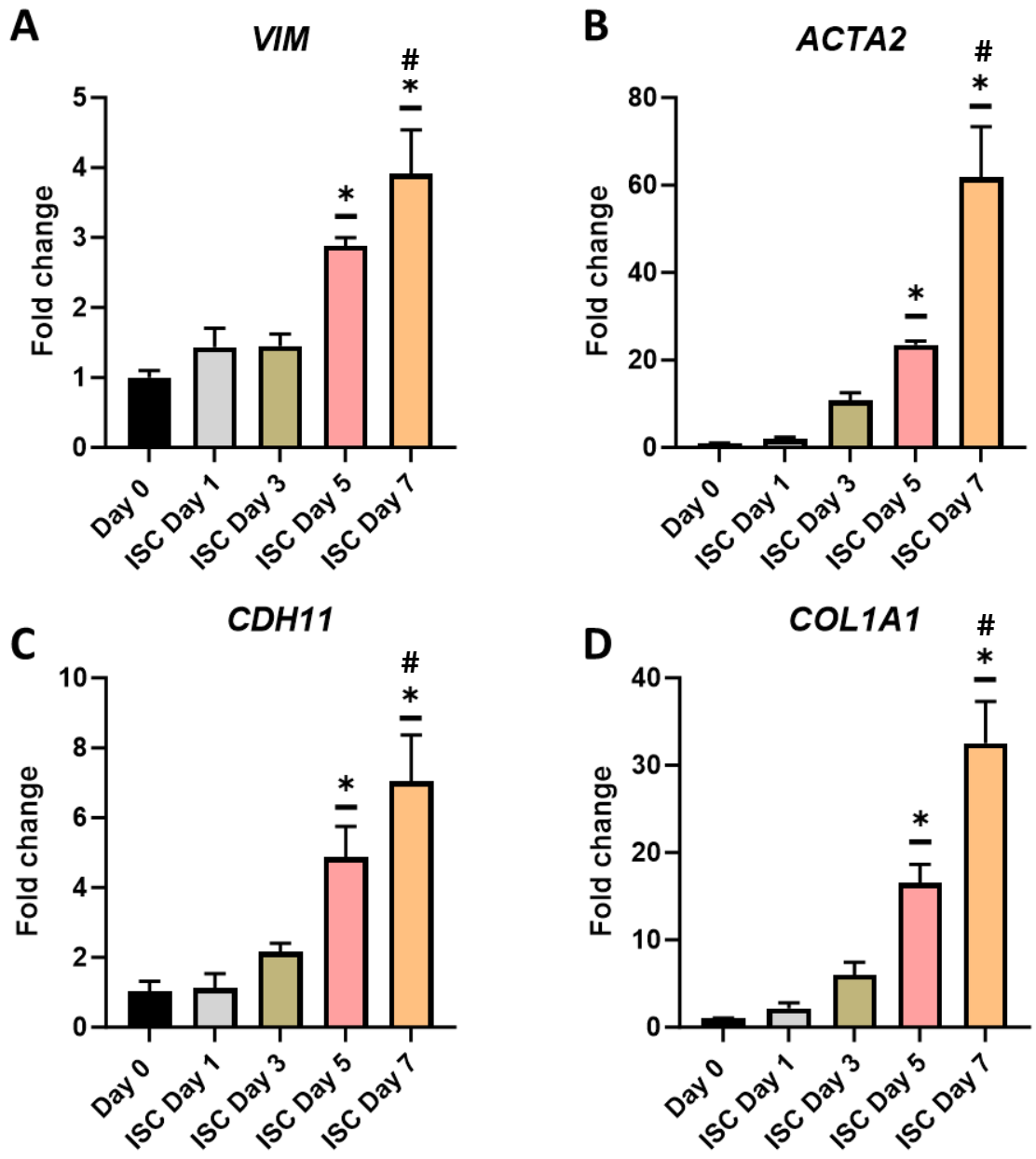

Figure 4.10: Representative rtq-RT PCR analysis of islets isolated and cultured from a 38-year-old male donor (LDIS355).

*Gene analysis was carried out for **(A)** mesenchymal gene vimentin (VIM), **(B)** smooth muscle alpha-actin gene (ACTA2), **(C)** cell surface and mesenchymal marker cadherin-11 (CDH11), and **(D)** a connective tissue gene collagen type 1 alpha 1 (COL1A1). Data are mean±SD data, n = 3 samples per condition. Gene expression presented as fold change was normalised to Day 0 control. A one-way ANOVA with a Tukey post hoc test was used. Significant difference is represented by $p < 0.05$ (**A**, **B**, **C** and **D**) ISC Day 5 and 7 vs Day 0, ISC Day 1 and 3 (*). (**A**, **B**, **C** and **D**) ISC Day 7 vs ISC Day 5 (#). Representative of studies undertaken in four separate donors.*

4.3.1.3 COL1A1 concentration increased gradually in the secretome samples of human ISC model

Stellate cells are known to mediate fibrosis by secreting COL1A1. Following on from increased COL1A1 gene expression ***(Figure 4.11)***, the concentration of COL1A1 protein secreted into the medium by the ISC model was determined by ELISA (Chapter 2 **2.2.8**). COL1A1 protein increased progressively in the secretome samples collected at Day 1, Day 3, Day 5, and Day 7 ISC culture ***(Figure 4.11)***. There was a significant increase in COL1A1 protein secretion (pg/ml) in Day 5 and Day 7 secretome samples of donor LDIS328 when compared to Day 1 and Day 3 ($p < 0.05$) ***(Figure 4.11 A)***. Combined analysis of ISC secretome collected from four different donors (LDIS328, LDIS335, LDIS353 and LDIS355) demonstrated COL1A1 secretion, presented as the average fold change calculated by normalising data of ISC secretion to Day 1***(Figure 4.11 B)***. This analysis confirmed that COL1A1 secretion in ISC model gradually increased from Day 1 with an average fold-change around 3, increasing further to around 10-fold by Day 7 ***(Figure 4.11 B).*** Day 5 COL1A1 secretion in the single donor study ***(Figure 4.11 A)*** was significantly higher than Day1 but significance was lost in the combined study ***(Figure 4.11 B)***. This could be due to biological variation in the individual donor-derived islet preparations used for ISC model. Hence, one representative study as well as the combined analysis were presented. These findings further supported successful establishment of a functional ISC model through demonstration of increased COL1A1 secretion in primary culture.

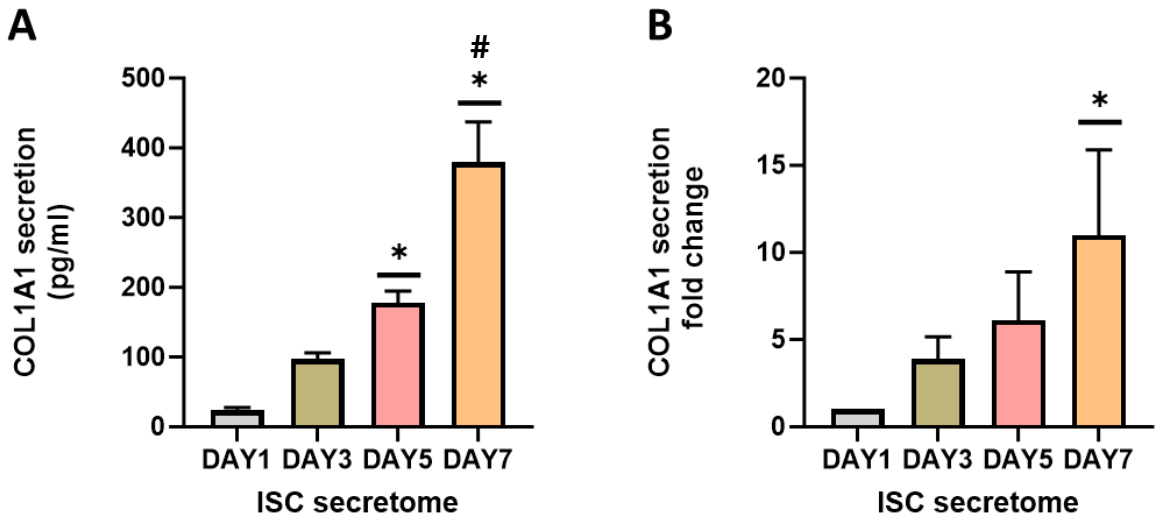

Figure 4.11: COL1A1 secretion in ISC model determined by sandwich ELISA.

(A) *Analysis for COL1A1 fold concentration in ISC secretome obtained from a single donor (LDIS328). Data represented as mean±SD for 3 experimental replicates.* ***(B)*** *A combined analysis for COL1A1 secretion fold-change in ISC secretome obtained from 4 donors (n = 4) (LDIS328, LDIS335, LDIS353 and LDIS355). Data represented as mean±SD for 3 experimental replicates. A one-way ANOVA with a Tukey post hoc test was used. $p < 0.05$ indicates the significant difference: Day 5 and Day 7 vs Day 1 and 3 (*), Day 7 vs Day 5 (#).*

4.3.1.4 MSD secretome analysis illustrated increase inflammatory molecule secretion during 7-day ISC culture

Following validation of the human ISC model through IF staining for vimentin and α-SMA, rtq-RT PCR gene analysis for mesenchymal and stellate cell markers, and quantification of secreted COL1A1 in ISC secretome. Further analysis of the secretome content, at the different time points in a single donor study, was conducted by Dr. Lee Borthwick using a multiplex biomarker assay (MSD) based on a selected fibrosis-associated secreted peptides (Chapter 2 **2.2.8**). Changes in cytokine secretion across the culture period of ISC model of donor LDIS328 are shown in ***Figure 4.12***. Day 5 secretome demonstrated the highest concentration of TGF-β1, TGF-β2, IL-1β**,** IL-1Ra, IL-6**,** IL-8 ***(Figure 4.12 A-F).*** Secreted TNF-α increased gradually and was slightly higher in Day 7 compared to Day 5 ***(Figure 4.12 G)***.

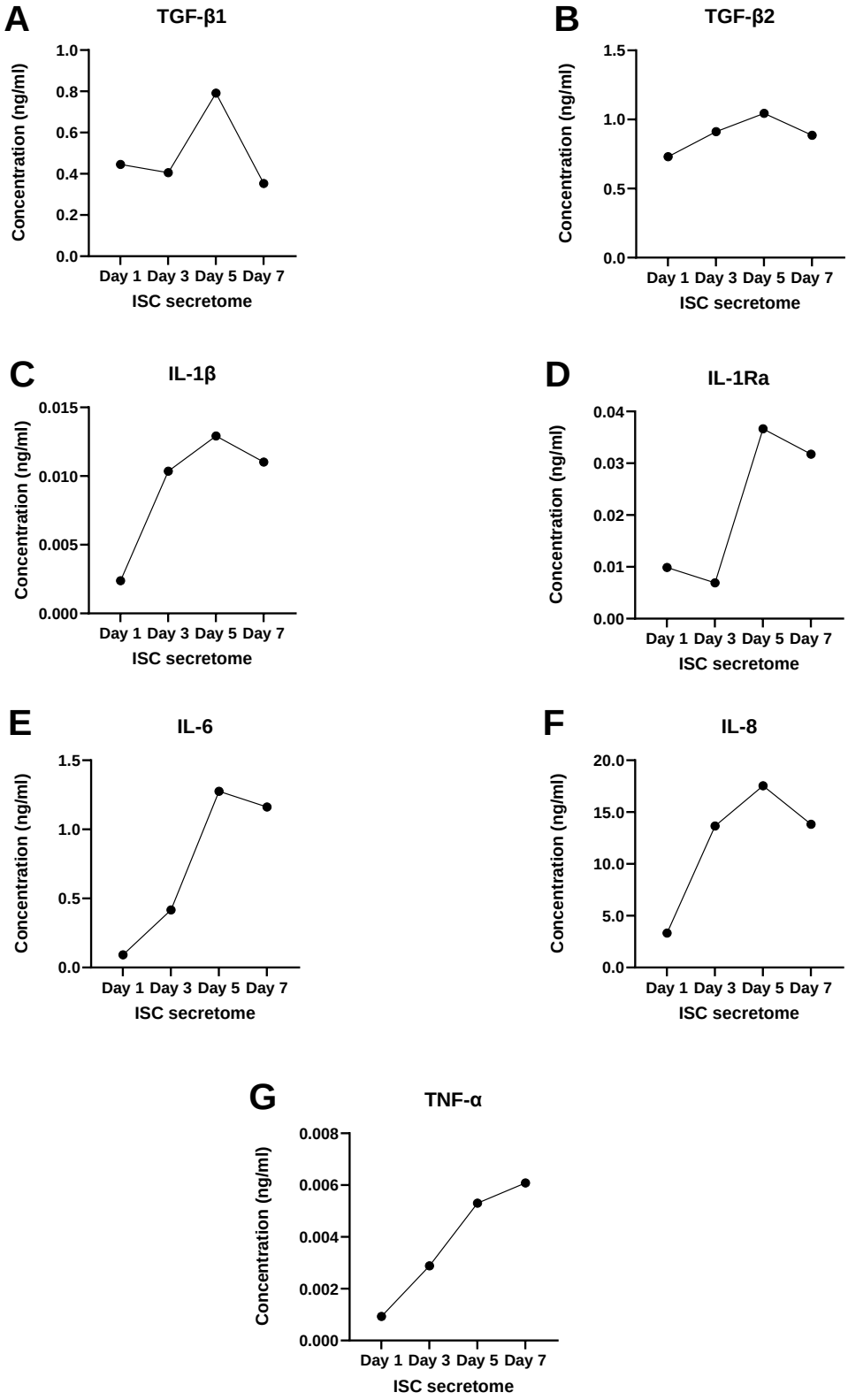

Figure 4.12: An increase in cytokines concentration (ng/ml) found in in ISC secretome of LDIS328 ISC model across the culture period.

(A) *TGF- β1,* ***(B)*** *TGF- β2,* ***(C)*** *IL-1β,* ***(D)*** *IL-1Ra,* ***(E)*** *IL-6,* ***(F)*** *IL-8,* ***(G)*** *TNF-α.*

MSD analysis also provided an overview of some chemokine subfamilies such as the CXC family (C-X-C motif chemokine) consisting of different chemokines including CXCL-1 (CXC ligand 1), CXCL-10 (CXC ligand 10), CXCL-12 (CXC ligand 12) and the CC (C-C motif chemokine) family including CCL-2 (CC ligand 2), CCL-4 (CC ligand 4) and MIP-1α (macrophage inflammatory protein-1α). These chemokines are known for their roles in inflammation and were shown to be present in elevated concentrations in ISC secretome across the culture period of ISCs from the LDIS328 donor ***(Figure 4.13)***.

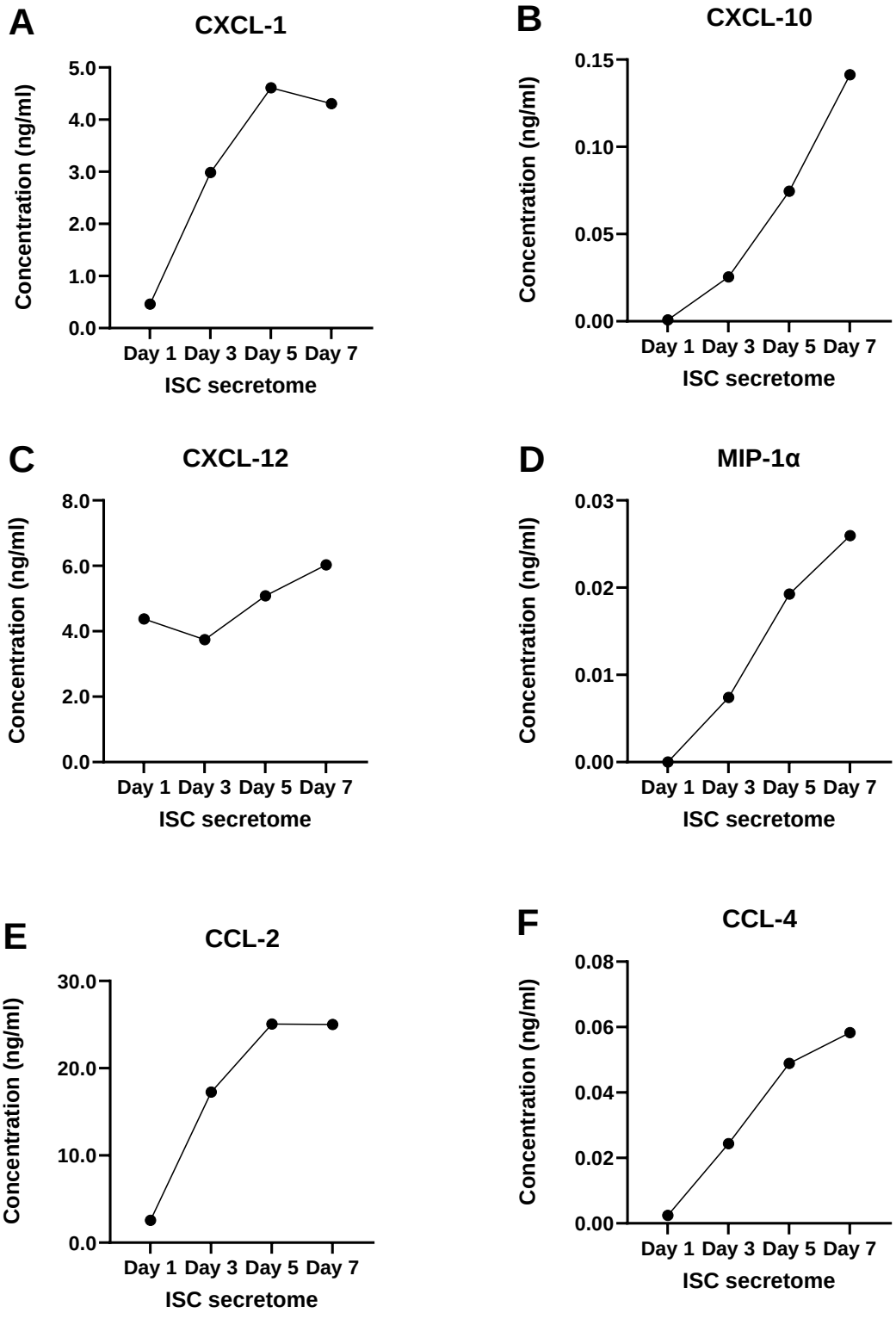

Figure 4.13: MDS derived data of chemokine (ng/ml) found in in ISC secretome of LDIS328 ISC model.

*C-X-C motif chemokine **(A)** CXCL-1: CXC ligand 1, **(B)** CXCL-10: CXC ligand 10, **(C)** CXCL-12: CXC ligand 12, **(D)** MIP-1α: macrophage inflammatory protein-1α, **(E)** CCL-2: C-C motif chemokine ligand 2 and **(F)** CCL-4: CC ligand 4.*

YKL-40 also known as chitinase-3-like protein 1 (CHI3L1) and TARC (thymus and activation-regulated chemokine) are chemokines associated with inflammation. MSD data of ISC secretome of LDIS328 ISC model shown in ***(Figure 4.14)***, demonstrated that both chemokines concentrations elevation across the culture period of ISCs. Secreted YKL-40 was the highest in Day 7 (~ 0.25 ng/ml) comparred to Day 1, 3 and 5 secretome ***(Figure 4.14 A)***. Whereas, Day 5 secretome illustrated the highest TARC concentration (~ 3.4 ng/ml) compared to Day 1, 3 and 7 ***(Figure 4.14 B)***.

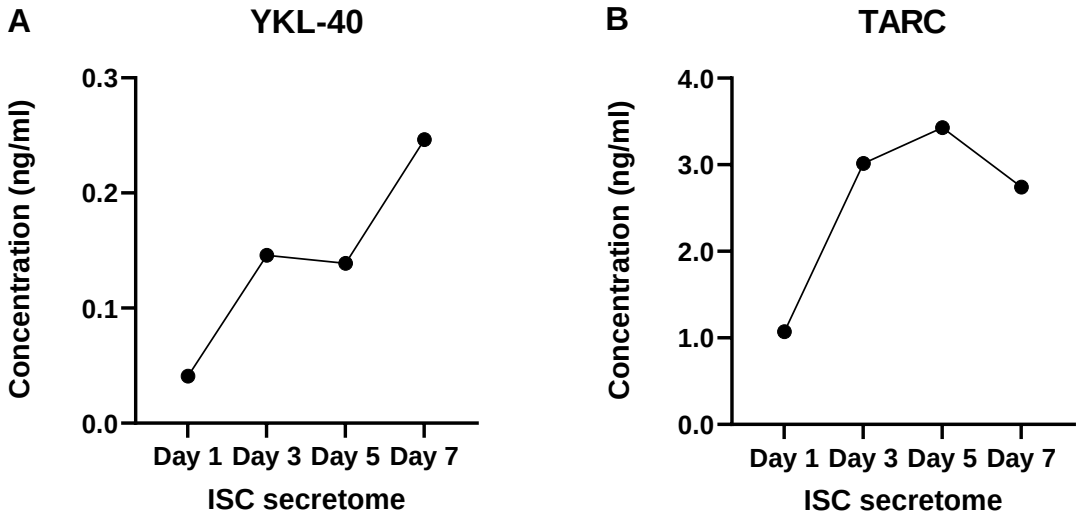

Figure 4.14: MSD-derived data of inflammation-associated biomarkers in ISC secretome (LDIS328).

(A) *YKL-40: also known as chitinase-3-like protein 1 and* ***(B)*** *TARC: thymus and activation-regulated chemokine.*

An overview of the hormonal secretions within the secretome was also provided by MSD data. Secreted proinsulin concentration in ISC secretome was similar at Day 1, 3 and 5 (~ 0.36- 0.43 pmol/L) and appeared to increase at Day 7 (0.86 pmol/L) ***(Figure 4.15 A)***. Insulin secretion was similar across culture days (~ 8.6 pmol/L) ***(Figure 4.15 B)***. Glucagon secretion appeared similar across culture days (~ 22.9-25 pmol/L) ***(Figure 4.15 C)***; whereas pancreatic polypeptide appeared to fall from Day 3 (~ 6.4 pmol/L) to Day 7 (~ 2.9 pmol/L) ***(Figure 4.15 D)***. Overall, hormonal secretion from cultured islets did not show drastic changes across the days of culture.

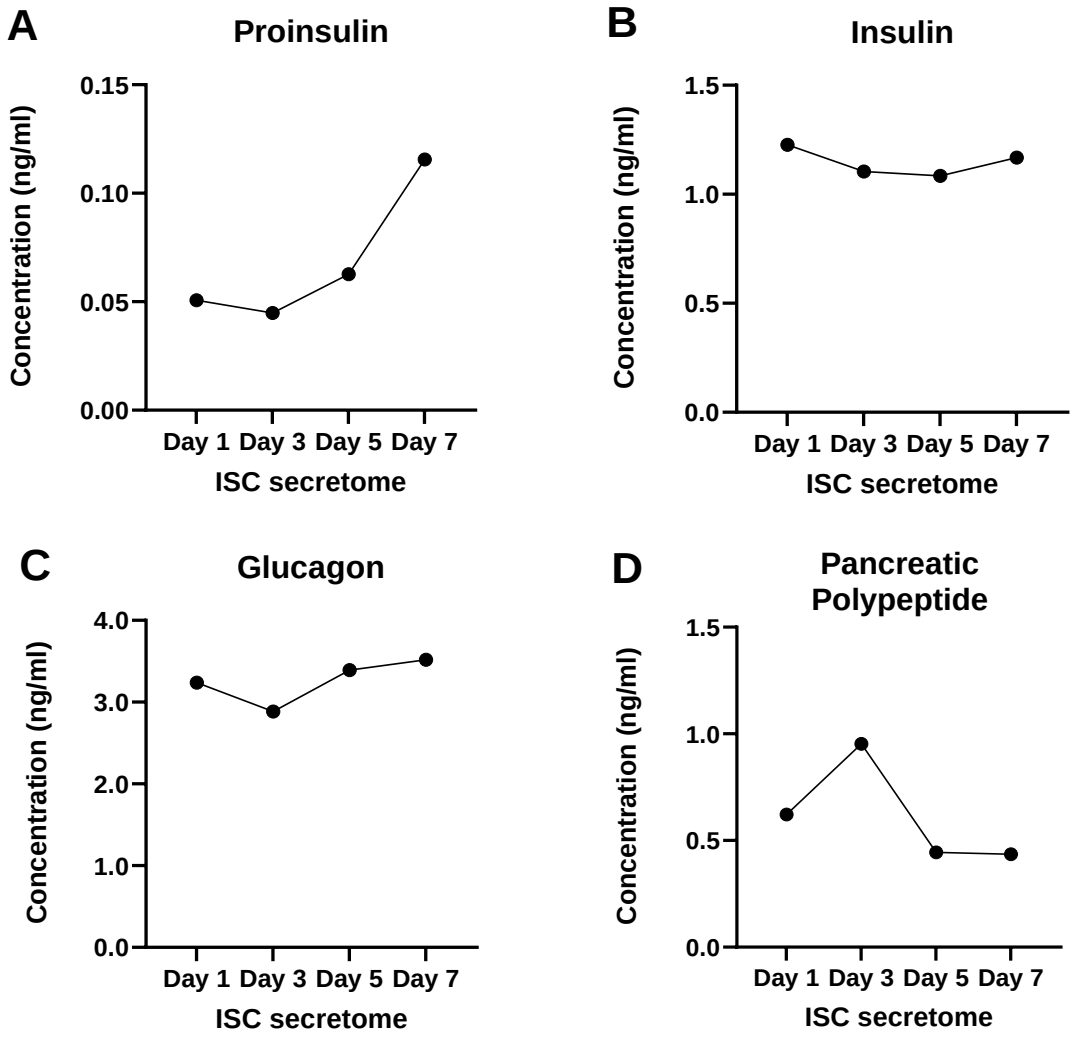

Figure 4.15: MDS derived hormonal concentrations (ng/ml) in the secretome of LDIS 328 ISC model. ***(A)*** *Proinsulin,* ***(B)*** *insulin,* ***(C)*** *glucagon and* ***(D)*** *polypeptide.*

4.3.2 Impact of ISC secretome on INS-1E viability and gene expression

4.3.2.1 24 h treatment with cytokines impacted significantly on INS-1E cell viability

In initial studies, the impact of cytokines on INS-1E viability was investigated. I tested different combinations of cytokine treatments (ng/ml) of different concentrations, as well as using chlorpromazine as a positive control for this experiment to investigate their impact in INS-1E cell viability. INS-1E cells at Passages 84-89 were plated on a 24-well plate and incubated overnight then treated with cytokine for 24 h, then an MTT assay was carried out (Chapter 2 **2.3.2** and **2.3.4**). A significant decrease ($p < 0.05$) in mean cell viability with all cytokine treatments (ng/ml) as well as chlorpromazine (200 µM) compared to control was seen ***Figure 4.16***. Cytokine treatments that showed the highest maintained viability compared to the rest of the treatments were Cytokine Mix 1: 1 ng/ml IL-1β, 20 ng/ml INF-γ, 10 ng/ml TNF-α, and Cytokine Mix 2: 1 ng/ml IL-1β, 20 ng/ml INF-γ, 50 ng/ml TNF-α. They illustrated a 70-80% mean viability relative to control.

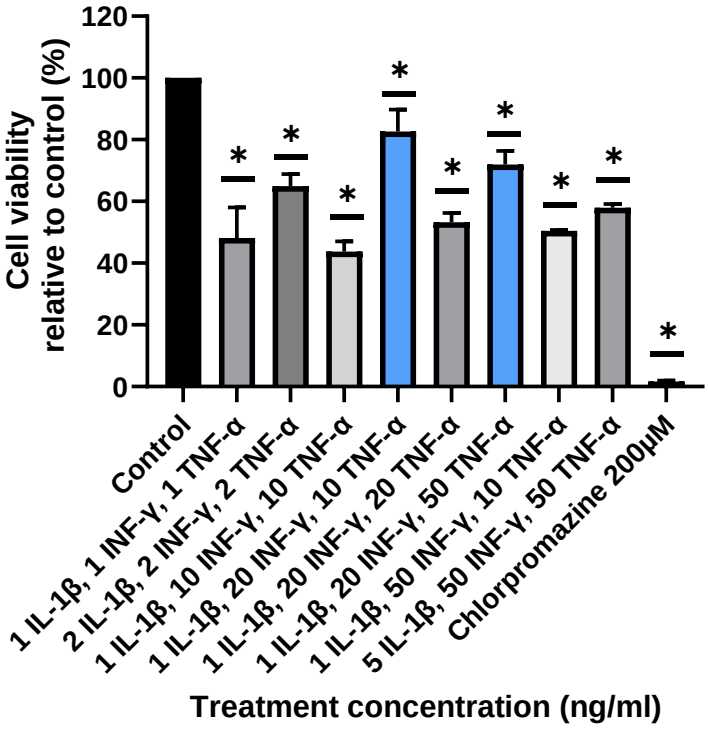

Figure 4.16: INS-1E mean cell viability relative to control (%) following a 24 h cytokine mix treatment (ng/ml) and a positive control treatment using chlorpromazine (200 µM).

Represented data are mean±SD (n = 3 wells per treatment). Blue bars represented the two cytokine mixtures with least impact on INS-1E viability. One-way ANOVA statistical test was carried out followed by a Tukey post hoc test. Significant difference is represented by $p < 0.05$, (*) indicates that treatments were statistically significant to control. Data presented of one single study (n = 1).

Consequently, these two mixtures of cytokines demonstrating an impact on INS-1E cell viability (~70-80%) without excess toxicity were further investigated as shown in ***Figure 10.17***. An individual study illustrated that both Cytokine Mixtures 1 and 2 impacted INS-1E cell viability significantly ($p < 0.05$) (25% and 75%, respectively) compared to control ***(Figure 10.17 A)***. Combined data from three independent biological studies illustrated in ***Figure 10.17 B*** showed Cytokine Mix 2 consistently led to mean cell viability of ~70% compared to the control. In contrast, Cytokine Mix 1 had a more significant and variable impact on INS-1E mean cell viability compared to the control (~45%). As a result, Cytokine Mix 2 (referred to as Cytokine Mix in following INS-1E studies) was favoured due to demonstrating lower and more consistent impact on cell viability making it a suitable positive control for further experiments. Both individual and combined studies are shown due to variability between studies observed following cytokine incubation.

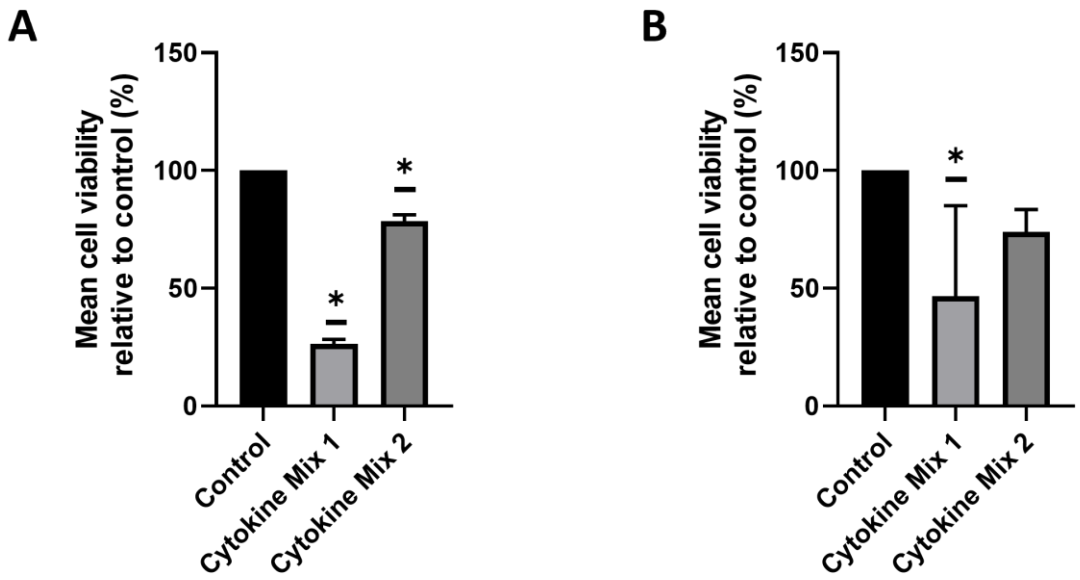

Figure 4.17: INS-1E mean cell viability relative to control (%) following a 24 h cytokine mix treatment (ng/ml). Cytokine Mix 1 (1 ng/ml IL-1β, 20 ng/ml INF-γ, 10 ng/ml TNF-α) and cytokine Mix 2 (1 ng/ml IL-1β, 20 ng/ml INF-γ, 50 ng/ml TNF-α).

*(**A**) One independent biological study (n = 1), (**B**) a combined study of three independent biological studies (N=3). Represented data illustrated mean±SD. One-way ANOVA statistical test was carried out followed by an LSD Fisher's post hoc test. Significant difference compared to control is represented by $p < 0.05$ (*).*

4.3.2.2 24 h treatment with RPMI media had no impact on INS-1E cell viability

ISC primary culture from three donors (LDIS326, LDIS328 and LDIS335) was set-up using RPMI media (#21875-034, Gibco, Thermo Fisher, Waltham, USA) as detailed in Chapter 2 **2.2.2,** addressed here as "ISC RPMI". Whereas, set-ups of ISC primary culture of three donors (LDIS354, LDIS355 and LDIS359) used the INS-1E RPMI medium (#R8758, Sigma-Aldrich, Missouri, USA) addressed here as "INS-1E RPMI". Prior to setting-up experiments assessing the impact of ISC secretome on INS-1E cells, it was essential to test the impact of ISC RPMI media on INS-1E cell viability first. This was carried out using an MTT assay as detailed in Chapter 2 **2.3.4**. Analysis of individual and three combined independent biological studies confirmed the absence of significant difference in INS-1E mean cell viability following 24 h incubation with INS-1E RPMI media alone, ISC RPMI media alone or a 1:1 mixture of these two media ***(Figure 4.18)***. The individual and combined studies were shown to illustrate the similarity in cell viability between studies.

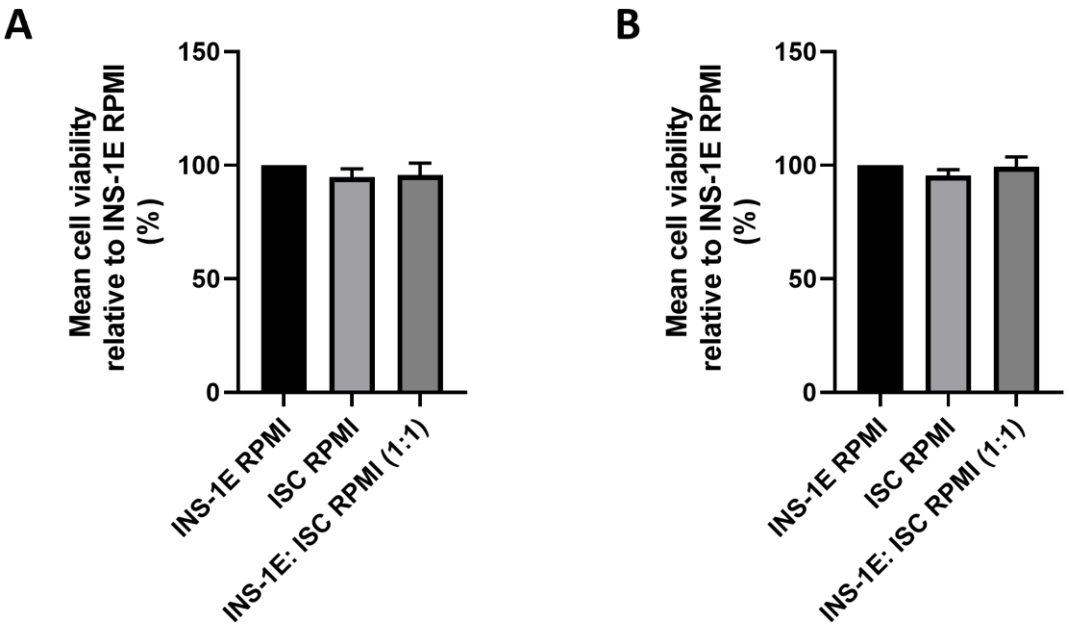

Figure 4.18: INS-1E mean cell viability relative to control (%) following a 24 h incubation with INS-1E RPMI media (#R8758, Sigma-Aldrich, Missouri, USA), ISC RPMI media (#21875-034, Gibco, Thermo Fisher, Waltham, USA) or a 1:1 dilution of both media.

*(**A**) One independent biological study (N=1), **B)** A combined analysis of three independent biological studies (N=3). Represented data illustrated mean±SD. One-way ANOVA statistical test was carried out followed by an LSD Fisher's post hoc test. No statistical significance difference between the treatments.*

4.3.2.3 24 h treatment with ISC secretome had no impact on INS-1E cell viability

To investigate the impact of ISC secretome (collected as detailed in Chapter 2 **2.3.3**) on INS-1E cell viability, cells were treated for 24 h with ISC secretome collected at Day 1, 3, 5 and 7 diluted in a 1:1 mixture with INS-1E RPMI media and a Cytokine Mix positive control (1 ng/ml IL-1β, 20 ng/ml INF-γ, 50 ng/ml TNF-α) (Chapter 2 **2.3.2**). Then an MTT assay was conducted (Chapter 2 **2.3.4**). MTT cell viability assay of individual ***(Figure 4.19 A)*** and combined three independent biological studies ***(Figure 4.19 B)*** illustrated the absence of a significant difference in INS-1E mean cell viability following the 24 h media treatments with ISC secretome, when compared to control (a 1:1 dilution of INS-1E RPMI: ISC RPMI). However, INS-1E cell viability treated with the Cytokine Mix was significantly reduced ($p < 0.05$) to ~60% mean cell viability compared to Control (1:1) ***(Figure 4.19)***. The individual and combined studies were shown to illustrate the similarity in cell viability between studies following ISC secretome and cytokine treatments.

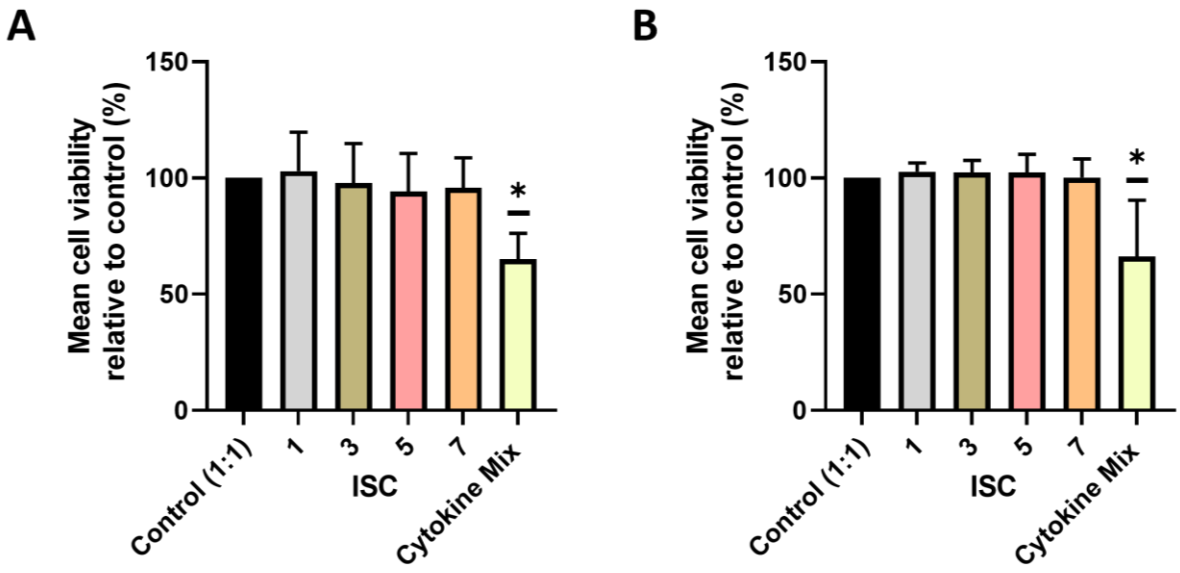

Figure 4.19: INS-1E mean cell viability relative to control (%) determined by an MTT assay following a 24 h treatment with ISC secretome Day 1, 3, 5, and 7 and a Cytokine Mix (1 IL-1β, 20 INF-γ, 50 TNF-α) ng/ml.

(A) *An independent biological study (n = 1),* ***(B)*** *a combined study of three independent biological studies (n = 3). Represented data illustrates mean±SD of 3 readings. One-way ANOVA statistical test was conducted followed by a Tukey post hoc test. Significant difference of (*) $p < 0.05$ compared to Control (1:1).*

4.3.2.4 rtq-RT PCR analysis illustrated no significant impact of ISC secretome on the expression of INS-1E function-related genes

To investigate the impact of ISC secretome on INS-1E genes associated with β-cell function, rtq-RT PCR gene expression analysis was carried out (Chapter 2 **2.3.3**) for the following genes: *Pdx1*, a key regulator of insulin gene expression, via regulating insulin expression and secretion; insulin associated genes *Ins1* and *Ins1*; *Slc2a2* gene that encodes for GLUT2, a glucose transporter, and *Slc30a8* which encodes for the zinc transporter ZnT8, that plays a key role in zinc homeostasis which is crucial for insulin secretion.

The three independent studies were presented due to variability observed in each study which could have arisen from the biological variability between ISC samples derived from separate human donor islet preparations. In one study, *Pdx1* expression was decreased in INS-1E cells treated with ISC secretome (donor LDIS335) with a significant decrease ($p < 0.05$) in ISC Day 7 sample compared to control (1:1) ***(Figure 4.20 A)***. *Ins1* and *Ins2* gene expression were significantly higher ($p < 0.05$) in INS-1E cells treated with ISC secretome compared to Control (1:1) ***(Figure 4.20 B*** and ***C)***. *Slc2a3* and *Slc30a8* gene expression was not significantly different in treated samples compared to Control (1:1), but a possible trend towards decreasing expression was observed in ISC secretome treated cells ***(Figure 4.20 D*** and ***E)***.

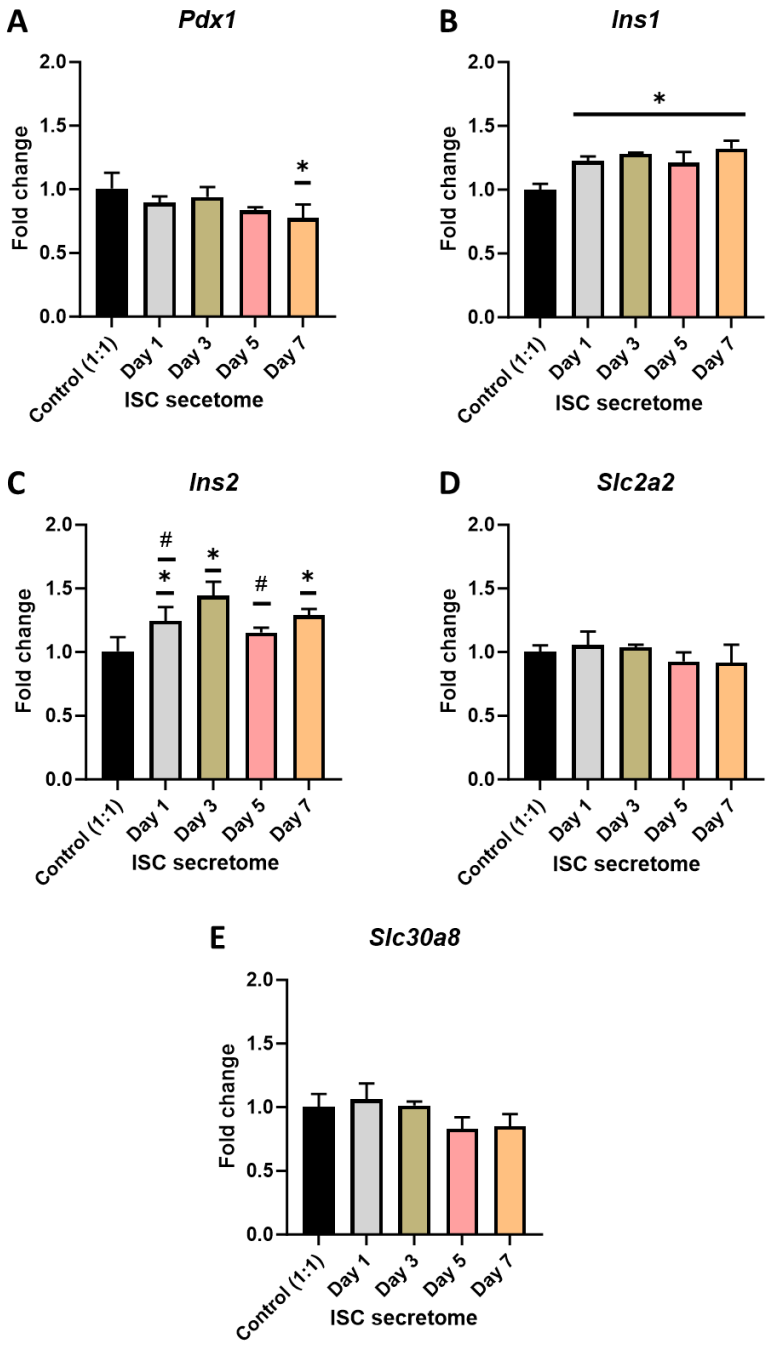

Figure 4.20: qRT-PCR analysis of INS-1E cells following a 24 h treatment with ISC secretome of Day 1, 3, 5 and 7 extracted from ISC model form a 53-year-old male donor LDIS335.

*Analysis was carried out for **(A)** β-cell transcription factor (Pdx1), (**B** and **C**) insulin associated genes (Ins1 and Ins2), **(D)** glucose transporter encoding gene (Slc2a2), **(E)** zinc transporter encoding gene (Slc30a8). Represented data illustrated as mean±SD obtained from three experimental samples. Control is a 1:1 dilution media. Gene expression presented by fold-change was normalised to control. One-way ANOVA statistical test followed by a Tukey post hoc test was conducted. Significant difference represented by (* or #), $p < 0.05$. **(A)** ISC Day 7 vs Control (1:1). **(B)** ISC Day 1, 3, 5 and 7 vs Control (1:1). **(C)** ISC Day 1, 3 and 7 vs Control represented by (*) and ISC Day 3 vs ISC Day 1 and 5 represented by (#). **(D** and E) Not significantly difference.*

rtq-RT PCR analysis of INS-1E cells treated with ISC secretome from a second donor (LDIS355), illustrated that *Pdx1* expression was not significantly different in INS-1E cells compared to control (1:1) ***(Figure 4.21 A)***. *Ins1* and *Ins2* gene expression appeared generally higher in INS-1E cells treated with ISC secretome with a significant increase ($p < 0.05$) of *Ins1* in ISC Day 7 sample and *Ins2* in ISC Day 1 and Day 3 samples compared to control ***(Figure 4.21 B*** and ***C)***. *Slc2a2* gene expression was not significantly different compared to control (***Figure 4.21 D)***. Whereas *Slc30a8* gene expression was significantly reduced in samples of ISC Day 3, 5 and 7 ***(Figure 4.21 E)***.

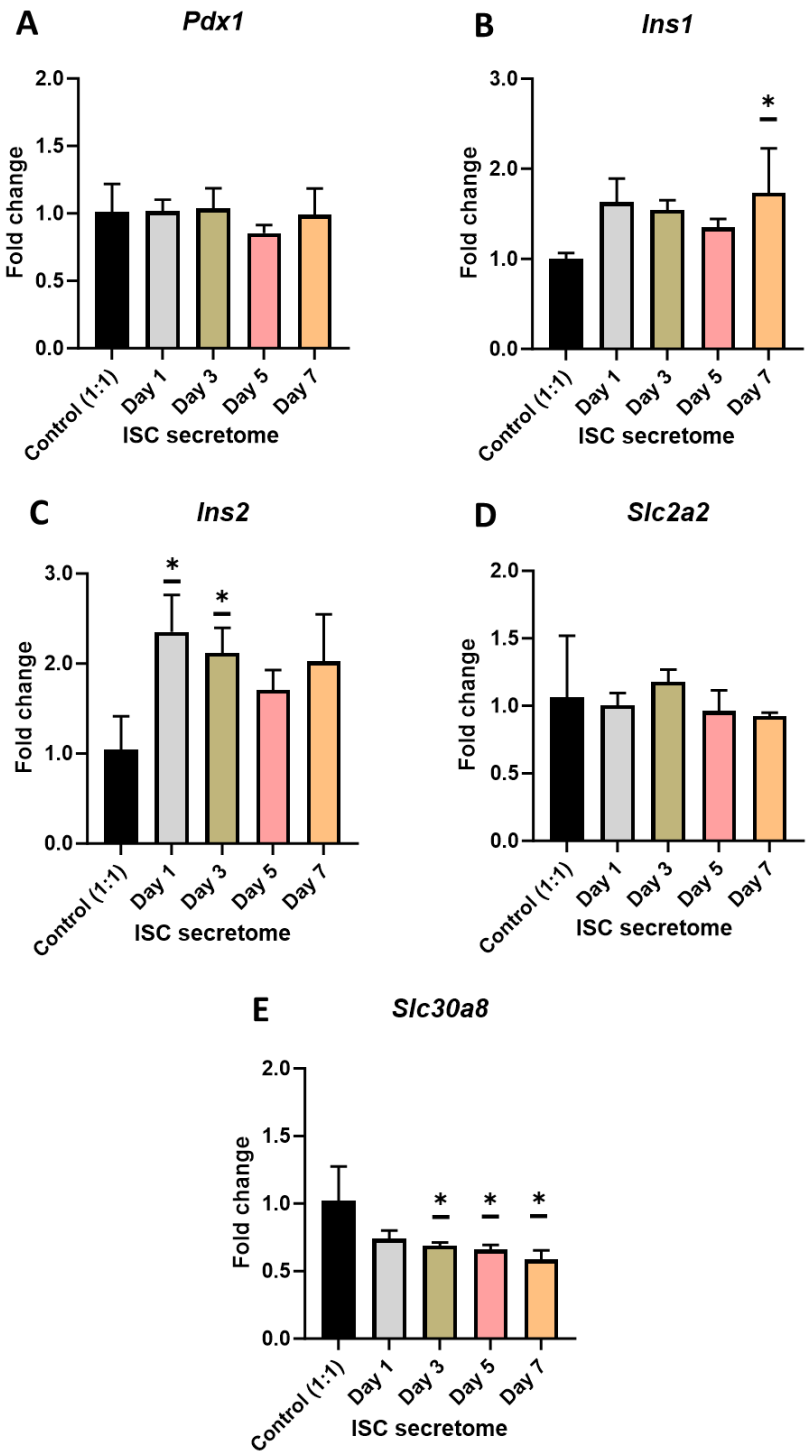

Figure 4.21: qRT-PCR analysis of INS-1E cells following a 24 h treatment with ISC secretome of Day 1, 3, 5 and 7 extracted from ISC model form a 38-year-old male donor LDIS355.

*Analysis was carried out for **(A)** β-cell transcription factor (Pdx1), (**B** and **C**) insulin associated genes (Ins1 and Ins2), **(D)** glucose transporter encoding gene (Slc2a2), **(E)** zinc transporter encoding gene (Slc30a8). 1:1 dilution media. Gene expression presented by fold-change was normalised to Control (1:1). One-way ANOVA statistical test followed by a Tukey post hoc test was conducted. Significant difference represented by (*), $p < 0.05$. (**A**) Not significantly different. (**B**) ISC Day 7 vs Control (1:1). (**C**) ISC Day 1 and 3 vs Control (1:1). (**D**) Not significantly different. (**E**) ISC Day 3, 5 and 7 vs Control (1:1).*

INS-1E gene expression data of rtq-RT PCR experiment carried out using LDIS328 ISC secretome was similar to Control (1:1), although statistical testing did show some degree of variation at specific time points ***Figure 4.22***.

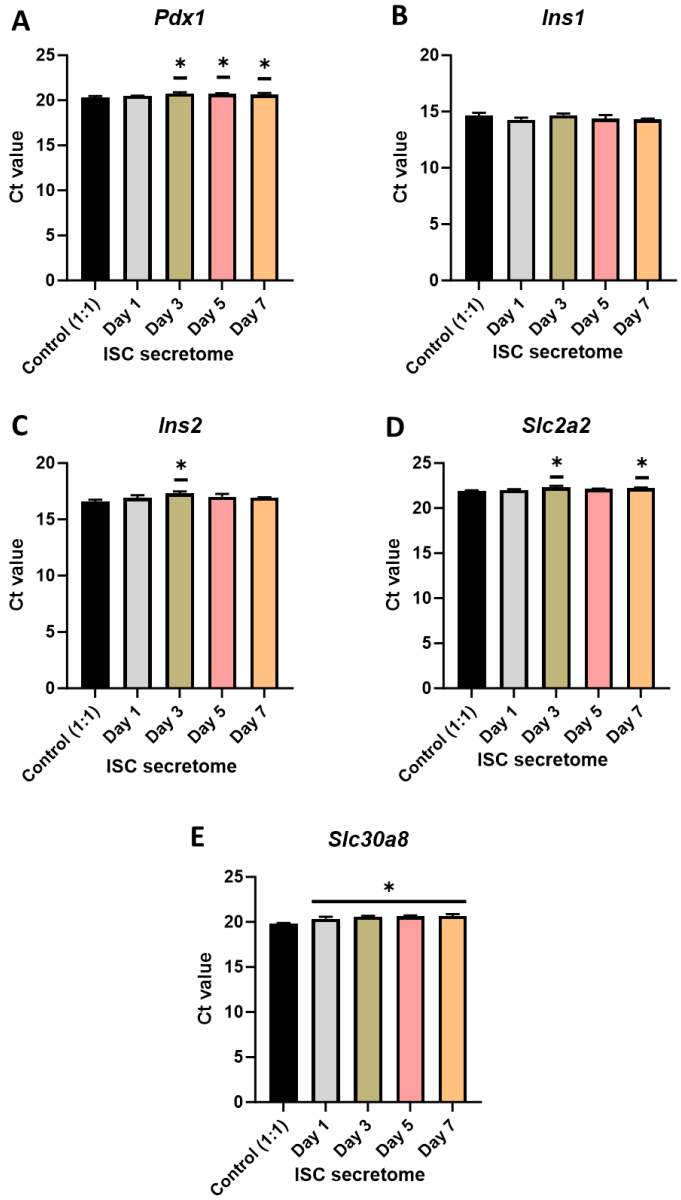

Figure 4.22: qRT-PCR analysis of INS-1E cells following a 24 h treatment with ISC secretome of Day 1, 3, 5 and 7 extracted from ISC model form a 53-year-old female donor LDIS328.

*Analysis was carried out for **(A)** β-cell transcription factor (Pdx1), (**B** and **C**) insulin associated genes (Ins1 and Ins2), **(D)** glucose transporter encoding gene (Slc2a2), **(E)** zinc transporter encoding gene (Slc30a8). Represented data illustrated as mean±SD data obtained from three experimental samples. Control is a 1:1 dilution media. Gene expression presented by ct values. One-way ANOVA statistical test followed by a Tukey post hoc test was conducted. Significant difference compared is represented by (*), $p < 0.05$. **(A)** ISC Day 3, 5 and 7 vs Control (1:1). **(B)** Not significantly different. **(C)** ISC Day 3 vs Control (1:1). **(D)** ISC Day 3 and 7 vs Control (1:1). **(E)** ISC Day 1, 3, 5 and 7 vs Control (1:1).*

Combined rtq-RT PCR data of donors LDIS335 and LDIS355 illustrated in ***Figure 4.23***, supported a possible increase in *Ins1* and *Ins2* and possible decrease in *Slc30a8* gene expression on incubation with ISC-conditioned medium with no consistent changes in expression of the other genes tested. Statistical analysis for the combined studies was not conducted as the rtq-RT PCR study of LDIS328 donor ***(Figure 4.22)*** could not be included.

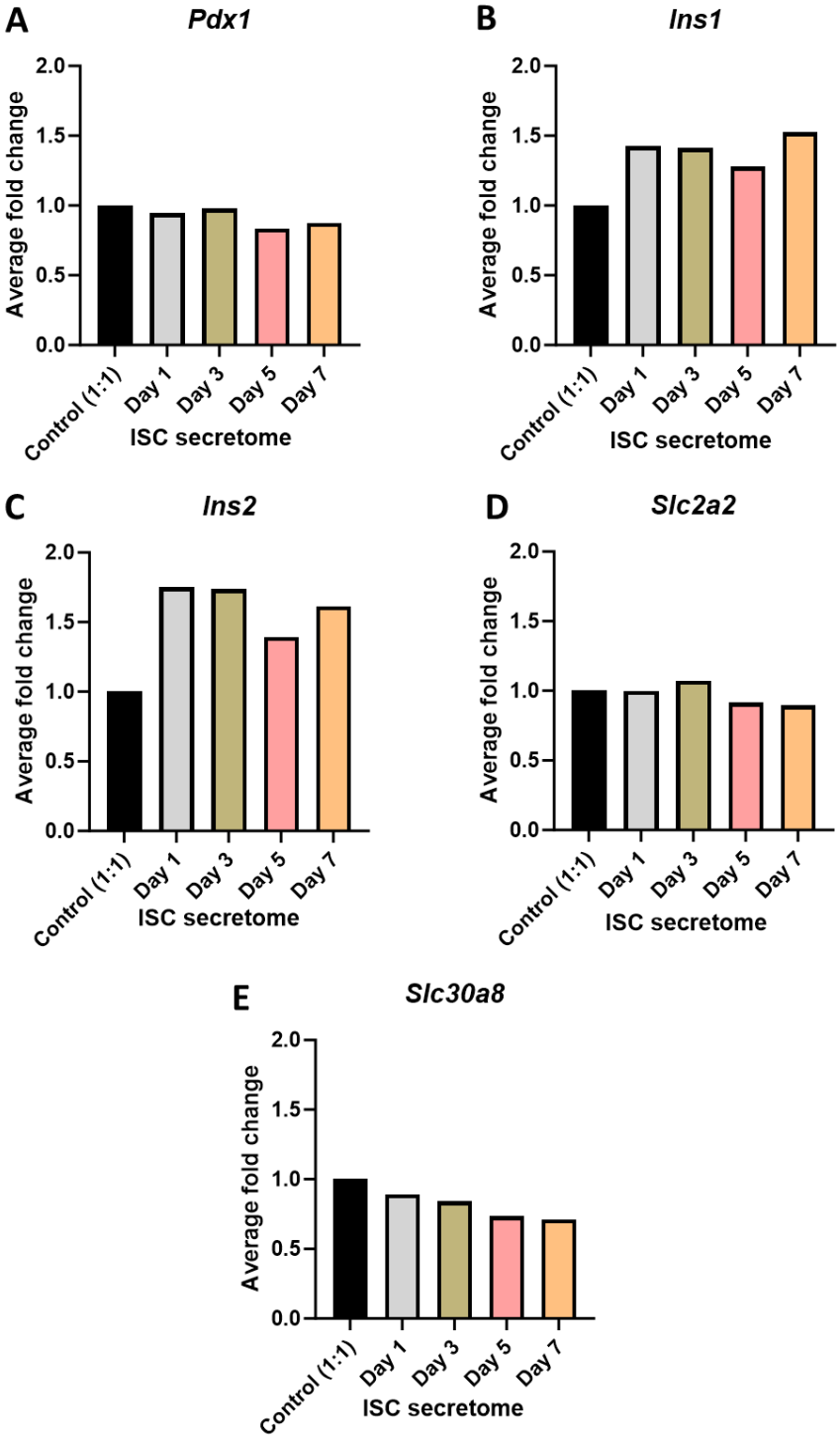

Figure 4.23: qRT-PCR analysis of INS-1E cells following a 24 h treatment with ISC secretome of Day 1, 3, 5 and 7 extracted from ISC model form two donors LDIS335 and LDIS355.

(A) *β-cell transcription factor (Pdx1),* ***(B*** *and* ***C)*** *insulin associated genes (Ins1 and Ins2),* ***(D)*** *glucose transporter encoding gene (Slc2a2),* ***(E)*** *zinc transporter encoding gene (Slc30a8). Gene expression presented by fold-change, which was normalised to Control (1:1). Represented data illustrated as the mean obtained from two independent biological studies. Statistical analysis was not applicable.*

4.3.3 Impact of ISC secretome on EndoC-βH1 cell viability and function

4.3.3.1 72 h treatment with ISC secretome decreases EndoC-βH1 cell viability

EndoC-βH1 cells were seeded at a density of 70,000 cells/well in a 96-well plate and incubated overnight at 37 °C. Then, a 72 h treatment with ISC secretome followed by an MTS assay experiment were conducted to investigate cell viability (Chapter 2 **2.3.5**, **2.3.6 - 2.3.11)**. Cell viability was presented as an optical density (mg^{-1}/well). EndoC-βH1 cell viability was assessed using MTS assay following a 72 h incubation with the control for the study consisting of 1:1 medium dilution (DMEM media: RPMI media) and a positive Cytokine Mix control, consisting of (1 ng/ml IL-1β, 20 ng/ml INF-γ, 20 ng/ml TNF-α), as previously published (Tsonkova et al., 2018). This cytokine mix concentration was not the same as the cytokine mix used to treat INS-1E. The individual study and the combined analyses of four independent biological studies illustrated the trend towards reduction in cell viability of EndoC-βH1 cells treated the Cytokine Mix but this reduction was not significant when compared to the control (1:1) ***(Figure 4.24)***.

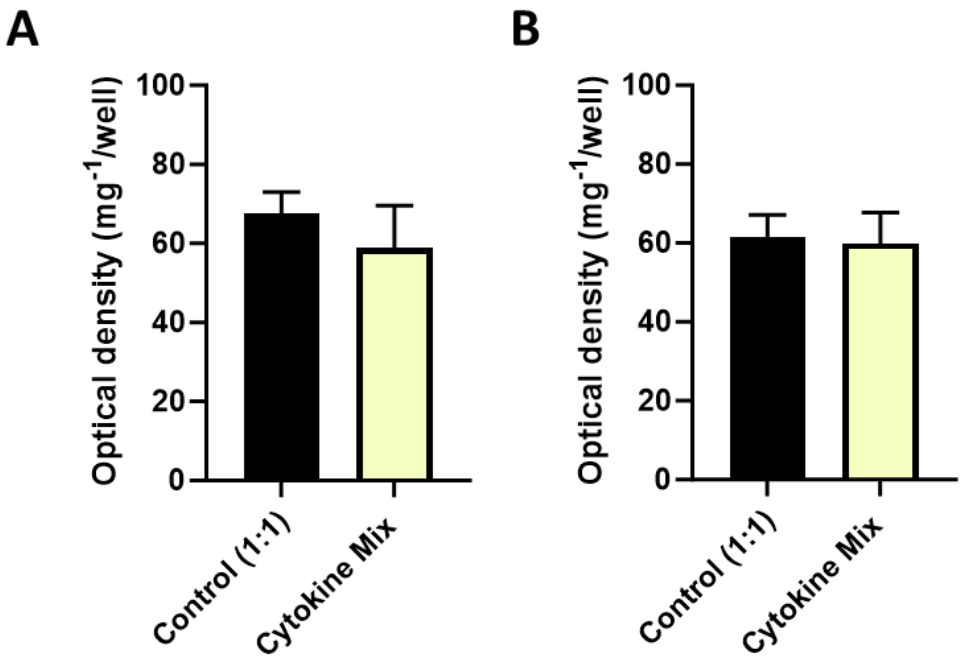

Figure 4.24: EndoC-βH1 cell viability determined by an MTS assay following a 72 h treatment with a Control 1:1 dilution (DMEM media: RPMI media) and a Cytokine Mix treatment (1 ng/ml IL-1β, 20 ng/ml INF-γ, 20 ng/ml TNF-α).

(A) *One independent biological study (n = 1),* ***B)*** *a combined study of four independent biological studies (n = 4). Represented data illustrated as mean±SD of four experimental samples. Statistical analyses were carried out using unpaired student's t test. No statistically significant difference was found.*

An individual study illustrated a decreased cell viability of EndoC-βH1 cells treated with LDIS335 ISC secretome of different days ***(Figure 4.25 A)***. This decrease in viability was significant ($p < 0.05$) in ISC Day 7 compared to Day 1 and Day 3. A combined analysis of the four individual studies illustrated a significant reduction ($p < 0.05$) in EndoC-βH1 cell viability treated with Day 7 ISC secretome compared to Day 3 ***(Figure 4.25 B)***. The individual and combined studies were shown to illustrate the significant reduction in cells viability presented by the optical density (mg-1/well) of EndoC-βH1 cells following ISC secretome treatment with Day 7 conditioned medium.

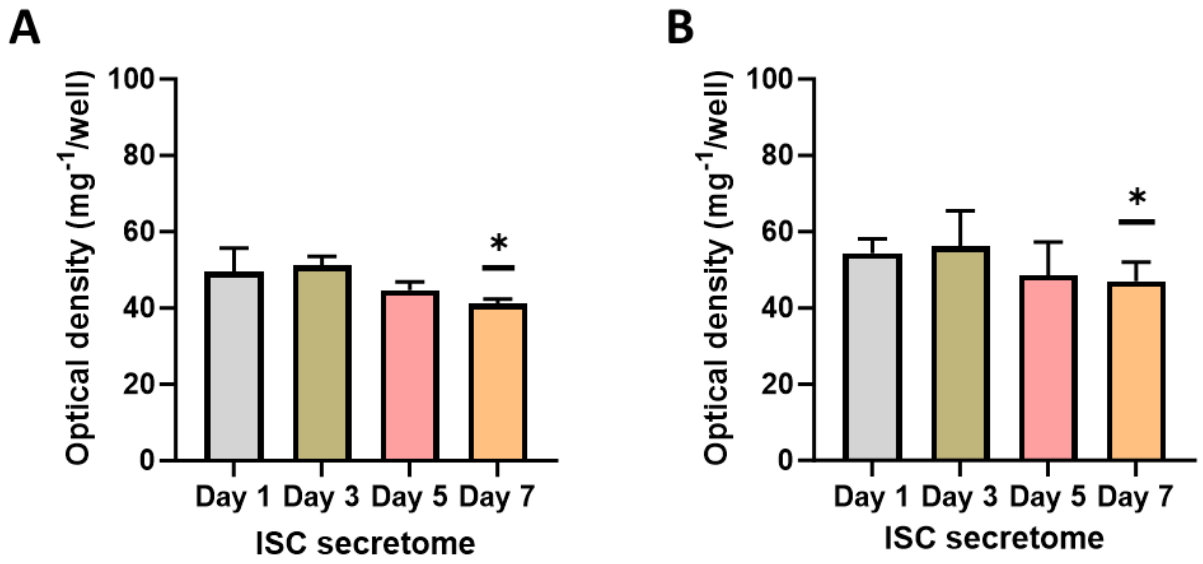

Figure 4.25: EndoC-βH1 cell viability determined by an MTS assay following a 72 h treatment with ISC secretome collected at culture Day 1, 3, 5, and 7 (LDIS 328, 335, 355 and 359).

(A) *One independent biological study (n = 1),* ***(B)*** *a combined study of four independent biological studies (n = 4). Represented data illustrated as mean±SD of four experimental samples. One-way ANOVA statistical test followed by a Tukey post hoc test was conducted. Significant difference represented by (*), p < 0.05.* ***(A)*** *Day 7 vs Day 1 and Day 3.* ***(B)*** *Day 7 vs Day 3.*

4.3.3.2 EndoC-βH1 insulin secretion assay following 72 h ISC secretome treatment

EndoC-βH1 cells were seeded at a density of 180,000 cell/well in a coated 48-well plate and incubated overnight at 37 °C. Then, a 72 h treatment with ISC secretome and a positive control Cytokine Mix (1 ng/ml IL-1β, 20 ng/ml INF-γ, 20 ng/ml TNF-α) treatment were conducted. Glucose-stimulated insulin secretion assay was undertaken to assess EndoC-βH1 cell function. Experiments were conducted as described in Chapter 2 (**2.3.7** - **2.3.10**).

Total protein (mg/well) quantification using a BCA assay (Chapter 2 **2.3.8**) was conducted to assess total protein content of EndoC-βH1 cells across the different treatments of low (1 mM) and high (20 mM) glucose conditions. Combined three independent biological studies illustrated in ***Figure 4.26*** (**A**) showed no significant change in total protein (mg/well) measured in Control 1:1 dilution (DMEM media: RPMI media) and Cytokine Mix. Likewise, there was no change in total protein content of high glucose stimulated EndoC-βH1 cells treated with ISC secretome collected from Day 1, 3, 5 and 7 in culture ***(Figure 4.26 B)***. This was also the case with low glucose stimulated EndoC-βH1 cells treated with ISC secretome from Day 1, 3 and 5. Whereas, total protein content in low glucose stimulated EndoC-βH1 cells treated with ISC secretome from Day 7 was significantly higher ($p < 0.05$) compared to low glucose stimulated EndoC-βH1 cells treated with ISC secretome from Day 1 ***(Figure 4.26 B)***.

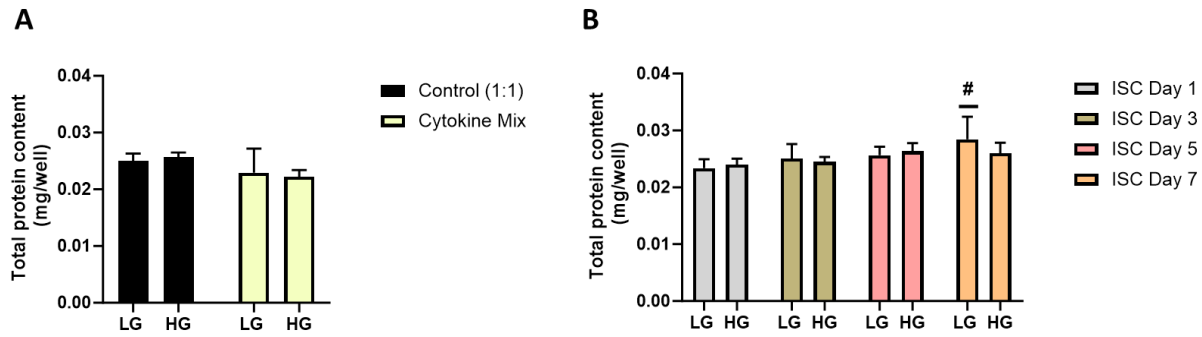

Figure 4.26: Total protein content of EndoC-βH1 cells (mg/well) quantified using BCA assay following a 72 h treatment and GSIS assay.

GSIS assay was carried out on EndoC-βH1 cells after stimulation with 1 mM glucose (low glucose; LG) and 20 mM glucose (high glucose; HG). ***(A)*** *Total protein content (mg/well) of EndoC-βH1 cells following a 72 h treatment with Control 1:1 dilution (DMEM media: RPMI media) and Cytokine Mix (1 ng/ml IL-1β, 20 ng/ml INF-γ, 20 ng/ml TNF-α). Represented data illustrated as mean±SD of three independent biological replicates (n = 3). Two-way ANOVA statistical test followed by LSD Fisher's post hoc test was conducted. No significant difference ($p < 0.05$) was found.* ***(B)*** *Total protein content (mg/well) of EndoC-βH1 cells following a 72 h treatment with ISC secretome Day 1, 3, 5, and 7. Two-way ANOVA statistical test followed by Tukey post hoc test was conducted. Significant difference represented by $p < 0.05$ between LG data (#). (#) ISC Day 7 LG vs ISC Day 1 LG.*

Insulin secretion in EndoC-βH1 cells following a 72 h treatment with control medium and ISC seceretome of different days and a 1 h glucose stimulation (1mM or 20 mM) assay, was investigated. Human Mercodia Insulin direct sandwich ELISA was used (Chapter 2 **2.3.9**). Combined analysis of three independent studies illustrated that secreted insulin (pmol/mg protein/h) was significantlly decresed ($p < 0.05$) at basal and stimulated levels in the Cytokine Mix treated cells compared with Control medium dilution (1:1) (DMEM media: RPMI media

(Figure 4.27 A). Compared to EndoC-βH1 cells treated with Day 1 ISC secretome at high glucose, insulin secretion of EndoC-βH1 cells treated with Day 3, 5 and 7 ISC secretome was significantly reduced ($p < 0.05$) ***(Figure 4.27 C)***. The calclulated insulin secretion stimulation index of the two groups was not significantly different ***(Figure 4.27 B*** and ***D)***.

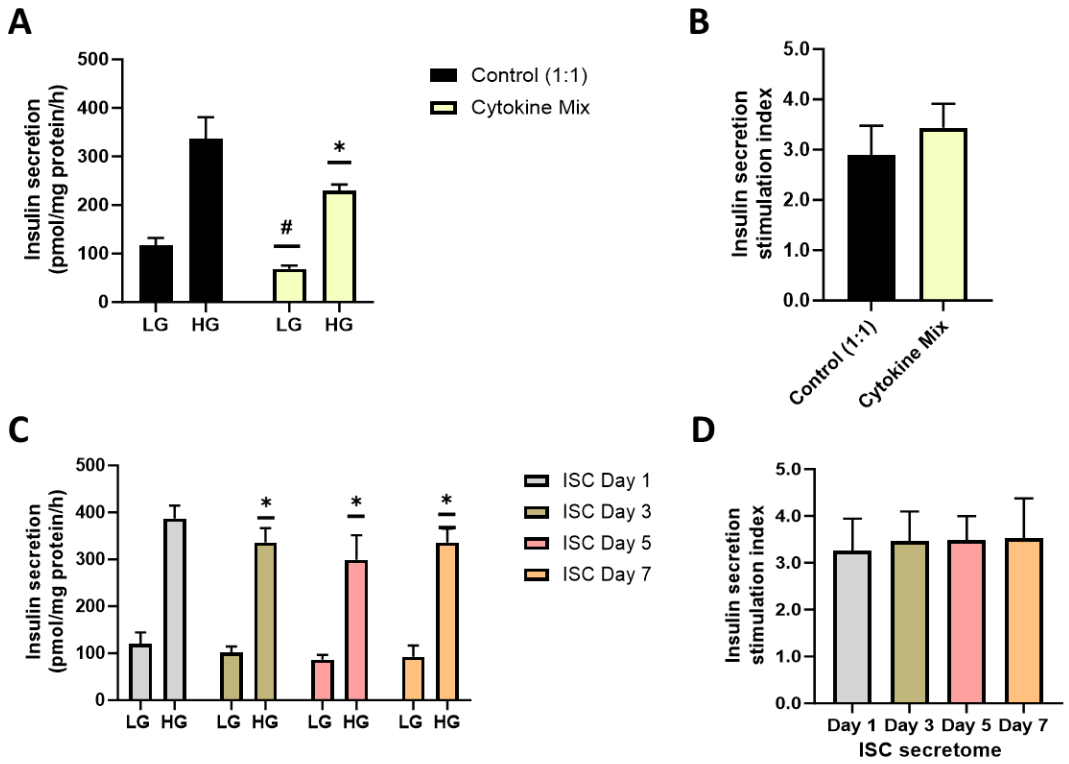

Figure 4.27: Insulin secretion of EndoC-βH1 cells (pmol/mg protein/h) following a 72 h hour treatment and GSIS assay.

GSIS assay was carried on on EndoC-βH1 cells after stimulation with 1 mM glucose (low glucose; LG) and 20 mM glucose (high glucose; HG). ***(A)*** *Insulin secretion (pmol/mg protein/h) of EndoC-βH1 cells following a 72 h treatment with Control 1:1 dilution (DMEM media: RPMI media) and Cytokine Mix (1 ng/ml IL-1β, 20 ng/ml INF-γ, 20 ng/ml TNF-α). Represented data illustrated as mean±SD of three independent biological replicates (n = 3). Two-way ANOVA statistical test followed by LSD Fisher's post hoc test was conducted. Significant difference represented by $p < 0.05$ between LG data (#) and between HG data (*). (#) Cytokine Mix LG vs Control (1:1) LG, (*) Cytokine Mix HG vs Control (1:1) HG.* ***(B)*** *Insulin secretion stimulation index of* ***(A)****. Unpaired student t-test was conducted. No significant difference was found.* ***(C)*** *Insulin secretion (pmol/mg protein/h) of EndoC-βH1 cells following a 72 h treatment with ISC secretome Day 1, 3, 5, and 7. Two-way ANOVA statistical test followed by Tukey post hoc test was conducted. Significant difference represented by $p < 0.05$. Significant difference represented by $p < 0.05$ between HG data (*). (*) ISC Day 3, Day 5 and Day 7 HG vs ISC Day 1 HG.* ***(D)*** *Insulin secretion stimulation index of* ***(C)****. One-way ANOVA statistical test followed by Tukey post hoc test was conducted. No significant difference was found.*

Insulin content (pmol/mg protein) in both low and high glucose treated cells was significantly reduced ($p < 0.05$) after treatment with Cytokine Mix compared to Control medium dilution (1:1) low and high glucose conditions, respectively ***(Figure 4.28 A)***. Insulin content of EndoC-βH1 cells treated with ISC secretome from Day 5 and 7 showed lower insulin content at high glucose compared to Day 1 ISC secretome ***(Figure 4.28 B)***. The decreased insulin content of ISC Day 5 was significantly lower ($p < 0.05$) compared with Day 1. There was no significant change in insulin content between ISC secretome treated cells after low glucose incubation.

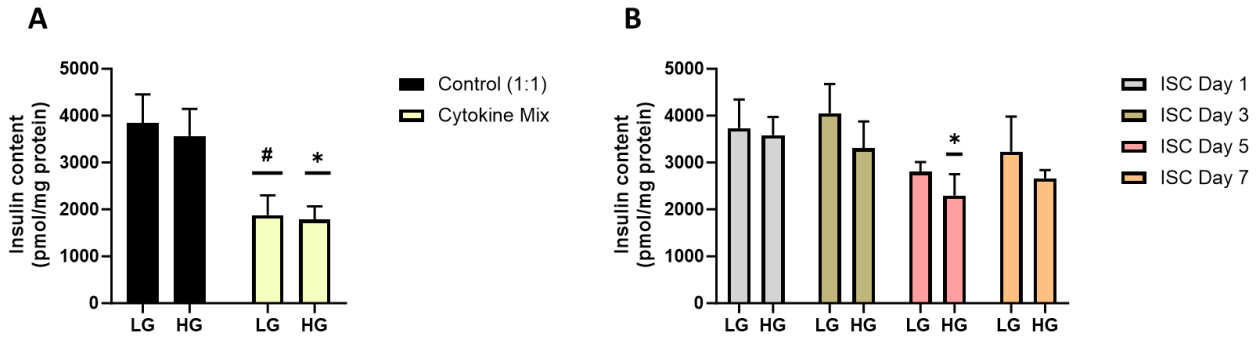

Figure 4.28: Insulin content of EndoC-βH1 cells (pmol/mg protein) following a 72 h hour treatment and GSIS assay.

GSIS assay was carried on on EndoC-βH1 cells after stimulation with 1 mM glucose (low glucose; LG) and 20 mM glucose (high glucose; HG). ***(A)*** *Insulin content (pmol/mg protein) of EndoC-βH1 cells following a 72 h treatment with Control 1:1 dilution (DMEM media: RPMI media) and Cytokine Mix (1 ng/ml IL-1β, 20 ng/ml INF-γ, 20 ng/ml TNF-α). Represented data illustrated as mean±SD of three independent biological replicates (n = 3). Two-way ANOVA statistical test followed by LSD Fisher's post hoc test was conducted. Significant difference represented by $p < 0.05$ between LG data (#) and between HG data (*). (#) Cytokine Mix LG vs Control (1:1) LG, (*) Cytokine Mix HG vs Control (1:1) HG.* ***(B)*** *Insulin content (pmol/mg protein) of EndoC-βH1 cells following a 72 h treatment with ISC secretome Day 1, 3, 5, and 7. Two-way ANOVA statistical test followed by Tukey post hoc test was conducted. Significant difference represented by $p < 0.05$ between LG data (#) and between HG data (*). (*) ISC Day 5 HG vs ISC Day 1 HG.*

Proinsulin secretion was investigated using Human Mercodia proinsulin direct sandwich ELISA (Chapter 2 **2.3.10**). Combined analysis of three independent studies illustrated that secreted proinsulin (pmol/mg protein/h) was significantlly increased ($p < 0.05$) after high glucose stimulation in the Cytokine Mix treated cells when compared to Control media dilution (1:1) ***(Figure 4.29 A)***. EndoC-βH1 cells treated with ISC secretome demonstrated no significant difference in proinsulin secretion among the different days ***(Figure 4.29 C)***. The calclulated proinsulin secretion stimulation index of the two groups was not significantly different ***(Figure 4.29 B*** and ***D)***.

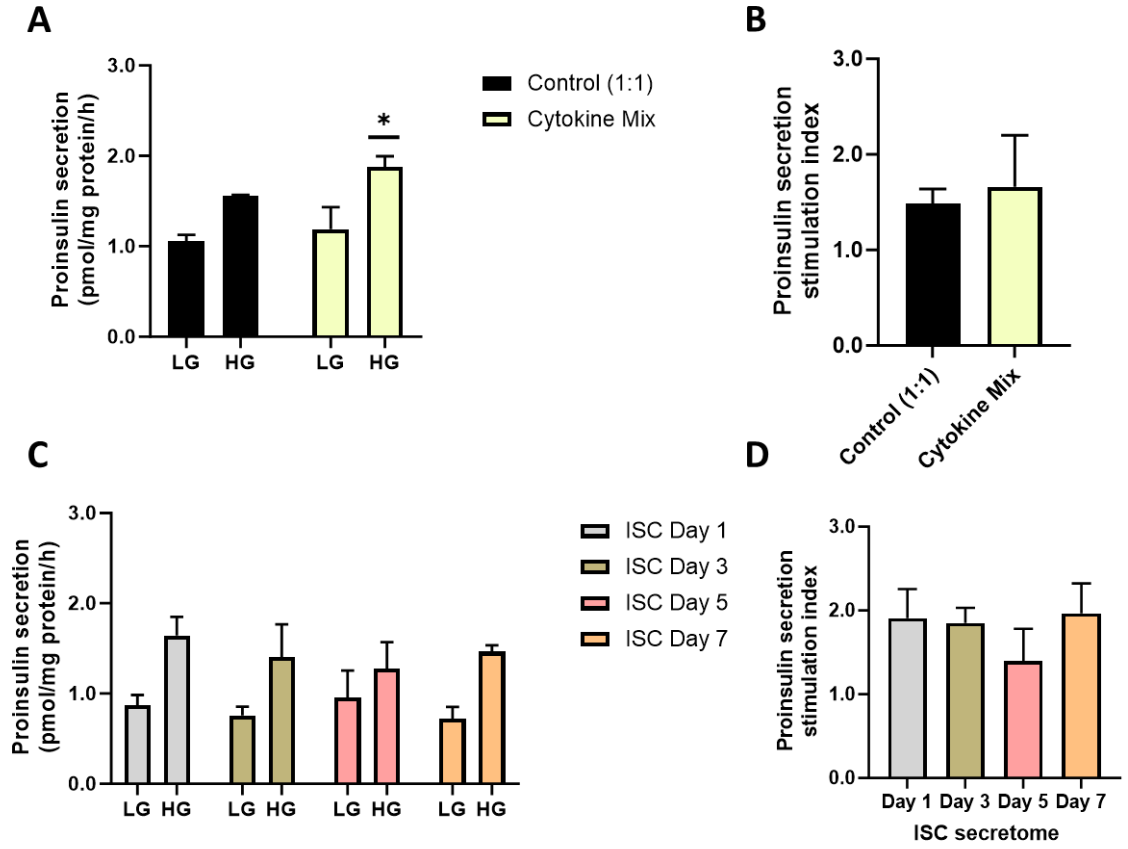

Figure 4.29: Proinsulin secretion of EndoC-βH1 cells (pmol/mg protein/h) following a 72 h hour treatment and GSIS assay.

GSIS assay was carried out on EndoC-βH1 cells after stimulation with 1 mM glucose (low glucose; LG) and 20 mM glucose (high glucose; HG). ***(A)*** *Proinsulin secretion (pmol/mg protein/h) of EndoC-βH1 cells following a 72 h treatment with Control 1:1 dilution (DMEM media: RPMI media) and Cytokine Mix (1 ng/ml IL-1β, 20 ng/ml INF-γ, 20 ng/ml TNF-α). Represented data illustrated as mean±SD of three independent biological replicates (n = 3). Two-way ANOVA statistical test followed by LSD Fisher's post hoc test was conducted. Significant difference represented by $p < 0.05$ between HG data (*). (*) Cytokine Mix HG vs Control (1:1) HG.* ***(B)*** *Proinsulin secretion stimulation index of* ***(A)****. Unpaired student t-test was conducted. No significant difference was found.* ***(C)*** *Proinsulin secretion (pmol/mg protein/h) of EndoC-βH1 cells following a 72 h treatment with ISC secretome Day 1, 3, 5, and 7. Two-way ANOVA statistical test followed by Tukey post hoc test was conducted. Significant difference represented by $p < 0.05$. No significant difference was found between LG data and between HG data.* ***(D)*** *Proinsulin secretion stimulation index of* ***(C)****. One-way ANOVA statistical test followed by Tukey post hoc test was conducted. No significant difference was found.*

Proinsulin content of EndoC-βH1 cells after stimulation with 1 mM glucose (low glucose; LG) and 20 mM glucose (high glucose; HG) was not significantly different in the Cytokine Mix compared to Control medium dilution (1:1) (***Figure 4.30 A***). Proinsulin content of EndoC-βH1cell treated with ISC secretome Day 5 and 7 showed significantly lower proinsulin content at high glucose compared to ISC Day 1 (***Figure 4.30 B***). There was no significant change in proinsulin content between ISC secretome treated cells of low glucose.

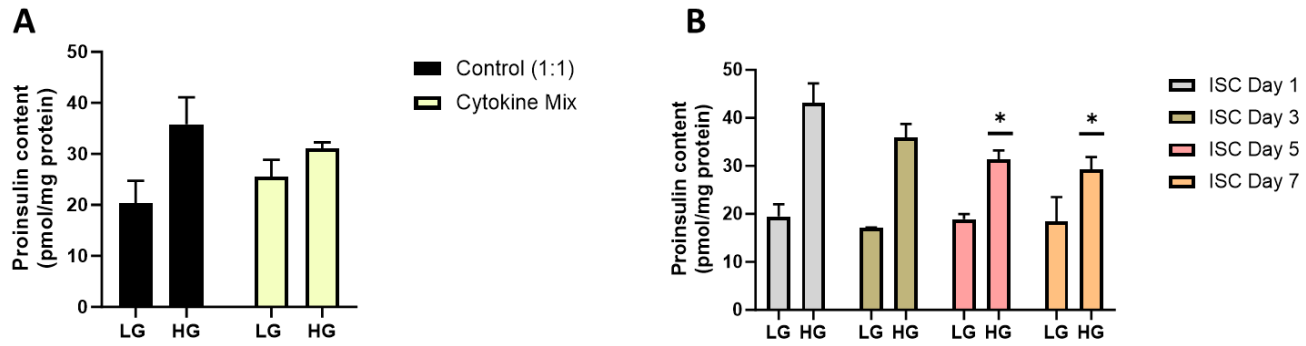

Figure 4.30: Proinsulin content of EndoC-βH1 cells (pmol/mg protein) following a 72 h hour treatment and GSIS assay.

GSIS assay was carried on on EndoC-βH1 cells after stimulation with 1 mM glucose (low glucose; LG) and 20 mM glucose (high glucose; HG). ***(A)*** *Proinsulin content (pmol/mg protein) of EndoC-βH1 cells following a 72 h treatment with Control 1:1 dilution (DMEM media: RPMI media) and Cytokine Mix (1 ng/ml IL-1β, 20 ng/ml INF-γ, 20 ng/ml TNF-α). Represented data illustrated as mean±SD of three independent biological replicates (n = 3). Two-way ANOVA statistical test followed by LSD Fisher's post hoc test was conducted.* ***(B)*** *Proinsulin content (pmol/mg protein) of EndoC-βH1 cells following a 72 h treatment with ISC secretome Day 1, 3, 5, and 7. Two-way ANOVA statistical test followed by Tukey post hoc test was conducted. Significant difference represented by $p < 0.05$ between LG data (#) and between HG data (*). (*) ISC Day 5 HG and ISC Day 7 vs ISC Day 1 HG.*

To further assess EndoC-βH1 function and the ability to synthesis and produce insulin, proinsulin:insulin ratio was calculated (total proinsulin/total insulin). In Cytokine Mix treated EndoC-βH1 cells, proinsulin:insulin was significantly increased by approximately ~1.9 fold in low glucose and by ~ 1.6 fold at high glucose treated wells ***(Figure 4.31 A)***. Proinsulin:insulin ratio of EndoC-βH1cell treated with ISC secretome showed ISC Day 5 to be significantly higher ($p < 0.05$) to ISC Day 1 at high glucose ***(Figure 4.31 B)***. There was no significant change in proinsulin:insulin ratio calculated between ISC secretome treated cells of low glucose.

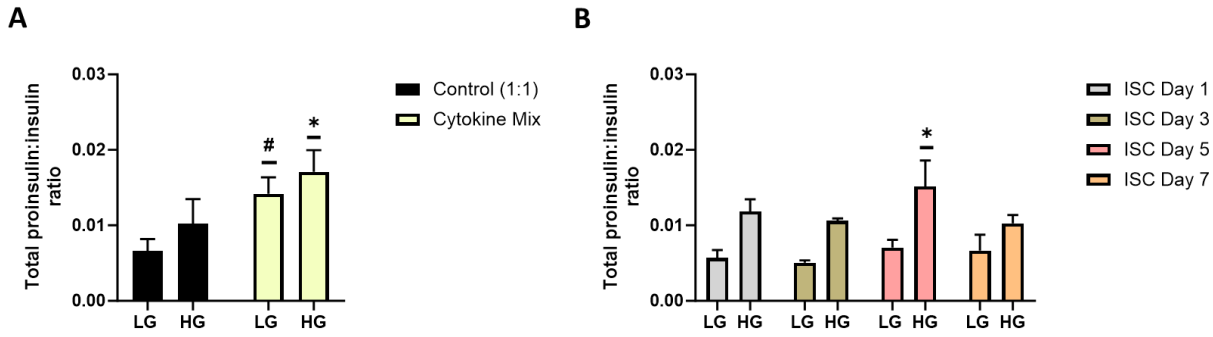

Figure 4.31: Quantification of proinsulin:insulin ratio of EndoC-βH1 cells following a 72 h hour treatment and GSIS assay.

GSIS assay was carried out on EndoC-βH1 cells after stimulation with 1 mM glucose (low glucose; LG) and 20 mM glucose (high glucose; HG). ***(A)*** *Proinsulin:insulin ratio of EndoC-βH1 cells following a 72 h treatment with Control 1:1 dilution (DMEM media: RPMI media) and Cytokine Mix (1 ng/ml IL-1β, 20 ng/ml INF-γ, 20 ng/ml TNF-α). Represented data illustrates mean±SD of three independent biological replicates (n = 3). Two-way ANOVA statistical test followed by LSD Fisher's post hoc test was conducted. Significant difference represented by p < 0.05 between LG data (#) and between HG data (*). (#) Cytokine Mix LG vs Control (1:1) LG, (*) Cytokine Mix HG vs Control (1:1) HG.* ***(B)*** *Proinsulin:insulin ratio of EndoC-βH1 cells following a 72 h treatment with ISC secretome Day 1, 3, 5, and 7. Two-way ANOVA statistical test followed by Tukey post hoc test was conducted. Significant difference represented by p < 0.05 between LG data (#) and between HG data (*). (*) ISC Day 5 HG vs ISC Day 3 and 7 HG.*

4.4 Discussion

4.4.1 Overview

Type 3c diabetes is a secondary outcome of diseases affecting the exocrine pancreas including chronic pancreatitis and cystic fibrosis. The pancreatic histopathology of these diseases is characterised by extensive replacement of the exocrine parenchyma with fibrotic tissue, as well as the presence of intra- and peri-islet fibrosis associated with impaired β-cell function. PaSCs are known to be key mediators of fibrosis in multiple tissues. Stellate cells present in islets are called islet stellate cells (ISCs) and have been proposed to impact on islet function. Following on from results obtained in Chapter 3, revealing the presence of activated PaSCs within the fibrotic regions around ducts and islets and within islets, the work summarised in this chapter aimed to establish an *in vitro* primary human ISC model using isolated islets from human donors none of whom had established diabetes (Chapter 2 ***Table 2.5***). Also, this chapter examined the content of the ISC model secretome and investigated its impact on viability and function of β-cell lines.

4.4.2 Establishment of a primary human ISC model

Isolated islets over seven days adhered to the culture plates, with growth of cells emanating from the edges of islets and continuing to grow and proliferate through Day 5 and Day 7, ultimately forming a confluent monolayer of cells ***(Figure 4.3)***. These cells were bipolar in shape exhibiting a fibroblast-like morphology and were further examined to confirm their nature as ISCs. Immunofluorescence staining of paraffin-embedded Day 0 islets confirmed insulin and glucagon expression, but also positive staining for vimentin and α-SMA within islets in cells with either a circular or elongated appearance, with no co-localisation with insulin or glucagon ***(Figure 4.4*** and ***Figure 4.7)***. It is important to note that, in addition to stellate cells, contractile pericytes lining small blood vessels and capillaries mediating vascular responses in islets express both markers (Kramann et al., 2015; Sakhneny et al., 2021; Tamayo et al., 2022). Pericytes have been reported to be a reservoir for progenitor cells that can transdifferentiate into myofibroblasts in response to injury and are themselves key mediators of injury-induced organ fibrosis (Kramann et al., 2015).

Immunofluorescence staining of spindle-like and or star-like outgrowing cells at culture Day 3, 5 and 7 were negative for both insulin and glucagon but positive for both vimentin and α-SMA ***(Figure 4.5*** and ***Figure 4.8)***. Vimentin has been reported to be expressed by islet stellate cells (Zang et al., 2015; Zha et al., 2016). The expression of α-SMA has been reported as the

most used marker for stellate cell activation (Apte et al., 1998; Bachem et al., 1998; Zha et al., 2016). Gene expression analysis undertaken using rtq-RT PCR confirmed an increase in the expression of genes associated with stellate cell activation over the culture period ***(Figure 4.10)***. These markers included vimentin, α-SMA encoding gene *ACTA2*, *CDH11* and *COL1A1* ***(Figure 4.10)***. ISC secretome analysis confirmed the functional activation of stellate cells illustrated by the increase in COL1A1 secretion over time in culture ***(Figure 4.11)***. Furthermore, MSD secretome analysis also evidenced stellate cell activation through increasing secretion of proinflammatory cytokines including TGF-β1, TGF-β2, IL-1, IL-6, IL-8 and TNF-α and secretion of chemokines and inflammatory biomarkers including CXCL-1, CXCL-10, CXCL-12, CCL-2 and MIP-1α over the culture period of ISCs ***(Figure 4.12***, ***Figure 4.13*** and ***Figure 4.14)***. Isolated islets from neonatal CF ferrets cultured for 9 days demonstrated a significant increase ($p < 0.01$) in IL-6 secretion when compared to wild-type islets, and proposed that this secretion was not coming from endocrine cells but other cells within islets (Sun et al., 2017). This study also demonstrated the presence of activated PaSCs in CF ferret pancreas via α-SMA$^+$ and desmin$^+$ staining compared to a quiescent state in wild-type CF ferrets (Sun et al., 2017). Together, these findings align with literature findings demonstrating that activated stellate cells are α-SMA$^+$ and vimentin$^+$ and secrete ECM proteins including COL1A1, inflammatory markers such as TGF-β, IL-1, IL-6, IL-8, TNF-α and CXCL and CCL chemokines (Elsässerm et al., 1989; Apte et al., 1998, 1999; Bachem et al., 1998; Kuroda et al., 1998; Gabbiani, 2003; Erkan et al., 2012; Zhao et al., 2018).

4.4.3 The impact of ISC secretome on β-cell viability and function

Initially, experiments setting out to investigate the impact of ISC secretome on INS-1E cell metabolic activity using MTT assay, as an indicator of cell viability, showed no significant change in mean cell viability of treated cells compared to the Control (1:1) ***(Figure 4.19)***. These results contradicted the findings of Zha et al., (2014) where INS-1E cell metabolic activity, assessed using cell counting kit-8 (CCK-8) following PaSCs secretome treatment, was observed to decrease INS-1E cell viability. Although both studies used the secretome in a 1:1 dilution, some of the factors that may have contributed to the difference in observed in the results include the source of stellate cells, whereby Zha et al., (2014) study used stellate cells derived from a rat pancreas, whereas we used stellate cells derived from isolated human islets. There were also differences in treatment time (24 h in our study and 48 h in Zha et al., (2014) study) and in the viability assays used (MTT assay in our study and CCK-8 assay in Zha et al., (2014) study). Both cell viability assays used assess cell metabolic activity, yet CCK-8 assay

uses water-soluble tetrazolium-8, whereas MTT uses water-insoluble tetrazolium that requires solubilisation solvents such as isopropanol to dissolve formazan crystals, which are used as indicative marker of metabolically active cells in both assays.

EndoC-βH1 cells used in this study were also treated with ISC secretome in a 1:1 dilution for 72 h and their viability was assessed using an MTS assay. Incubation of EndoC-βH1 cells treated with Day 7 ISC secretome led to a significant decrease in mean cell viability when compared to EndoC-βH1 cells treated with Day 1 ISC secretome ***(Figure 4.25)***. Cytokine combinations including IL-1β, INF-γ and TNF-α have been reported to decrease EndoC-βH1 cell viability (measured using neutral red uptake assay) in a time-related manner, whereby a 24 h cytokine treatment reduced the viability by ~25% and by ~45% following 48 h cytokine treatment (Oleson et al., 2015). Moreover, studies have reported that cytokine combination of IL-1β, INF-γ and TNF-α demonstrated a reduction of human islet cell viability in a time-dependent manner (Rabinovitch et al., 1990; Corbett et al., 1993; Eizirik et al., 1994; Arnush et al., 1998). The impact of ISC secretome on EndoC- βH1 cell viability could be mediated by the cytokines within the secretome and potentially those identified by MSD assay. Interestingly, EndoC-βH1 cells treated with Cytokine Mix, showed no change in cell viability when compared to Control (1:1).

ISCs are considered as a subgroup of PaSCs and both have been reported to be associated with islet fibrosis and islet cell dysfunction as they enhance β-cell apoptosis and reduce β-cell function (Li et al., 2016; Zha et al., 2016). Previous rodent studies have reported that activated PaSCs could reduce β-cell viability, reduce insulin secretion and induce cell death and apoptosis, when β-cell lines either directly co-cultured with activated PaSCs or treated with conditioned medium of activated PaSCs (Kikuta et al., 2013; Zha et al., 2014; Zang et al., 2015). PaSC co-culture mediated β-cell apoptosis has been associated with mitochondrial depolarization and the activation of the caspase pathway (Kikuta et al., 2013). Studies investigating the impact of PaSCs or ISCs conditioned medium on human β-cell lines has not been tested previously, which further strengthens the findings reported in this chapter.

EndoC-βH1 insulin secretion in the presence of high glucose was significantly reduced following a 72 h treatment with Day 3, 5 and 7 ISC secretome compared to Day 1 ISC secretome ***(Figure 4.27 C)***. Following these findings, insulin content was assessed and was also decreased suggesting that insulin biosynthesis might have been impacted ***(Figure 4.28 B)***. Therefore, proinsulin measurements were evaluated. Proinsulin secretion was found

unchanged but there was a significant decrease ($p < 0.05$) in proinsulin content in EndoC-βH1 treated with Day 5 and 7 ISC secretome ***(Figure 4.29 C*** and ***Figure 4.30 B)***. The reduction in proinsulin content as well as insulin content could be due to decreased biosynthesis and decreased processing due to possible ER stress. It could be suggested that ER stress was induced in response to ISC secretome containing proinflammatory cytokines produced by activated ISCs, impacting on proinsulin folding. Previously reported, proinflammatory cytokines such as IL-1β, INF-γ and TNF-α have been implicated in β-cell dysfunction during early stage and progression of diabetes (Eizirik et al., 1996; Donath et al., 2003; ; Eizirik et al., 2009). In line with these observations, EndoC-βH1 cells treated with the Cytokine Mix (1 ng/ml IL-1β, 20 ng/ml INF-γ, 20 ng/ml TNF-α) had reduced in insulin secretion, insulin content and proinsulin content when compared to the Control (1:1) ***(Figure 4.27 A, Figure 4.28 A*** and ***Figure 4.30 A)***.

The increase in proinsulin:insulin ratio observed in EndoC-βH1 cells treated with ISC secretome Day 5 (at 20 mM) and treated with the Cytokine Mix (at both 1 mM basal and 20 mM stimulated glucose concentrations) along with increased levels of secreted proinsulin in the later treatment ***(Figure 4.31*** and ***Figure 4.29 A)***, could further support the idea that a defect in proinsulin processing is associated with decreased insulin secretion and increased EndoC-βH1 cell dysfunction. It is suggested that the increase in secretory demands on β-cells in response to high glucose levels during diabetes, may contribute to the increase in proinsulin:insulin ratio, yet the main mechanisms behind this is still questioned in the literature (Mezza et al., 2018). In people with CF, the progression towards CFRD has been associated with impaired insulin secretion along with increased β-cell stress demonstrated by elevated fasting proinsulin:insulin ratio (Nielsen et al., 2023). The current studies suggest a role for intrapancreatic cytokines in mediating this stress and that ISCs may be a source of these mediators in the CF pancreas.

In summary we have successfully established a 2D human primary islet-derived stellate cell (ISC) model *in vitro* and demonstrated activation through α-SMA and vimentin positive immunofluorescence staining, the increased expression of selected genes and collagen / profibrotic molecule secretion. Findings in this chapter demonstrated that ISCs secretome exhibited an impact on β-cell viability and function. Further investigations are required to uncover the underlying mechanisms and understand the potential signalling molecules within the ISCs secretome and the pathways leading to β-cell dysfunction, reduced insulin secretion and ultimately development of T3c diabetes. These studies could foster the development of

therapies that could target the activation of PaSCs and ISCs to prevent islet fibrosis and limit β-cell dysfunction.

4.4.4 Study limitations

The work presented in this chapter could be further improved by limiting some of the factors that might have influenced the results. For example, additional repeats of ISC secretome studies using secretome of ISCs from different human islet donors, to reduce biological variability induced by batch difference. ISCs could be cultured using EndoC-βH1 medium to limit the impact of different medium constitution on EndoC-βH1 cell function, which could enable the comparisons of ISC secretome of different days to a 100% EndoC-βH1 medium as a more 'healthy' control. Also, studies could be repeated more than three times to ensure that they are truly representative.

Chapter 5: Transcriptomic analysis of human CF *post-mortem* pancreatic tissue and EndoC-βH1 cells following incubation with ISC secretome

5.1 Introduction

The work presented in this chapter follows on from the Chapter 3 and 4 studies, aiming to delve deeper into the molecular mechanisms and pathways underlying the results reported in the previous chapters.

5.1.1 CF molecular mechanisms

Architectural remodelling and morphological changes observed in CF and CFRD pancreata as the disease progress include ductal lumen dilatation, exocrine parenchyma loss and replacement with fibrotic tissue and/or adipocytes (Löhr et al., 1989; Olivier et al., 2012; Sun et al., 2014; Yi et al., 2016; Bogdani et al., 2017; Rotti et al., 2018; Rickels et al., 2020). The systematic pattern-based approach I established and reported in Chapter 3 highlighted how these morphological observations changed across the different pathological patterns as the disease progressed. However, there have been no previous deeper transcriptomic analysis studies providing more detail regarding the changes in gene expression associated with these progressive pathological changes. In addition, there is limited information on the mechanisms and cellular phenotypes which contribute to β-cell impairment and ultimately lead to the development of CFRD.

The NanoString nCounter analysis platform provides a useful tool to enable transcriptome profiling on CF pancreatic samples due to its high sensitivity, specificity, and power for the investigation of molecular mechanisms and disease pathways. NanoString technology uses a direct digital fluorescent barcode system to enable the detection and measurement of a specific nucleic acid in a single panel, with no further amplification (Veldman-Jones et al., 2015; Pedrosa et al., 2023). Another advantage of using NanoString is its ability to enable gene expression profiling in samples with poor RNA quality such as FFPE samples (Veldman-Jones et al., 2015).

The pancreas is one of the most challenging organs for meaningful transcriptomic analysis due to exocrine enzymatic activity that could impact on molecular integrity. Initially I extracted RNA from *post-mortem* CF tissue for bulk RNA sequencing, but RNA quality was unfortunately of insufficient quality. The high sensitivity and specificity of NanoString nCounter analysis made the technique a more suitable approach to provide detailed molecular

information from our very limited *post-mortem* CF tissue. It is clearly important to gain further understanding of the changes in gene expression which underlie the different CF patterns reported in Chapter 3. This chapter aimed to utilise the historic CF human tissue for transcriptomic analysis.

5.1.2 Bulk cell RNA-Sequencing of EndoC-βH1 cell following ISC secretome treatment

The underlying mechanisms of islet fibrosis development, pancreatic β-cell dysfunction and apoptosis in T3c diabetes are still unknown. Activated PaSCs and ISCs have been shown to play a critical role in the development of islet fibrosis with a postulated impact on β-cell dysfunction (Li et al., 2016; Zha et al., 2016). However, the gene expression changes leading to altered β-cell phenotype, function, and survival following incubation with ISC secretome remain unknown. After successfully establishing the ISC model and investigating the impact of secretome on β-cell function in Chapter 4, I set out to undertake RNA sequencing in EndoC-βH1 cells following incubation with ISC-conditioned medium.

5.2 Aim

The studies reported in this chapter aimed to conduct transcriptomic phenotyping of CF pancreatic tissue and EndoC-βH1 cells following treatment with ISC secretome.

- **Objective 1:** Investigate the differentially expressed genes and identify possible signalling pathways associated with the morphological and cellular changes across CF pancreatic tissue of different morphological patterns, by performing a NanoString nCounter analysis.
- **Objective 2:** Investigate the impact of ISC secretome on EndoC-βH1 cell transcriptome by performing bulk-RNA sequencing and exploring possible upregulated and downregulated gene expression pathways.

5.3 Results

5.3.1 NanoString nCounter analysis in control and CF human tissue samples

NanoString nCounter analysis was performed successfully in three controls and nine CF samples (Chapter 2 ***Table 2.4***). Sample selection was carried out based on morphological patterns, previously reported in Chapter 3, and each pattern was represented by three samples for RNA extraction. Two blocks from each of CF Case 22 and 29, one with Pattern 2 histopathology and one with Pattern 3 were chosen (***Table 2.2***). Hence, the nine CF samples were derived from seven CF cases. NanoString analysis was carried out using the nCounter® Human Fibrosis V2 Panel which captures the key pathways and processes defining fibrosis comprising 760 predefined target genes along with 10 internal reference genes, 6 of which were used for data normalisation (ACAD9, ARMH3, CNOT10, GUSB, MTMR14, NUBP1). Data were analysed using the ROSALIND® program which uses the NanoString nCounter® Advanced Analysis protocol. ROSALIND® was developed by ROSALIND, Inc. (San Diego, California, USA).

5.3.1.1 Gene expression analysis by NanoString

An initial exploration of the transcriptome profile of the samples was enabled using a multidimensional scaling (MDS) plot, revealing the separation between control and CF samples as observed in ***Figure 5.1***. Pattern 1 CF samples clustered separately from later-stage CF samples with closer co-localisation of Pattern 2 and Pattern 3 samples.

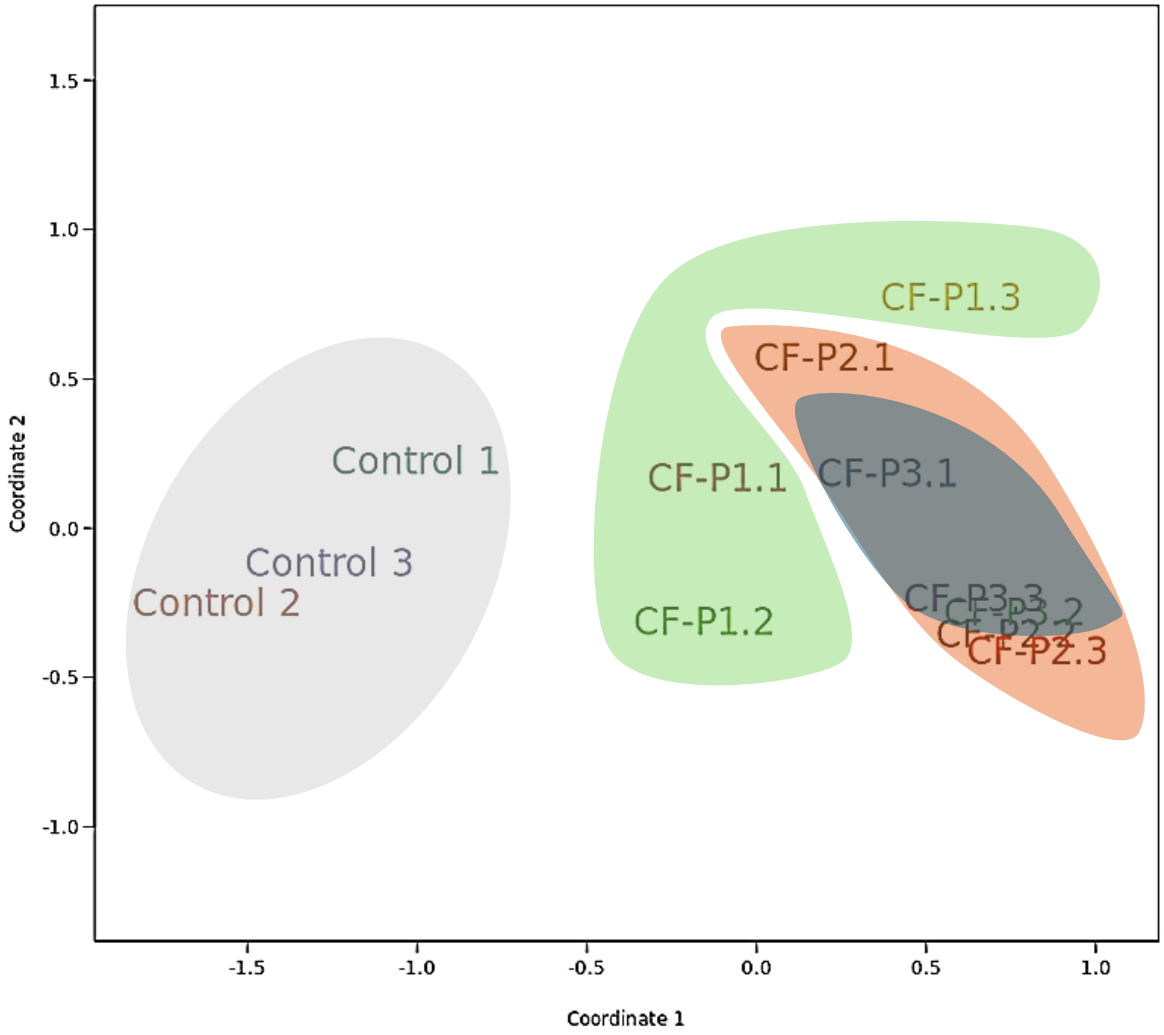

Figure 5.1: Multidimensional scaling (MDS) plot demonstrated an initial exploration of NanoString gene expression data a clear separation of three control samples and nine CF samples.

Control samples (1-3) highlighted in grey. CF Pattern 1 samples (CF-P1.1, CF-P1.2 and CF-P1.3) highlighted in green. CF Pattern 2 samples (CF-P2.1, CF-P2.2 and CF-P2.3) highlighted in orange. CF Pattern 3 samples (CF-P3.1, CF-P3.2 and CF-P3.3) highlighted in steel blue.

5.3.1.2 Differential analysis of gene expression in CF compared to Control tissue blocks

Heatmaps were generated to visualise the differentially expressed genes in CF, which were significantly ($p < 0.05$) upregulated (by ≥ 1.5-fold change) or downregulated (by ≤ -1.5-fold change) compared to control ***(Figure 5.2)***. In total there were 55 upregulated genes in CF compared to control. Venn diagrams were designed to enable the visualisation of the distribution of the differentially expressed genes as the disease progressed. Compared to control, in early-stage CF Pattern 1 (fibroatrophic pattern) samples, 34 genes were upregulated ***(Figure 5.2 A)***, 40 genes were upregulated in advanced-stage CF Pattern 2 samples (fibroatrophic and lipoatrophic pattern) ***(Figure 5.2 B)***, whereas, 36 genes were upregulated in end-stage CF Pattern 3 samples (lipoatrophic pattern) ***(Figure 5.2 C)***.

Twenty-three of these genes were upregulated in all CF patterns compared to control. The differentially expressed genes were grouped based on the associated pathways reported in the nCounter® Human Fibrosis V2 Panel used. Genes were associated with pathways including epithelial-mesenchymal-transition (EMT) pathway (*TGF-β1, ACTA2, CXCL-12 and CXC receptor-4: CXCR4*), Extracellular matrix (ECM) synthesis and degradation pathway (*COL4A1, COL4A2, COL5A3* and *COL16A1*), Adenosine pathway (Phosphodiesterase: *PDE2A* and Heparan sulphate proteoglycan 2: *HSPG2*), Phosphoinositide 3-kinase protein kinase B (PI3K-Akt) pathway (B-cell lymphoma-2: *BCL2* and Platelet-derived growth factor receptor beta: *PDGFRB*), Hippo pathway (Angiomotin like-2: *AMOTL2*), Notch pathway (Neurogenic locus notch homolog protein 3: *NOTCH3*) and Peroxisome proliferator-activated receptor (PPAR) signalling (Fatty acid-binding protein -4: *FABP4*) ***(Figure 5.2)***.

Genes that were only upregulated in CF Pattern 1 compared to control (10 genes) included genes associated with pathways such as collagen biosynthesis and modification and ECM synthesis and degradation pathways (*COL1A1, COL7A1 and COL3A1*), EMT and myofibroblast regulation pathways (Periostin: *POSTN*) and genes associated with hypoxia including hypoxia-inducible factor 3 alpha: *HIF3A* ***(Figure 5.2 A)***.

Genes that were only upregulated in CF Pattern 2 compared to control (eight genes) included genes associated with pathways such as EMT pathway (Neuropilin-2: *NRP2* and Matrix metalloproteinase-2: *MMP2*) and genes in TGF-β pathway (Thrombospondin-1: *THBS1* and Ring-box protein-1: *RBX1*) ***(Figure 5.2 B)***.

Genes that were only upregulated in CF Pattern 3 compared to control (five genes) included genes associated with pathways such as TGF-β pathway (Casitas B-lineage lymphoma: *CBL*),

insulin resistance (Nuclear receptor interacting protein-3: *NRIH3*), Notch pathway (Delta-like-4: *DLL4*) and Mechanistic target of rapamycin (mTOR) pathway (Ring Finger protein- 152: *RNF152* and ATPase H+ transporting V1 subunit E1: *ATP6V1E1*) ***(Figure 5.2 C)***.

Compared to control, CF Pattern 1 and CF Pattern 2 shared one upregulated gene that is associated with ECM synthesis (Nidogen-2: *NID2*) ***(Figure 5.2 A*** and ***B)***. Later-stage CF Patterns 2 and 3 shared eight upregulated genes including the gene Insulin-like growth factor 1 *(IGF1)*, which is associated with insulin signalling, mTOR pathway and PI3K-Akt pathway. Other genes are associated with EMT pathway (*VIM*), Do Novo lipogenesis pathway (Fatty acid synthase: *FASN*), ECM degradation pathway (Laminin C1: *LAMCI*) and autophagy (Microtubule-associated protein 1 light chain 3 alpha: *MAPILC3A*) ***(Figure 5.2 B*** and ***C)***.

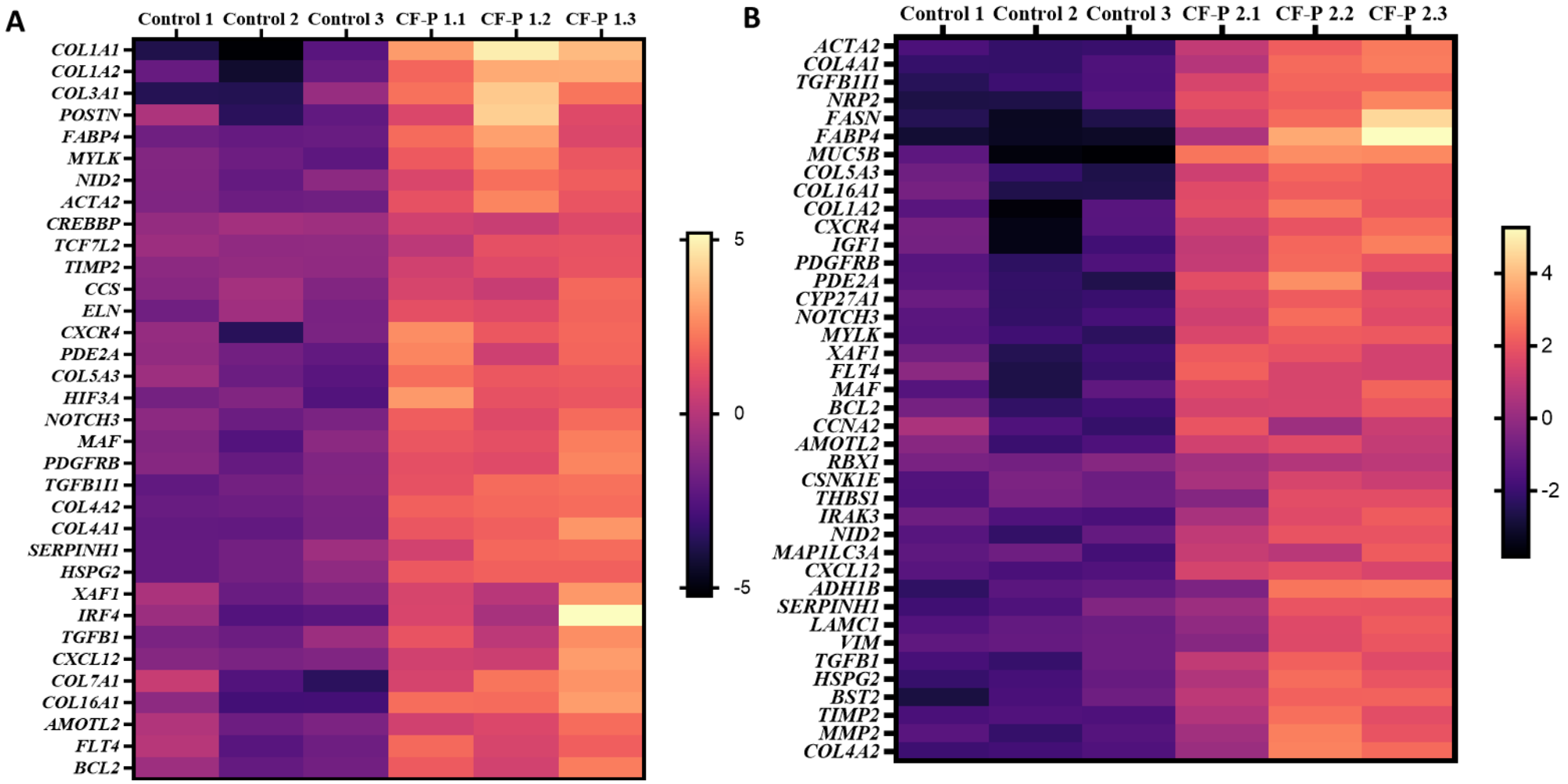
A
Control 1
Control 2
Control 3
CF-P 1.1
CF-P 1.2
CF-P 1.3
COL1A1
COL1A2
COL3A1
POSTN
FABP4
MYLK
NID2
ACTA2
CREBBP
TCF7L2
TIMP2
CCS
ELN
CXCR4
PDE2A
COL5A3
HIF3A
NOTCH3
MAF
PDGFRB
TGFB1I1
COL4A2
COL4A1
SERPINH1
HSPG2
XAF1
IRF4
TGFB1
CXCL12
COL7A1
COL16A1
AMOTL2
FLT4
BCL2
5
0
-5
B
Control 1
Control 2
Control 3
CF-P 2.1
CF-P 2.2
CF-P 2.3
ACTA2
COL4A1
TGFB1I1
NRP2
FASN
FABP4
MUC5B
COL5A3
COL16A1
COL1A2
CXCR4
IGF1
PDGFRB
PDE2A
CYP27A1
NOTCH3
MYLK
XAF1
FLT4
MAF
BCL2
CCNA2
AMOTL2
RBX1
CSNK1E
THBS1
IRAK3
NID2
MAP1LC3A
CXCL12
ADH1B
SERPINH1
LAMC1
VIM
TGFB1
HSPG2
BST2
TIMP2
MMP2
COL4A2
4
2
0
-2

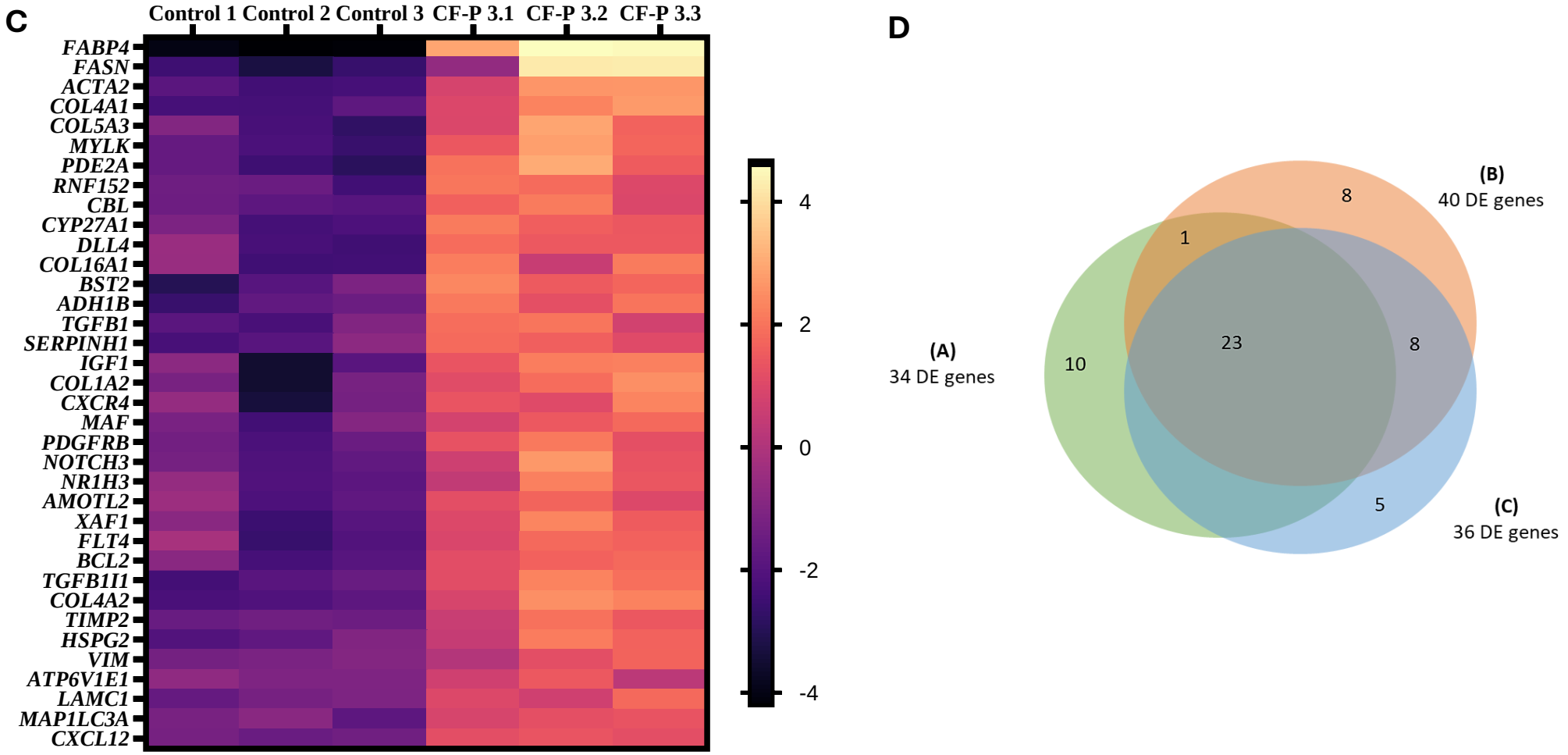

Figure 5.2: Visual illustrations of the 55 differentially upregulated genes in CF Patterns 1, 2 and 3 vs Control.

*Heatmaps demonstrated differentially expressed (DE) genes in (**A**) Control vs CF Pattern 1 (CF-P1), (**B**) control vs CF Pattern 2 (CF-P2) and (**C**) control vs CF Pattern 3 (CF-P3). Venn diagram illustrated the distribution of the 55 DE genes upregulated by ≥ 1.5-folds in CF Patterns 1, 2, and 3 compared to control (**D**). $p < 0.05$.*

Compared to control samples, 12 genes were downregulated in CF samples (≤ -1.5-fold change). Four genes were downregulated in early-stage CF Pattern 1 samples ***(Figure 5.3 A)***, eight genes were downregulated in advanced-stage CF Pattern 2 samples ***(Figure 5.3 B)***, whereas, 11 genes were downregulated in end-stage CF Pattern 3 samples ***(Figure 5.3 C)***. In all CF patterns, four genes were downregulated compared to control, including the gene *MMP7* which is associated with collagen biosynthesis and modification, ECM degradation, EMT and Wnt pathways. Four genes were downregulated in CF Pattern 3 compared to control samples, including Prolyl 4-hydroxylase beta subunit (*P4HB)* gene which is associated with collagen biosynthesis and modification, oxidative stress and proteotoxic stress. Another down-regulated gene is Presenilin (*PSEN2)* which is associated with the Notch pathway. Compared to control, later-stage CF Pattern 2 and CF Pattern 3 shared three downregulated genes that are associated with the EMT pathway (Ocludin: *OCLN*), fatty acid metabolism (Acyle-CoA synthetase medium-chain family member-3: *ACSM3*) and adenosine pathway and Complementary activation complement component-5 (*C5*).

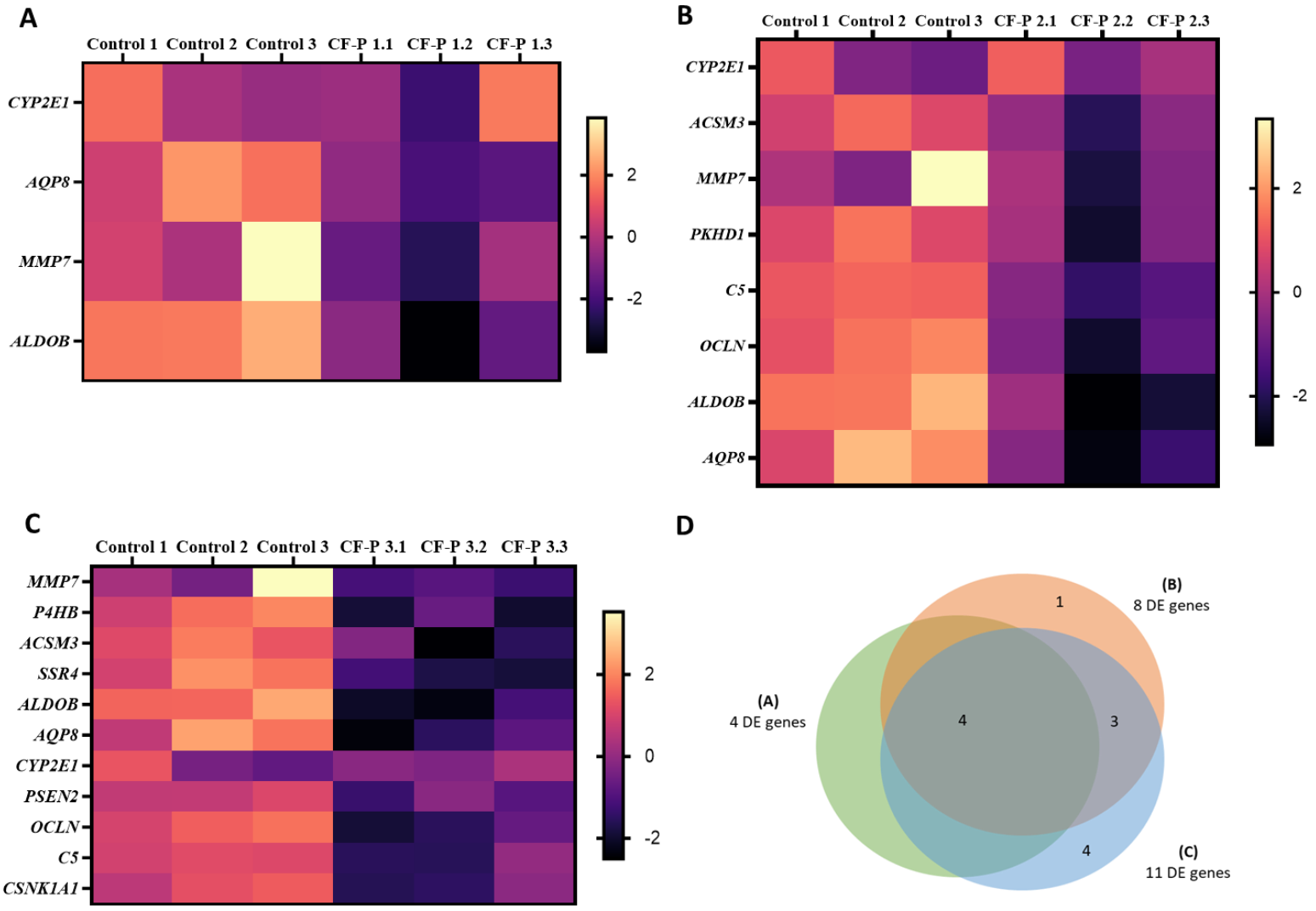

Figure 5.3: Visual illustrations of the 12 downregulated genes in CF Patterns 1, 2 and 3 vs Control.

*Heatmaps demonstrated differentially expressed (DE) genes in (**A**) Control vs CF Pattern 1 (CF-P1), (**B**) control vs CF Pattern 2 (CF-P2) and (**C**) control vs CF Pattern 3 (CF-P3). Venn-diagram illustrated 12 differentially expressed (DE) genes downregulated by ≤ -1.5-folds in CF patterns 1, 2, and 3 compared to control (**D**). $p<0.05$.*

5.3.1.3 Differential gene expression analysis between CF pathology patterns

Further analysis was undertaken to investigate the gene composition across CF patterns as the disease progresses. These comparison analyses were built whereby later-stage CF Patterns 2 and 3 were each compared to early-stage CF Pattern 1 (CF-P2 vs CF-P1 and CF-P3 vs CF-P1), and advanced-stage CF Pattern 2 was compared with Pattern 3 (CF-P3 vs CF-P2) ***(Figure 5.4)***.

Compared to early-stage CF samples, there were 28 upregulated genes in later-stage CF samples (≥ 1.5-fold change). Ten of these genes were upregulated in both advanced- and end-stage CF patterns compared to early-stage CF. These genes were associated with fatty acid metabolism pathways and gluconeogenesis: (Alcohol dehydrogenase 1B: *ADH1B*), fatty acid metabolism pathway and insulin resistance (Acetyl-CoA carboxylase beta: *ACACB*), ECM synthesis and TGF-β pathway (Serpin family G member-1: *SERPING1*) and PPAR signalling (Angiopoietin-like-4: *ANGPTL4* and Perilipin-4: *PLIN4*) ***(Figure 5.4 A*** and ***B)***.

Nine genes were upregulated in CF Pattern 2 compared to CF Pattern 1. These included genes associated with EMT pathway (Signal transducer and activator of transcription-5: *STAT5* and Early growth response-1: *EGR1*), Wnt pathway (Serpin family F member-1: *SERPINF1*) and insulin resistance (Sterol regulatory element-binding transcription factor-1: *SREBF1*) ***(Figure 5.4 A)***. Three genes were upregulated in CF Pattern 3 compared to CF Pattern 1, these genes are associated with EMT pathway (Germlin-1: *GREM1*) and insulin resistance, PI3K-Akt pathway and PPAR signalling (Phosphoenolpyruvate carboxykinase-1: *PCK1*) ***(Figure 5.4 B)***.

In CF Pattern 3, three genes were upregulated compared to CF Pattern 2, including genes associated with fatty acid metabolism pathway (Adiponectin receptor-1: *ADIPOR1*) and adenosine pathway (Glucagon-like peptide-1 receptor: *GLP1R*) ***(Figure 5.4 C)***. Three genes were only upregulated in CF Pattern 3 compared to both CF Patterns 1 and 2, these genes included genes associated with inflammation (C-reactive protein: *CRP*), neutrophil degradation (Fc gamma receptor 1A and 3B: *FGCGR3A/B*) and platelet degranulation and TLR-signalling (Fibrinogen alpha chain: *FGA*) ***(Figure 5.4 B*** and ***C)***.

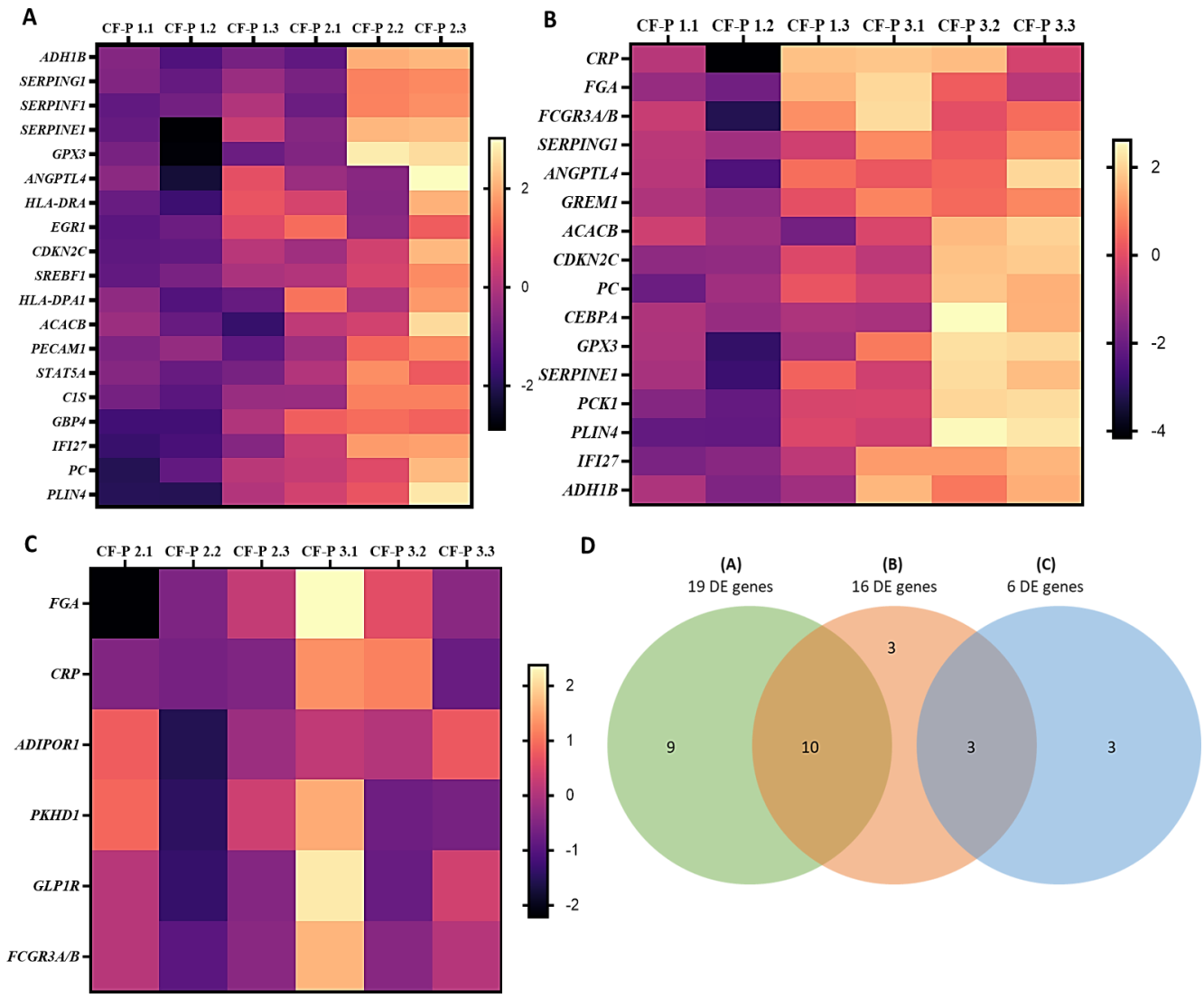

Figure 5.4: Visual illustrations of the 28 upregulated genes among CF Patterns 1, 2 and 3.

*Heatmaps demonstrated differentially expressed (DE) genes upregulated in (**A**) CF Pattern 2 vs CF Pattern 1 (CF-P2 vs CF-P1), (**B**) CF Pattern 3 vs CF Pattern 1 (CF-P3 vs CF-P1) and (**C**) CF Pattern 3 vs CF Pattern 2 (CF-P3 vs CF-P2). Venn diagram illustrating 28 differentially expressed (DE) genes upregulated by ≥ 1.5-folds among CF patterns according to the previously mentioned comparisons (**D**). $p < 0.05$.*

Compared to early-stage CF samples, there were 18 downregulated genes in advanced-stage CF samples (≤ -1.5-fold change) ***(Figure 5.5)***. Five of these genes were downregulated in both advanced-stage CF patterns compared to early-stage CF ***(Figure 5.5 A*** and ***B)***. These genes were associated with collagen biosynthesis and modification, ECM degradation and synthesis and PI3K-Akt pathway (*COL1A1*), ECM synthesis (Elastin: *ELN*), Hippo pathway (Ww domain containing-1: *WWC1*), and autophagy (Vesicle associated membrane protein-8: *VAMP8*) ***(Figure 5.5 A*** and ***B)***.

Only three genes were downregulated in CF Pattern 2 compared to CF Pattern 1 These genes included genes associated with platelet degranulation (Titin: *TTN*) and adenosine pathway (Faciogenital dysplasia 2: *FGD2*) ***(Figure 5.5 A)***. Three genes were downregulated in CF Pattern 3 compared to CF Pattern 1 including a gene associated with Notch pathway (*PSEN2*) and the *CFTR* gene ***(Figure 5.5 B)***.

In CF Pattern 3, six genes were downregulated compared to CF Pattern 2, including genes associated with NF-κB pathway (Phospholipase C gamma-2: *PLCG2* and Vascular cell adhesion molecule-1: *VCAM1*). One gene associated with fatty acid metabolism (Methylmalonyl-CoA mutase: *MMUT*) was downregulated in CF Pattern 3 compared to both CF Patterns 1 and 2 ***(Figure 5.5 C)***.

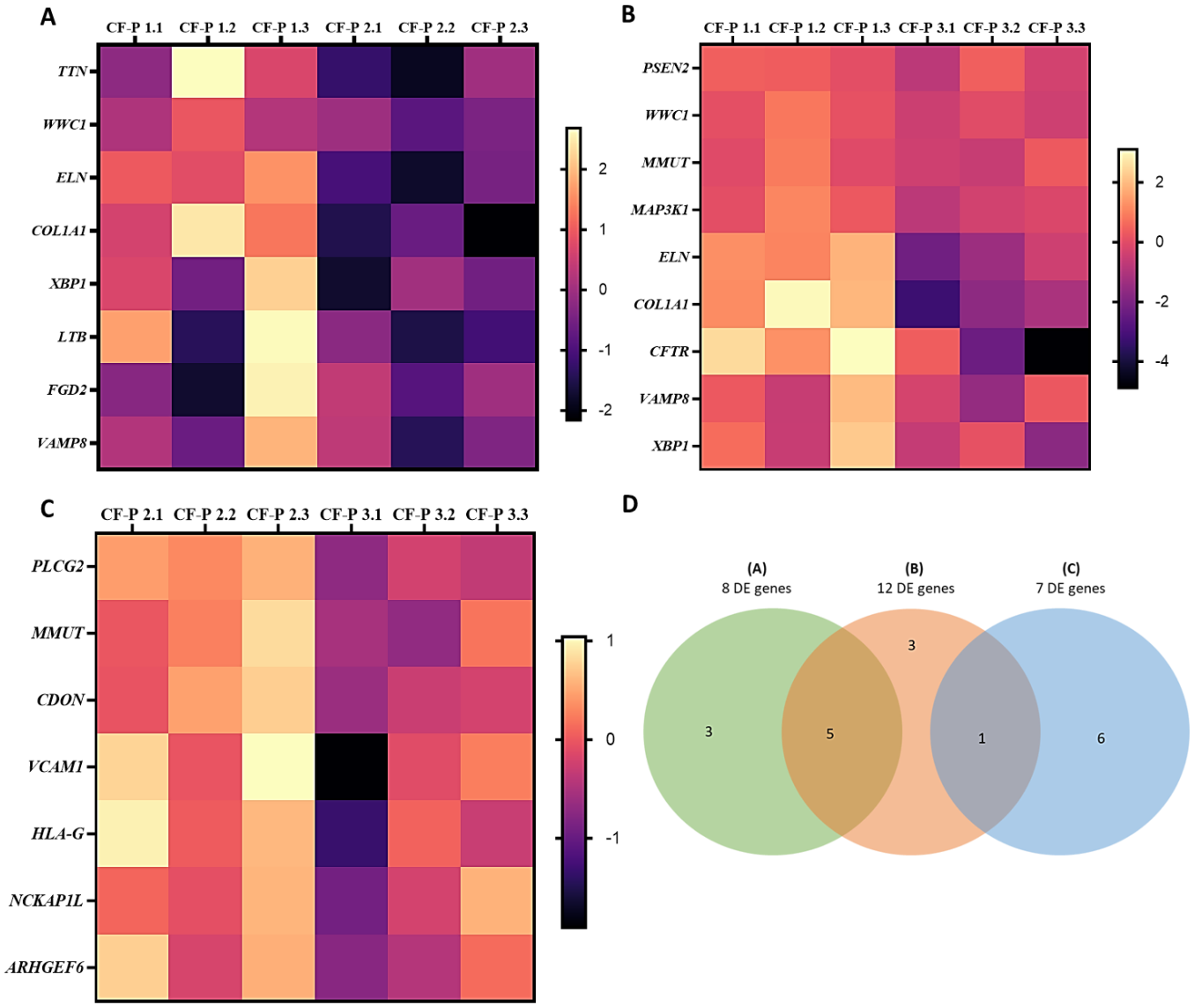

Figure 5.5: Visual illustrations of the 18 downregulated genes among CF Patterns 1, 2 and 3.

*Heatmaps demonstrated differentially expressed (DE) genes downregulated in (**A**) CF Pattern 2 vs CF Pattern 1 (CF-P2 vs CF-P1), (**B**) CF Pattern 3 vs CF Pattern 1 (CF-P3 vs CF-P1) and (**C**) CF Pattern 3 vs CF Pattern 2 (CF-P3 vs CF-P2). Venn diagram illustrating the 18 differentially downregulated by ≤ -1.5-folds among CF patterns genes according to the previously mentioned comparisons (**D**). $p < 0.05$.*

5.3.2 Bulk RNA-Sequencing of EndoC-βH1 cells following incubation with ISC secretome

To investigate EndoC-βH1 gene expression profile following 72 h treatment with ISC secretome, bulk RNA-Sequencing was conducted. Briefly, EndoC-βH1 cells were seeded at a density of 180,000 cell/well in a coated 48-well plate and were incubated overnight prior to starting the 72 h treatment with Control 1:1 dilution medium (labelled as Ctrl 2 in the following reported results), and ISC secretome collected at Days 1, 3, 5 and 7, which were prepared in a 1:1 ratio with EndoC-βH1 culture medium (Chapter 2 **2.3.5** and **2.3.6**). ISC secretome samples were obtained from three ISC batches (three separate donors: LDIS 328, LDIS 335 and LDIS 355). A Cytokine Mix comprising 1 ng/ml IL-1β, 20 ng/ml TNF-α and 20 ng/ml INF-γ was also used as a positive control. RNA extraction was carried out as described in Chapter 2 (**2.3.12**) and RNA-sequencing was performed to generate over 30 million single-end reads of 100 base pairs in length per sample. This was undertaken by the Genomic Core Facility, Newcastle University. Initial data analysis was undertaken by the Bioinformatics Support Unit, Newcastle University and I conducted further pathway analysis using Ingenuity Pathway Analysis (IPA) software (Qiagen, Valencia, California, USA).

5.3.2.1 Bulk RNA-Sequencing un-biased data analysis

Principal Component Analysis (PCA) was used as an exploratory measure to visualise the variability of gene expression in different samples (EndoC-βH1 cells treated with Ctrl 2 medium and ISC secretome collected at different days) deriving PC1 and PC2. PC1 reported 59.2% of variance within samples, whereas PC2 reported 33.4% ***(Figure 5.6)***. Ctrl 2 samples appeared to be clustered together, whereas EndoC-βH1 cells treated with ISC secretome collected at different days appeared to exhibit biological variation based on donors, whereby samples were grouped together according to donor ID. EndoC-βH1 cells treated with ISC secretome from Donor LDIS328 showed greater variability compared to the other samples ***(Figure 5.6)***. Another PCA plot containing EndoC-βH1 cells treated with ISC secretome of different days, Cytokine Mixture and Ctrl 1 (100% DMEM medium) was included in Appendix ***(Figure 7.1).***

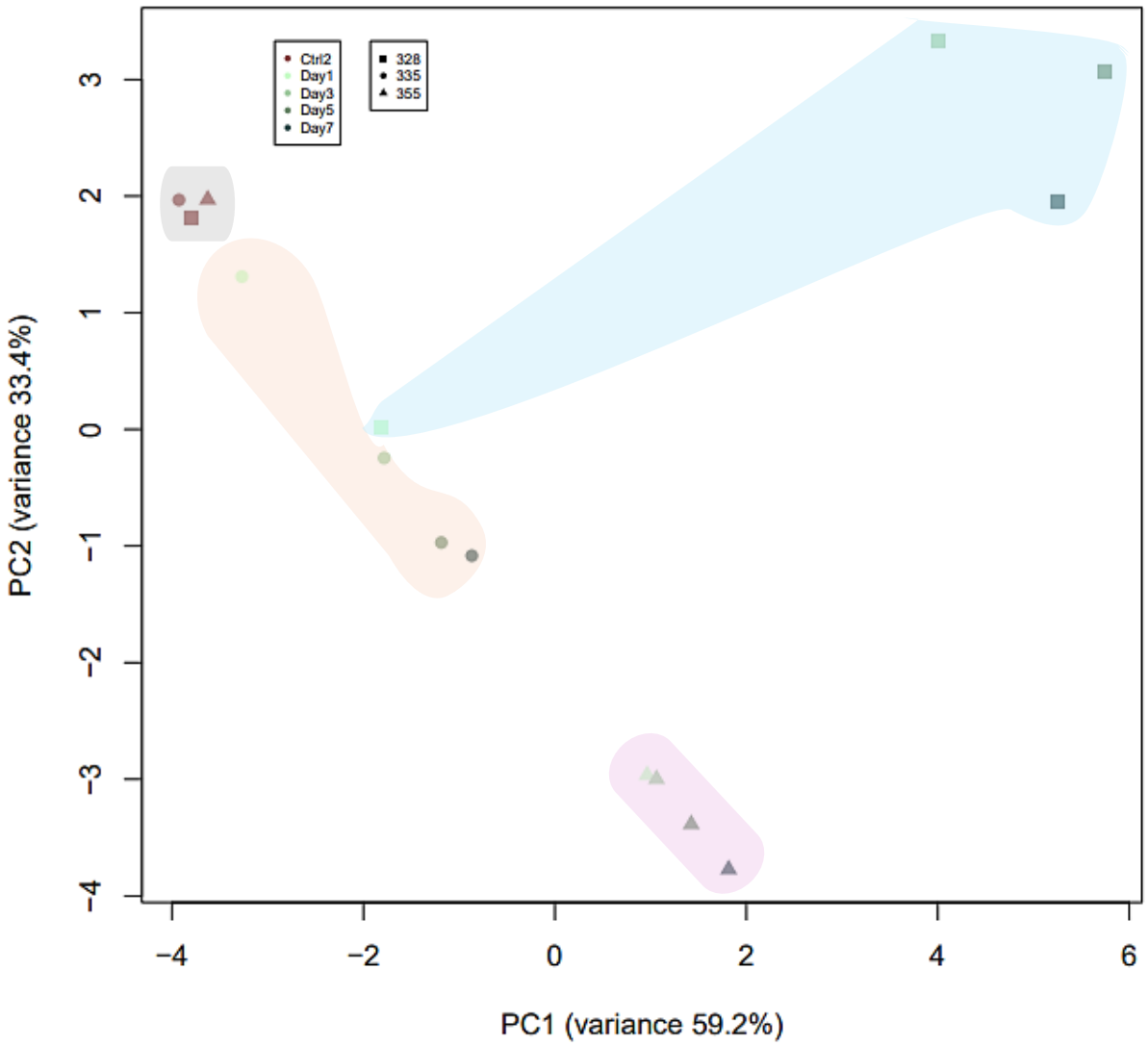

Figure 5.6: Principal Component Analysis (PCA) plot showing the variation of samples (EndoC-βH1 cells treated Ctrl 2 and ISC secretome of days 1, 3, 5 and 7) along the PC1 (59.2%) and PC2 (33.4%) axis.

Highlighted areas for EndoC-βH1 treated Ctrl2 (grey). EndoC-βH1 treated with LDIS328 ISC secretome (light yellow), LDIS335 ISC secretome (light orange) and LDIS355 ISC secretome (light blue).

Heatmaps of differentially expressed genes of Ctrl 2 vs treatment are included in Appendix (***Figure 7.8 - Figure 7.12***). The analysis reported that, compared to Ctrl 2, some of the differentially downregulated genes ($p < 0.05$) in EndoC-βH1 cells treated with ISC secretome include: β-cell identity genes: *PDX1*, *MafA* and *NKX 6.1 (*NK6 homeobox 1), ER stress gene X-box Binding Protein 1 *(XBP1).* Also, there was an upregulation in ER stress markers such as DNA Damage Inducible Transcript 3 (*DDIT3*) along with *XBP1* in Cytokine-treated EndoC-βH1 cells. Both treatments exhibited an increase in *Caspase 3* gene expression *(CASP3)* which is associated with the caspase pathway.

Pathway analysis was conducted using the IPA Software for each treatment condition vs Ctrl 2 and the top upregulated and downregulated pathways were graphed. For Ctrl 2 vs ISC secretome comparisons, the top five up- or down-regulated pathways for each condition were plotted based on significant gene expression ($p < 0.05$) of ± >1.5-fold change. Gene expression changes in EndoC-βH1 cells treated with all ISC donor conditioned media collected at all days of ISC culture were averaged and the top 10 significantly upregulated pathways and top five significantly downregulated pathways were plotted ***(Figure 5.7*** and ***Figure 5.8)***. To compare Ctrl 2 vs Cytokine Mix (1 ng/ml IL-1β, 20 ng/ml TNF-α and 20 ng/ml INF-γ), pathway analysis was conducted based on significant gene expression ($p < 0.05$) of ± 3-fold change due to the high variation in gene expression compared to Ctrl 2. The top five significantly upregulated and downregulated pathways are presented in ***Figure 5.9*** and ***Figure 5.10***. Graphical summaries of each treatment condition vs Ctrl 2 provided an overview of the key biological themes in the IPA analysis (See Appendix ***Figure 7.3 - Figure 7.7***). This shows visually the most significant genes identified during the core analysis and outlined their interactions with each other to provide a comprehensive picture of the cellular mechanisms, pathways, and key genes.

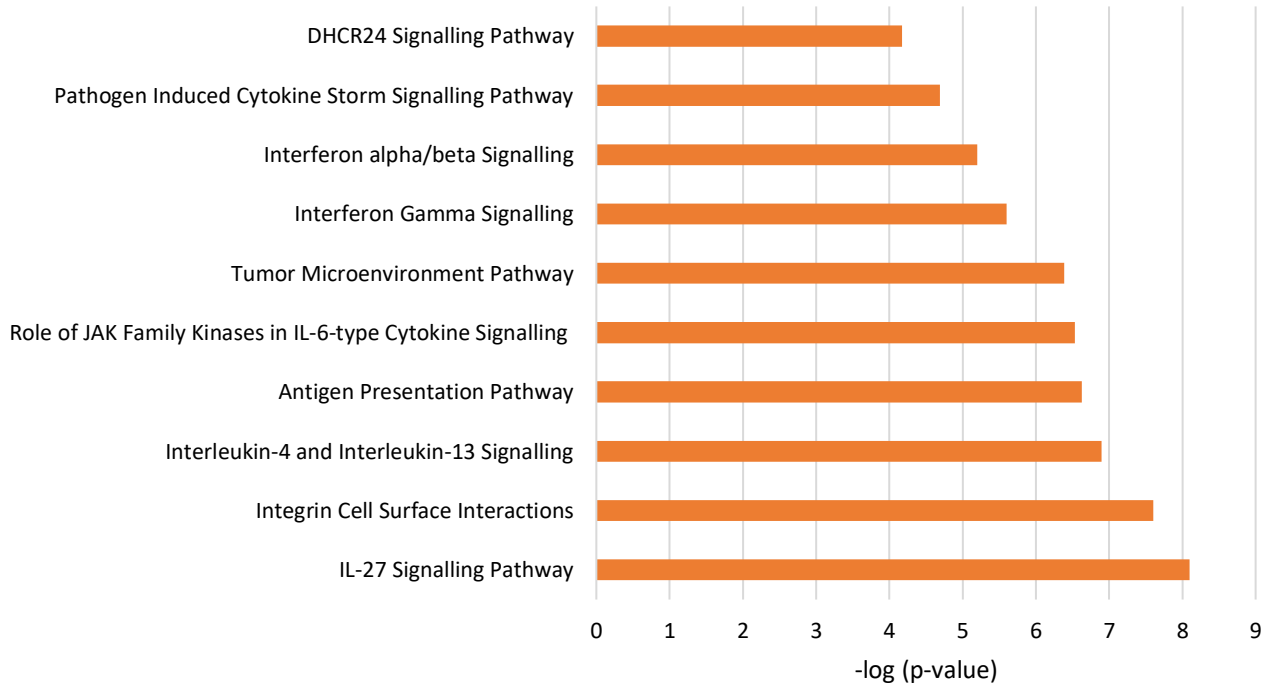

Figure 5.7: Top ten upregulated pathways in EndoC-βH1cells treated with ISC secretome. p<0.05.

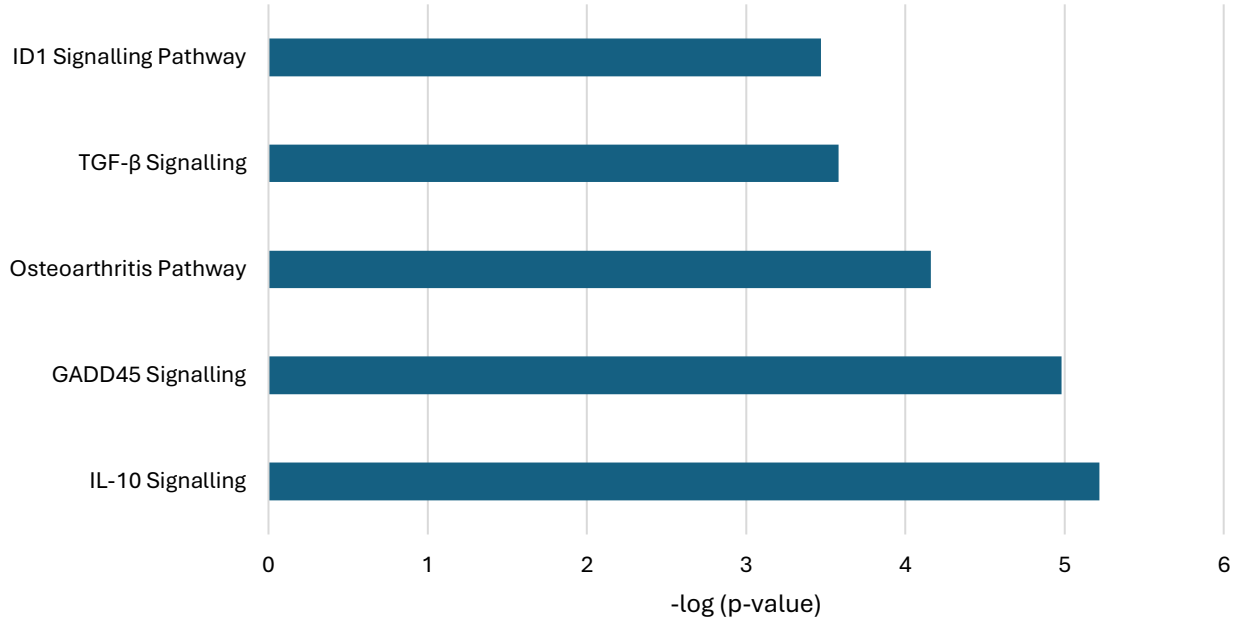

Figure 5.8: Top five downregulated pathways in EndoC-βH1 cells treated with ISC secretome. p<0.05.

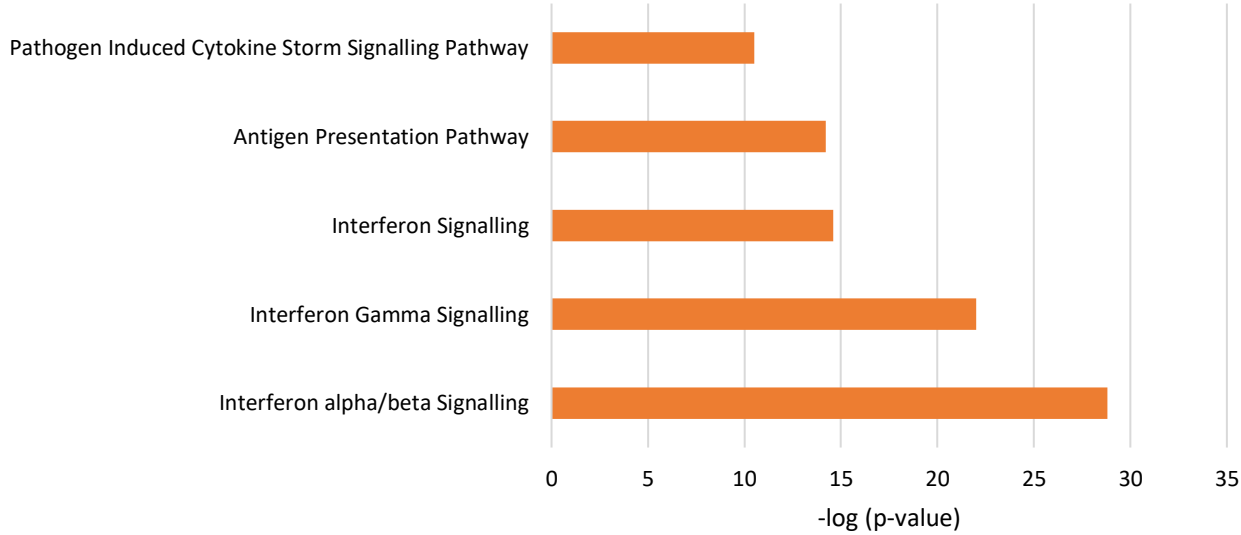

Figure 5.9: Top five upregulated pathways in EndoC-βH1 cells incubated with Cytokine Mix (1 ng/ml IL-1β, 20 ng/ml TNF-α and 20 ng/ml INF-γ). p<0.05.

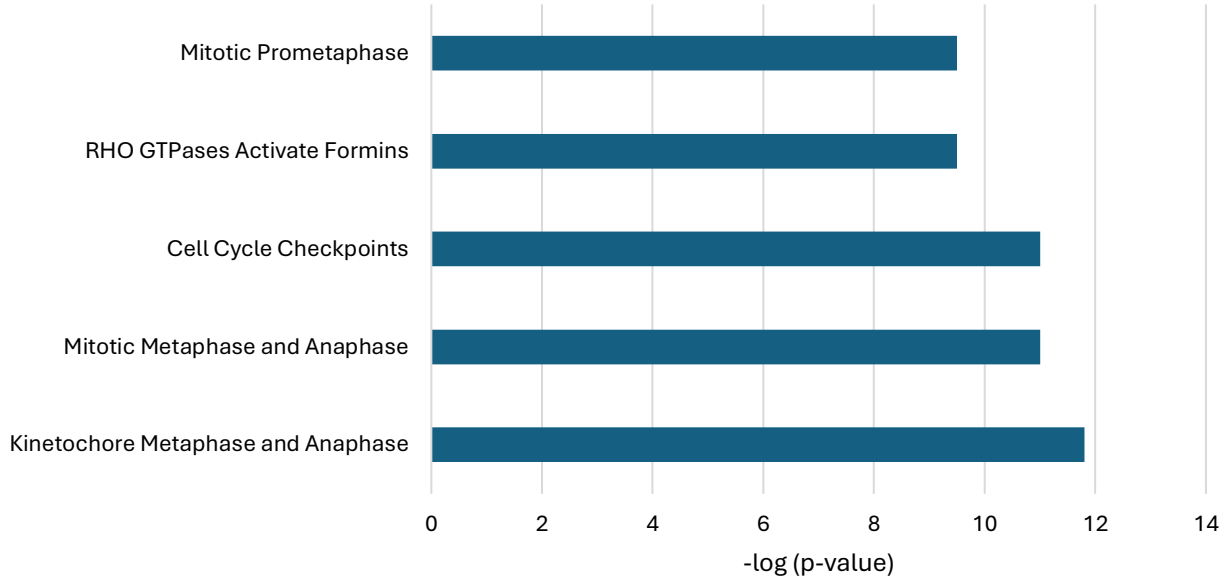

Figure 5.10: Top five downregulated pathways in EndoC-βH1 cells incubated with Cytokine Mix (1 ng/ml IL-1β, 20 ng/ml TNF-α and 20 ng/ml INF-γ). p<0.05.

Pathogen Induced Cytokine Storm Signalling Pathway was one of the upregulated pathways in EndoC-βH1 cells of ISC secretome treatment vs Ctrl 2 and Cytokine Mix treatment vs Ctrl 2. Examples of the pathway are illustrated for both treatments ***(Figure 5.11*** and ***Figure 5.13)***. Some of the top upregulated genes in this pathway associated with ISC secretome treatment included *COL3A1, COL5A2*, *COL6A2*, *COL9A1*, *STAT3* and *TGF-β1*. Whereas top upregulated genes associated with the Cytokine Mix treatment included *COL22A1*, *COL24A1*, *COL4A4*, *COL9A1*, *CXCL10*, *STAT1*, *STAT3* and *CASP7/8*.

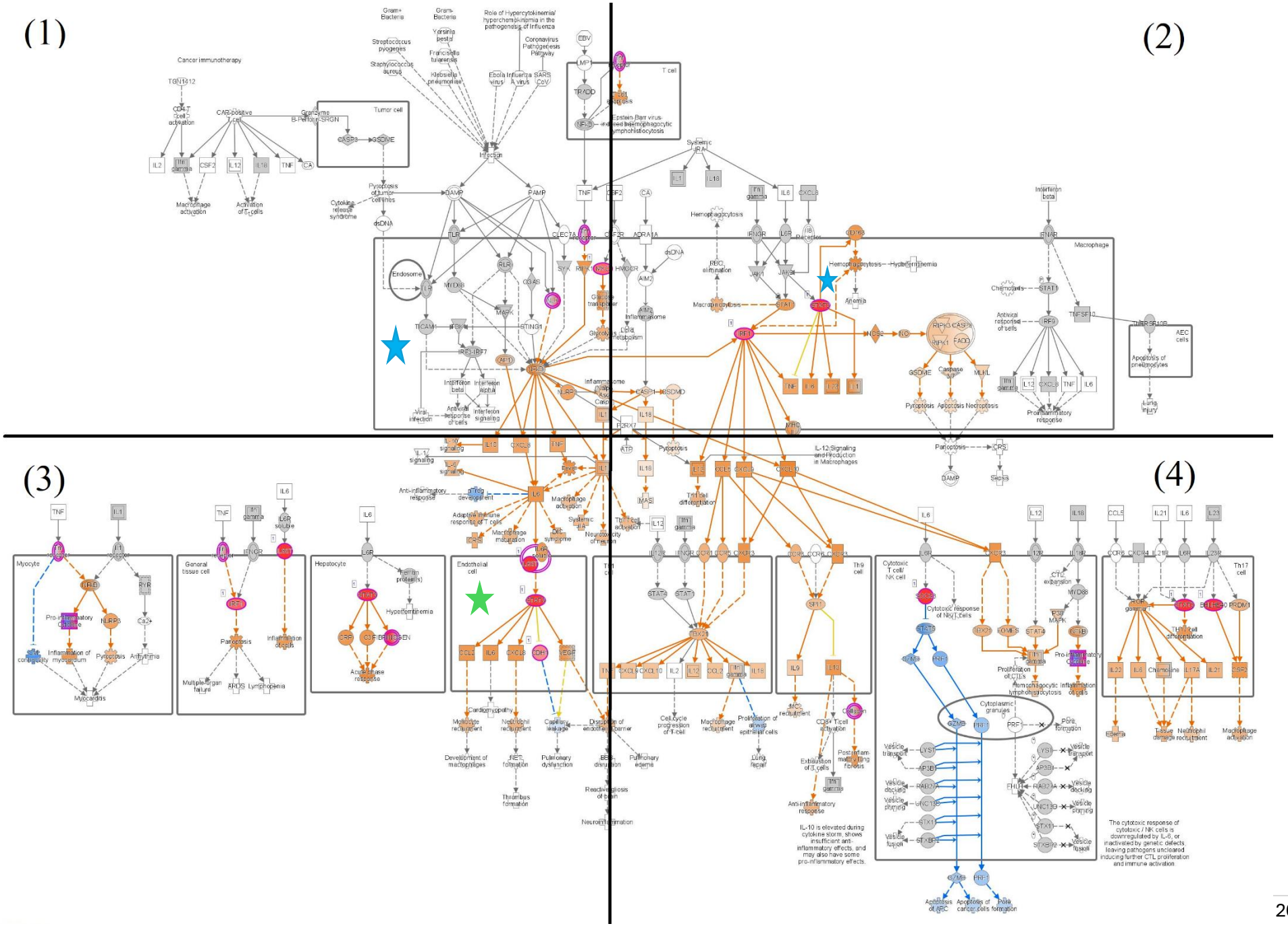
(1)
(2)
(3)
(4)
Cancer immunotherapy
Tumor cell
Infection
T cell
Macrophage
Endosome
Myocyte
General tissue cell
Hepatocyte
Endothelial cell
Cytotoxic T cell/ NK cell
Th9 cell
Th17 cell
Macrophage activation
Activation of T cells
Cytokine release syndrome
Pyroptosis
Apoptosis Necroptosis
Sepsis
Lung injury
Myocarditis
Cardiomyopathy
Thrombus formation
Pulmonary edema
Pulmonary dysfunction
Cytotoxic response of NK cells
Cytoplasmic granules
Apoptosis of APC
Apoptosis of cancer cells
Pore formation
IL-10 is elevated during cytokine storm, shows insufficient anti-inflammatory effects, and may also have some pro-inflammatory effects.
The cytotoxic response of cytotoxic / NK cells is downregulated by IL-6, or inactivated by genetic defects, leaving pathogens uncleared inducing further CTL proliferation and immune activation.

Figure 5.11: Illustration of the key genes involved in the Pathogen Induced Cytokine Storm Pathway in EndoC-βH1 cells treated with ISC secretome of Day 5.

The diagram is subdivided into four sections that are magnified in ***Figure 5.12****. Orange colour indicates predicated activation, blue: predicated inhibition. The darker the colour the greater increase/decrease in differential gene expression. Predicted relationships illustrated with lines: orange (leads to activation), blue (leads to inhibition), yellow (findings inconsistent with regards to downstream impact). Dashed lines indicate indirect relationship, whereas solid lines indicate direct relationship. The activation of IL-6 is enhanced by the upregulation of STAT3 and NF-κB (indicated by blue stars in sections 1,2 and 3). Further, the IL-6 influences the expression of STAT3 in Endothelial cells (indicated by a green star in section 3) which positively influences the expression of different genes such as CCL2, CXCL-8 and VEGF, that are associated with the recruitment of monocytes, neutrophils and disruption of endothelial barrier, respectively.*

(1)

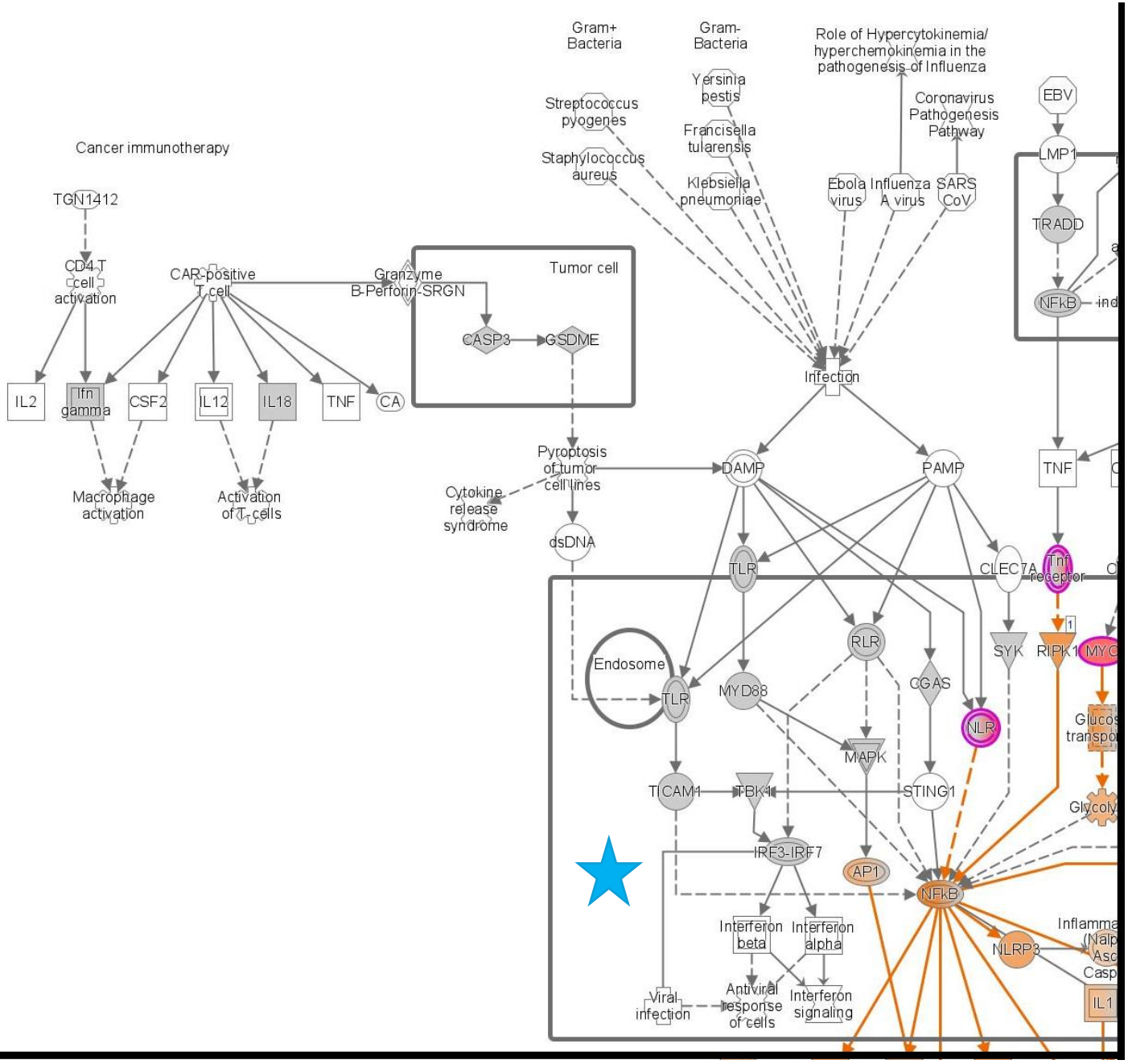
Gram+ Bacteria
Gram- Bacteria
Role of Hypercytokinemia/ hyperchemokinemia in the pathogenesis of Influenza
Yersinia pestis
Streptococcus pyogenes
Francisella tularensis
Coronavirus Pathogenesis Pathway
EBV
Staphylococcus aureus
Klebsiella pneumoniae
Ebola virus
Influenza A virus
SARS CoV
LMP1
Cancer immunotherapy
TRADD
TGN1412
CD4 T cell activation
CAR-positive T cell
Granzyme B-Perforin-SRGN
Tumor cell
NFkB
CASP3
GSDME
Infection
IL2
Ifn gamma
CSF2
IL12
IL18
TNF
CA
Pyroptosis of tumor cell lines
DAMP
PAMP
TNF
Macrophage activation
Activation of T cells
Cytokine release syndrome
dsDNA
TLR
CLEC7A
Tnf receptor
RLR
SYK
RIPK1
Endosome
TLR
MYD88
CGAS
NLR
MAPK
TICAM1
TBK1
STING1
IRF3-IRF7
AP1
NFkB
Interferon beta
Interferon alpha
NLRP3
Viral infection
Antiviral response of cells
Interferon signaling
IL1

(2)

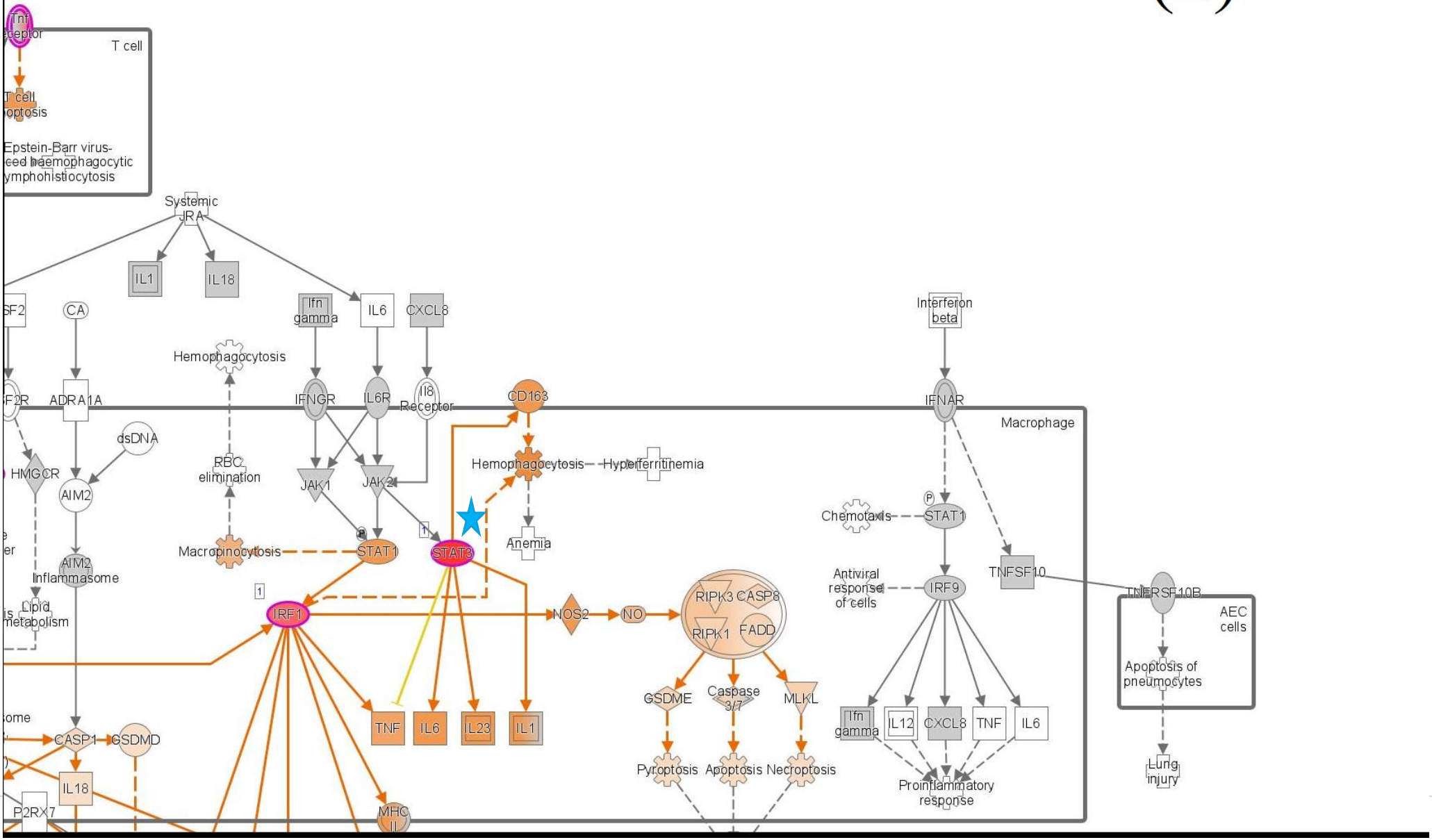
T cell
Epstein-Barr virus-
eed haemophagocytic
ymphohistiocytosis
Systemic
JRA
IL1
IL18
Ifn
gamma
IL6
CXCL8
Hemophagocytosis
IFNGR
IL6R
Receptor
CD163
Interferon
beta
IFNAR
Macrophage
ADRA1A
dsDNA
HMGCR
AIM2
RBC
elimination
JAK1
JAK2
Hemophagocytosis
Hyperferritinemia
Anemia
Macropinocytosis
STAT1
STAT3
Chemotaxis
Inflammasome
Lipid
metabolism
IRF1
NOS2
NO
RIPK3
CASP8
RIPK1
FADD
Antiviral
response
of cells
IRF9
TNFSF10
TNFRSF10B
AEC
cells
Apoptosis of
pneumocytes
GSDME
Caspase
3/7
MLKL
Pyroptosis
Apoptosis
Necroptosis
Ifn
gamma
IL12
CXCL8
TNF
IL6
Proinflammatory
response
Lung
injury
CASP1
GSDMD
IL18
P2RX7
TNF
IL6
IL23
IL1
MHC
II

(3)

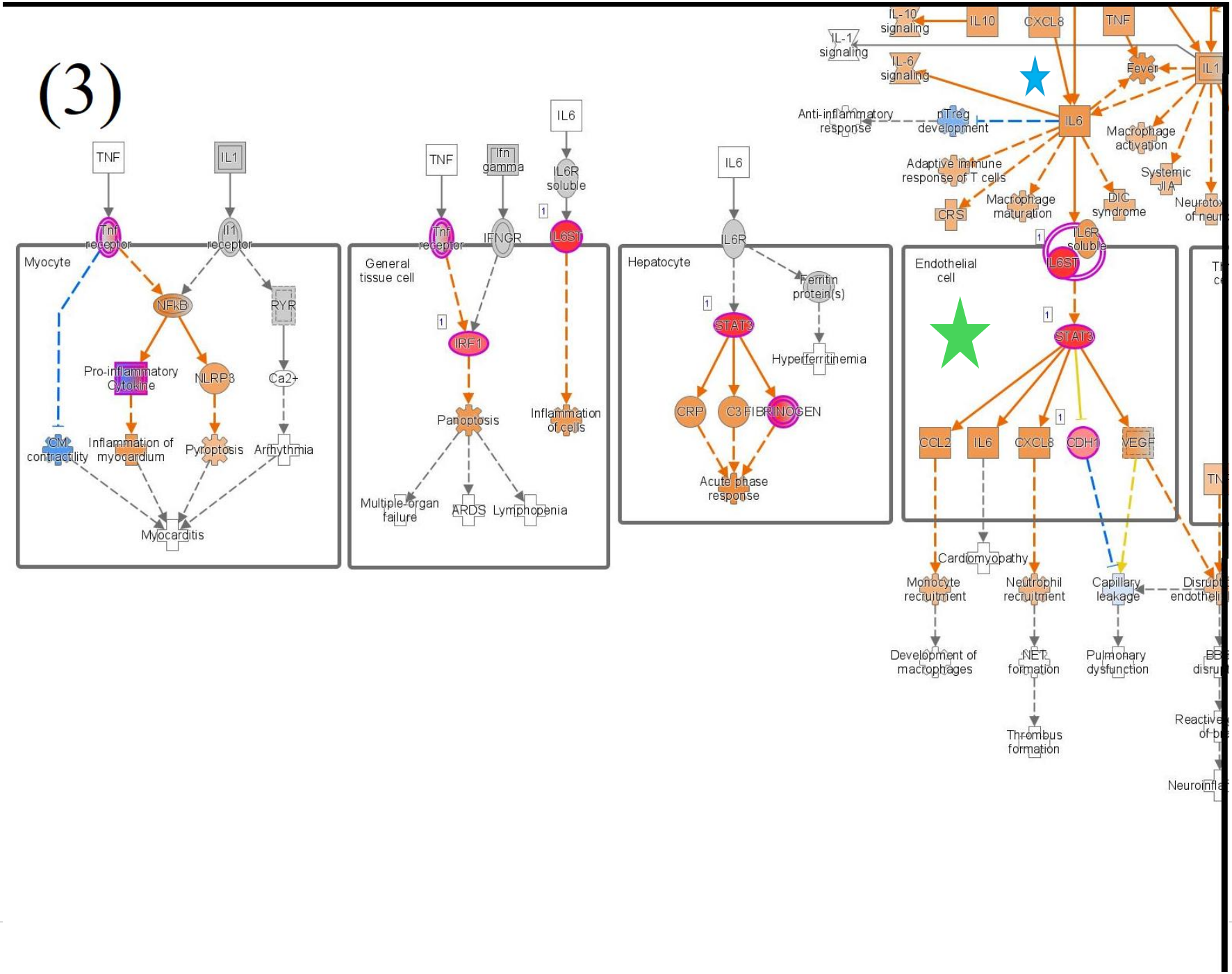
IL-10 signaling
IL10
CXCL8
TNF
IL-1 signaling
IL-6 signaling
Fever
IL1
Anti-inflammatory response
nTreg development
IL6
Macrophage activation
Adaptive immune response of T cells
Systemic JIA
Macrophage maturation
DIC syndrome
CRS
IL6R soluble
IL6ST
TNF
IL1
Tnf receptor
Il1 receptor
Myocyte
NFkB
RYR
Pro-inflammatory Cytokine
NLRP3
Ca2+
CM contractility
Inflammation of myocardium
Pyroptosis
Arrhythmia
Myocarditis
TNF
Ifn gamma
IL6
IL6R soluble
Tnf receptor
IFNGR
IL6ST
General tissue cell
IRF1
Panoptosis
Inflammation of cells
Multiple-organ failure
ARDS
Lymphopenia
IL6
IL6R
Hepatocyte
Ferritin protein(s)
STAT3
Hyperferritinemia
CRP
C3
FIBRINOGEN
Acute phase response
Endothelial cell
IL6R soluble
IL6ST
STAT3
CCL2
IL6
CXCL8
CDH1
VEGF
Cardiomyopathy
Monocyte recruitment
Neutrophil recruitment
Capillary leakage
Development of macrophages
NET formation
Pulmonary dysfunction
Thrombus formation

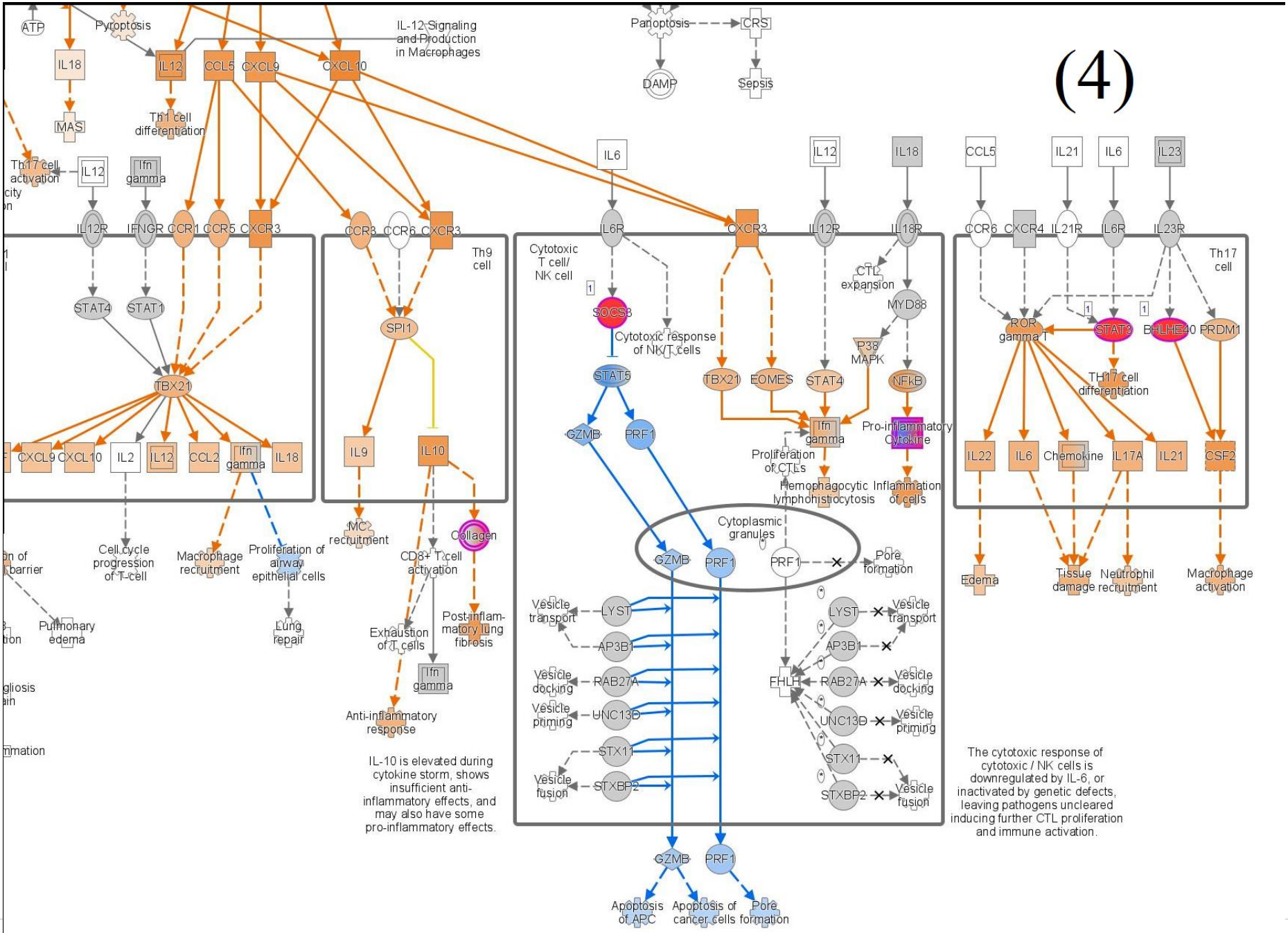
(4)
ATP
Pyroptosis
IL-12 Signaling and Production in Macrophages
Panoptosis
CRS
DAMP
Sepsis
IL18
IL12
CCL5
CXCL9
CXCL10
MAS
Th1 cell differentiation
Th17 cell activation
IL12
Ifn gamma
IL6
IL12
IL18
CCL5
IL21
IL6
IL23
IL12R
IFNGR
CCR1
CCR5
CXCR3
CCR8
CCR6
CXCR3
Th9 cell
IL6R
CXCR3
IL12R
IL18R
CCR6
CXCR4
IL21R
IL6R
IL23R
Th17 cell
Cytotoxic T cell/ NK cell
CTL expansion
MYD88
STAT4
STAT1
SPI1
SOCS3
Cytotoxic response of NK/T cells
P38 MAPK
ROR gamma T
STAT3
BHLHE40
PRDM1
TH17 cell differentiation
TBX21
STAT5
TBX21
EOMES
STAT4
NFkB
CXCL9
CXCL10
IL2
IL12
CCL2
Ifn gamma
IL18
IL9
IL10
GZMB
PRF1
Ifn gamma
Pro-inflammatory Cytokine
Proliferation of CTLs
Hemophagocytic lymphohistiocytosis
Inflammation of cells
IL22
IL6
Chemokine
IL17A
IL21
CSF2
Cytoplasmic granules
MC recruitment
Collagen
GZMB
PRF1
PRF1
Pore formation
Cell cycle progression of T-cell
Macrophage recruitment
Proliferation of airway epithelial cells
CD8+ T cell activation
Vesicle transport
LYST
AP3B1
Vesicle docking
RAB27A
Vesicle priming
UNC13D
STX11
Vesicle fusion
STXBP2
FHL1
Edema
Tissue damage
Neutrophil recruitment
Macrophage activation
Pulmonary edema
Lung repair
Exhaustion of T cells
Post-inflam-matory lung fibrosis
Ifn gamma
Anti-inflammatory response
IL-10 is elevated during cytokine storm, shows insufficient anti-inflammatory effects, and may also have some pro-inflammatory effects.
The cytotoxic response of cytotoxic / NK cells is downregulated by IL-6, or inactivated by genetic defects, leaving pathogens uncleared inducing further CTL proliferation and immune activation.
GZMB
PRF1
Apoptosis of APC
Apoptosis of cancer cells
Pore formation

Figure 5.12: Magnified diagrams of the key genes involved in the Pathogen Induced Cytokine Storm Pathway in EndoC-βH1 cells treated with ISC secretome of Day 5.

Magnified diagrams of ***Figure 5.11****. Orange colour indicates predicated activation, blue: predicated inhibition. The darker the colour the greater increase/decrease in differential gene expression. Predicted relationships illustrated with lines: orange (leads to activation), blue (leads to inhibition), yellow (findings inconsistent with regards to downstream impact). Dashed lines indicate indirect relationship, whereas solid lines indicate direct relationship. The activation of IL-6 is enhanced by the upregulation of STAT3 and NF-κB (indicated by blue stars in sections 1,2 and 3). Further, the IL-6 influences the expression of STAT3 in Endothelial cells (indicated by a green star in section 3) which positively influences the expression of different genes such as CCL2, CXCL-8 and VEGF, that are associated with the recruitment of monocytes, neutrophils and disruption of endothelial barrier, respectively.*

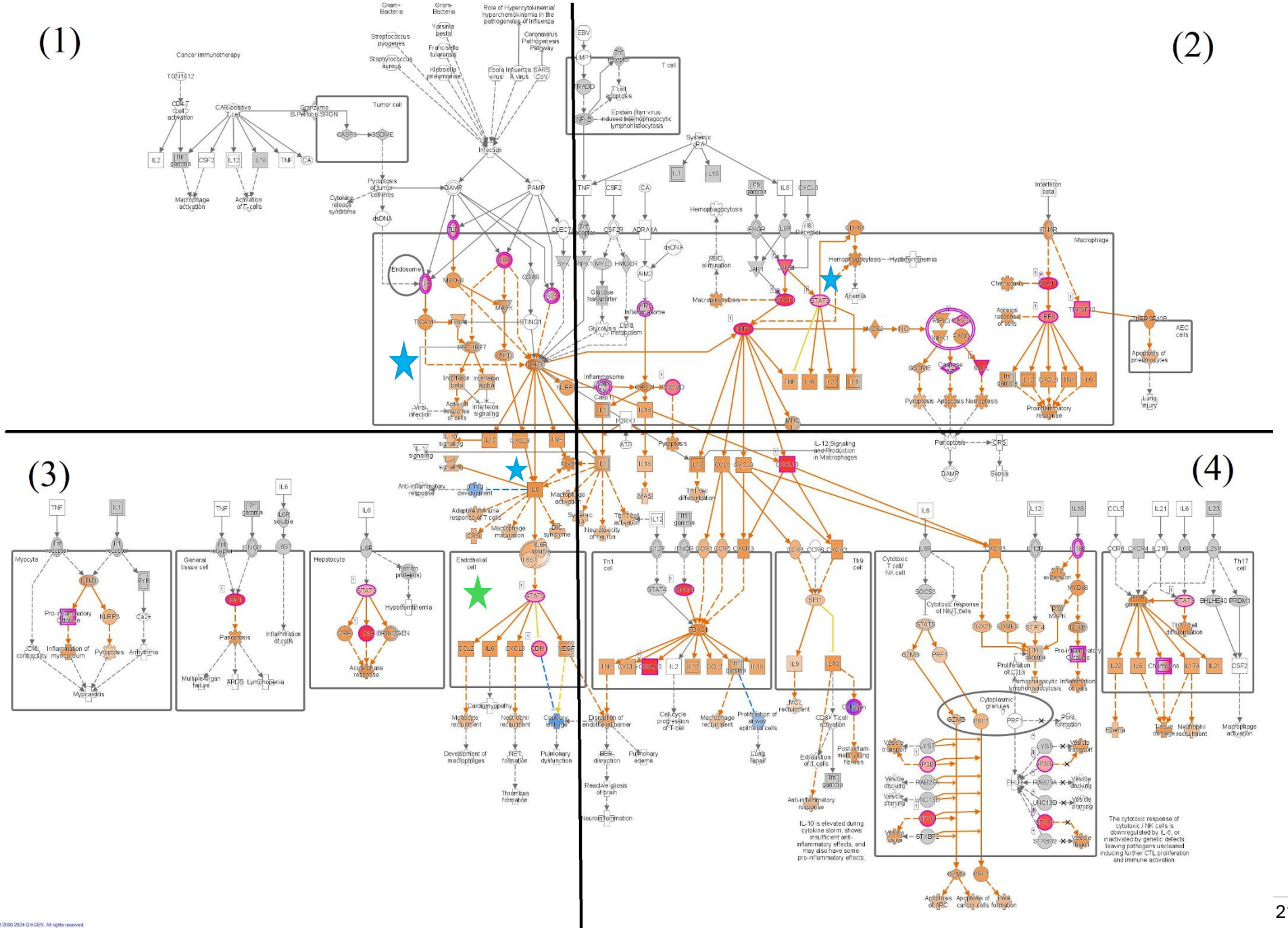

Figure 5.13: Illustration of the key genes involved in the Pathogen Induced Cytokine Storm Pathway in EndoC-βH1 cells treated with Cytokine Mix (1 ng/ml IL-1β, 20 ng/ml TNF-α and 20 ng/ml INF-γ).

The diagram is subdivided into four sections that are magnified in ***Figure 5.14****. Orange colour indicates predicated activation, blue: predicated inhibition. The darker the colour the greater increase/decrease in differential gene expression. Predicted relationships illustrated with lines: orange (leads to activation), blue (leads to inhibition), yellow (findings inconsistent with regards to downstream impact). Dashed lines indicate indirect relationship, whereas solid lines indicate direct relationship. The activation of IL-6 is enhanced by the upregulation of STAT3 and NF-κB (indicated by blue stars in sections 1,2 and 3). Further, the IL-6 influences the expression of STAT3 in Endothelial cells (indicated by a green star in section 3) which positively influences the expression of different genes such as CCL2, CXCL-8 and VEGF, that are associated with the recruitment of monocytes, neutrophils and disruption of endothelial barrier, respectively.*

(1)

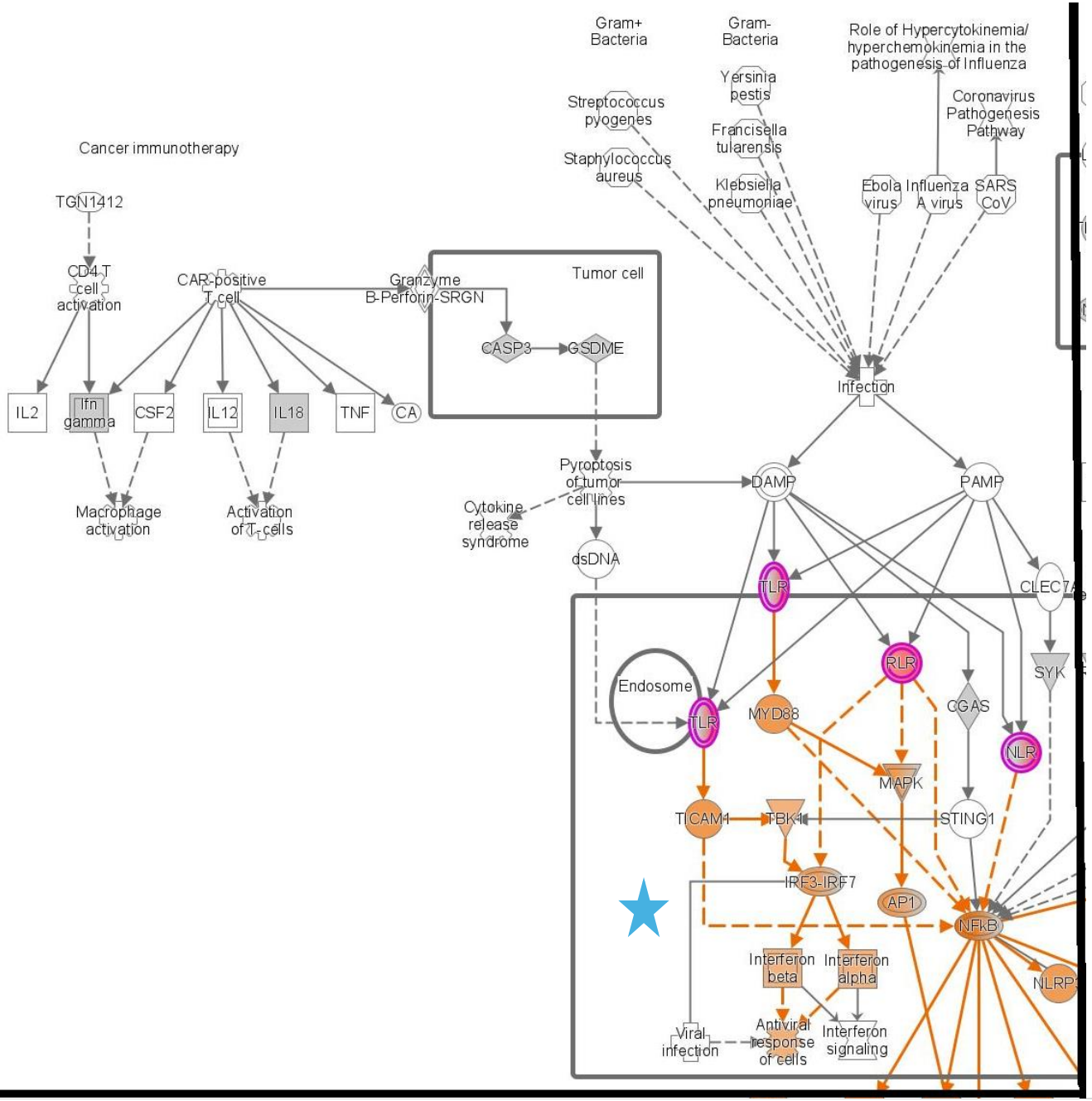
Gram+ Bacteria
Gram- Bacteria
Role of Hypercytokinemia/ hyperchemokinemia in the pathogenesis of Influenza
Yersinia pestis
Streptococcus pyogenes
Francisella tularensis
Coronavirus Pathogenesis Pathway
Staphylococcus aureus
Klebsiella pneumoniae
Ebola virus
Influenza A virus
SARS CoV
Cancer immunotherapy
TGN1412
CD4 T cell activation
CAR-positive T cell
Granzyme B-Perforin-SRGN
Tumor cell
CASP3
GSDME
Infection
IL2
Ifn gamma
CSF2
IL12
IL18
TNF
CA
Pyroptosis of tumor cell lines
DAMP
PAMP
Macrophage activation
Activation of T cells
Cytokine release syndrome
dsDNA
TLR
CLEC7A
RLR
SYK
Endosome
MYD88
CGAS
NLR
MAPK
TICAM1
TBK1
STING1
IRF3-IRF7
AP1
NFkB
Interferon beta
Interferon alpha
NLRP3
Viral infection
Antiviral response of cells
Interferon signaling

(2)

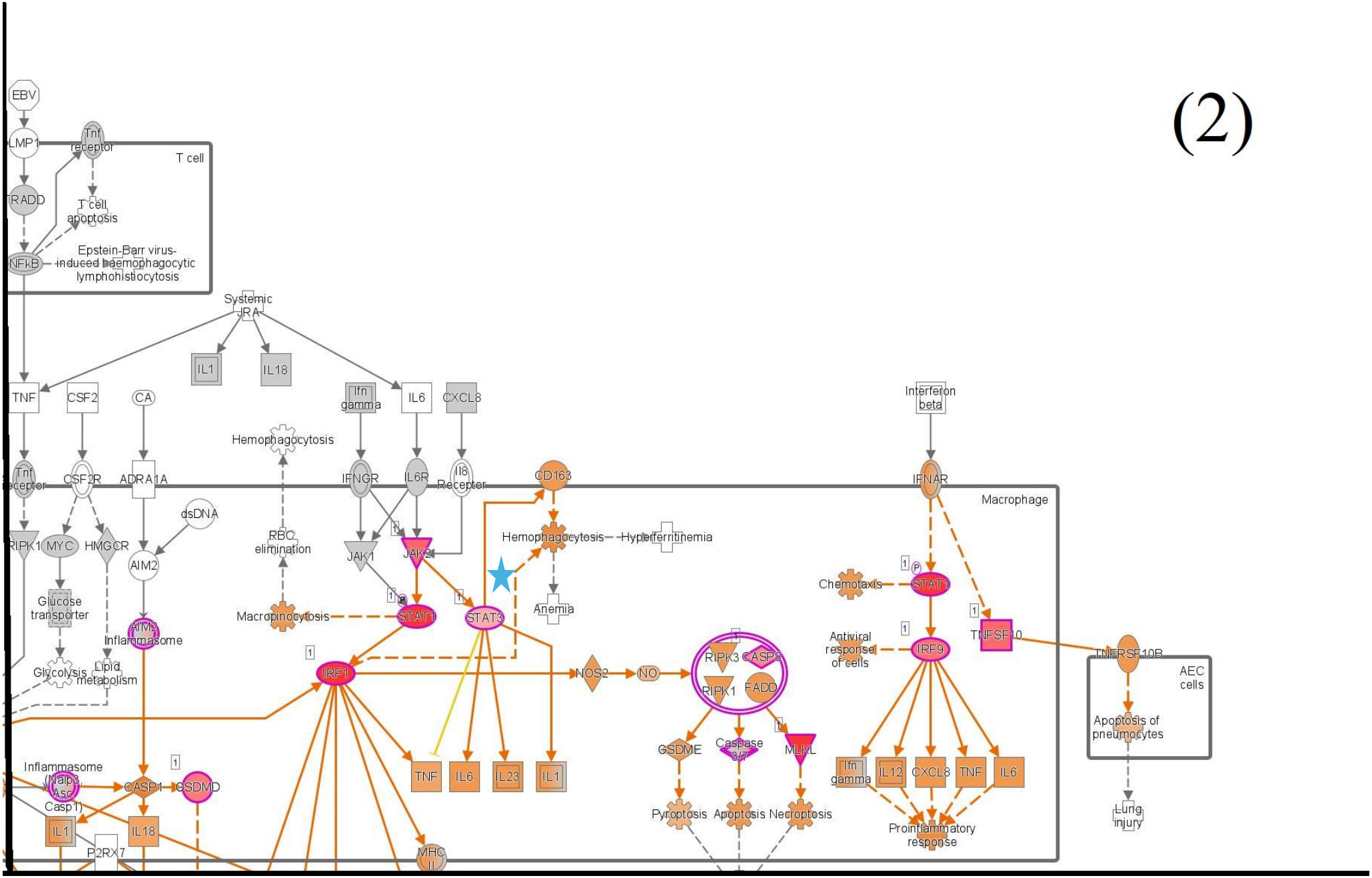
EBV
LMP1
Tnf receptor
T cell
TRADD
T cell apoptosis
NFkB
Epstein-Barr virus-induced haemophagocytic lymphohistiocytosis
Systemic JRA
IL1
IL18
TNF
CSF2
CA
Ifn gamma
IL6
CXCL8
Interferon beta
Hemophagocytosis
Tnf receptor
CSF2R
ADRA1A
IFNGR
IL6R
Il8 Receptor
CD163
IFNAR
Macrophage
dsDNA
RIPK1
MYC
HMGCR
AIM2
RBC elimination
JAK1
JAK2
Hemophagocytosis
Hyperferritinemia
Chemotaxis
STAT1
Glucose transporter
Macropinocytosis
STAT1
STAT3
Anemia
Antiviral response of cells
IRF9
TNFSF10
TNFRSF10B
AIM2 Inflammasome
Glycolysis
Lipid metabolism
IRF1
NOS2
NO
RIPK3
CASP8
RIPK1
FADD
AEC cells
Apoptosis of pneumocytes
Inflammasome (Nalp3, Asc, Casp1)
CASP1
GSDMD
TNF
IL6
IL23
IL1
GSDME
Caspase 3/7
MLKL
Ifn gamma
IL12
CXCL8
TNF
IL6
Lung injury
IL1
IL18
P2RX7
MHC II
Pyroptosis
Apoptosis
Necroptosis
Proinflammatory response

(3)

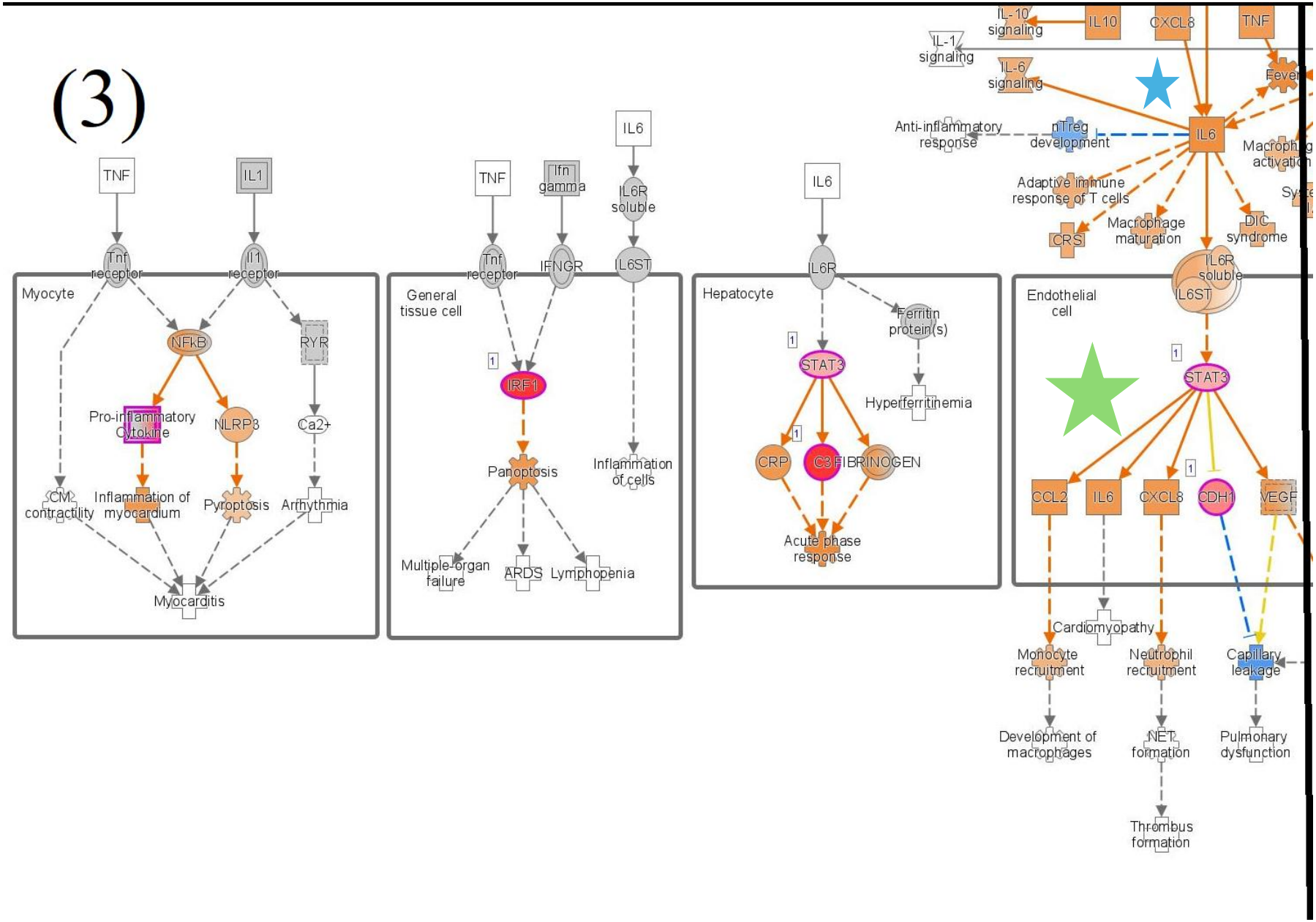
TNF
IL1
Tnf receptor
Il1 receptor
Myocyte
NFkB
RYR
Pro-inflammatory Cytokine
NLRP3
Ca2+
CM contractility
Inflammation of myocardium
Pyroptosis
Arrhythmia
Myocarditis
TNF
Ifn gamma
IL6
IL6R soluble
Tnf receptor
IFNGR
IL6ST
General tissue cell
1
IRF1
Panoptosis
Inflammation of cells
Multiple-organ failure
ARDS
Lymphopenia
IL6
IL6R
Hepatocyte
Ferritin protein(s)
1
STAT3
Hyperferritinemia
1
CRP
C3
FIBRINOGEN
Acute phase response
IL-10 signaling
IL10
CXCL8
TNF
IL-1 signaling
IL-6 signaling
Anti-inflammatory response
nTreg development
IL6
Adaptive immune response of T cells
Macrophage maturation
DIC syndrome
CRS
IL6R soluble
IL6ST
Endothelial cell
1
STAT3
1
CCL2
IL6
CXCL8
CDH1
VEGF
Cardiomyopathy
Monocyte recruitment
Neutrophil recruitment
Capillary leakage
Development of macrophages
NET formation
Pulmonary dysfunction
Thrombus formation

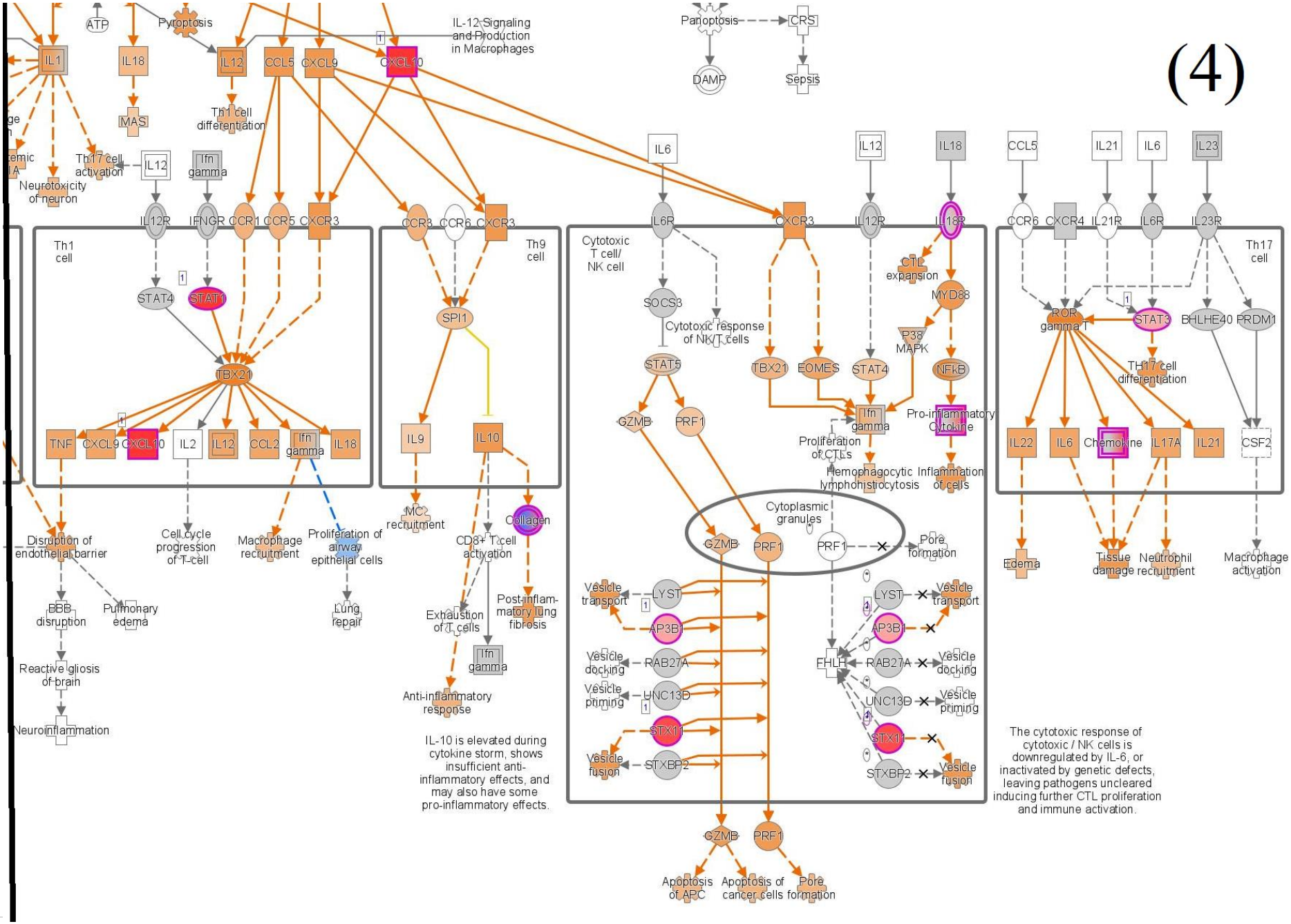
(4)
ATP
Pyroptosis
IL-12 Signaling and Production in Macrophages
Panoptosis
CRS
DAMP
Sepsis
IL1
IL18
IL12
CCL5
CXCL9
CXCL10
MAS
Th1 cell differentiation
Th17 cell activation
Neurotoxicity of neuron
Ifn gamma
IL12R
IFNGR
CCR1
CCR5
CXCR3
CCR8
CCR6
Th1 cell
Th9 cell
STAT4
STAT1
SPI1
TBX21
TNF
CXCL9
CXCL10
IL2
CCL2
IL9
IL10
Disruption of endothelial barrier
Cell cycle progression of T-cell
Macrophage recruitment
Proliferation of airway epithelial cells
MC recruitment
CD8+ T cell activation
Collagen
BBB disruption
Pulmonary edema
Lung repair
Exhaustion of T cells
Post-inflammatory lung fibrosis
Reactive gliosis of brain
Neuroinflammation
Anti-inflammatory response
IL-10 is elevated during cytokine storm, shows insufficient anti-inflammatory effects, and may also have some pro-inflammatory effects.
IL6
IL12
IL18
IL6R
CXCR3
IL12R
IL18R
Cytotoxic T cell/ NK cell
SOCS3
Cytotoxic response of NK/T cells
STAT5
TBX21
EOMES
STAT4
CTL expansion
MYD88
P38 MAPK
NFkB
GZMB
PRF1
Ifn gamma
Pro-inflammatory Cytokine
Proliferation of CTLs
Hemophagocytic lymphohistiocytosis
Inflammation of cells
Cytoplasmic granules
Pore formation
Vesicle transport
LYST
AP3B1
Vesicle docking
RAB27A
Vesicle priming
UNC13D
STX11
Vesicle fusion
STXBP2
FHL1
Apoptosis of APC
Apoptosis of cancer cells
Pore formation
CCL5
IL21
IL6
IL23
CCR6
CXCR4
IL21R
IL6R
IL23R
Th17 cell
ROR gamma T
STAT3
BHLHE40
PRDM1
TH17 cell differentiation
IL22
IL6
Chemokine
IL17A
IL21
CSF2
Edema
Tissue damage
Neutrophil recruitment
Macrophage activation
The cytotoxic response of cytotoxic / NK cells is downregulated by IL-6, or inactivated by genetic defects, leaving pathogens uncleared inducing further CTL proliferation and immune activation.

Figure 5.14: Magnified diagrams of the key genes involved in the Pathogen Induced Cytokine Storm Pathway in EndoC-βH1 cells treated with Cytokine Mix (1 ng/ml IL-1β, 20 ng/ml TNF-α and 20 ng/ml INF-γ).

Magnified diagrams of ***Figure 5.13****. Orange colour indicates predicated activation, blue: predicated inhibition. The darker the colour the greater increase/decrease in differential gene expression. Predicted relationships illustrated with lines: orange (leads to activation), blue (leads to inhibition), yellow (findings inconsistent with regards to downstream impact). Dashed lines indicate indirect relationship, whereas solid lines indicate direct relationship. The activation of IL-6 is enhanced by the upregulation of STAT3 and NF-κB (indicated by blue stars in sections 1,2 and 3). Further, the IL-6 influences the expression of STAT3 in Endothelial cells (indicated by a green star in section 3) which positively influences the expression of different genes such as CCL2, CXCL-8 and VEGF, that are associated with the recruitment of monocytes, neutrophils and disruption of endothelial barrier, respectively.*

5.4 Discussion

5.4.1 Overview

The molecular mechanisms leading to impaired insulin secretion in CF and the development of diabetes remain virtually entirely unknown. The work reported in this chapter aimed to undertake transcriptomic analysis to investigate differentially expressed genes in CF vs normal pancreas and a human β-cell line treated with ISC-conditioned medium to explore the potential signalling pathways associated with the morphological changes reported as CF progresses and the potential role of activated α-SMA^{+} cells. Also, to investigate changes in key transcripts reflecting EndoC-βH1 cell identity and survival following treatment with ISC secretome.

5.4.2 Why NanoString nCounter analysis?

Initially, it was intended to analyse RNA samples extracted from human CF tissue via bulk RNA-sequencing. But unlike the RNA samples extracted from QUOD controls, the library preparation procedure in the RNA samples extracted from the *post-mortem* Klöppel CF samples failed as seen in Appendix ***Figure 7.2***. This could be due to poor RNA integrity of CF samples due to them being *post-mortem* samples with possible prolonged ischaemia time. This may have yielded them fragile and susceptible to RNA degradation and unsuitability for reverse transcription necessary for cDNA synthesis and amplification. This unsuccessful method of investigating the transcriptome of CF samples led me to consider the use of more highly sensitive technique. NanoString nCounter analysis was undertaken, being highly sensitive / specific and capable of profiling gene expression in samples with poor RNA quality with no further additional steps such as cDNA synthesis and amplification (Veldman-Jones et al., 2015; Pedrosa et al., 2023). NanoString nCounter platform has been used in various clinical and research studies (Scott et al., 2013; Martin et al., 2014; Saba et al., 2015; Veldman-Jones et al., 2015; Pedrosa et al., 2023).

5.4.3 NanoString profiling of CF tissue enabled identification of possible associated pathways and biomarkers

NanoString nCounter analysis successfully undertaken on CF human fixed tissue was performed using the nCounter® Human Fibrosis V2 Panel consisting of 760 genes that encompass key fibrosis pathways and processes. Differential gene expression analysis of control and CF samples identified 55 key genes that were significantly ($p < 0.05$) overexpressed

(≥1.5-fold change) in CF tissue and were linked with various pathways ***(Figure 5.2)***. The EMT pathway appeared to be a key pathway regulating the different changes observed in CF tissue with many upregulated genes involved in EMT pathway such as *TGF-β1*, *ACTA2*, *CXCL*-12 and *CXCR4*. Compared to control, CF Pattern 1 and 2 biopsies were associated with fibrosis-associated changes in gene expression also revealing elevating levels of other EMT markers such as *POSTN*, *NRP2* and *MMP2*. Interestingly, later-stage CF exhibited another EMT marker *VIM* and upregulated genes associated with the *de novo* lipogenesis pathway (*FASN*), ECM degradation pathway (*LAMCI*) and autophagy (*MAPILC3A*), further reflecting the fibrotic changes observed within the diseased tissue. In CF, there was a reduction in genes associated with ECM degradation and biosynthesis pathways, which could explain the severe fibrotic changes represented by the abnormal deposition of collagen observed within the exocrine parenchyma and loss of normal tissue remodelling / repair ***(Figure 5.3)***.

Hart et al. (2018) investigated key transcripts associated with endocrine cell identity, maintenance and hormone secretion in islets isolated from five CF donors using whole-islet RNA sequencing (Hart et al., 2018). The study reported no gene expression changes in islets from CF donors when compared to control and suggested that the islet's genetic identity was preserved despite CF (Hart et al., 2018). This study had some limitations including the small sample size and the isolation procedure of islets which might have artefactually influenced islet gene expression and function and masked the true effect of CF *in vivo* (Hart et al., 2018). Having shown the presence of activated PaSCs in islets of CF ferrets, RNA expression analysis of isolated and cultured islets reported an increased levels of genes associated with PaSCs activation, fibrosis and inflammation including *acta2*, *IL-6* and *tgf-β1*, in keeping with a role for α-SMA positive cells within and around islets in driving endocrine cell dysfunction (Sun et al., 2017).

Up to date, no previous studies have reported bulk transcriptomic analysis of human CF pancreata. Our NanoString analysis has provided powerful new insights into potential cellular mechanisms and genes associated with CF changes and progression. The data of early- versus later-stage CF illustrated elevated levels of EMT and TGF-β associated genes that are possibly mediating the exocrine changes leading to destructive fibrotic tissue remodelling. Advanced- and end-stages CF exhibited an upregulation of genes associated with lipogenesis and fat metabolism pathways which could provide further insight into disease pathogenesis towards

global adipocyte replacement. The data also demonstrated reduction in genes associated with healthy ECM biosynthesis and degradation.

These gene signatures could serve as initial biomarkers for further studies that aim to investigate other genes associated within reported signalling pathways, which could contribute to β-cell impairment and eventually the development of CFRD. This promises potential development of pathway-specific targeted therapeutics which could prevent the onset of diabetes in CF.

5.4.4 Bulk RNA-Sequencing of EndoC-βH1 cells following ISC secretome treatment

EndoC-βH1 cells were treated for 72 h with ISC secretome collected at Days 1, 3, 5 and 7 in culture followed by RNA extraction and bulk RNA-Sequencing. PCA plot demonstrated different gene expression profiles of ISC secretome-treated versus control samples but also the variability in gene expression between donors rather than according to different duration of ISC culture, demonstrated significant variability between individual ISC donor cultures.

Differential gene expression analysis (Heatmaps in Appendix ***Figure 7.8*** - ***Figure 7.12***) revealed significant ($p < 0.05$) downregulation of some key β-cell identity genes (*PDX1*, *MafA* and *NKX 6.1*) in EndoC-βH1cells treated with ISC secretome. Beta-cell autophagy-related genes such as *BECN1* and *MAP1LC3B* were significantly increased in EndoC-βH1cells treated with ISC secretome as well as in the cytokine-treated positive control. These genes have been reported previously as markers of β-cell autophagy (Fujitani et al., 2009; Watada & Fujitani, 2015). Increased expression of the ER stress marker *DDIT3* (also known as *CHOP*) was seen during exposure of EndoC-βH5 cells to INF-γ alone (Frørup et al., 2023). ER stress induction in β-cells upon the exposure to our positive control could have taken place as there was a significant upregulation of *DDIT3* expression. *XBP1* is another ER stress gene that was upregulated in both of our study treatments.

Compared to the control, the upregulation of *CASP3* gene expression, encoding for caspase-3, in EndoC-βH1 cells treated with ISC Day 5 and the Cytokine Mix, could suggest the activation of the caspase pathway. Kikuta et al. (2013) have demonstrated that β-cell apoptosis was induced and was associated with the activation of the caspase pathway evidenced by increased levels of caspase-3 and caspase-9, when PaSCs were co-cultured with RIN-5F cells (Kikuta et al., 2013). Although *CASP9* gene expression was not significantly upregulated in EndoC-βH1

cells treated with ISC Day 5 and the Cytokine Mix, *CASP7* was significantly upregulated in the latter treatment, which supports another study reporting that EndoC-βH5 treated with the same cytokine treatment led to apoptotic caspase activation via cleaved and activated *CASP7* (Frørup et al., 2023).

Ingenuity pathway analysis elucidated the top up and down regulated biological pathways influenced by changes in gene expression in response to ISC secretome and Cytokine Mix treatments. The analysis explored the detailed molecular changes and revealed several significantly enriched pathways ($p < 0.05$), including the Pathogen Induced Cytokine Storm Pathway, which was significantly upregulated in both treatments ***(Figure 5.11*** and ***Figure 5.13)***. The pathway illustrated an activation of key molecules including STAT3, which is a key mediator of inflammatory processes. Yet, other differentially expressed genes in each pathway demonstrated a degree of variation ***(Figure 5.11*** and ***Figure 5.13)***. Interestingly, unlike the Cytokine Mix treatment, the graphical summaries (See Appendix ***Figure 7.3 - Figure 7.7***) of ISC secretome treatments, indicated some cellular events associated with proliferation and stimulation of connective tissue pathways, cell transformation, cell proliferation of fibroblasts in addition to other markers such as STAT3, IL-6, IL-1β. It could be suggested that EndoC-βH1 were responding to the stress induced by ISC secretome upon them through cytokine synthesis, whereby they themselves became proinflammatory and profibrotic rather than simply being the recipient of inflammatory and fibrotic signalling.

Rodent PaSC and ISC secretome-related studies reported primarily insulin-secretion analysis rather than transcriptomic analysis when investigating the impact of PaSCs and ISC secretome treatments on β-cell lines (Kikuta et al., 2013; Li et al., 2016; Zang et al., 2015; Zha et al., 2014). Following the treatment with ISC secretome, the reduction in β-cell function exhibited by decreased insulin secretion and insulin content observed in Chapter 4 studies, could be due to the downregulation of *PDX1*, *MafA* and *NKX 6.1* gene expression observed in this chapter. These genes could be further investigated at a protein level to provide detailed insight into how ISC secretome impacts on β-cell function and survival.

In summary, the NanoString data presented in this chapter revealed key genes overexpressed in CF tissue such as *TGF-β1* and *ACTA2* and other EMT and ECM markers. These data could contribute greatly to the understanding of the gene expression pathways underlying the

morphological changes observed in CF pancreata as the disease progresses. Following Chapter 4 studies reporting the impact of ISC secretome on EndoC-βH1 function, the RNA-seq data provided an insight into changes in EndoC-βH1 transcriptome and the possible activation of cytokine associated pathways in respond to the stress they are exposed to.

5.4.5 Study limitations

The work presented in this chapter has some limitations. No pancreatic tissue from very young control donors was available. Only nine samples (seven cases) were used from the CF tissue blocks provided kindly by Professor. Klöppel due to other factors that might influence the results such as the presence of lymph nodes, large blood vessels and grossly dilated ducts. The use of a fibrosis panel was a good choice considering the fibrotic changes observed in diseased tissue, yet a designed panel consisting of genes that are associated with β-cell identity and function could be further established. EndoC-βH1 studies were undertaken by myself in Sweden under Prof. Eliasson's guidance over a limited time, which only allowed three biological replicates of the studies. More repeats using ISC secretome from different donors could minimise the impact of biological variation within generated data.

Chapter 6: General Discussion

6.1 Overview

In 1938 “Cystic fibrosis of the pancreas” was first described by an American pathologist Dr. Dorothy Anderson, while working on autopsy studies of infants dying with malnutrition (Andersen, 1938) . Cystic fibrosis of the pancreas is characterised by ductal obstruction due to the build-up of mucus, which leads to acinar atrophy alongside fibrotic and lipoatrophic changes within the exocrine parenchyma (Lohr et al., 1989). As a result, 85-90% of CF cases develop exocrine pancreatic insufficiency and approximately around 2% of CF children, 20% of CF adolescents and 50% of CF adults develop CFRD (Baker et al., 2005; Kalnins et al., 2007; Moran et al., 2009; Hegyi et al., 2016; Kelsey et al., 2019; Olesen et al., 2020). Due to the limited access to human CF and CFRD pancreatic tissue and the difficulties in learning more from blood analytical tests or imaging of the diseased pancreas, the physiological, molecular and cellular mechanisms that play a role in the disease progression and exocrine-endocrine cross-talk leading to β-cell dysfunction and eventually the development of diabetes are not yet fully understood.

This thesis investigated morphological changes of fibrosis and fat replacement within human CF *post-mortem* pancreata as the disease progresses, and its relation to age. The natural history of the disease was elucidated through a designed semi-quantitative scoring system that assessed histopathological changes such as ductal dilation, acinar atrophy and ductal loss, and a robust AI quantitative analysis (HALO), which characterised the changes and possible associated drivers such as fibrosis and cellular players such as PaSCs within the exocrine and endocrine compartments of CF tissue. Following on from this, I established an *in vitro* primary human islet stellate cell (ISC) model to mimic the cell-mediated ‘stress’ environment which islets are exposed to in CF and/or CFRD pancreata. This model was used to assess β-cell function under the impact of proinflammatory mediators within the ISC secretome released following activation of ISCs in culture. Finally, I undertook transcriptomics phenotyping of human CF *post-mortem* pancreatic tissue and EndoC-βH1 cells following treatment with ISC secretome.

6.2 CF progression supported by exocrine changes

Löhr et al. (1989) have previously reported that the early- and end-stage of CF were represented by the fibrotic and the lipoatrophic patterns, respectively, to reflect the morphological changes

observed within the exocrine parenchyma. However, this thesis proposes that the disease progresses from an early-stage represented by fibrotic pattern alone, to the advanced-stage represented by a mixed fibrotic/lipoatrophic pattern to the end-stage represented by total replacement of the exocrine compartment with fatty tissue, progressing linearly with age ***(Figure 6.1)***. This could more meaningfully and accurately delineate the natural history of CF progression and the time-course associated with age and severity of pathological changes within the diseased tissue. The semi-quantitative analysis and AI-driven quantification based on phenotypic classification of the CF tissue further demonstrated the steady progression of the disease through ductal dilation/loss; acinar atrophy, exocrine pancreas fibrosis and islet remodelling. The loss of acinar area mirrored the increase in abnormal collagen deposition area which was then superseded by fatty tissue replacement.

Young CF pancreata (Premature–14-year-old) represented the early-stage of CF and were classified by CF Pattern 1, which exhibited fibroatrophic changes only. These cases revealed the preservation of the exocrine parenchyma with some mild alteration to pancreatic lobule structure, presence of intra-lobular collagen deposition, mild ductal dilation and mild acinar lumen dilation and acinar atrophy ***(Figure 6.1)***. These cases illustrated the absence of exocrine fat replacement or severe ductal dilation, which was also observed in young CF children of age < 1 year old in a study by Iannucci et al. (1984).

The advanced- and end-stages of the disease were illustrated by more severe changes within the exocrine parenchyma and CF tissue blocks (3–27-year-old). These were classified as CF Pattern 2 of a mixed pattern of fibrosis and fatty tissue replacement or the latter alone (CF Pattern 3). There was an observed extensive loss of exocrine parenchyma along with severe ductal dilation (mainly in CF Pattern 2) and ductal loss (mainly in CF Pattern 3) ***(Figure 6.1)***. The loss of acinar tissue, presence of ductal dilation and total replacement of the exocrine parenchyma were also observed in CF *post-mortem* pancreata during a qualitative analysis(Löhr et al., 1989). Although this and other studies before the current work have concluded that there may be two alternative end-stages (fibro-atrophic or lipo-atrophic) without reporting an inevitable sequential progression to global fat replacement

NanoString spatial analysis revealed associations between CF and key genes mediating pro-fibrotic EMT (*TGF-β1*, *ACTA2* and *CXCL-12*) and ECM synthesis / degradation pathways. As

disease progresses to later-stages, expression of genes associated with adipogenesis (*FABP4* and *FASN*) increased.

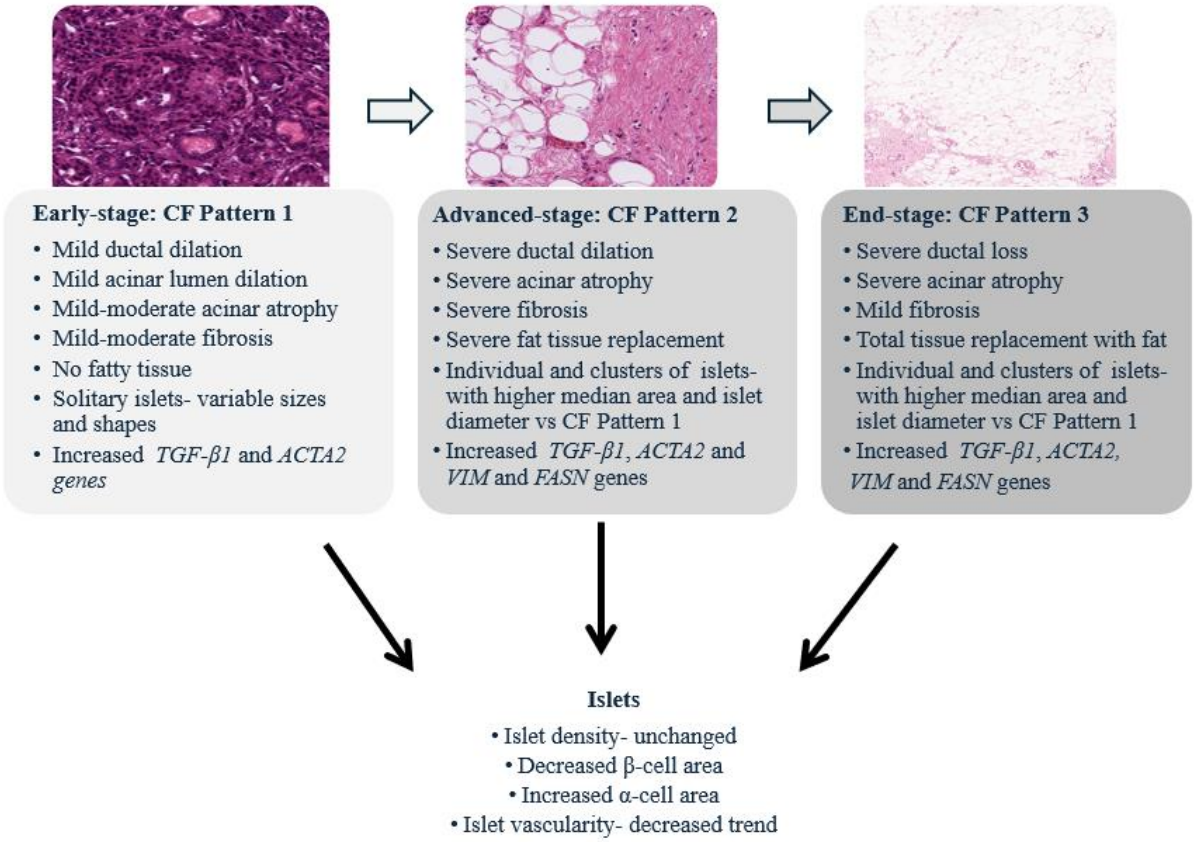

Figure 6.1: Diagram illustrating pancreatic changes as CF progresses.

Early-stage represented by CF Pattern 1: Fibroatrophic. Advanced-stage represented by CF Pattern 2: Fibroatrophic and lipoatrophic. End-stage represented by CF Pattern 3: Lipoatrophic.

6.3 CF progression supported by endocrine changes

Islets in early-stage CF were of varied sizes and shapes with presence of peri-islet fibrosis around some solitary islets. Islets in advanced- and end-stage CF appeared spared, varied in sizes (some are larger than early-stage CF islets) but disrupted and surrounded / infiltrated by collagen strands with adjacent adipocytes. These histological observations and increased islet remodelling with disease stage assessed by semi-quantitative scoring were supported by AI data showing islet diameter and median islet area of CF Pattern 2 and Pattern 3 to be higher compared to early-stage CF. Islets of CFRD pancreata have been reported to exhibit different sizes with a disorganised appearance (Iannucci et al., 1984, Abdul-Karim et al., 1986). In

addition, greater altered islet morphology was associated with lipoatrophic changes (Bogdani et al., 2017). CD31 quantification illustrated a reduction in islet vascularisation as the disease progressed. Together these findings associated with islet remodelling supported our proposed progression of the disease.

Although endocrine area and islet density remained unchanged in CF across Patterns 2 and 3 when compared to control pancreata, islet density of young donors was higher compared to the other two patterns and control. Yet, β-cell area and α-cell area represented by insulin^{+} and glucagon^{+} area [%], respectively, were decreased throughout CF stages even at birth (premature cases), suggesting that initial abnormalities contributing to islet dysfunction have taken place during in *utero* development. Beta-cell area is decreased in CF pancreata of young CF (< 4 years) and adult donors (Bogdani et al., 2017; Hart et al., 2018). There are contradicting findings of whether β-cell area is reduced in CFRD when compared to CF cases (Iannucci et al., 1984; Abdul-Karim et al., 1986; Soejima and Landing, 1986; Löhr et al., 1989; Bogdani et al., 2017). Alpha-cell area in human CF islets with and without CFRD have been reported to be increased (Löhr et al., 1989; Bogdani et al., 2017; Hart et al., 2018; Hull et al., 2018).

Delta-cells assessed by somatostatin $^{+}$ area [%] were increased in CF compared to control and this increase was mainly observed in the early-stage CF. This was supported by elevated δ-cell area in young CF (< 4 years) compared to control in Bogdani et al. (2017) study. Other studies reported the increase in δ-cell area in adolescent and adults with CF compared to control (Abdul-Karim et al., 1986; Löhr et al., 1989; Bogdani et al., 2017). Also, δ-cell area in adolescent and adults with CFRD compared to CF without diabetes was higher (Iannucci et al., 1984; Abdul-Karim et al., 1986; Soejima and Landing, 1986). Yet this finding was contradicted by Bogdani et al. (2017) reporting no change between CFRD and CF δ-cell area (Bogdani et al., 2017). AI quantification of pancreatic polypeptide^{+} area [%] illustrated no significant changes in CF compared to control. Other studies have shown an increased in pancreatic polypeptide^{+} area in young, adolescent and adults with CF (Löhr et al., 1989; Bogdani et al., 2017; Hull et al., 2018).

These findings highlight the importance of further investigating exocrine-to-endocrine cell cross-talk during disease progression moving beyond cross-sectional association studies, to be

able to elucidate the mechanisms behind the functional defects despite relatively preserved islet mass.

6.4 *In vitro* CF model mediated by stellate cells activation

In people with CF, impaired insulin secretion due to reduced β-cell function is central to the development of CFRD (Moran et al., 1991; Mohan et al., 2009; Merjaneh et al., 2015; Sheikh et al., 2017). Using CFTR knock out ferrets, total insulin content was lower in CF isolated islets compared to wild-type islets (Sun et al., 2017). Using a CF mouse model, possible defects in proinsulin processing and reduction in exocytosis and the number of insulin-containing granules at the cell membrane have been reported (Edlund et al., 2019).

In Chapter 3, it was demonstrated that insulin [%] area was reduced in CF along with increased presence of peri- and intra-islet fibrosis and observations of activated stellate cells expressing α-SMA within the fibrotic tissue and around the dilated ducts within the CF tissue. In Chapter 5, NanoString data revealed an increase in EMT markers such as *ACTA2* and *VIM* and ECM genes, which further supported stellate cell activation within the diseased tissue. However, cellular mechanisms impacting on β-cell function could not be elucidated as the generated data remain cross-sectional. Therefore, in Chapter 4 an *in vitro* primary human ISC model was established via culturing human islets (isolated from non-diabetic donors) over a course of 7 days in 2D adherent culture. Stellate cell presence and activation was confirmed by positive immunofluorescence staining for α-SMA and vimentin and increased gene expression of key transcripts of stellate cell activation and function - *ACTA2*, *VIM* and *COL1A1* via rtq-RT PCR analysis. ISC medium analysis confirmed COL1A1 secretion to be increased by 10-fold over the 7-day culture period. Additional ISC secretome analysis for selected fibrosis-associated peptides was conducted using MSD assay, confirmed the secretion of proinflammatory cytokines associated with fibrotic signalling such as TGF-β1, TGF-β2, IL-1, IL-6, IL-8 and TNF-α and secretion of chemokines and inflammatory biomarkers including CXCL-1, CXCL-10, CXCL-12, CCL-2 and MIP-1α over 7-days in culture. Together, these findings were supported by existing literature reporting that activated stellate cells are α-SMA$^+$ and vimentin$^+$ and secrete ECM proteins including COL1A1, inflammatory markers such as TGF-β, IL-1, IL-6, IL-8, TNF-α and CXCL and CCL chemokines (Elsässerm et al., 1989; Apte et al., 1998,

1999; Bachem et al., 1998; Kuroda et al., 1998; Gabbiani, 2003; Erkan et al., 2012; Zhao et al., 2018).

Having analysed the ISC secretome for the presence of inflammatory markers, functional studies using the EndoC-βH1 human β-cell line were conducted. EndoC-βH1 cells treated with ISC secretome exhibited a reduction in insulin content and secretion, which could be due to decreased reduced proinsulin biosynthesis possibly due to 1) Downregulation of *PDX1*, *MafA* and *NKX 6.1* gene expression. 2) The upregulation of β-cell autophagy-related genes such as *BECN1* and *MAP1LC3B.* 3) Upregulation of XBP1gene associated with ER stress. EndoC-βH1 cells treated with the Cytokine Mix reduced insulin content and secretion as well as proinsulin secretion and this could be due to elevated ER stress genes such as XBP1 and *DDIT3*. Day 5 ISC secretome-treated and cytokine treated EndoC-βH1 exhibited an increased proinsulin:insulin ratio which could be due to defects in proinsulin processing. Elevated fasting proinsulin:insulin ratio is associated with impaired insulin secretion during an oral glucose tolerance test in people with CF (Nielsen et al., 2023).

Having demonstrated an increase in *TGF-β1* in CF fixed tissue and the activation of stellate cells within the ISC model, we propose that TGF-β signalling may be driving stellate cell activation within the pancreas with cytokines such as IL-6 and IL-1β within the ISC secretome (but not necessarily TGF-β itself) mediating β-cell dysfunction. The IPA analysis of RNA-Seq data suggested that EndoC-βH1 cells were responding to the stress induced upon ISC secretome treatment through cytokine synthesis, whereby the treated endocrine cells became proinflammatory and pro-fibrotic rather than exclusively being the 'recipient' of inflammatory and fibrotic signalling from the ISC secretome. The current studies suggest a role for intrapancreatic cytokines in mediating this stress and that ISCs may be a source of these mediators in the CF pancreas.

Interestingly, pericytes lining small blood vessels and capillaries are also α-SMA$^+$ and vimentin$^+$. (Kramann et al., 2015; Sakhneny et al., 2021; Tamayo et al., 2022). These cells have been reported to be a source of progenitor cells which can further transdifferentiate into myofibroblasts in response to injury and are potential mediators of organ fibrosis (Kramann et al., 2015). It will be important to further characterise and investigate α-SMA$^+$ and vimentin$^+$

cells which may be activated stellate cells or pericytes driving peri- and intra-islet fibrosis environment by secreting profibrotic mediators and chemokines.

This ISC model established within this thesis has further potential for dynamically studying the interplay between pro-fibrotic stellate cells, the associated CF fibrotic environment and β-cell dysfunction. Co-culture systems could be set up and key changes in gene expression explored at the protein level.

6.5 Further experiments to test the hypotheses generated

Next steps to progress these studies could include:

1. Design of further AI pipelines and training classifiers to quantify additional changes within severely damaged CF tissue.
2. Further spatial analyses on the remaining human *post-mortem* CF tissue using a NanoString bespoke panel consisting of β-cell identity and function genes.
3. Spatial investigation and dynamic *in vitro* studies of the association between islet cell identity and function in CF pancreas to understand the mechanisms behind β-cell failure and α-cell dysfunction within CF and CFRD pancreata.
4. Assessment of ISC secretome content using ISC cultures established from more donors with no known pancreatic pathologies.
5. *In vitro* studies to assess potential for stellate cell transdifferentiation into adipocytes, then assess the impact of this adipogenic environment on β-cell lines.
6. Investigation of islet microvascular cells and pericytes as a potential source of stellate cells.

Our group is currently working on optimisation of a tissue imaging technique called MACSima, whereby tissue sections from donors with type 3c diabetes are being multiplex IF stained with specific protein markers associated with inflammation and fibrotic changes with the tissue as well as immune cells and endocrine phenotypic markers. Spatial relationships are being explored.

6.6 Conclusion

In conclusion, this thesis has enabled development and validation of novel approaches to study the patho-aetiology of CFRD including systematic approaches to semi-quantitative

tissue analysis and establishment of human *in vitro* models for dynamic functional studies of stellate cell collagen secretion / profibrotic signalling and the impact on β-cell gene expression in addition to (pro)insulin biosynthesis, processing and secretion. This work has provided a range of tools and approaches for further studies towards deeper understanding of underlying signalling pathways and ultimately development of novel therapeutic approaches with the aim of preventing progression to diabetes and the need for insulin therapy in people living with CF.

Chapter 7: Appendix

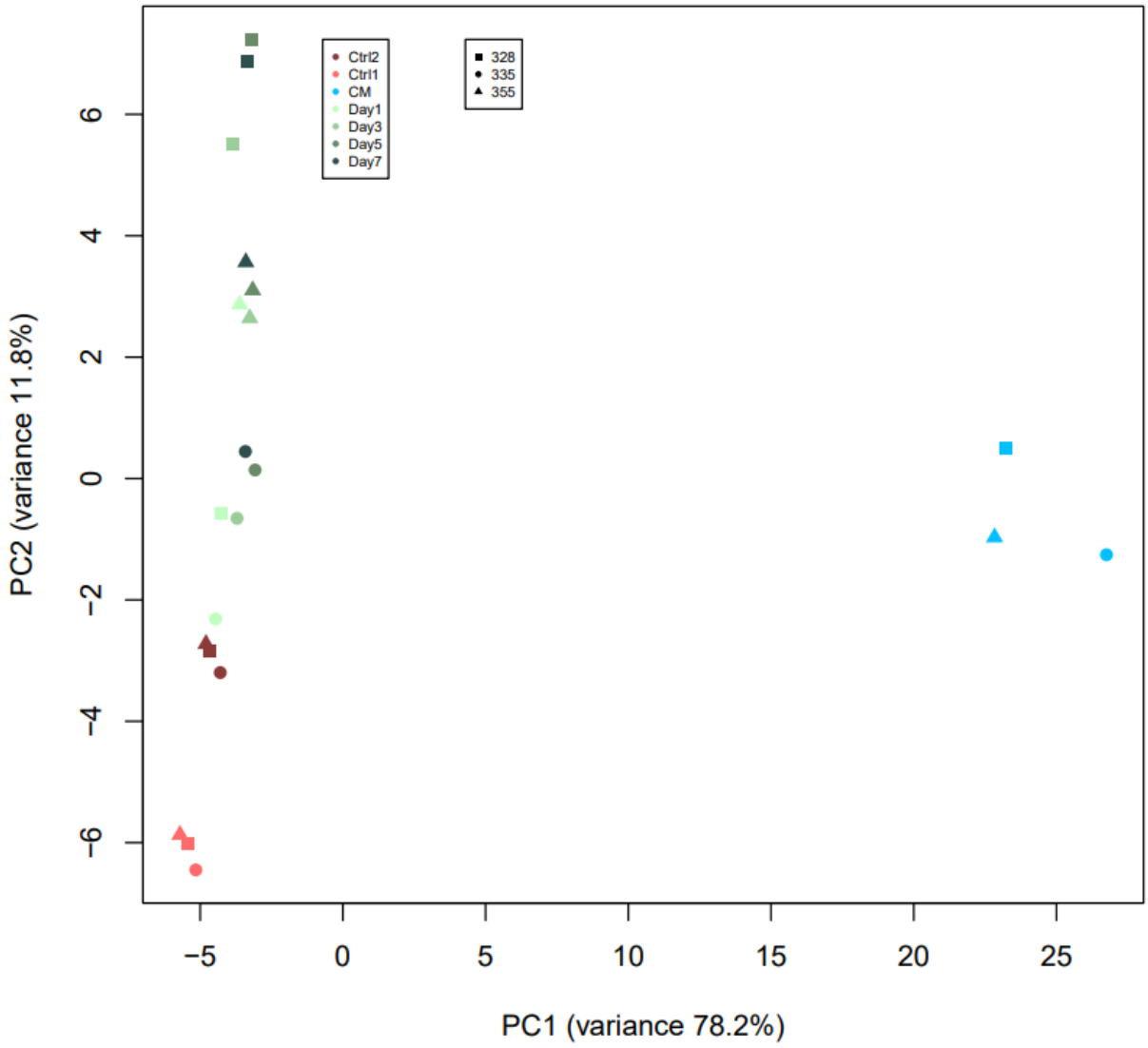

Figure 7.1: Principal Component Analysis (PCA) plot showing the variation of samples (EndoC-βH1 cells treated EndoC-βH1cells medium (Ctrl 1), control 1:1 dilution (Ctrl 2), ISC secretome of Days 1, 3, 5 and 7 and Cytokine Mix (CM) along the PC1 (78.2%) and PC2 (11.

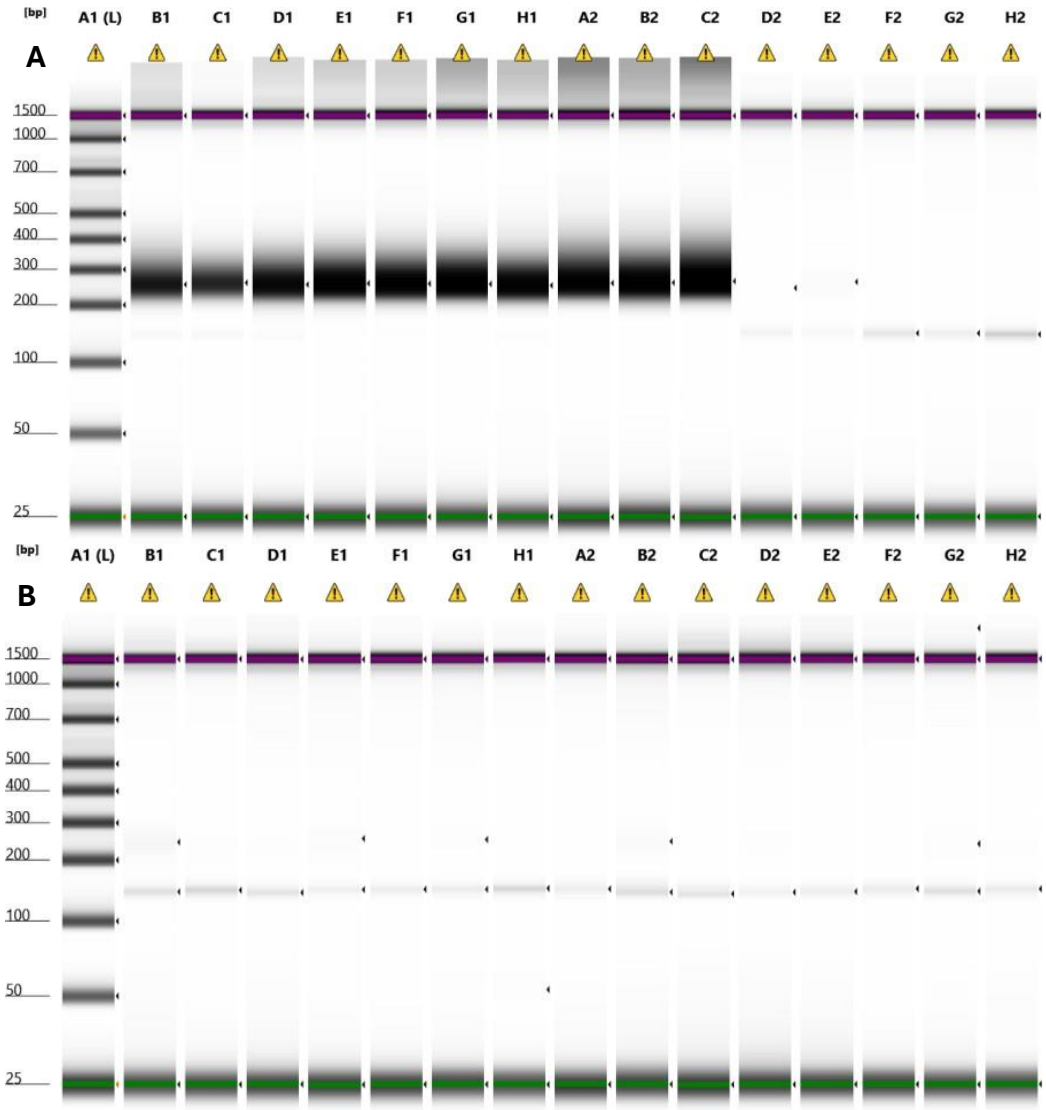

Figure 7.2: Library preparation traces for control and CF samples to undertake bulk RNA Sequencing.

*(**A**) Ten control samples B1-C2 and twenty CF samples (**A**) D2-H2 and (**B**) B1-H2. Ladder A1 in both (**A**) and (**B**).*

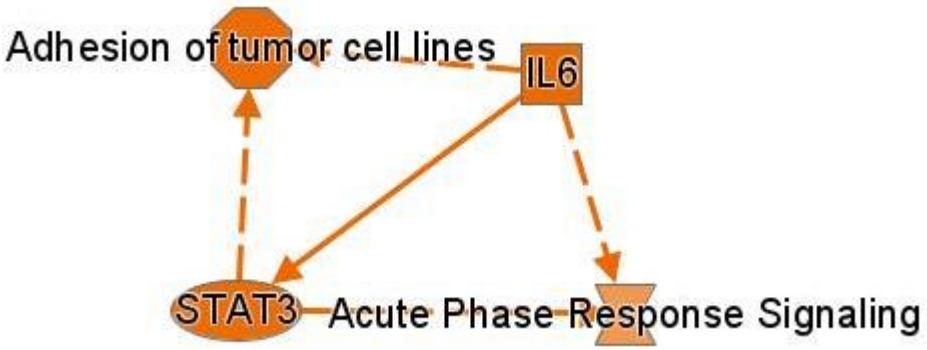

Figure 7.3: Graphical summary of EndoC-βH1cells treated with ISC secretome of Day 1 illustrated the key biological themes in the IPA analysis using the most significant genes identified in the core analysis.

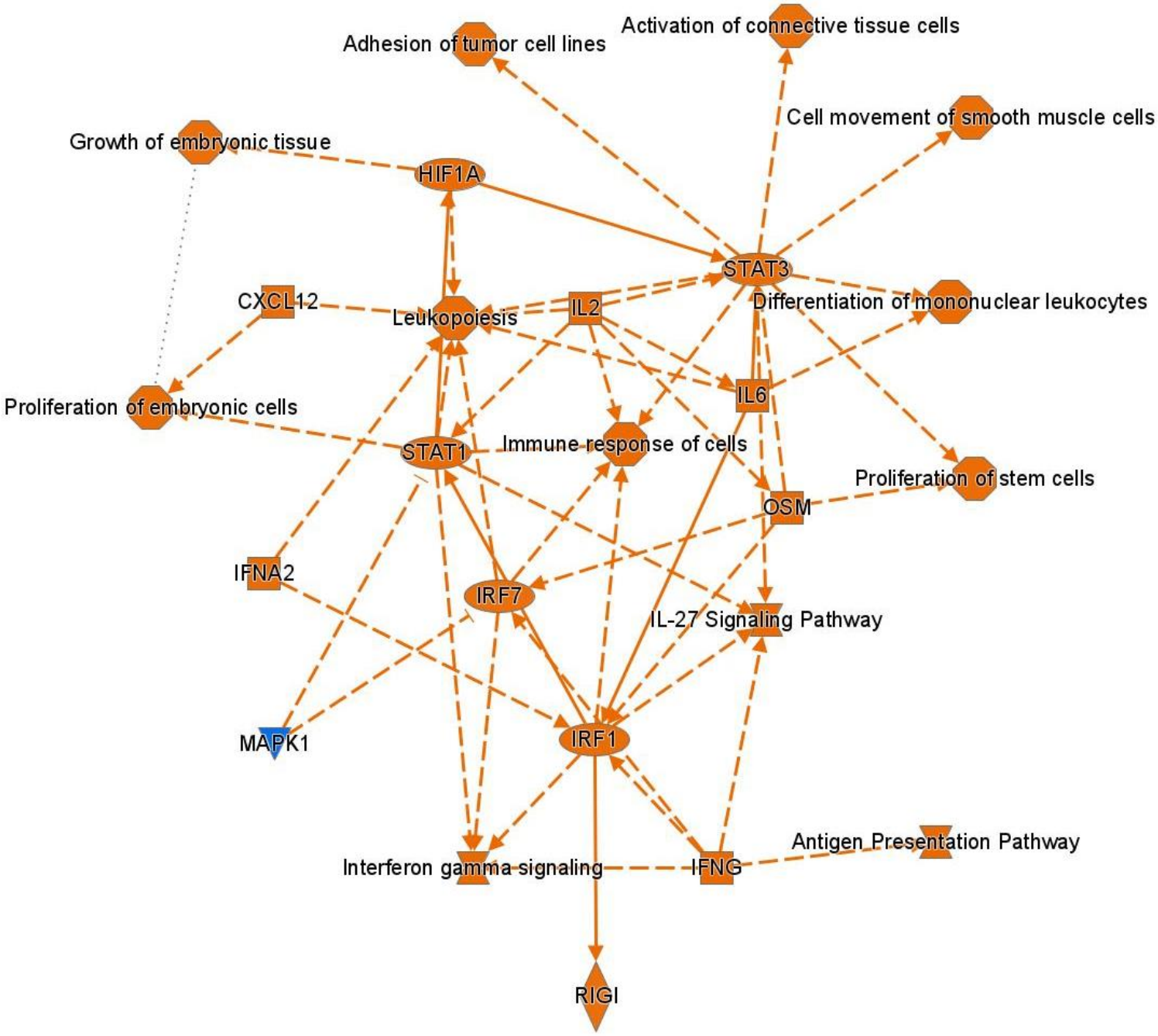
Activation of connective tissue cells
Adhesion of tumor cell lines
Cell movement of smooth muscle cells
Growth of embryonic tissue
HIF1A
STAT3
CXCL12
Leukopoiesis
IL2
Differentiation of mononuclear leukocytes
IL6
Proliferation of embryonic cells
STAT1
Immune response of cells
Proliferation of stem cells
OSM
IFNA2
IRF7
IL-27 Signaling Pathway
MAPK1
IRF1
Antigen Presentation Pathway
Interferon gamma signaling
IFNG
RIGI

Figure 7.4: Graphical summary of EndoC-βH1 cells treated with ISC secretome of Day 3 illustrated the key biological themes in the IPA analysis using the most significant genes identified in the core analysis.

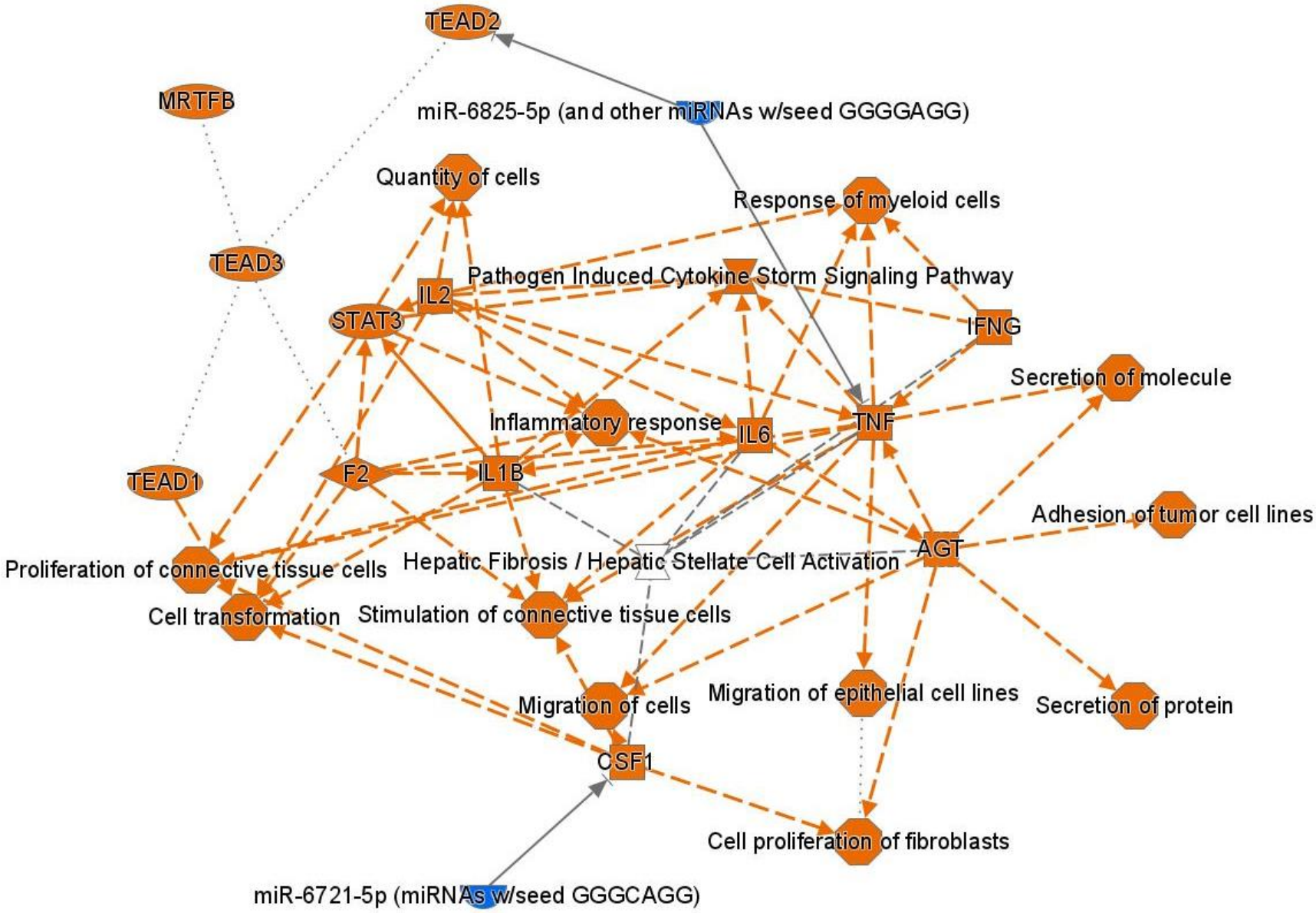
TEAD2
MRTFB
miR-6825-5p (and other miRNAs w/seed GGGGAGG)
Quantity of cells
Response of myeloid cells
TEAD3
Pathogen Induced Cytokine Storm Signaling Pathway
IL2
STAT3
IFNG
Secretion of molecule
Inflammatory response
IL6
TNF
TEAD1
F2
IL1B
Adhesion of tumor cell lines
AGT
Proliferation of connective tissue cells
Hepatic Fibrosis / Hepatic Stellate Cell Activation
Cell transformation
Stimulation of connective tissue cells
Migration of epithelial cell lines
Migration of cells
Secretion of protein
CSF1
Cell proliferation of fibroblasts
miR-6721-5p (miRNAs w/seed GGGCAGG)

Figure 7.5: Graphical summary of EndoC-βH1 cells treated with ISC secretome of Day 5 illustrated the key biological themes in the IPA analysis using the most significant genes identified in the core analysis.

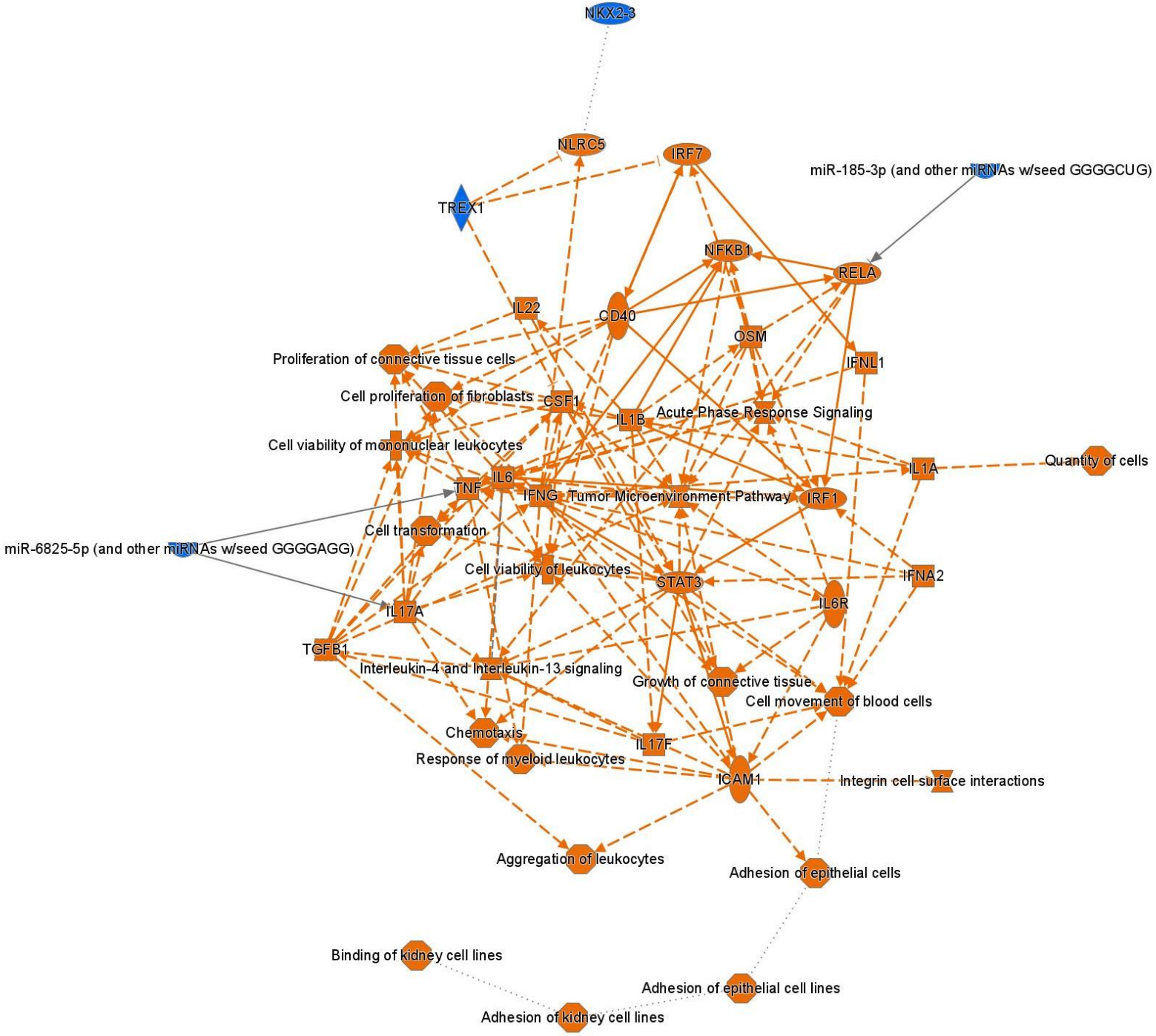
NKX2-3
NLRC5
IRF7
miR-185-3p (and other miRNAs w/seed GGGGCUG)
TREX1
NFKB1
RELA
IL22
CD40
OSM
Proliferation of connective tissue cells
IFNL1
Cell proliferation of fibroblasts
CSF1
IL1B
Acute Phase Response Signaling
Cell viability of mononuclear leukocytes
IL1A
Quantity of cells
IL6
TNF
IFNG
Tumor Microenvironment Pathway
IRF1
Cell transformation
miR-6825-5p (and other miRNAs w/seed GGGGAGG)
Cell viability of leukocytes
STAT3
IFNA2
IL17A
IL6R
TGFB1
Interleukin-4 and Interleukin-13 signaling
Growth of connective tissue
Cell movement of blood cells
Chemotaxis
IL17F
Response of myeloid leukocytes
ICAM1
Integrin cell-surface interactions
Aggregation of leukocytes
Adhesion of epithelial cells
Binding of kidney cell lines
Adhesion of epithelial cell lines
Adhesion of kidney cell lines

Figure 7.6: Graphical summary of EndoC-βH1 cells treated with ISC secretome of Day 7 illustrated the key biological themes in the IPA analysis using the most significant genes identified in the core analysis.

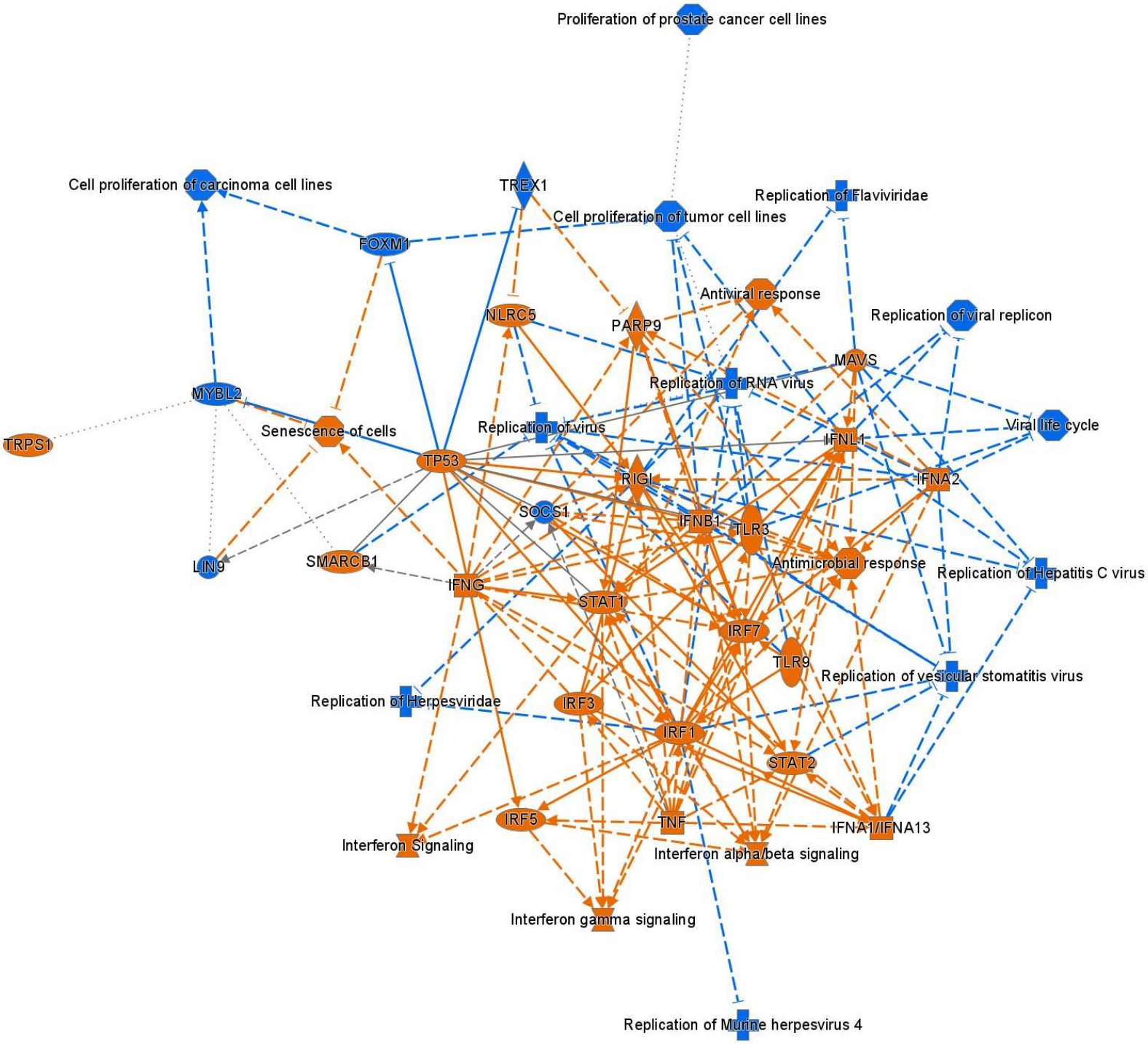
Proliferation of prostate cancer cell lines
Cell proliferation of carcinoma cell lines
TREX1
Cell proliferation of tumor cell lines
Replication of Flaviviridae
FOXM1
Antiviral response
NLRC5
PARP9
Replication of viral replicon
MAVS
MYBL2
Replication of RNA virus
TRPS1
Senescence of cells
Replication of virus
Viral life cycle
IFNL1
TP53
RIGI
IFNA2
SOCS1
IFNB1
TLR3
LIN9
SMARCB1
Antimicrobial response
Replication of Hepatitis C virus
IFNG
STAT1
IRF7
TLR9
Replication of vesicular stomatitis virus
Replication of Herpesviridae
IRF3
IRF1
STAT2
IRF5
TNF
IFNA1/IFNA13
Interferon Signaling
Interferon alpha/beta signaling
Interferon gamma signaling
Replication of Murine herpesvirus 4

Figure 7.7: Graphical summary of EndoC-βH1 cells treated with Cytokine Mix (1 ng/ml IL-1β, 20 ng/ml TNF-α and 20 ng/ml INF-γ) illustrated the key biological themes in the IPA analysis using the most significant genes identified in the core analysis.

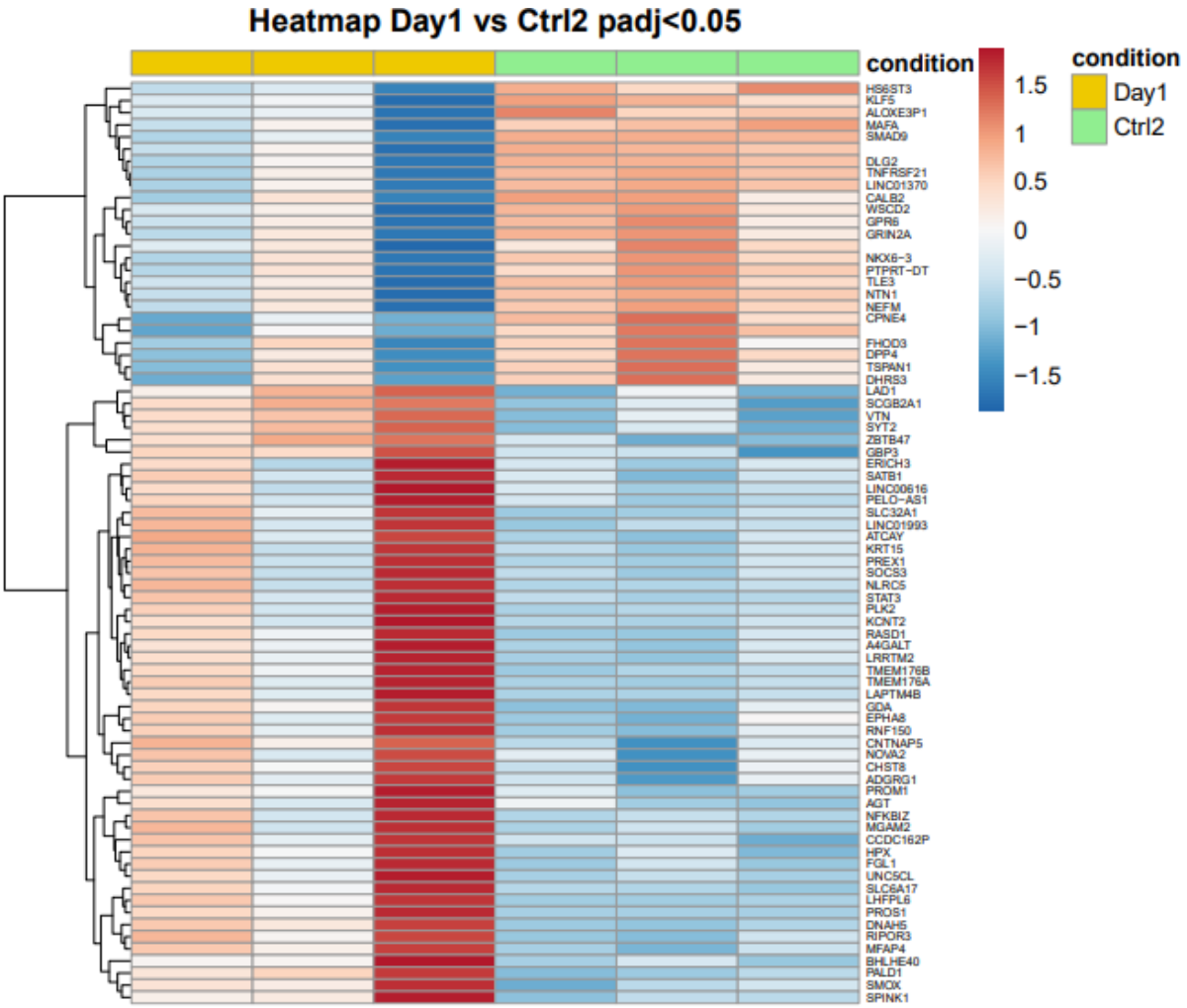

Figure 7.8: Differentially expressed genes of EndoC-βH1 cells treated with ISC secretome Day 1.

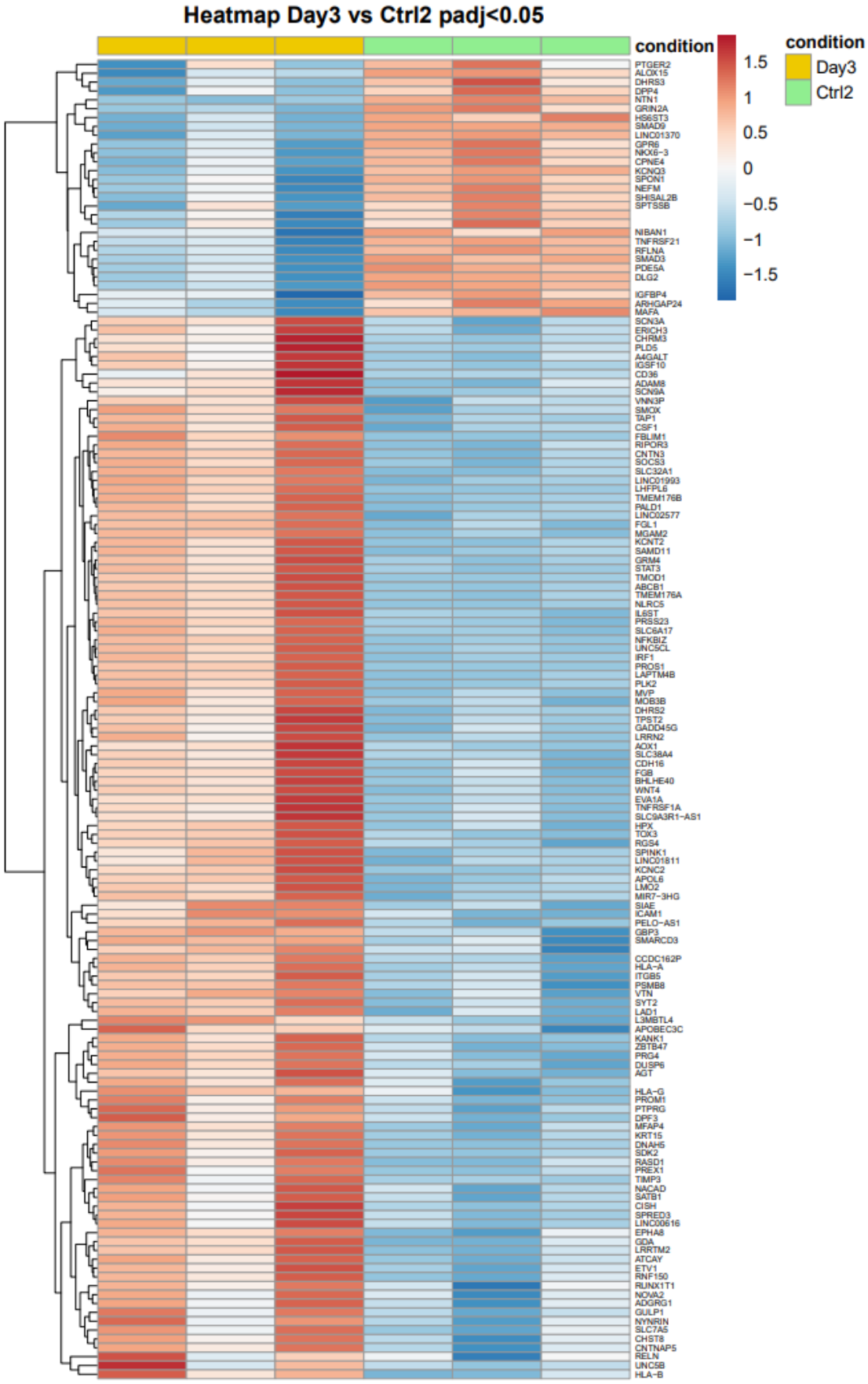

Figure 7.9: Differentially expressed genes of EndoC-βH1 cells treated with ISC secretome Day 3.

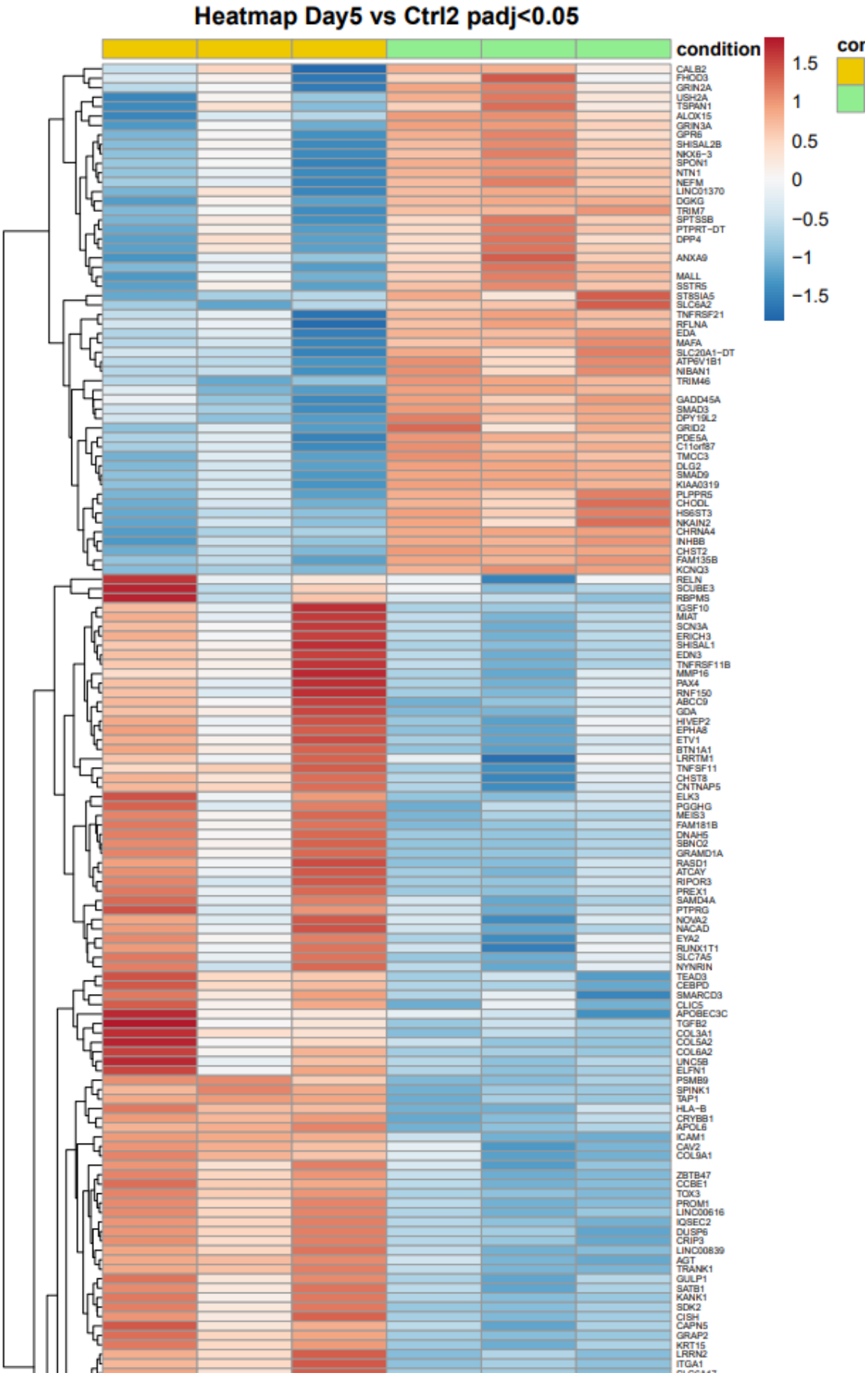
Heatmap Day5 vs Ctrl2 padj<0.05
condition
cor
1.5
1
0.5
0
−0.5
−1
−1.5
CALB2
FHOD3
GRIN2A
USH2A
TSPAN1
ALOX15
GRIN3A
GPR6
SHISAL2B
NKX6−3
SPON1
NTN1
NEFM
LINC01370
DGKG
TRIM7
SPTSSB
PTPRT−DT
DPP4
ANXA9
MALL
SSTR5
ST8SIA5
SLC6A2
TNFRSF21
RFLNA
EDA
MAFA
SLC20A1−DT
ATP6V1B1
NIBAN1
TRIM46
GADD45A
SMAD3
DPY19L2
GRID2
PDE5A
C11orf87
TMCC3
DLG2
SMAD9
KIAA0319
PLPPR5
CHODL
HS6ST3
NKAIN2
CHRNA4
INHBB
CHST2
FAM135B
KCNQ3
RELN
SCUBE3
RBPMS
IGSF10
MIAT
SCN3A
ERICH3
SHISAL1
EDN3
TNFRSF11B
MMP16
PAX4
RNF150
ABCC9
GDA
HIVEP2
EPHA8
ETV1
BTN1A1
LRRTM1
TNFSF11
CHST8
CNTNAP5
ELK3
PGGHG
MEIS3
FAM181B
DNAH5
SBNO2
GRAMD1A
RASD1
ATCAY
RIPOR3
PREX1
SAMD4A
PTPRG
NOVA2
NACAD
EYA2
RUNX1T1
SLC7A5
NYNRIN
TEAD3
CEBPD
SMARCD3
CLIC5
APOBEC3C
TGFB2
COL3A1
COL5A2
COL6A2
UNC5B
ELFN1
PSMB9
SPINK1
TAP1
HLA−B
CRYBB1
APOL6
ICAM1
CAV2
COL9A1
ZBTB47
CCBE1
TOX3
PROM1
LINC00616
IQSEC2
DUSP6
CRIP3
LINC00839
AQT
TRANK1
GULP1
SATB1
KANK1
SDK2
CISH
CAPN5
GRAP2
KRT15
LRRN2
ITGA1

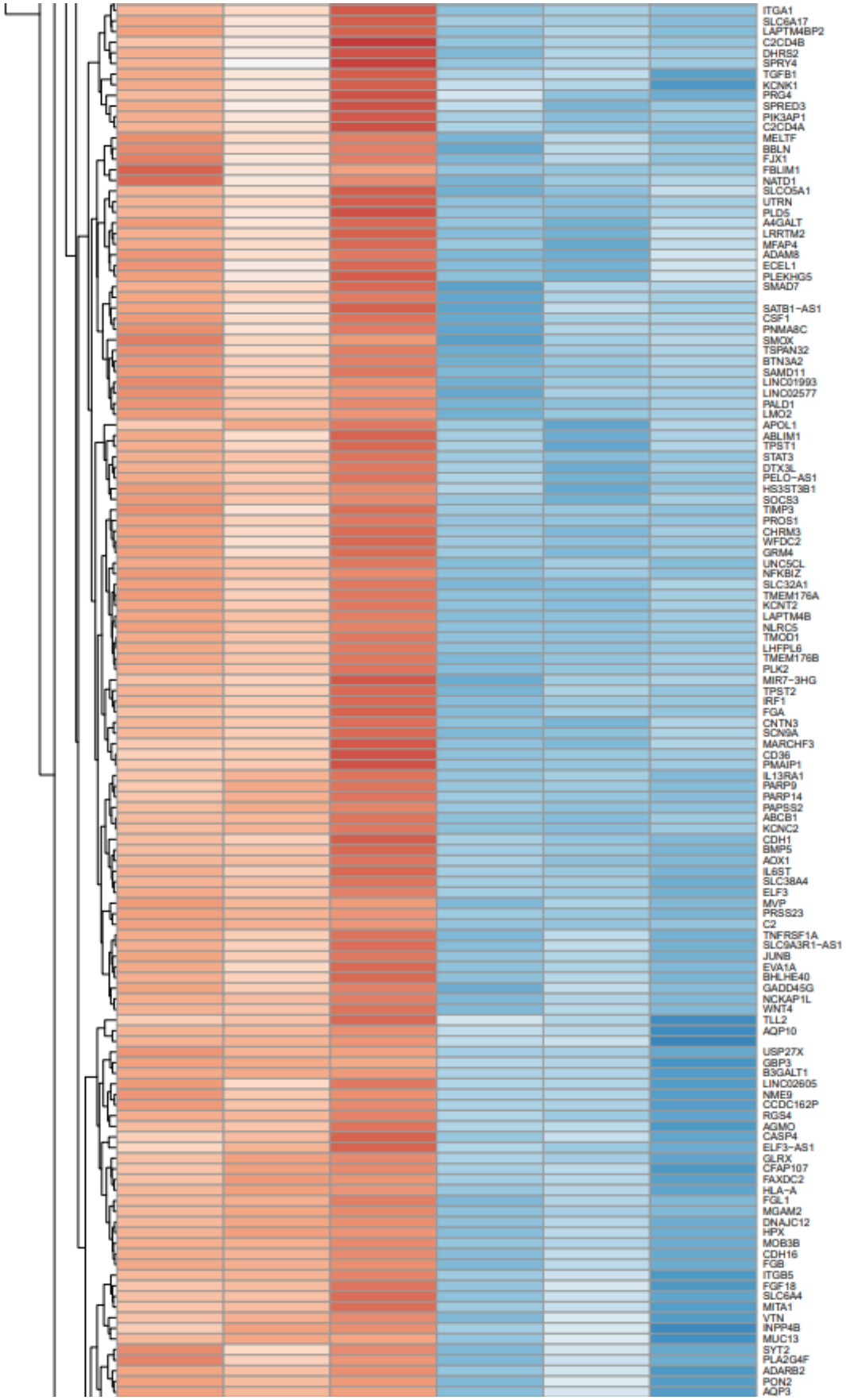

Figure 7.10: Differentially expressed genes of EndoC-βH1 cells treated with ISC secretome Day 5.

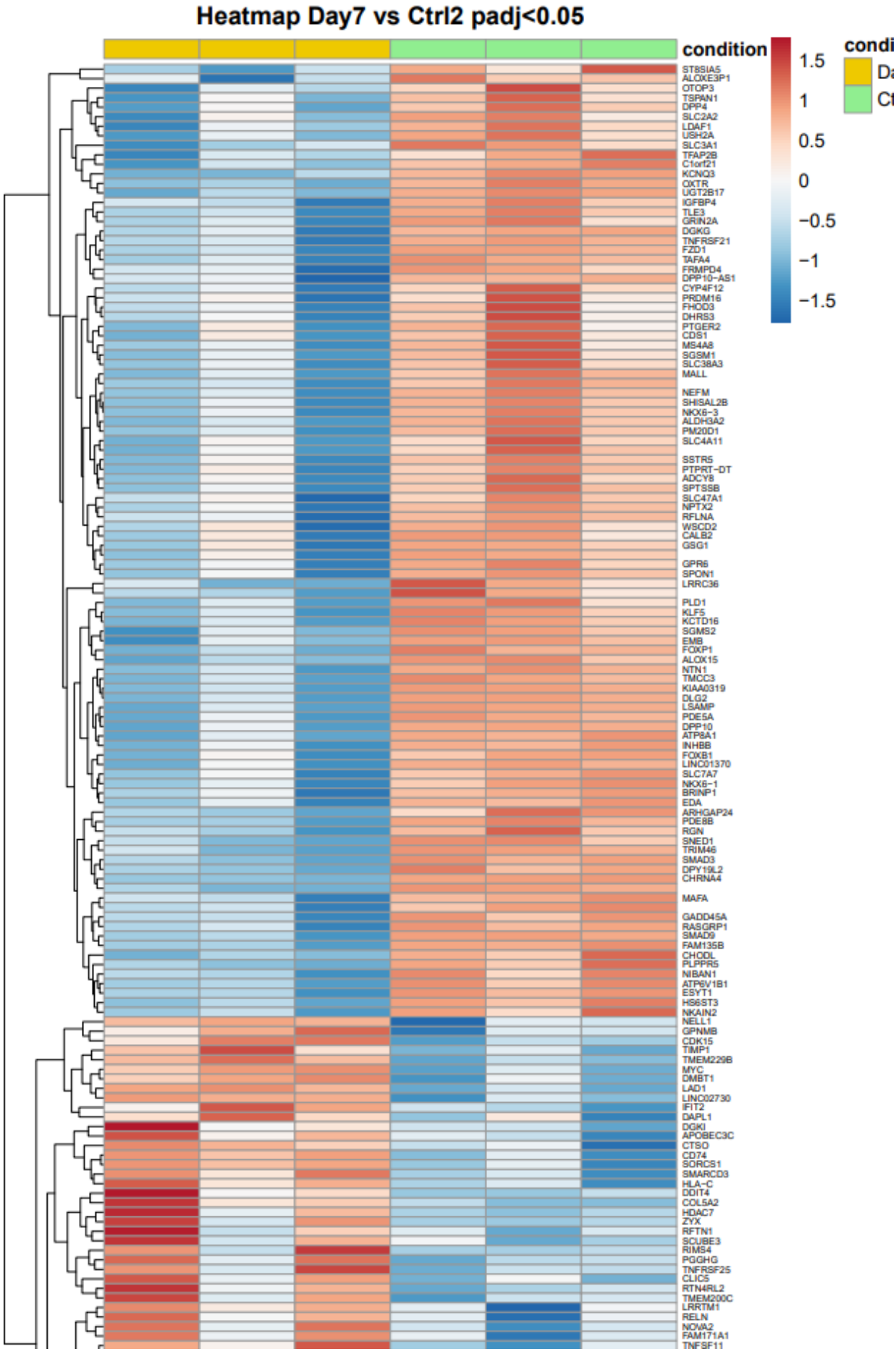
Heatmap Day7 vs Ctrl2 padj<0.05
condition
condi
Da
Ct
1.5
1
0.5
0
−0.5
−1
−1.5
ST8SIA5
ALOXE3P1
OTOP3
TSPAN1
DPP4
SLC2A2
LDAF1
USH2A
SLC3A1
TFAP2B
C1orf21
KCNQ3
OXTR
UGT2B17
IGFBP4
TLE3
GRIN2A
DGKG
TNFRSF21
FZD1
TAFA4
FRMPD4
DPP10−AS1
CYP4F12
PRDM16
FHOD3
DHRS3
PTGER2
CDS1
MS4A8
SGSM1
SLC38A3
MALL
NEFM
SHISAL2B
NKX6−3
ALDH3A2
PM20D1
SLC4A11
SSTR5
PTPRT−DT
ADCY8
SPTSSB
SLC47A1
NPTX2
RFLNA
WSCD2
CALB2
GSG1
GPR6
SPON1
LRRC36
PLD1
KLF5
KCTD16
SGMS2
EMB
FOXP1
ALOX15
NTN1
TMCC3
KIAA0319
DLG2
LSAMP
PDE5A
DPP10
ATP8A1
INHBB
FOXB1
LINC01370
SLC7A7
NKX6−1
BRINP1
EDA
ARHGAP24
PDE8B
RGN
SNED1
TRIM46
SMAD3
DPY19L2
CHRNA4
MAFA
GADD45A
RASGRP1
SMAD9
FAM135B
CHODL
PLPPR5
NIBAN1
ATP6V1B1
ESYT1
HS6ST3
NKAIN2
NELL1
GPNMB
CDK15
TIMP1
TMEM229B
MYC
DMBT1
LAD1
LINC02730
IFIT2
DAPL1
DGKI
APOBEC3C
CTSO
CD74
SORCS1
SMARCD3
HLA−C
DDIT4
COL5A2
HDAC7
ZYX
RFTN1
SCUBE3
RIMS4
PGGHG
TNFRSF25
CLIC5
RTN4RL2
TMEM200C
LRRTM1
RELN
NOVA2
FAM171A1
TNFSF11

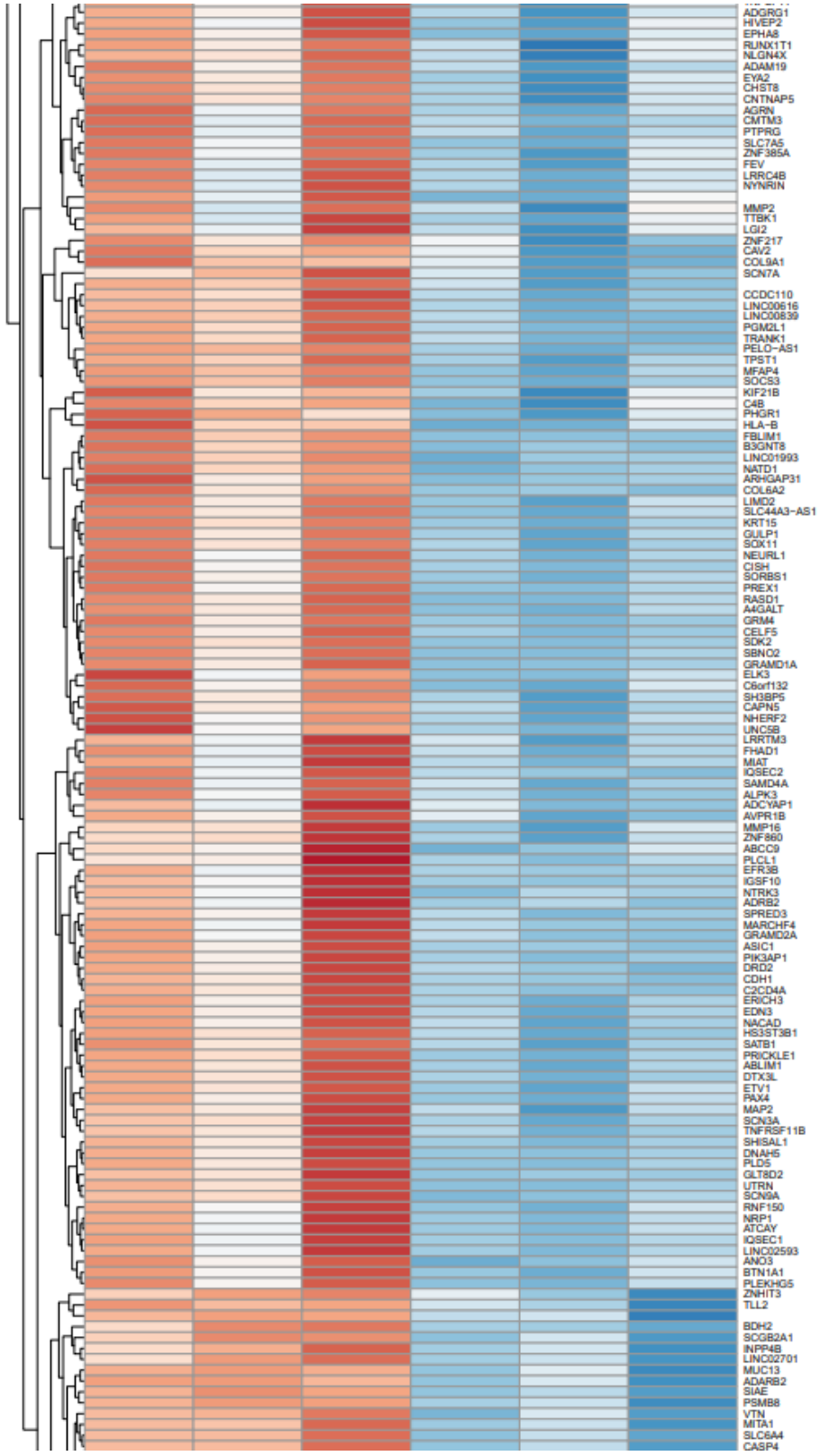

Figure 7.11: Differentially expressed genes of EndoC-βH1 cells treated with ISC secretome Day 7.

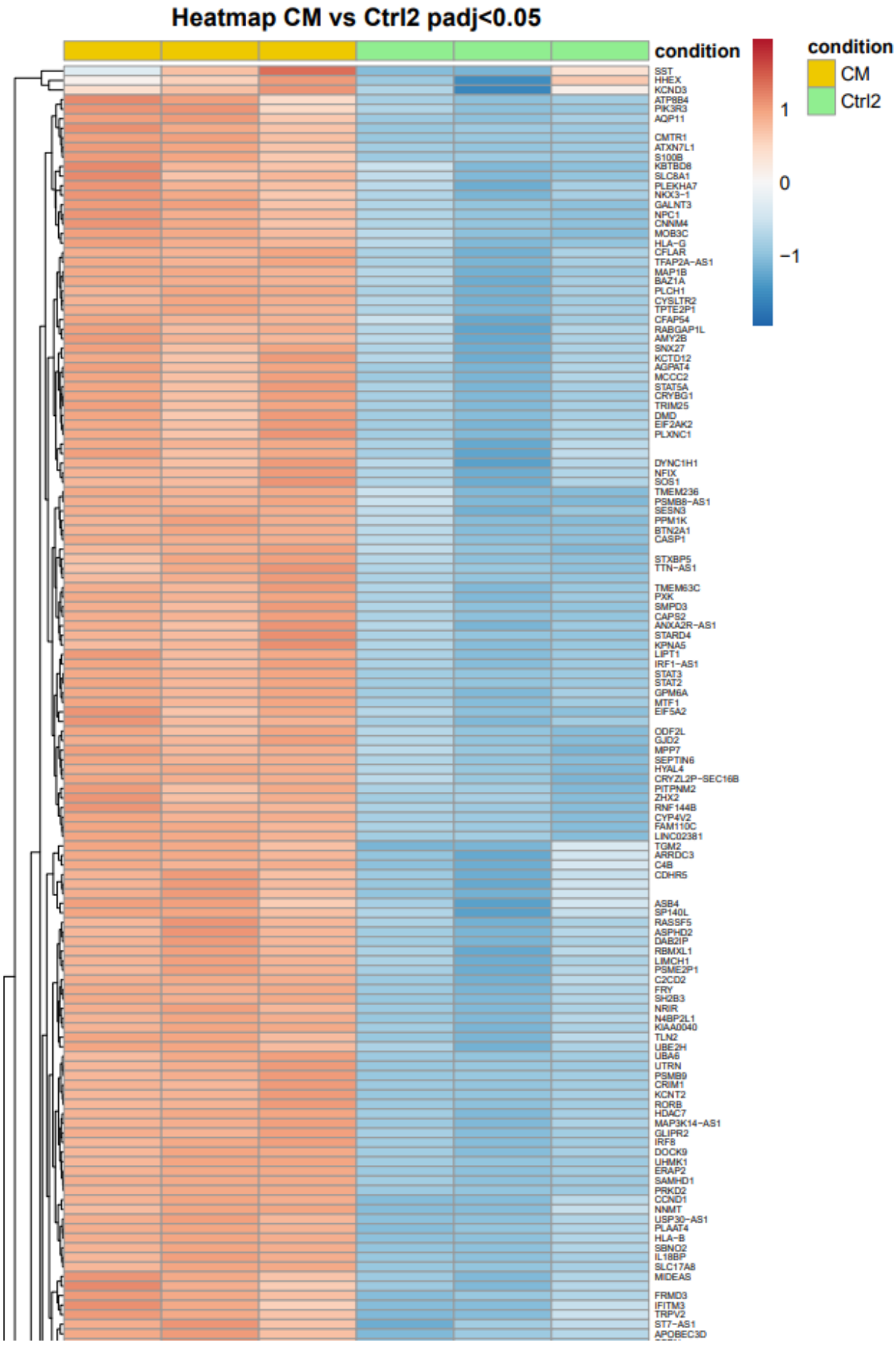
Heatmap CM vs Ctrl2 padj<0.05
condition
CM
Ctrl2
1
0
−1
SST
HHEX
KCND3
ATP8B4
PIK3R3
AQP11
CMTR1
ATXN7L1
S100B
KBTBD8
SLC8A1
PLEKHA7
NKX3−1
GALNT3
NPC1
CNNM4
MOB3C
HLA−G
CFLAR
TFAP2A−AS1
MAP1B
BAZ1A
PLCH1
CYSLTR2
TPTE2P1
CFAP54
RABGAP1L
AMY2B
SNX27
KCTD12
AGPAT4
MCCC2
STAT5A
CRYBG1
TRIM25
DMD
EIF2AK2
PLXNC1
DYNC1H1
NFIX
SOS1
TMEM236
PSMB8−AS1
SESN3
PPM1K
BTN2A1
CASP1
STXBP5
TTN−AS1
TMEM63C
PXK
SMPD3
CAPS2
ANXA2R−AS1
STARD4
KPNA5
LIPT1
IRF1−AS1
STAT3
STAT2
GPM6A
MTF1
EIF5A2
ODF2L
GJD2
MPP7
SEPTIN6
HYAL4
CRYZL2P−SEC16B
PITPNM2
ZHX2
RNF144B
CYP4V2
FAM110C
LINC02381
TGM2
ARRDC3
C4B
CDHR5
ASB4
SP140L
RASSF5
ASPHD2
DAB2IP
RBMXL1
LIMCH1
PSME2P1
C2CD2
FRY
SH2B3
NRIR
N4BP2L1
KIAA0040
TLN2
UBE2H
UBA6
UTRN
PSMB9
CRIM1
KCNT2
RORB
HDAC7
MAP3K14−AS1
GLIPR2
IRF8
DOCK9
UHMK1
ERAP2
SAMHD1
PRKD2
CCND1
NNMT
USP30−AS1
PLAAT4
HLA−B
SBNO2
IL18BP
SLC17A8
MIDEAS
FRMD3
IFITM3
TRPV2
ST7−AS1
APOBEC3D

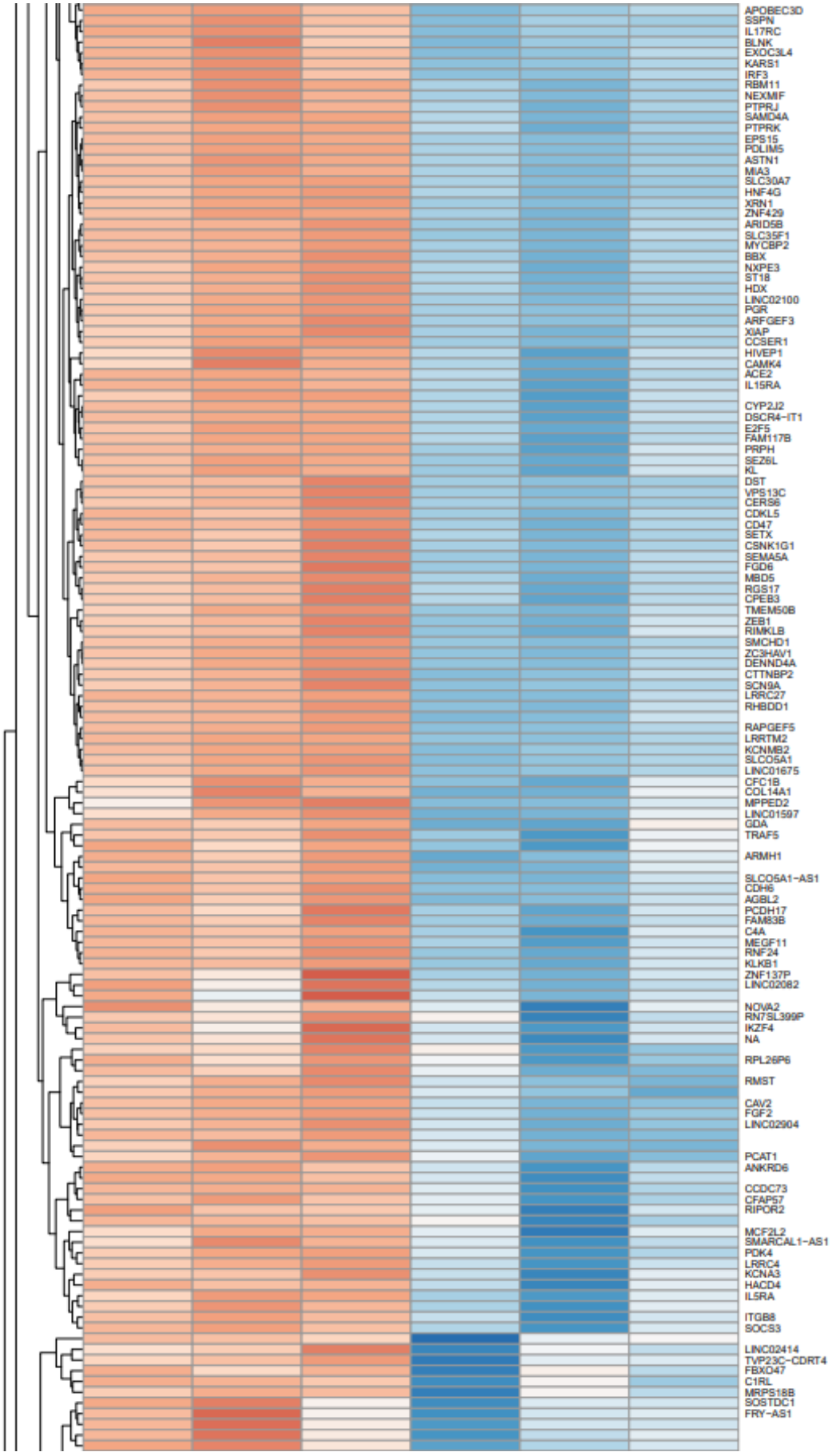
APOBEC3D
SSPN
IL17RC
BLNK
EXOC3L4
KARS1
IRF3
RBM11
NEXMIF
PTPRJ
SAMD4A
PTPRK
EPS15
PDLIM5
ASTN1
MIA3
SLC30A7
HNF4G
XRN1
ZNF429
ARID5B
SLC35F1
MYCBP2
BBX
NXPE3
ST18
HDX
LINC02100
PGR
ARFGEF3
XIAP
CCSER1
HIVEP1
CAMK4
ACE2
IL15RA
CYP2J2
DSCR4-IT1
E2F5
FAM117B
PRPH
SEZ6L
KL
DST
VPS13C
CERS6
CDKL5
CD47
SETX
CSNK1G1
SEMA5A
FGD6
MBD5
RGS17
CPEB3
TMEM50B
ZEB1
RIMKLB
SMCHD1
ZC3HAV1
DENND4A
CTTNBP2
SCN9A
LRRC27
RHBDD1
RAPGEF5
LRRTM2
KCNMB2
SLCO5A1
LINC01675
CFC1B
COL14A1
MPPED2
LINC01597
GDA
TRAF5
ARMH1
SLCO5A1-AS1
CDH6
AGBL2
PCDH17
FAM83B
C4A
MEGF11
RNF24
KLKB1
ZNF137P
LINC02082
NOVA2
RN7SL399P
IKZF4
NA
RPL26P6
RMST
CAV2
FGF2
LINC02904
PCAT1
ANKRD6
CCDC73
CFAP57
RIPOR2
MCF2L2
SMARCAL1-AS1
PDK4
LRRC4
KCNA3
HACD4
IL5RA
ITGB8
SOCS3
LINC02414
TVP23C-CDRT4
FBXO47
C1RL
MRPS18B
SOSTDC1
FRY-AS1

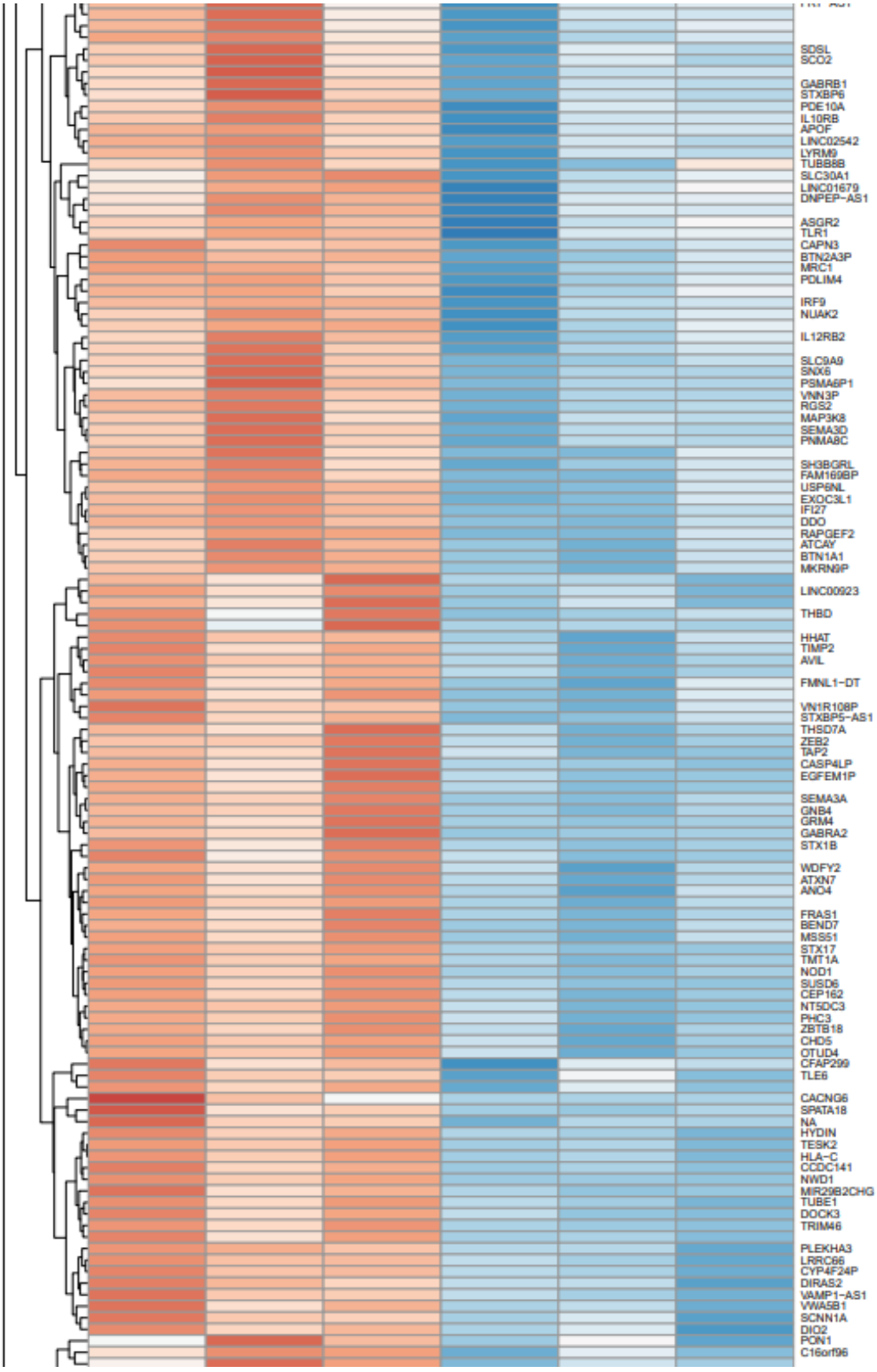
SDSL
SCO2
GABRB1
STXBP6
PDE10A
IL10RB
APOF
LINC02542
LYRM9
TUBB8B
SLC30A1
LINC01679
DNPEP-AS1
ASGR2
TLR1
CAPN3
BTN2A3P
MRC1
PDLIM4
IRF9
NUAK2
IL12RB2
SLC9A9
SNX6
PSMA6P1
VNN3P
RGS2
MAP3K8
SEMA3D
PNMA8C
SH3BGRL
FAM169BP
USP6NL
EXOC3L1
IFI27
DDO
RAPGEF2
ATCAY
BTN1A1
MKRN9P
LINC00923
THBD
HHAT
TIMP2
AVIL
FMNL1-DT
VN1R108P
STXBP5-AS1
THSD7A
ZEB2
TAP2
CASP4LP
EGFEM1P
SEMA3A
GNB4
GRM4
GABRA2
STX1B
WDFY2
ATXN7
ANO4
FRAS1
BEND7
MSS51
STX17
TMT1A
NOD1
SUSD6
CEP162
NT5DC3
PHC3
ZBTB18
CHD5
OTUD4
CFAP299
TLE6
CACNG6
SPATA18
NA
HYDIN
TESK2
HLA-C
CCDC141
NWD1
MIR29B2CHG
TUBE1
DOCK3
TRIM46
PLEKHA3
LRRC66
CYP4F24P
DIRAS2
VAMP1-AS1
VWA5B1
SCNN1A
DIO2
PON1
C16orf96

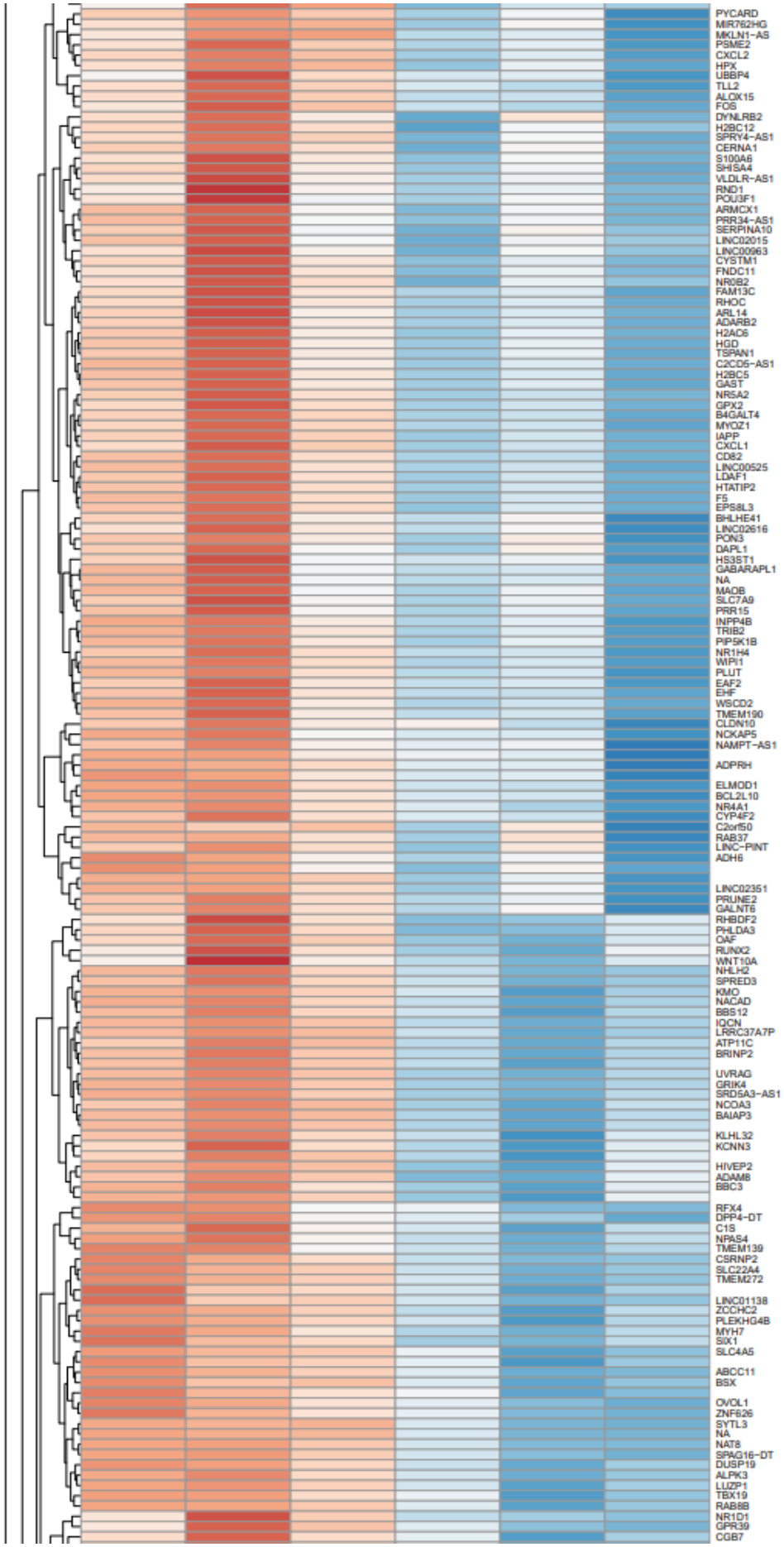
PYCARD
MIR762HG
MKLN1-AS
PSME2
CXCL2
HPX
UBBP4
TLL2
ALOX15
FOS
DYNLRB2
H2BC12
SPRY4-AS1
CERNA1
S100A6
SHISA4
VLDLR-AS1
RND1
POU3F1
ARMCX1
PRR34-AS1
SERPINA10
LINC02015
LINC00963
CYSTM1
FNDC11
NR0B2
FAM13C
RHOC
ARL14
ADARB2
H2AC6
HGD
TSPAN1
C2CD5-AS1
H2BC5
GAST
NR5A2
GPX2
B4GALT4
MYOZ1
IAPP
CXCL1
CD82
LINC00525
LDAF1
HTATIP2
F5
EPS8L3
BHLHE41
LINC02616
PCNX3
DAPL1
HS3ST1
GABARAPL1
NA
MAOB
SLC7A9
PRR15
INPP4B
TRIB2
PIP5K1B
NR1H4
WIPI1
PLUT
EAF2
EHF
WSCD2
TMEM190
CLDN10
NCKAP5
NAMPT-AS1
ADPRH
ELMOD1
BCL2L10
NR4A1
CYP4F2
C2orf50
RAB37
LINC-PINT
ADH6
LINC02351
PRUNE2
GALNT6
RHBDF2
PHLDA3
OAF
RUNX2
WNT10A
NHLH2
SPRED3
KMO
NACAD
BBS12
IQCN
LRRC37A7P
ATP11C
BRINP2
UVRAG
GRIK4
SRD5A3-AS1
NCOA3
BAIAP3
KLHL32
KCNN3
HIVEP2
ADAM8
BBC3
RFX4
DPP4-DT
C1S
NPAS4
TMEM139
CSRNP2
SLC22A4
TMEM272
LINC01138
ZCCHC2
PLEKHG4B
MYH7
SIX1
SLC4A5
ABCC11
BSX
OVOL1
ZNF626
SYTL3
NA
NAT8
SPAG16-DT
DUSP19
ALPK3
LUZP1
TBX19
RAB8B
NR1D1
GPR39
CGB7

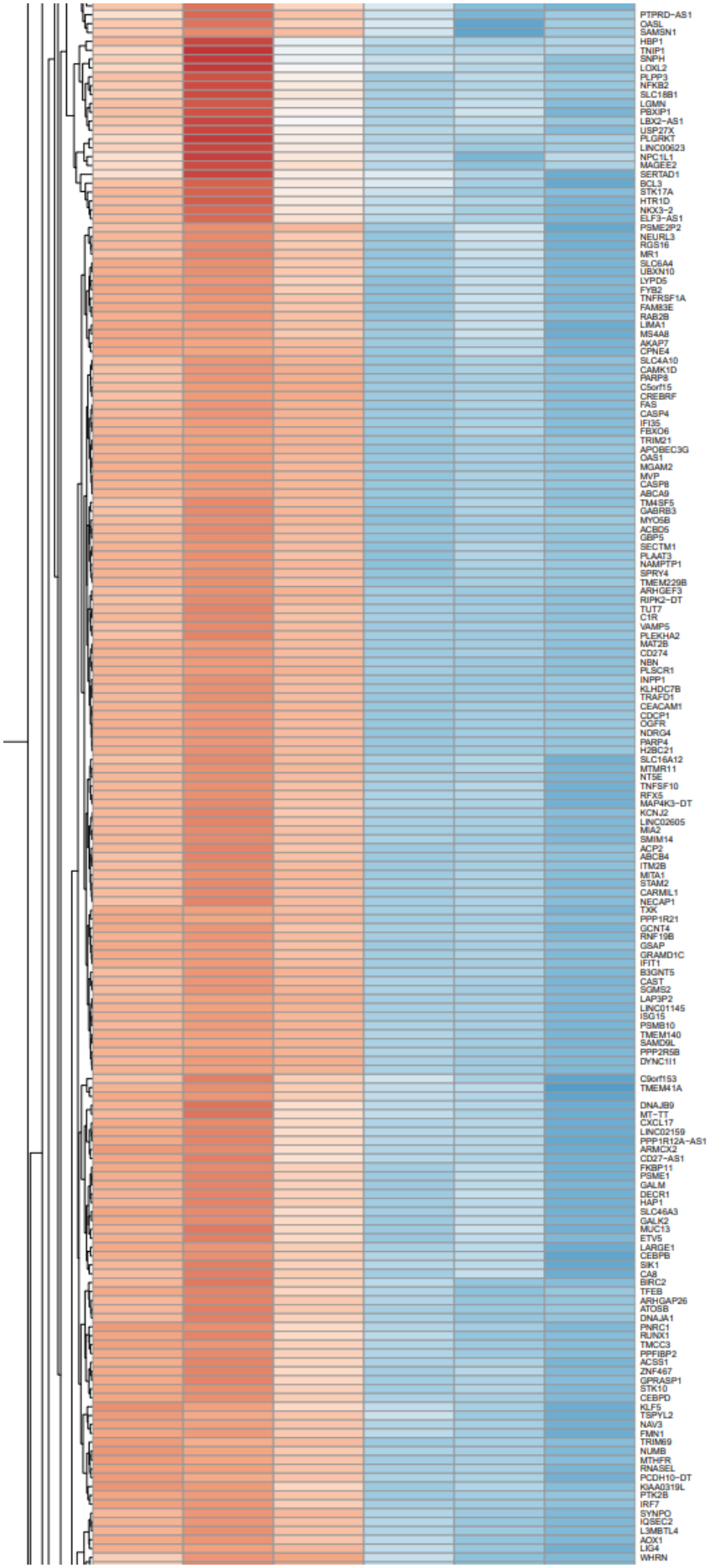
PTPRD-AS1
OASL
SAMSN1
HBP1
TNIP1
SNPH
LOXL2
PLPP3
NFKB2
SLC18B1
LGMN
PBXIP1
LBX2-AS1
USP27X
PLGRKT
LINC00623
NPC1L1
MAGEE2
SERTAD1
BCL3
STK17A
HTR1D
NKX3-2
ELF3-AS1
PSME2P2
NEURL3
RGS16
MR1
SLC6A4
UBXN10
LYPD5
FYB2
TNFRSF1A
FAM83E
RAB2B
LIMA1
MS4A8
AKAP7
CPNE4
SLC4A10
CAMK1D
PARP8
C5orf15
CREBRF
FAS
CASP4
IFI35
FBXO6
TRIM21
APOBEC3G
OAS1
MGAM2
MVP
CASP8
ABCA9
TM4SF5
GABRB3
MYO5B
ACBD5
GBP5
SECTM1
PLAAT3
NAMPTP1
SPRY4
TMEM229B
ARHGEF3
RIPK2-DT
TUT7
C1R
VAMP5
PLEKHA2
MAT2B
CD274
NBN
PLSCR1
INPP1
KLHDC7B
TRAFD1
CEACAM1
CDCP1
OGFR
NDRG4
PARP4
H2BC21
SLC16A12
MTMR11
NT5E
TNFSF10
RFX5
MAP4K3-DT
KCNJ2
LINC02605
MIA2
SMIM14
ACP2
ABCB4
ITM2B
MTA1
STAM2
CARMIL1
NECAP1
TXK
PPP1R21
GCNT4
RNF19B
GSAP
GRAMD1C
IFIT1
B3GNT5
CAST
SGMS2
LAP3P2
LINC01145
ISG15
PSMB10
TMEM140
SAMD9L
PPP2R5B
DYNC1I1
C9orf153
TMEM41A
DNAJB9
MT-TT
CXCL17
LINC02159
PPP1R12A-AS1
ARMCX2
CD27-AS1
FKBP11
PSME1
GALM
DECR1
HAP1
SLC46A3
GALK2
MUC13
ETV5
LARGE1
CEBPB
SIK1
CA8
BIRC2
TFEB
ARHGAP26
ATG5B
DNAJA1
PNRC1
RUNX1
TMCC3
PPFIBP2
ACSS1
ZNF467
GPRASP1
STK10
CEBPD
KLF5
TSPYL2
NAV3
FMN1
TRIM69
NUMB
MTHFR
RNASEL
PCDH10-DT
KIAA0319L
PTK2B
IRF7
SYNPO
IQSEC2
L3MBTL4
AOX1
LIG4
WHRN

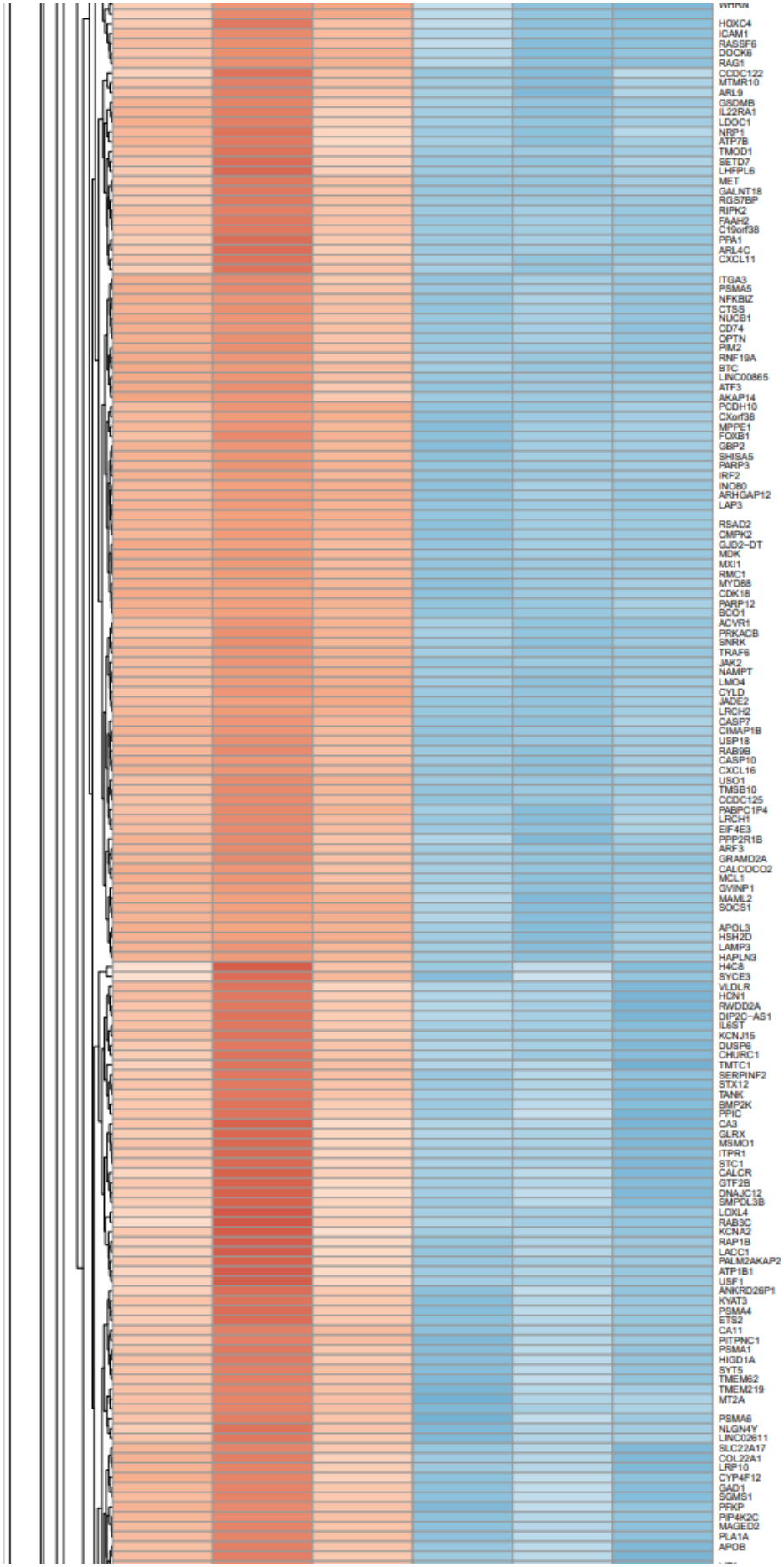
HOXC4
ICAM1
RASSF6
DOCK6
RAG1
CCDC122
MTMR10
ARL9
GSDMB
IL22RA1
LDOC1
NRP1
ATP7B
TMOD1
SETD7
LHFPL6
MET
GALNT18
RGS7BP
RIPK2
FAAH2
C19orf38
PPA1
ARL4C
CXCL11
ITGA3
PSMA5
NFKBIZ
CTSS
NUCB1
CD74
OPTN
PIM2
RNF19A
BTC
LINC00865
ATF3
AKAP14
PCDH10
CXorf38
MPPE1
FOXB1
GBP2
SHISA5
PARP3
IRF2
INO80
ARHGAP12
LAP3
RSAD2
CMPK2
CJD2-DT
MDK
MXI1
RMC1
MYD88
CDK18
PARP12
BCO1
ACVR1
PRKACB
SNRK
TRAF6
JAK2
NAMPT
LMO4
CYLD
JADE2
LRCH2
CASP7
CIMAP1B
USP18
RAB9B
CASP10
CXCL16
USO1
TMSB10
CCDC125
PABPC1P4
LRCH1
EIF4E3
PPP2R1B
ARF3
GRAMD2A
CALCOCO2
MCL1
GVINP1
MAML2
SOCS1
APOL3
HSH2D
LAMP3
HAPLN3
H4C8
SYCE3
VLDLR
HCN1
RWDD2A
DIP2C-AS1
IL6ST
KCNJ15
DUSP6
CHURC1
TMTC1
SERPINF2
STX12
TANK
BMP2K
PPIC
CA3
GLRX
MSMO1
ITPR1
STC1
CALCR
GTF2B
DNAJC12
SMPDL3B
LOXL4
RAB3C
KCNA2
RAP1B
LACC1
PALM2AKAP2
ATP1B1
USF1
ANKRD26P1
KYAT3
PSMA4
ETS2
CA11
PITPNC1
PSMA1
HIGD1A
SYT5
TMEM62
TMEM219
MT2A
PSMA6
NLGN4Y
LINC02811
SLC22A17
COL22A1
LRP10
CYP4F12
GAD1
SGMS1
PFKP
PIP4K2C
MAGED2
PLA1A
APOB

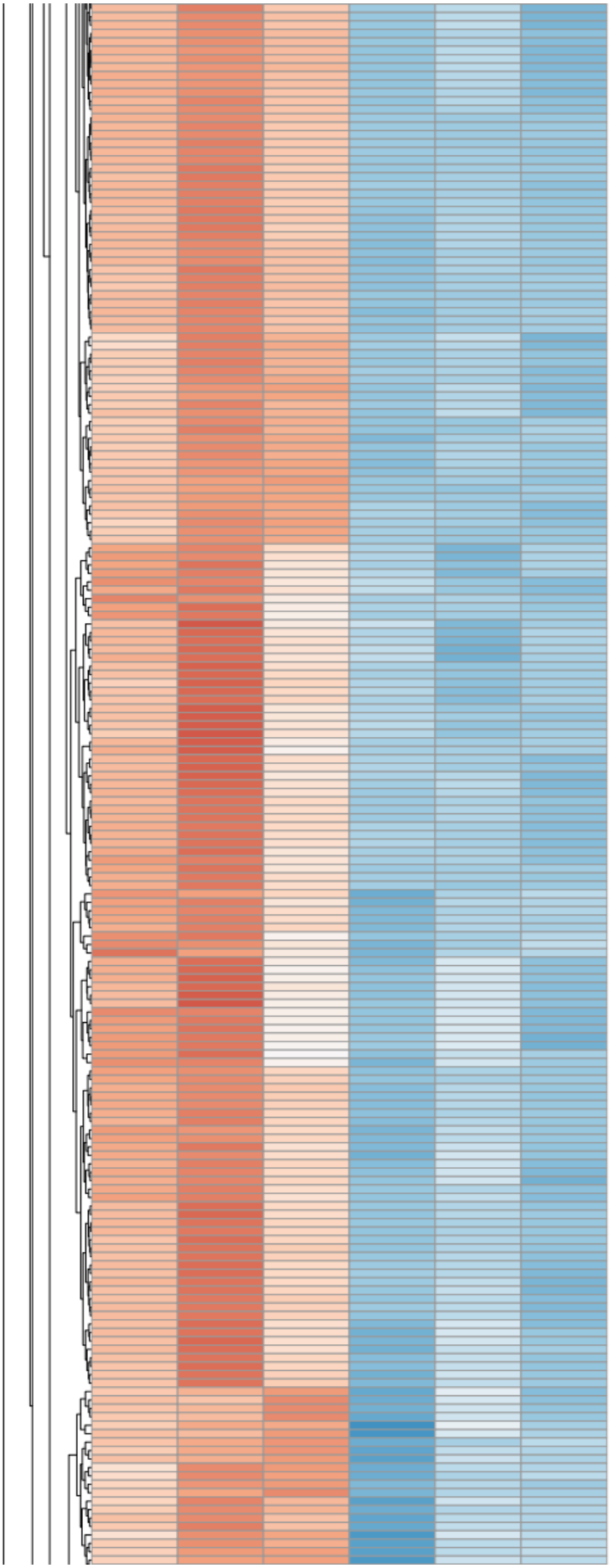
LIPA
C5AR1
IL18R1
PLEKHF2
ARSJ
FBXO7
UNC93B1
IFI6
ME3
UROS
CPQ
TDRD7
TYMP
LGALS14
SQWAHD
WDFY1
HOPX
MX2
LYSMD2
LIPH
RIPK4
ALAS1
FAM43A
PJA1
ZNF267
NT5C3A
BTBD9
TRO
EPB41L4B
ID1
RPS6KC1
MVB12A
CCDC71L
EHD3
RAB30
ACSS2
MAPRE2
CXCL10
PLCXD3
C19orf12
SLFN5
FNDC3B
VWA7
ABCA10
ADAMTSL3
ERLIN1
ENPP2
UBR1
RAB12
SLC12A7
USP15
BTBD8
ERP44
GALT
NPSR1−AS1
ABCB1
TNIK
IKZF2
TBK1
RAB27A
TMED7
RALB
GDPD1
ANKRD13C−DT
PXDC1
RASGRP1
C1orf116
LINC01522
MRPS30−DT
SYTL2
TMIE
EGR2
C3
CAPN5
PILRA
ZMYND15
BIRC3
LIMS1
C22orf42
DUSP5
ERN1
UBE2Z
CCDC159
DKK3
CHGA
RELB
NA
CLIP4
CFC1
TEX55
MST1R
FAM53B
MXD1
IL13RA1
ANKRD29
ELF3
ENPP5
TICAM1
MISP
LINC02717
SLC22A18
ADAMTS7P4
NFAM1
STYXL1
OAS2
TRPM4
STX4
DUSP10
H3C8
RRAS
TAPBP
PIK3IP1
SIRPA
CLU
NFATC2
TIMP1
GCNT2
PLA2G4F
ZNF396
FXYD3
PPP4R4
TNFRSF10B
HERC6
C1orf127
TSC22D4
DTNA
MPZL3
NCALD
TNFAIP3
PLEKHA4
FZD7
ICAM2
HPCAL4
RNASET2
PLA2G4C
MYO1A
ZFP36
GOLPH3L
NFE2L3
ACP5
JHY
ARHGAP18
LYN
HCCS
STX11
CX3CL1
VNN2
COQ10B
GC
ANXA7
BMP2
GOLM1
SHC3
LRMDA
TNFAIP2
LINC00237
MAPK8IP2
IGFBP3
CDKN1A
DYNLT1
ADGRG7
ALK
ABCC13
NEAT1
CADPS2
SERPINB9
FAM229B
SOHLH1
MAFF
MAGEA9
MICAL1
TCAF2C
ITIH6
PLEKHG7
NT5C3AP1
CIART
GADD45B
RHEBL1
L3HYPDH


ABCA8
CLDN9
SEMA6D
ATP10D
FTLP14
IRF2-DT
KCNC2
CDHR2
TSC22D1
NKAPP1
DSC2
DENND5B
DNAJC3-DT
ENDOD1
SP110
RBM43
GSTK1
CDK6
LRRN2
CTH
IL15
SLC37A1
CLIC5
B2M
NUDT16L2P
SLC29A7
ALMS1P1
DHX58
DRC1
PSTPIP2
METTL24
NIM1K
KLF4
TNFRSF14
GSDMD
ALS2CL
BMP3
GPBAR1
SERPINI2
SLC38A11
ABCD3P1
LPIN3
DENND2D
RHOU
RASSF8
PABIR3
JAK3
SLC35D2
CYP4F3
LINC02328
TENT5A
ANKFN1
PCGF5
MMAA
HSD17B7
TRIM14
CDH1
MLKL
COL24A1
NUGGC
NMNAT2
IFIT2
GBP3
UBE2L6
TNR
PIP4P2
B3GALT1
PARP10
HLA-A
AP3B1
NMI
IFIT5
ITGA6
HISLA
HPCAL1
GRAMD1B
MAX
ZNFX1
SERPINB9P1
ETV6
OAS3
ISG20
UBR2
EPSTI1
NUB1
FANCF
IFIH1
HELZ2
MX1
IFITM1
WARS1
SAMD9
FN1
SEC16B
TRIM56
WDR49
CTTNBP2NL
BTN2A2
PLEKHG1
TRANK1
ETV7
C6orf62
STARD5
CD44
PML
BTN3A1
ADAR
LMO7
APOL2
CASZ1
HLA-F
TRIM5
DGLUCY
SHFL
SCYL3
JAZF1
ELOVL7
TCAF2
IFIT3
ACY3
PATL2
LINC02577
CSF1
DCC
TFAP2A
CLMP
SIDT1
CALM3
SCML4
CASTOR3P
CLIP3
RAB19
SCN2A
BTN3A3
GBP1P1
DPYD
HERPUD1
GBP1
LGALS3BP
ERAP1
UBA7
MOV10
TAPBPL
DDX60
BTN3A2
BATF2
TAP1
DGKG
APOL6
RBCK1
NLRC5
C2
SLC28A3
PAXIP1-AS2
DTX3L
RNF213
SYNPO2
APOL1
ABTB2
PIK3AP1
RCN1
DNPEP
RUFY4
BISPR
STAT1
PARP9
APOBEC3F
PARP14
NEDD4L
IRF1
HEG1
TERT
RASGRP3
DDX60L
LY6E
HLA-H
IL7

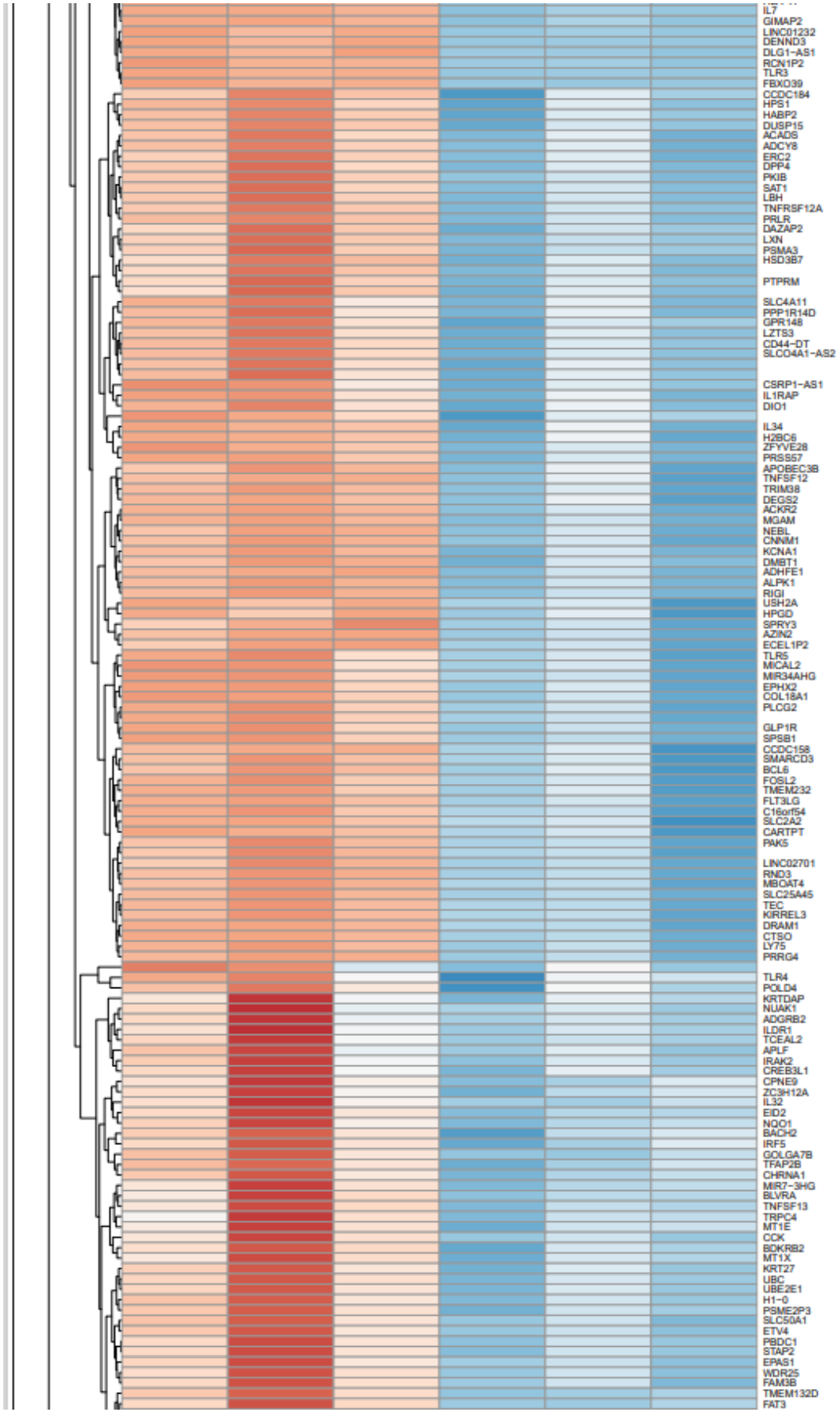
IL7
GIMAP2
LINC01232
DENND3
DLG1-AS1
RCN1P2
TLR3
FBXO39
CCDC184
HPS1
HABP2
DUSP15
ACADS
ADCY8
ERC2
DPP4
PKIB
SAT1
LBH
TNFRSF12A
PRLR
DAZAP2
LXN
PSMA3
HSD3B7
PTPRM
SLC4A11
PPP1R14D
GPR148
LZTS3
CD44-DT
SLC04A1-AS2
CSRP1-AS1
IL1RAP
DIO1
IL34
H2BC6
ZFYVE28
PRSS57
APOBEC3B
TNFSF12
TRIM38
DEGS2
ACKR2
MGAM
NEBL
CNNM1
KCNA1
DMST1
ADHFE1
ALPK1
RIGI
USH2A
HPGD
SPRY3
AZIN2
ECEL1P2
TLR5
MICAL2
MIR34AHG
EPHX2
COL18A1
PLCG2
GLP1R
SPSB1
CCDC158
SMARCD3
BCL6
FOSL2
TMEM232
FLT3LG
C16orf54
SLC2A2
CARTPT
PAK5
LINC02701
RND3
MBOAT4
SLC25A45
TEC
KIRREL3
DRAM1
CTSO
LY75
PRRG4
TLR4
POLD4
KRTDAP
NUAK1
ADGRB2
ILDR1
TCEAL2
APLF
IRAK2
CREB3L1
CPNE9
ZC3H12A
IL32
EID2
NQO1
BACH2
IRF5
GOLGA7B
TFAP2B
CHRNA1
MIR7-3HG
BLVRA
TNFSF13
TRPC4
MT1E
CCK
BDKRB2
MT1X
KRT27
UBC
UBE2E1
H1-0
PSME2P3
SLC50A1
ETV4
PBDC1
STAP2
EPAS1
WDR25
FAM3B
TMEM132D
FAT3

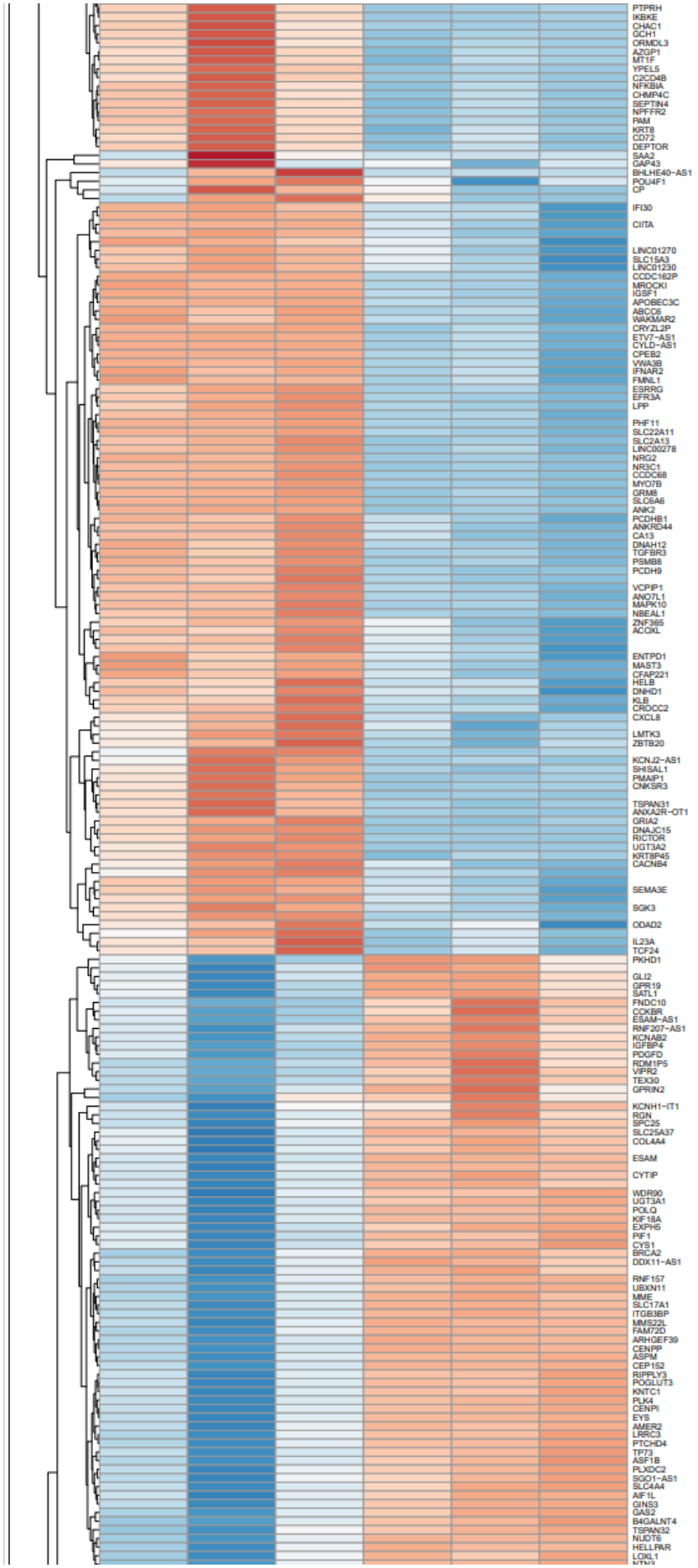
PTPRH
IKBKE
CHAC1
GCH1
ORMDL3
AZGP1
MT1F
YPEL5
C2CD4B
NFKBIA
CHMP4C
SEPTIN4
NPFFR2
PAM
KRT8
CD72
DEPTOR
SAA2
GAP43
BHLHE40-AS1
POU4F1
CP
IFI30
CIITA
LINC01270
SLC15A3
LINC01230
CCDC162P
MROCKI
IGSF1
APOBEC3C
ABCC6
WAKMAR2
CRYZL2P
ETV7-AS1
CYLD-AS1
CPEB2
VWA3B
IFNAR2
FMNL1
ESRRG
EFR3A
LPP
PHF11
SLC22A11
SLC2A13
LINC00278
NRG2
NR3C1
CCDC68
MYO7B
GRM8
SLC6A6
ANK2
PCDHB1
ANKRD44
CA13
DNAH12
TGFBR3
PSMB8
PCDH9
VCPIP1
AND7L1
MAPK10
NBEAL1
ZNF365
ACOXL
ENTPD1
MAST3
CFAP221
HELB
DNHD1
KLB
CROCC2
CXCL8
LMTK3
ZBTB20
KCNJ2-AS1
SHISAL1
PMAIP1
CNKSR3
TSPAN31
ANXA2R-OT1
GRIA2
DNAJC15
RICTOR
UGT3A2
KRT8P45
CACNB4
SEMA3E
SGK3
ODAD2
IL23A
TCF24
PKHD1
GLI2
GPR19
SATL1
FNDC10
CCKBR
ESAM-AS1
RNF207-AS1
KCNAB2
IGFBP4
PDGFD
RDM1P5
VIPR2
TEX30
GPRIN2
KCNH1-IT1
RGN
SPC25
SLC25A37
COL4A4
ESAM
CYTIP
WDR90
UGT3A1
POLQ
KIF18A
EXPH5
PIF1
CYS1
BRCA2
DDX11-AS1
RNF157
UBXN11
MME
SLC17A1
ITGB3BP
MMS22L
FAM72D
ARHGEF39
CENPP
ASPM
CEP152
RIPPLY3
POGLUT3
KNTC1
PLK4
CENPI
EYS
AMER2
LRRC3
PTCHD4
TP73
ASF1B
PLXDC2
SGO1-AS1
SLC4A4
AIF1L
GINS3
GAS2
B4GALNT4
TSPAN32
NUDT6
HELLPAR
LOXL1

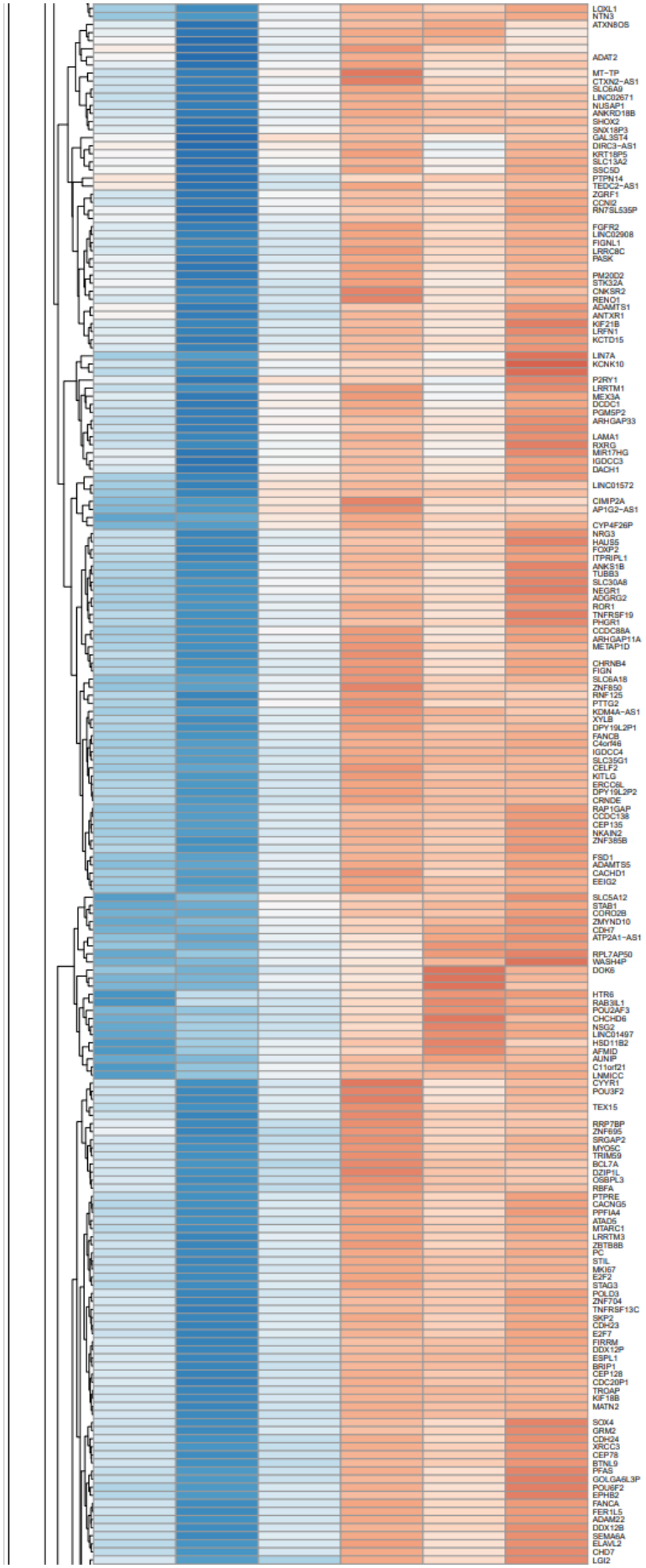
LOXL1
NTN3
ATXN8OS
ADAT2
MT-TP
CTXN2-AS1
SLC6A9
LINC02671
NUSAP1
ANKRD18B
SHOX2
SNX18P3
GAL3ST4
DIRC3-AS1
KRT18P5
SLC13A2
SSC5D
PTPN14
TEDC2-AS1
ZGRF1
CCNI2
RN7SL535P
FGFR2
LINC02908
FIGNL1
LRRC8C
PASK
PM20D2
STK32A
CNKSR2
RENO1
ADAMTS1
ANTXR1
KIF21B
LRFN1
KCTD15
LIN7A
KCNK10
P2RY1
LRRTM1
MEX3A
DCDC1
PGM5P2
ARHGAP33
LAMA1
RXRG
MIR17HG
IGDCC3
DACH1
LINC01572
CIMIP2A
AP1G2-AS1
CYP4F26P
NRG3
HAUS5
FOXP2
ITPRIPL1
ANKS1B
TUBB3
SLC30A8
NEGR1
ADGRG2
RORI
TNFRSF19
PHGR1
CODC88A
ARHGAP11A
METAP1D
CHRNB4
FIGN
SLC6A18
ZNF850
RNF125
PTTG2
KDM4A-AS1
XYLB
DPY19L2P1
FANCB
C4orf46
IGDCC4
SLC35G1
CELF2
KITLG
ERCC6L
DPY19L2P2
CRNDE
RAP1GAP
CCDC138
CEP135
NKAIN2
ZNF385B
FSD1
ADAMTS5
CACHD1
EEIG2
SLC5A12
STAB1
CORO2B
ZMYND10
CDH7
ATP2A1-AS1
RPL7AP50
WASH4P
DOK6
HTR6
RAB3IL1
POU2AF3
CHCHD6
NSG2
LINC01497
HSD11B2
AFMID
AUNIP
C11orf21
LNMICC
CYYR1
POU3F2
TEX15
RRP7BP
ZNF695
SRGAP2
MYO5C
TRIM59
BCL7A
DZIP1L
OSBPL3
RBFA
PTPRE
CACNG5
PPFIA4
ATAD5
MTARC1
LRRTM3
ZBTB8B
PC
STIL
MKI67
E2F2
STAG3
POLD3
ZNF704
TNFRSF13C
SKP2
CDH23
E2F7
FIRRM
DDX12P
ESPL1
BRIP1
CEP128
CDC20P1
TROAP
KIF18B
MATN2
SOX4
GRM2
CDH24
XRCC3
CEP78
BTNL9
PFAS
GOLGA8L3P
POU6F2
EPHB2
FANCA
FER1L5
ADAM22
DDX12B
SEMA6A
ELAVL2
CHD7
LGI2

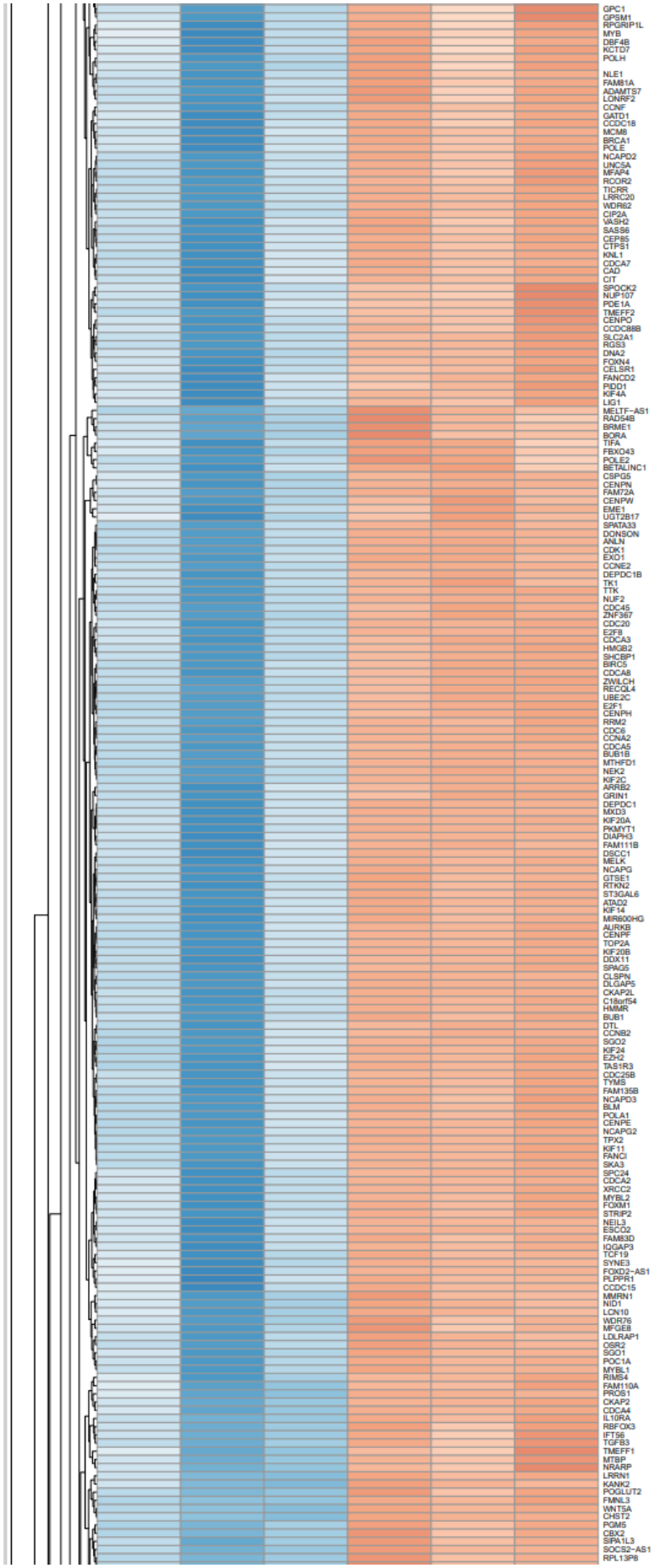
GPC1
GPSM1
RPGRIP1L
MYB
DBF4B
KCTD7
POLH
NLE1
FAM81A
ADAMTS7
LONRF2
CCNF
GATD1
CCDC18
MCM8
BRCA1
POLE
NCAPD2
UNC5A
MFAP4
RCOR2
TICRR
LRRC20
WDR62
CIP2A
VASH2
SASS6
CEP85
CTPS1
KNL1
CDCA7
CAD
CIT
SPOCK2
NUP107
PDE1A
TMEFF2
CENPO
CCDC88B
SLC2A1
RGS3
DNA2
FOXN4
CELSR1
FANCD2
PIDD1
KIF4A
LIG1
MELTF-AS1
RAD54B
BRME1
BORA
TIFA
FBXO43
POLE2
BETALINC1
CSPG5
CENPN
FAM72A
CENPW
EME1
UGT2B17
SPATA33
DONSON
ANLN
CDK1
EXO1
CCNE2
DEPDC1B
TK1
TTK
NUF2
CDC45
ZNF367
CDC20
E2F8
CDCA3
HMGB2
SHCBP1
BIRC5
CDCA8
ZWILCH
RECQL4
UBE2C
E2F1
CENPH
RRM2
CDC6
CCNA2
CDCA5
BUB1B
MTHFD1
NEK2
KIF2C
ARRB2
GRIN1
DEPDC1
MXD3
KIF20A
PKMYT1
DIAPH3
FAM111B
DSCC1
MELK
NCAPG
GTSE1
RTKN2
ST3GAL6
ATAD2
KIF14
MIR600HG
AURKB
CENPF
TOP2A
KIF20B
DDX11
SPAG5
CLSPN
DLGAP5
CKAP2L
C18orf54
HMMR
BUB1
DTL
CCNB2
SGO2
KIF24
EZH2
TAS1R3
CDC25B
TYMS
FAM135B
NCAPD3
BLM
POLA1
CENPE
NCAPG2
TPX2
KIF11
FANCI
SKA3
SPC24
CDCA2
XRCC2
MYBL2
FOXM1
STRIP2
NEIL3
ESCO2
FAM83D
IQGAP3
TCF19
SYNE3
FOXD2-AS1
PLPPR1
CCDC15
MMRN1
NID1
LCN10
WDR76
MFGE8
LDLRAP1
GSR2
SGO1
POC1A
MYBL1
RIMS4
FAM110A
PROS1
CKAP2
CDCA4
IL10RA
RBFOX3
IFT56
TGFB3
TMEFF1
MTBP
NRARP
LRRN1
KANK2
POGLUT2
FMNL3
WNT5A
CHST2
PGM5
CBX2
SIPA1L3
SOCS2-AS1
RPL13P8

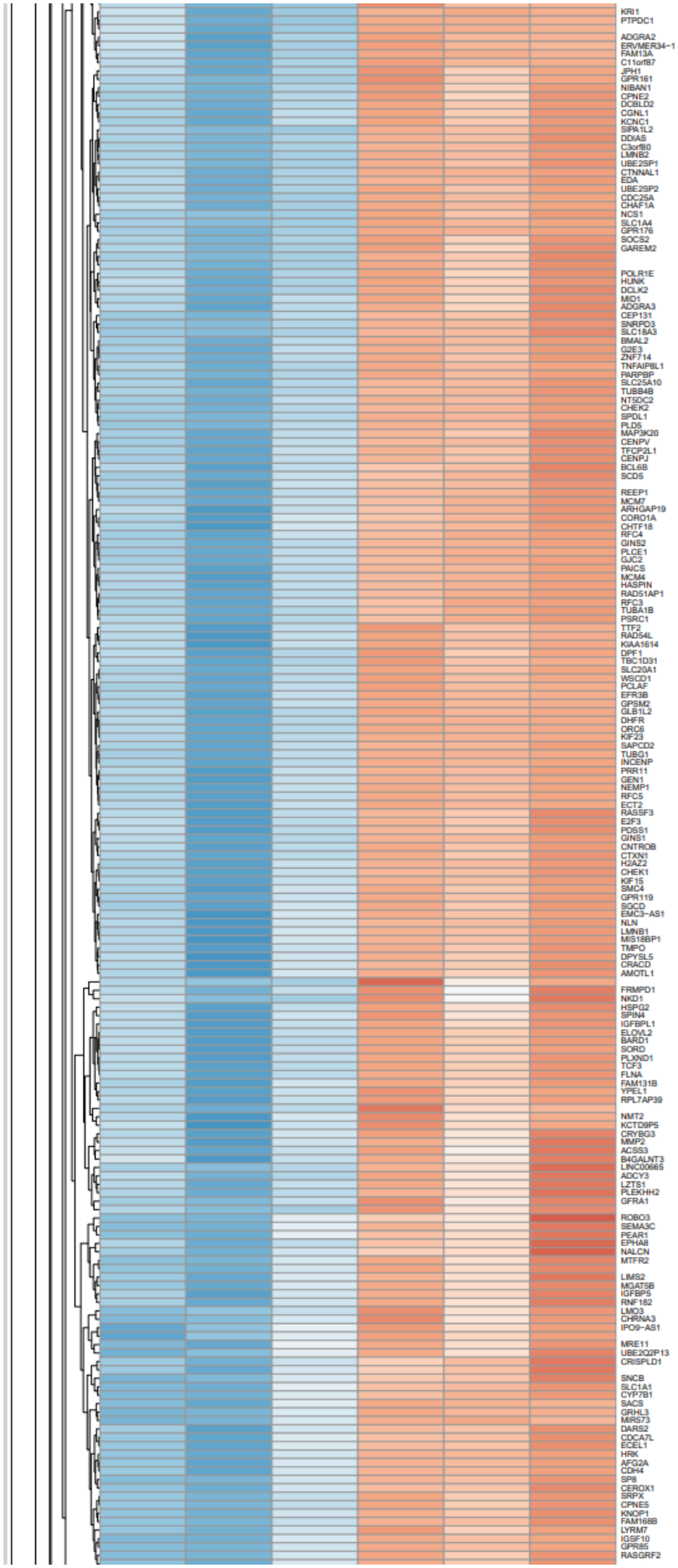
KRI1
PTPDC1
ADGRA2
ERVMER34-1
FAM13A
C11orf87
JPH1
GPR161
NIBAN1
CPNE2
DCBLD2
CGNL1
KCNC1
SIPA1L2
DDIAS
C3orf80
LMNB2
UBE2SP1
CTNNAL1
EDA
UBE2SP2
CDC25A
CHAF1A
NCS1
SLC1A4
GPR176
SOCS2
GAREM2
POLR1E
HUNK
DCLK2
MID1
ADGRA3
CEP131
SNRPD3
SLC18A3
BMAL2
G2E3
ZNF714
TNFAIP8L1
PARPBP
SLC25A10
TUBB4B
NT5DC2
CHEK2
SPDL1
PLD5
MAP3K20
CENPV
TFCP2L1
CENPJ
BCL6B
SCD5
REEP1
MCM7
ARHGAP19
CORO1A
CHTF18
RFC4
GINS2
PLCE1
GJC2
PAICS
MCM4
HASPIN
RAD51AP1
RFC3
TUBA1B
PSRC1
TTF2
RAD54L
KIAA1614
DPF1
TBC1D31
SLC20A1
WSCD1
PCLAF
EFR3B
GPSM2
GLB1L2
DHFR
ORC6
KIF23
SAPCD2
TUBG1
INCENP
PRR11
GEN1
NEMP1
RFC5
ECT2
RASSF3
E2F3
PDSS1
GINS1
CNTROB
CTXN1
H2AZ2
CHEK1
KIF15
SMC4
GPR119
SGCD
EMC3-AS1
NLN
LMNB1
MIS18BP1
TMPO
DPYSL5
CRACD
AMOTL1
FRMPD1
NKD1
HSPG2
SPIN4
IGFBPL1
ELOVL2
BARD1
SORD
PLXND1
TCF3
FLNA
FAM131B
YPEL1
RPL7AP39
NMT2
KCTD9P5
CRYBG3
MMP2
ACSS3
B4GALNT3
LINC00665
ADCY3
LZTS1
PLEKHH2
GFRA1
ROBO3
SEMA3C
PEAR1
EPHA8
NALCN
MTFR2
LIMS2
MGAT5B
IGFBP5
RNF182
LMO3
CHRNA3
IPO9-AS1
MRE11
UBE2Q2P13
CRISPLD1
SNCB
SLC1A1
CYP7B1
SACS
GRHL3
MIR573
DARS2
CDCA7L
ECEL1
HRK
AFG2A
CDH4
SP8
CEROX1
SRPX
CPNE5
KNOP1
FAM168B
LYRM7
IGSF10
GPR85
RASGRF2

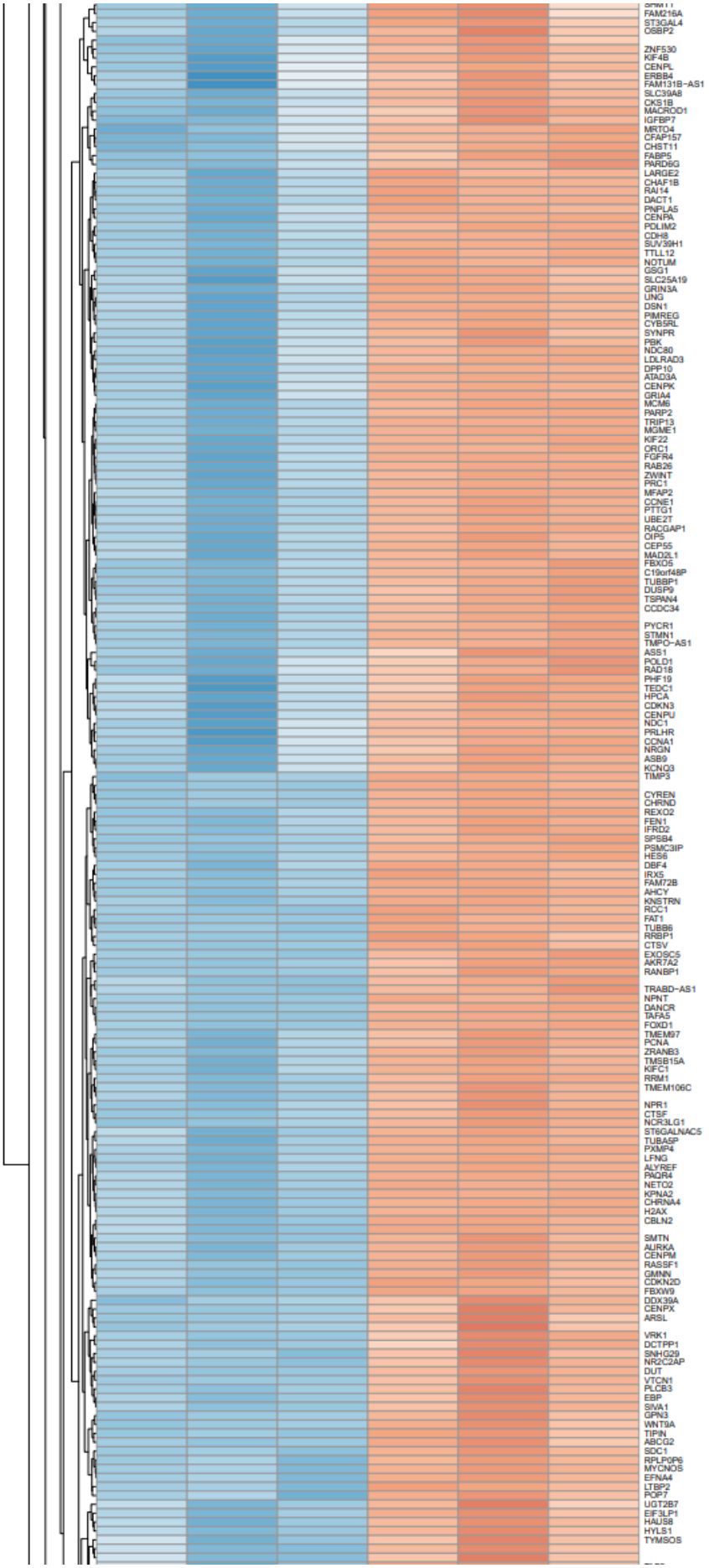
FAM216A
ST3GAL4
OSBP2
ZNF530
KIF4B
CENPL
ERBB4
FAM131B-AS1
SLC39A8
CKS1B
MACROD1
IGFBP7
MRTO4
CFAP157
CHST11
FABP5
PARD6G
LARGE2
CHAF1B
RAI14
DACT1
PNPLA5
CENPA
PDLIM2
CDH8
SUV39H1
TTLL12
NOTUM
GSG1
SLC25A19
GRIN3A
UNG
DSN1
PIMREG
CYB5RL
SYNPR
PBK
NDC80
LDLRAD3
DPP10
ATAD3A
CENPK
GRIA4
MCM6
PARP2
TRIP13
MGME1
KIF22
ORC1
FGFR4
RAB26
ZWINT
PRC1
MFAP2
CCNE1
PTTG1
UBE2T
RACGAP1
CIP5
CEP55
MAD2L1
FBXO5
C19orf48P
TUBBP1
DUSP9
TSPAN4
CCDC34
PYCR1
STMN1
TMPO-AS1
ASS1
POLD1
RAD18
PHF19
TEDC1
HPCA
CDKN3
CENPU
NDC1
PRLHR
CCNA1
NRGN
ASB9
KCNQ3
TIMP3
CYREN
CHRND
REXO2
FEN1
IFRD2
SPSB4
PSMC3IP
HES6
DBF4
IRX5
FAM72B
AHCY
KNSTRN
RCC1
FAT1
TUBB6
RRBP1
CTSV
EXOSC5
AKR7A2
RANBP1
TRABD-AS1
NPNT
DANCR
TAPA5
FOXD1
TMEM97
PCNA
ZRANB3
TMSB15A
KIFC1
RRM1
TMEM106C
NPR1
CTSF
NCR3LG1
ST6GALNAC5
TUBA5P
PXMP4
LFNG
ALYREF
PAQR4
NETO2
KPNA2
CHRNA4
H2AX
CBLN2
SMTN
AURKA
CENPM
RASSF1
GMNN
CDKN2D
FBXW9
DDX39A
CENPX
ARSL
VRK1
DCTPP1
SNHG29
NR2C2AP
DUT
VTCN1
PLCB3
EBP
SIVA1
GPN3
WNT9A
TIPIN
ABCG2
SDC1
RPLP0P6
MYCNOS
EFNA4
LTBP2
POP7
UGT2B7
EIF3LP1
HAUS8
HYLS1
TYMSOS

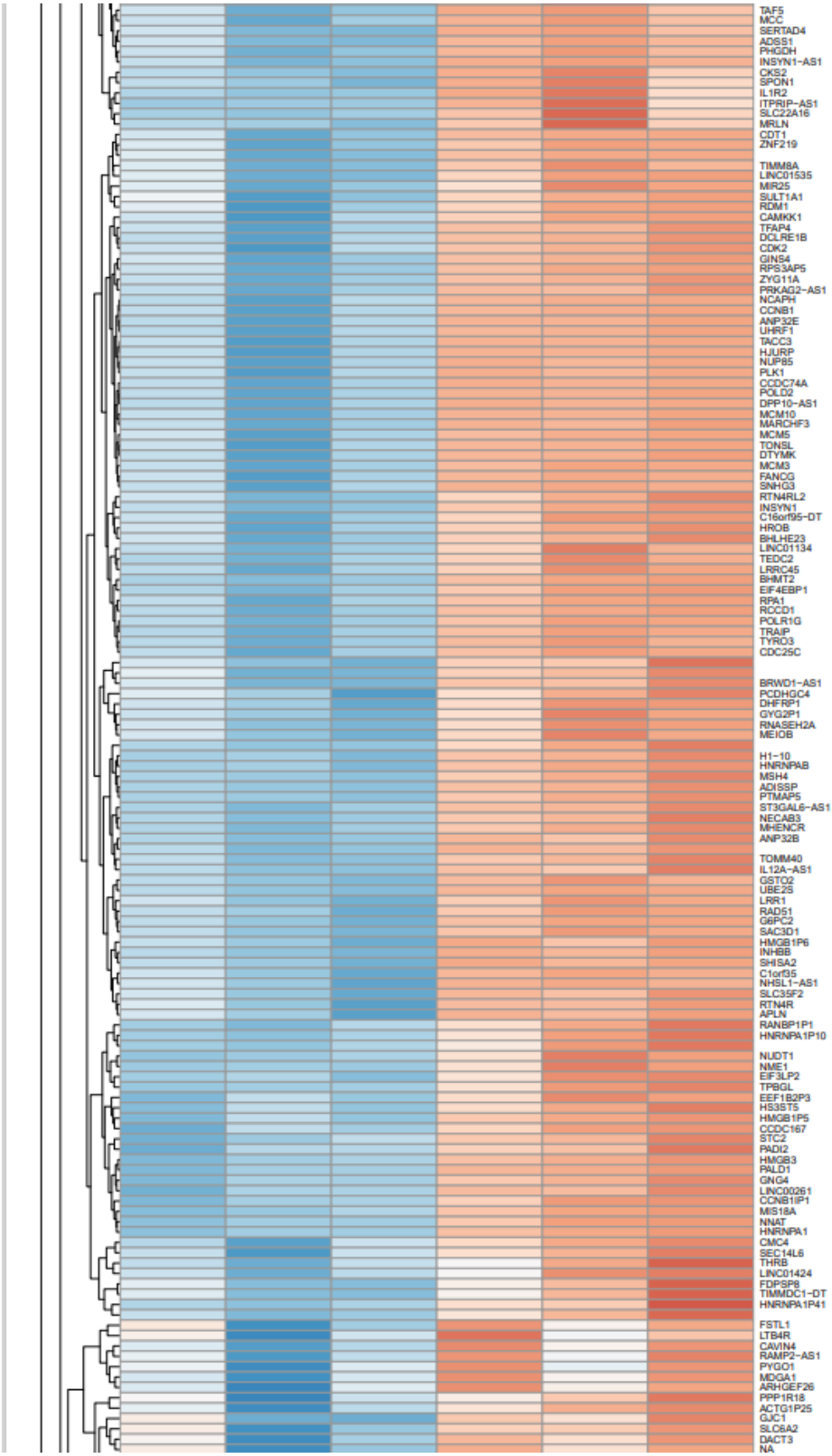
TAF5
MCC
SERTAD4
ADSS1
PHGDH
INSYN1-AS1
CKS2
SPON1
IL1R2
ITPRIP-AS1
SLC22A16
MRLN
CDT1
ZNF219
TIMM8A
LINC01535
MIR25
SULT1A1
RDM1
CAMKK1
TFAP4
DCLRE1B
CDK2
GINS4
RPS3AP5
ZYG11A
PRKAG2-AS1
NCAPH
CCNB1
ANP32E
UHRF1
TACC3
HJURP
NUP85
PLK1
CCDC74A
POLD2
DPP10-AS1
MCM10
MARCHF3
MCM5
TONSL
DTYMK
MCM3
FANCG
SNHG3
RTN4RL2
INSYN1
C16orf95-DT
HROB
BHLHE23
LINC01134
TEDC2
LRRC45
BHMT2
EIF4EBP1
RPA1
RCCD1
POLR1G
TRAIP
TYRO3
CDC25C
BRWD1-AS1
PCDHGC4
DHFRP1
GYG2P1
RNASEH2A
MEIOB
H1-10
HNRNPAB
MSH4
ADSSP
PTMAP5
ST3GAL6-AS1
NECAB3
MHENCR
ANP32B
TOMM40
IL12A-AS1
GSTO2
UBE2S
LRR1
RAD51
G6PC2
SAC3D1
HMGB1P6
INHBB
SHISA2
C1orf35
NHSL1-AS1
SLC35F2
RTN4R
APLN
RANBP1P1
HNRNPA1P10
NUDT1
NME1
EIF3LP2
TPBGL
EEF1B2P3
HS3ST5
HMGB1P5
CCDC167
STC2
PADI2
HMGB3
PALD1
GNG4
LINC00261
CCNB1IP1
MIS18A
NNAT
HNRNPA1
CMC4
SEC14L6
THRB
LINC01424
FDPSP6
TIMMDC1-DT
HNRNPA1P41
FSTL1
LTB4R
CAVIN4
RAMP2-AS1
PYGO1
MDGA1
ARHGEF26
PPP1R18
ACTG1P25
GJC1
SLC6A2
DACT3
NA

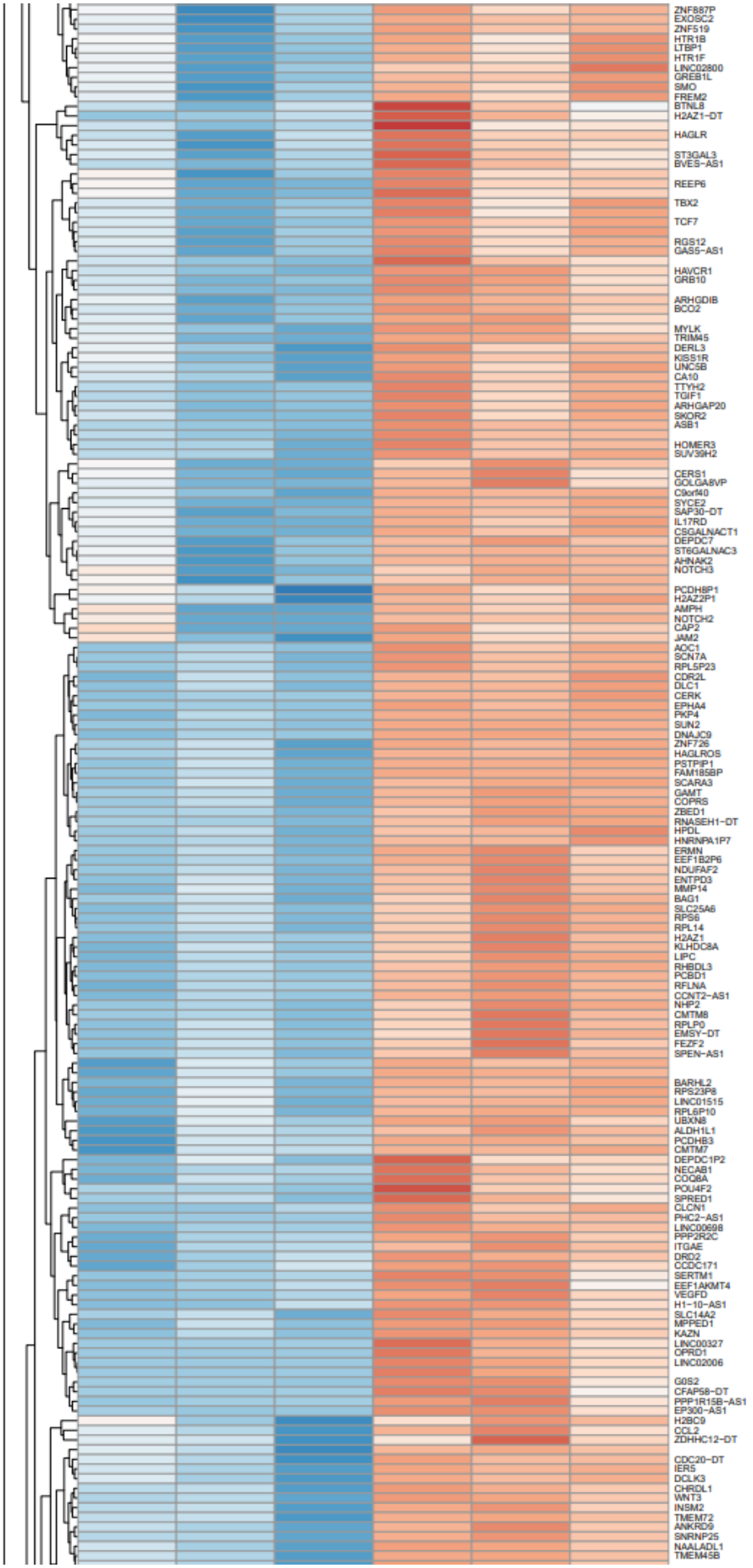
ZNF887P
EXOSC2
ZNF519
HTR1B
LTBP1
HTR1F
LINC02800
GREB1L
SMO
FREM2
BTNL8
H2AZ1-DT
HAGLR
ST3GAL3
BVES-AS1
REEP6
TBX2
TCF7
RGS12
GAS5-AS1
HAVCR1
GRB10
ARHGDIB
BCO2
MYLK
TRIM45
DERL3
KISS1R
UNC5B
CA10
TTYH2
TGIF1
ARHGAP20
SKOR2
ASB1
HOMER3
SUV39H2
CERS1
GOLGA8VP
C9orf40
SYCE2
SAP30-DT
IL17RD
CSGALNACT1
DEPDC7
ST6GALNAC3
AHNAK2
NOTCH3
PCDH8P1
H2AZ2P1
AMPH
NOTCH2
CAP2
JAM2
AOC1
SCN7A
RPL5P23
CDR2L
DLC1
CERK
EPHA4
PKP4
SUN2
DNAJC9
ZNF726
HAGLROS
PSTPIP1
FAM185BP
SCARA3
GAMT
COPRS
ZBED1
RNASEH1-DT
HPDL
HNRNPA1P7
ERMN
EEF1B2P6
NDUFAF2
ENTPD3
MMP14
BAG1
SLC25A6
RPS6
RPL14
H2AZ1
KLHDC8A
LIPC
RHBDL3
PCBD1
RFLNA
CCNT2-AS1
NHP2
CMTM8
RPLP0
EMSY-DT
FEZF2
SPEN-AS1
BARHL2
RPS23P8
LINC01515
RPL6P10
UBXN8
ALDH1L1
PCDHB3
CMTM7
DEPDC1P2
NECAB1
COQ8A
POU4F2
SPRED1
CLCN1
PHC2-AS1
LINC00698
PPP2R2C
ITGAE
DRD2
CCDC171
SERTM1
EEF1AKMT4
VEGFD
H1-10-AS1
SLC14A2
MPPED1
KAZN
LINC00327
OPRD1
LINC02006
G0S2
CFAP58-DT
PPP1R15B-AS1
EP300-AS1
H2BC9
CCL2
ZDHHC12-DT
CDC20-DT
IER5
DCLK3
CHRDL1
WNT3
INSM2
TMEM72
ANKRD9
SNRNP25
NAALADL1
TMEM45B

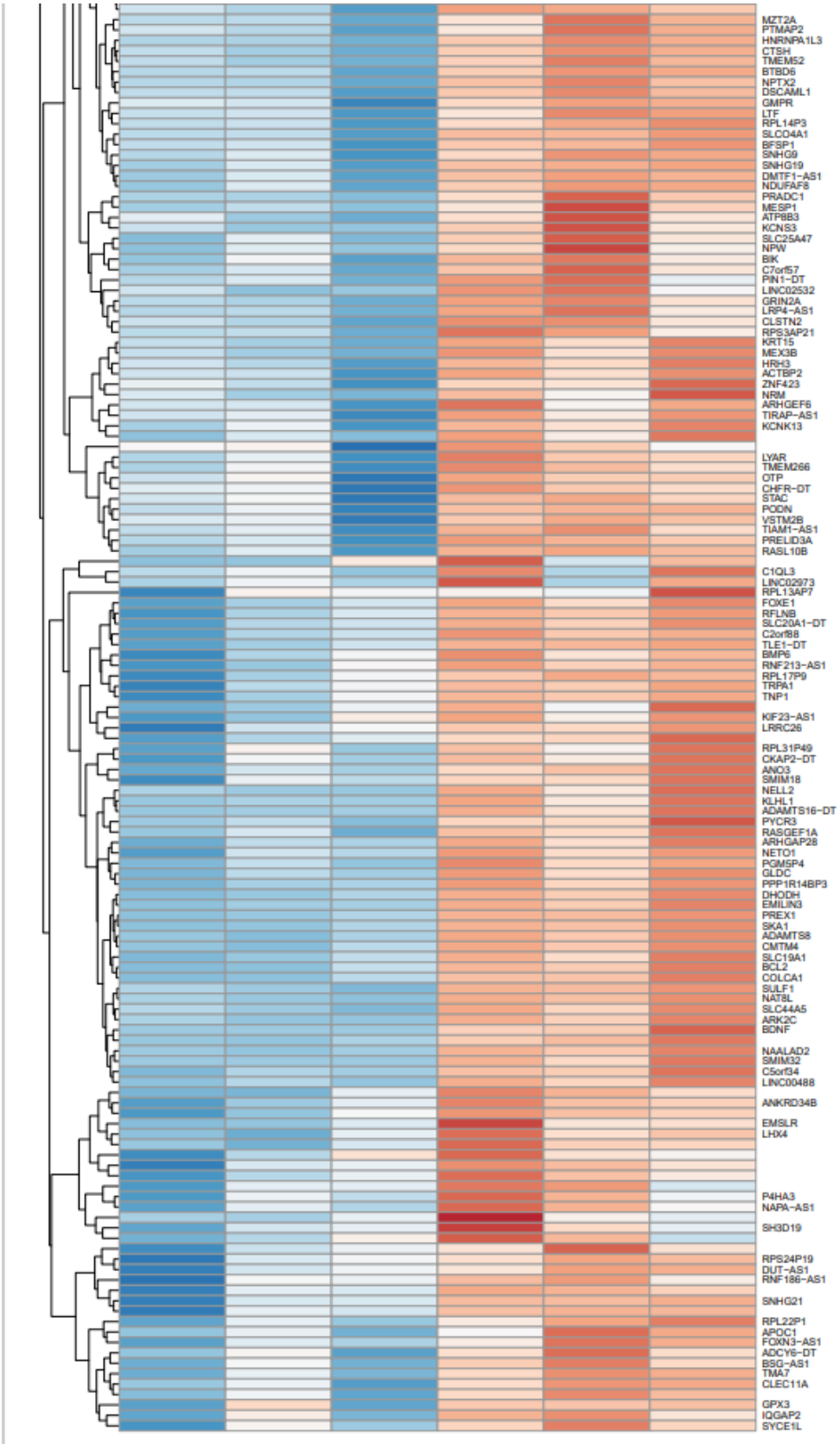

Figure 7.12: Differentially expressed genes of EndoC-βH1 cells treated with Cytokine Mix (1 ng/ml IL-1β, 20 ng/ml TNF-α and 20 ng/ml INF-γ).

Chapter 8: Bibliography

Abdul-Karim, F. W., Dahms, B. B., Velasco, M. E., & Rodman, H. M. (1986). Islets of Langerhans in adolescents and adults with cystic fibrosis. A quantitative study. Archives of Pathology & Laboratory Medicine, 110(7), 602–606.

Aleksic, T., Baumann, B., Wagner, M., Adler, G., Wirth, T., & Weber, C. K. (2007). Cellular immune reaction in the pancreas is induced by constitutively active IκB kinase-2. Gut, 56(2), 227–236. https://doi.org/10.1136/GUT.2005.084665

Alexandre-Heymann, L., Mallone, R., Boitard, C., & Scharfmann, R. (2019). Structure and function of the exocrine pancreas in patients with type 1 diabetes. Reviews in Endocrine & Metabolic Disorders, 20(2), 129–149. https://doi.org/10.1007/S11154-019-09501-3

Alfadhli, E. M. (2015). Gestational diabetes mellitus. Saudi Medical Journal, 36(4), 399–406. https://doi.org/10.15537/smj.2015.4.10307

Al-Mrabeh, A., Hollingsworth, K. G., Steven, S., & Taylor, R. (2016). Morphology of the pancreas in type 2 diabetes: effect of weight loss with or without normalisation of insulin secretory capacity. Diabetologia, 59(8), 1753–1759. https://doi.org/10.1007/s00125-016-3984-6

Andersen, D. H. (1938). Cystic fibrosis of the pancreas and its relation to celiac disease. American Journal of Diseases of Children, 56(2), 344. https://doi.org/10.1001/archpedi.1938.01980140114013

Anderson, M. S., & Bluestone, J. A. (2004). The Node Mouse: A Model of Immune Dysregulation. Http://Dx.Doi.Org/10.1146/Annurev.Immunol.23.021704.115643, 23, 447–485. https://doi.org/10.1146/ANNUREV.IMMUNOL.23.021704.115643

Anik, A., Çatli, G., Abaci, A., & Böber, E. (2015). Maturity-onset diabetes of the young (MODY): An update. In Journal of Pediatric Endocrinology and Metabolism (Vol. 28, Issues 3–4, pp. 251–263). Walter de Gruyter GmbH. https://doi.org/10.1515/jpem-2014-0384

Apte, M. V., Haber, P. S., Applegate, T. L., Norton, I. D., McCaughan, G. W., Korsten, M. A., Pirola, R. C., & Wilson, J. S. (1998). Periacinar stellate shaped cells in rat pancreas: Identification, isolation, and culture. Gut, 43(1), 128–133. https://doi.org/10.1136/gut.43.1.128

Apte, M. V., Haber, P. S., Darby, S. J., Rodgers, S. C., McCaughan, G. W., Korsten, M. A., Pirola, R. C., & Wilson, J. S. (1999). Pancreatic stellate cells are activated by proinflammatory cytokines: Implications for pancreatic fibrogenesis. Gut, 44(4), 534–541. https://doi.org/10.1136/gut.44.4.534

Apte, M. V., Pirola, R. C., & Wilson, J. S. (2012). Pancreatic stellate cells: A starring role in normal and diseased pancreas. In Frontiers in Physiology: Vol. 3 AUG. Frontiers Media SA. https://doi.org/10.3389/fphys.2012.00344

Arif, S., Leete, P., Nguyen, V., Marks, K., Nor, N. M., Estorninho, M., Kronenberg-Versteeg, D., Bingley, P. J., Todd, J. A., Guy, C., Dunger, D. B., Powrie, J., Willcox, A., Foulis, A. K., Richardson, S. J., Rinaldis, E. de, Morgan, N. G., Lorenc, A., & Peakman, M. (2014). Blood

and Islet Phenotypes Indicate Immunological Heterogeneity in Type 1 Diabetes. Diabetes, 63(11), 3835–3845. https://doi.org/10.2337/DB14-0365

Arnush, M., Heitmeier, M. R., Scarim, A. L., Marino, M. H., Manning, P. T., & Corbett, J. A. (1998). IL-1 produced and released endogenously within human islets inhibits β cell function. Journal of Clinical Investigation, 102(3), 516–526. https://doi.org/10.1172/JCI844

Arora, A., Behl, T., Sehgal, A., Singh, S., Sharma, N., Chigurupati, S., Kaur, R., Bhatia, S., Al-Harrasi, A., Vargas-De-La-Cruz, C., & Bungau, S. (2021). Free fatty acid receptor 1: a ray of hope in the therapy of type 2 diabetes mellitus. In Inflammopharmacology (Vol. 29, Issue 6, pp. 1625–1639). Springer Science and Business Media Deutschland GmbH. https://doi.org/10.1007/s10787-021-00879-8

Asensio, C., Cettour-Rose, P., Theander-Carrillo, C., Rohner-Jeanrenaud, F., & Muzzin, P. (2004). Changes in glycemia by leptin administration or high-fat feeding in rodent models of obesity/type 2 diabetes suggest a link between resistin expression and control of glucose homeostasis. Endocrinology, 145(5), 2206–2213. https://doi.org/10.1210/en.2003-1679

Association, American. Diabetes. (2018). Classification and diagnosis of diabetes: Standards of medical care in Diabetesd2018. Diabetes Care, 41(Supplement 1), S13–S27. https://doi.org/10.2337/dc18-S002

Atkinson, M. A., Bluestone, J. A., Eisenbarth, G. S., Hebrok, M., Herold, K. C., Accili, D., Pietropaolo, M., Arvan, P. R., Herrath, M. Von, Markel, D. S., & Rhodes, C. J. (2011). How Does Type 1 Diabetes Develop? Diabetes, 60(5), 1370–1379. https://doi.org/10.2337/DB10-1797

Atkinson, M. A., Campbell-Thompson, M., Kusmartseva, I., & Kaestner, K. H. (2020). Organisation of the human pancreas in health and in diabetes. In Diabetologia (Vol. 63, Issue 10, pp. 1966–1973). Springer. https://doi.org/10.1007/s00125-020-05203-7

Atkinson, M. A., Eisenbarth, G. S., & Michels, A. W. (2014). Type 1 diabetes. In The Lancet (Vol. 383, Issue 9911, pp. 69–82). Elsevier B.V. https://doi.org/10.1016/S0140-6736(13)60591-7

Avogaro, A., & Fadini, G. P. (2019). Microvascular complications in diabetes: A growing concern for cardiologists. International Journal of Cardiology, 291, 29–35. https://doi.org/10.1016/J.IJCARD.2019.02.030

Bachem, M. G., Schneider, E., Groß, H., Weidenbach, H., Schmid, R. M., Menke, A., Siech, M., Beger, H., Grunert, A., Grunert, G., & Adler, G. (1998). Identification, Culture, and Characterization of Pancreatic Stellate Cells in Rats and Humans.

Baker, S. S., Borowitz, D., & Baker, R. D. (2005). Pancreatic exocrine function in patients with cystic fibrosis. In Current Gastroenterology Reports (Vol. 7, Issue 3, pp. 227–233). Current Science Ltd. https://doi.org/10.1007/s11894-005-0039-4

Baldwin, A. (1996). The NF-kappa B and I kappa B proteins: new discoveries and insights. Annual Review of Immunology, 14, 649–681. https://doi.org/10.1146/ANNUREV.IMMUNOL.14.1.649

Barrio, R. (2015). Management of Endocrine Disease: Cystic fibrosis-related diabetes: novel pathogenic insights opening new therapeutic avenues. European Journal of Endocrinology, 172(4), R131–R141. https://doi.org/10.1530/EJE-14-0644

Baumann, B., Wagner, M., Aleksic, T., Von Wichert, G., Weber, C. K., Adler, G., & Wirth, T. (2007). Constitutive IKK2 activation in acinar cells is sufficient to induce pancreatitis in vivo. Journal of Clinical Investigation, 117(6), 1502–1513. https://doi.org/10.1172/JCI30876

Beckman, J. A., Paneni, F., Cosentino, F., & Creager, M. A. (2013). Diabetes and vascular disease: pathophysiology, clinical consequences, and medical therapy: part II. European Heart Journal, 34(31), 2444–2452. https://doi.org/10.1093/EURHEARTJ/EHT142

Bellin, M. D., Laguna, T., Leschyshyn, J., Regelmann, W., Dunitz, J., Billings, J., & Moran, A. (2013). Insulin secretion improves in cystic fibrosis following ivacaftor correction of CFTR: A small pilot study. Pediatric Diabetes, 14(6), 417–421. https://doi.org/10.1111/pedi.12026

Bethesda, M. (2017). Cystic Fibrosis Foundation Patient Registry Report 2016. Cystic Fibrosis Foundation.

Beyer, G., Habtezion, A., Werner, J., Lerch, M. M., & Mayerle, J. (2020). Chronic pancreatitis. The Lancet, 396(10249), 499–512. https://doi.org/10.1016/S0140-6736(20)31318-0

Blackman, S. M., Commander, C. W., Watson, C., Arcara, K. M., Strug, L. J., Stonebraker, J. R., Wright, F. A., Rommens, J. M., Sun, L., Pace, R. G., Norris, S. A., Durie, P. R., Drumm, M. L., Knowles, M. R., & Cutting, G. R. (2013). Genetic modifiers of cystic fibrosis-related diabetes. Diabetes, 62(10), 3627–3635. https://doi.org/10.2337/db13-0510

Bogdani, M., Blackman, S. M., Ridaura, C., Bellocq, J. P., Powers, A. C., & Aguilar-Bryan, L. (2017). Structural abnormalities in islets from very young children with cystic fibrosis may contribute to cystic fibrosis-related diabetes. Scientific Reports, 7(1), 1–11. https://doi.org/10.1038/s41598-017-17404-z

Böni-Schnetzler, M., & Meier, D. T. (2019). Islet inflammation in type 2 diabetes. Seminars in Immunopathology 2019 41:4, 41(4), 501–513. https://doi.org/10.1007/S00281-019-00745-4

Bonner-Weir, S., Inada, A., Yatoh, S., Li, W, C., Aye, T., Toshchi, E., & Sharma, A. (2008). Transdifferentiation of pancreatic ductal cells to endocrine beta-cells. Biochemical Society Transactions, 36(Pt 3), 353–356. https://doi.org/10.1042/BST0360353

Boom, A., Lybaert, P., Pollet, J., Jacobs, P., Jijakli, H., Golstein, P., Sener, A., Malaisse, W., & Beauwens, R. (2007). Expression and localization of cystic fibrosis transmembrane conductance regulator in the rat endocrine pancreas. Endocrine, 32(2), 197–205. https://doi.org/10.1007/S12020-007-9026-X

Booth, G., Kapral, M., Fung, K., & Tu, J. (2006). Relation between age and cardiovascular disease in men and women with diabetes compared with non-diabetic people: a population-based retrospective cohort study. Lancet (London, England), 368(9529), 29–36. https://doi.org/10.1016/S0140-6736(06)68967-8

Bottazzo, G., Florin-Christensen, A., & Doniach, D. (1974). Islet-cell antibodies in diabetes mellitus with autoimmune polyendocrine dificiencies. The Lancet, 304(7892), 1279–1283. https://doi.org/10.1016/S0140-6736(74)90140-8

Boucher, R. (2019). Muco-Obstructive Lung Diseases. The New England Journal of Medicine, 380(20), 1941–1953. https://doi.org/10.1056/NEJMRA1813799

Boyle, M. P., & De Boeck, K. (2013). A new era in the treatment of cystic fibrosis: correction of the underlying CFTR defect. The Lancet Respiratory Medicine, 1(2), 158–163. https://doi.org/10.1016/S2213-2600(12)70057-7

Brennan, A., & Beynon, J. (2015). Clinical updates in cystic fibrosis-related diabetes. Seminars in Respiratory and Critical Care Medicine, 36(2), 236–250. https://doi.org/10.1055/S-0035-1547319

Bridges, N., Rowe, R., & Holt, R. I. G. (2018). Unique challenges of cystic fibrosis-related diabetes. Diabetic Medicine: A Journal of the British Diabetic Association. https://doi.org/10.1111/dme.13652

Bruscia, E. M., & Bonfield, T. L. (2016). Cystic Fibrosis Lung Immunity: The Role of the Macrophage. Journal of Innate Immunity, 8(6), 550–563. https://doi.org/10.1159/000446825

Butler, A. E., & Misselbrook, D. (2020). Distinguishing between type 1 and type 2 diabetes. The BMJ, 370. https://doi.org/10.1136/bmj.m2998

Cano Megías, M., González Albarrán, O., Guisado Vasco, P., Lamas Ferreiro, A., & Máiz Carro, L. (2015). Insulin resistance, β-cell dysfunction and differences in curves of plasma glucose and insulin in the intermediate points of the standard glucose tolerance test in adults with cystic fibrosis. Endocrinología y Nutrición (English Edition), 62(2), 91–99. https://doi.org/10.1016/j.endoen.2015.02.001

Cantin, A. M., Hartl, D., Konstan, M. W., & Chmiel, J. F. (2015). Inflammation in cystic fibrosis lung disease: Pathogenesis and therapy. Journal of Cystic Fibrosis, 14(4), 419–430. https://doi.org/10.1016/J.JCF.2015.03.003

Carnegie, J. R., Robert-Cooperman, C. E., Wu, J., Young, R. A., Wolf, B. A., & Burkhardt, B. R. (2010). Characterization of the expression, localization, and secretion of PANDER in α-cells. Molecular and Cellular Endocrinology, 325(1–2), 36–45. https://doi.org/10.1016/j.mce.2010.05.008

Castellani, S., Di Gioia, S., di Toma, L., & Conese, M. (2018). Human cellular models for the investigation of lung inflammation and mucus production in cystic fibrosis. Analytical Cellular Pathology, 2018. https://doi.org/10.1155/2018/3839803

Castillo, J. J., Aplin, A., Akter, R., & Hull-Michelle, R. L. (2022). 13-OR: Cystic Fibrosis Donors Exhibit Striking Decrease in Pancreatic Islet and Exocrine Capillaries. Diabetes, 71(Supplement_1). https://doi.org/10.2337/db22-13-OR

Cell type atlas - CFTR - The Human Protein Atlas. (2021). Retrieved July 12, 2021, from https://www.proteinatlas.org/ENSG00000001626-CFTR/celltype/pancreas

Chalmers, J. D., Moffitt, K. L., Suarez-Cuartin, G., Sibila, O., Finch, S., Furrie, E., Dicker, A., Wrobel, K., Elborn, J. S., Walker, B., Martin, S. L., Marshall, S. E., Huang, J. T.-J., & Fardon, T. C. (2017). Neutrophil Elastase Activity Is Associated with Exacerbations and Lung Function Decline in Bronchiectasis. American Journal of Respiratory and Critical Care Medicine, 195(10), 1384. https://doi.org/10.1164/RCCM.201605-1027OC

Cnop, M., Welsh, N., Jonas, J. C., Jorns, A., Lenzen, S., & Eizirik, D. L. (2005). Mechanisms of pancreatic beta-cell death in type 1 and type 2 diabetes: many differences, few similarities. Diabetes, 54 Suppl 2(SUPPL. 2). https://doi.org/10.2337/DIABETES.54.SUPPL_2.S97

Cobo, I., Martinelli, P., Flández, M., Bakiri, L., Zhang, M., Carrillo-De-Santa-Pau, E., Jia, J., Lobo, V. J. S. A., Megías, D., Felipe, I., Del Pozo, N., Millán, I., Thommesen, L., Bruland, T., Olson, S. H., Smith, J., Schoonjans, K., Bamlet, W. R., Petersen, G. M., & Real, F. X. (2018). Transcriptional regulation by NR5A2 links differentiation and inflammation in the pancreas. Nature, 554(7693), 533–537. https://doi.org/10.1038/NATURE25751

Collier, J. J., Sparer, T. E., Karlstad, M. D., & Burke, S. J. (2017). Pancreatic islet inflammation: an emerging role for chemokines. Journal of Molecular Endocrinology, 59(1), R33–R46. https://doi.org/10.1530/JME-17-0042

Collins, S. (2018). Nutritional management of cystic fibrosis - an update for the 21st century. Paediatric Respiratory Reviews, 26, 4–6. https://doi.org/10.1016/J.PRRV.2017.03.006

Colombo, C., Foppiani, A., Bisogno, A., Gambazza, S., Daccò, V., Nazzari, E., Leone, A., Giana, A., Mari, A., & Battezzati, A. (2021). Lumacaftor/ivacaftor in cystic fibrosis: effects on glucose metabolism and insulin secretion. Journal of Endocrinological Investigation, 44(10), 2213–2218. https://doi.org/10.1007/s40618-021-01525-4

Concannon, P., Rich, S. S., & Nepom, G. T. (2009). Genetics of Type 1A Diabetes. New England Journal of Medicine, 360(16), 1646–1654. https://doi.org/10.1056/NEJMRA0808284

Cooper, J. D., Smyth, D. J., Walker, N. M., Stevens, H., Burren, O. S., Wallace, C., Greissl, C., Ramos-Lopez, E., Hyppönen, E., Dunger, D. B., Spector, T. D., Ouwehand, W. H., Wang, T. J., Badenhoop, K., & Todd, J. A. (2011). Inherited variation in vitamin D genes is associated with predisposition to autoimmune disease type 1 diabetes. Diabetes, 60(5), 1624–1631. https://doi.org/10.2337/DB10-1656

Corbett, J. A., Sweetland, M. A., Wang, J. L., Lancaster, J. R., & Mcdaniel, M. L. (1993). Nitric oxide mediates cytokine-induced inhibition of insulin secretion by human islets of Langerhans. In Proc. Natl. Acad. Sci. USA (Vol. 90). https://www.pnas.org

Cory, M., Moin, A. S. M., Moran, A., Rizza, R. A., Butler, P. C., Dhawan, S., & Butler, A. E. (2018). An Increase in Chromogranin A-Positive, Hormone-Negative Endocrine Cells in Pancreas in Cystic Fibrosis. Journal of the Endocrine Society, 2(9), 1058–1066. https://doi.org/10.1210/JS.2018-00143

Couce, M., O'Brien, T. D., Moran, A., Roche, P. C., & Butler, P. C. (1996). Diabetes mellitus in cystic fibrosis is characterized by islet amyloidosis. The Journal of Clinical Endocrinology & Metabolism, 81(3), 1267–1272. https://doi.org/10.1210/jcem.81.3.8772610

Criscimanna, A., Coudriet, G., Gittes, G., Piganelli, J., & Esni, F. (2014). Activated macrophages create lineage-specific microenvironments for pancreatic acinar- and β-cell regeneration in mice. Gastroenterology, 147(5), 1106-1118.e11. https://doi.org/10.1053/J.GASTRO.2014.08.008

Cystic Fibrosis Trust UK. (2024, July 2). CFRD - Cystic Fibrosis-Related Diabetes. https://www.cysticfibrosis.org.uk/what-is-cystic-fibrosis/how-does-cystic-fibrosis-affect-the-body/symptoms-of-cystic-fibrosis/cf-related-diabetes

Daneman, D. (2006). Type 1 diabetes. Lancet (London, England), 367(9513), 847–858. https://doi.org/10.1016/S0140-6736(06)68341-4

Despotes, K. A., & Donaldson, S. H. (2022). Current state of CFTR modulators for treatment of Cystic Fibrosis. In Current Opinion in Pharmacology (Vol. 65). Elsevier Ltd. https://doi.org/10.1016/j.coph.2022.102239

Di Fulvio, M., Bogdani, M,. Velasco, M., McMillen, T. S., Ridaura, C., Kelly, L., Almutairi, M. M., Kursan, S., Sajib, A. A., Hiriart, M., & Aguilar-Bryan, L. (2020). Heterogeneous expression of CFTR in insulin-secreting β-cells of the normal human islet. PloS One, 15(12). https://doi.org/10.1371/JOURNAL.PONE.0242749

Diakopoulos, K. N., Lesina, M., Wörmann, S., Song, L., Aichler, M., Schild, L., Artati, A., Römisch-Margl, W., Wartmann, T., Fischer, R., Kabiri, Y., Zischka, H., Halangk, W., Demir, I. E., Pilsak, C., Walch, A., Mantzoros, C. S., Steiner, J. M., Erkan, M., & Algül, H. (2015). Impaired autophagy induces chronic atrophic pancreatitis in mice via sex- and nutrition-dependent processes. Gastroenterology, 148(3), 626-638.e17. https://doi.org/10.1053/J.GASTRO.2014.12.003

Doan, L. V., & Madison, L. D. (2020). Cystic Fibrosis Related Diabetes. StatPearls.

Donath, M. Y., Böni-Schnetzler, M., Ellingsgaard, H., Halban, P. A., & Ehses, J. A. (2010). Cytokine production by islets in health and diabetes: Cellular origin, regulation and function. In Trends in Endocrinology and Metabolism (Vol. 21, Issue 5, pp. 261–267). Elsevier Current Trends. https://doi.org/10.1016/j.tem.2009.12.010

Donath, M. Y., Størling, J., Maedler, K., & Mandrup-Poulsen, T. (2003). Inflammatory mediators and islet β-cell failure: A link between type 1 and type 2 diabetes. In Journal of Molecular Medicine (Vol. 81, Issue 8, pp. 455–470). https://doi.org/10.1007/s00109-003-0450-y

Dotta, F., Censini, S., Halteren, A. G. S. van, Marselli, L., Masini, M., Dionisi, S., Mosca, F., Boggi, U., Muda, A. O., Prato, S. Del, Elliott, J. F., Covacci, A., Rappuoli, R., Roep, B. O., & Marchetti, P. (2007). Coxsackie B4 virus infection of β cells and natural killer cell insulitis in recent-onset type 1 diabetic patients. Proceedings of the National Academy of Sciences, 104(12), 5115–5120. https://doi.org/10.1073/PNAS.0700442104

Duncan, G. A., Jung, J., Hanes, J., & Suk, J. S. (2016). The Mucus Barrier to Inhaled Gene Therapy. Molecular Therapy, 24(12), 2043. https://doi.org/10.1038/MT.2016.182

Edlund, A., Barghouth, M., Huhn, M., Abels, M., Esguerra, J. S. E., Mollet, I. G., Sevdin, E., Wendt, A., Renstrom, E., Zhang, E., Weirup, N., Scholte, B. J., Flodstrom-Tullberg, M., & Eliasson, L. (2019). Defective exocytosis and processing of insulin in a cystic fibrosis mouse model. The Journal of Endocrinology, 241(1), 45–57. https://doi.org/10.1530/JOE-18-0570

Edlund, A., Esguerra, J. L., Wendt, A., Flodström-Tullberg, M., & Eliasson, L. (2014). CFTR and Anoctamin 1 (ANO1) contribute to cAMP amplified exocytosis and insulin secretion in human and murine pancreatic beta-cells. BMC Medicine 2014 12:1, 12(1), 1–12. https://doi.org/10.1186/1741-7015-12-87

Egea, P. F., Stroud, R. M., & Walter, P. (2005). Targeting proteins to membranes: Structure of the signal recognition particle. Current Opinion in Structural Biology, 15(2), 213–220. https://doi.org/10.1016/j.sbi.2005.03.007

Ehses, J. A., Perren, A., Eppler, E., Ribaux, P., Pospisilik, J. A., Maor-Cahn, R., Gueripel, X., Ellingsgaard, H., Schneider, M. K. J., Biollaz, G., Fontana, A., Reinecke, M., Homo-Delarche, F., & Donath, M. Y. (2007). Increased number of islet-associated macrophages in type 2 diabetes. Diabetes, 56(9), 2356–2370. https://doi.org/10.2337/db06-1650

Eizirik, D. L., Flodstriim, M., Karlsen, A. E., & Welsh, N. (1996). The harmony of the spheres: inducible nitric oxide synthase and related genes in pancreatic beta cells. In Diabetologia (Vol. 39).

Eizirik, D. L., Sandler, S., Welsh, N., Cetkovic-Cvrlje, M., Nieman, A., Geller, D. A., Pipeleers, D. G., Bendtzen, K., & Hellerström, C. (1994). Cytokines suppress human islet function irrespective of their effects on nitric oxide generation. Journal of Clinical Investigation, 93(5), 1968–1974. https://doi.org/10.1172/JCI117188

Ekblond, R. S., Nielsen, B. U., Højte, C., Almdal, T. P., Shaw, J., Pressler, T., Faurholt-Jepsen, D., & Mathiesen, I. H. M. (2023). Changes in glucose tolerance in people with cystic fibrosis after initiation of first-generation CFTR modulator treatment. Pediatric Pulmonology, 58(9), 2600–2609. https://doi.org/10.1002/ppul.26562

El Sayed, S. A., & Mukherjee, S. (2023). Physiology, Pancreas. StatPearls Publishing.

Elsässerm, H. P., Adler, G., & Kern, H. F. (1989). Fibroblast structure and function during regeneration from hormone-induced acute pancreatitis in the rat. Pancreas, 4(2), 169–178. https://doi.org/10.1097/00006676-198904000-00005

El-Sheikh, A., Suarez-Pinzon, W. L., Power, R. F., & Rabinovitch, A. (1999). Both CD4+and CD8+T cells are Required for IFN-γ Gene Expression in Pancreatic Islets and Autoimmune Diabetes Development in Biobreeding Rats. Journal of Autoimmunity, 12(2), 109–119. https://doi.org/10.1006/JAUT.1998.0264

Erkan, M., Adler, G., Apte, M. V., Bachem, M. G., Buchholz, M., Detlefsen, S., Esposito, I., Friess, H., Gress, T. M., Habisch, H. J., Hwang, R. F., Jaster, R., Kleeff, J., Klöppel, G., Kordes, C.,

Logsdon, C. D., Masamune, A., Michalski, C. W., Oh, J., & Wilson, J. (2012). StellaTUM: Current consensus and discussion on pancreatic stellate cell research. In Gut (Vol. 61, Issue 2, pp. 172–178). https://doi.org/10.1136/gutjnl-2011-301220

Erkan, M., Sunami, Y., Lampri, E. S., Sun, Z., Zhou, Y., Sun, B., Li, W., Zhou, J., Gao, F., Wang, X., & Cai, M. (2019). Pancreatic Stellate Cells: A Rising Translational Physiology Star as a Potential Stem Cell Type for Beta Cell Neogenesis Pancreatic Stellate Cells: A Rising Translational Physiology Star as a Potential Stem Cell Type for Beta Cell Neogenesis. Front. Physiol, 10, 218. https://doi.org/10.3389/fphys.2019.00218

Ewald, N., Kaufmann, C., Raspe, A., Kloer, H. U., Bretzel, R. G., & Hardt, P. D. (2012). Prevalence of diabetes mellitus secondary to pancreatic diseases (type 3c). Diabetes/Metabolism Research and Reviews, 28(4), 338–342. https://doi.org/10.1002/DMRR.2260

Farrell, P. M., White, T. B., Ren, C. L., Hempstead, S. E., Accurso, F., Derichs, N., Howenstine, S. E., McColley, S. A., Rock, M., Rosenfield, M., Sermet-Gaudelus, I., Southern, K. W., Marshall, B. C., & Sosnay, P. R. (2017). Diagnosis of Cystic Fibrosis: Consensus Guidelines from the Cystic Fibrosis Foundation. The Journal of Pediatrics, 181S, S4-S15.e1. https://doi.org/10.1016/J.JPEDS.2016.09.064

Feldmann, D., Couderc, R., Audrezet, M. P., Ferec, C., Bienvenu, T., Desgeorges, M., Claustres, M., Mittre, H., Blayau, M., Bozon, D., Malinge, M. C., Monnier, N., Bonnefont, J. P., Iron, A., Bieth, E., Dumur, V., Clavel, C., Cazeneuve, C., & Girodon, E. (2003). CFTR genotypes in patients with normal or borderline sweat chloride levels. Human Mutation, 22(4), 340. https://doi.org/10.1002/HUMU.9183

Françoise, A., & Héry-Arnaud, G. (2020). The Microbiome in Cystic Fibrosis Pulmonary Disease. Genes, 11(5). https://doi.org/10.3390/GENES11050536

Frørup, C., Gerwig, R., Svane, C. A. S., Mendes Lopes de Melo, J., Henriksen, K., Fløyel, T., Pociot, F., Kaur, S., & Størling, J. (2023). Characterization of the functional and transcriptomic effects of pro-inflammatory cytokines on human EndoC-βH5 beta cells. Frontiers in Endocrinology, 14. https://doi.org/10.3389/fendo.2023.1128523

Frossard, J. L., Hadengue, A., & Pastor, C. M. (2001). New serum markers for the detection of severe acute pancreatitis in humans. American Journal of Respiratory and Critical Care Medicine, 164(1), 162–170. https://doi.org/10.1164/ajrccm.164.1.2008026

Fu, Z., Gilbert, E. R., & Liu, D. (2013). Regulation of Insulin Synthesis and Secretion and Pancreatic Beta-Cell Dysfunction in Diabetes. In Curr Diabetes Rev (Vol. 9, Issue 1).

Fujitani, Y., Kawamori, R., & Watada, H. (2009). The role of autophagy in pancreatic β-cell and diabetes. Autophagy, 5(2), 280–282. https://doi.org/10.4161/auto.5.2.7656

Gabbiani, G. (2003). The myofibroblast in wound healing and fibrocontractive diseases. In Journal of Pathology (Vol. 200, Issue 4, pp. 500–503). Journal of Pathology. https://doi.org/10.1002/path.1427

Gaines, H., Jones, K. R., Lim, J., Medhi, N. F., Chen, S., & Scofield, R. H. (2021). Effect of CFTR modulator therapy on cystic fibrosis-related diabetes. Journal of Diabetes and Its Complications, 35(6). https://doi.org/10.1016/J.JDIACOMP.2020.107845

Gale, E. (2005). Type 1 diabetes in the young: the harvest of sorrow goes on. Diabetologia, 48(8), 1435–1438. https://doi.org/10.1007/S00125-005-1833-0

Galicia-Garcia, U., Benito-Vicente, A., Jebari, S., Larrea-Sebal, A., Siddiqi, H., Uribe, K. B., Ostolaza, H., & Martín, C. (2020). Pathophysiology of type 2 diabetes mellitus. In International Journal of Molecular Sciences (Vol. 21, Issue 17, pp. 1–34). MDPI AG. https://doi.org/10.3390/ijms21176275

Galindo, C. M., Ganzella, F. A. de, O., Klassen, G., Ramos, E. A. de, S., & Acco, A. (2022). Nuances of PFKFB3 Signaling in Breast Cancer. Clinical Breast Cancer, 22(4), e604–e614. https://doi.org/10.1016/j.clbc.2022.01.002

Goldfine, A. B., Fonseca, V., & Shoelson, S. E. (2011). Therapeutic Approaches to Target Inflammation in Type 2 Diabetes. Clinical Chemistry, 57(2), 162–167. https://doi.org/10.1373/CLINCHEM.2010.148833

Gordon, S., & Taylor, P. R. (2005). Monocyte and macrophage heterogeneity. Nature Reviews Immunology, 5(12), 953–964. https://doi.org/10.1038/NRI1733

Granger, J., & Remick, D. (2005). Acute pancreatitis: Models, markers, and mediators. Shock, 24(SUPPL. 1), 45–51. https://doi.org/10.1097/01.shk.0000191413.94461.b0

Gukovskaya, A. S., Gukovsky, I., Zaninovic, V., Song, M., Sandoval, D., Gukovsky, S., & Pandol, S. J. (1997). Pancreatic acinar cells produce, release, and respond to tumor necrosis factor-α. Role in regulating cell death and pancreatitis. Journal of Clinical Investigation, 100(7), 1853–1862. https://doi.org/10.1172/JCI119714

Gukovskaya, A. S., Mouria, M., Gukovsky, I., Reyes, C. N., Kasho, V. N., Faller, L. D., & Pandol, S. J. (2002). Ethanol metabolism and transcription factor activation in pancreatic acinar cells in rats. Gastroenterology, 122(1), 106–118. https://doi.org/10.1053/GAST.2002.30302

Gukovskaya, A. S., Vaquero, E., Zaninovic, V., Gorelick, F. S., Lusis, A. J., Brennan, M. L., Holland, S., & Pandol, S. J. (2002). Neutrophils and NADPH oxidase mediate intrapancreatic trypsin activation in murine experimental acute pancreatitis. Gastroenterology, 122(4), 974–984. https://doi.org/10.1053/GAST.2002.32409

Gukovsky, I., Gukovskaya, A. S., Blinman, T. A., Zaninovic, V., & Pandol, S. J. (1998). Early NF-κB activation is associated with hormone-induced pancreatitis. American Journal of Physiology - Gastrointestinal and Liver Physiology, 275(6 38-6). https://doi.org/10.1152/AJPGI.1998.275.6.G1402

Gukovsky, I., Li, N., Todoric, J., Gukovskaya, A., & Karin, M. (2013). Inflammation, autophagy, and obesity: Common features in the pathogenesis of pancreatitis and pancreatic cancer. Gastroenterology, 144(6). https://doi.org/10.1053/J.GASTRO.2013.02.007

Guo, J. H., Chen, H., Ruan, Y. C., Zhang, X. L., Zhang, X, H., Fok, K. L., Tsang, L. L., Yu, M. K., Huang, W. Q., Sun, X., Chung, Y. W., Jiang, X., Sohma, Y., & Chan, H. C. (2014). Glucose-induced electrical activities and insulin secretion in pancreatic islet β-cells are modulated by CFTR. Nature Communications, 5. https://doi.org/10.1038/NCOMMS5420

Guo, L., Sans, M. D., Hou, Y., Ernst, S. A., & Williams, J. A. (2012). C-Jun/AP-1 is required for CCK-induced pancreatic acinar cell dedifferentiation and DNA synthesis in vitro. American Journal of Physiology - Gastrointestinal and Liver Physiology, 302(12). https://doi.org/10.1152/AJPGI.00129.2010

Habtezion, A. (2015). Inflammation in acute and chronic pancreatitis. Current Opinion in Gastroenterology, 31(5), 395–399. https://doi.org/10.1097/MOG.0000000000000195

Haider, D. G., Schaller, G., Kapiotis, S., Maier, C., Luger, A., & Wolzt, M. (2006). The release of the adipocytokine visfatin is regulated by glucose and insulin. Diabetologia, 49(8), 1909–1914. https://doi.org/10.1007/s00125-006-0303-7

Haller, M., Atkinson, M., & Schatz, D. (2005). Type 1 diabetes mellitus: etiology, presentation, and management. Pediatric Clinics of North America, 52(6), 1553–1578. https://doi.org/10.1016/J.PCL.2005.07.006

Harjutsalo, V., Sjöberg, L., & Tuomilehto, J. (2008). Time trends in the incidence of type 1 diabetes in Finnish children: a cohort study. The Lancet, 371(9626), 1777–1782. https://doi.org/10.1016/S0140-6736(08)60765-5

Hart, N. J., Aramandla, R., Poffenberger, G., Fayolle, C., Thames, A. H., Bautista, A., Spigelman, A. F., Babon, J. A. B., DeNicola, M. E., Dadi, P. K., Bush, W. S., Balamurugan, A. N., Brissova, M., Dai, C., Prasad, N., Bottino, R., Jacobson, D. A., Drumm, M. L., Kent, S. C., & Powers, A. C. (2018). Cystic fibrosis-related diabetes is caused by islet loss and inflammation. JCI Insight, 3(8). https://doi.org/10.1172/jci.insight.98240

Hart, P. A., Bellin, M. D., Andersen, D. K., Bradley, D., Cruz-Monserrate, Z., Forsmark, C. E., Goodarzi, M. O., Habtezion, A., Korc, M., Kudva, Y. C., Pandol, S. J., Yadav, D., & Chari, S. T. (2016). Type 3c (pancreatogenic) diabetes mellitus secondary to chronic pancreatitis and pancreatic cancer. In The Lancet Gastroenterology and Hepatology (Vol. 1, Issue 3, pp. 226–237). Elsevier Ltd. https://doi.org/10.1016/S2468-1253(16)30106-6

Haugen, F., Jorgensen, A., Drevon, C. A., & Trayhurn, P. (2001). Inhibition by insulin of resistin gene expression in 3T3-L1 adipocytes. FEBS Letters, 507(1), 105–108. https://doi.org/10.1016/S0014-5793(01)02968-4

Hayes, D., McCoy, K., & Sheikh, S. (2014). Resolution of cystic fibrosis-related diabetes with ivacaftor therapy. American Journal of Respiratory and Critical Care Medicine, 190(5), 590–591. https://doi.org/10.1164/RCCM.201405-0882LE

Healey, D., Ozegbe, P., Arden, S., Chandler, P., Hutton, J., & Cooke, A. (1995). In vivo activity and in vitro specificity of CD4+ Th1 and Th2 cells derived from the spleens of diabetic NOD mice. The Journal of Clinical Investigation, 95(6), 2979–2985. https://doi.org/10.1172/JCI118006

Hegyi, P., Wilschanski, M., Muallem, S., Lukacs, G. L., Sahin-Tóth, M., Uc, A., Gray, M. A., Rakonczay, Z., & Maléth, J. (2016). CFTR: A new horizon in the pathomechanism and treatment of pancreatitis. Reviews of Physiology, Biochemistry and Pharmacology, 170, 37. https://doi.org/10.1007/112_2015_5002

Hogan, M. F., & Hull, R. L. (2017). The islet endothelial cell: a novel contributor to beta cell secretory dysfunction in diabetes. Diabetologia, 60(6), 952–959. https://doi.org/10.1007/s00125-017-4272-9

Hoque, R., Sohail, M., Malik, A., Sarwar, S., Luo, Y., Shah, A., Barrat, F., Flavell, R., Gorelick, F., Husain, S., & Mehal, W. (2011). TLR9 and the NLRP3 inflammasome link acinar cell death with inflammation in acute pancreatitis. Gastroenterology, 141(1), 358–369. https://doi.org/10.1053/J.GASTRO.2011.03.041

Huang, H., Yan, L., Daniluk, J., Gaiser, S., Chu, J., Wang, H., Li, Z. S., Logsdon, C. D., & Ji, B. (2013). Activation of nuclear factor-κB in acinar cells increases the severity of pancreatitis in mice. Gastroenterology, 144(1), 202–210. https://doi.org/10.1053/J.GASTRO.2012.09.059

Hull, R. L., Gibson, R. L., McNamara, S., Deutsch, G. H., Flinger, C. L., Frevert, C. W., Ramsey, B. W., & Sanda, S. (2018). Islet Interleukin-1β Immunoreactivity Is an Early Feature of Cystic Fibrosis That May Contribute to β-Cell Failure. Diabetes Care, 41(4), 823–830. https://doi.org/10.2337/DC17-1387

Humphreys, B. D., Lin, S. L., Kobayashi, A., Hudson, T. E., Nowlin, B. T., Bonventre, J. V., Valerius, M. T., McMahon, A. P., & Duffield, J. S. (2010). Fate tracing reveals the pericyte and not epithelial origin of myofibroblasts in kidney fibrosis. American Journal of Pathology, 176(1), 85–97. https://doi.org/10.2353/ajpath.2010.090517

Hunt, W. R., Zughaier, S. M., Guentert, D. E., Shenep, M. A., Koval, M., McCarty, N. A., & Hansen, J. M. (2014). Hyperglycemia impedes lung bacterial clearance in a murine model of cystic fibrosis-related diabetes. American Journal of Physiology - Lung Cellular and Molecular Physiology, 306(1), L43. https://doi.org/10.1152/AJPLUNG.00224.2013

Hutchings, P., Rosen, H., O'Reilly, L., Simpson, E., Gordon, S., & Cooke, A. (1990). Transfer of diabetes in mice prevented by blockade of adhesion-promoting receptor on macrophages. Nature 1990 348:6302, 348(6302), 639–642. https://doi.org/10.1038/348639a0

Iannucci, A., Mukai, K., Johnson, D., & Burke, B. (1984). Endocrine pancreas in cystic fibrosis: An immunohistochemical study [Article]. Human Pathology., 15(3), 278–284. https://doi.org/10.1016/S0046-8177(84)80191-4

Ikejiri, N. (1990). The Vitamin A-Storing Cells in the Human and Rat Pancreas. In THE KURUME MEDICAL JOURNAL (Vol. 37).

Imrie, J. R., Fagan, D. G., & Sturgess, J. M. (1979). Quantitative evaluation of the development of the exocrine pancreas in cystic fibrosis and control infants. The American Journal of Pathology, 95(3), 697–708.

Jallut, D., Golay, A., Munger, R., Frascarolo, P., Schutz, Y., Jéquier, E., & Felber, J. P. (1990). Impaired glucose tolerance and diabetes in obesity: A 6-year follow-up study of glucose metabolism. Metabolism - Clinical and Experimental, 39(10), 1068–1075. https://doi.org/10.1016/0026-0495(90)90168-C

Janet, L., Bernstein, L. E., Canavan, B., Torriani, M., Jackson, M. B., Ahima, R. S., & Grinspoon, S. K. (2007). Effects of TNF-α neutralization on adipocytokines and skeletal muscle adiposity in the metabolic syndrome. American Journal of Physiology - Endocrinology and Metabolism, 293(1), E102. https://doi.org/10.1152/ajpendo.00089.2007

Jansson, L., & Carlsson, P.-O. (2019). Pancreatic Blood Flow with Special Emphasis on Blood Perfusion of the Islets of Langerhans. Comprehensive Physiology, 9(2), 799–837. https://doi.org/10.1002/cphy.c160050

Jaques, R., Shakeel, A., & Hoyle, C. (2020). Novel therapeutic approaches for the management of cystic fibrosis. Multidisciplinary Respiratory Medicine, 15(1), 690. https://doi.org/10.4081/mrm.2020.690

Johnson, C. D., & Abu-Hilal, M. (2004). Persistent organ failure during the first week as a marker of fatal outcome in acute pancreatitis. Gut, 53(9), 1340–1344. https://doi.org/10.1136/GUT.2004.039883

Jurgens, C. A., Toukatly, M. N., Fligner, C. L., Udayasankar, J., Subramanian, S. L., Zraika, S., Aston-Mourney, K., Carr, D. B., Westermark, P., Westermark, G. T., Kahn, S. E., & Hull, R. L. (2011). β-Cell Loss and β-Cell Apoptosis in Human Type 2 Diabetes Are Related to Islet Amyloid Deposition. The American Journal of Pathology, 178(6), 2632. https://doi.org/10.1016/J.AJPATH.2011.02.036

Kalnins, D., Durie, P. R., & Pencharz, P. (2007). Nutritional management of cystic fibrosis patients. Current Opinion in Clinical Nutrition & Metabolic Care, 10(3), 348–354. https://doi.org/10.1097/MCO.0b013e3280a94f80

Katz, J., Benoist, C., & Mathis, D. (1995). T helper cell subsets in insulin-dependent diabetes. Science, 268(5214), 1185–1188. https://doi.org/10.1126/SCIENCE.7761837

Kayani, K., Mohammed, R., & Mohiaddin, H. (2018). Cystic fibrosis-related diabetes. Frontiers in Endocrinology, 9(FEB), 1–11. https://doi.org/10.3389/fendo.2018.00020

Kelly, A., De Leon, D. D., Sheikh, S., Camburn, D., Kubrak, C., Peleckis, A. J., Stefanovski, D., Hadjiliadis, D., Rickels, M. R., & Rubenstein, R. C. (2019). Islet hormone and incretin secretion in cystic fibrosis after four months of ivacaftor therapy. American Journal of Respiratory and Critical Care Medicine, 199(3), 342–351. https://doi.org/10.1164/rccm.201806-1018OC

Kelly, A., & Moran, A. (2013). Update on cystic fibrosis-related diabetes. In Journal of Cystic Fibrosis (Vol. 12, Issue 4, pp. 318–331). J Cyst Fibros. https://doi.org/10.1016/j.jcf.2013.02.008

Kelsey, R., Manderson Koivula, F. N., McClenaghan, N. H., & Kelly, C. (2019). Cystic Fibrosis–Related Diabetes: Pathophysiology and Therapeutic Challenges. Clinical Medicine Insights: Endocrinology and Diabetes, 12. https://doi.org/10.1177/1179551419851770

Kengne, A. P., Batty, G. D., Hamer, M., Stamatakis, E., & Czernichow, S. (2012). Association of C-Reactive Protein With Cardiovascular Disease Mortality According to Diabetes Status. Diabetes Care, 35(2), 396–403. https://doi.org/10.2337/DC11-1588

Kerem, E., Corey, M., Kerem, B. S., Rommens, J., Markiewicz, D., Levison, H., Tsui, L. C., & Durie, P. (1990). The relation between genotype and phenotype in cystic fibrosis--analysis of the most common mutation (delta F508). The New England Journal of Medicine, 323(22), 1517–1522. https://doi.org/10.1056/NEJM199011293232203

Kershenobich Stalnikowitz, D., & Weissbrod, A. B. (2003). Liver fibrosis and inflammation. A review. Annals of Hepatology, 2(4), 159–163.

Khan, D., Kelsey, R., Maheshwari, R. R., Stone, V. M., Hasib, A., Koivula, F. N. M., Watson, A., Harkin, S., Irwin, N., Shaw, J. A., McClenaghan, N. H., Venglovecz, V., Ébert, A., Flodström-Tullberg, M., White, M. G., & Kelly, C. (2019). Short-term CFTR inhibition reduces islet area in C57BL/6 mice. Scientific Reports 2019 9:1, 9(1), 1–11. https://doi.org/10.1038/s41598-019-47745-w

Kikuta, K., Masamune, A., Hamada, S., Takikawa, T., Nakano, E., & Shimosegawa, T. (2013). Pancreatic stellate cells reduce insulin expression and induce apoptosis in pancreatic β-cells. Biochemical and Biophysical Research Communications, 433(3), 292–297. https://doi.org/10.1016/j.bbrc.2013.02.095

Kim, J. J., Lee, E., Ryu, G. R., Ko, S. H., Ahn, Y. B., & Song, K. H. (2020). Hypoxia increases β-cell death by activating pancreatic stellate cells within the islet. Diabetes and Metabolism Journal, 44. https://doi.org/10.4093/dmj.2019.0181

Klöppel, G., Detlefsen, S., & Feyerabend, B. (2004). Fibrosis of the pancreas: The initial tissue damage and the resulting pattern. In Virchows Archiv (Vol. 445, Issue 1, pp. 1–8). https://doi.org/10.1007/s00428-004-1021-5

Koh, Y. H., Tamizhselvi, R., & Bhatia, M. (2010). Extracellular signal-regulated kinase 1/2 and c-Jun NH2-terminal kinase, through nuclear factor-κB and activator protein-1, contribute to caerulein-induced expression of substance P and neurokinin-1 receptors in pancreatic acinar cells. Journal of Pharmacology and Experimental Therapeutics, 332(3), 940–948. https://doi.org/10.1124/JPET.109.160416

Koivula, F. N. M., McClenaghan, N. H., Harper, A. G. S., & Kelly, C. (2016). Islet-intrinsic effects of CFTR mutation. Diabetologia, 59(7), 1350. https://doi.org/10.1007/S00125-016-3936-1

Konrad, K., Scheuing, N., Badenhoop, K., Borkenstein, M. H., Gohlke, B., Schöfl, C., Seufert, J., Thon, A., & Holl, R. W. (2013). Cystic fibrosis-related diabetes compared with type 1 and type 2 diabetes in adults. Diabetes/Metabolism Research and Reviews, 29(7), 568–575. https://doi.org/10.1002/dmrr.2429

Kramann, R., Schneider, R. K., Dirocco, D. P., Machado, F., Fleig, S., Bondzie, P. A., Henderson, J. M., Ebert, B. L., & Humphreys, B. D. (2015). Perivascular Gli1+ progenitors are key contributors to injury-induced organ fibrosis. Cell Stem Cell, 16(1), 51–66. https://doi.org/10.1016/j.stem.2014.11.004

Kristidis, P., Bozon, D., Corey, M., Markiewicz, D., Rommens, J., Tsui, L. C., & Durie, P. (1992). Genetic determination of exocrine pancreatic function in cystic fibrosis. American Journal of Human Genetics, 50(6), 1178–1184.

Kukko, M., Kimpimäki, T., Korhonen, S., Kupila, A., Simell, S., Veijola, R., Simell, T., Ilonen, J., Simell, O., & Knip, M. (2005). Dynamics of diabetes-associated autoantibodies in young children with human leukocyte antigen-conferred risk of type 1 diabetes recruited from the general population. Journal of Clinical Endocrinology and Metabolism, 90(5), 2712–2717. https://doi.org/10.1210/JC.2004-1371

Kuroda, J., Suda, K., & Hosokawa, Y. (1998). Periacinar collagenization in patients with chronic alcoholism. Pathology International, 48(11), 857–868. https://doi.org/10.1111/j.1440-1827.1998.tb03852.x

Löhr, M., Gocrtchen, P., Nizze, H., Gould, N. S., Gould, V. E., Oberholzer, M., Heitz, P. U., & Kloppel, G. (1989). Cystic fibrosis associated islet changes may provide a basis for diabetes An immunocytochemical and morphometrical study Virchows Arch& A Pathological Anatomy and Histopathology. In Virchows Archiv A Pathol Anat (Vol. 414).

LaPensee, C. R., Hugo, E. R., & Ben-Jonathan, N. (2008). Insulin stimulates interleukin-6 expression and release in LS14 human adipocytes through multiple signaling pathways. Endocrinology, 149(11), 5415–5422. https://doi.org/10.1210/en.2008-0549

Lawlor, N., George, J., Bolisetty, M., Kursawe, R., Sun, L., Sivakamasundari, V., Kycia, I., Robson, P., & Stitzel, M. L. (2017). Single-cell transcriptomes identify human islet cell signatures and reveal cell-type-specific expression changes in type 2 diabetes. Genome Research, 27(2), 208–222. https://doi.org/10.1101/gr.212720.116

Lee, E., Ryu, G. R., Ko, S. H., Ahn, Y. B., & Song, K. H. (2017). A role of pancreatic stellate cells in islet fibrosis and β-cell dysfunction in type 2 diabetes mellitus. Biochemical and Biophysical Research Communications, 485(2), 328–334. https://doi.org/10.1016/J.BBRC.2017.02.082

Lee, Y., Hirose, H., Ohneda, M., Johnson, J. H., McGarry, J. D., & Unger, R. H. (1994). Beta-cell lipotoxicity in the pathogenesis of non-insulin-dependent diabetes mellitus of obese rats: impairment in adipocyte-beta-cell relationships. Proceedings of the National Academy of Sciences of the United States of America, 91(23), 10878–10882. https://doi.org/10.1073/pnas.91.23.10878

Lehuen, A., Diana, J., Zaccone, P., & Cooke, A. (2010). Immune cell crosstalk in type 1 diabetes. Nature Reviews Immunology 2010 10:7, 10(7), 501–513. https://doi.org/10.1038/nri2787

Leighton, E., Sainsbury, C. A., & Jones, G. C. (2017). A Practical Review of C-Peptide Testing in Diabetes. Diabetes Therapy, 8(3), 475–487. https://doi.org/10.1007/s13300-017-0265-4

Lemelman, M. B., Letourneau, L., & Greeley, S. A. W. (2018). Neonatal Diabetes Mellitus: An Update on Diagnosis and Management. Clinics in Perinatology, 45(1), 41. https://doi.org/10.1016/J.CLP.2017.10.006

Leppkes, M., Maueröder, C., Hirth, S., Nowecki, S., Günther, C., Billmeier, U., Paulus, S., Biermann, M., Munoz, L. E., Hoffmann, M., Wildner, D., Croxford, A. L., Waisman, A., Mowen, K., Jenne, D. E., Krenn, V., Mayerle, J., Lerch, M. M., Schett, G., & Becker, C. (2016). Externalized decondensed neutrophil chromatin occludes pancreatic ducts and drives pancreatitis. Nature Communications, 7. https://doi.org/10.1038/NCOMMS10973

Leslie, R. D. (2010). Predicting adult-onset autoimmune diabetes clarity from complexity. Diabetes, 59(2), 330–331. https://doi.org/10.2337/DB09-1620

Li, F. F., Chen, B. J., Li, W., Li, L., Zha, M., Zhou, S., Bachem, M. G., & Sun, Z. L. (2016). Islet Stellate Cells Isolated from Fibrotic Islet of Goto-Kakizaki Rats Affect Biological Behavior of Beta-Cell. Journal of Diabetes Research, 2016. https://doi.org/10.1155/2016/6924593

Li, J., Klughammer, J., Farlik, M., Penz, T., Spittler, A., Barbieux, C., Berishvili, E., Bock, C., & Kubicek, S. (2016). Single-cell transcriptomes reveal characteristic features of human pancreatic islet cell types. EMBO Reports, 17(2), 178–187. https://doi.org/10.15252/embr.201540946

Liu, T., Zhang, L., Joo, D., & Sun, S. (2017). NF-κB signaling in inflammation. Signal Transduction and Targeted Therapy, 2. https://doi.org/10.1038/SIGTRANS.2017.23

Lomedico, P. T., Chan, S. J., Steiner, D. F., & Saunders, G. F. (1977). Immunological and chemical characterization of bovine preproinsulin. Journal of Biological Chemistry, 252(22), 7971–7978. https://doi.org/10.1016/s0021-9258(17)40921-5

Longnecker, D. S. (2021). Anatomy and Histology of the Pancreas. Pancreapedia: The Exocrine Pancreas Knowledge Base. https://doi.org/10.3998/PANC.2021.01

Lopes, M., Kutlu, B., Miani, M., Bang-Berthelsen, C. H., Storling, J., Pociot, F., Goodman, N., Hood, L., Welsh, N., Bontempi, G., & Eizirik, D. l. (2014). Temporal profiling of cytokine-induced genes in pancreatic β-cells by meta-analysis and network inference. Genomics, 103(4), 264–275. https://doi.org/10.1016/J.YGENO.2013.12.007

Lopes-Pacheco, M. (2016). CFTR Modulators: Shedding Light on Precision Medicine for Cystic Fibrosis. Frontiers in Pharmacology, 0(SEP), 275. https://doi.org/10.3389/FPHAR.2016.00275

Lopes-Pacheco, M. (2019). CFTR Modulators: The Changing Face of Cystic Fibrosis in the Era of Precision Medicine. Frontiers in Pharmacology, 10. https://doi.org/10.3389/FPHAR.2019.01662

Löhr, M., Goertchen, P., Nizze, H., Gould, N. S., Gould, V. E., Oberholzer, M., Heitz, Ph. U., & Kl�oppel, G. (1989). Cystic fibrosis associated islet changes may provide a basis for diabetes. Virchows Archiv A Pathological Anatomy and Histopathology, 414(2), 179–185. https://doi.org/10.1007/bf00718598

Macauley, M., Percival, K., Thelwall, P. E., Hollingsworth, K. G., & Taylor, R. (2015). Altered volume, morphology and composition of the pancreas in type 2 diabetes. PloS One, 10(5), e0126825. https://doi.org/10.1371/journal.pone.0126825

Maedler, K., Sergeev, P., Ehses, J. A., Mathe, Z., Bosco, D., Berney, T., Dayer, J. M., Reinecke, M., Halban, P. A., & Donath, M. Y. (2004). Leptin modulates β cell expression of IL-1 receptor antagonist and release of IL-1β in human islets. Proceedings of the National Academy of Sciences of the United States of America, 101(21), 8138–8143. https://doi.org/10.1073/pnas.0305683101

Marchetti, P. (2016). Islet inflammation in type 2 diabetes. Diabetologia, 59(4), 668–672. https://doi.org/10.1007/S00125-016-3875-X

Mareninova, O. A., Sendler, M., Malla, S. R., Yakubov, I., French, S. W., Tokhtaeva, E., Vagin, O., Oorschot, V., Lüllmann-Rauch, R., Blanz, J., Dawson, D., Klumperman, J., Lerch, M. M., Mayerle, J., Gukovsky, I., & Gukovskaya, A. S. (2015). Lysosome-Associated Membrane Proteins (LAMP) Maintain Pancreatic Acinar Cell Homeostasis: LAMP-2-Deficient Mice Develop Pancreatitis. CMGH, 1(6), 678–694. https://doi.org/10.1016/J.JCMGH.2015.07.006

Marques-Vidal, P., Schmid, R., Bochud, M., Bastardot, F., Känel, R. von, Paccaud, F., Glaus, J., Preisig, M., Waeber, G., & Vollenweider, P. (2012). Adipocytokines, Hepatic and Inflammatory Biomarkers and Incidence of Type 2 Diabetes. The CoLaus Study. PLOS ONE, 7(12), e51768. https://doi.org/10.1371/JOURNAL.PONE.0051768

Martin, J. W., Chilton-MacNeill, S., Koti, M., Van Wijnen, A. J., Squire, J. A., & Zielenska, M. (2014). Digital expression profiling identifies RUNX2, CDC5L, MDM2, RECQL4, and CDK4 as potential predictive biomarkers for neo-adjuvant chemotherapy response in paediatric osteosarcoma. PLoS ONE, 9(5), 1–8. https://doi.org/10.1371/journal.pone.0095843

Masamune, A., Kikuta, K., Watanabe, T., Satoh, K., Hirota, M., & Shimosegawa, T. (2008). Hypoxia stimulates pancreatic stellate cells to induce fibrosis and angiogenesis in pancreatic cancer. Am J Physiol Gastrointest Liver Physiol, 295, 709–717. https://doi.org/10.1152/ajpgi.90356.2008.-Pancreatic

Masamune, A., & Shimosegawa, T. (2009). Signal transduction in pancreatic stellate cells. In Journal of Gastroenterology (Vol. 44, Issue 4, pp. 249–260). https://doi.org/10.1007/s00535-009-0013-2

Masamune, A., Watanabe, T., Kikuta, K., & Shimosegawa, T. (2009). Roles of Pancreatic Stellate Cells in Pancreatic Inflammation and Fibrosis. Clinical Gastroenterology and Hepatology, 7(11 SUPPL.). https://doi.org/10.1016/j.cgh.2009.07.038

Mayerle, J., Schnekenburger, J., Krüger, B., Kellermann, J., Ruthenbürger, M., Weiss, F. U., Nalli, A., Domschke, W., & Lerch, M. M. (2005). Extracellular cleavage of E-cadherin by leukocyte elastase during acute experimental pancreatitis in rats. Gastroenterology, 129(4), 1251–1267. https://doi.org/10.1053/J.GASTRO.2005.08.002

Mayerle, J., Sendler, M., Hegyi, E., Beyer, G., Lerch, M. M., & Sahin-Tóth, M. (2019). Genetics and pathophysiology of pancreatitis. Gastroenterology, 156(7), 1951. https://doi.org/10.1053/J.GASTRO.2018.11.081

Means, A. L. (2013). Pancreatic stellate cells: Small cells with a big role in tissue homeostasis. In Laboratory Investigation (Vol. 93, Issue 1, pp. 4–7). Nature Publishing Group. https://doi.org/10.1038/labinvest.2012.161

Merjaneh, L., He, Q., Long, Q., Phillips, L. S., & Stecenko, A. A. (2015). Disposition index identifies defective beta-cell function in cystic fibrosis subjects with normal glucose tolerance. Journal of Cystic Fibrosis, 14(1), 135–141. https://doi.org/10.1016/j.jcf.2014.06.004

Mezza, T., Ferraro, P. M., Sun, V. A., Moffa, S., Cefalo, C. M. A., Quero, G., Cinti, F., Sorice, G. P., Pontecorvi, A., Folli, F., Mari, A., Alfieri, S., & Giaccari, A. (2018). Increased B-cell workload modulates proinsulin-to-insulin ratio in humans. Diabetes, 67(11), 2389–2396. https://doi.org/10.2337/db18-0279

Miller, B. J., Appel, M. C., O'Neil, J. J., & Wicker, L. S. (1988). Both the Lyt-2+ and L3T4+ T cell subsets are required for the transfer of diabetes in nonobese diabetic mice. The Journal of Immunology, 140(1).

Misgault, B., Chatron, E., Reynaud, Q., Touzet, S., Abely, M., Melly, L., Dominique, S., Troussier, F., Ronsin-Pradel, O., Gerardin, M., Mankikian, J., Cosson, L., Chiron, R., Bounyar, L., Porzio, M., Durieu, I., Weiss, L., Kessler, R., & Kessler, L. (2020). Effect of one-year lumacaftor–ivacaftor treatment on glucose tolerance abnormalities in cystic fibrosis patients. Journal of Cystic Fibrosis, 19(5), 712–716. https://doi.org/10.1016/j.jcf.2020.03.002

Mizukami, H., Takahashi, K., Inaba, W., Osonoi, S., Kamata, K., Tsuboi, K., & Yagihashi, S. (2014). Age-associated changes of islet endocrine cells and the effects of body mass index in Japanese. Journal of Diabetes Investigation, 5(1), 38–47. https://doi.org/10.1111/jdi.12118

Mohan, K., Miller, H., Burhan, H., Ledson, M. L., & Walshaw, M. J. (2008). Management of cystic fibrosis related diabetes: a survey of UK cystic fibrosis centers. Pediatric Pulmonology, 43(7), 642–647. https://doi.org/10.1002/PPUL.20831

Mohan, K., Miller, H., Dyce, P., Grainger, R., Hughes, R., Vora, J., Ledson, M., & Walshaw, M. (2009). Mechanisms of glucose intolerance in cystic fibrosis. Diabetic Medicine, 26(6), 582–588. https://doi.org/10.1111/j.1464-5491.2009.02738.x

Moheet, A., Beisang, D., Zhang, L., Sagel, S. D., VanDalfsen, J. M., Heltshe, S. L., Frederick, C., Mann, M., Antos, N., Billings, J., Rowe, S. M., & Moran, A. (2021). Lumacaftor/ivacaftor therapy fails to increase insulin secretion in F508del/F508del CF patients. Journal of Cystic Fibrosis, 20(2), 333–338. https://doi.org/10.1016/j.jcf.2020.09.001

Moran, A., Becker, D., Casella, S. J., Gottlieb, P. A., Kirkman, M. S., Marshall, B. C., & Slovis, B. (2010). Epidemiology, pathophysiology, and prognostic implications of cystic fibrosis-related diabetes: A technical review. In Diabetes Care (Vol. 33, Issue 12, pp. 2677–2683). American Diabetes Association. https://doi.org/10.2337/dc10-1279

Moran, A., Diem, P., Klein, D. J., Levitt, M. D., & Robertson, R. P. (1991). Pancreatic endocrine function in cystic fibrosis. The Journal of Pediatrics, 118(5), 715–723. https://doi.org/10.1016/s0022-3476(05)80032-0

Moran, A., Dunitz, J., Nathan, B., Saeed, A., Holme, B., & Thomas, W. (2009). Cystic Fibrosis–Related Diabetes: Current Trends in Prevalence, Incidence, and Mortality. Diabetes Care, 32(9), 1626. https://doi.org/10.2337/DC09-0586

Mueller-Brandes, C., Holl, R., Nastoll, M., & Ballmann, M. (2005). New criteria for impaired fasting glucose and screening for diabetes in cystic fibrosis. The European Respiratory Journal, 25(4), 715–717. https://doi.org/10.1183/09031936.05.00068104

Nathan, B. M., Laguna, T., & Moran, A. (2010). Recent trends in cystic fibrosis-related diabetes. In Current Opinion in Endocrinology, Diabetes and Obesity (Vol. 17, Issue 4, pp. 335–341). Curr Opin Endocrinol Diabetes Obes. https://doi.org/10.1097/MED.0b013e32833a780d

Nathan, D. M. (2014). The Diabetes Control and Complications Trial/Epidemiology of Diabetes Interventions and Complications Study at 30 Years: Overview. Diabetes Care, 37(1), 9–16. https://doi.org/10.2337/DC13-2112

NICE. (2024). Ivacaftor–tezacaftor–elexacaftor, tezacaftor–ivacaftor and lumacaftor–ivacaftor for treating cystic fibrosis. National Institute for Health and Care Excellence.

Nielsen, B. U., Mathiesen, I. H. M., Møller, R., Krogh-Madsen, R., Katzenstein, T. L., Pressler, T., Shaw, J. A. M., Ritz, C., Rickels, M. R., Stefanovski, D., Almdal, T. P., & Faurholt-Jepsen, D. (2023). Characterization of impaired beta and alpha cell function in response to an oral glucose challenge in cystic fibrosis: a cross-sectional study. Frontiers in Endocrinology, 14. https://doi.org/10.3389/fendo.2023.1249876

Nordmann, T. M., Dror, E., Schulze, F., Traub, S., Berishvili, E., Barbieux, C., Böni-Schnetzler, M., & Donath, M. Y. (2017). The Role of Inflammation in β-cell Dedifferentiation. Scientific Reports 2017 7:1, 7(1), 1–10. https://doi.org/10.1038/s41598-017-06731-w

Norris, A., Ode, K., Merjaneh, L., Sanda, S., Yi, Y., Sun, X., Engelhardt, J., & Hull, R. (2019). Survival in a bad neighborhood: pancreatic islets in cystic fibrosis. The Journal of Endocrinology, 241(1), R35–R50. https://doi.org/10.1530/JOE-18-0468

Ntimbane, T., Mailhot, G., Spahis, S., Rabasa-Lhoret, R., Kleme, M. L., Melloul, D., Brochiero, E., Berthiaume, Y., & Levy, E. (2016). CFTR silencing in pancreatic β-cells reveals a functional impact on glucose-stimulated insulin secretion and oxidative stress response. American Journal of Physiology. Endocrinology and Metabolism, 310(3), E200–E212. https://doi.org/10.1152/AJPENDO.00333.2015

Ntimbane, T., Krishnamoorthy, P., Hout, C., Legault, L., Jacob, S. V., Brunet, S., Levt, E., Gueraud, F., Lands, L. C., & Comte, B. (2008). Oxidative stress and cystic fibrosis-related diabetes: a pilot study in children. Journal of Cystic Fibrosis : Official Journal of the European Cystic Fibrosis Society, 7(5), 373–384. https://doi.org/10.1016/J.JCF.2008.01.004

Olesen, H. V., Drevinek, P., Gulmans, V. A., Hatziagorou, E., Jung, A., Mei-Zahav, M., Stojnic, N., Thomas, M., & Zolin, A. (2020). Cystic fibrosis related diabetes in Europe: Prevalence, risk factors and outcome; Olesen et al. Journal of Cystic Fibrosis: Official Journal of the European Cystic Fibrosis Society, 19(2), 321–327. https://doi.org/10.1016/J.JCF.2019.10.009

Oleson, B. J., McGraw, J. A., Broniowska, K. A., Annamalai, M., Chen, J., Bushkofsky, J. R., Davis, D. B., John Corbett, X. A., & Mathews, C. E. (2015). Distinct differences in the responses of the human pancreatic-cell line EndoC-H1 and human islets to proinflammatory cytokines. Am J Physiol Regul Integr Comp Physiol, 309, 525–534. https://doi.org/10.1152/ajpregu.00544.2014.-While

Olivier, A. K., Yi, Y., Sun, X., Sui, H., Liang, B., Hu, S., Xie, W., Fisher, J. T., Keiser, N. W., Lei, D., Zhou, W., Yan, Z., Li, G., Evans, T. I. A., Meyerholz, D. K., Wang, K., Stewart, Z. A., Norris, A. W., & Engelhardt, J. F. (2012). Abnormal endocrine pancreas function at birth in cystic fibrosis ferrets. Journal of Clinical Investigation, 122(10), 3755–3768. https://doi.org/10.1172/JCI60610

Omary, M. B., Lugea, A., Lowe, A. W., & Pandol, S. J. (2007). The pancreatic stellate cell: A star on the rise in pancreatic diseases. In Journal of Clinical Investigation (Vol. 117, Issue 1, pp. 50–59). American Society for Clinical Investigation. https://doi.org/10.1172/JCI30082

O'riordan, S. M. P., Robinson, P. D., Donaghue, K. C., & Moran, A. (2008). Management of cystic fibrosis-related diabetes. Pediatric Diabetes, 9(4 PART 1), 338–344. https://doi.org/10.1111/j.1399-5448.2008.00437.x

Pandol, S. J. (2010). Anatomy.

Papatheodorou, K., Papanas, N., Banach, M., Papazoglou, D., & Edmonds, M. (2016). Complications of Diabetes 2016. Journal of Diabetes Research, 2016. https://doi.org/10.1155/2016/6989453

Patzelt, C., Labrecque, A. D., Duguid, J. R., Carroll, R. J., Keim, P. S., Heinrikson, R. L., & Steiner, D. F. (1978). Detection and kinetic behavior of preproinsulin in pancreatic islets. Proceedings of the National Academy of Sciences of the United States of America, 75(3), 1260–1264. https://doi.org/10.1073/pnas.75.3.1260

Pedrosa, L., Araujo, I. K., Cuatrecasas, M., Soy, G., López, S., Maurel, J., Sánchez-Montes, C., Montironi, C., Saurí, T., Sendino, O., Pérez, F. M., Ausania, F., Fernández-Esparrach, G., Espósito, F. M., Vaquero, E. C., & Ginès, A. (2023). Targeted transcriptomic analysis of pancreatic adenocarcinoma in EUS-FNA samples by NanoString technology. Frontiers in Molecular Biosciences, 10(May), 1–9. https://doi.org/10.3389/fmolb.2023.1161893

Peiris, H., Bonder, C. S., Coates, P. T. H., Keating, D. J., & Jessup, C. F. (2014). The β-cell/EC axis: how do islet cells talk to each other? Diabetes, 63(1), 3–11. https://doi.org/10.2337/db13-0617

Perides, G., Weiss, E. R., Michael, E. S., Laukkarinen, J. M., Duffield, J. S., & Steer, M. L. (2011). TNF-α-dependent regulation of acute pancreatitis severity by Ly-6Chi monocytes in mice.

Journal of Biological Chemistry, 286(15), 13327–13335. https://doi.org/10.1074/JBC.M111.218388

Phillips, J. M., Parish, N. M., Raine, T., Bland, C., Sawyer, Y., De La Peña, H., & Cooke, A. (2009). Type 1 diabetes development requires both CD4+ and CD8 + T cells and can be reversed by non-depleting antibodies targeting both T cell populations. Review of Diabetic Studies, 6(2), 97–103. https://doi.org/10.1900/RDS.2009.6.97

Phillips, P. (2012). Pancreatic stellate cells and fibrosis. In Pancreatic Cancer and Tumor Microenvironment. Transworld Research Network. http://www.ncbi.nlm.nih.gov/pubmed/22876388

Plikus, M. V, Guerrero-Juarez, C. F., Ito, M., Li, Y. R., Dedhia, P. H., Zheng, Y., Shao, M., Gay, D. L., Ramos, R., Hsi, T.-C., Oh, J. W., Wang, X., Ramirez, A., Konopelski, S. E., Elzein, A., Wang, A., Supapannachart, R. J., Lee, H.-L., Lim, C. H., & Cotsarelis, G. (2017). Regeneration of fat cells from myofibroblasts during wound healing. Retrieved February 23, 2021, from http://science.sciencemag.org/

Prentice, B., Hameed, S., Verge, C., Ooi, C., Jaffe, A., & Widger, J. (2016). Diagnosing cystic fibrosis-related diabetes: current methods and challenges. Expert Review of Respiratory Medicine, 10(7), 799–811. https://doi.org/10.1080/17476348.2016.1190646

Rabinovitch, A., Sumoski, W., Rajotte, R. V, & Warnock, G. L. (1990). Cytotoxic Effects of Cytokines on Human Pancreatic Islet Cells in Monolayer Culture*. In Journal of Clinical Endocrinology and Metabolism (Vol. 71, Issue 1). https://academic.oup.com/jcem/article/71/1/152/2652590

Rafeeq, M. M., & Murad, H. A. S. (2017). Cystic fibrosis: current therapeutic targets and future approaches. Journal of Translational Medicine, 15(1), 84. https://doi.org/10.1186/S12967-017-1193-9

Ralhan, A., Laval, J., Lelis, F., Ballbach, M., Grund, C., Hector, A., & Hartl, D. (2016). Current Concepts and Controversies in Innate Immunity of Cystic Fibrosis Lung Disease. Journal of Innate Immunity, 8(6), 531–540. https://doi.org/10.1159/000446840

Richards, O. C., Raines, S. M., & Attie, A. D. (2010). The role of blood vessels, endothelial cells, and vascular pericytes in insulin secretion and peripheral insulin action. Endocrine Reviews, 31(3), 343–363. https://doi.org/10.1210/er.2009-0035

Richardson, S. J., Morgan, N. G., & Foulis, A. K. (2014). Pancreatic Pathology in Type 1 Diabetes Mellitus. Endocrine Pathology 2014 25:1, 25(1), 80–92. https://doi.org/10.1007/S12022-014-9297-8

Rickels, M. R., Norris, A. W., & Hull, R. L. (2020). A tale of two pancreases: exocrine pathology and endocrine dysfunction. Diabetologia 2020 63:10, 63(10), 2030–2039. https://doi.org/10.1007/S00125-020-05210-8

Riordan, J. R., Rommens, J. M., Kerem, B. S., Alon, N. O. A., Rozmahel, R., Grzelczak, Z., Zielenski, J., Lok, S. I., Plavsic, N., Chou, J. L., Drumm, M. L., Iannuzzi, M. C., Collins, F. S.,

& Tsui, L. C. (1989). Identification of the cystic fibrosis gene: Cloning and characterization of complementary DNA. Science, 245(4922), 1066–1073. https://doi.org/10.1126/science.2475911

Rodriguez-Calvo, T., Ekwall, O., Amirian, N., Zapardiel-Gonzalo, J., & Herrath, M. G. von. (2014). Increased Immune Cell Infiltration of the Exocrine Pancreas: A Possible Contribution to the Pathogenesis of Type 1 Diabetes. Diabetes, 63(11), 3880–3890. https://doi.org/10.2337/DB14-0549

Rose, V. De. (2002). Mechanisms and markers of airway inflammation in cystic fibrosis. European Respiratory Journal, 19(2), 333–340. https://doi.org/10.1183/09031936.02.00229202

Rotti, P. G., Xie, W., Poudel, A., Yi, Y., Sun, X., Tyler, S. R., Uc, A., Norris, A. W., Hara, M., Engelhardt, J. F., & Gibson-Corley, K. N. (2018a). Pancreatic and Islet Remodeling in Cystic Fibrosis Transmembrane Conductance Regulator (CFTR) Knockout Ferrets. American Journal of Pathology, 188(4), 876–890. https://doi.org/10.1016/j.ajpath.2017.12.015

Rubin, B. (2014). Cystic fibrosis: myths. mistakes, and dogma. Paediatric Respiratory Reviews, 15(1), 113–116. https://doi.org/10.1016/J.PRRV.2013.11.004

Saba, N. F., Wilson, M., Doho, G., DaSilva, J., Benjamin Isett, R., Newman, S., Chen, Z. G., Magliocca, K., & Rossi, M. R. (2015). Mutation and Transcriptional Profiling of Formalin-Fixed Paraffin Embedded Specimens as Companion Methods to Immunohistochemistry for Determining Therapeutic Targets in Oropharyngeal Squamous Cell Carcinoma (OPSCC): A Pilot of Proof of Principle. Head and Neck Pathology, 9(2), 223–235. https://doi.org/10.1007/s12105-014-0566-0

Sanders, N., Rudolph, C., Braeckmans, K., Smedt. S. C. DE., & Demeester, J. (2009). Extracellular barriers in respiratory gene therapy. Advanced Drug Delivery Reviews, 61(2), 115–127. https://doi.org/10.1016/J.ADDR.2008.09.011

Sandouk, Z., Khan, F., Khare, S., & Moran, A. (2021). Cystic fibrosis related diabetes (CFRD) prognosis. Journal of Clinical and Translational Endocrinology, 26. https://doi.org/10.1016/j.jcte.2021.100278

Schauer, C., Janko, C., Munoz, L. E., Zhao, Y., Kienhöfer, D., Frey, B., Lell, M., Manger, B., Rech, J., Naschberger, E., Holmdahl, R., Krenn, V., Harrer, T., Jeremic, I., Bilyy, R., Schett, G., Hoffmann, M., & Herrmann, M. (2014). Aggregated neutrophil extracellular traps limit inflammation by degrading cytokines and chemokines. Nature Medicine, 20(5), 511–517. https://doi.org/10.1038/NM.3547

Scott, D. W., Chan, F. C., Hong, F., Rogic, S., Tan, K. L., Meissner, B., Ben-Neriah, S., Boyle, M., Kridel, R., Telenius, A., Woolcock, B. W., Farinha, P., Fisher, R. I., Rimsza, L. M., Bartlett, N. L., Cheson, B. D., Shepherd, L. E., Advani, R. H., Connors, J. M., & Gascoyne, R. D. (2013). Gene expression-based model using formalin-fixed paraffin-embedded biopsies predicts overall survival in advanced-stage classical hodgkin lymphoma. Journal of Clinical Oncology, 31(6), 692–700. https://doi.org/10.1200/JCO.2012.43.4589

Seiron, P., Wiberg, A., Kuric, E., Krogvold, L., Jahnsen, F. L., Dahl-Jørgensen, K., Skog, O., & Korsgren, O. (2019). Characterisation of the endocrine pancreas in type 1 diabetes: islet size is maintained but islet number is markedly reduced. Journal of Pathology: Clinical Research, 5(4), 248–255. https://doi.org/10.1002/cjp2.140

Sell, H., Habich, C., & Eckel, J. (2012). Adaptive immunity in obesity and insulin resistance. Nature Reviews Endocrinology 2012 8:12, 8(12), 709–716. https://doi.org/10.1038/nrendo.2012.114

Sendler, M., Dummer, A., Weiss, F. U., Krüger, B., Wartmann, T., Scharffetter-Kochanek, K., Rooijen, N. Van, Malla, S. R., Aghdassi, A., Halangk, W., Lerch, M. M., & Mayerle, J. (2013). Tumour necrosis factor α secretion induces protease activation and acinar cell necrosis in acute experimental pancreatitis in mice. Gut, 62(3), 430–439. https://doi.org/10.1136/GUTJNL-2011-300771

Sendler, M., Beyer, G., Mahajan, U. M., Kauschke, V., Maertin, S., Schurmann, C., Homouth, G., Volker, U., Volzke, H., Halangk, W., Wartmann, C., Weiss, F. U., Hegyi, P., Lerch, M. M., & Mayerle, J. (2015). Complement Component 5 Mediates Development of Fibrosis, via Activation of Stellate Cells, in 2 Mouse Models of Chronic Pancreatitis. Gastroenterology, 149(3), 765e10-776.e10. https://doi.org/10.1053/J.GASTRO.2015.05.012

Sendler, M., Weiss, F. U., Golchert, J., Homuth, G., van den Brandt, C., Mahajan, U. M., Partecke, L. I., Döring, P., Gukovsky, I., Gukovskaya, A. S., Wagh, P. R., Lerch, M. M., & Mayerle, J. (2018). Cathepsin B-Mediated Activation of Trypsinogen in Endocytosing Macrophages Increases Severity of Pancreatitis in Mice. Gastroenterology, 154(3), 704-718.e10. https://doi.org/10.1053/J.GASTRO.2017.10.018

Sheikh, S., Gudipaty, L., De Leon, D. D., Hadjiliadis, D., Kubrak, C., Rosenfeld, N. K., Nyirjesy, S. C., Peleckis, A. J., Malik, S., Stefanovski, D., Cuchel, M., Rubenstein, R. C., Kelly, A., & Rickels, M. R. (2017). Reduced β-cell secretory capacity in pancreatic-insufficient, but not pancreatic-sufficient, cystic fibrosis despite normal glucose tolerance. Diabetes, 66(1), 134–144. https://doi.org/10.2337/db16-0394

Shu Jin Chan, Keim, P., & Steiner, D. F. (1976). Cell free synthesis of rat preproinsulins: Characterization and partial amino acid sequence determination. Proceedings of the National Academy of Sciences of the United States of America, 73(6), 1964–1968. https://doi.org/10.1073/pnas.73.6.1964

Soejima, K., & Landing, B. H. (1986). Pancreatic Islets in Older Patients with Cystic Fibrosis with and without Diabetes Mellitus: Morphometric and Immunocytologic Studies. Pediatric Pathology, 6(1), 25–46. https://doi.org/10.3109/15513818609025923

Soliman, A., DeSanctis, V., Yassin, M., Elalaily, R., & Eldarsy, N. E. (2014). Continuous glucose monitoring system and new era of early diagnosis of diabetes in high risk groups. Indian Journal of Endocrinology and Metabolism, 18(3), 274. https://doi.org/10.4103/2230-8210.131130

Sosnay, P., White, T. B., Farrell, P. M., Ren, C. L., Derichs, N., Howenstine, M. S., Nico, J. A., & Boeck, K. D. (2017). Diagnosis of Cystic Fibrosis in Nonscreened Populations. The Journal of Pediatrics, 181S, S52-S57.e2. https://doi.org/10.1016/J.JPEDS.2016.09.068

Steinle, A. U., Weidenbach, H., Wagner, M., Adler, G., & Schmid, R. M. (1999). NF-κB/Rel activation in cerulein pancreatitis. Gastroenterology, 116(2), 420–430. https://doi.org/10.1016/S0016-5085(99)70140-X

Stoltz, D., Meyerholz, D., & Welsh, M. (2015). Origins of cystic fibrosis lung disease. The New England Journal of Medicine, 372(4), 351–362. https://doi.org/10.1056/NEJMRA1300109

Street, M. E., Spaggiari, C., Ziveri, M. A., Rossi, M., Volta, C., Viani, I., Grzincich, G. L., Sartori, C., Zanzucchi, M., Raia, V., Terzi, C., Pisi, G., Zanetti, E., Boguszewski, M. C. S., Kamoi, T. O., & Bernasconi, S. (2012). Insulin production and resistance in cystic fibrosis: Effect of age, disease activity, and genotype. Journal of Endocrinological Investigation, 35(3), 246–253. https://doi.org/10.3275/7628

Strong, T., Smit, L. S., Turpin, S. V., Cole, J. L., Hon, C. T., Markiewicz, D., Petty, T. L. Craig, M. W., Rosenow, E. C., & Tsui, L. C. (1991). Cystic fibrosis gene mutation in two sisters with mild disease and normal sweat electrolyte levels. The New England Journal of Medicine, 325(23), 1630–1634. https://doi.org/10.1056/NEJM199112053252307

Sun, X., Olivier, A. K., Yi, Y., Pope, C. E., Hayden, H. S., Liang, B., Sui, H., Zhou, W., Hager, K. R., Zhang, Y., Liu, X., Yan, Z., Fisher, J. T., Keiser, N. W., Song, Y., Tyler, S. R., Goeken, J. A., Kinyon, J. M., Radey, M. C., & Engelhardt, J. F. (2014). Gastrointestinal pathology in juvenile and adult CFTR-knockout ferrets. American Journal of Pathology, 184(5), 1309–1322. https://doi.org/10.1016/j.ajpath.2014.01.035

Sun, X., Yan, Z., Yi, Y., Li, Z., Lei, D., Rogers, C. S., Chen, J., Zhang, Y., Welsh, M. J., Leno, G. H., & Engelhardt, J. F. (2008). Adeno-associated virus - Targeted disruption of the CFTR gene in cloned ferrets. Journal of Clinical Investigation, 118(4), 1578–1583. https://doi.org/10.1172/JCI34599

Sun, X., Yi, Y., Xie, W., Liang, B., Winter, M. C., He, N., Liu, X., Luo, M., Yang, Y., Larson Ode, K., Uc, A., Norris, A. W., & Engelhardt, J. F. (2017). CFTR Influences Beta Cell Function and Insulin Secretion Through Non-Cell Autonomous Exocrine-Derived Factors. https://doi.org/10.1210/en.2017-00187

Sun, Y., Zhou, Y., Shi, Y., Wang, S., Zhu, Y., Correspondence, X. H., Zhang, Y., Liu, K., Liang, R., Sun, P., Chang, X., Tang, W., Zhang, Y., Li, J., & Han, X. (2021). Expression of miRNA-29 in Pancreatic β Cells Promotes Inflammation and Diabetes via TRAF3. CellReports, 34, 108576. https://doi.org/10.1016/j.celrep.2020.108576

Tamayo, A., Gonçalves, L. M., Rodriguez-Diaz, R., Pereira, E., Canales, M., Caicedo, A., & Almaça, J. (2022). Pericyte Control of Blood Flow in Intraocular Islet Grafts Impacts Glucose Homeostasis in Mice. Diabetes, 71(8), 1679–1693. https://doi.org/10.2337/db21-1104

Taylor-Cousar, J. L., Robinson, P. D., Shteinberg, M., & Downey, D. G. (2023). CFTR modulator therapy: transforming the landscape of clinical care in cystic fibrosis. Lancet (London, England), 402(10408), 1171–1184. https://doi.org/10.1016/S0140-6736(23)01609-4

Taylor-Robinson, D., Archangelidi, O., Carr, S. B., Cosgriff, R., Gunn, E., Keogh, R. H., MacDougall, A., Newsome, S., Schlüter, D. K., Stanojevic, S., & Bilton, D. (2018). Data resource profile: The UK cystic fibrosis registry. International Journal of Epidemiology, 47(1), 9–10e. https://doi.org/10.1093/ije/dyx196

The Endocrine Pancreas | Anatomy and Physiology II. (2021). Retrieved July 19, 2021, from https://courses.lumenlearning.com/suny-ap2/chapter/the-endocrine-pancreas/

Thomassen, J. C., Mueller, M. I., Alejandre Alcazar, M. A., Rietschel, E., & van Koningsbruggen-Rietschel, S. (2018). Effect of Lumacaftor/Ivacaftor on glucose metabolism and insulin secretion in Phe508del homozygous cystic fibrosis patients. Journal of Cystic Fibrosis, 17(2), 271–275. https://doi.org/10.1016/j.jcf.2017.11.016

Thota, P., Perez-Lopez, F. R., Benites-Zapata, V. A., Pasupuleti, V., & Hernandez, A. V. (2017). Obesity-related insulin resistance in adolescents: a systematic review and meta-analysis of observational studies. Gynecological Endocrinology, 33(3), 179–184. https://doi.org/10.1080/09513590.2016.1273897

Tokarz, V. L., MacDonald, P. E., & Klip, A. (2018). The cell biology of systemic insulin function. In Journal of Cell Biology (Vol. 217, Issue 7, pp. 2273–2289). Rockefeller University Press. https://doi.org/10.1083/jcb.201802095

Tsabari, R., Elyashar, H. I., Cymberknowh, M. C., Breuer, O., Armoni, S., Livnat, G., Kerem, E., & Zngen, D. H. (2016). CFTR potentiator therapy ameliorates impaired insulin secretion in CF patients with a gating mutation. Journal of Cystic Fibrosis : Official Journal of the European Cystic Fibrosis Society, 15(3), e25–e27. https://doi.org/10.1016/J.JCF.2015.10.012

Tsalamandris, S., Antonopoulos, A. S., Oikonomou, E., Papamikroulis, G. A., Vogiatzi, G., Papaioannou, S., Deftereos, S., & Tousoulis, D. (2019). The role of inflammation in diabetes: Current concepts and future perspectives. In European Cardiology Review (Vol. 14, Issue 1, pp. 50–59). Radcliffe Cardiology. https://doi.org/10.15420/ecr.2018.33.1

Tsonkova, V. G., Sand, F. W., Wolf, X. A., Grunnet, L. G., Kirstine Ringgaard, A., Ingvorsen, C., Winkel, L., Kalisz, M., Dalgaard, K., Bruun, C., Fels, J. J., Helgstrand, C., Hastrup, S., Öberg, F. K., Vernet, E., Sandrini, M. P. B., Shaw, A. C., Jessen, C., Grønborg, M., & Frogne, T. (2018). The EndoC-βH1 cell line is a valid model of human beta cells and applicable for screenings to identify novel drug target candidates. Molecular Metabolism, 8, 144–157. https://doi.org/10.1016/j.molmet.2017.12.007

Turcios, N. L. (2020). Cystic Fibrosis Lung Disease: An Overview. Respiratory Care, 65(2), 233–251. https://doi.org/10.4187/RESPCARE.06697

Valle, A., Giamporcaro, G. M., Scavini, M., Stabilini, A., Grogan, P., Bianconi, E., Sebastiani, G., Masini, M., Maugeri, N., Porretti, L., Bonfanti, R., Meschi, F., Pellegrin, M. De, Lesma, A.,

Rossini, S., Piemonti, L., Marchetti, P., Dotta, F., Bosi, E., & Battaglia, M. (2013). Reduction of Circulating Neutrophils Precedes and Accompanies Type 1 Diabetes. Diabetes, 62(6), 2072–2077. https://doi.org/10.2337/DB12-1345

Van Ness-Otunnu, R., & Hack, J. B. (n.d.). Clinical Reviews HYPERGLYCEMIC CRISIS. https://doi.org/10.1016/j.jemermed.2013.03.040

Vanscoy, L., Blackman, S. M., Collaco, J. M., Bowers, A., Lai, T., Naughton, K., Algire, M., McWilliams, R., Beck, S., Hoover-Fong, J., Hamosh, A., Cutler, D., & Cutting. C. R. (2007). Heritability of lung disease severity in cystic fibrosis. American Journal of Respiratory and Critical Care Medicine, 175(10), 1036–1043. https://doi.org/10.1164/RCCM.200608-1164OC

Veldman-Jones, M. H., Brant, R., Rooney, C., Geh, C., Emery, H., Harbron, C. G., Wappett, M., Sharpe, A., Dymond, M., Barrett, J. C., Harrington, E. A., & Marshall, G. (2015). Evaluating robustness and sensitivity of the nanostring technologies ncounter platform to enable multiplexed gene expression analysis of clinical samples. Cancer Research, 75(13), 2587–2593. https://doi.org/10.1158/0008-5472.CAN-15-0262

Vonlaufen, A., Phillips, P. A., Xu, Z., Goldstein, D., Pirola, R. C., Wilson, J. S., & Apte, M. V. (2008). Pancreatic stellate cells and pancreatic cancer cells: An unholy alliance. In Cancer Research (Vol. 68, Issue 19, pp. 7707–7710). https://doi.org/10.1158/0008-5472.CAN-08-1132

Wang, C., Guan, Y., & Yang, J. (2010). Cytokines in the Progression of Pancreatic β-Cell Dysfunction. International Journal of Endocrinology, 2010. https://doi.org/10.1155/2010/515136

Wang, R., Klöppel, G., & Bouwens, L. (1995). Duct- to islet-cell differentiation and islet growth in the pancreas of duct-ligated adult rats. Diabetologia, 38(12), 1405–1411. https://doi.org/10.1007/BF00400600

Wang, X., Li, W., Chen, J., Zhao, S., Qiu, S., Yin, H., Carvalho, V., Zhou, Y., Shi, R., Hu, J., Li, S., Nijiati, M., & Sun, Z. (2018). A Transcriptional Sequencing Analysis of Islet Stellate Cell and Pancreatic Stellate Cell. Journal of Diabetes Research, 2018. https://doi.org/10.1155/2018/7361684

Watada, H., & Fujitani, Y. (2015). Minireview: Autophagy in pancreatic β-cells and its implication in diabetes. Molecular Endocrinology, 29(3), 338–348. https://doi.org/10.1210/me.2014-1367

Watari, N., Hotta, Y., & Mabuchi, Y. (1982). Morphological Studies on a Vitamin A-Storing Cell and its Complex with Macrophage Observed in Mouse Pancreatic Tissues following Excess Vitamin A Administration. In Okajimas Folia Anat. Jpn (Vol. 58, Issue 6).

Weiss, M. A. (2009). Proinsulin and the genetics of diabetes mellitus. In Journal of Biological Chemistry (Vol. 284, Issue 29, pp. 19159–19163). https://doi.org/10.1074/jbc.R109.009936

White, M. G., Maheshwari, R. R., Anderson, S. J., Berlinguer-Palmini, R., Jones, C., Richardson, S. J., Rotti, P. G., Armour, S. L., Ding, Y., Krasnogor, N., Engelhardt, J. F., Gray, M. A., Morgan, N. G., & Shaw, J. A. M. (2020). In situ analysis reveals that CFTR is expressed in only a small minority of β-cells in normal adult human pancreas. In Journal of Clinical Endocrinology and

Metabolism (Vol. 105, Issue 5, p. 1366). Endocrine Society. https://doi.org/10.1210/clinem/dgz209

Willcox, A., Richardson, S. J., Bone, A. J., Foulis, A. K., & Morgan, N. G. (2009). Analysis of islet inflammation in human type 1 diabetes. Clinical & Experimental Immunology, 155(2), 173–181. https://doi.org/10.1111/J.1365-2249.2008.03860.X

Wilschanski, M., & Novak, I. (2013). The cystic fibrosis of exocrine pancreas. Cold Spring Harbor Perspectives in Medicine, 3(5), a009746. https://doi.org/10.1101/cshperspect.a009746

Winkler, C., Lauber, C., Adler, K., Grallert, H., Illig, T., Ziegler, A. G., & Bonifacio, E. (2011). An interferon-induced helicase (IFIH1) gene polymorphism associates with different rates of progression from autoimmunity to type 1 diabetes. Diabetes, 60(2), 685–690. https://doi.org/10.2337/DB10-1269

Wu, N., Xu, X. F., Xin, J. Q., Fan, J. W., Wei, Y. Y., Peng, Q. X., Duan, L.-F., Wang, W., & Zhang, H. (2021). The effects of nuclear factor-kappa B in pancreatic stellate cells on inflammation and fibrosis of chronic pancreatitis. Journal of Cellular and Molecular Medicine, 25(4), 2213–2227. https://doi.org/10.1111/JCMM.16213

Xia, Y., Xie, Z., Huang, G., & Zhou, Z. (2019). Incidence and trend of type 1 diabetes and the underlying environmental determinants. In Diabetes/Metabolism Research and Reviews (Vol. 35, Issue 1, p. e3075). John Wiley and Sons Ltd. https://doi.org/10.1002/dmrr.3075

Xu, W., Gao, Z., Wu, J., & Wolf, B. A. (2005). Interferon-γ-induced regulation of the pancreatic derived cytokine FAM3B in islets and insulin-secreting βTC3 cells. Molecular and Cellular Endocrinology, 240(1–2), 74–81. https://doi.org/10.1016/j.mce.2005.05.010

Xue, J., Sharma, V., Hsieh, M. H., Chawla, A., Murali, R., Pandol, S. J., & Habtezion, A. (2015). Alternatively activated macrophages promote pancreatic fibrosis in chronic pancreatitis. Nature Communications, 6. https://doi.org/10.1038/NCOMMS8158

Yagihashi, S. (2017). Diabetes and pancreas size, does it matter? In Journal of Diabetes Investigation (Vol. 8, Issue 4, pp. 413–415). Blackwell Publishing. https://doi.org/10.1111/jdi.12590

Yang, Y., Kim, J. W., Park, H. S., Lee, E. Y., & Yoon, K. H. (2020). Pancreatic stellate cells in the islets as a novel target to preserve the pancreatic β-cell mass and function. In Journal of Diabetes Investigation (Vol. 11, Issue 2, pp. 268–280). Blackwell Publishing. https://doi.org/10.1111/jdi.13202

Yi, Y., Sun, X., Gibson-Corley, K., Xie, W., Liang, B., He, N., Tyler, S. R., Uc, A., Philipson, L. H., Wang, K., Hara, M., Ode, K. L., Norris, A. W., & Engelhardt, J. F. (2016). A transient metabolic recovery from early life glucose intolerance in cystic fibrosis ferrets occurs during pancreatic remodelling. Endocrinology, 157(5), 1852–1865. https://doi.org/10.1210/en.2015-1935

Ying, W., Fu, W., Lee, Y. S., & Olefsky, J. M. (2020). The role of macrophages in obesity-associated islet inflammation and β-cell abnormalities. In Nature Reviews Endocrinology (Vol. 16, Issue 2, pp. 81–90). Nature Research. https://doi.org/10.1038/s41574-019-0286-3

Zang, G., Sandberg, M., Carlsson, P. O., Welsh, N., Jansson, L., & Barbu, A. (2015). Activated pancreatic stellate cells can impair pancreatic islet function in mice. Upsala Journal of Medical Sciences, 120(3), 169–180. https://doi.org/10.3109/03009734.2015.1032453

Zha, M., Li, F., Xu, W., Chen, B., & Sun, Z. (2014). Isolation and characterization of islet stellate cells in rat. Islets, 6(2), e28701-1-e28701-7. https://doi.org/10.4161/ISL.28701

Zha, M., Xu, W., Jones, P. M., & Sun, Z. (2016). Isolation and characterization of human islet stellate cells. Experimental Cell Research, 341(1), 61–66. https://doi.org/10.1016/j.yexcr.2015.11.002

Zha, M., Xu, W., Zhai, Q., Li, F., Chen, B., & Sun, Z. (2014). High glucose aggravates the detrimental effects of pancreatic stellate cells on beta-cell function. International Journal of Endocrinology, 2014. https://doi.org/10.1155/2014/165612

Zhao, Q., Wei, Y., Pandol, S. J., Li, L., & Habtezion, A. (2018). STING Signaling Promotes Inflammation in Experimental Acute Pancreatitis. Gastroenterology, 154(6), 1822-1835.e2. https://doi.org/10.1053/J.GASTRO.2018.01.065

Zhou, Q., & Melton, D. A. (2018). Pancreas regeneration HHS Public Access. Nature, 557(7705), 351–358. https://doi.org/10.1038/s41586-018-0088-0.Pancreas

Zhou, Y., Li, W., Zhou, J., Chen, J., Wang, X., Cai, M., Li, F., Xu, W., Carlsson, P. O., & Sun, Z. (2019). Lipotoxicity reduces β cell survival through islet stellate cell activation regulated by lipid metabolism-related molecules. Experimental Cell Research, 380(1), 1–8. https://doi.org/10.1016/j.yexcr.2019.04.012